ANALYSIS AND MODELLING OF LAVA FLOW-FIELDS AND VOLCANO-TECTONICS PROCESSES WITH A FOCUS ON THE AL HARUJ VOLCANIC PROVINCE, CENTRAL LIBYA

A thesis submitted for the degree of Doctor of Philosophy at the University of London

Abdelsalam Salem Elshaafi

Rock Fractures and Fluid Flow Research Group
Department of Earth Sciences

October 2017

Declaration

I, Abdelsalam Salem Elshaafi, declare that this thesis and the work presented has been composed solely by myself and that it has not been submitted, in whole or in part, in any previous application for a degree or professional qualification unless otherwise stated. I am responsible for the data collection throughout this thesis, for the first authorship of the papers in the thesis and second authorship on one paper. Statements of my contribution are included on the first page of each paper. The collaborative contributions have been indicated clearly and acknowledged.

Signed

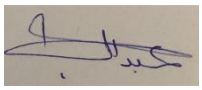

Dated

15/10/2017

Abstract

The thesis focuses mainly on various aspects of the volcano-tectonics processes in the Al Haruj Volcanic Province (AHVP), central Libya, as well as the emplacement and inflation of the Al-Halaq al Kabir lava flow field of the associated volcanic province. Six main volcanic clusters are identified in Libya. Each is thought to have been supplied with magmas from a deep-seated reservoir, most likely at the crust-mantle boundary. The magmatic overpressure in the AHVP is similar to that of typical regional feeder dykes in many other areas. Numerical modelling and field observations suggest that some feeder-dykes may have used steeply dipping normal-fault zones as part of their paths to the surface. Hence the various orientations of crater rows or volcanic fissures are likely to be partly controlled by the directions of pre-existing faults. Together the monogenetic volcanoes in the AHVP form two distinct density groups which are interpreted as separate volcanic systems. Each system is thought to be fed by a deep-seated and very extensive magma reservoir. From the eruptive volumes and the density distributions of the volcanoes, we estimate the volumes of the reservoirs. Numerical models are used to investigate local variation in the stress field resulting from general doming of the area during the late Miocene, as well as local loading by magma reservoirs, including the effects of various mechanical properties of the crustal layers, so as to explain the variation in space and time of the volcanic activity in this part of Libya. The inflation features are used to understand better the emplacement mechanism. The preferred pathways beneath upper lava crust are most favourable for thermally efficient lava delivery from the vent system to the distal portion of the lava flow field in the Al Haruj region. Numerical models suggest stress interaction between the six volcanic systems, encouraging shared dykes. The present work also investigates the mechanics of central volcanoes and caldera collapses in the Tibesti Volcanic Province (TVP), NW Chad.

Acknowledgments

First and forever thanks to God for everything. All gratitude is due to Almighty ”Allah” the Lord of the world who guided and aided me in bringing forth this work. Undertaking this Ph.D. thesis has been a life-changing experience for me and it would never have been achievable without the support and invaluable guidance that I regularly received from my supervisor Professor Agust Gudmundsson during these past four years. He has been a tremendous mentor for me. I would like to express my deepest sincere gratitude to him for encouraging my research and for allowing me to grow as a research earth scientist. I thank him for the great opportunity to study in details, for the first time, the volcano-tectonics of Libya and adjacent area and publish unique papers about these important regions. His advice on both research as well as on my career have been irreplaceable. Special thanks are dedicated to my advisor Professor Dave Mattey for his valuable remarks; constructive comments and suggestions during up-grade. I am eternally grateful to the examiners Professor Thorvaldur Thordarson and Dr. Domenico Chiarella who greatly contributed to improving the final version of Ph.D. thesis and provided interesting insights and ideas during the thesis defence. I would like to thank Dr. John Browning from University College London for helping me to develop my background in volcanology and being incredibly supportive. Also for his valuable advice, confidential assistance and fruitful discussions are greatly appreciated. I want to thank Dr. Nora Lecoeur for introducing me to numerical modelling, particularly to Comsol Multiphysics software, and offering support in this when needed. I am grateful for continuous support from Mr. Nathaniel Forbes Inskip who was heavily assistance for preparing samples and measurement of dynamic Young’s modulus at the Rock and Ice Physics Laboratory at University College London (UCL). Special thanks to him, Mr. Kayode Adeoye and Dr. John Browning again for reading and re-reading various sections of my thesis. My thanks go to Dr. Laura Christie from Educational Development for reading and re-reading several sections of my thesis. I would like to thank Awad Bilal and Basim Mohamed who are good classmates and were always willing to help and give their best suggestions. Special thanks are extended to Mr. Zayed Al Gharyanie from Schlumberger, for providing data about the properties of rock mechanics in the Sirt Basin. I gratefully acknowledge the full funding received towards my Ph.D. from the Libyan Ministry of Higher Education and Scientific Research. My thanks are also extended to Mr. Abdulhamed Shahlol who is Seismic Interpretation Superintendent from Arabian Gulf Oil Company, Benghazi-Libya, for providing seismic surveys of Zallah field. I feel obliged to express gratitude to the Head of Industrial Research Centre (IRC), Tripoli, and Director of the Geological Research and Mining Department and Director of Mapping Department for their encouragement and kind support during the fieldwork and other logistics. Appreciations also expressed to geologists of the Industrial Research Centre (IRC); Mr. Abdullah Buagrab, Mr. Abdullah Garbee, Mr. Naji Buzaid and Mr. Khalid Trish for their invaluable help on the fieldwork. I wish to express my appreciation to Dr. Özgür Karaoğlu from Eskişehir Osmangazi University, Department of Geological Engineering, and Dr. Mohamed Salah from the Department of Geology, the American University of Beirut for their great contributions to our published paper about Ağrı Dağı (Ararat) volcano, Eastern Turkey. I am very grateful to the members of the Department of Earth Sciences, Royal Holloway University of London for their moral assistance and helping me ease into life in Egham. It is hoped that the results of this thesis will meet the interest which they have given. I would also like to thank my parents, brothers, and sisters. They were always supporting me spiritually throughout my life and encouraging me with their best wishes. Last but not the least; I would like to give massive thanks to my wife, Rima Balhola and my sons, Salem and Belal. She always was cheering me up and calm me down and stood by me through good and hard times.

Table of Contents

List of figures

List of tables

Chapter 1: Introduction

1.1 Overview

The Neogene – Quaternary volcanism within the African and Eurasian plates is widely distributed and reflects a change in the plate tectonic regime, most likely are related to the changing stress fields and patterns of mantle convection (Guiraud and Bellion, 1995; Janssen et al. 1995; Cloetingh and VanWees, 2005; Cloetinghet al., 2005; Abadi et. al., 2008). The volcanoes are commonly classified into polygenetic and monogenetic based on several criteria. These criteria are mainly concerned with mode of eruption, volcanic eruptive volume, frequency of volcanic eruptions, magma source, stability of the volcanic conduits, and the mechanisms of the magma generations (Sato et al., 1990).

Monogenetic volcanoes strictly erupt only once but are defined as volcanoes that produce small eruptive volumes (typically ≤ 1 km^3) over a short-lived eruption duration (typically ≤ 10 years) with a wide range of eruptive styles, such as lava shields, scoria cone, spatter cones, tuff cones and maars (Fig. 1.1) (Németh and Kereszturi, 2015). The eruptive styles are mainly dependent upon magmatic effusion rate, composition of magma and bulk ratio of water-magma interaction (Houghton et al. 1999; Parfitt 2004, Valentine and White 2012; Valentine and Cortes 2013; van Otterloo et al. 2013; Valentine and de Vries 2014; Valentine et al. 2014; Németh and Kereszturi, 2015). Modern results from high resolution geochemical data (e.g., Jankovics et al. 2012; Valentine 2012; McGee et al. 2013) indicate that monogenetic volcanoes can illustrate systematic geochemical variations indicating the processes of melt differentiation. The monogenetic volcanism can be the result of an individual continuous eruptive phase or many discontinuous small eruptions (number of eruptive pluses) that can be fed from one or multiple magma batches (Németh and Kereszturi, 2015).

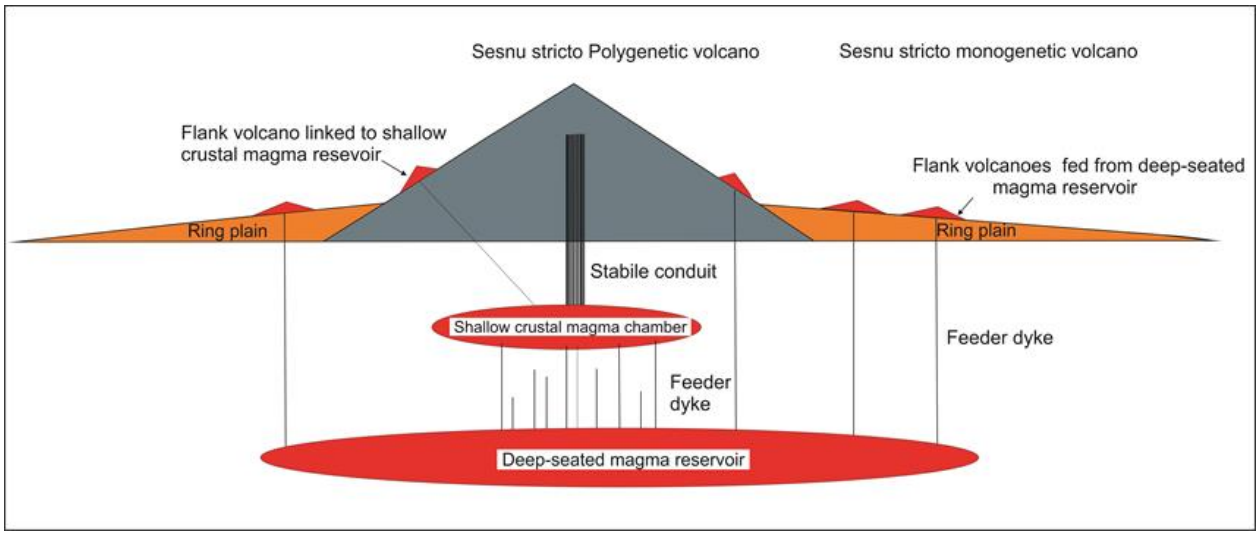

Figure 1.1. A schematic illustration of polygenetic and monogenetic volcanoes. The eruptive volume of a polygenetic volcano is characterised by cumulative eruptive volume that are several orders of magnitude greater than that of a typical monogenetic volcano. The long-lived polygenetic volcanoes formed by stabile conduit system from shallow crustal magma chamber, while short-lived monogenetic volcanoes formed through movable conduit from a deep-seated magma reservoir or even from shallow crustal magma chamber. Not to scale (modified from Németh and Kereszturi, 2015).

A single volcanic eruption may consist of several eruptive phases, which might take several months to years or even decades (Fisher and Schmincke, 1984, Thordarson and Self, 1998; Thordarson and Hoskuldsson, 2008). By contrast, polygenetic volcanoes are defined as volcanoes that erupt many times over long-lived period of time (tens of thousands of years to millions of years) through steady eruption via a stable of volcanic conduits, such as stratovolcanoes, shield volcanoes and calderas (Fig. 1.1). Therefore, polygenetic volcanoes commonly have volumes several orders of magnitude larger than monogenetic volcanoes. Sato et al. (1990) inferred from geochemical data from the central part of the Cameroon volcanic line that the polygenetic volcanoes were generated by partial melting of the upwelling asthenosphere diaper beneath the African plate, whereas the monogenetic volcanoes were generated by melting of the lowest part of the subcontinental lithosphere. Németh and Kereszturi (2015) have recently determined key parameters (eruptive volume, time period of eruption, the eruption style and number of volcanic conduits) that can be used to distinguish between

monogenetic and polygenetic volcanoes. Many examples from various polygenetic and monogenetic volcanoes on Earth are cited throughout the thesis in comparison to the study areas.

Although much volcanism occurs at plate boundaries, there is some volcanism generated within the plate interior. The highly voluminous volcanism within intraplate region is termed hotspots such as Hawaii, Iceland, and Louisville in the Pacific hemisphere. In addition, the massive flood basalt provinces within continents are thought to be produced above mantle plumes, such as Columbia River Basalt Group (CRBG) and Deccan Traps in India (Courtillot and Renne, 2003; Barry et al., 2010).The mantle plume theory, despite not being universally agreed upon, gives a global framework to understand better volcanism within the plate interiors. The hotspots are believed to be underlain by a large plume of anomalously hot mantle and caused high degree of melting in the mantle and consequently produced enormous volumes of basalt magma (Pirajno, 2004).

Courtillot et al. (2003) have identified three origins of hotspots on Earth which correspond to distinct mantle boundary layers as follows. (i) The primary hotspots may originate directly from the deepest part of the lower primary hotspots (Courtillot et al., 2003). (ii) The mantle plume seems to be generated in the lowermost mantle or at the core-mantle boundary and rise slowly through the mantle by buoyancy flux (>10^3 kg s^{-1}). The secondary hotspots are generated due to impinging of the plume stem (Richards et al., 1989; Cazenave et al., 1989; Pirajno, 2004). (iii) The Andersonian hotspots have been linked to asthenosphere and most likely related to tensile stresses in the lithosphere and decompression melting (Anderson, 1998; 2000).

There are five main intra-continental volcanic provinces in the North Africa, known as Gharyan –Tibesti volcanic provinces (Fig. 1.2). They represent the Neogene – Quaternary outpouring volcanic activity and arranged generally NW – SE linear trend which cover a total area exceeding 95,000 km^2 (Goudarzi, 1980; Lustrino et al., 2012; Busrewil, 2012). Those volcanic provinces are organised from the Mediterranean Sea coastline toward the Libyan – Chadian border as follows: (i) Gharyan Volcanic Province (GVP) in northwest of Tripoli (ii) As Sawda Volcanic Province (SVP) at the westernmost of the Sirt Basin (iii) Al Haruj Volcanic Provinces (AHVP) in the central Libya (iv) Nuqay Volcanic Province (NVP) at southernmost of Libya and (v) Tibesti Volcanic Province (TVP) at northwest of Chad. In addition, the minor volcanic occurrences of Jabal Al Hasawinah at the west of SVP as well as the ring dykes of Jabal Awayant are situated in the extreme southeast of Libya (Busrewil and Wadsworth, 1980; Elshaafi and Gudmundsson, 2016). Although these major five volcanic provinces (Gharyan – Tibesti volcanic provinces) form one of the largest volcanic fields in NW Africa, they have not been investigated in detail regarding volcano-tectonic evolution, origin of magmatism and mechanism of lava emplacement.

The present work mainly focuses on various aspects of the volcano-tectonics processes in the late Miocene – Holocene Al Haruj Volcanic Province (AHVP), central Libya, and the emplacement and inflation of the Al-Halaq al Kabir lava flow field of the associated volcanic province. This study also investigates the possibility of mechanical interaction and stress transfer between the main volcanic systems throughout Libyan territory. Owing to the absence of central volcanoes and collapse calderas in the AHVP, this thesis examines the mechanics of central volcanoes and collapse calderas at the late Miocene – Pleistocene Tibesti Volcanic Province (TVP), NW Chad. There are great differences between the AHVP and the late Miocene – Pleistocene Tibesti volcanic province (TVP), NW Chad, regards to volcano-tectonic aspects, the eruptive styles and production of materials.

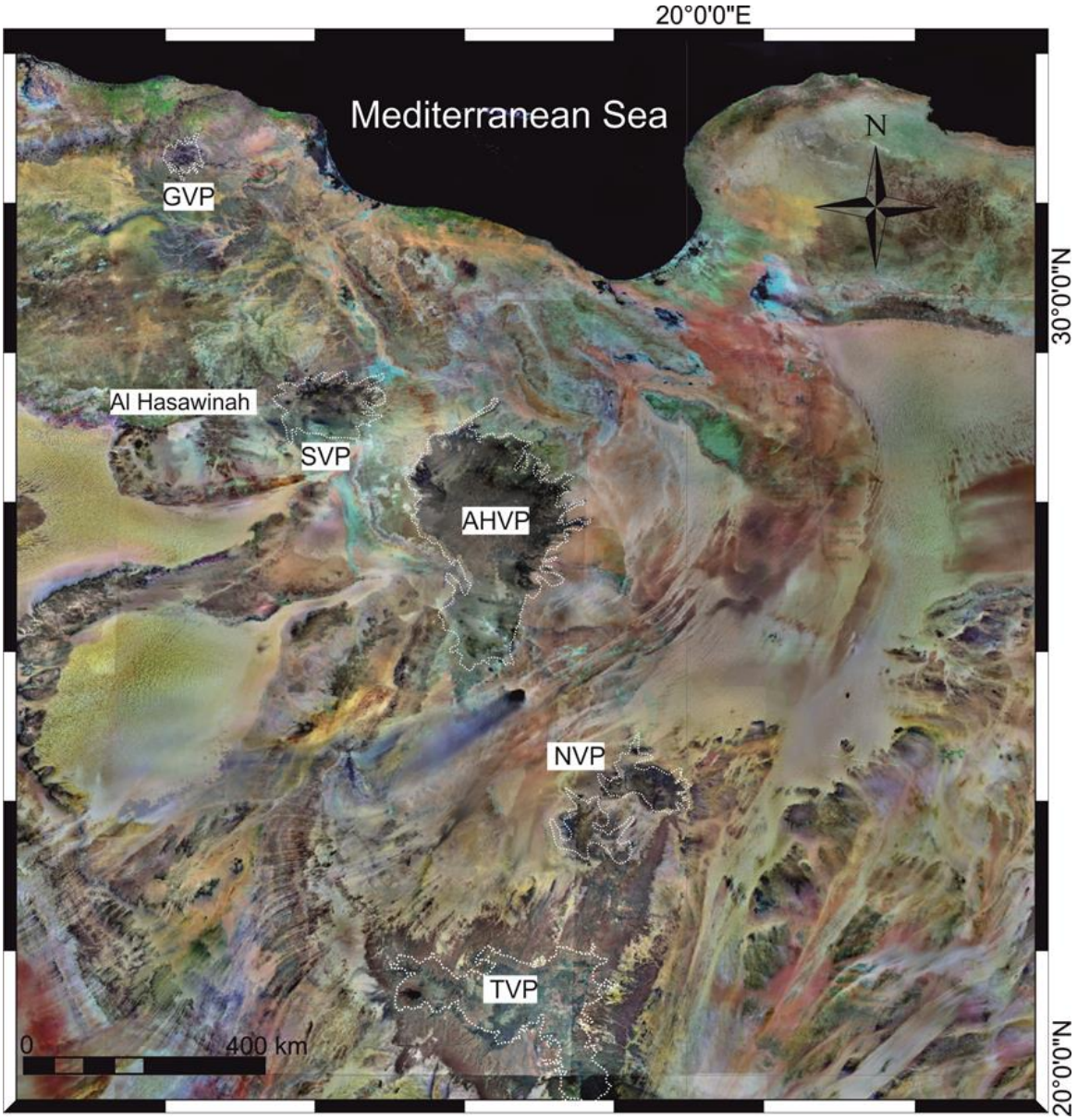

Figure 1.2. Landsat ETM+ image (adapted from Satellite Imaging Corporation) showing the distribution of the Tibesti – Gharyan volcanic provinces. The boundaries of volcanic provinces are indicated by dotted n white lines. GVP; Gharyan Volcanic Province, SVP; Sawda Volcanic Province, AHVP; Al Haruj Volcanic Province; NVP; Nuqay Volcanic Province, TVP; Tibesti Volcanic Province

The thesis provides an analytical approach for calculating volume of magma reservoirs from the volume of lava shields at the AHVP. Additionally, this analytical method has also been applied to estimate the source volume needed to supply two large basaltic lava flows at the Ağrı Dağı (Arart) stratovolcano, Eastern Turkey.

1.2 Aims of the present work

The aims of the present study, using a range of techniques, are as follows:

- To obtain data on the aspect (length/thickness) ratios of dykes and volcanic fissures at the AHVP from multisource high-resolution remote sensing images and field observations in order to calculate the magmatic overpressure (P_0) at the time of dyke emplaced for understanding better the volcano-tectonics in the AHVP. This method has important implications as a potential way to estimate the minimum magma overpressure necessary for a dyke to have the opportunity of erupting, thereby adding important data in order to make a realistic assessment of volcanic hazards. In addition, using the length/thickness ratios of fissures and dykes to estimate volume of injected material.

- To analyse and explore the conditions that favour the development of the dykes that fed the AHVP and construct numerical models for magma transport through the Earth's crust in the AHVP. The ultimate aim is to integrate numerical modelling, volcano-structural analysis, as well as spatial density and alignment of volcanic vents, in order to propose alternative mechanisms for magma-fault interaction coherent with tectonics alignments that elucidate how magma migrate through the Earth's crust to feed an eruption.

- To describe the morphologies inflation features in the AHVP (e.g., tumuli and lava rise plateaus) from more recent lava flows (the Al-Halaq al Kabir lava field) that are an indication their mode and style of emplacement. The aspect (height/width) ratios of tumuli are compared with morphology and aspect (height/width) ratios to the tumuli which have been studied in Icelandic Holocene lava shields (monogenetic shield volcanoes). The maximum and minimum axis for tumuli and lava rise plateaus are

measured in plan-view in order to find plan aspect ratios. The plan aspect ratios are then used to analytical and numerical models of tumuli and lava rise plateaus in order to estimate over-magmatic pressure and tensile stress that caused deflection and extension fractures respectively. Such data (plan aspect ratios) are also a crucial due to they could be applied to understanding remotely sensed observation of lava flows on other planetary surfaces (e.g., Moon and Mars).

- Compilation data on height as well as basal diameter of lava shields within the AHVP from satellite imagery and available geological maps through using ArcGIS10.1 in order to provide density maps of monogenetic volcanoes (crater cones, lava shields, and maars) so as to define the dimensions of the two main volcanic systems that constitute the AHVP. These data are taken as an indication of geometry of the magma reservoirs beneath the Al Haruj region. Subsequently, the areas and lengths of the axes of the two magma reservoirs beneath the AHVP have been calculated through ArcGIS 10.1.

- To provide data on the size and areal distributions of the lava shields on the AHVP, and compare them, as regards volume, with similar shields in Iceland. For comparison, polygenetic shield volcanoes from the Galapagos and Hawaii are included in some of the plots.

- Use numerical modelling results to explain, crudely, the size, age, and areal distribution of the lava shields in the AHVP with references to the local stresses and loading history of the inferred source magma reservoirs in particular.

- Identify spatial density and alignment of volcanic eruptions that allowed evaluating the relation between volcanism and tectonics of this Pliocene-Holocene intracontinental basalt province in order to investigate the feasibility of creating the volcano-tectonic model for the AHVP. It is a crucial to determine the tectonic controls on magmatism so as to evaluate

the possible renewal of volcanic activity in the AHVP due to this volcanic field may still be potentially volcanically active.

- To test the possibility of mechanical interaction between magma sources for four principal volcanic provinces in Libya (Gharyan, As Sawda, Al Haruj and Nuqay), in order to explore and analyse how stress interaction between nearby volcanic systems may contribute for formation or rejuvenation shear (faults) and extension fractures (e.g., dykes). In fact, the stress may be transferred between volcanic and seismic zones in extension tectonic regimes (cf. Gudmundsson et al., 2008). The spatial distributions of volcanic eruptions or monogenetic volcanoes within those volcanic provinces in Libya were examined and presented on a density map. ArcGIS was used to georeferenced raster images of the geological maps of these volcanic provinces as a guide to plot crater of these volcanoes. The magma reservoirs were modelled as circular hole field-scale in two-dimensional (2-D) and modelled as oblate ellipsoids (penny shaped or sill-like) with a thickness of 2 km penny-shaped in three-dimensional (3-D) with magmatic excess pressure 5 MPa at depth of 35 km corresponding to the crust-mantle boundary. The minimum diameter of reservoir for each volcanic system was roughly estimated at around 66 km by tracing the boundary of the greatest amount of volcanoes from density volcanic eruptions map.

- To provide a model to explain the formation of the central volcanoes (constructive structure) and calderas (destructive structure) as a consequence of the existence of a shallow magma chamber for the Tibesti Volcanic Province (TVP). Finite element methods (FEM) are used here to calculate the local stress field associated with magma chamber to better understand the volcano-tectonics mechanism for the TVP. Magma chambers are modelled here as a hole (circular) and oblate ellipsoids (penny-shaped, or sill-like) within the Earth's crust and subject to various loading conditions. The three main loading conditions considered are (i) the excess magmatic pressure within magma chamber, (ii) tensile

stresses represent the remote or field stress as well as (iii) the compressive stress at the bottom of the crust during the end of Miocene due to accumulation magma at lower crust or at the crust-mantle boundary and subsequently caused regional swelling or uplift. The results indicate that the uplift doming at the lower crust played major role to generate three major calderas respectively, while excess magmatic pressure and far-field stress as loadings are only favoured to form constructive volcano (radial dykes and inclined sheets) rather than collapse caldera (ring-faults and ring-dykes). Basaltic rocks mainly produced at peripheral of province and meantime followed each collapse caldera, but the intermediate and acid rocks are produced in the central parts.

- To explore the feeding mechanism of the large-volume basaltic lava flows at Ağrı Dağı (Ararat) volcano, Eastern Turkey, in the absence of evidence of volcano-tectonic forcing contributing to the generation of the lava flows.

1.3 Thesis plan

Two chapters and one appendix of this thesis are presented as peer-reviewed and published papers and one chapter in the second revision with some corrections before considered for publication in Tectonophysics. Two chapters are in preparation for publication in international scientific journals as well. Each of these chapters can be considered as separate study but all fit together as a part of a general volcanotectonic investigation and lava emplacement. The main methodologies frameworks have been used in this thesis are presented in Chapter 4. This chapter involves selecting a suitable research design, choosing and applying proper procedures for data collection and modelling. All measurements are subject to erroneous that are critically evaluated and accompanied by statement of the associated error or uncertainty. The tectonic evolution and palaeographic of Libya and North Africa at large scale are summarised in Chapter 3 with attention on the tectonic of the Sirt Basin due to the Al Haruj Volcanic Province (AHVP) is

located at the south-western margin of the Sirt Basin, one of the main structural elements of North Africa. It follows that the volcano-tectonic evolution of the Al Haruj region and history is strongly related to the tectonic evolution of the Sirt Basin.

Chapter 5 gives the first detailed description of the AHVP, and its volcanotectonic structures and evolution. In particular, we present the result of a study of over 400 lava shields, crater cones, maars, 47 feeder-dykes/volcanic fissures, and about 1000 related (mostly normal) faults. We show that, despite the great depth of origin of the magma (≈ 35 km), the magmatic overpressure is similar to that of typical regional feeder dykes in many other areas. We also show that some of the dykes may have used steeply dipping faults as parts of their paths and that the volcanic field can be divided into two subfields, the northern one of which may still be active.

Chapter 6 provides, for the first time, data on the size and areal distributions of 55 lava shields on the Al Haruj Volcanic Province (AHVP) that are mostly restricted to the north and southern parts and date from late Miocene to (at least) the end of Pleistocene (some activity extends into Holocene), and compare them, as regards volumes, with similar shields in Iceland. For comparison, polygenetic shield volcanoes from the Galapagos and Hawaii are also included in some of the plots. In particular, we show that the typical radius and height of lava shields on the AHVP are much closer to monogenetic lava shields in Iceland than polygenetic shield volcanoes on Hawaii and Galapagos and that the volumes of shields and their areal distributions have gradually decreased over time.

We also show that all the monogenetic volcanoes (shields, crater cones, and maars) form two distinct density groups, which we interpret as a separate volcanic systems. We propose that each system is fed by a deep-seated and very extensive magma reservoir. The density distribution of the volcanoes in each system, plotted as eruption points or sites, has a roughly elliptical surface expression, suggesting similar plan-view geometry of the source reservoirs. From the eruptive volumes and the density distributions of the

volcanoes, we estimate the volumes of the reservoirs. In addition, we made several numerical models in order to investigate local variation in the stress field resulting from general doming of the area during the late Miocene, as well as local loading by magma reservoirs, including the effects of various mechanical properties of the crustal layers, so as to explain the variation in space and time of the volcanic activity in this part of Libya.

Chapter 7 reports the results of detailed measurements of several hundreds of lava rise plateaus and tumuli at the distal portion of the Al-Halaq al Kabir lava field using field observations as well as ArcGIS10.1. These inflation features are used to understand better the emplacement mechanism in the Al Haruj region. Lava tubes played significant role in the transport of lava from the vent system to the distal portion of the flow field. Laboratory experiments are employed to determine dynamic Young's modulus for the basaltic rocks in the study area. Analytical and numerical approaches used to estimate the maximum tensile stress in the inflated upper crust which suggest theoretical stresses orders of magnitude higher than the tensile strengths of rocks. The tensile stresses induced by the effect of inflation are more than sufficient to result in brittle failure at the surface of the of the Al-Halaq al Kabir lava flow field. Tumuli observed in the area are remarkably similar in morphology and aspect (height/width) ratios to the flow-lobe tumuli which have been examined in Holocene lava shields (monogenetic shield volcanoes) in Iceland by Rossi and Gudmundsson (1996) at the distal portion of flow field, similar our study site. This geometric similarity suggests that they may have been emplaced through an analogous mechanism.

Chapter 8 provides new data on volcanic eruption centres in Libyan territory and combines this data with a suite of finite element numerical models in order to infer the relative location of magma reservoirs, and test, for the first time the possibility of mechanical interaction and stress transfer between the main volcanic systems of Libya. The spatial distributions of volcanic craters within these volcanic provinces were examined and presented on a density map using ArcGIS 10.1. Six main volcanic clusters are identified in this study so that an individual magma reservoir may have existence beneath each

maximum amount of volcanic craters. The crustal thickness may be variable along Libyan volcanic zone where each magma reservoir may be mainly drawn magma from a limited region where the crustal thickness attains a relative minimum that strongly correlated to the current basement elevated areas.

The magma reservoirs modelled as two-dimensional sill-like in 2-D and penny-shaped in 3-D within the elastic lower crust with length 66 km and thickness 2 km. The numerical models indicate, and the field data propose that the volcanic systems in Libya predominately interact mechanically with the nearby volcanic system even the great distance separates between them. In addition, the present numerical models explain why most of volcanoes in Libya have been erupted within or in the space between the four principal volcanic provinces. We also show that the high tensile and shear stresses concentration zones between the magma reservoirs that are nearly coincidence with extension (dykes and volcanic fissures) and shear (faults) fractures dominated in the area. There is considerable observational evidence supporting the numerical modelling findings.

Chapter 9 considers the mechanisms of central volcanoes and caldera collapses at the late Miocene – late Pleistocene Tibesti Volcanic Province, northernmost Chad. The variety of volcanic products along the TVP range from contemporaneous basaltic to acidic, during the end of Miocene to late Pleistocene, propose that the magma in this volcanic field may be comparatively derived from double magma sources. While the Al Haruj Volcanic Province, central Libya, is commonly supplied through single magma reservoir, most likely at the crust-mantle boundary and only produced basaltic lava flows.

We present many numerical models with various loadings to better understand the volcano-tectonic evolution and spatial and temporal distribution of the major volcanic units for this volcanic province. We infer that the stress fields associated with excess magmatic pressure or regional field stress as loading are only favourable to form constructive volcano (radial

dykes and inclined sheets) and mostly associated with small volcanic eruptive materials. By contrast, stress fields associated with the doming at the lower crust owing to accumulation of magma is favourable for initiation ring-faults at the surface or at shallow depth leading to emplacement of ring-dykes from lateral ends of existence shallow crustal magma chamber that subsequently led to subsidence block roof (piston-like caldera subsidence) and squeeze out most of magma in the chamber.

Appendix (C) deals with the multidisciplinary study of the Pliocene - Holocene Ağrı Dağı (Arart) stratovolcano, Eastern Turkey. This paper focuses on the most recent major eruptive phase that culminated with the eruption of two large-volume mafic lava flows of 3.2 km^3 and 0.6 km^3, respectively. Since it is unusual for stratovolcanoes to produce such large basaltic eruptions, we integrated different data (analytical, numerical models, seismic tomographic images along with geochemical data) to improve our understanding the conditions that triggered two large basaltic lava flows. They also convincingly demonstrated the presence and location of multiple magma chambers/reservoirs. This study is of interest also for social applications like contributing to a better local knowledge for volcanic hazard assessment due to this stratovolcano has at least four historical volcanic eruptions. Chapter 10 discuses and evaluates our results in the light of the methods and techniques used throughout thesis. Finally, chapter 11 involves briefly summary along with how the work can be ongoing into future researches.

Chapter 2: Literature review

2.1 Introduction

The Gharyan – Tibesti volcanic provinces are spatially related to two structural trends; early Palaeozoic structural elements of a prevalent NW–SE to NNW–SSE direction (parallel to the Red Sea) and late Palaeozoic to Mesozoic structures (Hercynian Orogeny) with a general E–W to ENE–WSW trend (parallel to East Africa rift) (Fig.2.1) (Woller and Fediuk, 1980). These two orthogonal trends represent regional structures, which have played a significant role in the geological evolution of this region, particularly on the location of thermal uplifts and magmatism (Woller and Fediuk, 1980; Radivojević et al., 2015). The Cenozoic Libyan magmas are most likely related to reactivation of these pre-existing megastructures during lithospheric stretching and asthenospheric upwelling as a result collision between the African and European plates since the late Jurassic (Bardintzeff et al., 2012; Stuart et al., 2014). Furthermore, at large scale there are two giant structural lineaments, namely Tibesti Lineament and Taoudenni lineament. They were identified by Guiraud et al. (2000) based on satellite imagery and digital elevation models (Fig. 2.1b). The Tibesti Lineament extends around 6,000 km length NW–SE striking from Algeria to Kenya while the Taoudenni lineament extends around 3,000 km length NE–SW striking along the northern margins of Taudenni Basin and the Hoggar Massif. Both giant lineaments are more or less parallel with the regional structural elements have been suggested by Woller and Fedick (1980) in Libyan territory.

The Gharyan – Tibesti volcanic provinces, however, are strongly correlated to the current basement elevated areas. The basement highs seem to be reflected subcrustal arching where magma might have preferentially penetrated. Alternatively, this might be difficulty in piercing thick sedimentary

sequence. The Precambrian crystalline rocks in Libyan territory are exposed in narrow and comparatively small areas such as Jabal al Hasawinah, west of the SVP and inlier of Dur Quassah west of the AHVP, whereas large areas at Tibesti massif at Libyan – Chadian border (Fig. 2.1). Therefore, it seems the attenuation of the Earth's crust within these specific areas during Palaeozoic and Mesozoic period is one of the main contributions that encourage to the outflowing of five principal volcanic provinces during the Tertiary up to Holocene time (Busrewil and Oun, 1991; Goudarzi, 1980; El-Makhrouf, 1988; Less et al., 2006). The following sections describe volcanological and tectonic aspects of the relevant volcanic provinces and pays particular attention to the AHVP.

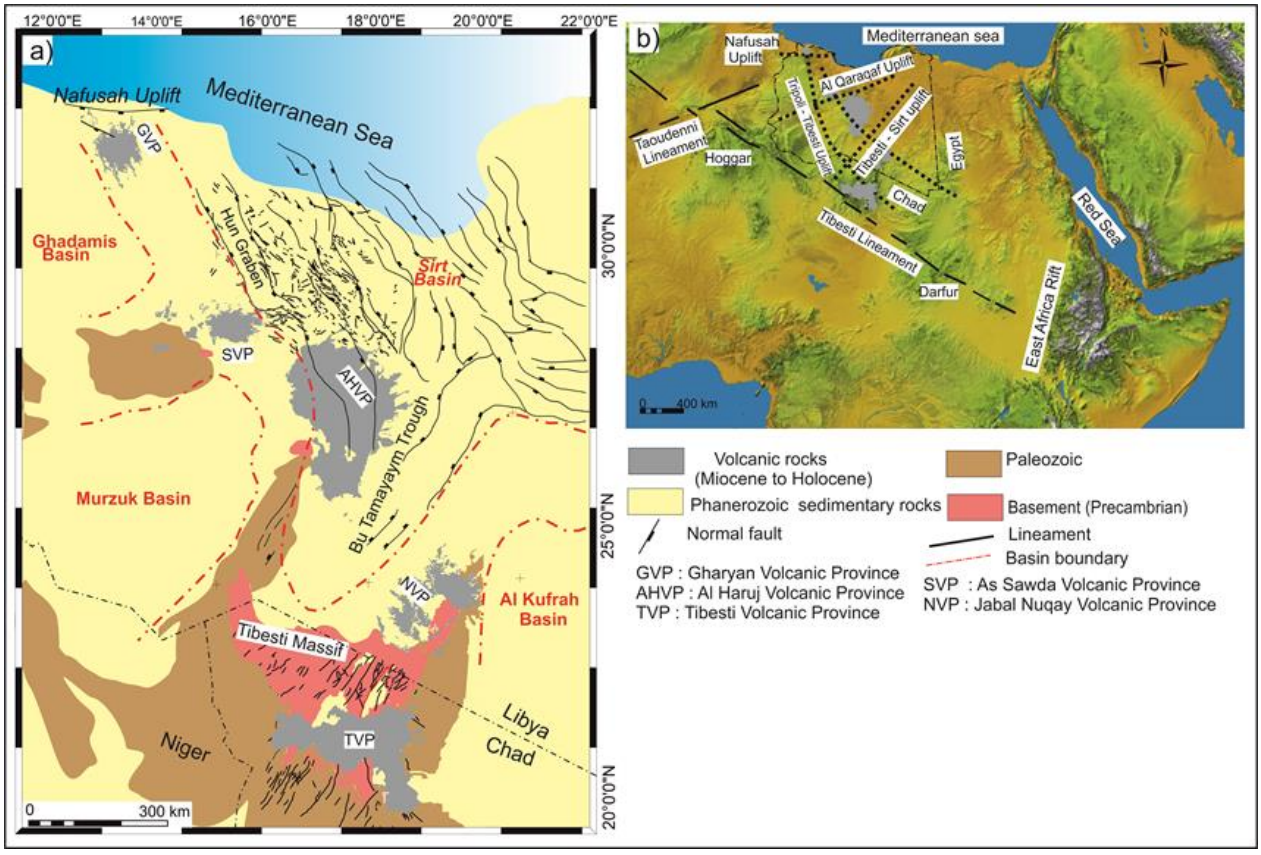

Figure 2.1. a) Simplified geological map showing the distribution of the Tibesti – Gharyan volcanic provinces (modified from Abadi et al., 2008; Deniel et al., 2015). b) Digital elevation map (from Shuttle Radar Topography Mission – SRTM data) shows two main orthogonal structural trends through the Libyan territory based on Woller and Fediuck (1980) which are more or less parallel with the mega-lineaments (Tibesti and Taoudenni Lineaments) were identified by Guiraud et al. (2000).

2.2 Al Haruj Volcanic Province (AHVP) (late Miocene to Holocene)

The Al Haruj Volcanic Province (AHVP) represents the largest part of the five extensive Gharyan – Tibesti volcanic provinces which are considered to be typical within plate (Busrewil and Suwesi, 1993; Peregi et al., 2003; Less et al., 2006). The AHVP developed during the end of Miocene up through Holocene time and has been linked to the rifting and tectonic evolution of the rifting of the Sirt Basin (Busrewil and Suwesi, 1993; Cvetkovic et al., 2010; Busrewil, 2012). The AHVP shows many similarities with the other three main mafic volcanic fields in the Libyan Territory (Gharyan, As Sawda and Nuqay volcanic fields) while it varies from Tibesti Volcanic Province (TVP), particularly in terms of volcano-tectonic mechanism, volcanic style, and products materials. For example, the lava flows of the Neogene – Quaternary Libya's volcanism are dominated by basaltic rocks with a minor amount of phonolites at Gharayn Volcanic Province (GVP). The basaltic lava flows are mainly associated with lava shields and scoria cones and absence of any collapse caldera or central volcanoes at Libya's volcanism. By contrast, the Tibesti Volcanic Province (TVP) is almost entirely made of ignimbrites, trachyte along with basaltic lavas which are characterised by predominately of collapse calderas and bimodal central volcanoes.

The AHVP is primarily made of sizeable alkaline to transitional basalts and subordinate sub-alkaline basalts; whereas more differentiated volcanic rocks are not observed (Busrewil and Suwesi, 1993; Peregi et al., 2003; Less et al., 2006). The area of the AHVP has been calculated using ArcGIS 10.1 which covers a total an area of approximately 42,000 km^2. It has been subdivided into two subprovinces from the north to the south based on morphology, age and thickness of lava flows (Busrewil and Suwesi, 1993; Peregi et al., 2003). The main and youngest subprovince is called Jabal Al Haruj al Aswad (the Black Mountain) or the Al Haruj al Aswad Subprovince (AHAS), which is mainly considered to be younger than Pliocene. Whereas the Jabal Al Haruj al Abyad (the White Mountain) or the Al Haruj al Abyad

Subprovince (AHAB) falls in the southern part of the main body which is slightly prolonged in a direction of a NNW–SSE trending zone (Peregi et al., 2003; Less et al., 2006; Martin and Nemeth, 2006; Al-Hafdth and El-Shaafi., 2015). However, the Al Haruj al Aswad Subprovince (AHAS) is dominated by large shield volcanoes setting on a lava plateau, while Al Haruj al Abyad Subprovince (AHAB) comprises clusters of scoria, spatters cones and maars aligned NW–SE to NNW–SSE trend (Martin and Nemeth, 2006; Abdel-al et al., 2013). A relatively large lava plateau was built during the first volcanic phase, and the magma seems to have been emitted as extremely fluid via several hundred of volcanic fissures. Most of the feeding fissures cannot be recognised in the field or from high-resolution remote sensing because they have been covered by more recent eruption products (Busrewil et al., 1996; Busrewil, 2012).

The surface features of the old volcanic phases are strongly eroded while the more recent volcanic phases have been well-preserved and show the primary features of pahoehoe lava flows which indicate that the volcanic activity was continued into Holocene (Busrewil and Suwesi, 1993; Busrewil, 2012). The differences in appearance and morphology between various volcanic phases have produced conspicuous topographic features, easily recognised in the field as well as on the aerial photographs and satellite images (Busrewil, and Suwesi, 1993; Peregi et al., 2003; Less et al., 2006). The surface exposures of the old lava flows are generally massive angular-blocky to sub-angular and composed of a pale grey colour and commonly have tension fractures (Fig. 2.2a). By contrast, the surfaces expressions of recent lava flows are extremely fresh, largely unaffected by weathering, coal black lava rocks, vesicular and show ropy pahoehoe flow structure and characterised by predominately inflation structures, such as tumuli and lava rises (Fig. 2.2b). Those basaltic rocks are generally disconformably overlying the older sequence of sedimentary rocks (Eocene to middle Miocene); (Fig. 2.2c). However, an elucidation of the origin and volcano-tectonics of this widespread Tertiary to Quaternary intra-continental volcanic rocks for the AHVP in particular and the Ghyaran – Tibesti volcanic provinces in general

are often controversial topic in the literature. They involve contrasting tectonic processes related to magma generation, such as lithospheric an extension and mantle plume upwelling (e.g., Peregi et al., 2003).

Figure 2.2. Field photographs showing a) large-blocky outcrop of an old basalt flow, b) a ropy pahoehoe lava in a more recent basalt flow (probably Holocene), c) the lower part calcareous sandstone of Maradah Formation (Lower – Middle Miocene) capped by blocky basaltic rocks in Wadi Al Bagar, the northeastern part of the AHVP. Note the persons at the top of photo for scale.

2.2.1 Physiography, accessibility and climate

The overall landscape of Al Haruj area that of is a vast plateau. It is mainly characterised by hilly, undulating hummocky morphology having numerous steep lava fronts, blocky lava field as well as tumuli and lava rises transversed by intermittent of desert sand dunes and dotted by kipukas (Busrewil and Suwessi, 1993; Busrewil, 2012; Al-Hafdth and El-Shaafi., 2015).

The AHVP rises above the surrounding area, and the average relief is around 700 m above sea level in the northern part of the AHAS. However, it reaches between 550 to 600 m above sea level in the southern part of the AHAB (Salem, 2014) (Fig. 2.3). The large spread of the lava flows appears to be mainly due to the flat the paleo-relief whereas the lava flows at periphery exhibited distinct elongation that run-off within paleo- valleys (cf. Yahiaoui et al. 2014). Although, the Al Haruj region was inhabited in prehistoric time as proven from prehistoric tools, where lithic was found from many sites within the Al Haruj (Busrewil et al., 1996; Busrewil, 1996). Currently, the whole area of the Al Haruj is uninhabited, with no permanent settlement (Busrewil and Suwesi, 1993; Salem, 2014). However, it contains some oil fields for national and international oil companies because the Al Haruj region contains some important hydrocarbons reservoirs (Fig. 2.4). The Al Haruj area is accessible through several villages such as Zallah, Hun, Soknah, Al Fugaha and Temessah in the northwest, on dirt road or tracks so that a four wheel drive vehicle is an essential to access the study area. However, the Al Haruj region is cut by many valleys flowing generally from west-southwest toward east-southeast. These valleys radiate from the central part of the Al Haruj al Aswad Subprovince (AHAS) to their tributaries branching non-systematically in various directions.

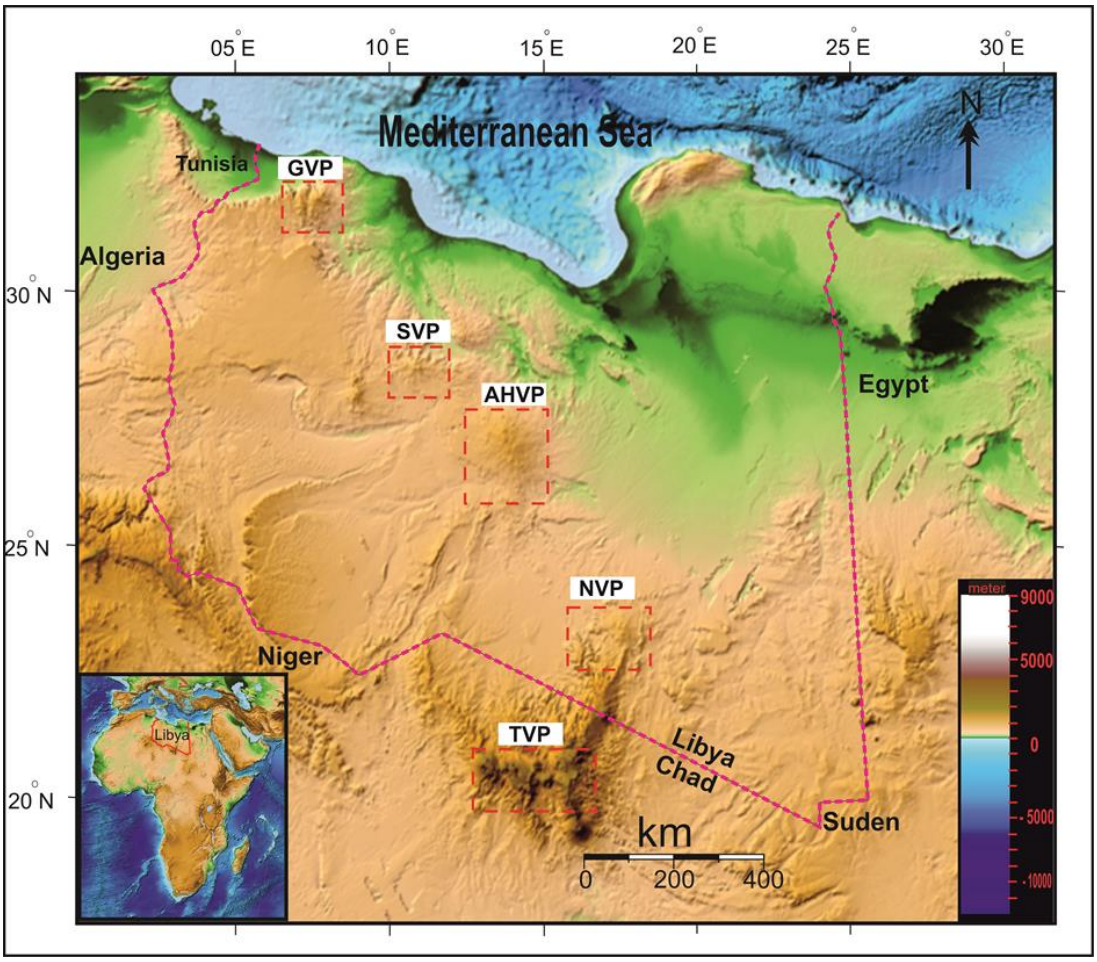

Figure 2.3. Relief map showing the locations and elevations of the main five volcanic provinces (a digital elevation model at 90 m spatial resolution is taken from ETOPO1 Ice Surface Global Relief Model, 2009).

The surface topography of Al Haruj is characterised by widespread small shallow depressions, known as kipuka or Balta in a local Arabic name. Kipukas are surrounded by lava flows and characterised by flat bottomed Quaternary sediments, varying in diameter from about a few hundreds of meters to several kilometres. This feature commonly forms when lava surrounds a hill or topographic high at the time of the lava emplacement (Peregi et al., 2003). During lava emplacement and inflation processes, the surface topography generally begins to be reversed, high areas (e.g., kipukas) in the terrain become low whereas low areas become lava rises and tumuli (Self et al., 1998).Therefore, the kipukas are now depressions among the lava tongues and inflation features. They are commonly filled by

Quaternary sediments of yellow colour, which are partly of aeolian origin and may be derived from the surrounding slopes of sedimentary rocks (Fig. 2.5). The kipukas are readily recognisable on satellite image as small white spots within more recent lava flows. (Busrewil and Suwesi, 1993; Peregi et al., 2003; Less et al., 2006). The climate in this region is very arid, and with an annually but erratic rainfall between October and April which ranges from 15 to 30 mm/year. The average temperature in June and July is around 37˚C, whereas in December and January, it is less than 10˚C. The humidity is about 22% in June and July (Goudarzi, 1970; Busrewil and Suwesi, 1993). Furthermore, the winter is typically Saharan, very cold at night and warm during the day; it is hot in the summer with occasional sand storms. Acacia tortilles and Ziziphus lotus are the main flora growing in this area. Annuals herbs and grasses provide a ground cover over the kibukas and valleys banks (Busrewil and Suwesi, 1993). Nevertheless, as the AHVP is quite remote as mentioned earlier, it is rather inaccessible and an extremely tough terrain. The field works were carried shared with the team of Industrial Research Centre (IRC), Tripoli, who were doing field work as part of the geological mapping project of SE Libya.

2.2.2 Volcano-tectonic evolution of the AHVP

The Al Haruj al Aswad Subprovince (AHAS) represents the northern of the AHVP and characterised by more than 100 m thickness of volcanic sequence and dozens of large lava shields (Peregi et al., 2003). Lavas emitted in the central parts of this subprovince were captured by radial erosional pattern along the periphery, so that the volcanic pile gradually decreases in thickness towards the margins (Fig. 2.2c). The Al Haruj al Abyad Subprovince (AHAB) is situated in the southern part of the main body of the AHVP which is slightly elongated toward NNW–SSE (Peregi et al., 2003;Martin and Nemeth, 2006; Less et al., 2006) (Fig. 2.4).

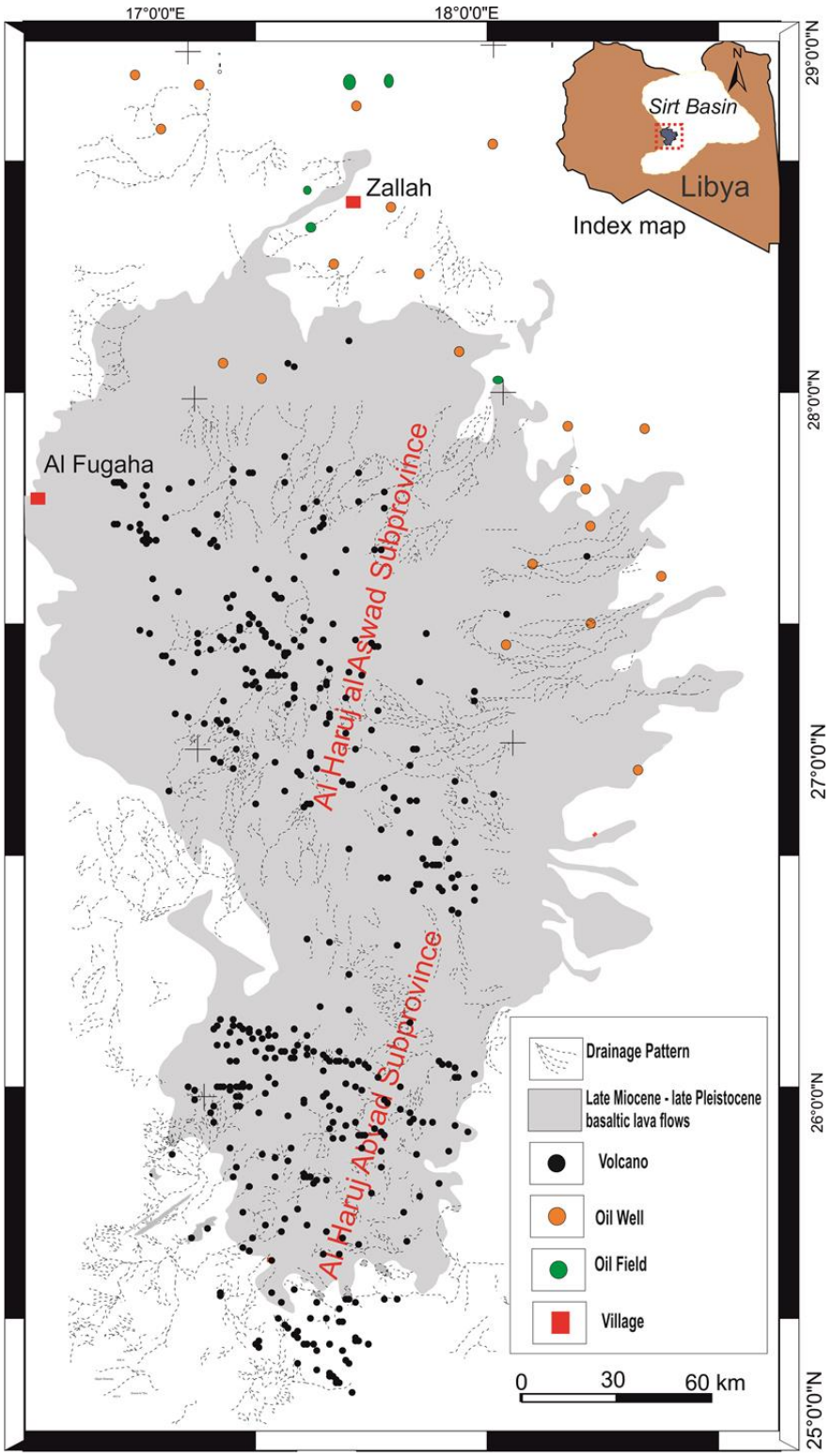

Figure 2.4. Sketch map showing the drainage pattern of the AHVP and areal distribution of volcanoes inferred from the available geological maps of the Al Haruj region (Vesely, 1985; Busrewil and Suwesi, 1993; Peregi et al., 2003 and Less et al., 2006). The AHVP has been divided into the Al Haruj al Aswad Subprovince (AHAS) in the north and the Al Haruj al Abyad Subprovince (AHAB) in the south.

It consists of more than several hundreds of small lava shields and scoria cones forming linear vent systems indicative of volcanic fissures. Neogene sedimentary rocks in many locations in the AHAB were not covered by basaltic lava flows (Pacific Survey, 1979; Less et al., 2006).

However, the lava flows of the whole AHVP have been classified by Busrewil and Suwesi (1993) into six major volcanic phases or groups and each volcanic phase was subdivided into subphases (Fig. 2.6). There are several criteria that can be used to differentiate between volcanic phases as follows; (i) colour variation and morphological characteristics of the basaltic lava flows observable on Landsat images together with aerial photographs of different scales, (ii) drainage pattern and density of basaltic lava flows detectable on multispectral Landsat images and on the aerial photographs, (iii) degree of weathering of basaltic rocks, (iii) sequence of superposition of the lava flows, (iv) morphological and lithological characteristics observable in the field, (v) K/Ar age method and palaeomagentic measurements (Table 2.1) (Busrewil and Suwesi, 1993; Peregi et al., 2003; Peregi et al., 2006). Each volcanic phase has certain period of time and specific characteristics in the field and on multispectral satellite imagery that can be used to identify it (e.g., Fig. 2.2a, b).

The average total thickness of basaltic rocks in the central parts of the AHVP does not exceed 150 m and gradually decreases to several meters in the margins, based on measurements in various parts of the province. The average accumulated thickness is much small compared with areal distribution of the volcanic flows (Pacific Aero Survey, 1979; Peregi et al., 2003). Figure 2.6 showing the areal distribution and order of the six main volcanic phases in the AHVP from the late Miocene to Holocene. The division of the volcanic phases is based on the above listed criteria that have been carefully used by Busrewil and Suwesi (1993), Peregi et al. (2003), Less et al. (2006) for mapping the entire AHVP. The area of each volcanic phase has been calculated during this study by using ArcGIS 10.1 along with

detailed published geological maps as a baseline. Subsequently, the volume for each volcanic province crudely estimated based on the average maximum thickness for each individual volcanic phase in the field (Busrewil and Suwesi, 1993; Peregi et al., 2003; Peregi et al., 2006) (Fig. 2.6b, c).

Figure 2.5. Photograph showing kipuka formed in-between the lava tongues. The depression is covered by thick argillaceous, aeolian and fluvial sediments of mostly silt and sand with common mud cracks as seen in the up right corner. The view is to the west.

The production rate of eruptive materials at the AHVP has generally declined over time from the end of Miocene up through Holocene. More specifically, around 231 km^3, erupted (volcanic phase I) during the late Miocene - early Pliocene, while only 11.5 km^3 erupted (volcanic phase VI) during late Pleistocene-Holocene. Hence the decrease in lava production over time is evidently sizeable, and may be greater than that indicated in Fig. 2.6. In

addition, most of the previous studies on the AHVP (e.g., Peregi et al., 2006; Bardintzeff et al., 2012) suggest that the primary magma derived from a common parental source with different degrees of partial melting. Further detail about the lava coverage decrease with time is covered in Chapter 6. Despite, the AHVP representing one of the largest among volcanic provinces in North Africa with an area of approximately 42,000 km^2, modern investigations are relatively few, and most of the literature has been produced in relation to regional mapping primarily because of the relatively difficult ground-access to this region.

Nonetheless, the origin and volcano-tectonics of the AHVP are debated and various interpretations based on geochemical data are available. Until now the existing models have been mostly centred on two hypotheses. Some authors consider the region to be a hotspot mantle plume beneath the region. By contrast, other authors completely rule out the mantle plume theory. For example, Klitzsch (2000) suggests that the magmatism of the AHVP resulted from tension produced by reactivation of three major structural elements which are NW–SE trending Palaeozoic (South Al Haruj Uplift), the NE–SW trending Tibesti – Sirt uplift (Hercynian Orogeny) and the continuation of the Cretaceous – Tertiary Hun graben (Fig. 2.1). In contrast to other volcanic provinces in Libya, these three tectonic elements played a significant role in geological development of the Al Haruj volcanic province. This most likely account partly for the large size of the AHVP compared to the sizes of the other volcanic provinces in Libya (Farahat et al., 2006).

The primary magmas are considered to have been produced as a consequence of lithospheric delamination. The primary magmas derived from the mantle commonly never undergo fractional crystallisation, assimilation, or magma mixing that would yield high Mg values (>0.7), high Ni (>1000 ppm), high Cr (>400-500 ppm) and low SiO_2 < 50% (Wilson, 2007). Therefore, the primitive magmas can be considered as representative original mantle. Nixon et al. (2011) inferred from new geochemical database

in the AHVP that the primary magmas were originated at depths of 70 and 74 km for tholeiitic and alkali magmas. The primary magmas ascend through the mantle by porous flow (Scott and Stevenson 1986). Subsequently, they are normally accumulated at the Moho discontinuity as a pool or puddle to form magma reservoir. The primary magmas at this place were then undergone to fractional crystallization that led to reduce Mg concentrations in the melt. The magma types are generally defined mainly based on the silica content (SiO_2) into (i) mafic ($SiO_2 \leq 53\%$), (ii) intermediate ($SiO_2 \leq 63\%$) and (iii) felsic magma ($SiO_2 > 63\%$ to 70%). These differences in silica content are directly related to differences in temperature, viscosity as well as gas content (Winter, 2010).

The primary magma in the AHVP may be associated with the rifting of the Sirt Basin, inducing low degree partial melting at depth in the upwelling asthenosphere. The degree of partial melting in the mantle is important so as to determine the type of magma is produced (Wilson, 2007), since Nixon et al. (2011) concluded from new geochemical data that the primary magma in the AHVP are produced at partial melt of 13.5% and 18.9% for tholeiitic and alkali magmas, respectively. The discrete volcanic phases in the AHVP might be corresponded to periods of rejuvenation of pre-existing fault system in response to late Tertiary extensional tectonic events that most likely related to Africa-Eurasia convergence (Cvetkovic´ et al., 2010).

Busrewil (1996) inferred from the aerial distribution of more recent lava flows (volcanic phase V and VI) along NW–SE and NE–SW and from alignment of shield volcanoes along with scoria and spatter cones that the AHVP is probably related to the intersecting fault system of Dur al Qussah and prolongation of Hun graben. Therefore, the rising magma may have propagated along the planes of the weakness at the crossing of these two main tensional structural elements. Thus, the pre-existing basement faults may have played a major role in the tectonic evolution of the AHVP and the whole Gharayn – Tibesti volcanic provinces.

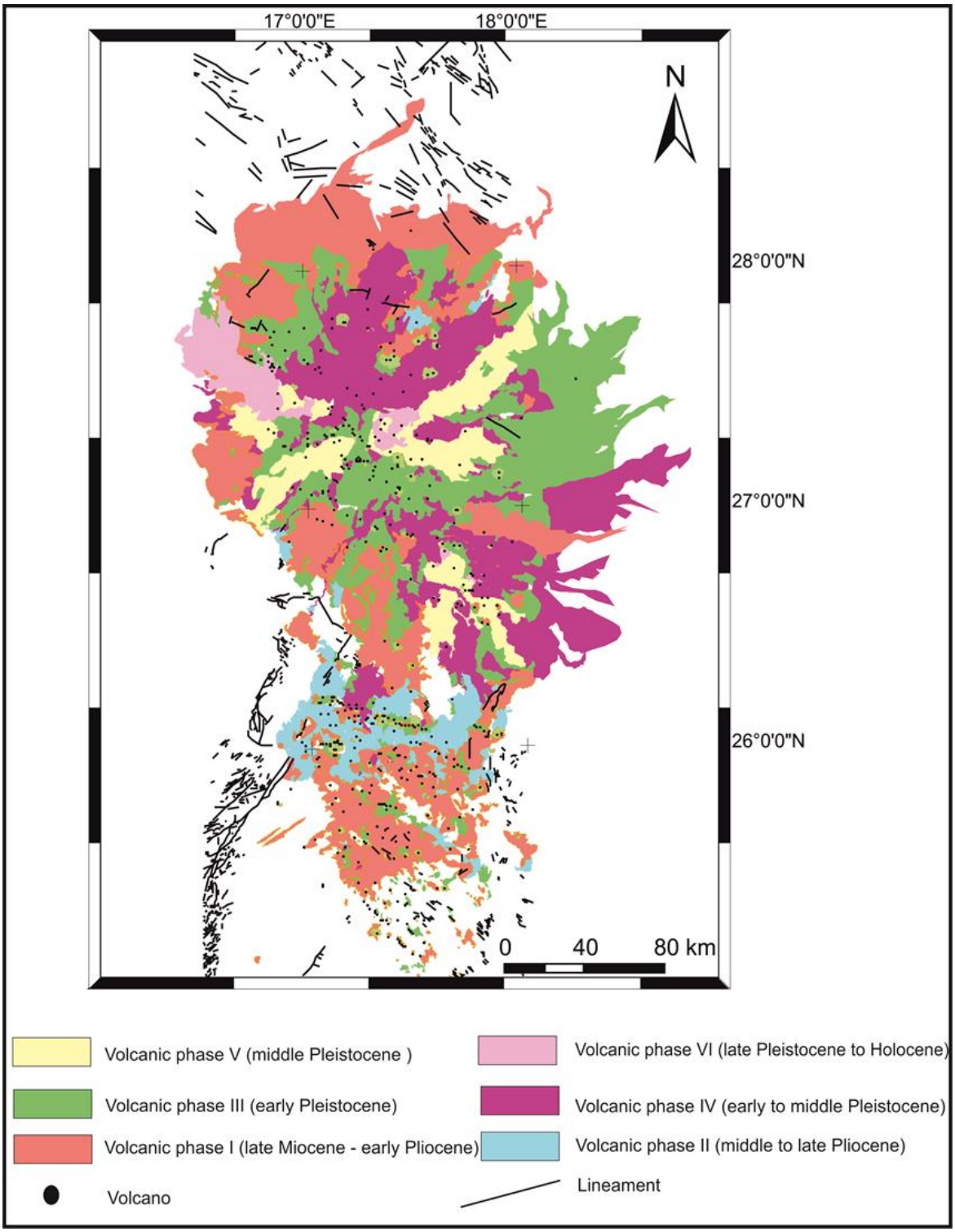

Figure 2.6. Geological map of the Al Haruj Volcanic Province (AHVP) showing the distribution of the major six volcanic phases, volcanoes (including shield volcanoes and scoria cones) as well as structural elements that inferred by integrating satellite imagery with the existing geological maps (modified after Woller, 1984; Vesely, 1985; Busrewil and Suwesi, 1993; Peregi et al., 2003; Less et al., 2006).

Alternatively, model of mantle plume has been supported by some studies beneath the Al Haruj region (e.g., Hegazzy, 1999). He suggests that the origin of Libyan magmatism, along the NNW–SSE linear trend of Libyan volcanic provinces and their decrease in age from NNW toward SSE direction is due to motion of the region over a fixed mantle plume that led to systematic change in the location of volcanism throughout Libyan territory with time from northwest at Ghyaryan Volcanic Province (GVP) to extreme southeast at the Nuqay Volcanic Province (NVP) at Libyan – Chadian border (Fig. 2.1). However, the structural and magmatic patterns of these volcanic provinces are thought to be complex and episodic for such simple model to work (Farahat et al., 2006). Besides, Burk (1996) proposes that North African intraplate volcanism is related to mantle plumes in the underlying asthenosphere. Ebinger and Sleep (1998) suggest that nearly all of the volcanic activities in North and Central Africa such as Darfur, Tibesti and Cameroon are most likely associated with the Afar plume, since plume materials flowing laterally beneath the lithosphere and feeding these volcanic edifices (Azzouni-Sekkal et al., 2007). But the relatively low magmatic temperature that has been obtained through the studied peridotite xenoliths (spinel lherzolites) (Peregi et al., 2003; Less et al., 2006) from the Al Haruj al Abyad Subprovince, do not support the presence of a mantle plume underneath the Al Haruj region but It rather suggests the existence of relatively cold lithosphere.

Furthermore, the tomographic model of Lie´geois et al. (2005) also does not support existence mantle hotspots beneath Libyan volcanic provinces. This model assumes that the shallow mantle is warmer with melt fractions at depths between 100 km to 150 km. This estimated depth is in good agreement to the depths of 80-150 km reported from geobarometry and isotopic studies on Al Haruj and Waw an Namous lavas and lithospheric mantle xenoliths (Bardintzeff et al., 2012). The relatively low $^{3}He/^{4}He$ isotope signature of Gharyan xenoliths in particular and the Cenozoic volcanic rocks of NW Africa in general suggest that the sublithospheric component of the erupted magmas originates within the upper mantle (Pik et al., 2006;

Beccaluva et al., 2008). Farahat et al. (2006) have mentioned that the Libyan is most likely related to the large Afro–Arabian rift system that extends from Turkey to Mozambique. This rift system is thought to have developed episodically rather than continuous. Radiometric age dating of the eastern rift in Kenya has been evolved in three major pulses from Eocene (44–38 Ma), Middle Miocene (16–11 Ma) and Pliocene to Holocene (5–0 Ma).These timespans are generally contemporaneous with ages of Libyan volcanic activity; for example, the AHVP correspond to the third episode whereas Gharyan volcanic province was contemporaneous with whole three episodes.

Peregi et al. (2003) have inferred that it is extremely difficult to decide whether or not AHVP was related to the extension of lithosphere passive rifting or active rifting associated with upwelling mantle plume. The primitive mantle normalized multi-element patterns of most of these mafic rocks are highly enriched in incompatible trace elements, similar to within plate basalts, particularly oceanic island basalts (OIB) spectrum (St Helena-type) which represent basaltic melts an enriched asthenospheric mantle source, most likely associated with uprising mantle plume (Asran and Aboazom, 2004). St. Helena is formed by mantle plume similar to that of many volcanic islands, such as Hawaii. This type of volcanism is long-lived (tens to hundreds of thousands of years) and characterised by steady eruption though volcanic conduits resulting in the formation of composite stratovolcanoes (polygenetic volcanism). The average total thickness of lavas is much larger than the area distribution of volcanic flows. By contrast, the origin of volcanism at the AHVP may be related to lithospheric stretching due to rifting of the Sirt Basin that produce small eruptive volumes over a short period of time to form only scoria cones or small lava shields (monogenetic volcanism). Hence the average sequence thickness in the AHVP is much smaller than the areal distribution of the volcanic flows as already mentioned. Farahat et al. (2006) also postulated that the linear trend of the Libyan volcanism and their decrease in age from NNW towards SSE is highly probably related to variations intraplate extensional field stresses.

Continental rifting is commonly associated with asthenospheric upwelling with high heat flow, but there is some argument as the mechanism involved.

The structures have been observed by Cvetkovic´ et al. (2010) in the AHVP are most likely related to the late evolution of the Sirt Basin during Paleocene to Miocene, producing rejuvenation of pre-existing structural element from the Tibesti-Sirt environment in response to convergence of African and European plates that are characterised by NE–SW tension and perpendicular compression. It seems to have partially controlled the volcanic activity in the Al Haruj region. Yahiaoui et al. (2014) suggest that the Al Haruj - Waw an Namous region would represent the eastern border of the Murzuq craton where the In-Ezzane volcanic field, in Algeria, is situated in the same framework on the western border of the Murzuq craton at the triple junction of Algeria, Niger, and Libya, as evidenced by their similar isotopic signatures (Bardintzeff et al., 2012). Therefore, those volcanic fields represent similar mantle domain within the circum cratonic mantle lying beneath the Murzuq craton. Furthermore, Stuart et al. (2014) have inferred from new geochemical and isotope data from four main volcanic provinces of Libya that the locations of these volcanic provinces have not changed systematically with a time in a way that is suggestive of plate motion over fixed mantle plume. Therefore, the Neogene volcanism up through recent time seems to be related to reactivation of pre-existing structures that have been resulted in response to approaching of Europe and Africa since Jurassic time.

To sum up, volcanic activities in the AHVP has been periodic with difference in their duration indicating that the volcano-tectonics is mainly controlled by reactivations of pre-existing fault systems during Neogene time. Therefore, it has commonly believed that extension and shear fractures enhance volcanic activity (Fig. 2.7) (Le Corvec et al., 2013). In addition, the more recent lava flows (volcanic phase V and volcanic phase VI) have been cutting by a NW–SE set of faults that indicate the reactivation of these faults obviously

postdated the volcanic activity in the AHVP. It can be suggested the basement faults are still tectonically active (Busrewil et al., 1996).

2.2.3 Previous Investigations of the AHVP

Many authors have been studied and reported on the different occurrences of basaltic rocks in this province, some of who provided remarkably useful information (Peregi et al., 2003; Less et al., 2006). It is important to mention that most previous studies of the AHVP were based on separated studies discussing the northern subprovince (the Al Haruj al Aswad Subprovince) and southern subprovince (the Al Haruj al Abyad Subprovince) as independent provinces which make the volcano-tectonic evolution of the whole AHVP ambiguous.

The first geological reference to the AHVP commenced by Hornman (1802) who mentioned the presence of basaltic lava flows and volcanic cones. He gave brief account of the Black Mountains existing in the central part of Libya while Palaeozoic in southernmost of Libya had been studied by Overweg (1851). Further data have been added by later geologists (Busrewil and Suwesi, 1993). The first authentic geological maps in the regional scale of the central and southern parts of Libya and a more detailed field works were carried out during 1930s and 1940s (during Libya was colony under Italy), mainly by Italian geologists under the supervision of Desio (1934, 1936, 1937). He undertook a geological reconnaissance trips to parts of the Al Haruj (Al Aswad and Al Abyad) and highlighted the youthfulness of lava flow east of Al Fuqaha town and stressed their similitude to Etna effusive. Subsequently, Bellair et al. (1952) gave a brief geological description of this relatively remote region and identified two episodes of basaltic activity, both of which were assumed to be post-Oligocene based on morphological features of lava flows and cross cutting relationships with Oligocene host rock. The earlier episode produced a broad lava plateau, whereas the later

activity gave rise to a series of shield volcanoes and scoria cones that mostly concentrated in the central and southern parts of the AHVP (Peregi et al., 2003; less et al., 2006).

2.2.3.1 Volcanic phases and age dating of the AHVP

The first attempt to distinguish individual basaltic lava flows within the AHVP was made by Klitzsch (1967, 1968). He established the first comprehensive division of the different lava flows and recognized six major and a minor basalt lava flows on the basis of remote sensing in conjunction with several reconnaissance field trips. He also mentioned that the basaltic lava flows were produced episodically rather than continuously. The preliminary geological map of the AHVP was produced by complementary of aerial photo mosaics of scale 1:250,000 using indices like the surface appearance of the basalt flows, development stage of the drainage system with morphological of lava flow in the field (Peregi et al., 2003). Assaf et al. (1973) provided data on the radioactive materials in the Precambrian granite rocks of the Dor el Qussah inlier west of the AHVP using scintillometer. The scintillometric measurements were done by trenching and pitting in the anomalous areas, but they found only minor precipitations of radioactive materials.

In general terms, the basaltic rocks of the Al Haruj volcanic field occur with time span running from the late Miocene to late Pleistocene according to age dating by number of authors in the period from 1974 to 2012 (Table 2.1). Nixon et al. (2011) suggest that the Al Haruj volcanic activity lasted until pre-historic time or until 3.2 ka. Excellent preservation of inflation features, such tumuli and lava rises for last volcanic phase (phase VI) strongly supported their results. In addition, Busrewil et al. (1996) suggest that the volcanic activity commenced in the late Miocene and extended up to the pre-historic time, where more recent lava flows (volcanic phase V and phase VI) must have been post-Neolithic in age due to field studies indicating both of these

phases did not use of pre-historic sites and thus most likely erupted after Neolithic age. Rocks from the older lava flows (volcanic phases I, II, III and IV) were widely employed as Neolithic stone weapons. The age dating results indicate that the volcanism of the Al Haruj region is contemporaneous with the last distinct basaltic phase of the Al Gharyan volcanic province and with In-Ezzane volcanic district (Yahiaoui et al., 2014) and with the second volcanic event of Nuqay Volcanic Province (Radivojević et al., 2015) as well as with Tibesti Volcanic Province (Deniel et al., 2015).

The first radiometric age dating of the mafic rocks from the Al Haruj province has been done by Pesce (1966), who considered them as being from late Pliocene (3.6-2.5 Ma) based on K/Ar determination. Subsequently, Ade-Hall et al. (1974) used similar method accompanied with palaeomagnetic measurements indicating that the volcanic activity started in late Miocene and lasted until the end of Pleistocene (6-0.4 Ma), with most of the lava flows presently exposed being younger than Pliocene (Less et al., 2006). Busrewil and Wadsworth (1980; 1983) published first crucial data on geochemistry and petrology of the basic volcanic rocks of the Al Haruj al Aswad Subprovince. They inferred that the volcanic rocks belonging to the alkali association ranging from olivine basalt to hawaiite of the alkali series. Furthermore, they also provided works on tectonic setting of the different rocks representing different volcanic phases. From the 1980s until the beginning of 21th century a number of new a systematic regional maps and booklets have been published by Industrial Research Centre (IRC), Tripoli, as part of the programme of regional mapping of whole Libya of 1: 250,000 scale. These publications are considered as most recent and best studies on the AHVP (Table 2.1).

Woller (1984) has provided a geological map and booklet on the southwestern part of the Al Haruj al Aswad Subprovince, and showed that the volcanics span the range from alkaline to hawaiite. Vesely (1985) later identified three lava flows (F0, F1, F2) existence in the northernmost part of

AHAS and most of them are classified as transitional or mildly alkaline basalts (hypersthene and olivine-normative). K/Ar radiometric determination on the earliest lava flow package (F0) gave age ranging from 8–6.7Ma. Corresponding to the Tortonian-Messinian. Himmali and Oun (1991) studied two suites of basaltic rocks, from northernmost of the AHVP, derived from a mantle source with variable depth and degrees of partial melting. This magma was contaminated during residence in the crustal magma chamber. Oun et al. (1998) studied geochemistry, petrology and tectonic evolution of the Dor el Qussah basement inlier west of the AHVP and they inferred that the timespan of Dor el Qussah granitoid complex is 550-580 Ma, that is, at the end of the Pan-African orogeny.

Relatively modern and more comprehensive volcanic eruption scheme for the Al Haruj al Aswad Subprovince (AHAS) established by Busrewil and Suwesi (1993), based on the study of the basaltic rocks in the central part of the AHVP. They divided the lava flows into six major volcanic phases as mentioned above. Furthermore, Al Haruj al Abyad Subprovince (AHAB) has been investigated by Peregi et al. (2003) who adopted similar principle of Busrewil and Suwesi (1993). In addition, they considered age dating for major volcanic phases based on K/Ar age determination combined with paleomagnetic measurement. They show that the volcanic activity continued from 5.27 Ma to about 0.5 Ma, corresponding to a time-span from early Pliocene to late Pleistocene (Table 2.1). Furthermore, the basaltic rocks have high MgO value >7% suggesting only a small degree of magma differentiation and slow ascent of the magmas from their mantle source regions as evidenced by the absence of ultra-mafic xenoliths in these lavas. The main volcanic eruptions of the AHVP are presented in the simplified geological map in Figure (2.6). The composition of the individual lavas is rather uniform cannot be distinguished using petrology and geochemistry alone (Peregi et al., 2003; Less et al., 2006). This volcanic province is enormous size due to dominantly extruded from both thousands of feeding fissures and central volcanoes (Busrewil and Suwesi, 1993).

Asren and Aboazom (2004) concluded that the Al Haruj province vary from subalkaline to alkaline within plate affinities and magma was derived by partial melting of asthenospheric mantle source. More evolved rocks such as trachyte and phonolite were not recorded in this region. They also demonstrated high field strength elements of mafic rocks have a resemblance to oceanic plateau basalts that is suggestive of mantle plume source. Nemeth et al. (2003) point out that the eruptive phase of most volcanic cones and some shield volcanoes at the Al Haruj al Abyad Subprovince are characterised by Hawaiian-style lava fountaining. They also mentioned coherent lava tubes situated on the flank of the shield volcanoes. The absence of evidence of chilling of juvenile fragments that seem to be the volcanisms of the Al Haruj al Abyad Subvolcanic (AHAB) existed in the terrestrial environment in an area of minimum water availability rather than phreatomagmatic origin.

Martin and Nemeth (2006) suggest that the pyroclastic rocks have been preserved in the southwestern part of the Al Haruj al Abyad Subprovince (AHAB) indicating eruption with fountaining activity to Strombolian type eruptions and formation of scoria cones. In addition, some of the cones have relatively deep craters with low limbs resembling a maar structure. Consequently the magmatic fragmentation of the uprising melt changed to magma/water interaction which demonstrates the potential role of phreatomagmatism where leading to explosive events that have withdrawn the top of the volcanic cones and caused maar-like structure. In addition, Martin and Nemeth (2006) have given detailed analyses of deposits persevered on scoria cones in the AHAB and on their architecture. So that they have classified the scoria cones in this region into four different types on the basis of their pyroclastic stratigraphy, an area surrounding cone, morphology of cone as well as its relationship with the kind of the preserved pyroclastic units which indicate that the variety in the eruptive styles and mechanisms during emplacement. The great diversity of scoria cones from

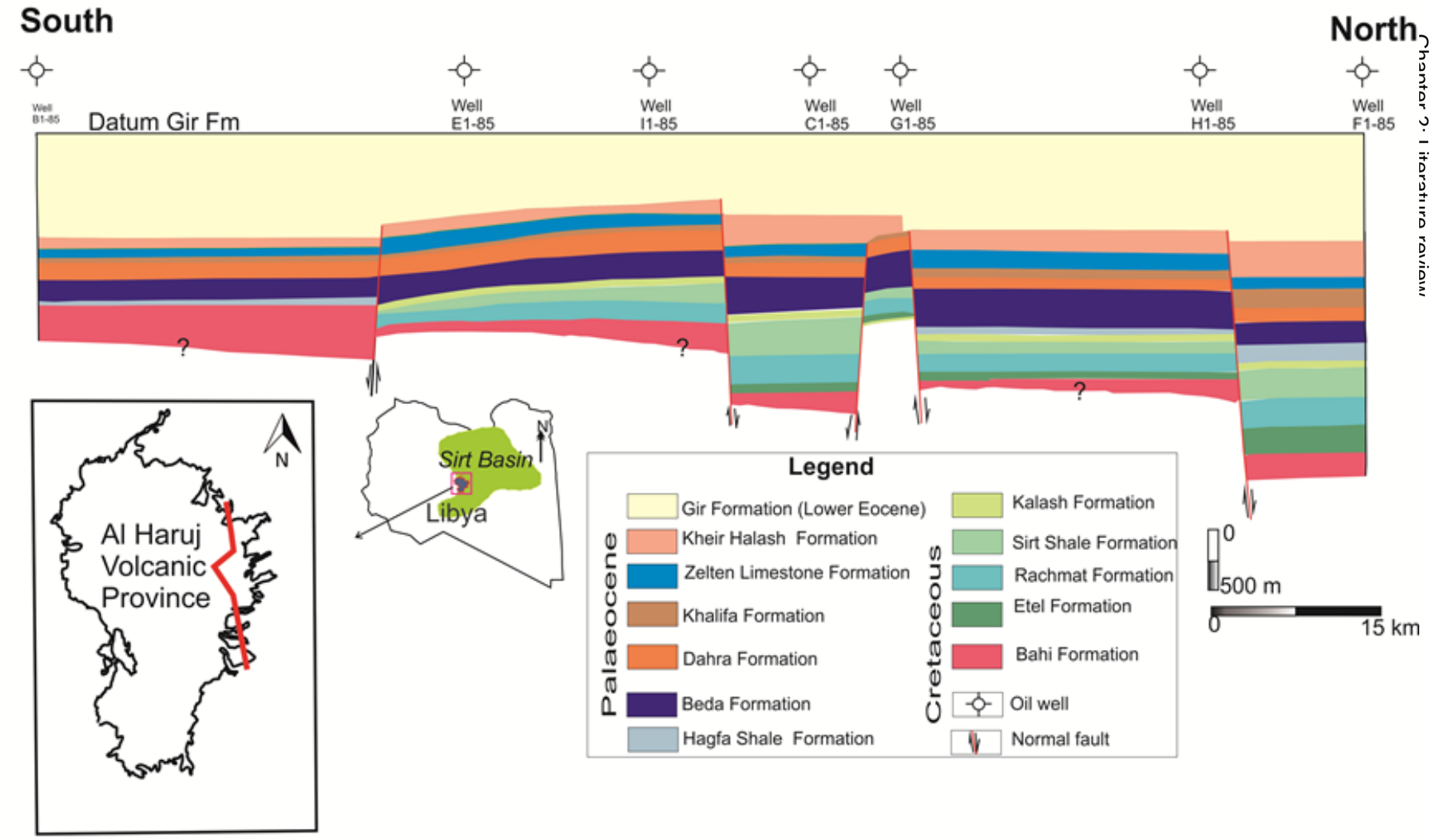

Figure 2.7. South–north cross section showing stratigraphy and structural through the eastern part of the Al Haruj volcanic field (modified from Busrewil et al., 1996).

type (I) to type (IV) displays gradual transitions between Hawaiian lava fountaining to Strombolian type eruptions which reveal differences in bedding and grain sizes of pyroclastic units among scoria cones.

Farahat et al. (2006) studied the mineral chemistry of the basic volcanic rocks in the western part of AHAS to evaluate the petrogenetic and geotectonic evolution of the province. They suggest that the tholeiitic basalts and alkaline basalts of this region represent pre-rift and rift stages respectively, whereas alkaline basalts created by a lower degree of partial melting than tholeiite of the common source but at greater depth. They mentioned that the olivine phenocrysts have fosterite content in the range 75% to 80% or significantly lower than the FO content in peridotite and CaO content higher than olivine in peridotite. In addition, olivines contain spinel as inclusions. Hence, these olivine crystals are considered as phenocrysts rather than xenocrysts as implied by previous studies. Moreover, the temperature and pressure obtained in range from 750° to 1100° C and from 0.46 to 0.73 GPa, respectively, according to the compositions of clinopyroxene, Ti – Fe oxides, olivine spinel as well as oxygen fugacity. The lower limit of temperatures seems to be very low, but Farahat et al. (2006) propose that the more evolved basalts may be produced at a relatively lower temperature.

Nemeth et al. (2008) mentioned that tumuli are widespread in the Al Haruj al Abyad Subprovince (AHAB) and are very similar in form and structure as those identified in Iceland by Rossi and Gudmundsson (1996). They suggested lava supply rate of 1–5 m^3/s in the Al Haruj al Abyad Subprovince, which is similar to the rate obtained in Iceland by Rossi and Gudmundsson (1996). The lava tubes are not recognised at the southern part of the AHVP but the alignments of tumuli propose the presence of narrow internal pathways within a hummocky flow (Self et al., 1998; Thordarson and Self, 1998; Duraiswami et al., 2001; Bernardi et al., 2015). The distributary tube systems are used to transport lava to the distal parts of flow filed (Self et al.,

1998; Glaze et al., 2005). Moreover, Less et al. (2006) have mapped the southernmost part of AHAB and Waw Alkabier area, where they applied similar principles as previous researchers in order to divide basaltic lava flows into five volcanic phases and precise age determination for each volcanic phase since they used K/Ar and isochron together with paleomagnetic measurements. Measurements of age dating for five major phases gave age ranging from 7.94 Ma to 0.5 Ma for the formation of the volcanic rocks in the Al Haruj al Abyad Subprovince which correspond to late Miocene to Quaternary (Table 2.1).

Cvetkovic et al. (2010) used conventional K/Ar method for dating the earlier five volcanic phases in the eastern part of the Al Haruj al Aswad Subprovince. The results revealed ages from around 5.4 Ma to 0.5 Ma. These results are consistent with age dating of Peregi et al. (2003) (Table 2.1). The AHVP was formed by series of episodically volcanic events from the end of Miocene up through Holocene as is revealed by the characteristics of the lava flows in the field and on the multispectral satellite imagery. Each volcanic phase is marked by multi-flow basaltic lobes or units that may be produced by a multi-episode of a single eruption as lava flow field (cf. Thorardorson and Self, 1998).

Author (s)	Ade-Hall et al (1974)	Peregi et al. (2003)	Less et al. (2006)	Cevtkovic et al. (2010)	Bardintzeff et al. (2012)	Nixon et al. (2011)
Age dating Method	(K/Ar)	(K/Ar)	(K/Ar)	(K/Ar)	Unspiked K/Ar	^{3}He
Volcanic Phase VI	0.4 Ma (late Pleistocene)	0.10 - 0.50 (late to middle Pleistocene)	----------	0.5 Ma (late Pleistocene)	0.2 Ma (late Pleistocene)	3 ka (Holocene)
Volcanic Phase V		0.15 - 0.78 (middle Pleistocene)	0.30 - 0.50 (late to middle Pleistocene)			
Volcanic Phase IV		0.34 - 1.22 Ma (early to middle Pleistocene)	0.50 - 1.22 Ma (early to middle Pleistocene)			
Volcanic Phase III		1.22 - 1.77 Ma (early Pleistocene)	1.22 - 1.77 Ma (early Pleistocene)			
Volcanic Phase II		1.46 - 2.24 Ma (late Pliocene)	1.77 - 3.31 Ma (late Pliocene)			
Volcanic Phase I	6.0 Ma (late Miocene)	2.73 - 5.27 Ma. (early to late Pliocene)	3.67 - 7.94 (late Miocene to early Pliocene)	5.4 Ma (late Miocene)	8.1 Ma (late Miocene)	5.27 Ma (early Pliocene)

Table 2.1. Age dating of the AHVP throughout the last four decades based on the work many authors.

These rocks are mainly olivine transitional basalt and somewhat primitive rocks (MgO# values around 10%). The transition from tholeiitic to alkali basalts type have been clarified by many researchers which is well-established in many Oceanic Islands Basalts (OIBs) (e.g., Hawaiian Islands and Galapagos Islands) (Middlemost, 1975; Bardintzeff et al., 1994) . The term transitional basalt or mild alkaline is commonly used to describe rocks that are chemically intermediate between alkali and tholeiitic basalts on the basis of total alkali silica diagram (TAS). There are other discrimination diagrams are suggested by Middlemost (1975) to distinguish between tholeiitic, alkali and transitional basalts. Cvetkovic et al. (2010) have also mentioned that the trace element pattern of the Al Haruj volcanic province are alike to the pattern of Oceanic Island Basalts (OIBs) and generated by around 5% partial melting of garnet-bearing peridotitic source. But in the absence of isotope data, can only speculate on the role of crustal contamination on the evolution of the Al Haruj volcanic province (Cvetkovic et al., 2010).

Bardintzeff et al. (2012) used unconventional unspiked K/Ar age dating method to obtain the age for two samples from extremely southernmost part of the Al Haruj al Abyad Subprovince (between the AHVP and Waw Namus area). They found their ages of 8.1 and 0.2 Ma respectively. These ages are younger and older than previous age determinations. Moreover, they inferred that the basaltic rocks underwent to variable degrees of partial melting of mantle source with depth causative sources between 80 km to 150 km (within upper mantle) as already stated. Abdel-al et al. (2013) classified the basaltic rocks in the AHAB into three major groups based on their trace elements concentration, each featuring different degrees of partial melting. Also they identified that many of dykes intersect the basaltic lava flows and Tertiary sedimentary rocks. These dykes mainly have NW–SE to NNW–SSE trending strikes which are parallel with major fault pattern in the Sirt Basin. Minority of dykes trend NNE–SSW to N–S and has acute angle to the first fault system. They also mentioned that there are many similarities between the AHVP and other intra-plate alkaline basaltic fields within the North Africa,

such as the western Shalate in SE Desert of Egypt and the volcanic rocks of Meidob in NW Sudan. Stuart et al. (2014) Have recently used new geochemical data (major, trace and Rare Earth Element, Sr-Nd-Pb isotopes ratios as well as cosmogentic ^{3}He) on the basis of new regional basaltic database from various volcanic provinces in Libyan territory. They inferred that evolution of the basalts (alkali to sub-alkali) was dominated by fractional crystallization with little evidence of crustal contamination. In addition, they concluded that basaltic magmas were generated by 5 to 15 % melts of heterogeneous sub-lithosphere mantle as well as Nd and Sr isotopic composition of the Al Haruj Volcanic Province and the Ghayran Volcanic Province (0.5128-0.51294 and 0.703-0.704) are similar to Etna and Pantelleria in southern Italy.

2.3 Tibesti Volcanic Province (TVP) (late Miocene to Pleistocene)

The Tibesti Massif or the Tibesti Mountains is located in the central Sahara desert, mostly in north-western Chad and extend into north-eastern Niger and southernmost Libya which covers an area around 100,000 km^2 (Permenter and Oppenheimer 2007; Deniel et al., 2015) (Fig. 2.8). It is a dome with elevations in excess of 3,000 m above the sea level with late Miocene to end of Pleistocene volcanic field in the southern half of the mountains and covers area an around 29,000 km^2. The Tibesti Volcanic Province (TVP), at the north-western of Chad, is considered as the southernmost extension of the four main volcanic provinces in Libyan territory (Fig. 2.1). There are great differences between the Tibesti Volcanic Province and other volcanic provinces in regards to volcano-tectonics processes, the eruptive style, and production of volcanic materials despite that they are contemporaneous. The lava flows of Libya's volcanism are generally predominated by alkali to transitional basaltic rocks with minor amount of phonolites and trachyte (e.g., Stuart et al., 2014; Radivojević et al., 2015). The TVP is almost entirely made of ignimbrites, trachyte and

basaltic lava flows along with recent minor andesitic-trachyte (Deniel et al., 2015).

Despite the TVP is enormous and represents the second largest in size among the Tibesti – Gharyan volcanic provinces, very little is known about it due to inaccessibility because of a series conflicts at Libyan – Chadian border, since 1979 to 1989 between Libyan and Chadian forces and remains extremely hazardous for ground-based expedition, even at present. Therefore, most of the literature dates back to the early fifties to the seventies, for example Wacrenier et al. (1958); who established the first geological map. Subsequently, Vincent (1960, 1963, and 1970) provided critical data on the geology and structure of the Precambrian Tibesti massif, where he divided the Precambrian basement underlying the TVP into Lower Tibestian in the eastern part and Upper Tibestian in the western part. He classified the volcanic units in the TVP into plateau volcanism, central bimodal volcanoes and shield volcanoes and estimated volume of plateau volcanism is around 10,00 km^3. He also classified collapse caldera into (i) classic collapse calderas and (ii) pesudocalderas associated with elevated domes. Subsequently, Malin (1977) inferred from remote sensing data that the large volcanoes within the Tibesti mountains (e.g., Emi Koussi) are comparable Elysium Mons and the Martian volcanoes (e.g., Olympus Mons and the Tharsis Montes) and he concluded that the sources of magma for these volcanic provinces are stationary relative to the surface (Permenter and Oppenheimer 2007). Furthermore, the modern studies on this fascinating volcanic region are also still very few and sparse commonly by Guiraud et al. (2000); Gourgaud and Vincent (2004); Permenter and Oppenheimer (2007); Deniel et al. (2015).

2.3.1 Main volcanic units at the Tibesti Volcanic Province

In the Tibesti mountains, a large volume of late Miocene – Pleistocene volcanic rocks (TVP) is exposed in the southern part and have been classified into five main volcanic units by Deniel et al. (2015), based on field relationships, volcanological, geochronological data and petrological, as follows (Fig. 2.8); i) Plateau volcanism (17– 8 Ma) consists of alkaline olivine basalt lavas covering area about 29,000 km^2. The basalt lavas are associated with trachytic to phonolite plugs. This volcanic unit represents the oldest volcanic rocks in the TVP and plateau volcanism (17– 8 Ma) in the TVP overlaps in time with basaltic lavas of the As Sawda Volcanic Province (16-8 Ma), central Libya (Ade-Hall et al. 1974; Woller and Fediuk 1980; Bardintzeff et al., 2012). ii) The main volcanism spreads toward central part of the province at the end of Miocene or between 8 and 5 Ma, forming four large compositionally similar bimodal volcanic centres (Yega, Oye, Toom and Tieroko) (Fig. 2.8). Those central volcanoes are exposed over an area about 2.700 km^2 and form an eroded plateau. Each central volcano consists of two distinct stages. The first stage consists mainly of basaltic lava emplaced at the margins while the second stage consists of rhyolites lava flow formed at the core (Deniel et al., 2015). This volcanic unit was followed by iii) three major calderas respectively and produced of three large ignimbritic volcanoes (> 100 km^3) as follows; Voon caldera (7–5 Ma), Emi Koussi caldera (2.4–1.33 Ma), and Yirrigue caldera (0.43 Ma) (Deniel et al., 2015). iv) The recent basaltic volcanism resuming again after initial basaltic plateau (volcanic unit a) at 7–5 Ma to 0.43 Ma which produced scoria pyroclastic cones and lava flows. This volcanic unit is apparently consistent with age and composition of the volcanic phases at the Haruj Volcanic Province (AHVP) (Table 2.1).

Some of the basaltic activity occurred along rims of calderas and interior of the calderas. However, each major caldera-forming episode coincided with existence shallow crustal magma chamber, the initiation of mafic volcanism around the rim of caldera and migration of the focus of further ignimbrite to

other places of the Tibesti region due the local stress field associated around the old magma chamber is not favourable to feed it from deeper magma reservoir. This local stress field (compressive stress) generated due the up-doming at the lower crust or crust-mantle boundary (magma accumulation). In turn, the new magma chamber would be formed on either or both sides of the old magma chamber. This mechanism will discuss in detail in the chapter (9). v) Last volcanic activity within the TVP has been observed at rim of Yirrigue caldera in the Tarso Tosside Volcanic Complex and produced andesitic-trachyte (100 ka). This volcanism as well as Tarso Tousside and Emi Koussi fumarole are considered as potentially active (www.volcano.si.edu; Permenter and Oppenheimer, 2007).

The basement rocks underlying the TVP were emplaced during the Late Precambrian (Pan-African orogeny), accompanied by intense deformation, shearing and metamorphism and subdivided into the Lower Tibestain (T1) and Upper Tibestain (T2) which are separated by unconformity or contact (Fig. 2.8). The former basement unit is exposed in the eastern part and made up of high-grade metamorphic rocks while the latter basement unit consists of low-grade metasedimentary rocks (Deniel et al., 2015). It was followed by post-orogenic magmatism until the early Cambrian intruded by different types of granites and elucidated as the early manifestation of the Caledonian orogeny (Klitzch, 2000; Peregi et al., 2003, Deniel et al., 2015). The Caledonian orogeny was accompanied by the formation of the NW–SE trending extended as much as more than several hundred kilometres, such as Tripoli – Tibesti Uplift that is subparallel to the Al Haruj Uplift and among others. The TVP is also influenced by perpendicular structures during the Hercynian orogeny (late Jurassic – early Cretaceous) were superimposed over the earlier Pan-African system (Fig. 2.8). The NE–SW striking Sirt – Tibesti uplift (Sirt Arch) has been formed during this period. The elevated Precambrian of central Sahara was actively eroded during most of the Palaeozoic and produced a large volume of clastic materials and subsequently largely formed the Palaeozoic hydrocarbon reservoirs in the Murzuq Basin, SW Libya (Peregi et al., 2003). Deniel et al. (2015) suggest that the volcano-tectonic in the TVP was influenced by two tensional lines,

namely, the great NW–SE Tassilian flexure to the southwest and a major NE–NE Yebbigue fault zone to the east. They are obviously consistent with two orthogonal regional structures elements that were interpreted by Woller and Fediuk (1980) (Fig. 2.1).

The present distribution of the main volcanic units on the TVP is given in Figure (2.8). It is only a guideline to whole the volcanic province which involves delineation of different types of volcano-tectonic elements together with their assignment to the relevant volcanic events. Consequently, we will build up the present work according to this comprehensive and concise division was provided by Deniel et al. (2015). Nevertheless, the other three volcanic provinces (Gharyan, As Sawda and Nuqay) in Libya are beyond scope during the present work so that they are briefly summarised as follows;

2.4 Gharyan Volcanic Province (GVP) (late Miocene to Pleistocene)

Gharyan volcanic province is the smallest among the five main volcanic fields (Fig. 2.1), and form generally continuous sheet in the central part of Jabal Nafusah which has been active from the late Miocene to late Pleistocene and lies at the intersection of two major structural elements; the NNW–SSE trending Tripoli – Tibesti Uplift axis formed in the early Palaeozoic and the E–W trending Nafusah Uplift formed during the late Palaeozoic to Mesozoic time (Fig. 2.1) (Goudarzi, 1980; Busrewil and Suwesi, 1993).

This volcanic field made up of three distinct phases, an early unit of large plateau lava eruption has hypersthene-normative (tholiite), subsequently the second phase of small phonolitic domes and trachyte, and finally a rejuvenation volcanic phase was characterized by basanitic composition (Almond et al., 1974; Al-Hafdh and Jafeer, 2014). The modern age dating for the major pluses of basalt volcanism in this volcanic province using

(40Ar/39Ar) chronology by Saurt et al. (2014) indicates that the basaltic rocks were produced over 6 Ma to 2 Ma which is contemporaneous with the volcanism in both the Al Haruj and Naquy volcanic provinces (from the end of Miocene to Pleistocene). In addition, they inferred that phonolites were produced over short period time at 8.1 Ma, alternatives to previous age determinations that were 40 – 50 Ma (early to middle Eocene) (e.g., Almond et al., 1974; Busrewil and Wadsworth 1980). Therefore, the new age of phonolites age is also simultaneous with the volcanism of Gharyan –Tibesti volcanic provinces. Mechanical interaction between them during active time may encourage s volcanic and tectonic events, seismogenic faulting, and dyke sharing between volcanic provinces.

2.5 As Sawda Volcanic Province (SVP) (Miocene)

The As Sawda or Sawda is situated in the westernmost of the Sirt Basin at the intersection of the early Palaeozoic the Al Haruj Uplift with the late Palaeozoic to Mesozoic Al Qarqaf Uplift (Woller and Fediuk, 1980) (Fig. 2.1). This volcanic province covers an area approximately 5,902 km^2; probably this figure is underestimation due to lack of detail geological map about it compared with the other volcanic provinces. Further to the SW of As Sawda volcanic field, the location of the small volcanic field of Jabal Al Hasawinah is tectonically related to the Tertiary reactivation of two intersecting major elements in southern Libya, early Palaeozoic NNW–SSW Tripoli – Tibesti Uplift and the Hercynian ENE–WSW, Al Qarqaf Uplift.

This tectonic movement developed in the evolution of two neighbouring structural domes on N–S axis (namely Wadi Bardan and Wadi Darman domes), in cores of which the basement granite of Pan-African Orogeny is exposed (Busrewil and Oun, 1991). However, the volcanic rocks of As Sawda consist of alkaline and tholeiite basalts along with minor phonolitic

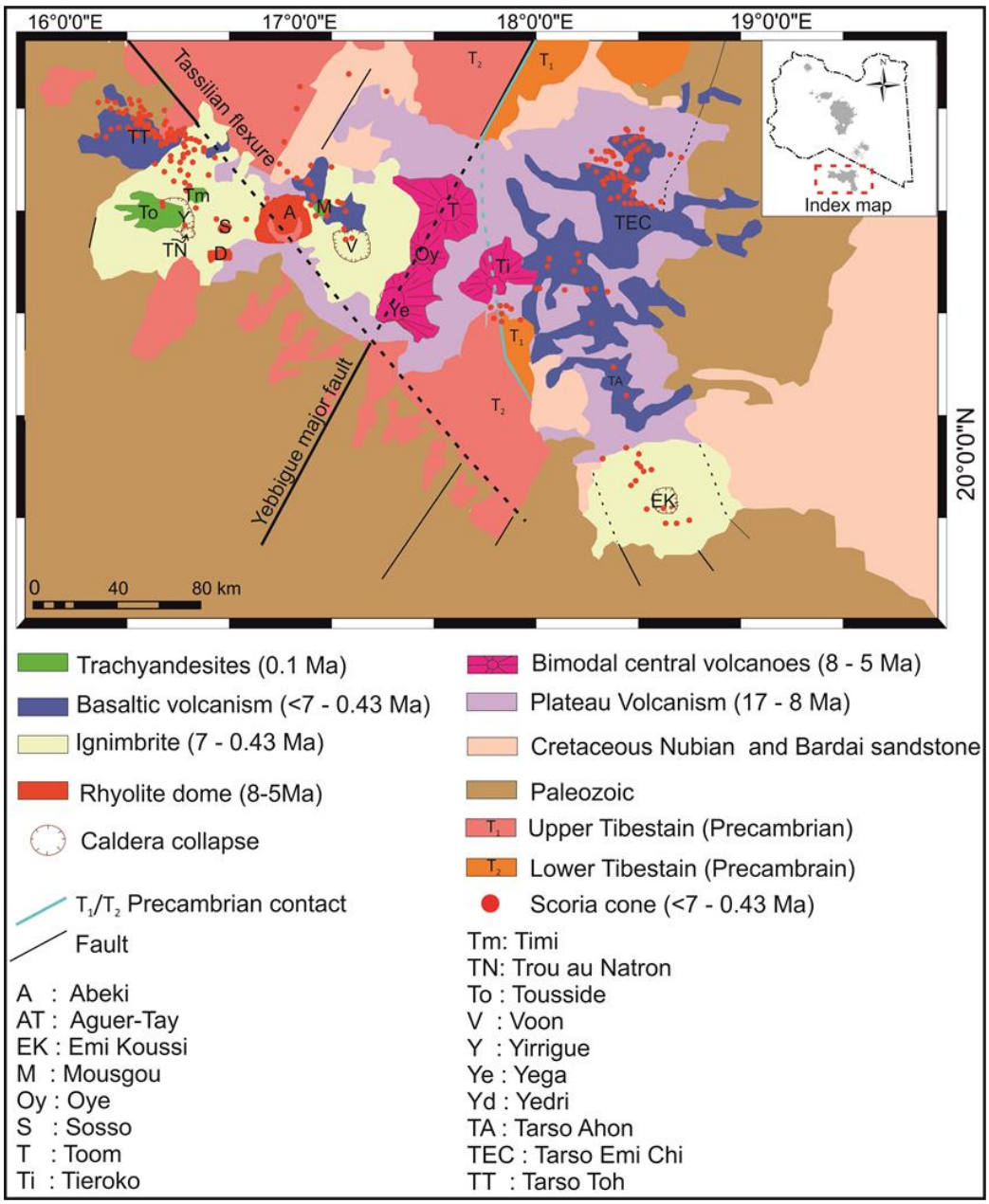

Figure 2.8. Simplified geological map of the Tibesti Volcanic Province showing the distribution of the five main volcanic units and tectonic framework. The dashed red box in the inset map shows the location. Three collapse calderas are indicated by pale yellow (colour with associated large volume of ignimbrites (> 100km^3) that are aligned NW-SE linear trend. While three bimodal central volcanoes are marked by pink colour that are extended NE-SW trend along Yebbigue major fault. Scoria cones are indicated by red spots. The Precambrian rocks were divided into the Lower Tibestain (T1) and Upper Tibestain (T2). (modified from Permenter and Oppenheimer, 2007; Deniel et al., 2015).

rocks and have timespan between 16 and 8 Ma (Ade-Hall et al. 1974; Woller and Fediuk 1980), while Jabal Al Hasawinah made up of basalts and basanites, trachytes and phonolites being subordinate, which are dated between 24.9 and 15.7 Ma (Jurak 1978). The new age dating of basaltic rocks of Jabal Al Hasawinah and As Sawda inferred that erupted between 23 Ma and 10 Ma (Saurt et al., 2014).

2.6 Nuqay Volcanic Province (NVP) (Middle Miocene to Pleistocene)

This volcanic province consists of two main volcanic events. The first event occurred from the middle Miocene up to the Pliocene and produced mainly alkaline to sub-alkaline basaltic rocks (tholeiitic) while the second event extends from late Pliocene up to Pleistocene time which produced basanite spatter to scoria pyroclastic cones and subsidiary flow-lobes lava flow (Radivojević et al. 2015). The second volcanic episode is apparently consistent with age and composition of the main volcanic phases of the Haruj Volcanic Province (AHVP). However, the NVP covers an area around 11,655 km^2 and considered as the third largest among Gharayn –Tibesti volcanic provinces. New geochronology data during the last few years show that volcanism in Libya was to a degree contempoareous, that is, overlapped, during certain periods of time in three of the provinces (Nixon et al., 2011; Bardintzeff et al., 2012; Stuart et al., 2014; Radivojević et al., 2015). Before these geochronology data, it was generally believed that volcanism in Libya showed a gradual decrease in their age from the northwest, namely the Gharyan Volcanic Province, towards the southeast, that is, to the Nuqay Volcanic Province (e.g., Hegazi, 1999).

2.7 Geometry and morphology of fractures

The Al Haruj Volcanic Province (AHVP) is thought to have been produced by hundreds of feeding fissures and dyke (Busrewi and Suwesi, 1993; Busrewil et al., 1996; Busrewil, 2012). Most of these fissures and dykes are now covered by more recent volcanic phases (volcanic phase V & Phase VI) (Busrewil et al., 1996; Busrewil, 2012) (Fig. 2.6). Those extension fractures that have been recognised in the field, as well as on multispectral satellite imagery, are predominately located along the periphery of the main body of the volcanic field. Field and remote sensing investigations indicate that most of the lineaments in the AHVP are normal faults and extensional fractures (volcanic fissures and dykes) (Peregi et al., 2003; Less et al., 2006).

The methodology used in the present study utilised a combination of existing geological maps and multi-source high-resolution remote sensing images. Satellite imagery available from Google Earth (GE) hosts high-resolution imagery (Potere et al., 2008) using a digital elevation model (DEM) data collected by NASA Shutter Radar Topography Mission (SRTM) with imagery resolution ranges from 15 meters to 15 centimetres. The volcano-tectonic analysis has been made using the latest satellite imagery available on GE over the studied areas. These images permit the location and precise mapping of volcanoes, dykes, volcanic fissures, lava rise plateaus, tumuli and faults in the frame of a Geographic Information System (GIS), as long as published geological maps are used as a baseline. This method is considered as a powerful tool for volcano-tectonic and physical volcanology studies when size, remoteness, arid and inhospitable field areas induce difficulties of ground-based access (Drury, 2001; Rajesh, 2004; Koch and Mather, 1997, Chorowicz and Deroin, 2003; Peña and Abdelsalam, 2006; Solomon and Ghebreab, 2008; Chen et al., 2014; Abdunaser and McCaffrey, 2014; Chorowicz and Benissa, 2016). The Al Haruj Volcanic Province (AHVP) and the Tibesti Volcanic Province (TVP) certainly fall within this description.

The areal distribution of each volcanic phase and lineaments interpreted as volcano-tectonic structures were measured using ArcGIS 10.1. The geometry of each lineament is defined by its strike, length and thickness or aperture (paleo-opening) (Gudmundsson, 2011). The definition of the main

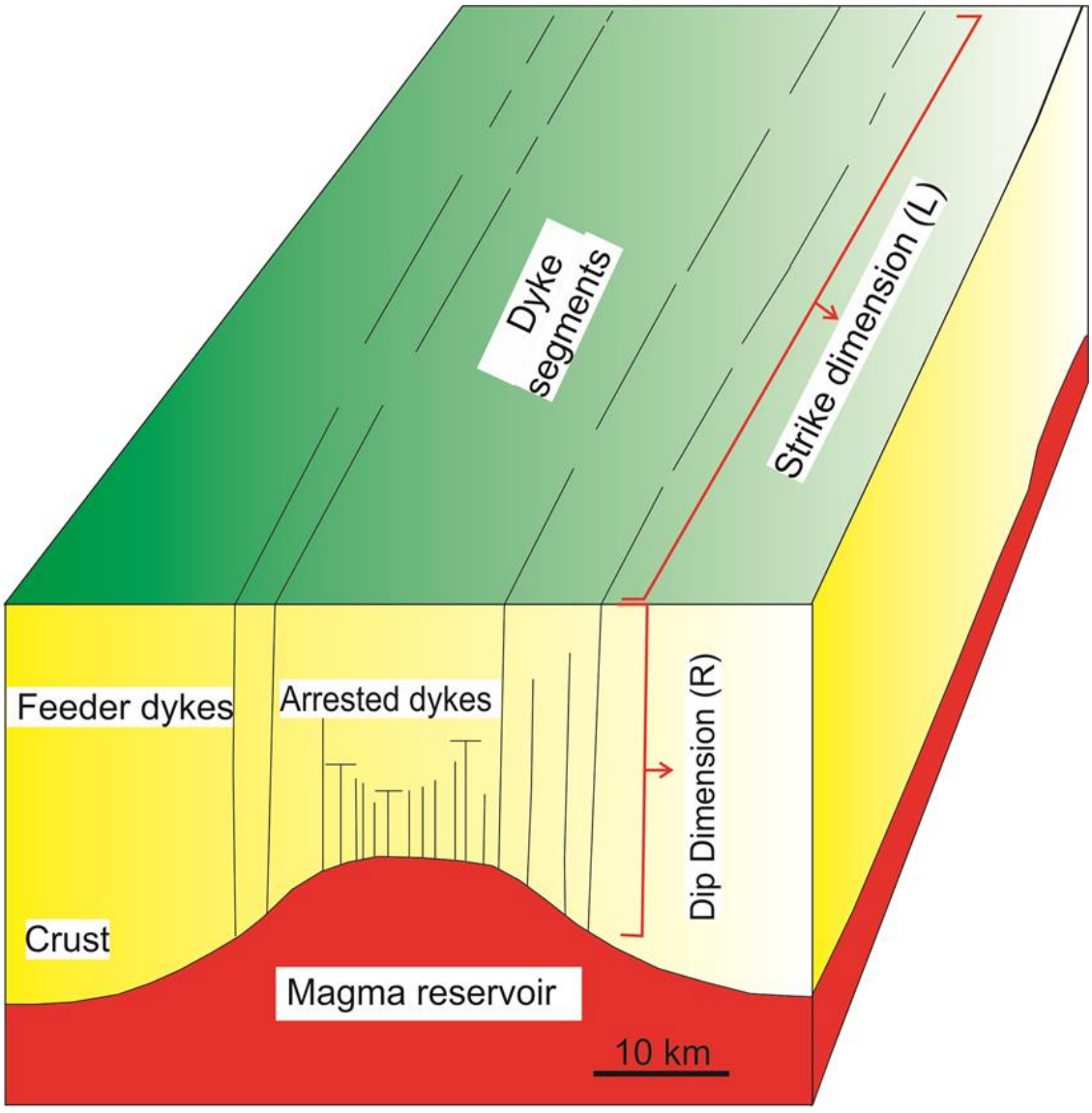

Figure 2.9. Schematic illustration of feeder dykes and arrested dykes. Feeder dykes are propagated from one free surface (magma reservoir) to another free surface (the Earth's surface), as such they can be modelled as through thickness cracks (mode I). The strike dimension (L) is often larger than the dip dimension (R), thereby, dip is the controlling dimension. The arrested dykes are, conversely, modelled as partial through thickness cracks (mode I). Most dykes are usually arrested at depth due to differences in mechanical properties between various strata at the Earth's crust (modified after Gudmundsson, 2015).

fracture pattern is acquired by analysing the azimuth frequency distribution of lineaments, lineament length and thickness distribution as well as lineament density (Wise et al., 1985; Zakir etal., 1999; Francesco and D'Orazio, 2003). Orientation and length of fractures including faults, fissures, and dykes, are extracted from satellite imagery and available geologic maps of the study area. These shear and extension fractures are mainly confined to areas where bedrock is not covered by lava flows or Quaternary sand dunes. The data are consequently grouped based on types and ages, and then the GEOrient software is implemented to plot the directions of fissures, dykes and shear fractures in a rose diagram.

2.7.1 Magmatic overpressure during dyke emplacement

Magma injects from a magma chamber or reservoir as a dyke and/or an inclined sheet, the geometry of which is governed by both the regional and local tectonic stress field (Le Corvec et al., 2013) (Fig. 2.9). The geometric and kinematic features of dykes are utilised as paleostress indicators (Nakamura, 1977; Nakamura et al., 1977; Zoback et al., 1989; Bosworth et al., 1992; Suter et al., 1992; Bosworth and Strecker, 1997; Chorowicz et al., 1997; Paulsen and Wilson, 2009). Dykes are essentially extension fractures (mode I cracks) (Babiker and Gudmundsson, 2004). Therefore, the maximum principal compressive stresses σ_1 coexist parallel to the plane of the dykes whereas minimum compressive (maximum tensile) stress σ_3 is perpendicular to the plane of the dyke (Gudmundsson, 2011; Browning and Gudmundsson, 2015). A dyke propagates from its source when the condition of equation (2.1) is met at any points in the walls or roof of the magma chamber (Fig. 3.4) (Babiker and Gudmundsson, 2004; Gudmundsson, 2011);

$$p_l + p_e = \sigma_3 + T_0 \qquad (2.1)$$

where p_e is the excess pressure in the source of magma and p_l represents the lithostatic stress , and σ_3, T_0 are the minimum compressive principal stress and in situ tensile strength respectively.

When dyke commences to transmit up to layers, its magmatic overpressure P_0 at the surface is given by (Gudmundsson, 2011);

$$p_o = p_e + (\rho_r - \rho_m)gh + \sigma_d \quad (2.2)$$

Here is ρ_r the average density of the host rock, ρ_m is the average density of the magma in the dyke, g is acceleration due to gravity, h is the dip dimension and σ_d is the differential stress (the difference between the maximum principal stress σ_1 and the minimum principal horizontal stress σ_3 where dyke is observed (Kusumoto et al., 2013). The magmatic overpressure p_0 depends on the excess pressure p_e in the magma chamber, on the buoyancy effect $(\rho_r - \rho_m)$ as well as the state of stress of the host rock. During volcanic eruptions, the overpressure p_0 of the feeder dyke is a crucial constraint on the mechanism of the eruption, as it has primary influences on the volumetric or effusion flow rate throughout the associated volcanic fissure (Gudmundsson, 2011).

Magmatic overpressures can be estimated from aspect (length/aperture) ratio of dykes and volcanic fissures making assumptions elastic behaviour of the host rock (Delaney and Pollard, 1981; Pollard and Segall, 1987; Kusumoto et al., 2013). Equation (2.3) proposes that magmatic overpressure during the dyke propagation is constant, as a first approximation, particularly when there is limited data as to the exact thickness of dykes and volcanic fissures (Becerril et al., 2013);

$$\Delta u = \frac{2L\left(1-\nu^2\right)P_0}{E} \tag{2.3}$$

where ν represents Poisson's ratio of the host rock, E is Young's modulus, Δu is the maximum opening or thickness of the dyke, and L is dimension (horizontal length) of the dyke of the dyke which is related to its strike dimension (Fig. 2.9). The maximum opening is considered as the average aperture (thickness of dyke). Most dykes have relatively smooth and flat elliptical variations in their thickness (Becerril et al., 2013), and P_0 is the magmatic overpressure in the dyke at its time of emplacement. When viewed from overhead it is clear that dykes and volcanic fissures largely appear as segments. These segments are modelled as a single fracture when tips of the fragments are separated by little space relative (≈10%) to the length (cf. Babiker and Gudmundsson, 2004). These segments behave mechanically as an individual continuous fracture (Fig. 2.10) (Gudmundsson, 2011).

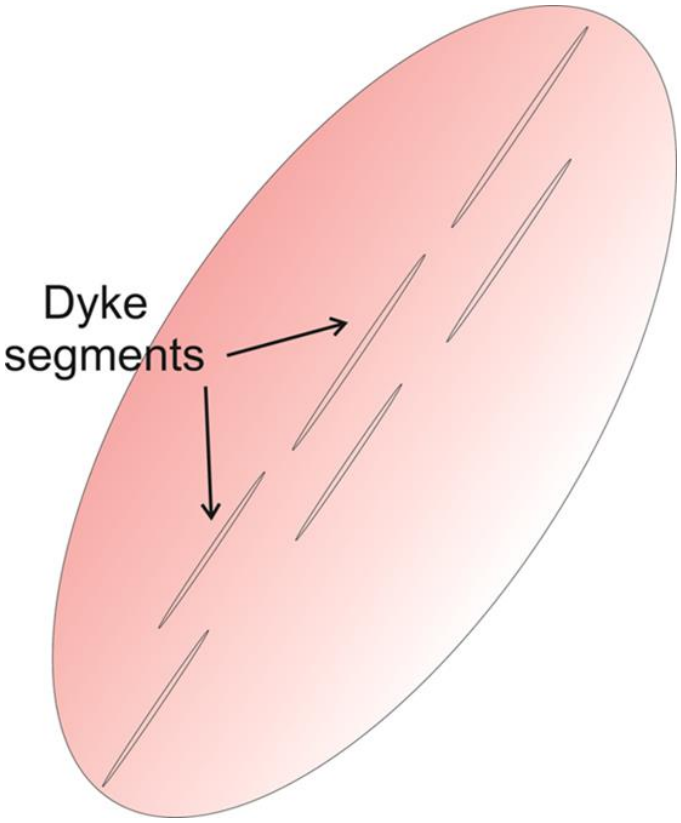

Figure 2.10. Segments of dykes are modelled as a single dyke as the tips of the segments are separated by much less distance than the lengths. The length equals the total length of dyke segments (modified after Gudmundsson, 2011).

2.7.2 Mechanisms controlling the propagation of dykes

Most eruptions on Earth are fed by dykes and inclined sheets, so understanding the mechanics of dyke and inclined sheet emplacement and propagation through the Earth's crust is important for a better of volcano-tectonics processes. Development of models to explain how magma transports through the Earth's crust have benefited from 3D seismic reflection data (Thomson and Hutton, 2004; Planke et al. 2005; Cartwright and Hansen, 2006; Hansen and Cartwright, 2006; Thomson and Schofield, 2008; Sevensen et al. 2012; McClay et al., 2013; Holt et al., 2014). For example, sharp contrast horizontal continuous layers interpreted as magma can extend laterally for up to several tens of kilometres and form various morphologies such as concave-up and saucer shaped (Cartwright and Hansen, 2006; Hansen and Cartwright, 2006). Magma can also be transported as vertical features from the magma reservoir through fluid-driven fractures (Clemens and Mawer 1992; Winter 2010; Holt et al., 2014) (Fig. 2.11a, b).

The analysis and modelling of the spatial distribution of volcanoes and dykes at the AHVP during this study led us to a new interpretation of the dynamics of magma propagation of the AHVP. It is crucial to decipher the major processes and mechanisms that control dyke and an inclined sheet propagation. When dykes or inclined sheets propagate from magma source and meets contact (discontinuity), the fracture responds in one of four ways (Fig. 2.11c), the dyke penetrates the contact, propagates to the surface and form an eruption, 2) the dyke becomes arrested at the contact, 3) the dykes becomes deflected in one direction or 4) in two directions at the contact. Local stresses in rock layers partly control dyke propagation along a potential fracture path. Subsequently, the local stress relies on the mechanical properties of these strata, their contacts and other factors as will be discussed later in Chapter 5.

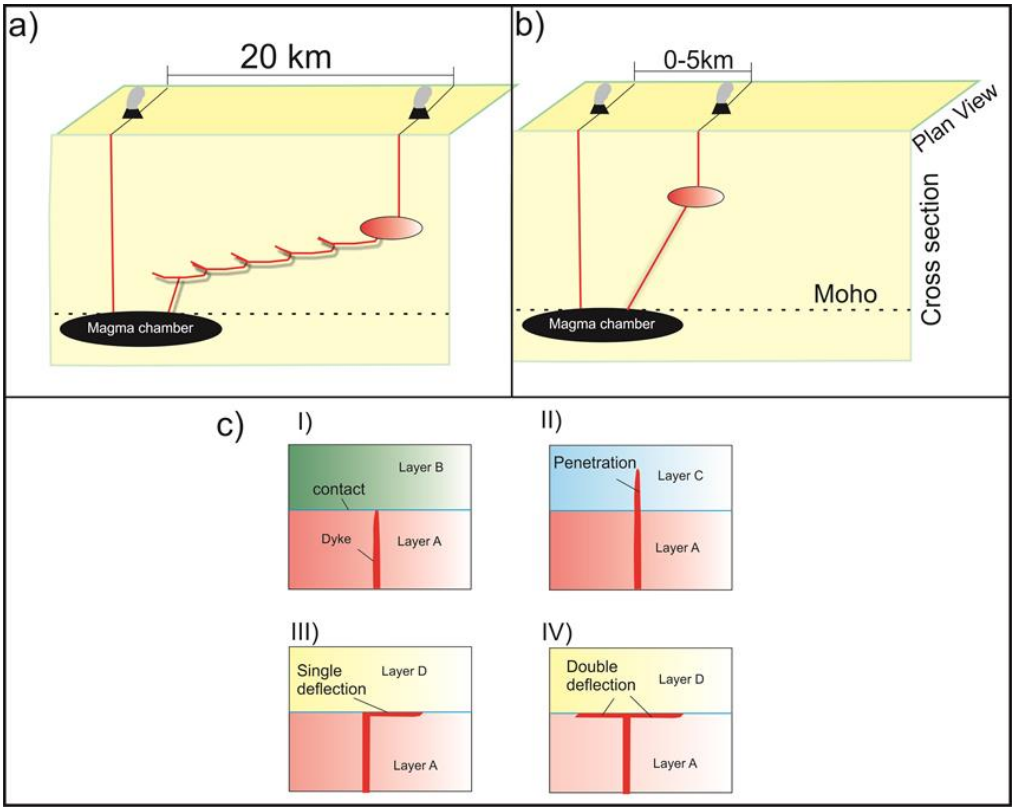

Figure 2.11. Two models used to infer how magma transports from magma reservoir to feed eruptions. a) Horizontal model of magma propagation. This model supposes that most magma rises laterally through the Earth's crust to form interconnected sills. b) This is a traditional model where magma uses vertical hydrofractures (dykes) and high angle faults as conduits to feed eruptions (Modified after Holt et al., 2014). c) Dyke only has four ways when meet contact/discontinuity. The dyke may I) become arrested; II) penetrated the discontinuity or become deflected to form sill either; III) in one direction; or IV) in two directions (modified after Barnett and Gudmundsson, 2014).

Chapter 3: Regional geology and tectonics of central Libya

3.1 Introduction

The plate tectonic history of Libya has been clarified over the last four decades during with intensive research in deep seismic profiling and deep drilling oil wells works which are being extended to the whole territory of Libya as a result of new subsurface data (Peregi et al., 2003; Less et al., 2006).The tectonic development of North Africa generally involves an alternating of long periods of predominately gentle basins subsidence or rifting and short periods of compressional events (Klitzsch, 1970; Guiraud et al., 2005; Saadi et al., 2011). Libya, located at the north central margin of the African continent, developed over a platform of cratonic basins (Fig. 2.1). The major diastrophic disturbances include the Pan-African, Caledonian and Hercynian orogenies and disturbances also extended during Cretaceous, middle Tertiary, Oligocene through Miocene and Holocene time leading to produce major structural and tectonic features. However, the influences of the main tectonic events were generally broad, and compressional folds are not common (Goudarzi, 1980; Al-Heety, 2013; Chorowics and Benissa, 2016).

In general terms, during the Palaeozoic and early Mesozoic the development tectonic of Libyan tectonics was controlled by the evolution of Gondwana and Pangaea. While through the late Mesozoic and Cenozoic times was governed by the evolution of Tethys and the Mediterranean Sea due to the North Africa situated on the leading edge of Gondwana (Hallett, 2002; Peregi et al., 2003). Noticeable also were eustatic sea-level fluctuations associated with global climatic changes that played an important role in sedimentation cycles (Guiraud et al., 2005). The stratigraphic sequence from the Neo-Proterozoic to Quaternary allows reconstruction of the tectonic history and paleogeography of North Africa (Guiraud et al., 2005). This chapter shall attempt to summarise hereafter the tectonic

evolution and paleogeographic of Libya and North Africa at large scale and pay special attention to the Sirt Basin domain, located in the central part of Libya.

3.2 Late Precambrian to late Silurian (≈ 1300-422 Ma)

The Rodinia supercontinent, during Meso-Proterozoic, was constructed by around twenty identifiable Archean and Palaeo-Proterozoic cratons (Hallett, 2002). Subsequently, it started to break-up during the Neo-Proterozoic then reassembled again of the component plates into the new supercontinent called Pannotia (also known as the Vendian supercontinent) in the late Neo-proterozoic. During this phase, cratonic blocks of western Rodinia was rotated clockwise and translated relatively towards the west whereas eastern Rodinia cratonic blocks were rotated anticlockwise direction and displace relatively eastwards (Hallett, 2002; Fig. 3.1).

There was accompanied by a variety of processes, called Pan-African Orogeny, during which some of the Archean cratonic margins were extensive remobilised and frequently focused ascending magmas, leading to refertilisation of the subcontinental lithospheric mantle (SCLM) (Begg et al., 2009). Components of North Africa were emplaced along shear zones which marked by a broad of collisional deformation (Less et al., 2006; Fig. 3.2). These deformations involve crustal reactivation, subduction, and production of granites and extensive displacement of crustal blocks. Most of the exposed basement of Libya and Tibesti massif at the northernmost of Chad has been influenced by these processes (Rogers, 1980). The acidic rocks of the Upper Tibestian in the western Jabal Tibesti, on Libyan – Chadian border, form part of this remobilised belt and the basement outcrops of the Dor el Qussah inlier west of the Al Haruj Volcanic Province and the small inliers of Precambrian metamorphic rocks on the Al Qaraqaf Arch belong to the Pan-African suite of rocks in Libya (Hallett, 2002; Less et al., 2006; Fig. 2.1). In addition, subsurface data from hydrocarbon wells suggest that this

suit of rocks extent through the Murzuq Basin, the Tibesti arch as well as southern part of the Sirt Basin (Hallett, 2002).

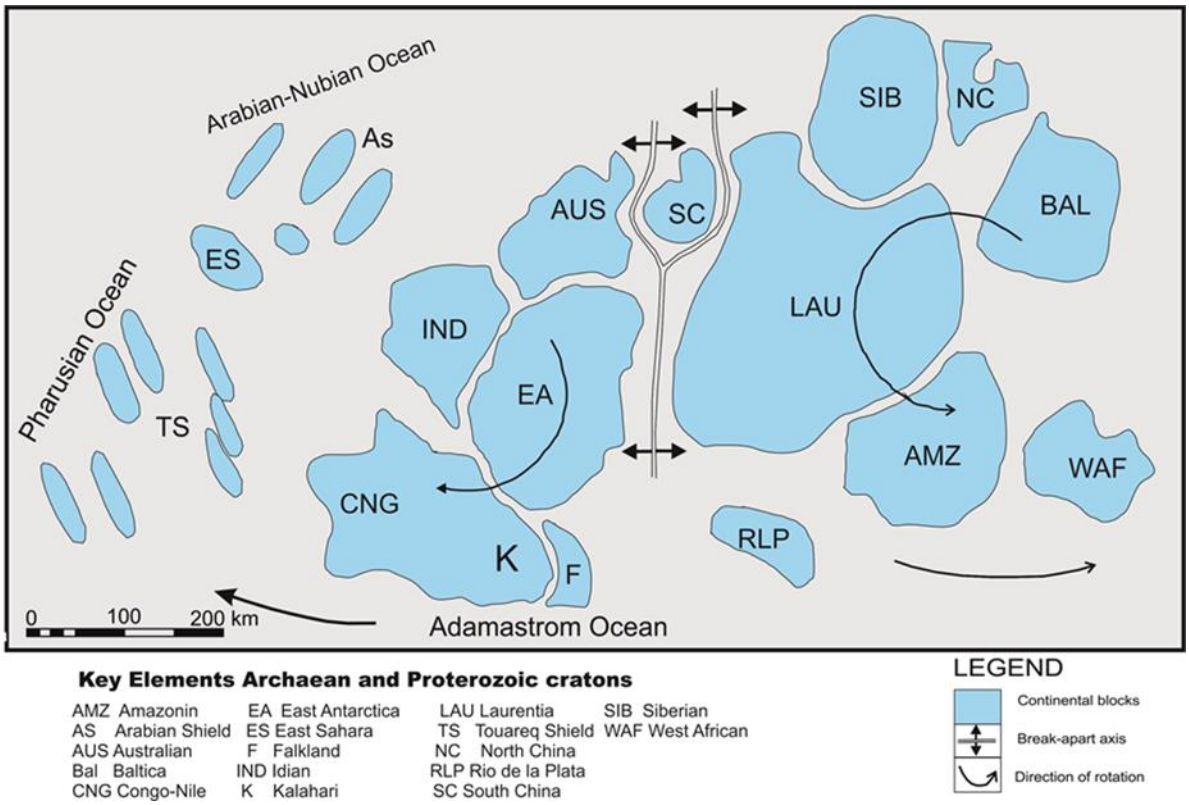

Figure 3.1. Cartoon showing the break-up of Rodinia supercontinent commenced during the early Neo-Proterozoic (1000 to 700 Ma). Oceanic microplates in the Pharusian Ocean in the western part jointed to form the Touareq Shield of North Africa whereas they were formed the Arabian Shield in the northwestern part of the Arabian Nubian Ocean (modified from Unrug et al., 1996; Hallett, 2002).

During the earliest Palaeozoic was related to the breaking up of the Pannotia supercontinent and to gathering the southern continental assemblage which constituted Gondwana in the latest Pan-African Orogeny from early Ordovician to Jurassic time (Begg et al., 2009; Fig. 3.3). The formation and breakup of Gondwana is considered as the major tectonic evolution of Africa (Montgomery, 1994, Saadi et al., 2011). The southern margin of Gondwana was characterised by mountain building, convergence and subduction tectonics, whereas the North African formed part of the massive margin of western Gondwana since the early Palaeozoic and the emergent internal

parts of the supercontinent which provided the source area of the terrigenous clastic materials (Less et al., 2006). The early Palaeozoic rocks in the North Africa have been classified into three meg-acycles sequence. The first cycle, dominantly transgressive in character, represents a maximum flooding event, which followed by regressive cycle, whereas the third cycle is terminated by the basal Silurian marine transgression (Hallett, 2002).

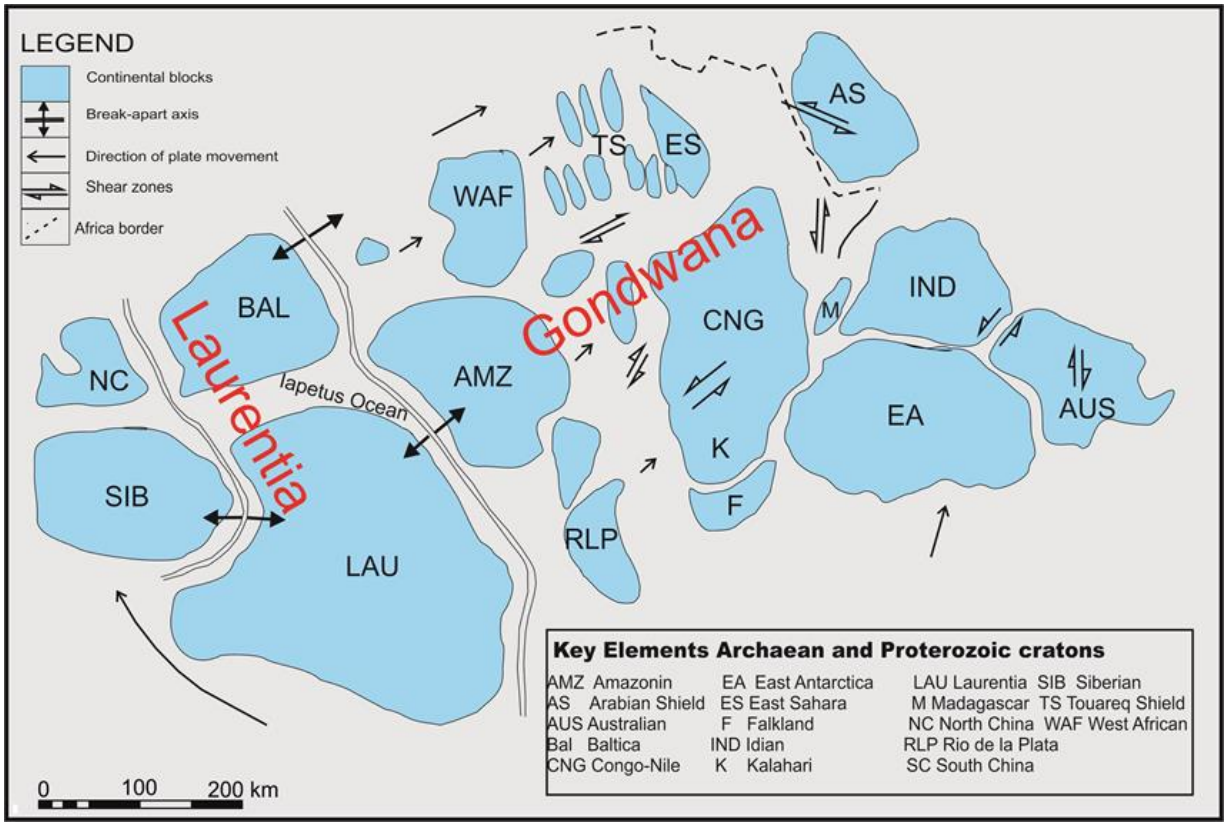

Figure 3.2. Cartoon showing the division of the Pannotia supercontinent into Laurentia and Gondwana during Cambrian time (modified from Unrug et al., 1996; Hallett, 2002).

Moreover, during the early Palaeozoic western Gondwana was located closer to the South Pole than the present-day and glacial conditions prevailed over much of the region during the Ordovician. The Ordovician formations in southern Libya are made up of sandstone strata containing abundance of traces fossils (e.g. Tigillites and Cruziana), indicating

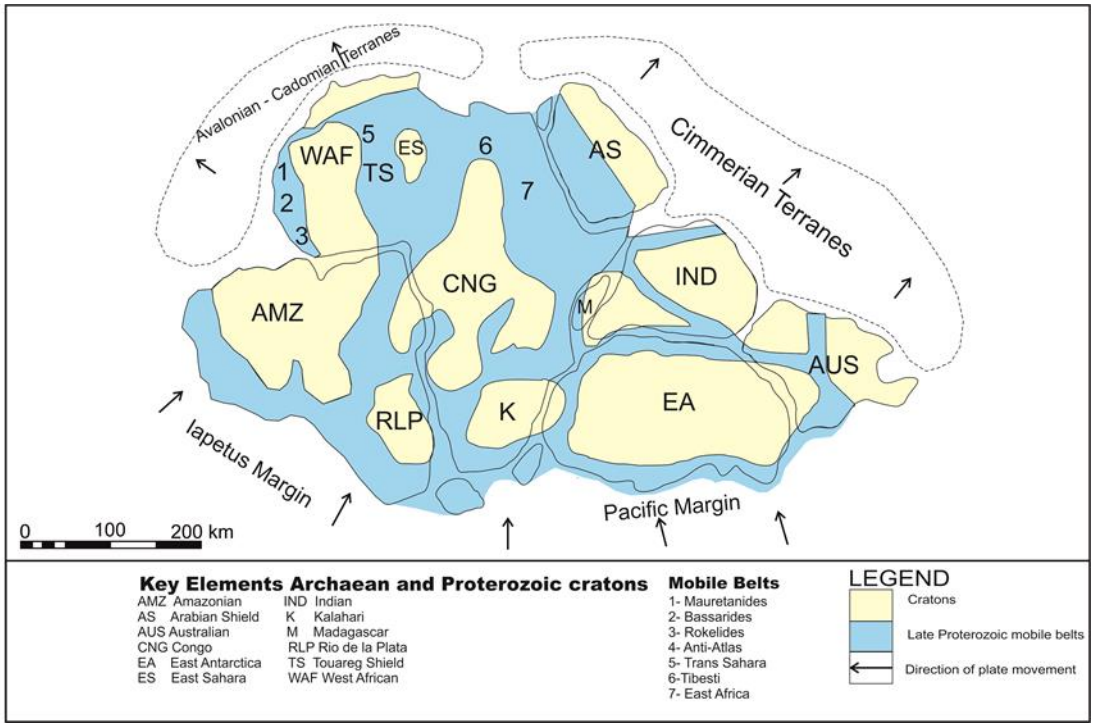

Figure 3.3. Cartoon showing the craton blocks stitched together during the Pan-African Orogeny. The tectonic architecture of Africa comprises of several stable Archean cratonic and surrounded by younger Proterozoic mobile belts (modified from Unrug et al. 1996; Hallett 2002). The weakened margins of cratons have frequently been reactivated during cycles of rifting, subduction and renewed accretion (Begg et al., 2009).

significantly deeper shallow marine depositional conditions than in the Cambrian (Brenchley, et al. 1994; Semtner and Klitzsch, 1994; Sutcliffe, et al. 2000; Hallett, 2002; Peregi et al., 2003). The climate following this event became warmer once again which caused rapid melting of the ice sheets to the south which led to consecutive major transgression in the earliest Silurian and deposited thick black shales (organic-rich graptolites shale). These form the primary hydrocarbon source rocks in the North Africa (e.g., the Tanezzuft Formation in the Murzuq Basin), then followed by pro-delta and deltaic high-stand deposits, e.g., the shallow marine of the Akakus Formation as common oil reservoir in Murzuq Basin (Boote et al., 1998; Hallett, 2002; Guiraud et al., 2005; Less et al., 2006; Chorowicz and Benissa, 2016). Sedimentation was generally ceased during the Silurian-Devonian transition due to a drop in global sea level and tectonic instability (Guiraud et al., 2005).

The latest Pan-African orogeny was expressed by unconformities on the Ordovician sequence (Peregi et al., 2003; Less et al., 2006). This event was followed by collision of Laurentia (North America) with Africa in the late Silurian-early Devonian forming a series broad of NW–SE to N–S uplifts and grabens which include the Tihemboka High, the Murzuq – Jadu Trough, the Dor el Qussah Trough, Kalanshio Trough as well as the Tripoli –Tibisti Uplifts. These structural elements were controlled deposition during the early Palaeozoic in Libya (Goudarzi,1980; Ziegler, 1988; Scotese and McKerrow, 1990; Kröner, 1991; Echikh, 1998; Boote et al., 1998; Chorowicz and Benissa, 2016; Fig. 2.4).

3.3 Early Devonian to middle Triassic (≈ 422-242 Ma)

The early Devonian sequence can be divided into four sedimentary cycles which are dominated by widespread deltaic complex and terminated by uplift and erosion during the middle Devonian. During this period, the western part of Libya became subject to extensive tectonic deformations, representing the first event of Hercynian orogeny. This event played a major role to effect on the geological development of the North Africa when Laurasia supercontinent collided with the northwestern margin of western Gondwana where an episode of extensive erosion on the limbs of Al Qaraqaf Arch and deposition of continental sandstone formations, e.g. Tadrat Formation in Murzuq Basin (Hallett, 2002; Peregi et al., 2003; Guiraud et al., 2005).The middle and late Devonian were marked by a flooding event leading to the deposition organic-rich shale (Guiraud et al., 2005). During the middle Carboniferous-Permian growing the intensity of the collision between Gondwana and Laurasia led to the development of Atlas Mountains and produced flooding event in Libya, followed that uplifted and extensive erosion which reached its peak during the late Carboniferous (Hallett, 2002; Chorowicz and Benissa, 2016).

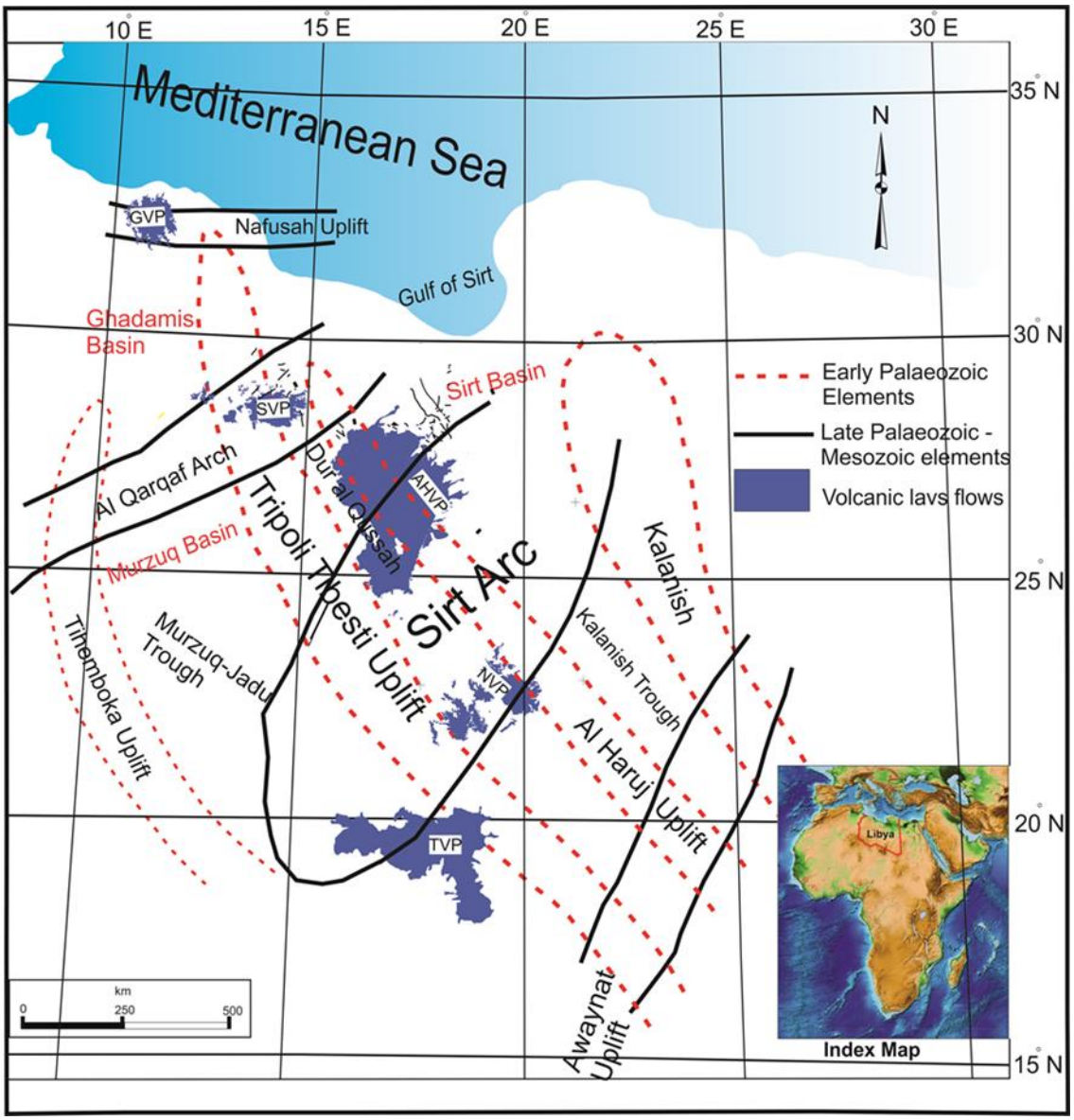

Figure 3.4. Hercynian structural elements with E–W to NE–SW trends, indicated by solid black lines, were superimposed over the early Palaeozoic structural elements, indicated by dashed red lines (modified after Klitzsch, 1971; Anketell, 1996; Hallett, 2002). GVP; Gharyan Volcanic Province; SVP; As Sawda Volcanic Province; AHVP;Al Haruj Volcanic Province; NVP; Nuqay Volcanic Province; TVP; Tibesti Volcanic Province.

The southern part of Libya had been transported into a continental environment with superposition of the Hercynian trend over the Lower Palaeozoic trend which led to the destruction of the earlier structural elements with the formation new structural elements. The latter structural elements are nearly perpendicular to the former elements (Woller and

Fediuck, 1980; Peregi et al., 2003). There are newly formed E–W trending the Nafusah Uplift, NE–SW to ENE–WSW trending, Tibesti – Sirt uplift (Sirt Arch), Al Qarqaf Arch and Al Awaynat Uplift which destroyed the major parts of NW–SE to NNW–SSW of the Tripoli – Tibesti Uplift, Dor el Qussah Trough, South Haruj Uplift and Kalanshio Trough (Fig. 3.4). These structural elements led to separate of Ghadamis Basin from the Murzuq Basin and remains of the Dor el Qussah trough became the eastern part of the Muruzq Basin and parts of the South Al Haruj Uplift is much less clear due to covered by the later Tertiary to Quaternary extruded basaltic lava flows of the Al Haruj Volcanic province (AHVP) (Peregi et al., 2003; Less et al., 2006; Chorowics and Benissa, 2016). The Palaeozoic sequence of the central and southernmost part of Libya was dominated by folds and steep shear zones beginning at Emsian and continuing until Moscovian. They were characterised by compression stress which led to producing the inversion of Dur al Gussah trough (Oun et al., 1998; Peregi et al., 2003).

Alternatively, Chorowics and Benissa (2016) propose that the Qarqaf Arch, N70^{o}E, occurred due to transfer fault along duration extension and associated transcurrent movement during the Palaeozoic rather than regional compression stress. In addition, most folds occurrences in the NW Libya were related to folding along normal faults or due to gravity sliding of soft material along transfer fault zone (Chorowics and Benissa, 2016). However, all the main continental plates had formed a single supercontinent which called Pangea due to the collision between western Gondwana and Laurasia and continued until the Jurassic time, where a great strike-slip component and a major right-lateral shear zone were developed and extended along the line contact between them. Therefore, many of basins situated on the margin of the North African are governed by dextral shear zone such as the Sirt Basin (Hallett, 2002; Fig. 3.5).

The middle to late Permian was prevailed by tensional regime that encouraged magmatism as evidenced by basic volcanic rocks which have

been encountered offshore in many oil wells as well as granites dated as late Permian (256 Ma) on the Waddan horst, west Sirt Basin (Wilson and Guiraud, 1998; Hallett, 2002; Abadi et al., 2008). Moreover, microsyenite sills have been recorded in the Amal oil field, the eastern part of Sirt Basin, with a time span 245 Ma (Abadi et al., 2008). This time corresponds to the fragmentation of many small plates in the eastern Mediterranean as resulted of the intense dextral wrench strike with displacement around 400 km between Laurasia and Gondwana (Fig. 3.5). The Permian – Triassic transition time was marked by minor tectonic activity and slightly changes in the paleogeography (Echikh and Sola, 2000; Guiraud et al., 2005).

3.4 Triassic to late Cretaceous (≈ 242-66 Ma)

Pangea was commenced to the break-up during the late Triassic to middle Jurassic time that led to the opening of the Central Atlantic due to the separation of the northwest Africa from North America which was associated with melt generation and magma emplacement (Less et al., 2006; Abadi et al., 2008). Granodiorites have been penetrated in several oil wells on the Waddan Platform, the western part of Sirt Basin, as well as from Amal area that have been dated as 230 Ma (Carnian) and 207 Ma (Rhaetian) respectively (Abadi et al., 2008). The magmatic episodes may be provided significant insight into the timing and the evolution of plate geodynamics (White and McKenzie 1989; Suleiman et al., 2017).

Laurasia had totally separated from the Gondwana by the late of Jurassic (Hallett, 2002). The relative motion between African and European plates is crucial importance to the tectonic evolution of North Africa and the development of Tethys (Mediterranean Sea) between North Africa and Europe. Transgression of the Neotethys along Northern Africa which produced terrigenous to mixed marine sedimentation and predominated extensional tectonics during this period (Conant and Goudarzi, 1967; Gumati

and Kanes, 1985; Ziegler, 1988, 1992; Baird et al., 1996; Schroter, 1996; Hallett, 2002; Courel et al., 2003; Guiraud et al., 2005; Abadi, et. al., 2008; Chorowics and Benissa, 2016; Fig. 3.6). Several geodynamic and magmatic events were registered by the Jurassic times along the northwestern Africa which thus strongly influenced by transtensional movements (Guiraud et al., 2005). The continental rifting generally was very active during this time within entire the African plate and produced numerous NW–SE troughs as documented in many regions (Corti, 2009).

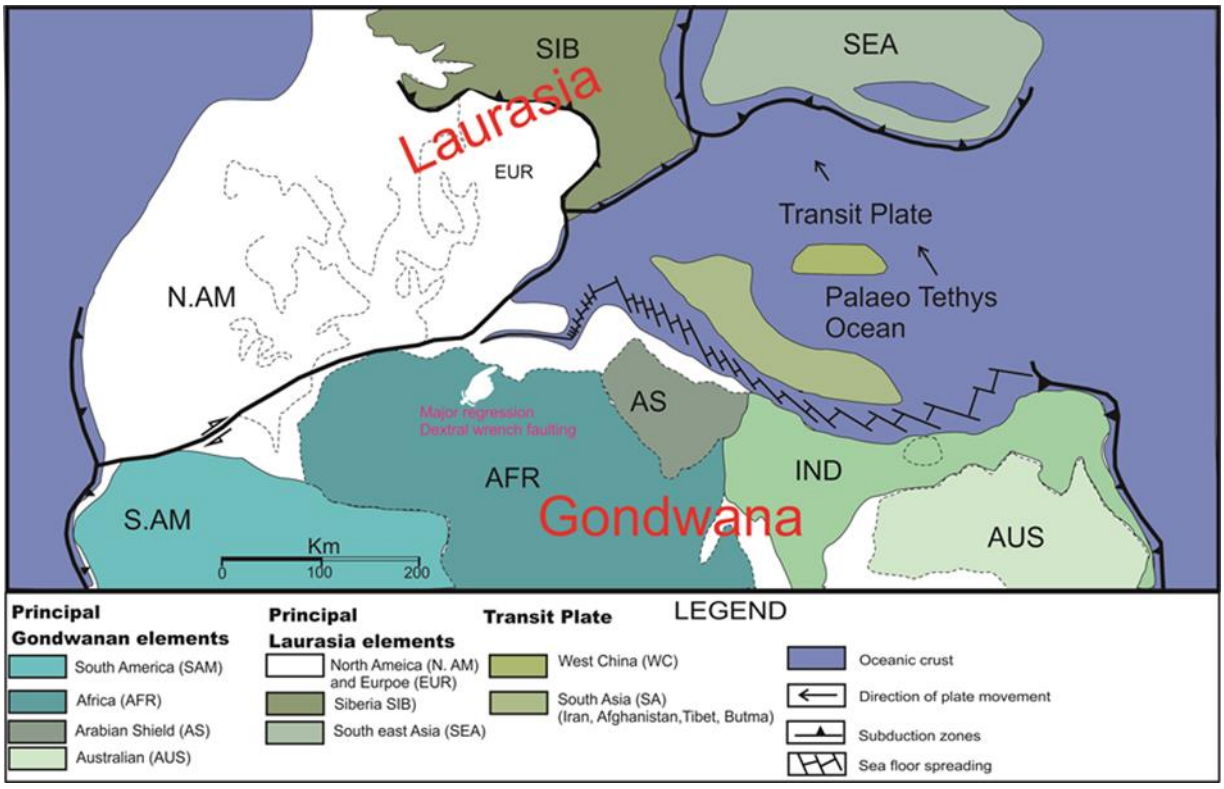

Figure 3.5. Pangea super-continent was established during the early Permian (256 Ma) due to the collision between Laurasia and Gondwana. Palaeo-Tethys ocean began to develop and rifting among West Gondwana and Laurasia (modified from Ricou, 1996; Hallett, 2002).

However, in the early Cretaceous, the seafloor spreading began in the central Atlantic that induced major changes in the drift of Africa relative to Europe from an ESE to E which produced the major shift in the position of the Mediterranean terranes. Subsequently, stretching and collapse of the Sirt

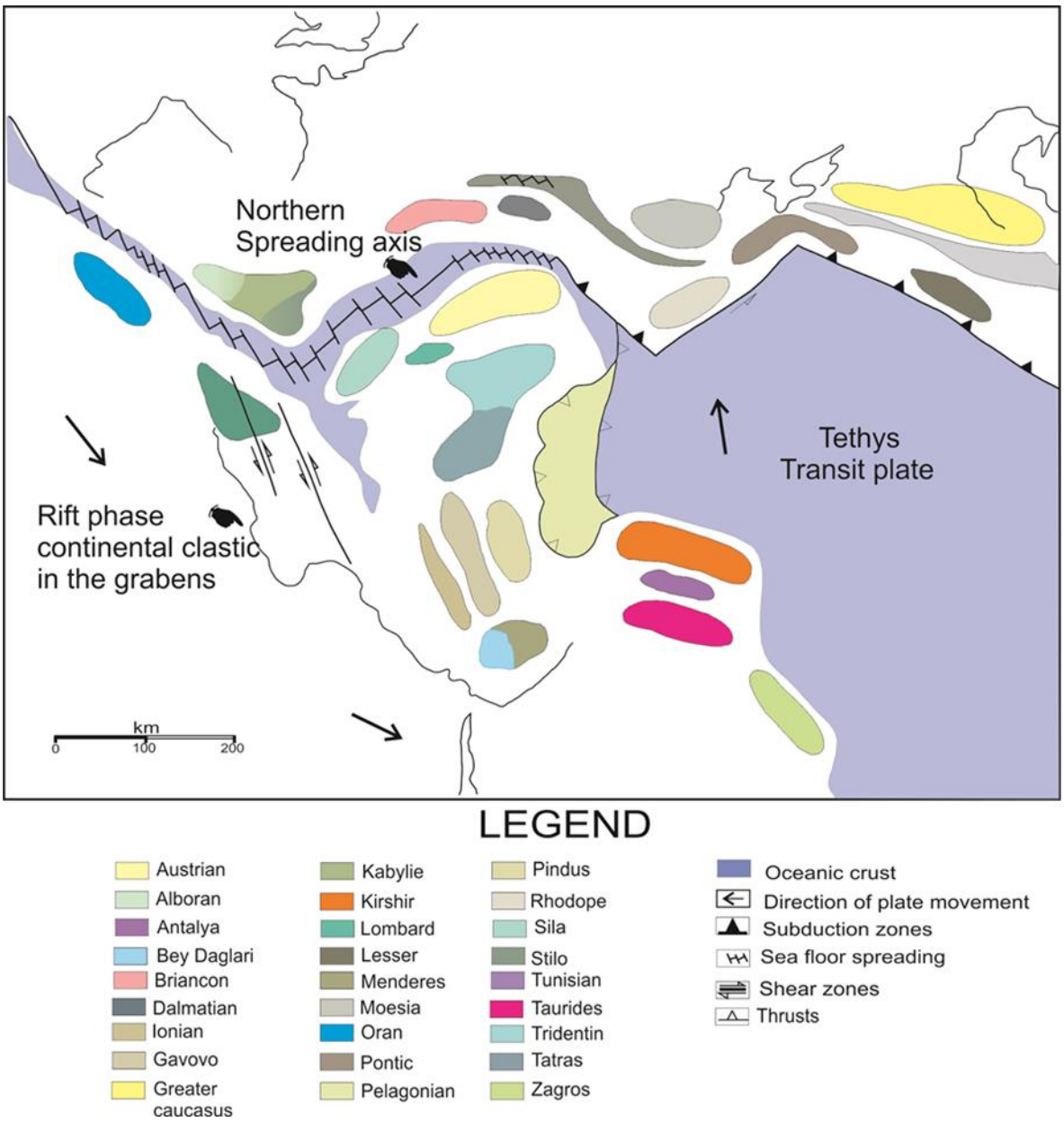

Figure 3.6. The break-up of Pangea led to establish sea floor spreading throughout the Mediterranean province as well as newly opening Atlantic during the mid-Jurassic. African plate was simultaneously moved eastward relative to Eurasia, resulting left shear zones in the western Mediterranean (modified from Dercourt et al., 1986; Hallett, 2002).

Arch was caused by detachment of Apulia plate and remaining what is now the Gulf of the Sirt (Hallett, 2002; Fig. 3.7). Active sea floor spreading adjacent to the African margin and the eastwards drifting of Africa, with the formation of horsts and grabens in NW–SE strike trending led to the formation of the Sirt Basin (Fig. 3.8). They were submerged by a marine

transgression during the Cenomanian and associated with warm global climates and the highest global Phanerozoic sea levels, which favoured the development of carbonate platforms (Dercourt et al 2000; Hallett, 2002; Philip, 2003; Guiraud et al., 2005). Many studies suggest that the northern Libyan margin basins commenced to create during Permian times along offshore domain, while onshore domain was formed during Cretaceous (e.g., Shegewi, 1992; Dercourt et al., 1993; Anketell, 1996; Abdunaser and McCaffrey, 2014). However, most of the central and southern Libya was undergone to widespread erosion and continental sedimentation from the mid-Permian to late Cretaceous, therefore a thick sequence of terrigenous sedimentary rocks was deposited in the Murzuq Bain during this period. By contrast, the Sirt arch was exposed to extensive erosion (Peregi et al., 2003). Guiraud et al., (1992) demonstrate that the Mesozoic – Tertiary tectonic evolution of the African plate is directly linked to the opening history of the Atlantic Ocean and related to the interaction of the Eurasian and African plates (Ziegter, 1992; Van Der Meer and Cloetingh, 1993).

During the Coniacian-Santonian the relative motion between African and Eurasian plates changed relatively from sinistral divergence to dextral convergence in NE direction and termination of sea floor spreading in the western Mediterranean. Meanwhile, Tethys began to close, reflecting the marked change in tectonic style that took place in the Santonian across the Mediterranean region and Africa. Therefore, the Santonian represents a compression phase associated with the continued NE movement of the African plate leading to inversion of Al Jabal al Akhadar Trough in NE Libya with folding roughly NNE–SSW axes (Hallett, 2002; Abadi et al., 2008). This regional compressive regime is present throughout the eastern Mediterranean region from Syria to form the Syrian arc fold system through Palestine to the Western Desert of Egypt. Subsequently, tension phase occurred in the latest Cretaceous (Campanian – Maastrichtian) along the southern margin of Tethys (Fig.3.9a) (Rohlich, 1991; Anketell and Ghellali, 1991; Guiraud et al., 1992; Abadi et al., 2008).

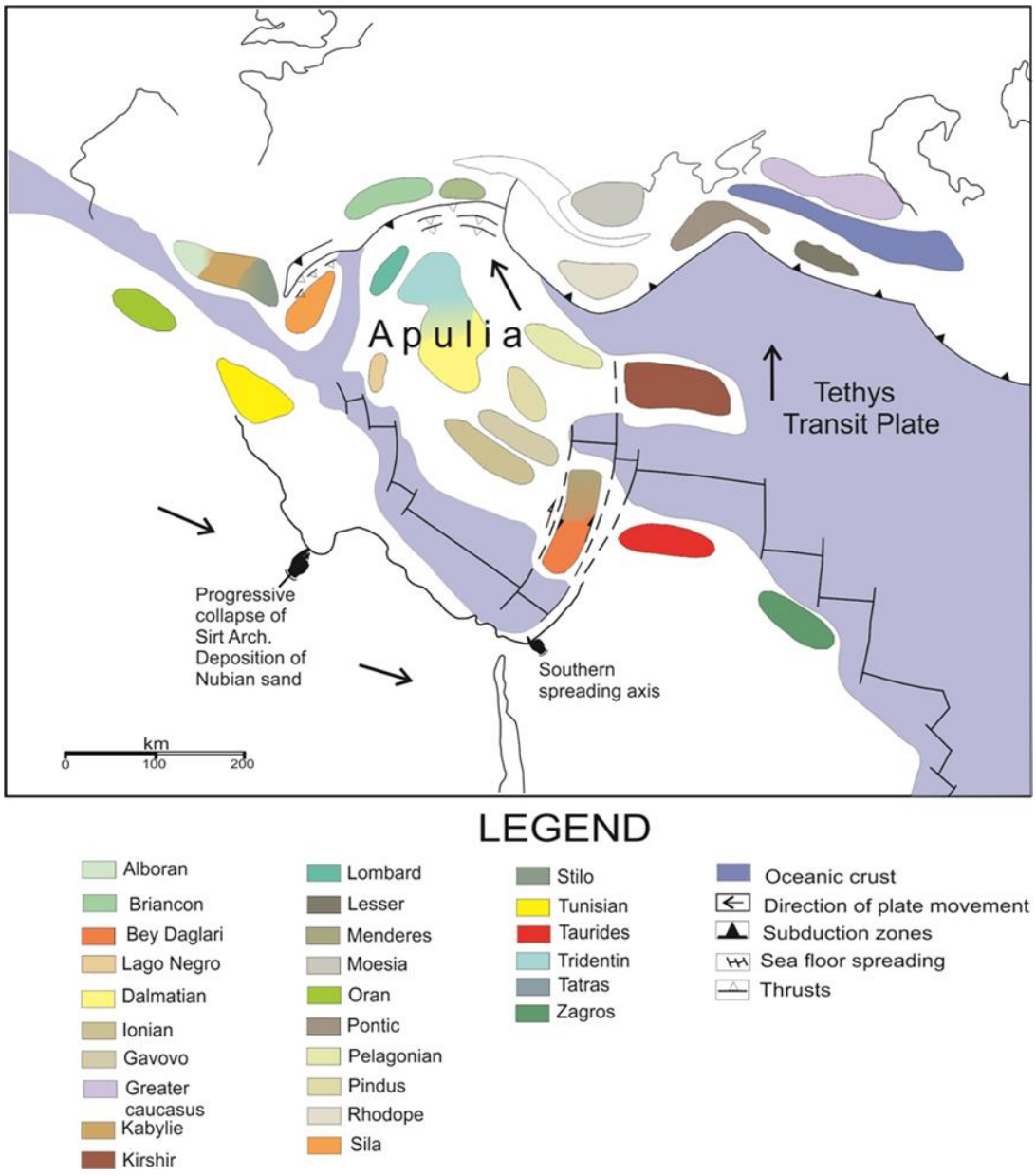

Figure 3.7. Sea floor spreading established in the early Cretaceous, leading to major changes of Mediterranean terranes (modified from Dercourt et al., 1986; Hallett, 2002).

3.5 Early Paleogene to Present day (≈66-0 Ma)

African plate ceased motion relative to European plate during the Paleocene (Rosenbaum et al., 2002), causing inactive faulting in the Sirt Basin with down-warping forming a structural sag. Then the late Eocene to the recent time was dominated by strong volcano-tectonics and ring intrusions have been dated as Eocene at Jabal Awayant on the border between Libya and

Sudan and this stage was marked by rapid and intense changes in the global climate (Woller and Fediuk, 1980; Andre, et al. 1991; Guiraud et al., 2005; Fig. 3.4). Followed that in the Oligocene the relative movement of African to Eurasian plates had been dramatically changed which led to several significant changes in the western Mediterranean and subsidence of the Hun Graben occurred during this period.

A major subsidence was still taking place in northern part of the Ajdabiya Trough, the eastern part of Sirt Basin (Abadi et al., 2008). Moreover, sedimentation of the Oligocene was influenced by the upper Eocene – early Oligocene uplift and erosion. The broad carbonate platforms in the early Tertiary have represented a major hydrocarbon reservoir in the Sirt Basin (Hallett, 2002). In addition, the Arabian shield commenced to break-up from the African plate throughout the rifting of the East African in the Oligocene leading subsequently to opening Red Sea and the Gulf of Aden during Miocene (Bosworth et al., 2005; Begg et al., 2009; Al Kwatli et al., 2012). Sebratah and Jifarah basins in the north-western part of Libya began to subsidence during late Paleocene to Eocene, simultaneously continued drift of Africa to the northeast with greater rotation to the east from the Miocene at rate of about 1cm per year. Whereas the rate movement of Arabian plate is around 3 cm per year which led to increase compression along the boundary between Arabia and Iran as well as rifting of the Red Sea has developed into an active spreading center (Hallett, 2002; McClusky et al., 2003; Al Kwatli et al., 2012).

Furthermore, Capitanio et al. (2012) suggest that the Jifarah Basin, Jabal Nafusah and the Hun Graben are consistent with age and trends of the Sicily Channel rift zone. The Dead Sea was subject to strike-slip faulting during mid-late Miocene, these events reflect the ENE tilting and minor folding of the Sirt Basin (Hallett, 2002). Subsequently, the motion of African plate relative to European plate changed during the Tortonian (8.5 Ma) from a NNE to NW which led to rejuvenation Hercynian faults WNW (Fig. 3.9b).

During this period was marked by thrusting and wrench faulting in offshore of Libya, marine sedimentary rocks in Cyrenaica, NE Libya. Meantime, uplift and erosion took place in western Libya which interpreted as upwelling mantle plume caused this uplifted as well as continued extensive subsidence in the whole of the Sirt Basin (Hallett, 2002; Guiraud et al., 2005). Subsequently large of basaltic lava flows (> 66,000 km^2) which were erupted along the axis of the Paleozoic Tripoli – Tibesti Uplift in the trend NNW–SSE from the Gharyan volcanic field at the coast of Mediterranean Sea to Nuqay at Libya – Chad border through the AHVP as well as at Tibesti Volcanic Province, in northernmost Chad (Anketell, 1996; Deniel et al., 2015). The Tripoli – Tibesti Uplift is considered by many studies as the junction between two African plates (East and West plates) according to paleo-stress field studies (Hallett, 2002). Reactivation of these ancient megastructures as the African and European continents gradually became closer since late Cretaceous may be one reason for the Libyan magmatisms (Bardintzeff et al., 2012; Staurt et al., 2014). The alignments eruptive vents/crater rows at the AHVP display the dominating strike of volcanic fissures/feeder-dykes namely WNW–ESE to NW–SE and NE to NNE, coinciding with the predominate orientations of these regional pre-existing structures. Therefore, some feeder-dykes may have used these ancient fractures as part of their paths to the surface.

Nevertheless, super-aridity occurred at the late Miocene (<11 Ma) in the central Libyan Sahara which caused the mass extinction of savanna climatic conditions and substantial antiquity of river basins at Lake Megafezzan, southwestern Sirt Basin (Hunslow et al., 2017). In addition, the level of sea water in the Mediterranean dramatically drawdown more than 500 m during the latest Miocene (Messinian time) and produced massive desiccation in the Mediterranean Sea, known as Messinian Salinity Crisis (MSC) (Gautier et al., 1994; Bache et al., 2009). The Messinian event has been evidenced by the presence layers of evaporites in outcrops of Sahabi area, west of Ajdabia city, and in many oil wells in the Sabratah Basin (Barr and Weegar, 1972;

Schäfer, et al, 1980; Hallett, 2002; Muftah et al., 2013; El-Shawaihdi et al., 2016).

3.6 Tectonic evolution of the Sirt Basin

The AHVP is mostly located within the Sirt Basin; thus its geological history is mainly related to the Sirt Basin tectonic evolution. The sedimentary record filling of the basin belongs to the late Mesozoic to Tertiary time which reaches a maximum thickness around 7,500 m in the Ajdabi Trough (Fig. 3.10). The Sirt Basin is situated within the North African passive continental margin and bounded on the north by the Mediterranean Sea, from the west by Al Qaraqf Arch, southeast by Az Aalmah Arch and from northeast by the Cyrenica platform which is considered as a continental rift (Fig. 3.11) (Futyan and Jawzi, 1996; Guiraud and Bosworth, 1997; Abdunaser and McCaffrey, 2014; Galushkin, 2016).

The basement rocks of the Sirt Basin have been penetrated by numerous oil wells which reveal the Pan-African remobilised, subsequently, deposition of sediments in the Kalanshio Trough during early Palaeozoic then uplift and erosion in the Devonian. So that the tectonic evolution of the Sirt Basin was initiated as positive Tibesti – Sirt arch, which was formed during the Hercynian Orogeny in the mid-Devonian due to inversion of the early Palaeozoic structure elements during the late Palaeozoic – early Mesozoic (Anketell, 1996). This major arch extended NE–SW from Chad towards Cyrenaica and was undergone to intensive faulting and deformation (Fig. 3.4). Consequently, major erosion led to a removal of the Paleozoic sediments over the crest of the arch. Some traces of Kalanshio Trough have been reported in the lower Palaeozoic succession beneath the AHVP as well as in the Al Fuqaha Depression (Bellini and Massa, 1980; Van Houten, 1980; Anketell, 1996; Pawellek 2007). Granites and mafic rocks, however, have been encountered from borehole data in the Sirt Basin which dated as early Cretaceous. Therefore, some studies suggest that the Sirt Arch was situated

over a fixed mantle plume led to stretched and weakened the overlying crust (Deunff and Massa, 1975; Belhaj, 1996; Echikh, 1998; Hallett, 2002).

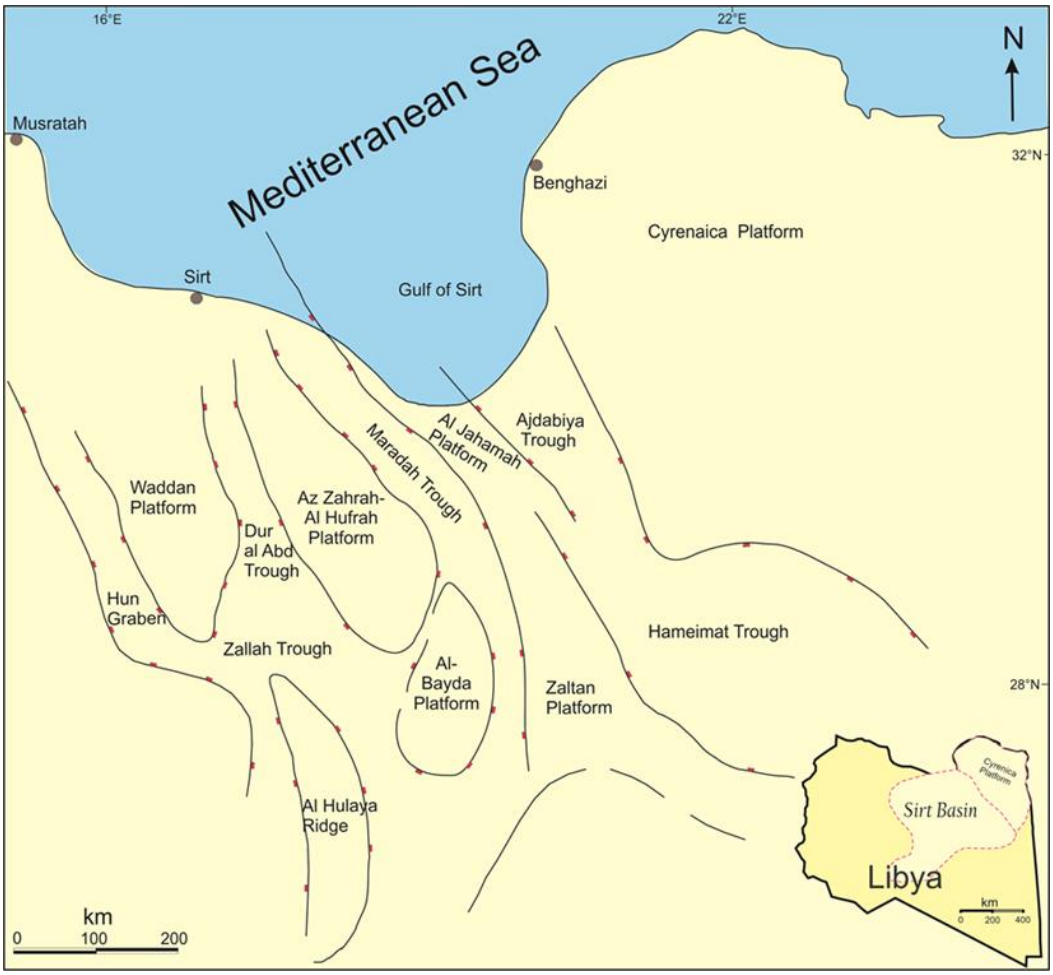

Figure 3.8. A generalised structural map showing the broad NW–SE structural patterns of the Sirt Basin that consist of grabens with intervening horsts produced from the collapse of the Sirt Arch (modified after Anketell, 1996).

However, the Sirt Basin is comprised of a series of platforms and troughs mainly orientated in NW–SE that commenced to evolve in the latest Jurassic and announced the dominant structural trends in the basin today (Fig. 3.8). The troughs gradually deepen eastwards providing a regional asymmetry to the structural shape of the Sirt Basin (Abdunaser and McCaffrey, 2014). The origin and tectonic evolution of the Sirt Basin have been attributed to different causes by many researches as well as the timing of the main tectonic phases is subject to open debate due to lack of deep hydrocarbon wells to

reach the basement in the trough areas as well as lack available high quality 3-D seismic surveys (Abadi et al., 2008, Abdunaser and McCaffrey, 2014).

Some suggestions from these numerous syntheses and models as to the timing and tectonic evolution of the Sirt Basin during the last few decades will be discussed here. For instance Schäfer et al. (1980) demonstrated that the drift velocity of the Saharah sub-plate was decreased relative to the east African sub-plate during the late Cretaceous in response to collision between Saharah sub-plate with European plate which continued drifting to the NE and led to extension and development of the Sirt Basin (Abdunaser and McCaffrey, 2014; Fig. 3.12). Thusu (1996) suggests that rifting of the Sirt Basin began in the Triassic or probably in the Permian associated with the initial opening of Neotethys (Stampfli, 2001). Baird et al. (1996) argue that the rifting of the Sirt Basin was active during Cenomanian to Campanian then infill rifting until the latest Maastrichtian. It was followed by inclining towards the NE during the Oligocene, whereas others suggest (e.g., Thusu, 1998) that the rifting started as early as Triassic and the syn-rift extended only from Triassic to early Cretaceous. The rift termination was marked by a thermal sag stage which gave rise to the Cenomanian marine transgression (Gras, 1996).

Gealey (1988) suggests that the rifting began in the mid-Cretaceous in response to extension along abroad transform zone extending through western Mediterranean into the Atlantic Ocean. Anketell (1996) presented evidence to indicate that the Sirt Basin created along the North African plate margin under sinistral strike-slip movement, rifting in the Hameimat Trough was obviously active in the Berriasian – Valanginian time while was active during the Aptian in the western part of the Sirt Basin. Ambrose (2000) suggests that dextral strike-slip influenced on the late Cretaceous tectonism in this region. Capitanio et al. (2009) propose that the tectonic development of the Sirt Basin derived from slab pull forces due to the evolution of the

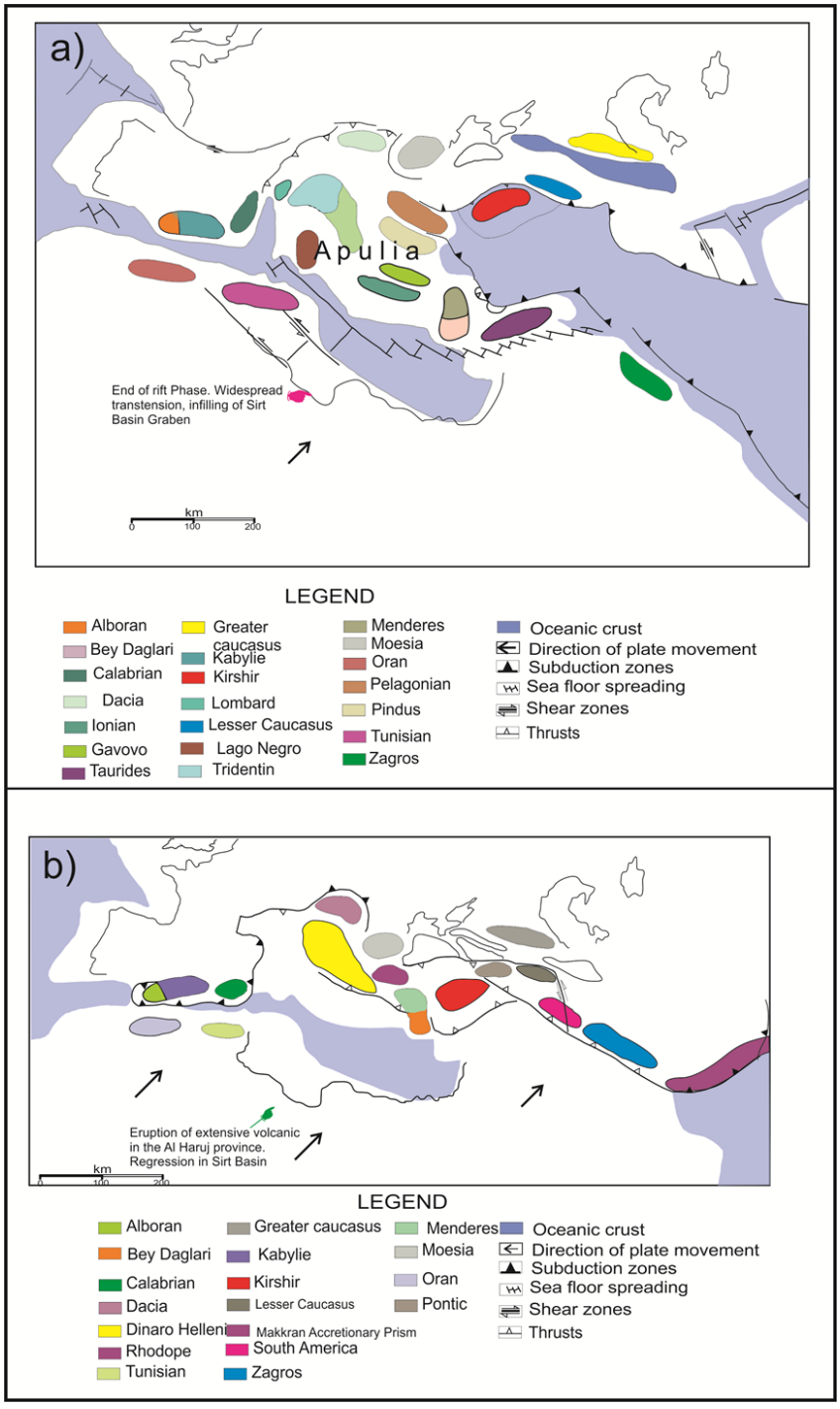

Figure 3.9. a) The relative motion of African plate changed from eastward to northeastward in the latest Cretaceous, causing ending of the seafloor spreading in part of the western Mediterranean and sinistral shearing zones in the North Africa (modified from Dercourt et al., 1986; Hallett, 2002). b) The relative motion of African plate to Eurasian plate changed from the north-eastward to the north-westward during the Eocene and Oligocene after that it went back toward northeast during the early Miocene, indicated by black arrows (modified from Dercourt et al., 1986; Hallett, 2002).

Hellenic subduction system. Hellenic extension caused differential faulting in the Sirt Basin during (Maastrichtian-Thanetian), subsequently grew at early Eocene (Yppresian), producing large extension in Sirt Basin. Abdunaser and McCaffrey (2014) suggest that the tectonic evolution of the Sirt Basin started as early as the Permian-Triassic until the Neogene which is characterised by a complex history of extension interrupted by strike-slip faults and compressional phases. Theses faults partly control the dyke paths in the uppermost crust in the western part of Sirt Basin (Elshaafi and Gudmundsson, 2016).

Additionally, Van Houten (1983) propose that the rifting was resulted by crustal thinning due to the passage of the area for a long period over a fixed mantle plume during the early Cretaceous that presumably produced change in state of stress within Africa plate (Hallett, 2002). Moreover, Burke and Dewey (1974) suggest that the Sirt Basin constitutes the failed arm of a triple junction among the Eurasian, African and Tethyan plates. It can be suggested that the NW trend of horsts and grabens, the SW trend of the Abu Tumayam Trough as well as E–W trend of the Hameimat Trough seem to form triple junction within Sirt Basin, due to crustal thinning over a fixed hotspot in the late Jurassic – Cretaceous time (Dercourt, et al. 1986; Gras; and Thusu, 1998; El-Makhrouf, 1988, 1996; Finetti and Del Ben, 2000; Van Houten, 1983; Anketell, 1996; Hallett, 2002).

Klitzch (1971) suggests that the basin formed in an intraplate setting due to shearing movements, resulting from the rotation of the Sahara platform in the west direction relative to Europe shearing movements. Guiraud and Maurin (1992) pointed out that the Sirt Basin was considered as one from a number of large NW trending troughs during early Cretaceous that opened due to NE extensional regime. While the central African fracture zone extended from Benue to Sudan that revealed strike-slip movements to produce pull-apart basins. The African plate was divided into a western Africa block or (subplate), an east African block subplate as well as a southern African sub-

plate (Fig. 3.12). The East African sub-plate was segregated from another sub-plates and moving towards the North in Berriasian to early Aptian, subsequently, changed toward the NE during the middle Aptian to late Albian (Guiraud and Maurin, 1992; Anketell, 1996; Abdunaser and McCaffrey, 2014).

Overall, the Sirt Basin was active at several stages and associated with series of tectonic events caused complex geodynamic system. Therefore, four main tectonic phases have been identified from the late Cretaceous to present day based on thickness variations and subsidence analysis, corresponding to plate reorganisation which is tied to the evolution of the Atlantic and Tethys (Gumati and Nairn, 1991; Van der Meer and Cloetingh, 1993; Baird et al.,1996; Schroter, 1996; Abadi, 2002; Galushkin, 2016).The stretching periods of the tectonic subsidence of the Sirt Basin have been punctuated by periods of tectonic quiescence and thermal subsidence, where stretching of the crust began at the trough centres then gradually transported to the crest of platforms (Abadi et al., 2008). The complex geodynamic evolution of the Sirt Basin was followed by the onset of extensive volcanic activity in the SW margin of the Sirt Basin (Fig. 3.13; Table 3.1).

3.6.1 Tectonic phase I (late Jurassic – early Cretaceous)

Limited subsidence commenced on the early rifting phase and was corroborated by magmatism as evidenced by granites have been dated 152–122 Ma and basic-intermediate volcanic rocks have been dated 148–127 Ma (Cahen et al., 1984; Rossi et al., 1991;Hallett and El-Ghoul, 1996 ; Gras and Thusu, 1998; Wilson and Guiraud, 1998; Abadi et al., 2008). Less intense subsidence was most pronounced in the western part of the Sirt Basin in the Dahra Platform, Zallah Trough, Hun Graben as well as Waddan Uplift with stretching β value less than 1.059 compared to the eastern part of the basin

in Hameimat and Sarir Troughs to be 1.21, 1.096 respectively (Abadi et al., 2008). The stretching β values are obtained from back-stripping geophysical results by Abadi et al. (2008).

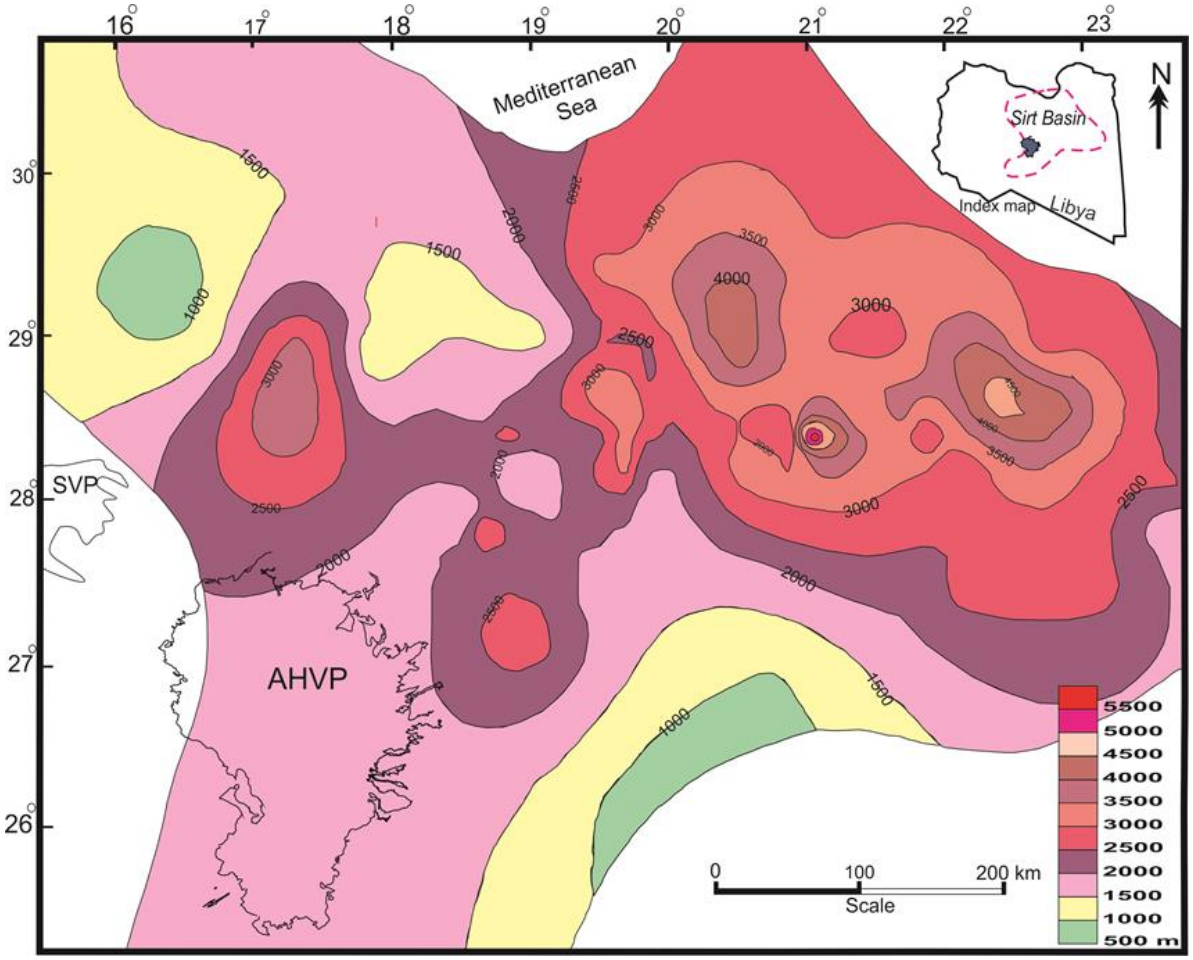

Figure 3.10. Isopach map showing the subsurface distribution of the sediment thickness in the Sirt Basin from the lower Cretaceous to Quaternary according to examined about 250 oil wells. The maximum thickness has been recorded in the eastern part of the basin at Ajdabi Trough (modified from Abadi et al., 2008).

The Apulian/Adriatic plate is a small tectonic plate carrying mainly continental crust that broke-up from Africa along a large transform fault in the early Cretaceous which led to increase instability and then the thinned and rifted Tibesti – Sirt Arch (Pawellek 2007; Abadi et al., 2008). The Tibesti – Sirt Arch collapsed during the Aptian producing in a rift basin with a NW–SE trending

horst and graben structure, and flooding of the collapsed area during Cenomanian. Subsidence and pull-apart took place in the Hameimat and Sarir Troughs, Messlah and South Sarir Horsts whereas the Jaghbub Trough on the Cyrenica Platform was created during the Berriasian – Valanginin (Hallett, 2002). All of these structural elements have roughly an E-W alignment (Fig. 3.11). Some studies suggest that the Abue Tumayam Trough formed at the same time with opposed direction in the NNE–SSW due to inherited of pre-existing structure (e.g., Wennekers et al., 1996; El-Hawat et al., 1996; Rasul, 2000; Sinha and Mriheel, 1996; Hallett, 2002). Klitzsch (1971) proposed that the central part of Libya developed as evolved into a high-elevation region (Sirt Arch) during Hercynian Orogeny, followed by collapsed associated with a rejuvenation of pre-existing structural elements. The Sirt Basin was mainly filled up by continental sandstone of Nubian Formation and subjected to erosion into the late Cretaceous (Tawadros, 2001, Abdunaser and McCaffrey, 2014). Nubian Sandstone refers to a diversity of sedimentary rocks deposited on the Precambrian basement in the central Libya and many other places in North Africa. The formation contains continental sandstones with thin beds of marine limestones, and marls and its timespan ranging from upper Cambrian to lower Cretaceous (Issawi , 19972). The earliest faulting in the Sirt Basin is existed in the Hameimat - Sarir troughs and began in early Cretaceous time (Berriqsian – Valanginian) and trended E–W and WSW–ESE (AGOCO, 1980). These faults probably controlled fragmentation of the plate margin along a Sabratah – Cyrenica shear zone (Anketell, 1996).

3.6.2 Tectonic phase II (late Cretaceous) (Cenomanian–Maastrichtian)

During the late Cretaceous, the African plate has been changed movement direction that led to the stretching of the cratonic lithosphere and fragmentation in the North Africa and major basin subsidence faults (Gumati and Kanes, 1985; Gumati and Nairn, 1991). This tectonic phase has been subdivided into five tectonic sub-phases by Abadi et al. (2008) based on an automated forward modelling technique that reflects existence of a complex

tectonic evolution. There are exhibited strongly subsidence variations in spatial and temporal, and the greatest stretching was recorded in this phase with β value of 1.26.

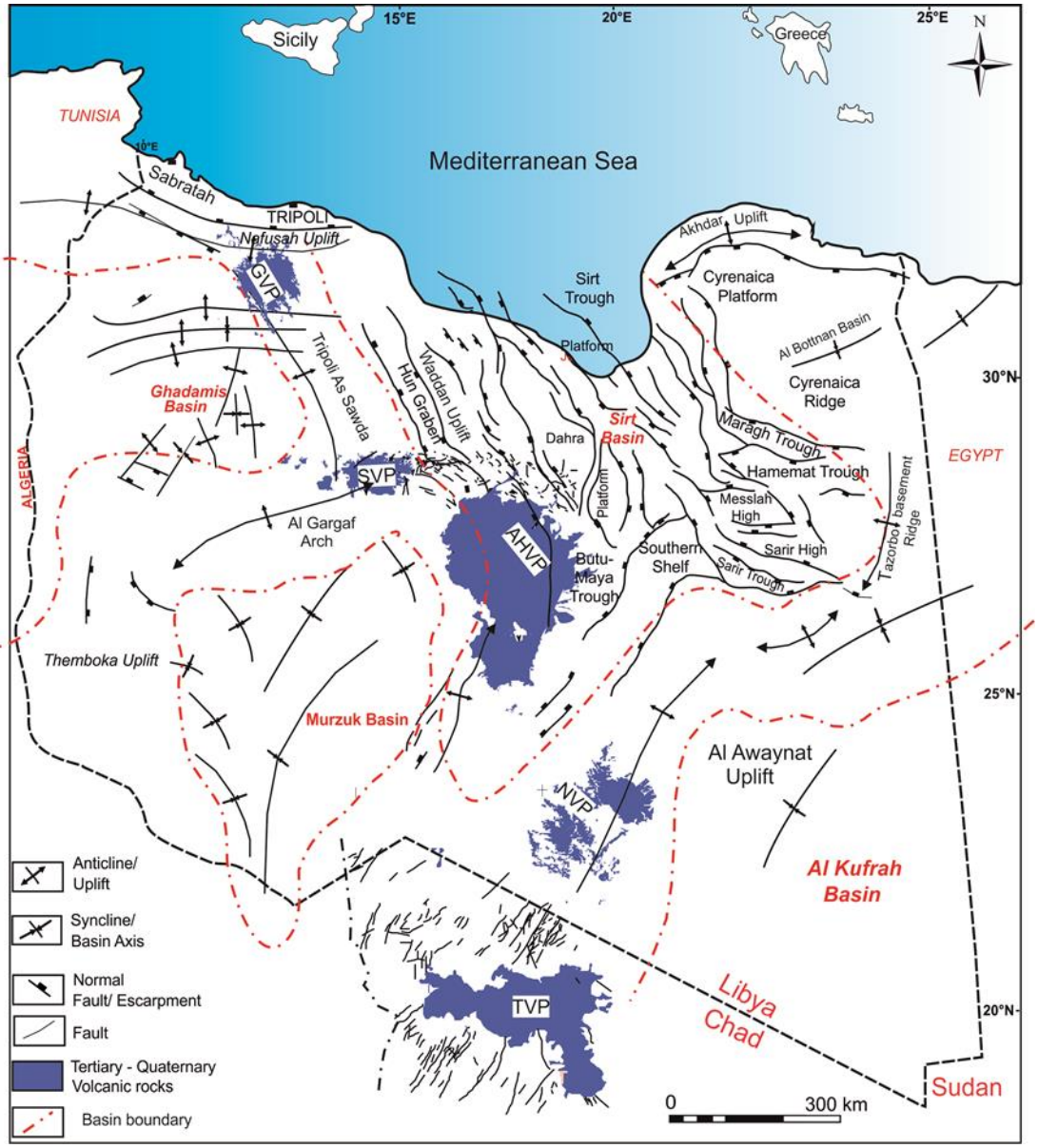

Figure 3.11. Tectonic map showing the major structural elements of the Sirt Basin and adjacent areas (modified after Mouzughi and Taleb, 1981; Ambrose, 2000; Abadi et al., 2008).

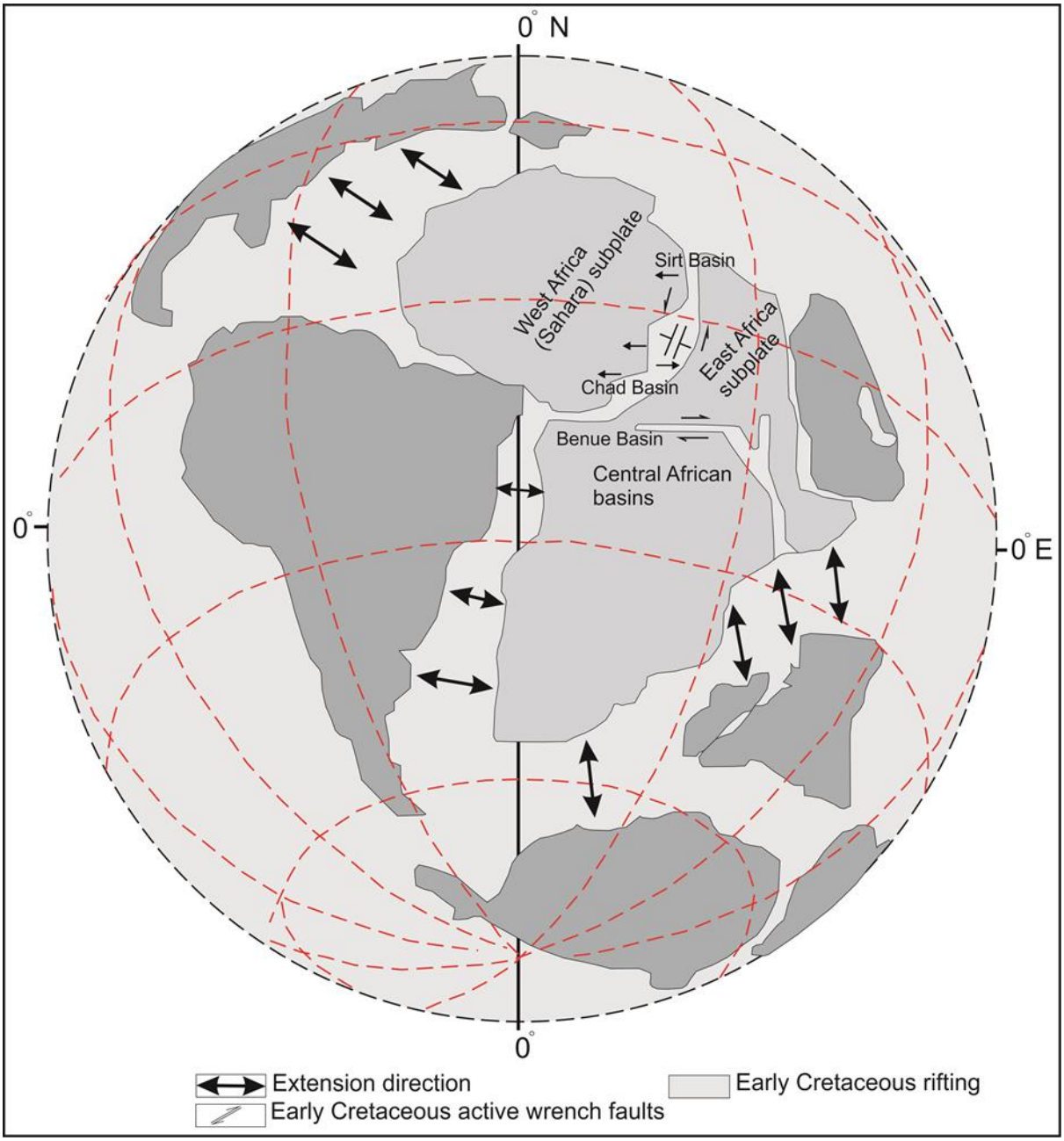

Figure 3.12. Subdivision of Africa into major blocks during the early Cretaceous. The Sirt Basin is situated at the tip of the Sirt-Benue fracture zone (modified from Fairhead and Green, 1989; Fairhead and Binks, 1991; Guiraud and Maurin, 1992; Anketell, 1996; Abdunaser and McCaffrey, 2014).

The great difference in subsidence rate during this tectonic phase most likely are related to change in the stress field regime interacting with the basin structure (Abadi et al. 2008; Galushkin, 2016). Subsequently, in the

Maastrichtian, the subsidence of the Sirt Basin became less variation in the space whereas the subsidence in the Ajedabia Trough continued intensively (Fig. 3.14). It was followed by minor subsidence and mild inversion in the Jabal al Akhadar anticlinorium, NE Libya, during the Santonian and Coniacian (Ziegler, 1988; Anketell, 1996; Guiraud et al., 2001, Abadi et al., 2008). During the late Cretaceous, the magmatism became larger in response to extensive rifting and sinistral strike slip faulting on the offshore Pelagian Shelf and volcanic rocks (trachyte) have been reported in the Sirt Basin and dated as early Palaeocene (Abadi et al., 2008). During the latest of Cretaceous most of the area had submerged under the sea and shale rich organic material (source rock of kerogen) was deposited in the troughs. Then subsidence was continued and formation extensive of the platform carbonates (reservoirs above horsts) (Abdunaser and McCaffrey, 2014).

3.6.3 Tectonic phase III (early Palaeocene – early Eocene)

The Palaeocene rifting phase was marked by an a rapid subsidence rates of the Sirt Basin due to the relative motions of the African and Eurasian plates during the opening of the Atlantic Ocean and the development of the Tethys (Mediterranean Sea) on the foreland of the African plate (Van der Meer and Cloetingh, 1993; Anketell, 1996; Abadi et al., 2008). It is associated with differential fault tectonics and reactivation of basement faults (Fig.3.15). Simultaneously, dextral strike-slip fault movement expressed along the coastal plain of Libya from Sabratah to Cyrenica leading to increase rift subsidence in the Sirt Basin during Palaeocene-early Eocene, indicating NE–SW extensional stresses (Anketell, 1996, Guiraud et al., 2001; Hallett, 2002).

Furthermore, a number of fault zones exposed in the western part of Sirt Basin were interpreted as initiated by sinistral strike slip fault (Less et al., 2006). It can be suggested that the rifting of the Sirt Basin can be explained by both dip-slip extensional and strike-slip tectonics (Kumati, 1981, Abdunaser and McCaffrey, 2014; Galushkin, 2016). Meanwhile, lithosphere

isostatically responds to a significant crustal extension (Van Der Meer and Cloetingh, 1993), and magmatic rocks have been recorded in the Tunisian-

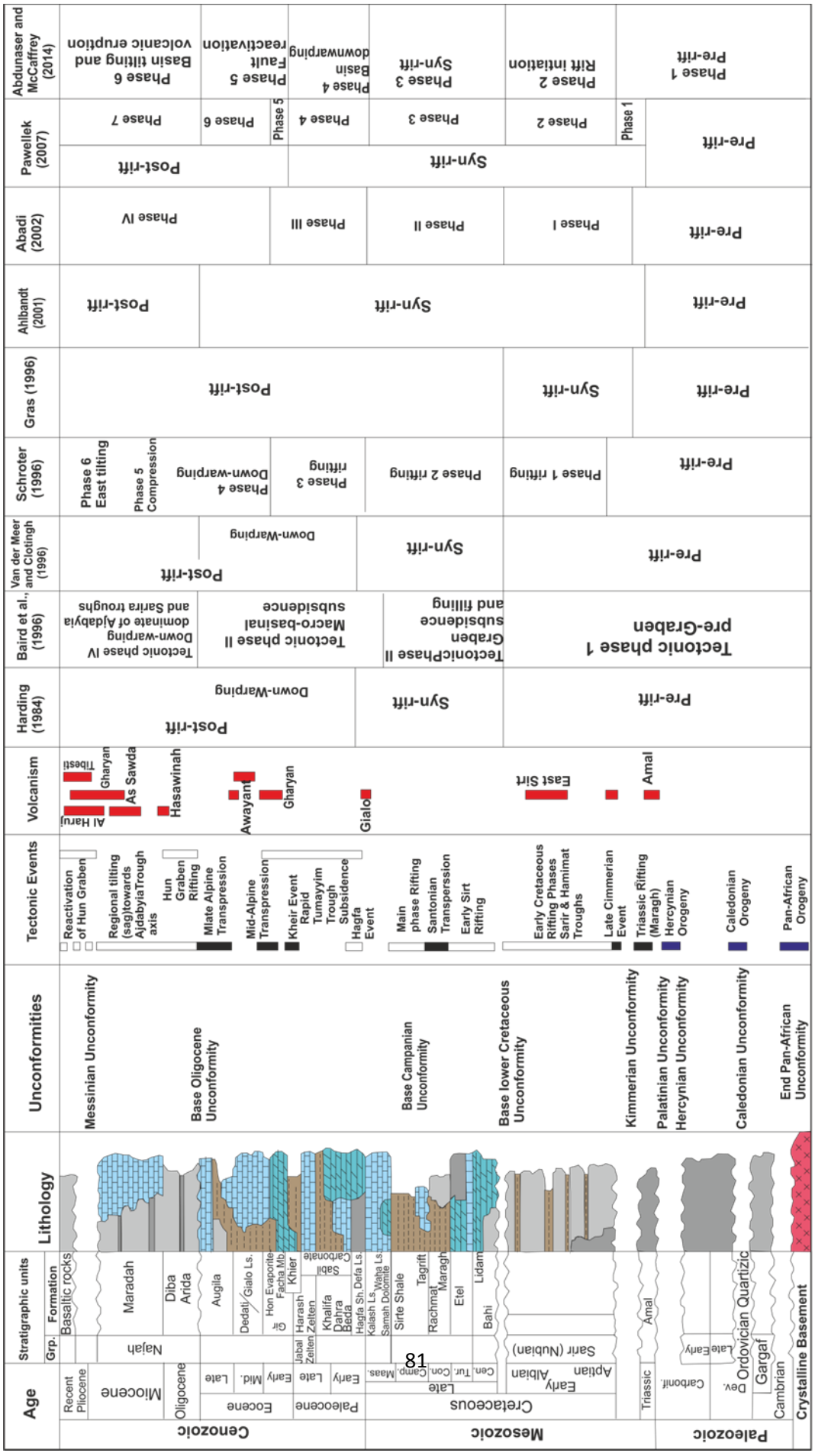

Table 3.1. Generalised tectonostratigraphic of the Sirt Basin area (modified after Guiraud et al., 2005; Abdunaser and McCaffrey, 2014).

Sicilian-Libya region which are given age as the late Cretaceous (Fig. 3.11) (Hammuda et al., 1991; Guiraud and Bosworth, 1997). In addition, the major volcanic activity of Gharyan volcanic field, located in the northwestern of the Sirt Basin, has timespan in ranging from the early Eocene to Pliocene based on K/Ar age dating method (Wilson and Guiraud, 1992, Al-Hafdth and Jafeer, 2014). Two main tectonic phases subsidence occurred in the Sirt Basin were separated by a tectonically quiescent phase during the Maastrichtian (Busrewil et al., 1996). They were followed by the early Eocene transgression leading to evaporitic and dolomitic deposition due to inversion tectonic to the north-eastern Libya at the Jabal Al Akhader anticlinorium (Abadi et al., 2008).

3.6.4 Tectonic IV (Post-rift stage) (middle Eocene to Holocene)

Subsidence and flexural bending occurred during this tectonic phase in response to thermal contraction of the lithosphere and vertical loading by sediments with a thickness of hundreds of meters. The highest subsidence during this tectonic phase occurred in Ajedabia Trough and Zelten Platform (eastern part of the Sirt Basin) (Hallett, 2002; Abadi et al., 2008). Thermal subsidence can be explained by an intraplate compression as a result the collisional coupling of Africa and Europe and subsequent stress release related to change in Atlantic geometry (Van Der Meer and Cloetingh, 1993). Syn-sedimentary reactivation of NW–SE pre-existing extensional faults occurred during the Oligocene in the SW part of the basin at the Al Haruj region that contributed to en-échelon pattern and right stepping asymmetric relay ramps (Peregi et al., 2003; Fodor et al., 2005; Less et al., 2006).

Moreover, the western part of the Sirt Basin was affected by the highest erosion amplitudes led to removing as much as 1000 m during the last 10 Ma (Gumati and Schamel, 1988; Galushkin, 2016) (Fig. 3.13). It is most likely related to a significant topographic doming in this area which was marked by the widespread volcanic activity of the Gharyan – Tibesti volcanic fields.

Those volcanisms can be explained by mantle upwelling in the absence of faulting during post-rift stage (Skogseid, 1994). The asthenospheric rise caused decompression partial melting at various levels and created later magma reservoirs at the crust-mantle boundary (Cvetkovic et al., 2010; Elshaafi and Gudmundsson, 2017). Lithospheric folding was most likely associated with the mantle upwelling as found in many areas in European plate (Hallett, 2002; Cloetingh and Van Wees, 2005). In addition, dykes associated with magmatic activity in the southwestern part of the Sirt Basin may have contributed to an elevated heat flow which led to enhancement maturation levels of kerogen (Gumati and Schamel, 1988 Abadi et al., 2008).

Furthermore, magmatism in the Gharayn – Tibesti volcanic provinces in general and the Al Haruj Volcanic province in particular, postdates peak extension of the Sirt Basin. Therefore, the thinning of lithosphere cannot be the directly related to the melt generation. It is noteworthy that this mafic volcanism took place mostly at the south-western periphery of the Sirt Basin rather than in central region that underwent to significant thinning. However, the rifting of the Sirt Basin has affected the sedimentary sequence of the late Cretaceous – Tertiary in the central and southern part of Libya. The major effect was mainly a tensional stress NE–SW to E–W in the southernmost part of the Sirt Basin which is primarily characterized by NW–SE trending normal fault, conjugate strike-slip faults with displacement less than 100 m as well as drape folds (Peregi et al., 2003; Fodor et al., 2005, Less et al., 2006). In contrast, the direction of tension along the Dor el Qussah basement inlier, west of the AHVP, and Abu Tumayam sub-basin, southeastern of the AHVP, were generally trending the NNE–SW as opposed to major trend of the Sirt Basin NW–SE. Therefore, this structural trend was inherited from ancient structural elements which could influence the geometry of the southernmost of the Sirt Basin (Fig. 3.11) (Less et al., 2006).

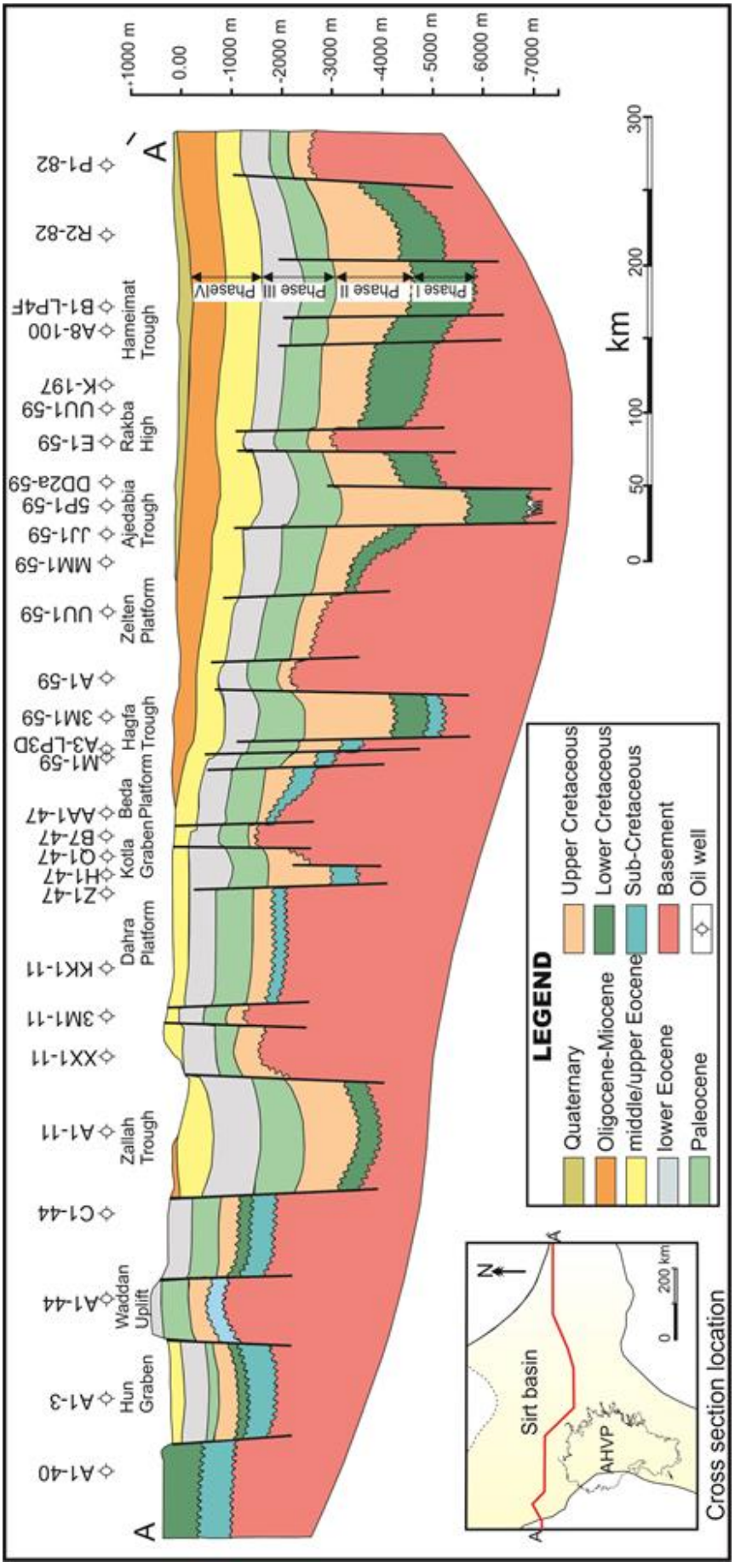

Figure 3.13. East–west cross section showing structural, tectonic phases and thickness of sediments in the Sirt Basin (modified from Abadi et al., 2008).

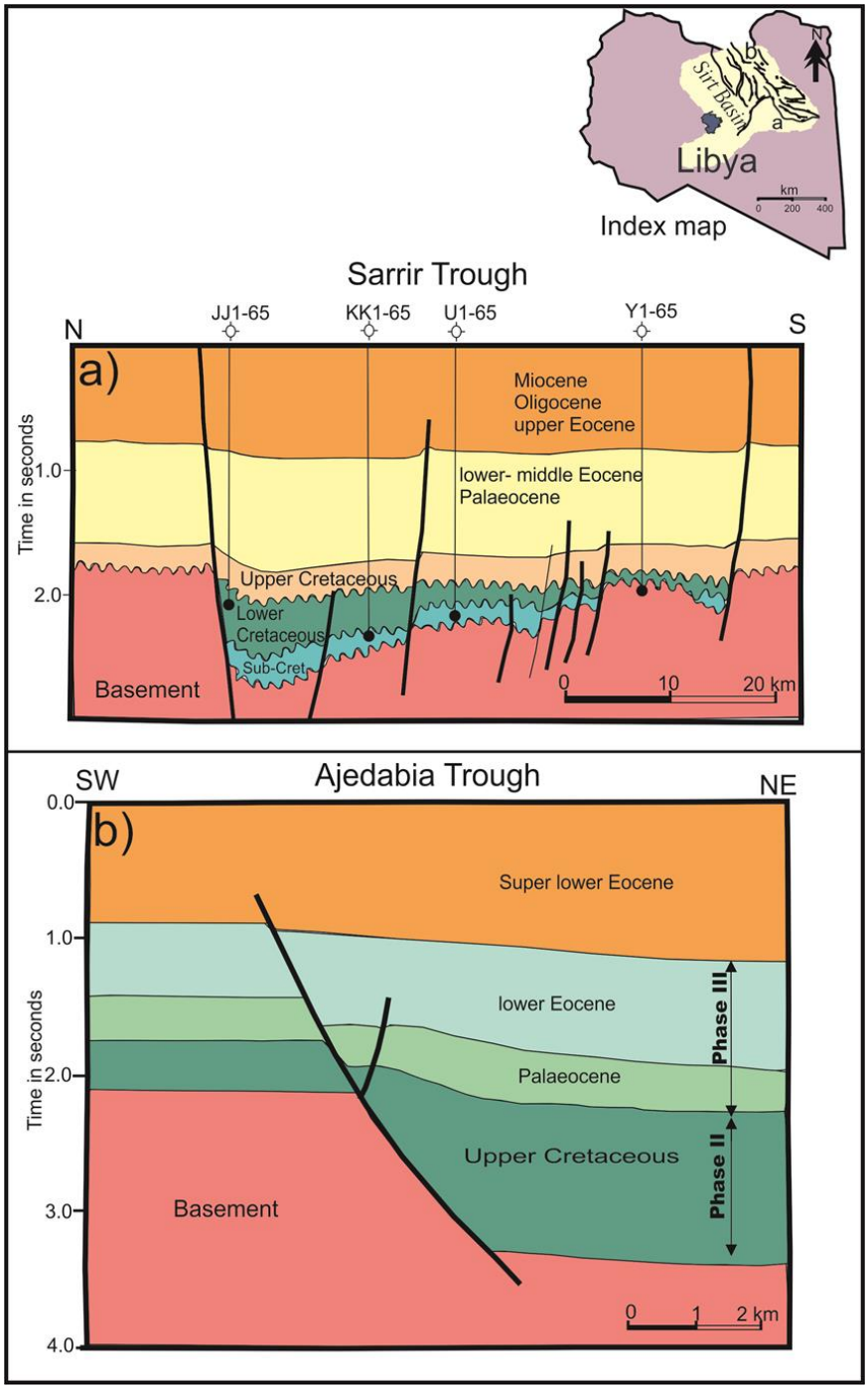

Figure 3.14. a) Schematic cross section of the Sarir Trough, SE of the Sirt Basin, reconstructed from seismic reflection line NC171-91-55. Note major tectonic phases were governed by high angle normal faults of the basement (modified from Gras and Thusu, 1998; Abadi et al., 2008). b) Cross section in the area separates the Ajedabia Trough from Zelten Platform according to interpreted seismic section (modified after Skuce, 1996; Abadi et al., 2008).

Moreover, the geodynamic processes contributing to basin subsidence include stretching of the lithosphere during the rifting phase (McKenzie, 1978; Van Der Meer and Cloetingh, 1993; Galushkin, 2016), and thermal upward displacement of the lithosphere-asthenosphere boundary. The total crustal stretching estimated for the entire of the Sirt Basin from early Cretaceous to Miocene is around 1.4 β a value derived from back-stripping geophysical technique as mentioned earlier. If assuming the initial thickness of the Earth's crust to be 35 km, then the sediment accumulation in the Sirt Basin has to have been in the order of 7 km (Abadi et al., 2008). Stretching factor (β) along the rift of the Sirt Basin is presumed to increase with decreasing crustal thickness. Nevertheless, an extension of the crust within the Sirt Basin region produced thermal and convective processes that led to thinning of the lithosphere in association with magmatic underplating and mantle injected melts into the crust (Ziegler 1992; Van Der Meer and Cloetingh, 1993). Magma reservoirs beneath this region most likely have produced the widespread basaltic lava flows in the western part of the Sirt Basin at As Sawda and the AHVP, respectively (Fig. 3.11). The basin tilting was followed by slightly basin inversion and activation of volcanic fissures that represented post-rift stage of the Sirt Basin. This event was most likely related to Alpine Orogeny in the Post-Eocene (Farahat et al., 2006; Cvetkovic´ et al., 2010). It was contemporaneous with the development of the Red Sea, Gulf of Aden and breakup of the Arabian shield from African plate (Binks and Fairhead, 1992; Al-Kwatli et al., 2012).

3.7 Stratigraphic sequence of the Sirt Basin and the Al Haruj region

The Precambrian crystalline basement and Cambrian – Ordovician clastic sedimentary rocks in the Sirt Basin are overlying by Mesozoic and Cenozoic sedimentary succession (Table 3.2). The sedimentary sequences in the Sirt Basin are marked by cycles of major transgressions and regressions, producing in extremely variable of marine, continental and transitional

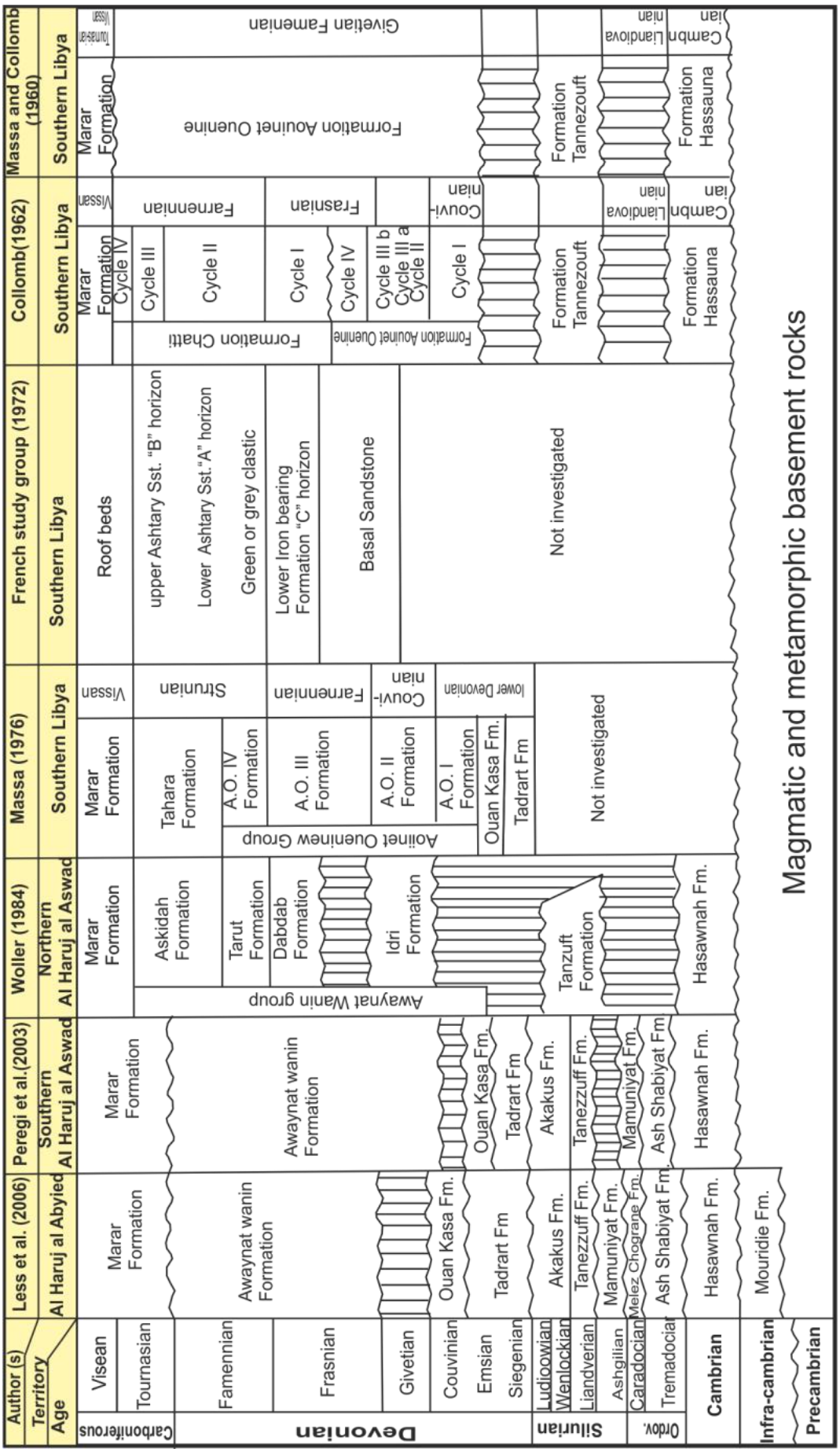

Table 3.2. Stratigraphic subdivisions from Cambrian to Carboniferous of the central and southern part of Libya (modified from Less et al., 2006).

deposit environments reflecting the complex geodynamic evolution of the Sirt Basin (Hallett, 2002; Abdunaser and McCaffrey, 2014). The real complexities of the uppermost crust in the Sirt Basin have strong effects on the mechanics on mechanics of dyke emplacement and propagation as discussed in detail in Chapter 6. The Mesozoic rift sediments (tectonic phase I first megacycle) composes of continental – marine clastic rocks of Nubian sandstones of early Cretaceous time, and scarce coccolith strata units depending on location in the basin which is separated by the Hercynian unconformity from the underlying granitic and metamorphic rocks. The base of the early Cretaceous is characterized by the unconformity which indicates a significant change from Nubian sandstone continental to the marine environment (Hallett, 2002). Marine clastics are preserved in a thick section in the troughs whereas carbonate rocks come out on the platforms and highs (tectonic phase II). The Mesozoic sedimentary rocks exhibit more lateral and vertical variations in thickness and lithology than the overlying Tertiary sedimentary rock (Table 3.3).

The Palaeocene sequence was deposited a relatively during inactive structural time with basin down-warping creating a structural sag during thermal subsidence and climaxed carbonate in the Palaeocene indicate that open marine environment (Parsons et al., 1980; Abdunaser and McCaffrey, 2014). These are overlain by large quantities of evaporites, limestone, and dolomite comprising the Kheir, Gir, Gialo and Gedir Formations that were deposited in the early Eocene (tectonic phase III). It appears to be associated with a strong reactivation of faulting recorded during Eocene than Palaeocene. They are marked by differences in thickness of sediment during late Eocene (Anketell and Kumati, 1991; Abdunaser and McCaffrey, 2014). Subsequently, the basin was beginning to deposit terminal continental during the late Eocene to Miocene (post-rift stage)(tectonic Phase IV), Bishimah Formation (early Eocene), Aljir Formation (Middle Eocene), Wadi Thamat Formation (Terrigenous clastic sedimentary rocks (late Eocene – Oligocene) was overlain by shallow marine rocks of Qarat Jahanam Member of Maradah Formation (early Miocene) (Hallett, 2002). A final tectonic phase of a post-rifting stage is coincident with extrusion of basaltic lava during the late

Miocene to late Pleistocene (Table 3.3) (Cvetokivc et al. 2010). The paleo-water depth of the upper Cretaceous – Tertiary sequence in the Sirt Basin has been estimated by planktonic and benthonic foraminifera around 200 m (Bezan, 1996; Muftah; 1996; Abadi, et al. 2008). The Quaternary sedimentary rocks in the Al Haruj region (south–western part of the Sirt Basin) is calcareous sandstone of Brak Member (Al Mahruqah Formation) with sabkha, deluvial, prouvial, sand dunes as well as kipukas (Less et al., 2006).

3.8 Ancient and modern Libyan stress field regime

The recent World Stress Map (2015) in Figure (3.16) is indicated very rare studies have been published on the present-day stress regime particularly in Libya and North Africa at large scale due to the lack suitably located stress field indicators (Bosworth, 2008). There are generally ambiguous regarding the regional stress field in this region. However, the first attempt to measure in situ the regional Libyan present-day stress field was done by Schäfer et al. (1980) who measured in situ rock strain at 26 sites that extended from Tuisian-Libyan border to Jabal Al akhadar in the northeast and to Hun Graben and the Jufrah oasis in the Southwest (Fig. 3.17).

The in-situ crustal stress in Libya was inferred from overcoring measurements Schäfer et al. (1980). Overcoring used to calculate the in-situ stress from strain relief around the borehole. The physical properties (e.g., Young's modulus) of rocks have been selected for measurements are similar and known, but their ages very widely (Triassic to Holocene). Therefore, in situ stress can be calculated from the observed elastic strains (Bosworth, 2008). Schäfer et al. (1980) concluded from the overcoring data that the present-day horizontal stresses have a large degree of scatter and complexities and range from tensile to compressive depending on the location. The direction of maximum compressive horizontal stress and minimum horizontal stress displayed over a large area. Most tensile stress values range between 5 MPa to 15 MPa.

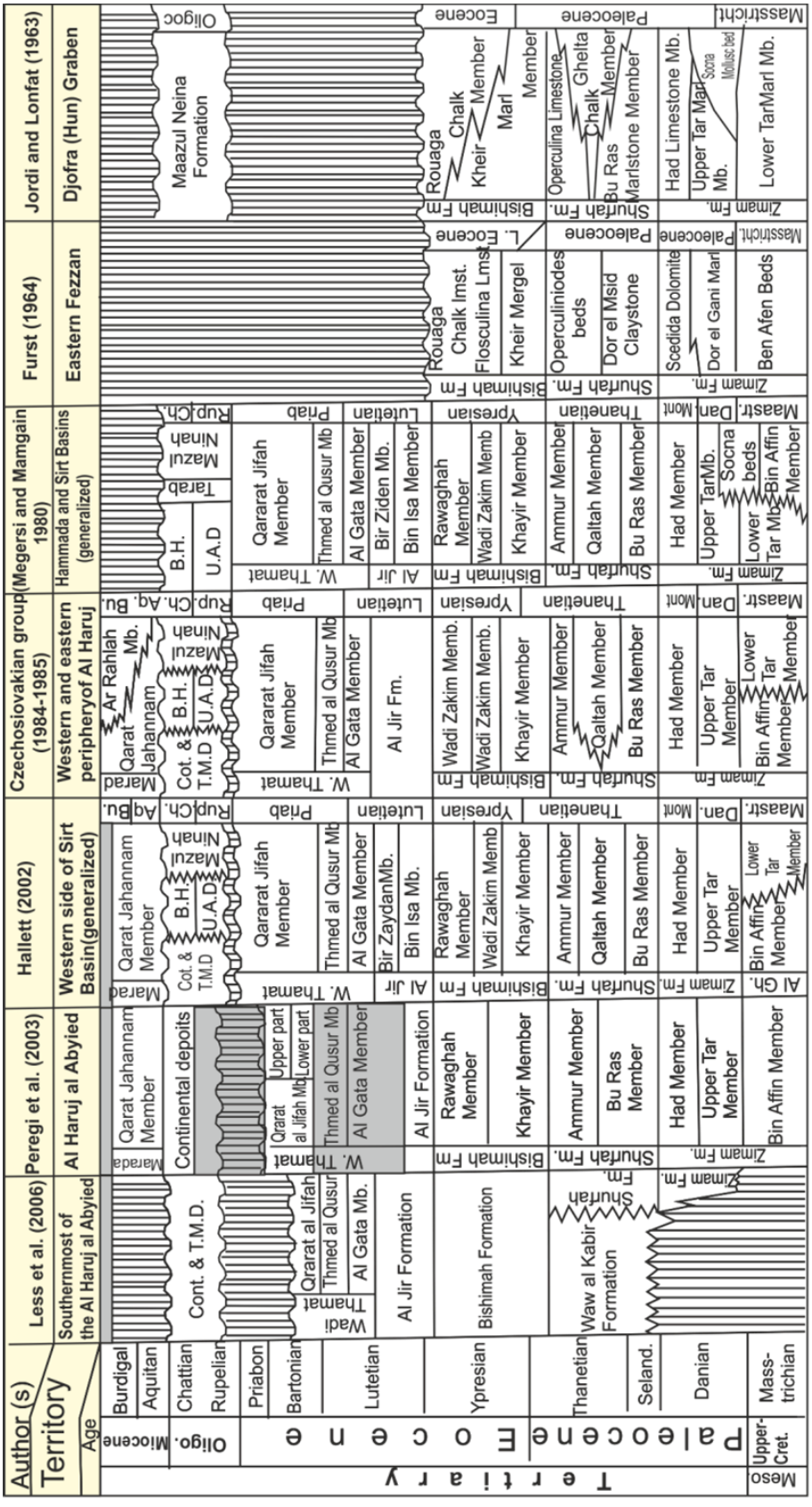

Table 3.3. Stratigraphic subdivisions of the central and southern part of Libya from late Cretaceous to Miocene (modified from Less et al., 2006).

Three distinct stress domains have been recognised for the complexities of the Libyan stress regimes by Schäfer et al. (1980) as follows; (i) the western domain extending from Tunisia border to the western shoulder of the Hun Graben region, has a NW–SE maximum horizontal compressive stress (Fig. 3.17). (ii) The second in situ stress domain occurs in the central Libya that includes the entire Sirt Basin and characterised by a NE–SW direction. While (iii) the eastern Libyan domain occurs along the Jabal Al Akhadar anticlinorium that extends from Benghazi to the Tobark city in the easternmost of Libya. The western and eastern domains are characterised by compression regime much higher than central domain as a result of approaching the African plate to European plate in the last 10 million years, as estimated by Schäfer et al. (1980) which are considered to be responsible for the increased seismic activity in those zones (Hassen, 1983).The stress regime in the central Libya may be rotated from extensional through most of the Mesozoic and Cenozoic to compressional mode since the early Miocene.

Suleiman and Doser (1995) are used earthquakes focal mechanisms in the vicinity of Hun Graben during the last century to calculate the present-day stress field orientation and stress regime. They mainly analysed two large aftershocks of 1935 (Mb=7.1) earthquake and three other in Hun Graben earthquakes and interpreted as a mixture of strike slip and normal faulting with compression axis WNW–ESE (97o) (Fig. 3.17). But Westaway (1990, 1996) obtained significantly different results for the earthquakes focal mechanisms of the Hun Graben. He was interpreted to have occurred as oblique dextral strike-slip movement on NW–SE trending normal faults and kinematic model incorporates E–W extension a cross the Hun Graben.

Borehole breakouts can be used to infer present-day stress field (Gough and Bell, 1981; Bosworth, 2008). Breakouts occur when the tensile stress around the borehole reaches the maximum tensile strength of the rock, generally 0.5-9 MPa and most commonly 2-4 MPa (Gudmundsson, 2011). In order to understand the complexities of the Libyan stress regime, borehole breakouts were measured in many oil wells in the eastern part of the Sirt

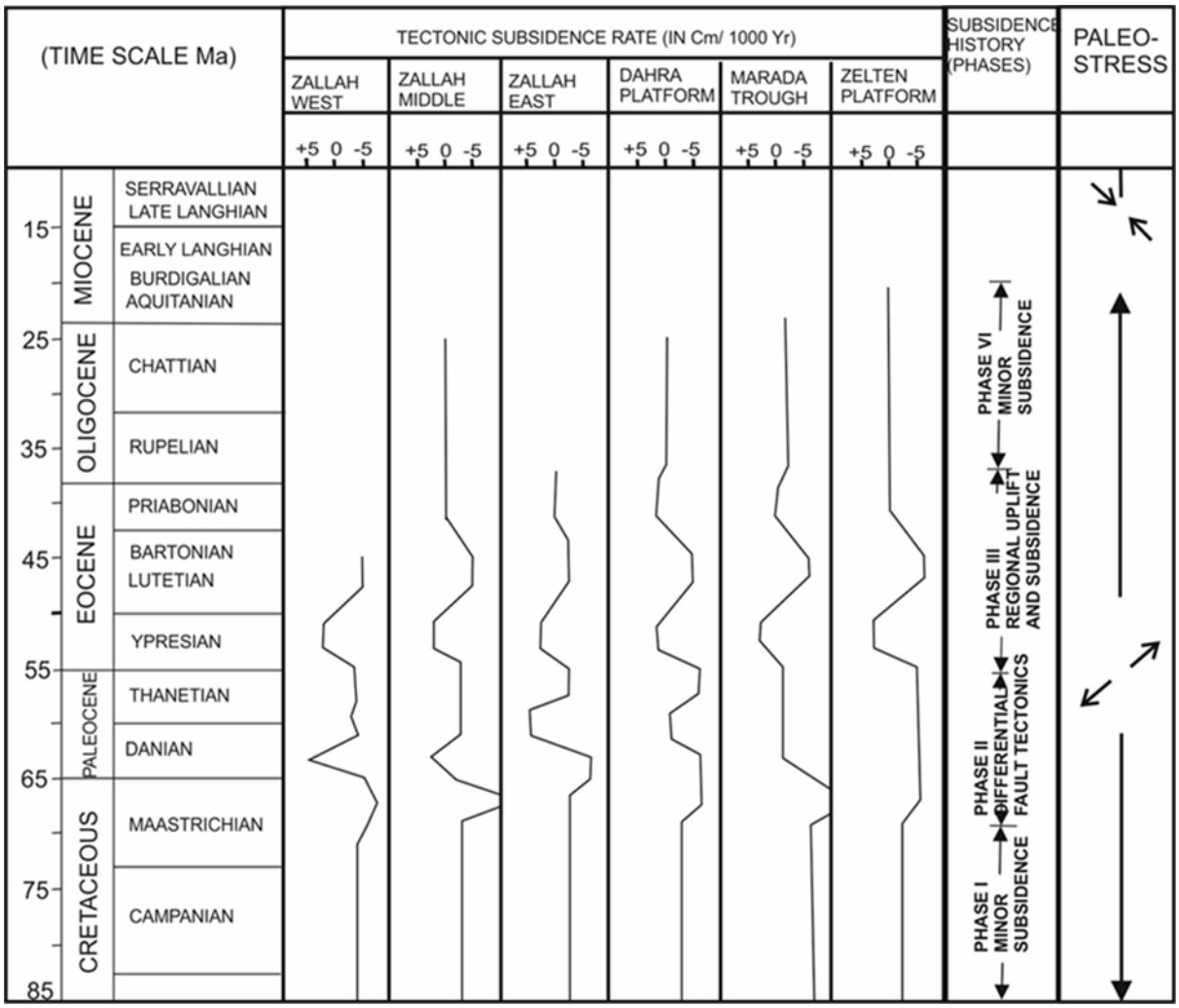

Figure 3.15. Tectonic evolution and paleo-stress of the Sirt Basin (modified after Schäfer et al., 1980; Van Deer Meer and Cloetingh, 1993).

Basin (Hameimat Trough) by used calliper logs and drilling-induced hydrofracture which demonstrated WNW–ENE orientation (Bosworth, 2008). It is widely consistent with volcanic crater alignments in the Al Haruj Volcanic Province (AHVP) (Fig. 3.17) (Peregi et al., 2003; Less et al., 2006, Bosworth, 2008; Elshaafi and Gudmundsson, 2016). This conclusion is not in agreement with overcoring data of Schäfer et al. (1980) in the vicinity of Hun Graben. Furthermore, Bosworth (2008) concluded from borehole breakouts data and drilling- induced hydro-fractures the existence complex transition stress field zone in the Mediterranean offshore that is extended from Egypt to Algeria passes through Libya and Tunisia (Fig. 3.17). This transitional zone separates between the North Africa and Mediterranean Basin since the maximum compressive horizontal stress is predominately E–

W oriented in the North Africa whereas it is primarily N–S oriented in the Mediterranean basin. The rapid lateral and vertical changes in the stress field regime with the upper crust and limited of data presented make a fairly broad range of uncertainty. Fortunately, the orthogonal interconnected fractures produced due to this complex transition stress field zone (Fig. 3.17), regardless of the mechanisms mixed up that may encourage hydrocarbon production (Bosworth, 2008). Further analysis is thus required for improve our understanding the complexities of the Libyan stress field.

Van Der Meer and Cloetingh (1993) demonstrate that the long-term trend of the palaeo-stress was changed from tension during the Cretaceous - early Neogene to compression in the late Neogene to Quaternary (Fig. 3.15). The trend of pale-stresses supposed that the late Palaeocene - early Eocene terminating of the rifting and variation faulting phase was associated with major relaxation of tensional stresses, subsequent renewed accumulation and relaxation during the middle Eocene giving way to a compressional stress regime during in the late Tertiary (Van Der Meer and Cloetingh, 1993). Ritsema (1975) supposed that most of the NW Africa is subjected to a recent NW–SE oriented horizontal compressive stresses. In addition, Sestini (1984) suggests that a post Eocene phase dominated by compressional events throughout the North Africa margin. Guiraud et al. (1992) suggest that these compressional events to major stage in the collision between African and European, which can be correlated with a change in opening direction of the Central Atlantic. Therefore, many of rifted basins in the Mediterranean are subject to a late Neogene increase in subsidence that can be related to late stage compression as a result of the Africa – Europe collision (Van Der Meer and Cloetingh, 1993). Le Pichon et al. (1988) pointed out that a change in the relative movement direction between African and European plates from left lateral translation to convergence commenced during the Late Cretaceous (about 90 Ma ago) involving the progressive closure of the remains Tethyan Oceanic domains which coincide with the initial rifting stage of the Sirt Basin (Van Der Meer and Cloetingh, 1993). At the present time, the NW–SE compression reflects part of the relative slow convergence between Africa and Eurasia (Azzouni-Sekkal et al., 2007).

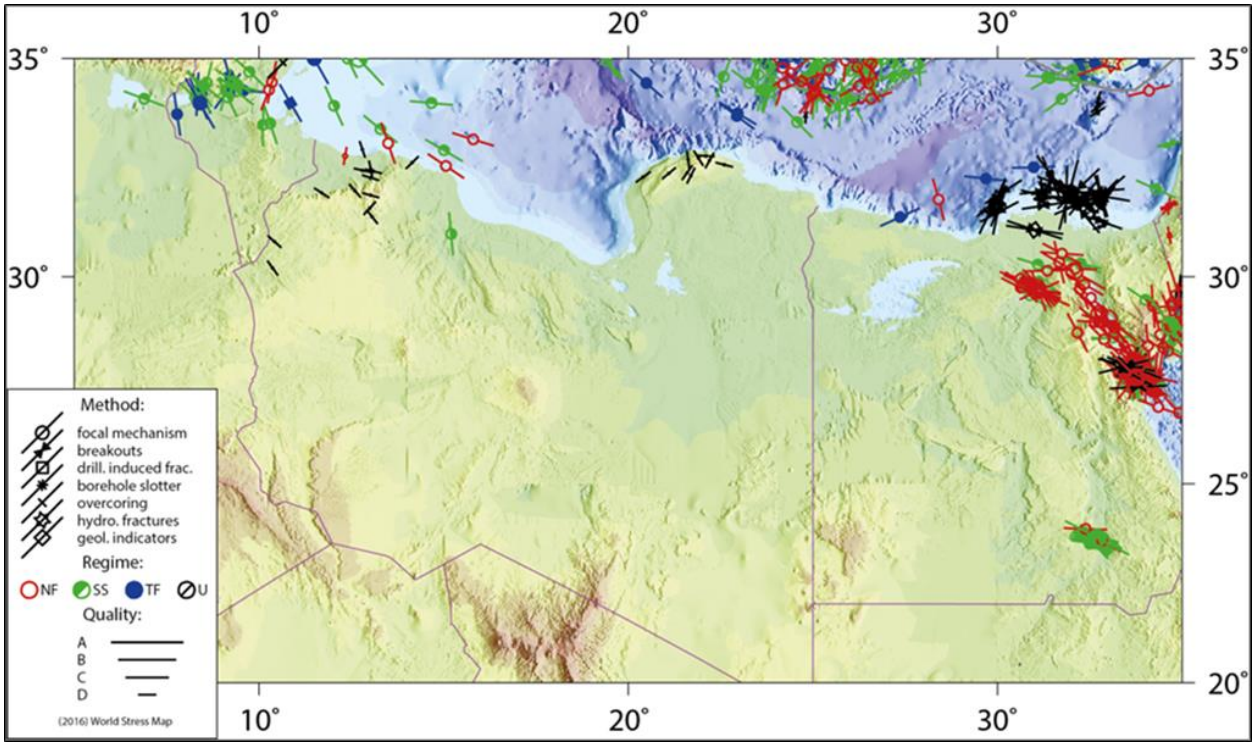

Figure 3.16. The recent World Stress Map of present-day stress field for Libya and Neighbour countries. Note the central and southern part of Libya does not have any data. Sticks mention the maximum horizontal compressive stress with indicator type and quality shown in legend inset (Zoback et al. 1992; Reinecker et al. 2015).

By contrast, Peregi et al. (2003) and Less et al. (2006) inferred based on volcanic vent alignments and paleo-fault kinematic indicators that the Sirt Basin remains tectonically active today, and extension is presently highly oblique WNW–ESE to NW–SE oriented. The occurrence NW–SE set of normal faults which cross-cut the more recent lava flows in the AHVP is also indication of a tectonically active basin (Cvetkovic et al., 2010).Thus the development regional tensional regime was most likely responsible for the occurrence of the magmatic activity. It coincides with the opening of the southern Hun Graben commenced in the late Miocene and carried on until

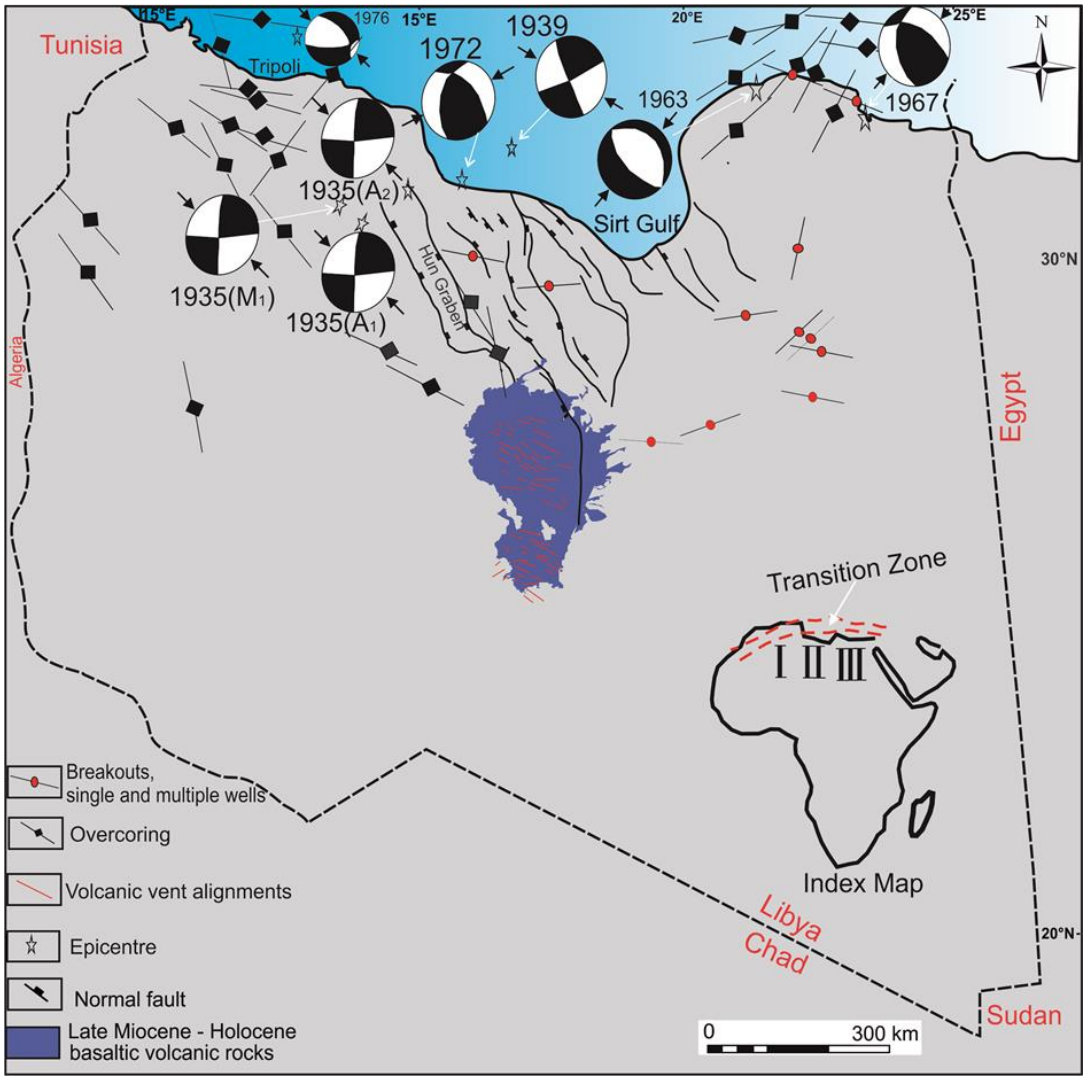

Figure 3.17. Present-day stress field for northern Libya inferred from various techniques; (i) outcrop overcoring at 26 sites (modified from Schäfer et al., 1980; Bowsworth, 2008), (ii) earthquake focal mechanisms during the last one hundred years. A mixed of strike-slip and normal events predominates in the Hun Graben for the 1935 and 1939 sequences, demonstrating WNW compression. Black quadrants of stereonets indicate tensional axes while black arrows denote strike of P-axes. Earthquake focal mechanisms are taken from Suleiman and Doser (1995), iii) borehole breakouts from oil wells in the eastern Sirt Basin. Sticks represent the maximum compressive stress. Breakout data are taken from Bosworth (2008), (iv) volcanic vent alignments (Elshaafi and Gudmundsson, 2016). The inset map shown locations of three stress domain zones have been suggested by Schäfer et al. (1980), and complex transition zone, is indicated by dashed red lines, has been supposed by Bosworth (2008).

nowadays (Table 3.1). Furthermore, Westaway (1996) suggests that the Sirt Basin and Pelagian Shelf, according to plate tectonic analyses, create active tilting extension at a rate ~1 mm/year during the recent time due to the continuing rotation of Calabrian terrains (Hallett, 2002).

3.9 Seismicity of Libya

Libya, situated on the Mediterranean foreland of the African shield, has encountered a significant intraplate tectonism and differential in seismic hazard throughout the territory due to the relative approaching between the African and Eurasian plates (Suleiman et al., 2004). The potential problem for the seismicity of Libya in the last three decades was the absence of seismic monitoring stations or any seismological service where the first Libyan seismological network has been installed since 2005. Thus, the locations of earthquakes can be determined within ±35 km in depth and ±0.5 degrees in latitude and longitude (Hassen, 1983). In addition, faults have not been sufficiently investigated to yield the certain information about recent activity needed to be able to predict earthquake occurrence in Libya (Hassen, 1983). Therefore information on seismicity related to the seismo-tectonic setting in Libya must be obtained from an instrumental recording of international seismology, nearby seismic stations exist in Rome, Athens as well as in Egypt (Hassen, 1983; Al-Heety, 2013).

However, the majority of seismic activity of Libya is particularly concentrated in three zones, (i) near Hun Graben domain, (ii) NE Libya (Cyrenica platform) domain and (iii) NW Libya domain. The location of earthquakes is close to the transition zones between the stress zones in northern Libya. 61 earthquakes of different magnitudes have been recorded in Libya for the period from 1900 to 2005 and a low heat flow have been recorded in this region that suggest the deep intraplate seismicity (Fig. 3.18a) (Nyblade et al., 1996; Al-Heety, 2013). In general terms, activity of earthquakes seems to be concentrated in two regions, the first of which is the Hun Graben area

between 15° to 17°E whereas the second is located between 21° to 25°E in the eastern part of Libya (Fig. 3.18c).

Seismicity of Libya has been classified into four categories by Hassen (1983) based on observed and expected magnitude seismic activity (Fig. 3.18b). The highest magnitude is concentrated around Hun Graben (north-central Libya) and NE Libya, whereas the southern part of Libya is considered to be seismically stable (Al-Heety, 2013). Statistical analysis was also made by Hassen (1983) to evaluate the frequency-magnitude relation of seismic activity in Libya during the period from 1963 to 1982. He inferred that around 140 earthquakes would be occurred in Libya with magnitude equal or greater than 5 every 100 years, while one earthquake would be expected with magnitude equal or more than 7 every 100 years.

Although Libya is generally considered as a low to an intermediate seismic region, some areas have experienced large earthquakes during the last two centuries. At the beginning of 19th century, many earthquakes associated with aftershocks have been recognised in Libya. In 1935 seismic stations in many parts of the world recorded a series of the earth-shock with epicentres in the Hun Graben region. The strongest of these earthquakes had recorded magnitude (7.1), and two of the aftershocks recorded magnitudes of 6.0 and 6.5 (Hassen, 1983; Johnston 1989; Suleiman and Doser, 1995). The same region was shaken by two major earthquakes of magnitudes more than 5 in 1939 and 1941. Subsequently, a number of earthquakes have been recorded in the Hun Graben during 2000 and 2001. The Hun Graben is defined as a prominent rift valley feature, extends NNW trend from the City of Hun in the south to Al Qaddahia town in the north. The situations of epicentre have been determined during the period 1935 to 2001 which are clustered in the similar trend of the Hun Graben seismic activity appears to be condensed along the eastern side of the Hun Graben (Suleiman et al., 2001; Suleiman et al., 2004). Therefore, the Hun graben of the western of the Sirt Basin is still tectonically active and manifested in the surface topography, and

substantial fault displacement can be mapped at the surface (Suleiman and Doser, 1995; Suleiman et al 2004).

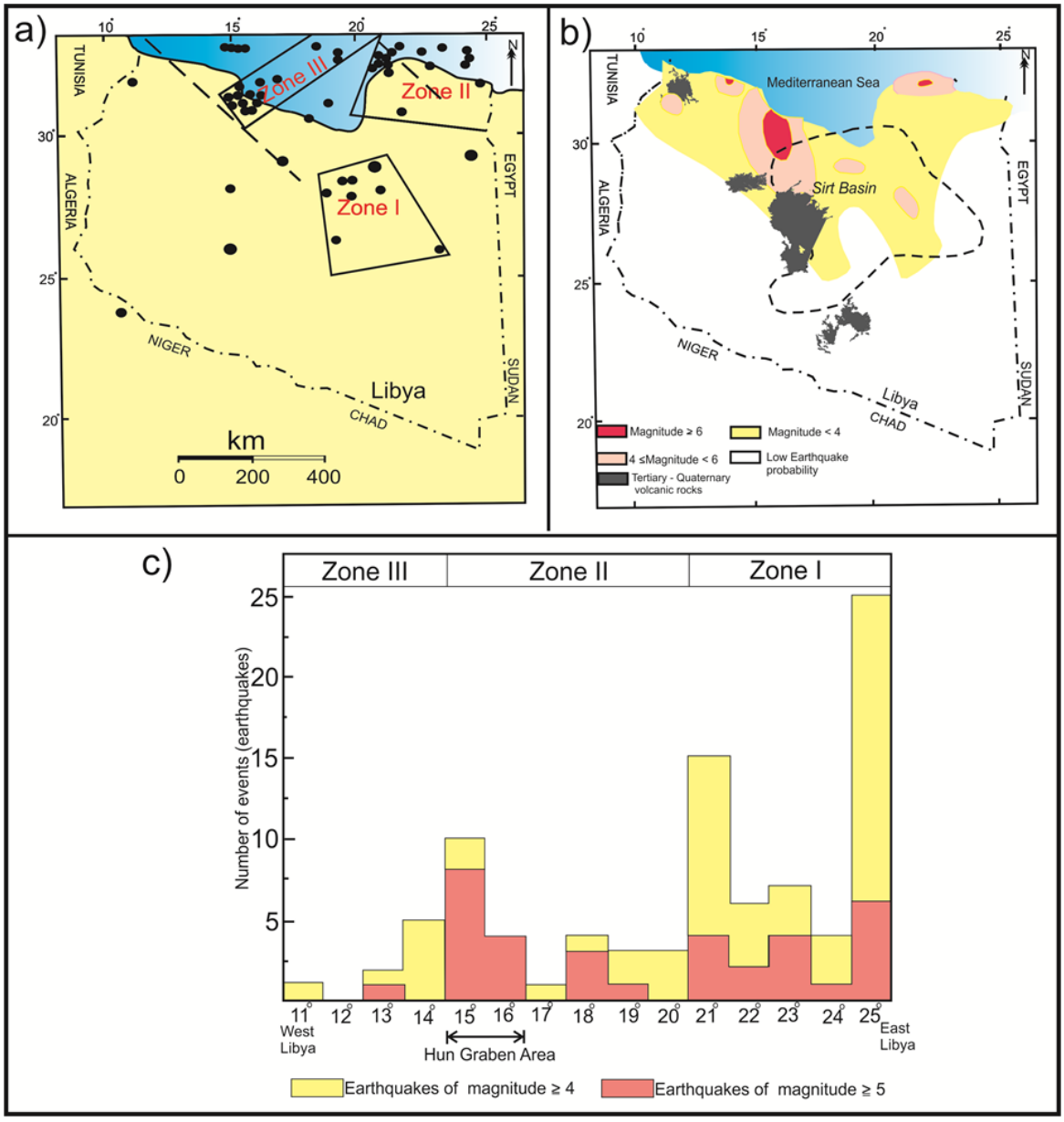

Figure 3.18. a) Distribution of epicentres of the earthquakes in Libya during the period from 1900 to 2005 (modified from Al-Heety, 2013). b) Showing seismicity of Libya subdivided into four categories based on the magnitude of the earthquake (modified from Hassen, 1983). c) Histogram shows the magnitude and distribution of the earthquakes for the period from 1903 to 1981 in Libya (modified from Hassen, 1983).

Furthermore, Boote et al. (2012) propose that the rifting of the Sirt Basin may still be active in offshore as well as in the Hun Graben area during the present-day (Abdunaser and McCaffrey, 2014). Schäfer et al. (1980) pointed out that the Hun Graben area represents a transitional zone from NE–SW stress domain to NW–SE stress domain which epicentres are clustered at that region. It can be suggested a stress concentration along this transition zone that is responsible for powerful earthquakes (Hassen, 1983).

Other common earthquake had recorded in Al-Marj city, Jabal al Al Khadar area NE Libya, in 1963 with the magnitude 5.3. It was followed by five aftershocks; all of magnitudes are greater than 4 (Hassen, 1983). Many faults have recognised in this area cutting Tertiary carbonate rocks that seem to be responsible for the earthquakes in this zone. The epicentre of this earthquake was situated close the in situ stress site 18 (the highest compressive stress) (Fig. 3.17) that was measured by Schäfer et al. (1980). Despite this earthquake manifested a release of energy much less than the 1935 earthquake at Hun Garben, it was caused heavily damage due to several reasons; (i) attributed to shallow focal depth, (ii) the presence of alluvium underlying Al-Marej city and extensive use of mud and stone in older structures. By contrast, Hun Graben area was not reported tremendous damage, although it was stronger, because Hun Graben area is an uninhabited area (Hassan, 1983; Suleiman et al., 2004). Al-Heety (2013) has mentioned that the epicentres of Libya correspond to the distribution of the major tectonic features. It can be suggested that the reactivation of pre-existing faults and variations of local stress regime are considered as causative mechanisms for seismicity in Libya. Most of these earthquakes are located along the Mediterranean coast which is dominated by NW–SE compressional mechanisms related to the collision between Europe and Africa (Craig et al., 2011). Majority of earthquakes in Libya occur at depths between 30–35 km (Al-Heety, 2013), thus increased seismogenic thickness corresponds to thick lithosphere underlain the region (Priestley and McKenzie, 2006; Craig et al., 2011)

Chapter 4: Research methodologies

4.1 Introduction

This chapter introduces the research methodologies applied in this study. The research workflow is given in Figure (4.1). The workflow involved selecting a suitable research outline method by choosing and using appropriate procedures for data collection and modelling.

4.2 Data compilation during fieldwork at the AHVP

The AHVP is remote and rather inaccessible and has difficult terrain, so the fieldwork of this research was shared with a team from the Industrial Research Centre (IRC), Tripoli, who were doing fieldwork as part of a geological mapping project in SE Libya. Prior to commencing any fieldwork, ascertain localities were selected, and access to the sites was negotiated. Many of the rugged localities were accessed only through valleys and seismic truck roads. The seismic truck roads in the Al Haruj region have been created by many oil companies during geophysical surveys (e.g., Fig. 4.2). Most of the fieldwork was carried out on more recent lava flows in the north-eastern part of the AHVP (Fig. 4.3). Field measurements are collected with standard geologic field equipment. Compass clinometer was used in the field to measure the dip and strike of faults, extension fractures, and dykes while a standard tape measure was utilised to record dimensions of various volcanic features.

The investigated basaltic rocks in the entire Al Haruj Volcanic Province (AHVP) show varied colours and morphologies on the Landsat imagery,

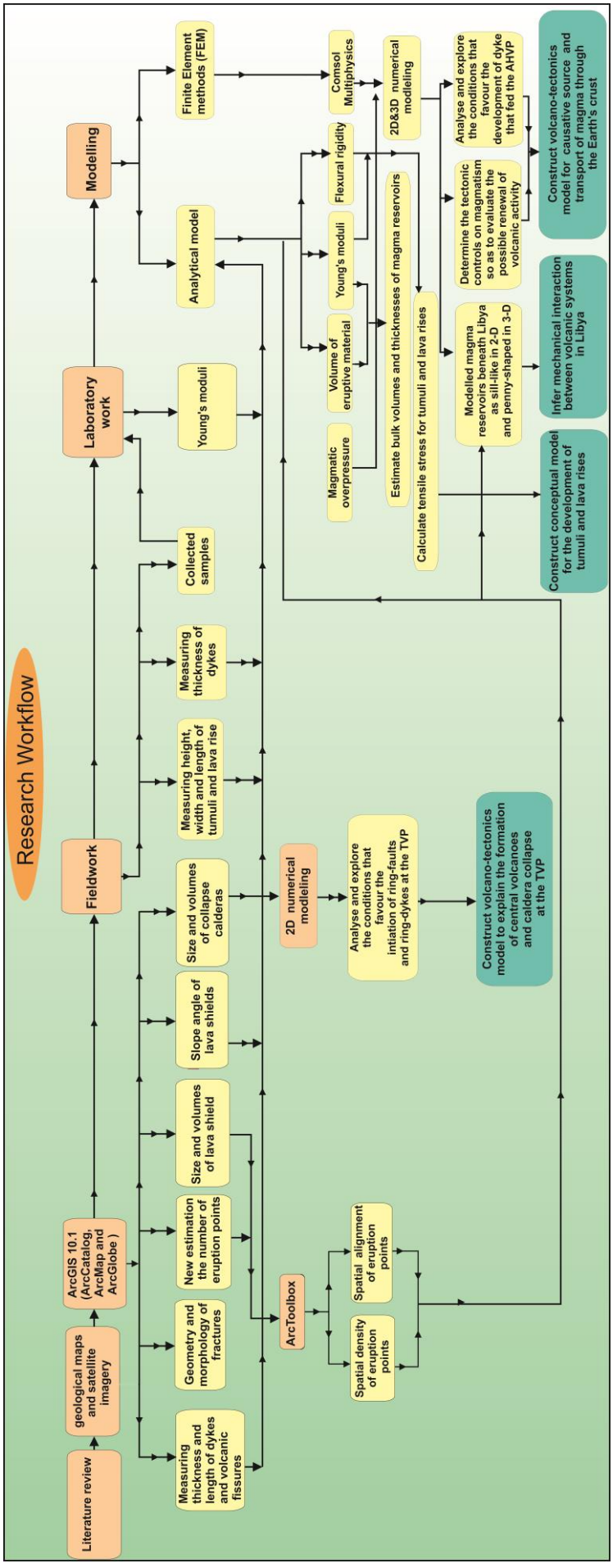

Figure 4.1. Research workflow showing main methodologies, techniques and ultimate aims.

implying that were produced episodically rather than continuously (Busrewil and Suwesi, 1993; Peregi et al., 2003; Less et al., 2006).The stratigraphic volcanic sequence in the northern part of AHVP has been subdivided by earlier studies (e.g., Busrewil and Suwesi, 1993) into six major volcanic phases based on several factors used complementary; (i) the colour variation of lava flows on multispectral satellite imagery, (ii) drainage pattern density observable on aerial photographs, and (iii) morphological characteristics and degree of erosion processes observed in the field. The NE part of the Al Haruj region has not yet been studied in regards to physical volcanology. Hence further attention is needed, especially as the area hosts the youngest volcanic phases in the Al Haruj volcanic province and therefore presents the greatest risk of future volcanic activity in the region. The recent volcanic units are easily recognisable on satellite imagery owing to outstanding moonscape morphologies and well-preserved pahoehoe lava structures. These units tend to be coal black with a braided pattern of lava flows, often having small pits at their peripheral parts and dotted by a great number of small flat depressions that are filled with fine sediments. The surfaces of lava flow fields exhibit linear and relatively semi-equant tumuli in plan-view as well as lava rise plateaus. While the exposures of the older volcanic units, on the Landsat image, appear as grey to pale grey tone and are low lying and relatively flat relief (e.g., Less et al., 2006).

The Al-Halaq al Kabir lava field has been previously mapped by Busrewi and Suwesi, (1993) and mapped as volcanic phase VI. During this study, we treated the unit of Busrewi and Suwesi, (1993) as an individual lava flow field. The Al-Halaq al Kabir lava field is restricted to the central part of the AHVP (Fig. 4.3). The map of Busrewi and Suwesi, (1993) was used as a primary guideline for the fieldwork campaign. Numerous lava rise structures, including tumuli developed in the medial and distal portions of the Al-Halaq al Kabir lava flow field during the last eruption (sometime during the Holocene) in the central part of the Al Haruj Volcanic Province (AHVP). These inflation features can be used to better understand the emplacement mechanism and to estimate duration of tumuli and lava rise plateaus in part of the Al Haruj

region. Fieldwork involved describing morphologies and measurements of tumuli cross sections, surface profiles and axial inflation/circumferential crack depths as well as a sampling of the lava in order to determine physical properties such as Young's modulus and density, the latter are discussed in detail in section 4.7.

Figure 4.2. Field photograph showing a seismic truck road which provided access to some rough/rural sites. The seismic truck roads are made by oil companies during seismic operations. Note the person in the middle road (indicated by the red ellipse) provides scale.

The duration of formation of flow lobe has been estimated by Hon et al. (1994) who inferred a positive correlation between the thickness of the upper lava crust and the square-root of time during owing to conductive cooling;

$$t = 164.8C^2 \qquad (4.1)$$

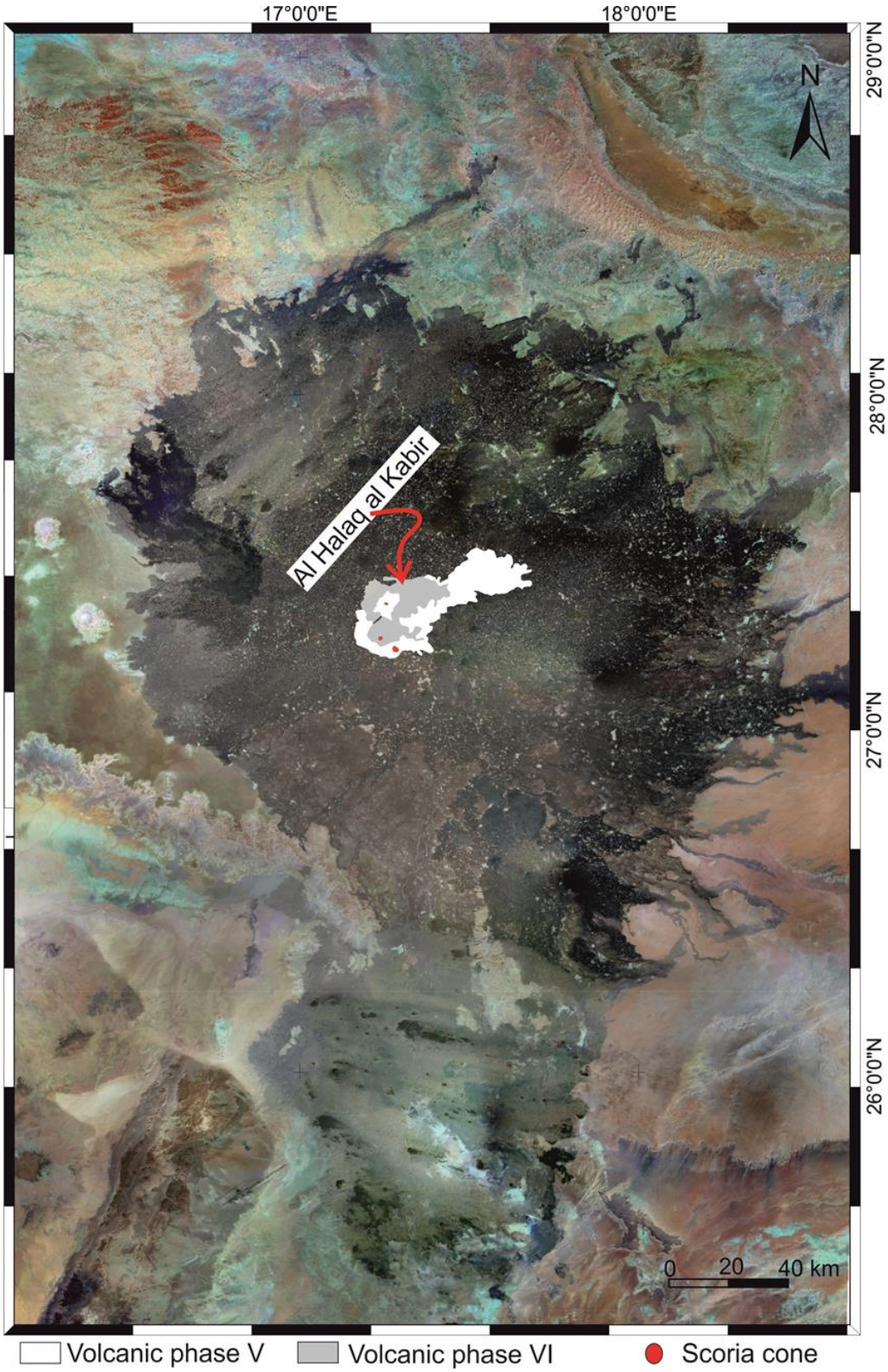

Figure 4.3. Landsat ETM+ image showing the extent of the Al-Halaq al Kabir lava flow field which represent the most recent lava flows at the AHVP. This lava flow field originated from a vent system (red spots) and generally flowed north-east for over 20 km (adapted from Satellite Imaging Corporation).

where t is the time in hours during which inflation occurs and C is the thickness of the upper vesicular crust or maximum depth measured in inflation cracks (Fig. 4.4) (Hon et al 1994;Thordarson and Self 1998). This cooling model is currently widely using to estimate lava flow field duration for (e.g., Thordarson and Self 1998; Thordarson, 2000; Mattsson and Höskuldsson, 2005; Thordarson and Höskuldsson, 2008). Such data are extremely important for understanding better lava emplacement and assessment hazards. In order to provide data for analytical and numerical models, detailed measurements of dimensions, maximum and minimum diameters of lava rises and large tumuli in plan-view have been taken using ArcGIS10.1. The emplacement and inflation of the Al-Halaq al Kabir lava flow field are covered in further detail in Chapter 7.

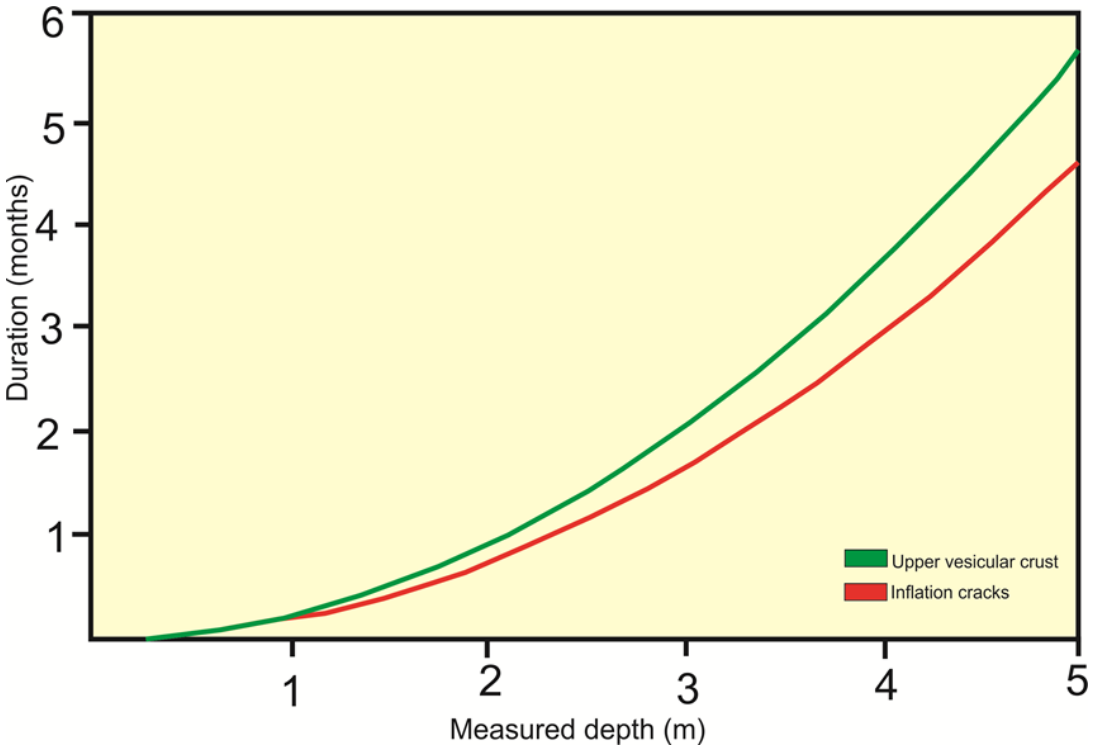

Figure 4.4. Estimated duration of tumuli formation using a thickness of the upper lava crust and axial inflation cracks. The curves were plotted using the equation of Hon et al. (1994). There is a difference of about 10% in duration timescales between that estimated from the thickness of the upper vesicular crust (UVC) and the length of axial inflation crack depths (modified from Cashman and Kauahikaua, 1997; Mattsson et al., 2005).

4.3 Numerical modelling

Numerical models have been increasingly applied to analysing structures and fluid flow in recent years as an alternative or compliment procedure to analytical solutions once the constitutive equations become more complex. Numerical models give more realistic results than other models where they can allow the implementation of mechanical heterogeneities within the Earth's crust with real scale (Andrew, 2008; Henk et al., 2013; Bagnardi, 2014; Hickey et al., 2013; Hickey and Gottsmann, 2014). The Finite Element Method (FEM) is one of many types of numerical models in which continuous systems are discretised into numerous simple and small pieces termed finite elements (Deb, 2009; Henk et al., 2013). It is inevitable to construct an assumption for each individual element. This assumption is considered as the basis for the evolution of finite element analysis procedure. The set of simultaneous equations are subsequently elaborated for describing the constitutive equation with regard to discrete nodal point values of the primary variable. After that, each of these elements is integrated by proper compatibility relations among them and a global set of simultaneous equations is acquired (Deb, 2009).

The application of loads and boundary conditions are eventually manipulated to the global set of simultaneous equations, and these equations are solved implicitly using a workstation (Deb, 2009). Modelling using the finite element method can be carried out with multiple rock strata having different values of toughness and Young's modulus and applied to multiple loading and boundary conditions, in order to obtain the likely intricacies and yield realistic of the magmatic plumbing system dynamics (Hickey and Gottsmann, 2014). This approach can also save enormous amounts of time and money with accuracy (Grosfils, 2007; Deb, 2009; Hickey et al., 2013). The finite element methods are used in this study to calculate the local stress fields associated with magma reservoir/chamber and dyke propagation. Thus the FEM is considered as an excellent facility to analyse and interpret magma plumbing

systems and is widely applied to analyse and explain the mechanisms of caldera collapse and improve understanding of how magma transports through the Earth's crust (cf. Andrew, 2008; Barnett and Gudmundsson, 2014; Hickey and Gottsmann, 2014; Browning and Gudmundsson, 2015; Karaoğlu et al., 2016). Improvement in computing speed and digital storage capacity produces versatile finite element method (FEM) software (Deb, 2009; Hickey and Gottsmann, 2014), such as Ansys (www.Ansys.com) and Comsol Multiphysics (www.comsol.com). A series of numerical models have been run to explain conditions of dykes deflection and arrest within strata or at stratum contacts or other discontinuities, alternatively, how dykes are emplaced and propagated to build up volcanic edifice on the surface. The magma chamber/reservoir was generally modelled in all study areas as a hole for a two-dimensional model or penny-shaped, sill-like, in three-dimension within the Earth's crust and subject to various loading conditions. All numerical models were performed in this thesis using Comsol Multiphysics (www.comsol.com).

4.3.1 Comsol Muliphysics

Comsol Multiphysics is a finite element analysis (FEM), solver and simulation software package for various physics applications (Barnett and Gudmundsson, 2014). It is extremely well-tested (Hickey and Gottsmann, 2014, Browning, 2015). Comsol enables the creation of two-dimensional and three-dimensional models and stress visualisation behaviour of structures which allow to the user to elucidate results more efficiently. There are three main stages to producing a numerical model using the Solid Mechanics module of Comsol. This module solves Navier-Cauchy equations for linear elastic stress as a result of load application and boundary conditions (Browning, 2015) (Fig.4.5). First of all, a pre-processing stage involves the input of geologically relevant geometries using the Structural Mechanics

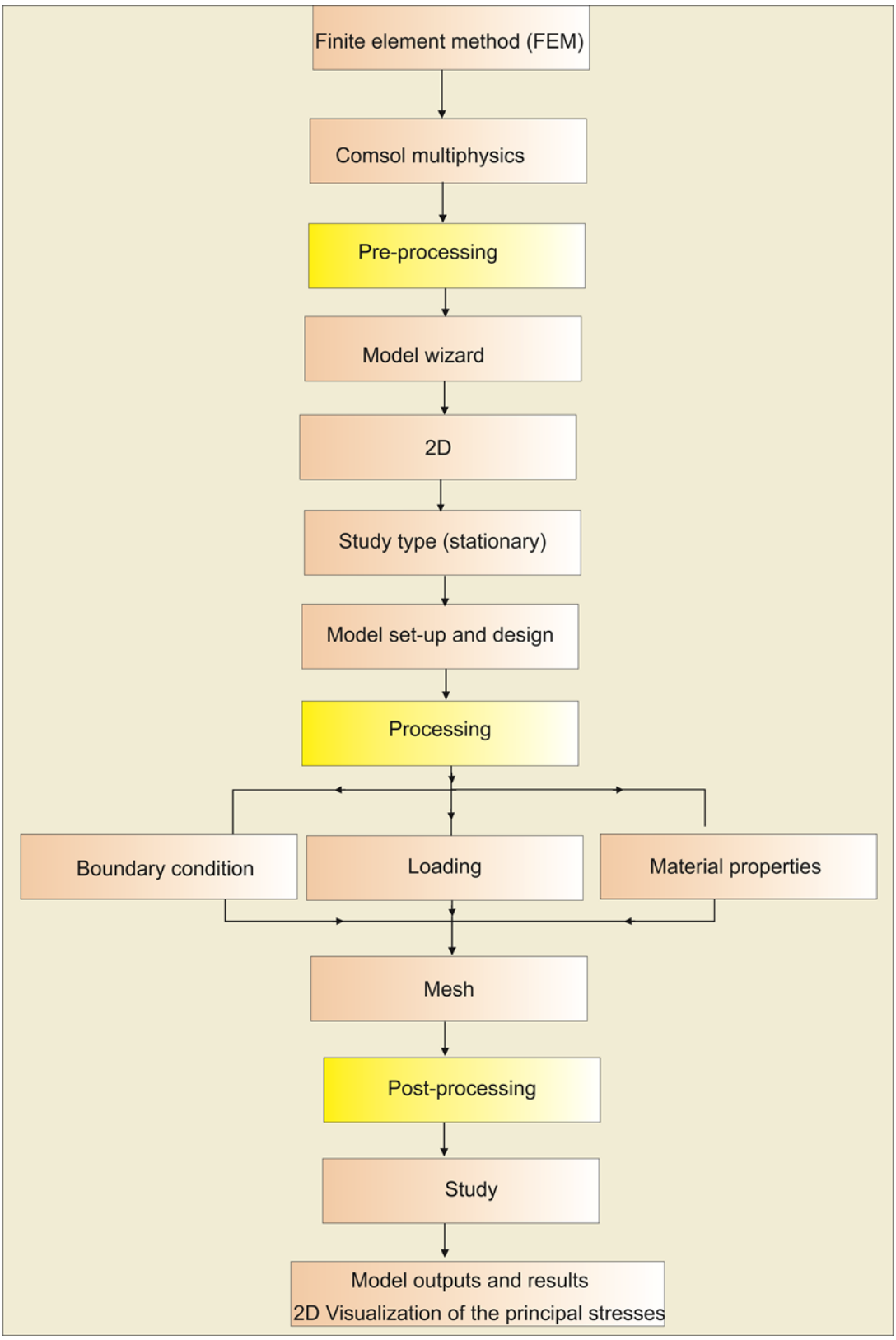

Figure 4.5. Workflow showing the main processes to produce a numerical model using Comsol Multiphysics.

module and selecting the stationary study since time does not have influence on the model. The geological structures were designed in CorelDRAW X7 and imported into Comsol with a DXF format. Dykes and magma chamber/reservoir is always modelled as cavity. It is important to mention that geometries are not situated near to the edge of the model where they will be later fastened to avoid rigid body rotation and displacement.

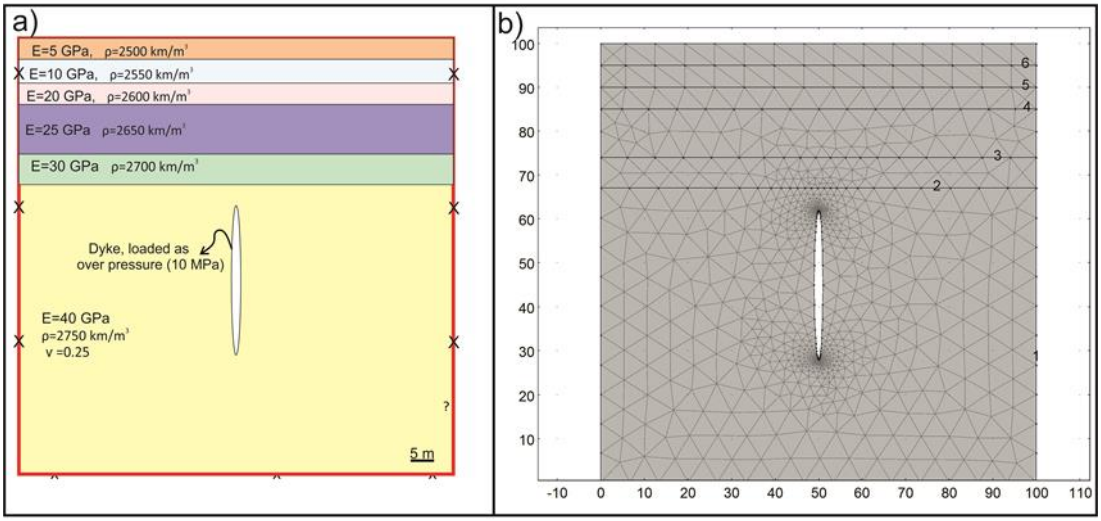

Figure 4.6. a) Configuration of the finite element model (FEM) shows geometries and mechanical properties (Young's moduli and densities) that represent heterogeneity in the Earth's crust. The model is fixed at the bottom and lateral edges to avoid any rotation or displacement in these places. The dyke is modelled as an elliptical cavity with a magmatic overpressure of 10 MPa as the only loading. b) A triangular mesh finite element was used for the inner part of the model. Note the mesh has been made to be the highest resolution around tips of the dyke with minimum size ≈ 1 m whilst triangular meshes become wider at the distal areas with maximum element size ≈ 12 m.

Secondly, analysis or process stage where suitable values for the geological geometries are set. These parameters involve, for example, Young's modulus, Poisson's ratio, rock density, loading (magmatic overpressure or excess pressure) (Fig. 4.6a). The full range of model details, including descriptions of input parameters are given in Chapters 5 to 9 on the basis of the nature of the scientific problem. The boundary conditions are often applied to the lateral ends of the model to simulate remote-field tectonic stresses. Models were fixed at the bottom and/or later edges to avoid rigid

body rotation and translation (displacement being zero in all directions). Elastic material models are considered as linear elastic through Hooke's law.

The entire volume of the model is discretised into triangular or quadrilateral mesh elements or other simple convex polygons in order to produce a suitable solution for calculating stress (Fig.4.6b). Triangular meshes were used during this study for all two-dimensional models. Mesh elements differ in size throughout models providing fine scale close to an area of interest but become coarser in far away from stress concentrations (Fig. 4.6b). The last process in numerical modelling is called post-processing, here Comsol Multiphysics produces a variety of graphic tools which can be used to critically evaluate and assess the distribution of stress. The magnitude of the maximum tensile principal and shear stresses are always presented as colour contours in mega-pascals whilst the maximum compressive stress are plotted as trajectories (cones or arrows) alongside the colour contours of the maximum tensile stress to identify the propagation path of dyke. A dyke is primarily an extension fracture and hence propagates in the direction of the maximum compressive principal stress. Figure 4.7 shows a two-dimensional and three-dimensional visualization of the model result for shallow a magma chamber subjected to two different types of loading. Firstly, internal magmatic pressure (5 MPa), using excess pressure in the magma chamber in all models rather than total pressure, due to the effects of gravity are automatically considered (Gudmundsson, 2012). Secondly, the far-field extensional regime has a value of -5 MPa as the loading so as to be in agreement with the commonly measured maximum in situ tensile strength of rock (Gudmundsson, 20016). The tensile stress at the surface cannot exceed the maximum in-situ tensile strength and is thus generally less than 6 MPa (Gudmundsson et al., 2008). This topic is covered in more detail in Chapters 5, 6 and 8. However, results of numerical models are always associated with a small carton illustrating the area modelled, type of loading, boundary conditions and the area given in the result.

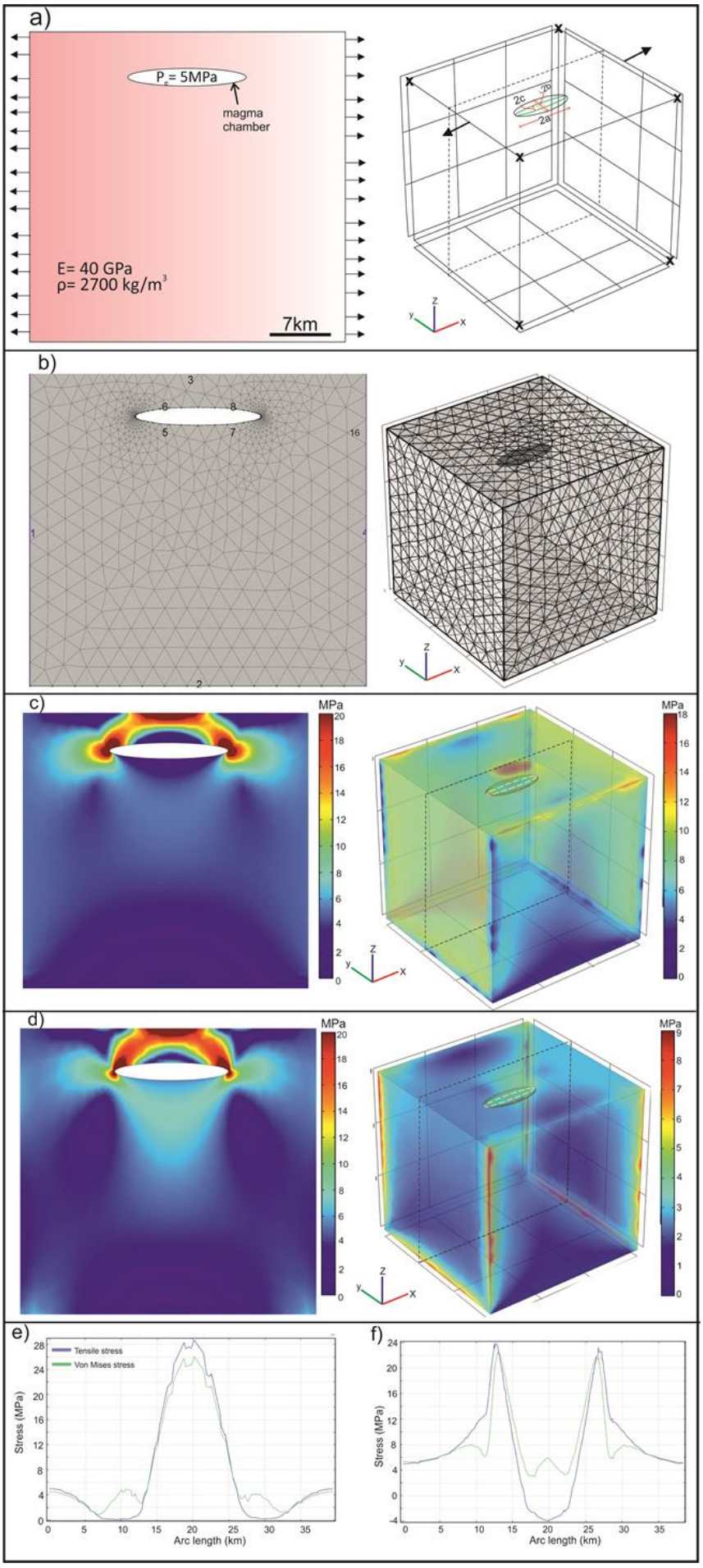

Figure 4.7. a) 2-D and 3-D numerical model setups on the left and right side respectively. Model setups showing an oblate ellipsoidal magma chamber within an elastic homogenous host rock subject to internal magmatic excess pressure (5 MPa) and far-field extension(-5MPa) as loading, indicated by black arrows. The length (2a), width (2b) and thickness (2c) of the magma chamber in 3-D model setup are indicated by red arrows. b) Both models are discretised the entire volume into free triangular elements for 2-D and tetrahedral elements for 3-D with maximum resolution at the lateral tips of magma chamber. The model results show (c) the maximum tensile stress σ_3 and (d) Von Mises (shear) stress τ which is mainly concentrated at the lateral ends of the magma chamber and above at the Earth's free surface. e) Magnitude of tensile and shear stresses along a horizontal plane at surface (free surface). f) Magnitude of tensile and shear stresses along a horizontal plane above the magma chamber.

In this thesis, all numerical models were created according to the tectonic setting of each specific area with varying levels of complexity. Different values of static Young's modulus or elastic modulus and density are used in some models to correspond with heterogeneity and anisotropy within the Earth's crust. The Young's modulus is a measure of the stiffness of a solid material and defined as the relationship between stress and strain in the one-dimensional Hooke's law and is revealed by the slope of the stress-strain curve (Jaeger, et al., 2007). Poisson's ratio of most rocks is in the range of 0.1-0.3 (Pollard and Fletcher, 2005). Similar values have been obtained in laboratory tests on extracted core samples from the Sirt Basin (Qiu et al., 2008). The Poisson's ratio used in all numerical models in this thesis allocated a typical average value of 0.25 (Gudmundsson, 2011).

4..4 Geographic Information System (ArcGIS) Technique

This approach is a computerised database management system used to capture, manage, retrieve, analyse and visualise spatial information using a broad range of spatial operations and functions to produce a high-resolution image (Burrough and Andrew, 1996). Data were used in ArcGIS 10.1 that are mostly collected from published geological maps, satellite imagery, and field observations. The hard copies of the geological maps are transferred into a digital medium through the use of geo-referencing capabilities (Fig. 4.8). Data are georeferenced to the coordinates of a particular system (WGS 1984) that allows accurate placement of geological features such as lava shields, scoria cones, and faults and maintains the spatial relationships between mapped features. Therefore, referenced data can be overlaid to a better understand relationships, patterns, and trends between volcanoes and structural elements. In addition, ArcGIS is utilised to link the spatial and attribute data. Spatial refers to how geographic space is visually represented such as the X Y coordinates of a volcano eruption would be its spatial data. Attribute data describe the spatial data, and in ArcGIS are stored in the attribute table that stores quantitative and descriptive data (Hall, 2014).

There are two basic spatial data types used to enter data into ArcGIS where it is stored in a digital format. Raster (gridded) data are discrete cells arranged in a rigid row by column format such as satellite imagery and aerial photography. Each cell stores a value, for instance, elevation or chemical concentration that represents continuous data (Hall, 2014). Vector data conversely uses points, polylines, polygons and triangulated irregular networks (TINs) to represent geological features (non-continuous data) on the Earth's surface like volcanoes and lineaments. Most commercial GIS systems provide facilities for both types of data. Each vector dataset consists of a main shape file (.shp) and extensions (an index file (.shx) and a dBASE (.dbf) (Hall, 2014).

4.4.1 Spatial density of volcanic eruptions

Lava shields, scoria cones, spatter cones, dykes, volcanic fissures, and maars were identified using published geological maps combined with satellite imagery. The geologic maps of the AHVP exhibit numerous eruption points, including both the Al Haruj al Aswad and the al Abyad subprovinces. These maps originate from a series of publications during the last three decades by Woller (1984); Vesely (1985); Busrewil and Suwesi (1993); Peregi et al. (2003); Less et al. (2006). Some of the volcanoes do not correlate closely with satellite imagery during this study, particularly with old published geological maps where the error reaches to hundreds of meters. Therefore, this study allowed us to correct geographic coordinates of some lava shields at the AHVP. Except for these geological maps and limited studies of eruptions types, little is known about volcano-tectonic structures and long term volcanic activity, mechanism of lava emplacement of the AHVP from early Pliocene up to present time. The exact number of eruption points in the entire AHVP was previously undetermined. In this thesis, a new estimation of the number of volcanic points was performed, on the basis of integrating remote sensing imagery with the geologic maps of the region.

ArcGlobe 10.1 is used to plot volcanic eruptions accurately, fissures and the distribution of lava flows using the zoom, pan, and tilt functions (Lesti et al., 2008; Boyce, 2013). The volcanic points are recognized on this satellite

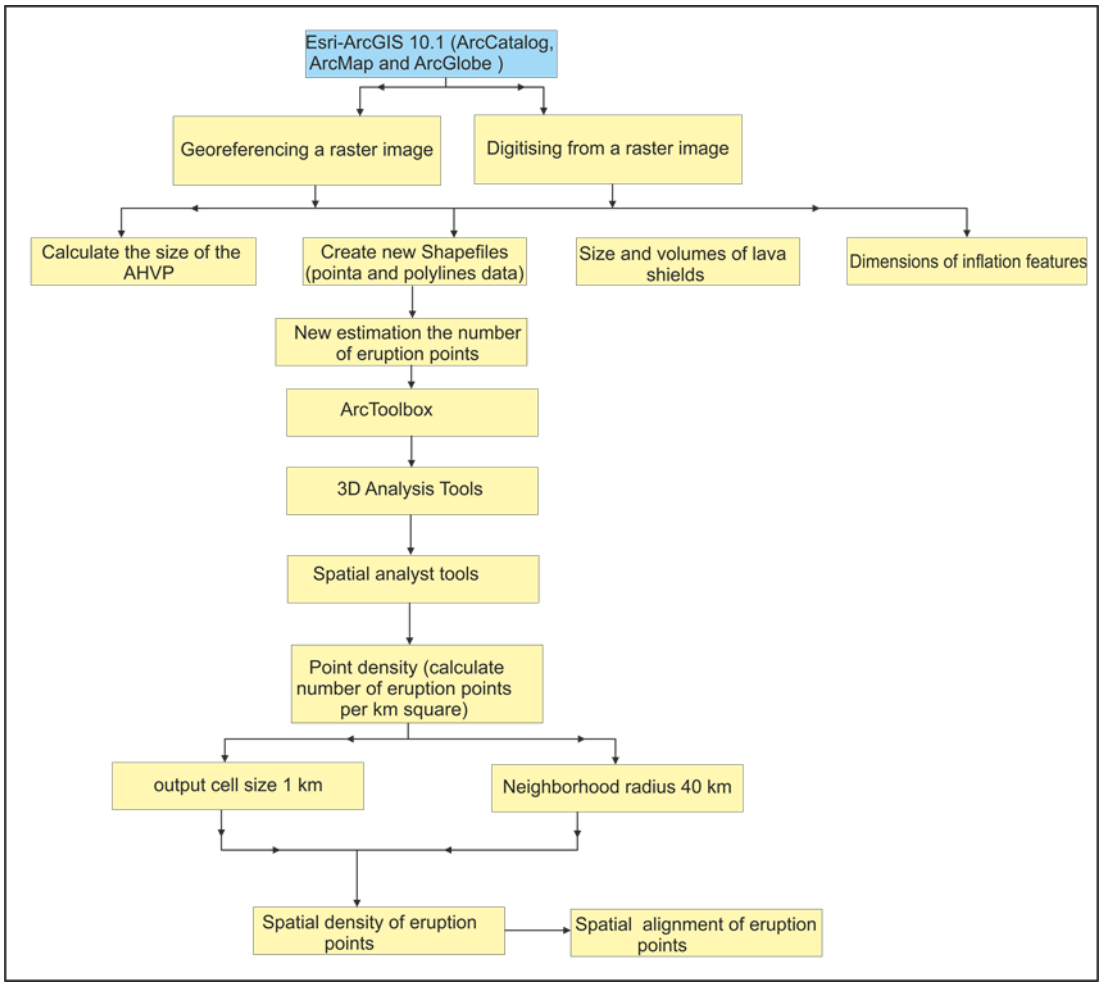

Figure 4.8. Data processing workflow of ArcGIS gives an overview of the steps in creating spatial density and alignment of volcanoes along with calculate the size of lava-shields in the AHVP.

imagery and saved in point shape files (.shp) which allow features like coordinates and their associated placemarks to be displayed on geospatial software ArcGIS 10.1 (Fig. 4.8). The volcanic edifices are generally characterised by circular morphology either in positive relief features such as lava shields and volcanic cones or in negative relief features formed destructive activity such as maars, calderas, and craters (Lesti et al., 2008). Both constructive and destructive volcanic activity can occur in the same volcanic edifice (Nakamura, 1977, Lesti et al., 2008). The recognition of

these volcanic features is made according to their features. The perfect geometric resolution of satellite imagery through ArcGIS has allowed the identification most of the volcanic vents.

The spatial distribution of volcanic eruptions was analysed by processing a density map through ArcGIS 10.1. A point density map is defined by calculating a magnitude of events per square kilometre that fall within a circular neighbourhood with a given radius around each cell (Silverman, 1986). A neighbourhood is defined around each raster cell centre, and the cumulative number of points that fall within the neighbourhood is calculated and divided by the area of the neighbourhood (Silverman, 1986). The density map is computed using a search radius value of 40 km to highlight the large crust scale distribution on the constructed density map (Lesti et al., 2008), and an output raster cell size of 1 km as computed by ArcToolbox, 3D Analyst Tools. Then Spatial Analyst Tools (Fig. 4.9) calculates a density of eruption points that fall within a neighbourhood of 40 km around each cell. Large values of radius produce a more generalised density raster and do not change the calculated density values. In spite the fact that more points will fall inside the larger neighbourhood, this number will be divided by a larger area when calculating the density. The main effect of a greater radius is that density is calculated considering a larger number of points (Silverman, 1986). The density distribution map is interpreted the main relative maxima accumulated of volcanic eruptions and overall trend. In other words, the monogenetic volcano/eruption site density map shows the number of volcanoes per square kilometre using the total number of volcanoes that fall within a circular neighbourhood (40 km) around each cell as follows;

$$Volcano \quad density = \frac{Total \quad number \quad of \quad volcanoes}{Area \quad of \quad a \quad circular \quad neighbourhood} \qquad (4.2)$$

The volcano density map consequently subdivided into several zones or classes based on the intensity of volcanoes per unit area (Fig. 4.9).

4.4.2 Spatial alignment of volcanic eruptions

Alignments of eruptive structures are obvious through the satellite imagery, which contain at least three volcanic cones that are traced on ArcGlobe 10.1 and saved in polyline shape files (.shp). These files are then displayed within ArcGIS 10.1 (Fig. 4.8). Each alignment is marked by orientation, length, edge coordinate and number of the volcanic eruption (density). Subsequently,

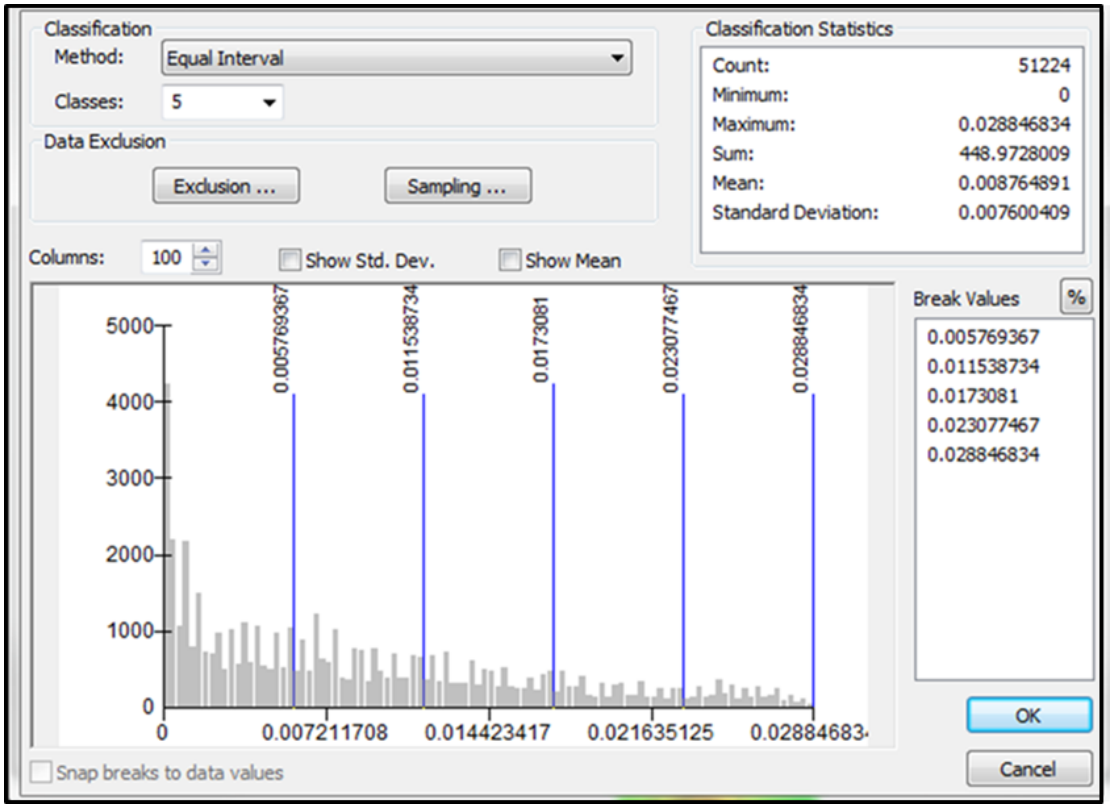

Figure 4.9. Dialog box showing the statistics data and break values for intensity of volcanoes per square kilometre within a circular neighbourhood 40 km.

GEOrient software 9.1 is executed to plot the direction of alignments in rose diagrams. The spatial distribution of alignments was analysed with each recognised area in AHVP. The orientation of feeder dykes in the AHVP can be inferred from volcanic alignments and morphology. Therefore, these alignments can be used to deduce the paleostress field during the dyke

emplacement (Bosworth 2008; Paulsen and Wilson, 2009). Further detail is covered in chapter 5, 6, and 8.

4.5 Size, distribution and slope of lava shields

The location, basal radius, and height of lava shields are extracted from high-resolution land sat images and available geological maps. The base of a volcano is determined where the generally equidistant around volcano become somewhat wider and flat (Hasenaka, 1994). In cases where the bases of two or more volcanoes overlap, the height is recorded at the rim of the overlap (Hasenaka, 1994). The basal radius of volcano is calculated based on the principal of triangular. The volume of lava shields is generally computed by approximating its shape as a truncated cone for flat-topped volcanoes (Fig. 4.10);

$$V\,(volume \quad of\ truncated \quad cone) \quad = \quad \frac{1}{3}\pi(r_1^2 + r_1 + r_1 r_2 + r_2^2)h \tag{4.3}$$

where $r_1\ and\ r_2$ are the base and top radius of shield volcanoes, respectively, whereas h is height.

Cone shape is also used for calculation conical-topped volcanoes.

$$volume(volume \quad of\ cone) = \pi r^2 \frac{h}{3} \tag{4.4}$$

Slope angle is estimated as the tangent of the height to basal radius ratio $\left(\tan^{-1}(H/R)\right)$, for example (Fig. 4.11). It is effectively a method to explain the tendency of the steepness of the lava shields and useful to compare the Al Haruj volcanic province with other terrestrial shield volcanoes such as Iceland and Hawaiian.

The geometry area of volcanoes and volcanic fissures can be calculated using ArcGIS with several steps. The polygon shape.file is created in ArcCatalog and then imported into ArcMap to calculate the area of the volcanic feature (Fig.4.11). ArcGIS uses planimetric algorithms to calculate geometry such as area. The ArcGIS needs to work with projected coordinate systems (PCS) rather than geographic coordinate systems in order to calculate areas (Hall, 2014). Frequency histograms and statistical analyses for height, basal radius, and slope angle as well as volume of lava shields were created by Excel software for distinctions between different volcanoes within the AHVP.

The delineation of different types of volcano-tectonic elements at the Tibesti Volcanic Province (TVP) together with their assignment to the relevant volcanic events the main volcanic units of the Tibesti Volcanic Province (TVP) was studied in a detail by using ArcGIS 10.1 along with detailed geological map created by Deniel, et al. (2015) as a baseline. The geometry of each volcanic unit at this volcanic province is defined by its length, width

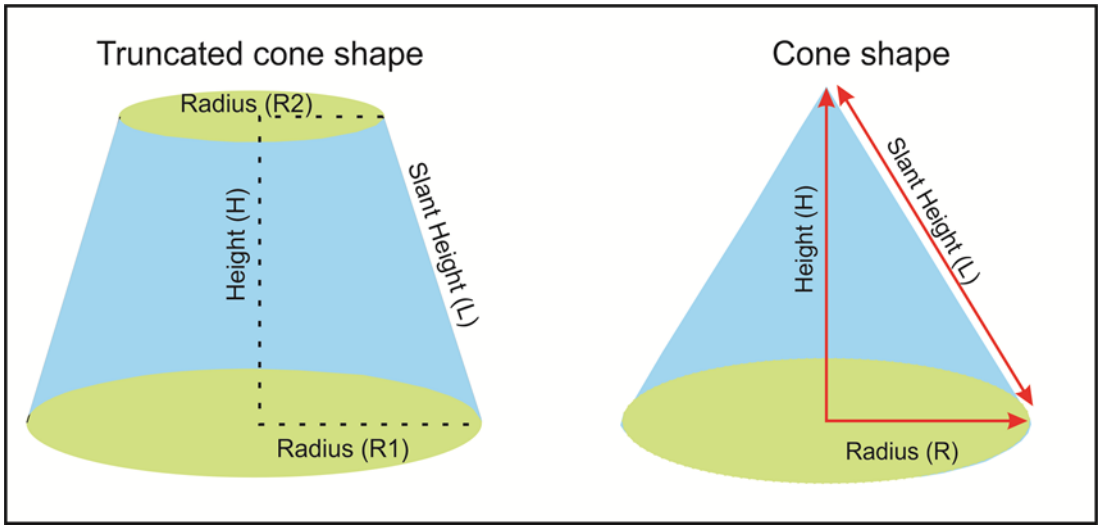

Figure 4.10. Conical shapes are assumed in calculating lava shields volume.

(diameters), area, volume and depth or thickness. Subsequently, the area of the collapse caldera at the TVP used to estimate the cross-sectional area of the associated magma chamber (cf. Marti et al., 1994; Marti and Gudmundsson, 2000; Acocella, 2007). The subject is studied further detail in Chapter 9.

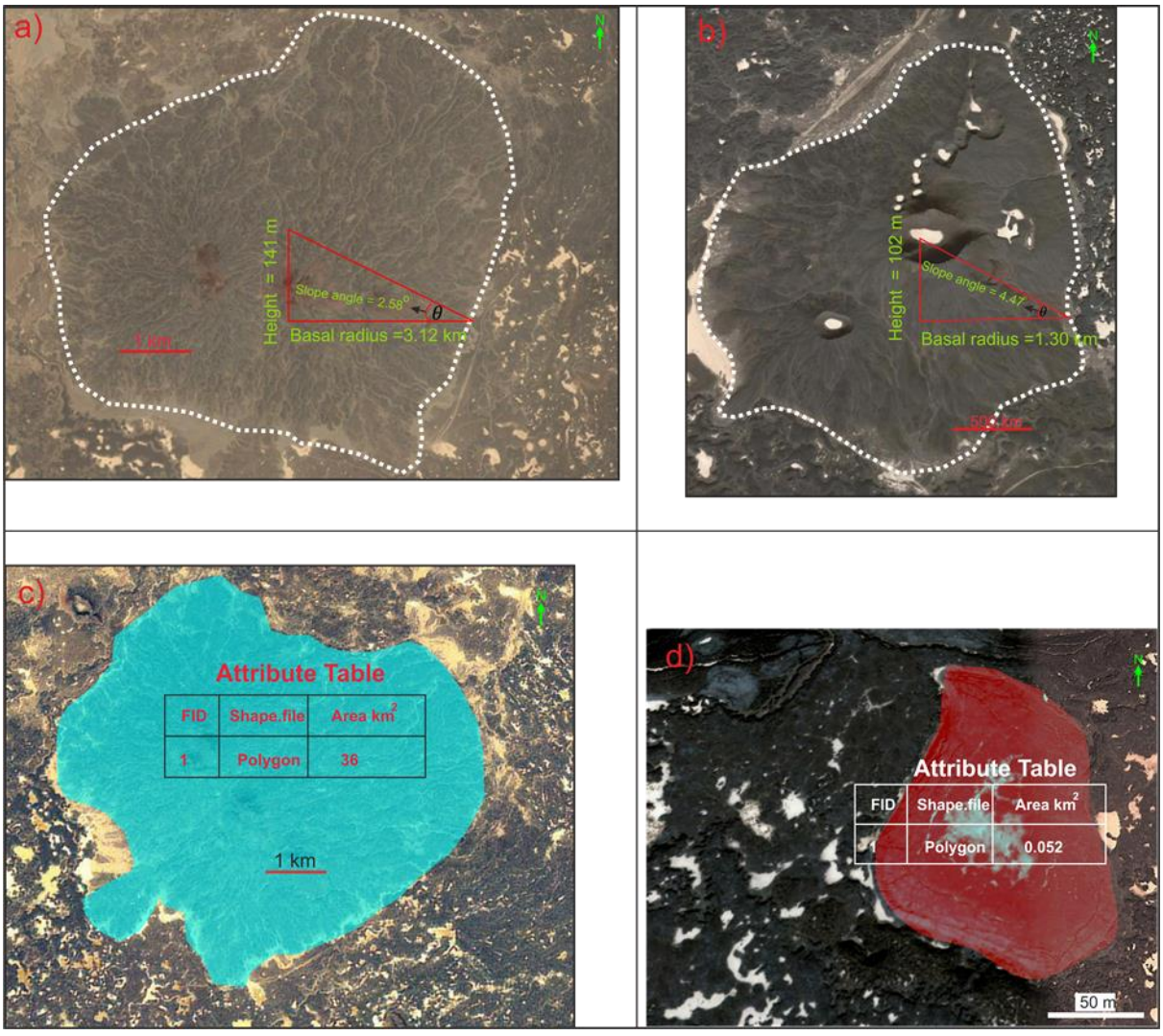

Figure 4..11. Slope angles of lava shields have been calculated from height and basal radius of the shields. a) Lava shield for the first volcanic phase while b) lava shield for the third volcanic phase. The cross-sectional area of lava shield (c) and lava rise (d) have been calculated using ArcGIS 10.1 and associated with attribute table.

4.6 Using the ground-based data and satellite imagery to evaluate error

Lengths and thicknesses of dykes, and areas and heights of lava shields as well as areas and diameters of inflation features were measured from satellite imagery, independent estimates for some of these volcanic features obtained using field surveys. The latter data were used as an accuracy assessment for critical evaluating uncertainty or error and considered here as true or reference value. The error is generally defined as the difference between a measured value and its actual value (reference value) (Dodge, 2003). The percentage of error can be found by this equation;

$$The\ \ percentage\ \ error\ = \frac{Difference\ \ between\ \ field\ \ and\ \ remote\ \ measured}{Length\ \ or\ \ thickness\ \ measured\ \ in\ \ the\ \ field} * 100 \quad (4.5)$$

The images are detailed enough in the three studies areas with high resolution leading to reduced errors as far as practicable. Images are allowed precisely mapping various volcanic features particularly in the Al Haruj and Tibesti volcanic provinces. Figure (4.12) involves two examples to explain to how estimated error percentage. Figure (4.12a) illustrates the same feeder dyke as observed in the field and on the satellite imagery. The measured thickness of this dyke in the field was 0.72 m while its thickness measured from satellite imagery as 0.80 m. The difference between field and remote measurement in this case was around 0.08 m. From Eq. (4.5) the percentage of error for thickness is approximately ±10%. Similarly, the length measured in the field was 14 m whereas from satellite imagery was 13 m. Hence the percentage of error this case was ±7%. Figure (4.12b) shows a volcanic fissure observed in the field with a thickness (paleo-opening) of approximately 1.1 m while on the satellite imagery its thickness is around 1.2 m. In meanwhile its length in the field was 175 m and on satellite imagery is 170 m. Hence the errors for thickness and length from Eq. (4.5) are 14% and 3% respectively. Furthermore, the perfect correlation of determinations of thicknesses (aperture or paleo-opening) (R^2=0.99) and lengths (R^2=0.99) for 16 points measured in the field and from satellite images at scattered locations at the AHVP which indicates a sufficient and accurate method (cf.

Chen et al., 2014) (Fig. 4.13a, b). However, the percentage of error obviously gradually decreases with increasing thickness and length of dyke/volcanic fissure due to the resolution becoming higher and more confident, particularly when the areas and heights/depths for lava shields and collapse calderas are measured.

Figure 4.12. a) Large ridge (probably a volcanic plug or neck) in the north-eastern of the AHVP which is dissected by several dykes. One of these dykes is marked by red ellipse on the left. The same dyke is marked by red ellipse on the satellite imagery. b) Volcanic fissure observed in the field on the left and the same volcanic fissure recognised on the satellite imagery on the right. The inset map shows the location.

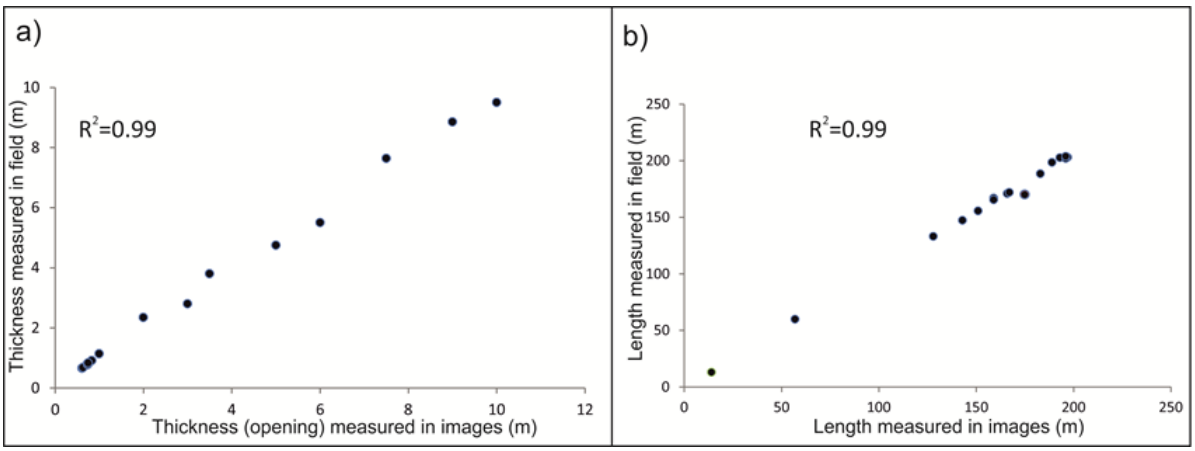

Figure 4.13. Graphics showing the relationship between 16 points measured in the field and from satellite imagery at the AHVP (a) thickness (paleo-opening) and (b) length. R^2 is coefficient of determination.

4.7 Dynamic Young's modulus using ultrasonic wave velocities

The texture, mineral, and chemical composition of most basaltic rocks entire AHVP exhibit great similarity (Busrewi and Suwesi, 1993; Peregi et al., 2003; Less et al., 2006; Cvetkovic´ et al., 2010). During this study, four samples were collected from fresh and more recent lava flows at the NE part of the AHVP in order to measure their Young's moduli. The Young moduli, then, have been used to calculate flexural rigidly for those rocks in order to estimate magmatic over-pressure caused inflation features.

Two alternative techniques are commonly used to determine the Young's modulus of rocks; (i) ultrasonic wave velocities are used to determine dynamic Young's modulus, whilst (ii) uniaxial compressive strength (UCS) tests are used to measure static Young's modulus through measuring the stress and strain as the sample in compressed. The present study is employed the former method then used certain equations in order to estimate the static Young's modulus. However, the sample preparation and ultrasonic wave velocity measurements have been done at the Rock and Ice Physics Laboratory at University College of London (UCL). All core samples

used in this study were taken from the upper lava crust of inflation features. The ultrasonic wave velocity measurements were made parallel to the core axis but also at different intervals radially around the core axis in as illustrated in Fig (3.14a).

A DPR300 35MHz Ultrasonic pulser/receiver was connected to an Agilent Technologies 1.5 GHz oscilloscope and was used to excite a Panametrics V103 P-wave transducer at 1 MHz resonance frequency. Waveforms captured from an identical transducer were subsequently displayed on the digital oscilloscope (Fig. 4.14b). The time difference between the initial pulse and the first arrival was measured as the P-wave travelled through the sample. This procedure was repeated with polarised S-wave transducers in order to measure the travel time for an S-wave to cross the sample. P-waves reached the transducer prior to the S-waves due to their higher velocity. Therefore, P-waves are usually hidden by the arrival of S-waves, but the amplitude of S-waves is often greater than the P-waves. Subsequently the sample is rotated to measure anisotropy within the same sample (Fig.4.14a). Acoustic wave velocities are calculated from the measured time of compression (P) and shear (S) waves to cross the sample (Fig. 4.14c). The P-wave velocity rather than S-wave velocity measurements are commonly used to calculate the sample anisotropy as there is greater amount of confidence in the P-wave velocity readings (Modi et al., 2016). Therefore the P-wave anisotropy throughout the samples in different orientations can be found by equation (4.6), given by Benson et al. (2005);

$$P_V = \frac{\left(v_{p\max} - v_{p\min}\right)}{v_{pmean}} \tag{4.6}$$

P_V is the anisotropy parameter and $v_{p\max,}$ $v_{p\min}$, v_{pmean} is the maximum, minimum and average P-wave velocities respectively. Thus the P-wave anisotropy of the four samples in the multiple orientations (axial and radial) is less than 10 % which indicates that the basaltic rocks at the AHVP little anisotropy, and can be considered as isotropic or weakly anisotropic.

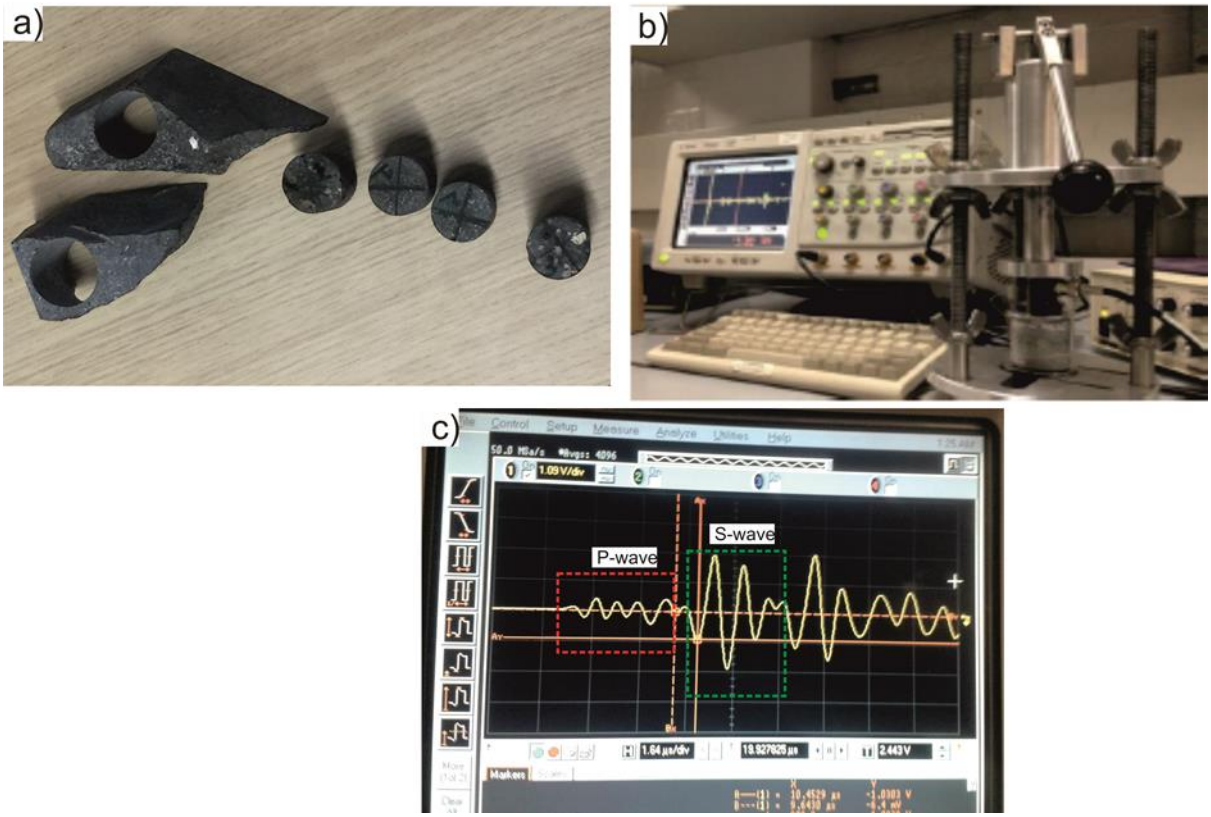

Figure 4.14. a) The core holes are around 29 mm in diameter, and the cores produced from these holes are 25 mm in diameter. The lines marked on the samples refer to a function of azimuth to measure anisotropy within each sample in various orientations. b) Oscilloscope and jig were used for measuring ultrasonic velocities. c) The first arrival P-waves are indicated by the red box while S-waves are characterised by greater amplitude and marked by the green box.

The P and S-wave velocities and bulk density are used to calculate the dynamic Young's modulus based on equation (4.7) (Jaeger et al., 2007);

$$E_{dyn} = \frac{V_s^2 \rho \left[3\left(V_p^2 / V_s^2 \right) - 4 \right]}{\left(V_p / V_s \right)^2 - 1} \tag{4.7}$$

where E_{dyn} is dynamic Young's modulus, V_p is the compression seismic velocity, V_s is the shear seismic velocity, ρ represents the bulk density of the core sample where it is found from mass and volume (kg/m^3). The relationships between the static and dynamic moduli for different rock types

are somewhat complex (Eissa and Kazi, 1988, Brotons et al., 2015). There are many investigations that try to correlate the static and dynamic moduli for different types of rocks (e.g. Christaras et al., 1994; Brotons et al., 2015). For example; Eissa and Kazi (1988) performed a statistical relation to estimate the static E_{st} from dynamic Young's modulus E_{dyn} that may be crudely valid for all rock types as follows;

$$E_{st} = 0.74E_{dyn} - 0.82 \quad (4.8)$$

From laboratory measurements, the dynamic modulus is usually approximately twice that of the static modulus, but in the field, this ratio varies from 1.5 to 9.1 for most volcanic rocks depending on many factors such as fractures, cavities, and planes of weakness (Gudmundsson, 1990). In addition, the in-situ Young's modulus is likely to be lower (1.5 to 5 times) than the core-sample (Gudmundsson, 2011).

Chapter 5: Volcano-tectonics of the Al Haruj Volcanic Province, Central Libya

Journal of Volcanology and Geothermal Research

Abdelsalam Elshaafi and Agust Gudmundsson

http://dx.doi.org/10.1016/j.jvolgeores.2016.06.025

Statement of contribution:

The origin idea, methodology, computation and creation of models were developed by AE.

Fieldwork and satellite measurements conducted by AE

Writing the initial draft was made by AE and later critical review and commentary from co-author

All illustrations were prepared by AE, with later adjustments and modifications from co-author.

Interpreted data and discussions were done by AE and specifically critical revision from co-author.

Journal of Volcanology and Geothermal Research 325 (2016) 189–202

Contents lists available at ScienceDirect

Journal of Volcanology and Geothermal Research

journal homepage: www.elsevier.com/locate/jvolgeores

Volcano-tectonics of the Al Haruj Volcanic Province, Central Libya

Abdelsalam Elshaafi *, Agust Gudmundsson

Department of Earth Sciences, Royal Holloway University of London, Egham TW20 0EX, UK

ARTICLE INFO

Article history:
Received 7 March 2016
Received in revised form 15 June 2016
Accepted 30 June 2016
Available online 4 July 2016

Keywords:
Lava shields
Pyroclastic cones
Volcanic fissures
Feeder-dykes
Local stresses
Magma paths

ABSTRACT

The Al Haruj intra-continental Volcanic Province (AHVP), located at the south-western margin of the Sirt Basin, hosts the most extensive and recent volcanic activity in Libya - which is considered typical for plate interiors. From north to south the AHVP is divided into two subprovinces, namely Al Haruj al Aswad and Al Haruj al Abiyad. The total area of the AHVP is around 42,000 km^2. Despite the great size of the AHVP, its volcano-tectonic evolution and activity have received very little attention and are poorly documented and understood. Here we present new field data, and analytical and numerical results, on the volcano-tectonics of the AHVP. The length/thickness ratio of 47 dykes and volcanic fissures were measured to estimate magmatic overpressure at the time of eruption. The average dyke (length/thickness) ratio of 421 indicates magmatic overpressures during the associate fissure eruptions of 8–19 MPa (depending on host-rock elastic properties). Spatial distributions of 432 monogenetic eruptions sites/points (lava shields, pyroclastic cones) in the AHVP reveal two main clusters, one in the south and another in the north. Aligned eruptive vents show the dominating strike of volcanic fissures/feeder-dykes as WNW-ESE to NW-SE, coinciding with the orientation of one of main fracture/fault zones. Numerical modelling and field observations suggest that some feeder-dykes may have used steeply dipping normal-fault zones as part of their paths to the surface.

1. Introduction

The Al Haruj Volcanic Province (AHVP) is the largest volcanic province in Libya, the other three being the Gharyan Province in north-western Tripoli, the Jabal as Sawda Volcanic Province, located between Jabal Gharyan Volcanic Province and the AHVP, and the Jabal Nuqay Volcanic Province which is situated close to Tibesti Mountain at the Libyan-Chadian border (Fig. 1a; Al-Hafdh and El-Shaafi, 2015). All four are considered typical intra-plate volcanic provinces. The AHVP developed from early Pliocene up to late Pleistocene and has been linked to the tectonic evolution of the rifting of the Sirt Basin (Less et al., 2006; Cvetković et al., 2010; Bardintzeff et al., 2012).

The AHVP is primarily composed of lava flows, mostly transitional to alkaline basalts and subsidiary sub-alkaline. More evolved volcanic rocks have not been observed (Busrewil and Suwesi, 1993; Peregi et al., 2003; Al-Hafdh and El-Shaafi, 2015). The area of the AHVP calculated using ArcGIS 10.1 during this study is around 42,000 km^2. The AHVP is here divided into two subprovinces based on volcano-morphological features and thicknesses of lava flows (Fig. 1b; Peregi et al., 2003). The main subprovince, which also shows the most recent volcanic activity, is the one located in the north. It is named the Al Haruj al Aswad Subprovince (AHAS) (the Black Mountain) and is mainly composed of lava flows younger than Pliocene (Busrewil and Suwesi, 1993; Busrewil, 1996). The other subprovince is located in the south and named the Al Haruj al Abyied Subprovince (AHBS) (the White Mountain). Both subprovinces belong to an area that is slightly prolonged in the NNW-SSE direction (Peregi et al., 2003; Less et al., 2006; Al-Hafdh and El-Shaafi, 2015). The Al Haruj al Aswad Subprovince consists mainly of large lava shields on a lava plateau, while the Al Haruj al Abyied Subprovince consists primarily of clusters of scoria cones and spatter cones, mostly aligned NW-SE (Martin and Németh, 2006).

A wide lava plateau was built during the first volcanic phases (early Pliocene), primarily through eruptions of low-viscosity pahoehoe lava flows issued from several hundred volcanic fissures, some of which also generated blocky flows (Busrewil and Suwesi, 1993). Many of volcanic fissures are covered by subsequent lava flows and thus difficult to recognise in the field and on remote-sensing images (Busrewil and Suwesi, 1993; Busrewil, 2012). Many of the topographic features, such as tumuli and lava rises, however, are easily recognised in the field as well as on the aerial photographs and satellite images.

The principal aim of this paper is to present new volcano-tectonic data and models on the AHVP with a view of understanding its volcano-tectonic evolution. The data include feeder-dykes and volcanic fissures, lava shields and pyroclastic (scoria) cones, including their spatial distributions and orientations in relation to the main fault zones in the area. We use the data to estimate magmatic overpressures during

* Corresponding author.
E-mail addresses: abdelsalamelshaafi@yahoo.co.uk (A. Elshaafi), a.gudmundsson@rhul.ac.uk (A. Gudmundsson).

http://dx.doi.org/10.1016/j.jvolgeores.2016.06.025
0377-0273/

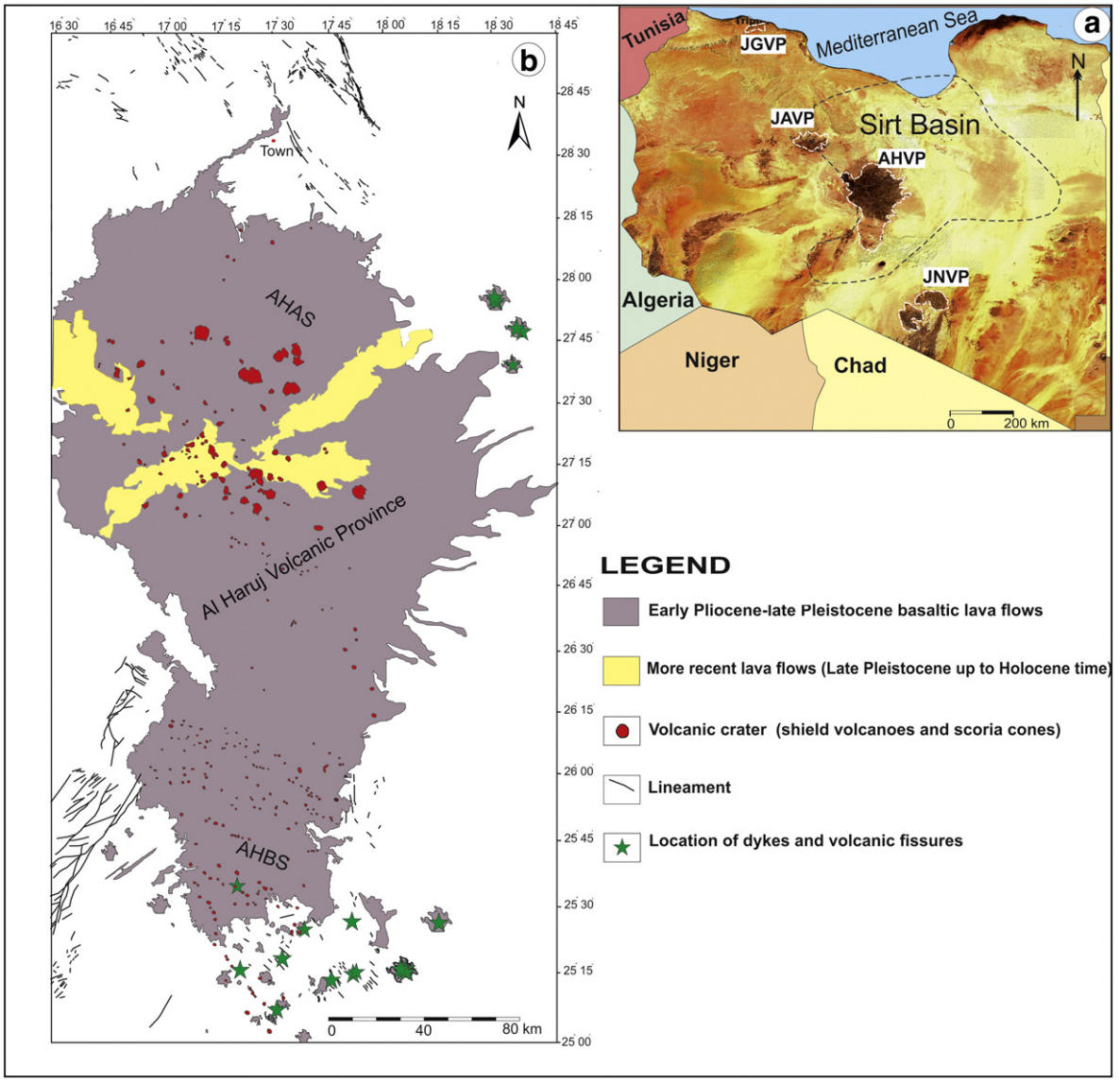

Fig. 1. a) Satellite image shows the four main occurrence of Tertiary–Quaternary volcanic provinces in Libya which are situated along the axis of the Palaeozoic Tripoli Tibesti Uplift. The Al Haruj Volcanic Province (AHVP) is located at the south-western margin of the Sirt Basin, Central Libya. b) Geological map showing the main structural elements and distribution of eruption points or eruptive centres and more recent lava flows on the Al Haruj Volcanic Province. Green stars indicate the location of dykes and volcanic fissures. Some of the dykes were mapped by Less et al. (2006). JGVP = Jabal Gharyan Volcanic Province, JAVP = Jabal as Sawda Volcanic Province, JNVP = Jabal Nuqay Volcanic Province, AHAS = Al Haruj al Aswad Subprovince, AHBS = Al Haruj al Abyied Subprovince.

fissure eruptions and numerical models to illustrate how some of the dykes may have used steeply dipping normal-fault zones, which are abundant in the area, as part of their paths to the surface.

2. Geological background of the AHVP

The Al Haruj Volcanic Province (AHVP) is located at the south-western margin of the Sirt Basin, one of the main structural elements of North Africa. It follows that the AHVP volcano-tectonic evolution and history is strongly related to the tectonic evolution of the Sirt Basin (Fig. 2). The origin of the volcanism in the Al Haruj province and its volcanic-tectonic evolution are still poorly constrained despite more than five decades of intensive hydrocarbon exploration and the discovery of numerous oil and gas fields in the Sirt Basin.

Many different models have been suggested for the geodynamic setting of the AHVP. Burke (1996) suggests that the Miocene volcanism of Libya was related to the passage of African plate over a relatively fixed asthenosphere hotspot or plume. This is currently not regarded as a very plausible model because (1) the time-related migration of volcanic provinces does not fit well with the movement of the African plate (Farahat et al., 2006; Mohamed, 2014), and (2) peridotite xenoliths indicate a cold lithosphere rather than hotspot at the time of volcanism (Peregi et al., 2003; Less et al., 2006).

Alternatively, Klitzsch (2000) suggests that the volcanic products of the AHVP relate to relative tensile stresses associated with the reactivation of three major structural elements. These elements are (1) the NW-SE trending Palaeozoic South Al Haruj Uplift, (2) the NE-SW trending Tibesti-Sirt Uplift (Hercynian Orogeny), and (3) the continuation of the Cretaceous–Tertiary Hun Graben (Peregi et al., 2003). In contrast to the other volcanic provinces in Libya, the AHVP is associated with major structural elements that have affected its volcano-tectonic development and may, partly, be the reason for the great size of the AHVP (Farahat et al., 2006).

The primary magmas may have been produced in relation to lithospheric delamination. This is plausible given the rifting of the Sirt Basin since early Cretaceous, inducing low-degree partial melting at depth in the upwelling asthenosphere (Less et al., 2006). Also, the discrete volcanic phases of the AHVP may partly relate to periods of

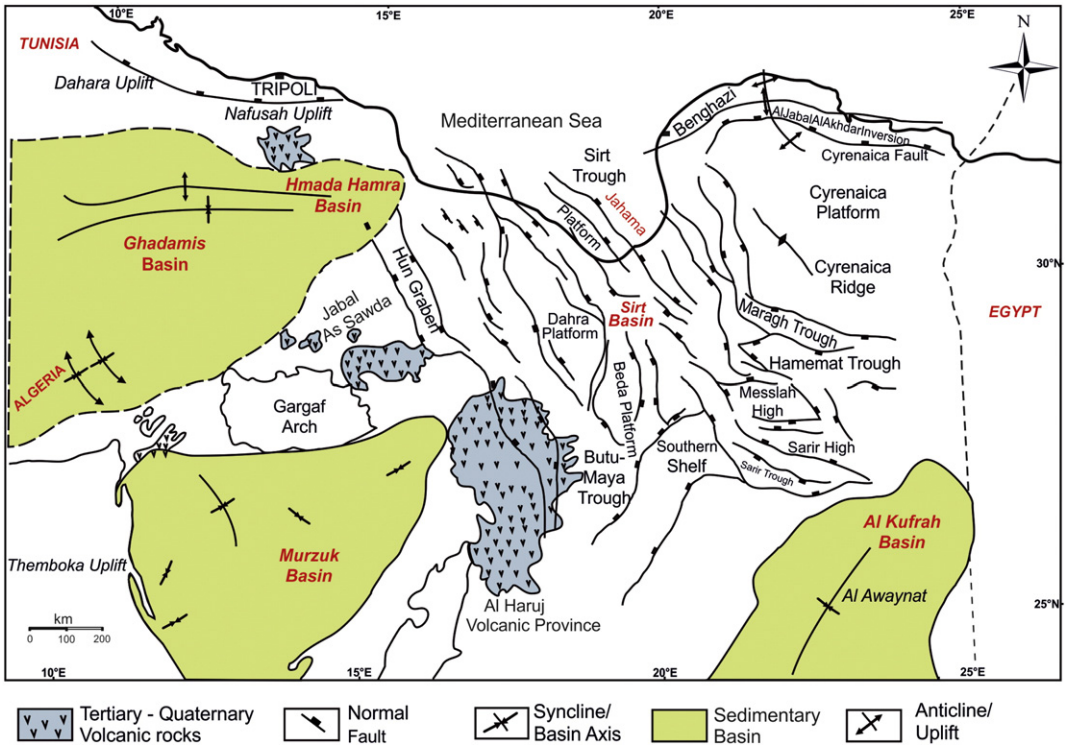

Fig. 2. Tectonic map showing major structural elements of the Sirt Basin.
(Modified after Mouzughi and Taleb, 1981; Ambrose, 2000; Abadi et al., 2008).

rejuvenation of pre-existing fault system in response to late Tertiary extensional tectonic events most likely related to Africa-Eurasia convergence (Cvetković et al., 2010). But the time gap between the main syn-rift phases of the Sirt Basin (late Cretaceous–Eocene) and the volcanism (from early Pliocene to late Pleistocene) is still largely unexplained and debated.

Many authors (i.e. Less et al., 2006) have suggested the magma of the AHVP migrated partly along crustal weaknesses. Yet, the exact process of magma channelling along such weaknesses has not been analysed. Here we explore the role of volcano-tectonics at a crustal scale in the evolution and activity of the AHVP and suggest an alternative mechanism for magma-fault interaction, including new field data and numerical models on volcano-tectonic interactions and stress fields. In particular, we notice and explore several aspects of the activity of the AHVP, including (1) while AHVP covers a large area, the cumulative thickness of the basaltic sequence generally does not exceed 140 m (Pacific Aero Survey, 1979; Peregi et al., 2003), which may indicate low eruption rates (Le Corvec et al., 2013). (2) The magma is generally poorly evolved, indicating lack of significant differentiation stages during magma ascent. (3) Concentrations of major and some trace elements in the eruptive show narrow variations, suggesting magma origin through melting of similar sources and that the magma underwent similar subsequent fractionation processes (Peregi et al., 2003; Less et al., 2006).

3. Geometry and morphology of fractures

The Al Haruj Volcanic Province (AHVP) is thought to have been dominantly extruded from hundreds of feeder-dykes whose surface expressions are volcanic fissures, most of which, however, are covered by more recent lava flows (Busrewil and Suwesi, 1993; Busrewil, 1996). Some of the dykes and volcanic fissures, as well as numerous normal faults, can be seen in the field as well as on Landsat images (Fig. 3).

Field and remote sensing investigations indicate that most of the lineaments in the AHVP are normal faults and extension fractures, some of the extension fractures being volcanic fissures and dykes (Peregi et al., 2003; Less et al., 2006). The geometry and morphology of these lineaments were studied in more detail using ArcGIS 10.1 and multi-source high-resolution remote sensing images for instance the satellite imagery available on Google Earth (2015) for the central part of Libya. Digital elevation model (DEM) and data collected by the NASA Shutter Radar Topography Mission (SRTM) were also used. Google Earth imagery provides three-dimensional geospatial data through Keyhole Mark-up Language (KML). In AHVP, the images are detailed enough so as to provide a resolution of about 2.5 m multispectral at nadir (Abdunaser and McCaffrey, 2014) and allow measurements of the geometries of volcanoes, volcanic fissures, and dykes. The present study confirms that high-resolution remote sensing is an efficient and accurate complementary method to traditional field measurements of lineaments and volcanoes in arid and remote areas (cf. Drury, 2001; Rajesh, 2004; Chen et al., 2014; Abdunaser and McCaffrey, 2014) such the AHVP.

To define the main fracture patterns we analysed the azimuth frequency distributions of lineaments, lineament length and dyke-thickness distributions, as well as lineament densities (Wise et al., 1985; Abebe et al., 1998; Zakir et al., 1999; Francesco and D'Orazio, 2003). The faults and the extension fractures are mainly confined to scattered areas around the main province that range in size from a few to several dozen square kilometres. The bedrocks in these areas are not usually covered with lava flows or Quaternary sand dunes (Fig. 1b). The data are consequently grouped based on types, and then GEOrient software was used to plot the directions of fissures, dykes, and faults on rose diagrams.

4. Extension fractures

The only published studies on volcanic fissures and dykes in the Al Haruj Volcanic Province are those by Less et al. (2006). The dykes strike mainly from NW – SE to NNW–SSE, directions which are generally parallel to the strike of major faults in the Sirt Basin and similar to the trend of inferred and observed volcanic fissures. A minor dyke trend, from

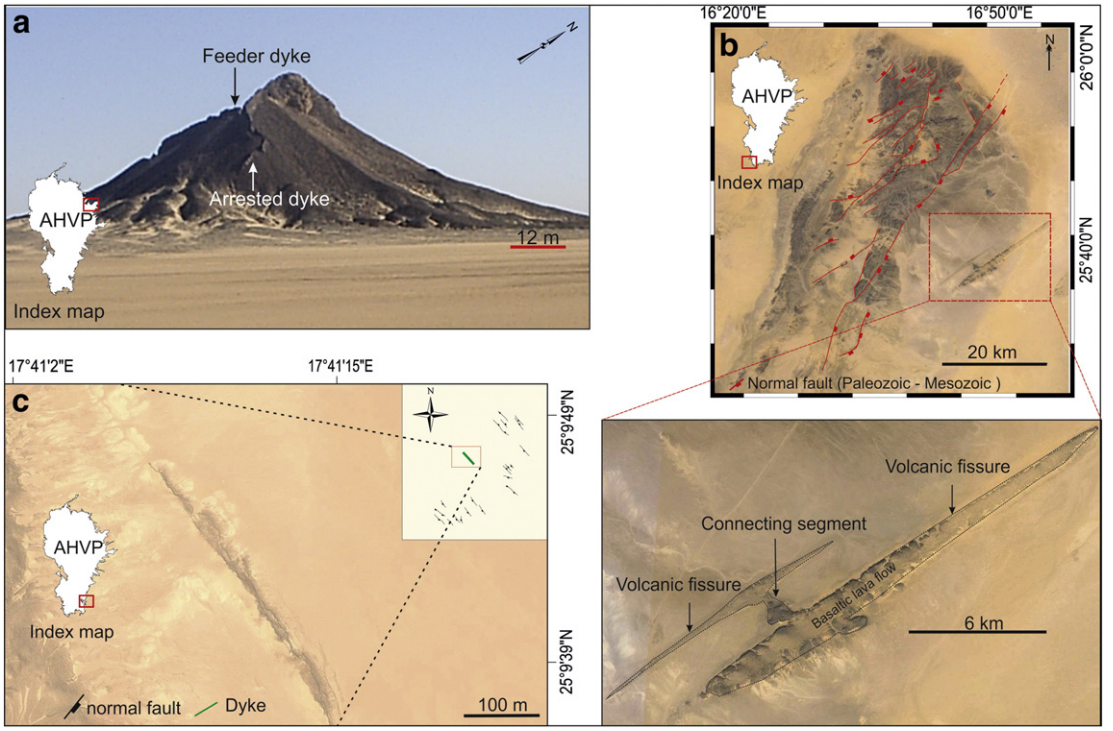

Fig. 3. a) Field photograph of large ridge (probably volcanic plug or neck) in the north-eastern of the AHVP known as Glyab Al-Baroad that is dissected by several dykes (arrows), which also contribute to the ridge formation. The ridge stands tens of metres above its surroundings, being more resistant to erosion than Miocene host rock (Maradah Formation, calcareous sandstones). The inset map shows the location. b) Landsat images showing two ridges of Dur Qrarat Amhamed in the southernmost part of the AHVP. These are interpreted as volcanic fissures (adapted from Google Earth). Both volcanic ridges constitute long NE-SW trending fissures as well as short WSW-ESE trending connecting segments. Normal faults are taken from Less et al. (2006). c) Segmented dykes are modelled as individual fractures when the nearby tips of the segments are spaced at short distances in relation to the segment lengths. Here the maximum dyke thickness is 0.8 m (adapted from Google Earth). The inset map shows Oligocene-Miocene normal faults. The segments of dykes have similar trend as the faults. Faults were mapped by Less et al. (2006).

NNE-SSW to NE-SW, may be related to inheritance of Palaeozoic crustal weaknesses (Less et al., 2006).

The thicknesses of the dyke segments are commonly 0.5–2 m thick (Fig. 4), while some may be as thick as 20 m, and their lengths are mostly 0.1–1 km (Less et al., 2006). These figures are similar to those of regional dykes in many other volcanic areas (Gudmundsson, 1995; Babiker and Gudmundsson, 2004). Some dykes in the eastern and southwestern part of the AHVP form ridges (Fig. 3a, b). All dykes and volcanic fissures, as seen in the field and on satellite images, are segmented. Such segmented extension fractures, however, are normally modelled as single fractures or cracks when the nearby ends of the segments are separated by less than 10% of the segment lengths, in which case the segments act mechanically essentially as a continuous fractures (Fig. 3c; Gudmundsson, 2011a). Remote sensing images have been used to extract length, thickness, and strike of 47 dyke segments and volcanic fissures around margins of the Al Haruj Volcanic Province (Table 1, Appendix I), all parameters that are important when considering the mechanics of dyke emplacement and associated stress fields (Babiker and Gudmundsson, 2004). The relation between lengths and thicknesses of these extension fractures is roughly linear (Fig. 4), in agreement with standard fracture-mechanics theory (Gudmundsson, 2011a).

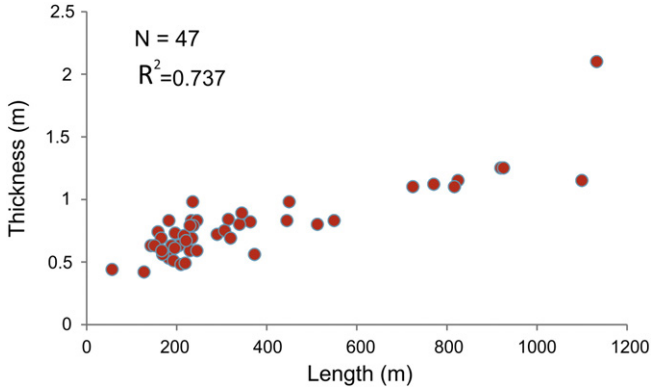

Fig. 4. Diagram showing a roughly linear correlation between length and thickness of 47 dyke segments and volcanic fissures on the AHVP. R^2 is the coefficient of determination.

4.1. Magmatic overpressure of the Al Haruj Volcanic Province

A magma chamber ruptures and injects a dyke when the conditions of Eq. (1) are met at any location in the walls or roof of the chamber, regardless the shape of the chamber (Browning et al., 2015):

$$p_l + p_e = \sigma_3 + T_0 \quad (1)$$

where p_e is the excess magmatic pressure in the chamber at the time of rupture, that is, the difference between the total magma pressure p_t and lithostatic stress p_l, and σ_3 and T_0 are the minimum compressive (maximum tensile) principal stress and the in situ tensile strength of the chamber host rock, respectively. As the dyke begins to propagate up into the roof of the chamber, the magma overpressure in the dyke becomes:

$$p_o = p_e + (\rho_r - \rho_m)gh + \sigma_d \quad (2)$$

where ρ_r is the host-rock density, ρ_m is the magma density, g is acceleration due to gravity, h is the dip dimension and σ_d is the differential stress at the level where the dyke is observed for a feeder-dyke (volcanic fissure) at the surface (Gudmundsson, 1990, 2011a).

The magmatic overpressure p_0 measures the difference between the total magma pressure and the minimum principal compressive stress

σ_3, which acts normal to the dyke; p_0 increases up along the dyke fracture so long as the buoyancy term $(\rho_r - \rho_m)gh$ is positive. During fissure eruptions, the overpressure p_0 has large effects on the volumetric flow or effusion rate (Gudmundsson, 1990, 2011a; Kusumoto et al., 2013).

From the aspect (strike dimension/thickness) ratio of the dyke, its overpressure p_o at the time of its formation can be calculated. The following equation supposes the magmatic overpressure is constant, which is a good first approximation generally and particularly when there is limited data as to the exact thickness variations of dykes and volcanic fissures (Becerril et al., 2013):

$$p_o = \frac{\Delta u E}{2L(1-\nu^2)} \quad (3)$$

Here ν is Poisson's ratio of the host rock, E its Young's modulus, Δu the maximum aperture or thickness of the dyke, and L the strike dimension (horizontal length) of the dyke. Dykes are primarily extension fractures that are modelled as either through cracks (when feeders) or part-through cracks (when arrested). In particular, feeder-dykes extend from one free surface (the source magma chamber) to another one, namely the Earth's surface (Fig. 5; cf. Gudmundsson, 2011a). Non-feeders propagate from one free surface (the source magma chamber) and then become arrested at some depth below the surface, usually at contacts between mechanically dissimilar layers (Gudmundsson, 2011b).

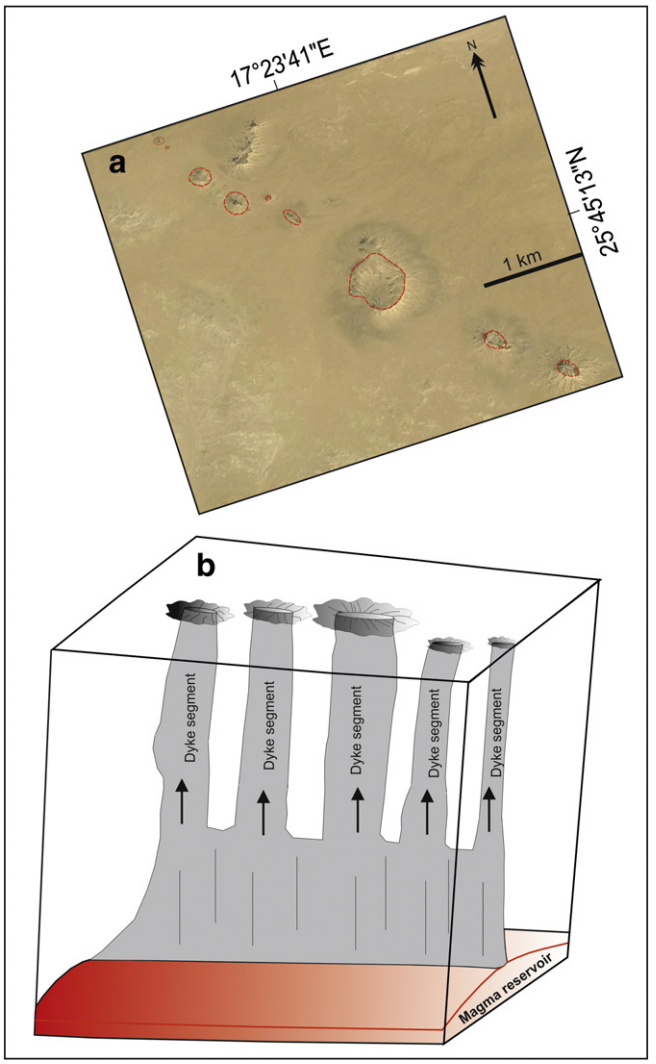

Fig. 5. a) Image showing several eruption points/centres fed by a segmented dyke (adapted from Google Earth). b) Schematic illustration of a segmented dyke, the segments being extension fractures (mode I cracks). When the dyke, as here, extends from one free surface (magma chamber) to another free surface (Earth's surface), it is modelled as a through crack. The dyke length or strike dimension is smaller than the height or dip dimension. Therefore, the strike dimension is the controlling dimension. (Modified after Gudmundsson, 2011a).

Lengths of measured dykes and volcanic fissures at AHVP range from 57 m to 1133 m and their thicknesses or openings (palaeo-apertures) from 0.42 m to 2.1 m (Appendix I). The estimated uncertainties or errors in the measurements are 5% for length and 15% for thickness. Most of the dykes and fissures strike NW-SE. The average aspect (length or strike dimension/thickness) ratio is 421, which is within a factor of 2 for aspect ratio estimates from other areas (Becerril et al., 2013). The aspect ratio depends much on the stiffness or Young's modulus of the host rocks where the dykes/fissures are measured.

The static Young modulus (E) of the uppermost crust of the Sirt Basin, based on drill-core samples, is estimated in the range of 8–20 GPa (Qui et al., 2008). The basement rocks in the south western portion of the Sirt Basin are mostly granodiorite, granite, and metamorphic rocks and overlain by around 2000 m of various types of sedimentary rocks. The in-situ Young's modulus is likely to be lower than the core-sample modulus (Gudmundsson, 2011a) and is here assumed in the range of 7–15 GPa. Poisson's ratio ν of most rocks is in the range 0.2–0.3; we use the typical average value of 0.25 (Gudmundsson, 2011a), which is similar to ν values obtained in laboratory tests on core samples in the Sirt Basin (Qui et al., 2008). We assume the strike dimension (outcrop length) to be the controlling dimension, that is, smaller than the dip dimension (depth to the source magma chamber). This follows because the depths to the magma chambers (the dip dimension) in the AHVP is estimated at 35–55 km (Peregi et al., 2003), many times larger than the measured strike dimensions of the dykes.

From Eq. (3), using the measured aspect ratios and inferred elastic properties of the host rock, the magmatic overpressure of individual dykes can be estimated. For the average aspect ratio, magmatic overpressure is from 8 MPa ($E = 7$ GPa) to 19 MPa ($E = 15$). These results are very reasonable. The lower value (8 MPa) is similar to those obtained in many other studies from different volcanic provinces (Delaney and Pollard, 1981; Poland et al., 2008; Geshi et al., 2010; Kusumoto et al., 2013) and is close to the maximum in-situ tensile strength of rocks (Gudmundsson, 2011a; Kusumoto et al., 2013). The higher value (19 MPa) is similar to those obtained in areas where, like in the AHVP, the depth of origin of the basaltic magma forming the dykes is great (Becerril et al., 2013).

5. Magma propagation from the source chamber

Nearly all eruptions are fed by dykes and inclined sheets. Understanding the mechanics of dyke emplacement and propagation through the Earth's crust (e.g., Gudmundsson et al., 2014) is therefore crucial for a better understanding of volcano-tectonic processes in general and those operating in the AHVP in particular. Dykes occur mainly in elongated swarms outside the main volcanic system, whereas the shield volcanoes and scoria cones are mostly confined to the northern, central as well as the southernmost of this province (Fig. 1b).

While the Al Haruj area is located within the most important hydrocarbon sedimentary basin in Africa, the details of the geometry of sills, dykes, and inclined sheets that eventually fed the eruptions are still poorly understood. In the past few years, many models on intrusions in sedimentary basins have been developed, focusing mostly on sill emplacement (Planke et al., 2005; Cartwright and Hansen, 2006; Polteau et al., 2008; Thomson and Schofield, 2008; Gudmundsson and Løtveit, 2012; Holt et al., 2014). Sills can propagate laterally within basins for tens or hundreds of kilometres and attain various shapes (Cartwright and Hansen, 2006; Hansen and Cartwright, 2006; Gudmundsson and Løtveit, 2012; Barnett and Gudmundsson, 2014). However, magma transport to the surface is mostly through dykes, and outside central

volcanoes (where inclined sheets are common) almost exclusively so. Here we therefore focus on dyke propagation.

5.1. Mechanics controlling the propagation of dyke

When a dyke injected from a source magma chamber meets a discontinuity such as a contact, it can respond in one of four ways: (a) become arrested at the contact, (b) penetrate the contact and continue its propagation towards the surface (perhaps eventually erupting), and (c) change into sill through and single deflection or (d) double deflection along the contact (Gudmundsson, 2011b; Barnett and Gudmundsson, 2014). Arrest or deflection of a dyke at a contact is controlled by three main mechanisms, namely:

a) Stress barriers (layers where the principals stresses have rotated so as to become unfavourable for dyke propagation)
b) The Cook-Gordon debonding or delamination (induced dyke-parallel tensile stress opens the contact ahead of the propagating dyke tip)
c) Elastic mismatch (relates to change in Young's modulus across a contact in relation to the contact properties and material toughness)

Several numerical models on dyke deflection and arrest were made using Comsol Multiphysics (5.1) (www.comsol.com), a finite element (FEM) software package for various physics and engineering applications (Tabatabaian, 2014). The dykes are modelled as elliptical holes subject to constant magmatic overpressure of 10 MPa (the typical value based on the above range of 8–19 MPa estimated above). The vertical dimension or height of the model is taken as a unit and all the layers have the same Poisson's ratio, 0.25, and density, 2500 kg/m^3. The models are fastened at the edges to avoid rigid-body rotation and translation. The direction of dyke propagation is inferred from the trajectories or ticks showing the direction of the maximum principal compressive stress σ_1. The contours of the calculated maximum principal tensile stress, σ_3, are also shown.

For a homogeneous and isotropic crust, so long as there is magmatic overpressure in the dyke it should reach the surface as a feeder (Gudmundsson, 2011a). Field observations, however, show that most dykes become arrested at contacts between layers in anisotropic (layered) crustal segments (Gudmundsson, 2011b; Browning and Gudmundsson, 2015) and are thus non-feeder dykes. The dykes may stop altogether at the contacts, or change into sills – which have the potential of developing into shallow magma chambers. Our numerical models illustrate how arrest can occur in relation to the three main arrest conditions indicated above, which we now discuss in more detail.

5.1.1. Stress barrier (the rotation of the principal stresses at the contact between layers)

This mechanism operates when a dyke meets a layer with local stress field that is unfavourable to dyke propagation (Barnett and Gudmundsson, 2014; Tibaldi, 2015); namely, the maximum compressive principal stress field σ_1 is rotated 90° so as to become horizontal. Examples include contact where across which Young's modulus changes abruptly (Fig. 6). Stress barrier thus partly control the frequency with which injected dykes reach the surface to feed eruptions (Gudmundsson et al., 2010).

5.1.2. Cook-Gorden debonding mechanism

The dyke-parallel tensile stress induced ahead of propagating dyke is about 20% of the induced tensile stress of perpendicular to the dyke (Fig. 7a) and can open up contact ahead of dyke tip if it reaches the tensile strength T_0 of the contact (0.5–9 MPa and most commonly 2–5 MPa; Gudmundsson, 2011a). On meeting the open contact then, depending on the magmatic overpressure, the dyke either becomes arrested or changes into a sill (Barnett and Gudmundsson, 2014) (Fig. 7b, c).

5.1.3. Elastic mismatch

This mechanism operates when there is an abrupt change in the elastic properties, particularly in Young's modulus, across a contact (cf. He and Hutchinson, 1989). More specifically, when a dyke meets a contract, the ratio of strain energy release rate (a measure of material toughness or resistance to fracture) for dyke deflection (into a sill) along the contact G_d to that of dyke penetration G_p, both in relation to Dundurs elastic mismatch parameter, α (Fig. 8; Gudmundsson, 2011a, 2011b) may control what happens to the dyke. There is little difference in the elastic strain energy release rate for a single or double deflection. For negative values of Dundurs elastic mismatch parameter, layer 1 (the dyke-hosting layer) is stiffer than layer 2 and there is little tendency to dyke deflection along the contact. However, as the stiffness of layer 1 increases in relation to that of layer 2, the tendency to dyke deflection along the contact greatly increases. If there is no Young's modulus mismatch across the contact dyke deflection occurs only if contact material toughness is about 26% of the toughness of the rock on the other side of the contact. When the elastic mismatch increases (to the right), however, dyke deflection will occur even the contact toughness becomes equal to and higher than the toughness of layer 1.

6. Spatial density of volcanic eruptions

The spatial distributions of 432 volcanic eruptions points (monogenetic volcanoes) were examined and are presented on a density map (Fig. 9). ArcGlobe 10.1 was utilised to plot the volcanic vents, with the

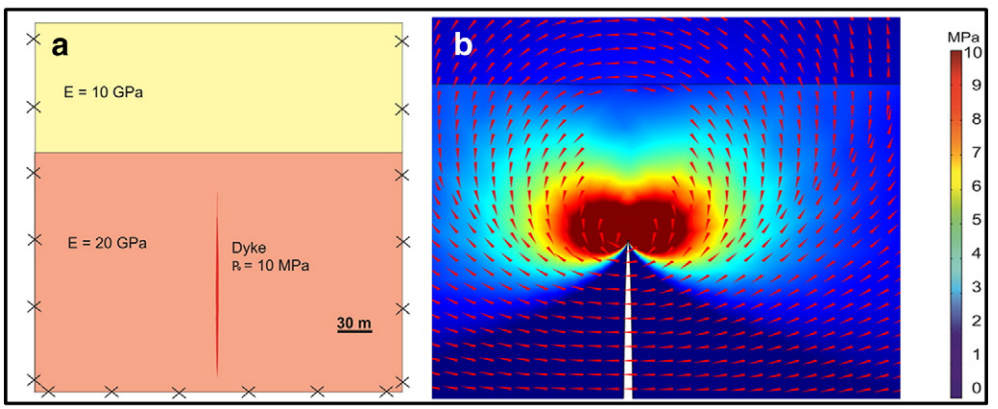

Fig. 6. a) Model setup of two layers with different mechanical properties, the lower layer hosting a dyke. b) Numerical model results showing the stress trajectories of the maximum principal compressive stress σ_1 represented by red arrows, while the colour contours represent maximum principal tensile stressσ_3. This model and subsequent models are fixed at the sides, indicated by crosses, to avoid rigid body rotation and translation.

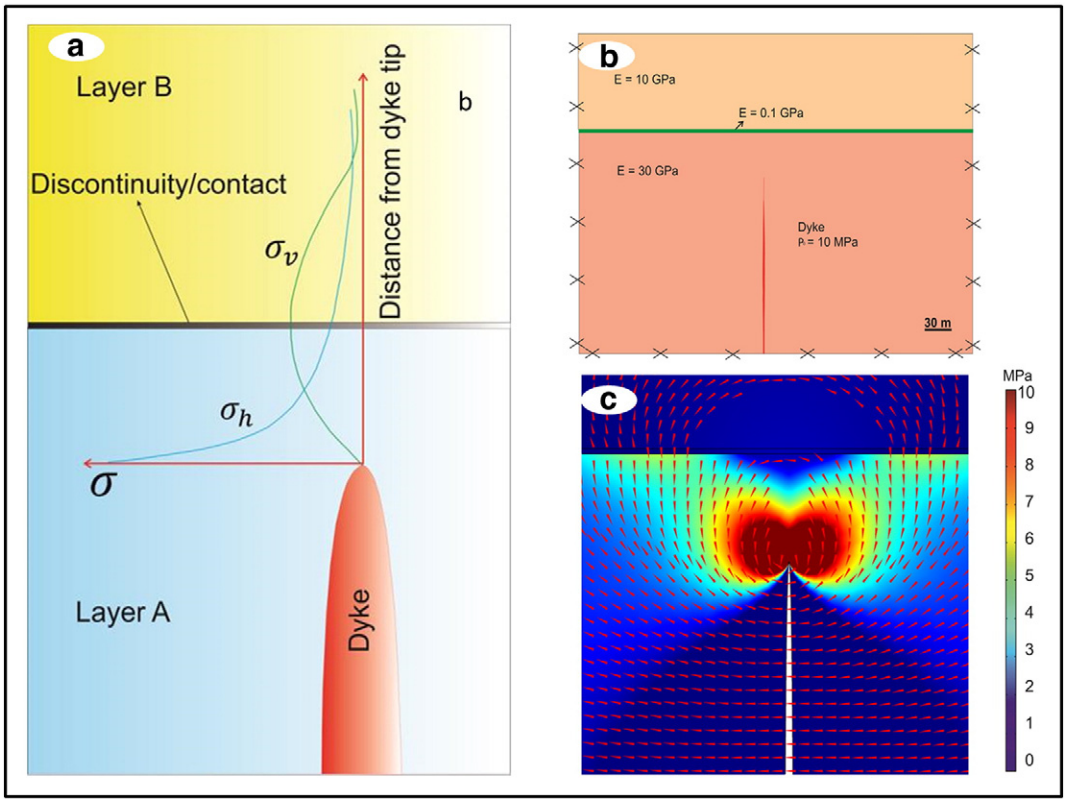

Fig. 7. a) The dyke-parallel tensile stress at the head of propagating dyke is about 20% of the tensile stress perpendicular to the dyke and may open up a weak (low tensile-strength) contact or discontinuity at ahead of the dyke. This is known as Cook-Gordon debonding or delamination mechanism (modified after Thouless and Parmigiani, 2007; cf. Gudmundsson, 2011a). b) A weak contact (green) is modelled as soft thin layer that is located between two stiffer layers. c) Model results showing rotated ticks (trajectories) of σ_1. When a dyke reaches this contact the dyke may become arrested or deflected along the contact depending on magmatic overpressure of the dyke, the contact strength, and the magnitudes of the principal stresses.

shape files of volcanoes imported into ArcMap10.1. The density map calculates the frequency of eruption points or eruptive centres that fall within a neighbourhood around each raster cell. A neighbourhood is defined around each cell centre, and then the cumulative number of eruption points/centres is divided by the area of the neighbourhood.

The spatial density map is drawn by ArcGIS 10.1 for a search radius of 40 km, producing a generalised output raster (Lesti et al., 2008), gives the volcano distribution and density variation in the area. Fractures were added to the map through georeferenced raster images of the geological maps of the AHVP as a guide.

Only volcanoes with clear boundaries were compiled, the main types being lava shields, pyroclastic or scoria cones, and (a few) maars. The volcanic points are clearly clustered (Fig. 9), and some are associated with volcanic fissures. There are two main density subzones. The first occurs in the northern part of the AHVP and is mainly composed of large lava shields and some scoria cones – these constitute the most recent eruption sites in the area. The second occurs in the southern part of the AHVP and is primarily composed of scoria cones, with comparatively few lava shields, yielding smaller eruptions, on average, than in the northern cluster. The lowest frequency of eruption points/centres occurs in the central area between the northern and the southern cluster (Fig. 9). The volcanic fissures (lineaments) are primary WNW-trending, coinciding with the general trend of the main volcanic zone/crustal weakness/fracture zone in the area.

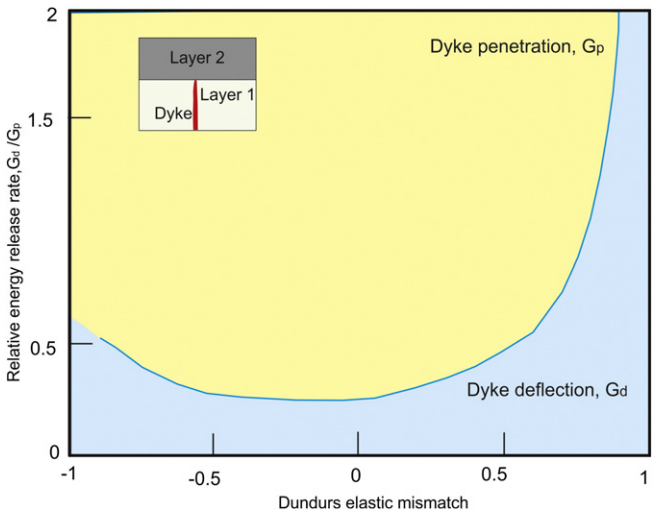

Fig. 8. Schematic illustration of the mechanism of elastic mismatch and material toughness for deflection or penetration of a dyke when it meets a contact. Dyke penetration mainly occurs when Dundurs elastic mismatch across the contact equals zero. The Dundurs parameter becomes negative when the layer hosting the dyke (layer 1) is stiffer than the layer above the contact (layer 2), whereby the dyke has a little propensity to deflection into a sill along the contact. Alternatively, when the Dundurs parameter becomes positive the dyke has great tendency to deflect into sill along the contact.
(Modified after He and Hutchinson, 1989; Hutchinson, 1996).

7. Spatial alignment of volcanic eruptions

The volcanic fissures were obtained through alignments of volcanic points (Fig. 10). When more than one possible alignment could be made, elongate craters are used as an indication of the general trend and the vents along that trend are joined, following a standard method (Paulsen and Wilson, 2009). The strike of the aligned vents is then assumed to coincide with that of a volcanic fissure/feeder-dyke when more recent flows cover part of the fissure.

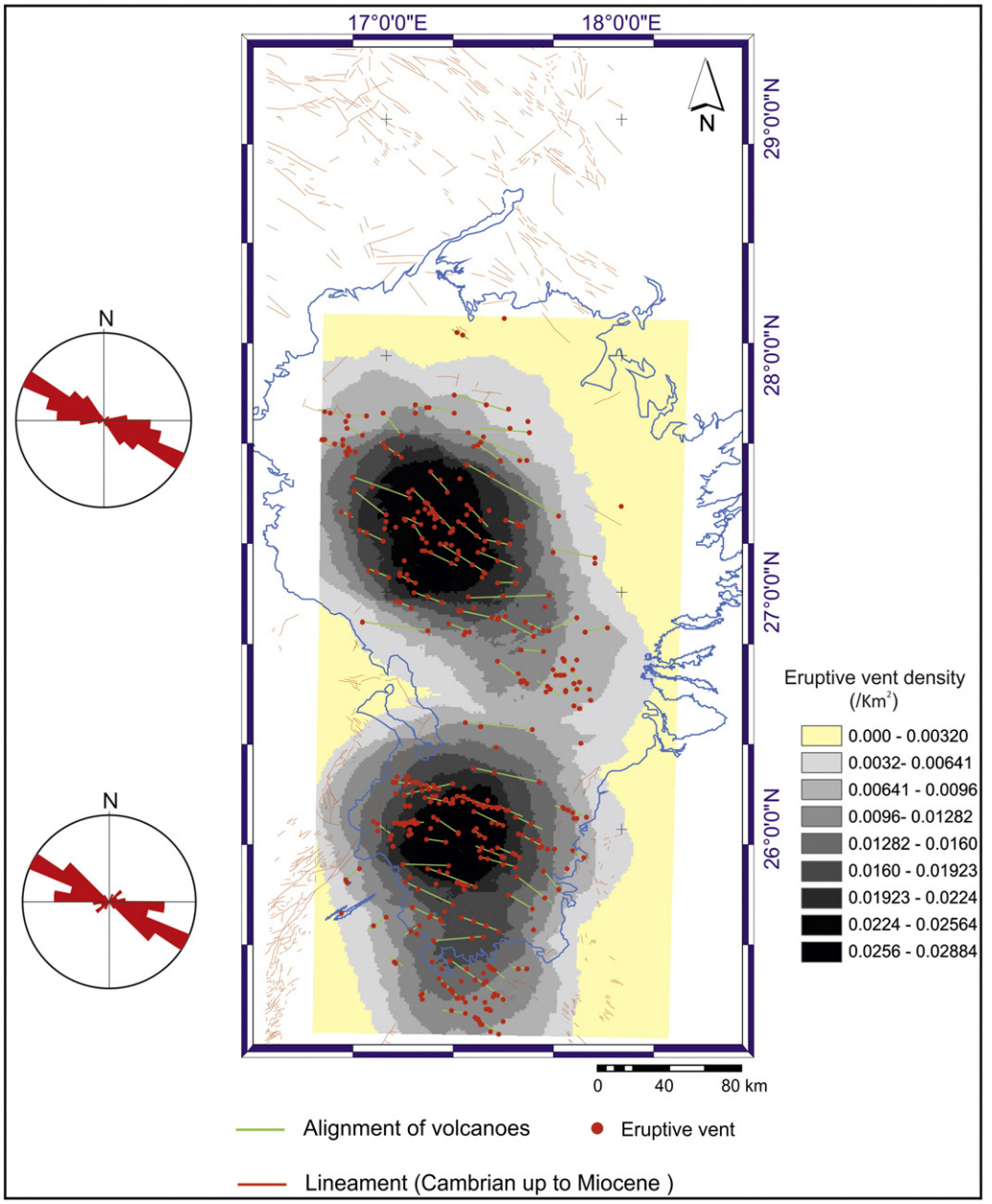

Fig. 9. Density map of the volcanoes of the AHVP. In total 432 eruption points/centres were mapped in this study, most of which are lava shields (small monogentic shield volcanoes) and pyroclastic (scoria) cones. Spatial alignments of the volcanoes, as inferred from satellite imagery, and their trends are plotted in rose diagrams for each density maximum zone. The locations of the lineaments are taken from, Busrewil and Suwesi (1993); Peregi et al. (2003); Less et al. (2006), and Abdunaser and McCaffrey (2014).

The rose diagrams for the strike of volcanic fissures, made using the GEOrient software, show that WNW-ESE trends dominate, with small NE-SW subsets. Rose diagrams for some 1000 (mostly normal) faults, extension fractures and alignments of volcanoes in the area show two main sets (Fig. 11a,b,c). One set strikes WNW-ESE, while other set of strikes between NE and ENE, which is similar to that of some of the large volcanic ridges in the area (Fig. 3a,b). The length-size distribution of these fractures is roughly log-normal, as is common for fractures (Fig. 11a,b,c; Babiker and Gudmundsson, 2004).

8. Structural evolution of the Al Haruj Volcanic Province

The tectonic evolution of the AHVP may be divided into five main deformation episodes or phases (Peregi et al., 2003), each of which is characterised by structural elements that differ in orientation (and thus in associated stress fields) and timing from the elements of other phases (Appendix II). The main structural features in the area relate to Phase IV and V, which occurred during Palaeogene–Quaternary and can be linked to the most recent evolution of the Sirt Basin (Cvetković et al., 2010). In particular, during phase IV most of the Al Haruj region was subject to NE-SW oriented tension, roughly perpendicular to main structural elements in the northern and central parts of the area (Less et al., 2006). Similarly trending structural elements have been identified in the central and western parts of the Sirt Basin (Anketell, 1996; Abadi et al., 2008; Abdunaser and McCaffrey, 2015).

In contrast to the local stress field of the AHVP, the regional stress field for the whole area, including the Sirt Basin, relates to NW-SE compression and NE-SW extension (Appendix III; Less et al., 2006). Abdunaser and McCaffrey (2015) inferred from 2D seismic lines and borehole data that the structure of the south-western part of the Sirt

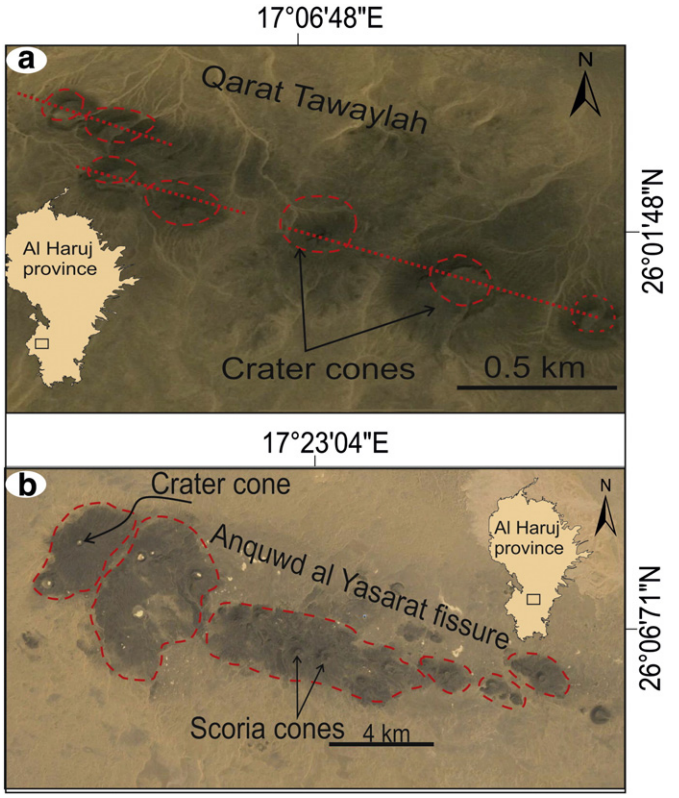

Fig. 10. Satellite images (adapted from Google Earth) showing examples of spatial alignment of volcanic eruption points/centres in the southern portion of the AHVP. a) NW-SE trending alignments of volcanoes. The long axes of the craters and alignments mark the strike orientation the subsurface feeder-dykes (cf. Paulsen and Wilson, 2009). b) WNW-ESE trend inferred from several pyroclastic/scoria cones. The inset maps provided the location.

Basin is primarily composed of high-angle normal faults striking NNW-SSE and related to late Cretaceous to Eocene extensional tectonics superimposed on inherited Pan-African basement structures (early Palaeozoic) and pre-existing Hercynian structures (late Palaeozoic-early Mesozoic) (Fig. 12). Pre-existing structural elements are likely to have affected the volcanic activity in the AHVP, to which we turn now.

9. Discussion

9.1. Role of pre-existing fracture zones in providing magma paths

One principal question that arises is why and how magma reaches the surface in the AHVP, and what the relation is, if any, between the volcanic activity in AHVP and the tectonic activity in the nearby Sirt Basin. Here we discuss the interaction between faults and dykes, both with reference to earlier data and models as well as our own results.

During the last two decades a substantial amount of deep hydrocarbon wells have been drilled throughout the Sirt Basin. Using these data, Busrewil et al. (2012) suggest that the Cretaceous basaltic rocks (100–130 Ma) within the Nubain clastics in Al Hameimat Trough, NE Sirt Basin, were fed by dykes that may partly have used high angle normal faults as paths (Fig. 13). It is well known that dykes use pre-existing structures, primarily joints but sometimes high-angle (primarily normal) faults, to form their paths (Delaney et al., 1986; Gudmundsson, 2011a; Gudmundsson et al., 2010; Magee et al., 2013; Bedard et al., 2012; Tibaldi, 2015), so the idea is worth analysing.

Fault zones are composed of two main mechanical units or zones, a fault core and a fault damage zone (Fig. 14). In large fault zones the damage zone may reach thickness of up to a few kilometres, but is more commonly of the order of tens to hundreds of metres (Gudmundsson et al., 2010). The damage zone may contain breccia, but is characterised by fractures whose frequency varies (mostly irregularly) with distance from the core. By contrast, the core, commonly several metres thick in major fault zones, consists primarily of gouge and breccia. The boundary between damage zone and host rock vary along the fault and change spatially and temporarily with the evolution of the fault zone in active fault whereas in inactive faults the contact between them is generally sharp (Gudmundsson, 2011a).

When a dyke approaches a mechanically weak discontinuity (i.e., one with low tensile strength) such as an active fault, the dyke may open up the discontinuity and, depending on the magmatic overpressure and the local stress field, enter the discontinuity. This is known from field observations and also from numerical models. For example, many dykes have been observed to follow steep normal faults for a while, both in the active and in the palaeo-rift zones of Iceland (Gudmundsson, 1995). Numerical models (Gudmundsson et al., 2010) show that a dyke meeting with a steep and mechanically weak normal fault tends to open up the fault and then use it as a part of the dyke path. Thus, although most dykes do not use faults as channels, the potential for a steep, active and weak normal fault to form a part of a dyke path is well established.

To explore this possibility further, we considered the interaction between a mechanically strong fault and a propagating dyke. More specifically, we model the core of the fault as stiff in relation to the damage zone. The idea here is to test if such fault zones might also function as a channel for magma. The core may become stiff primarily in two ways. First, through compaction and secondary mineralisation; second, through being injected by earlier dykes. It is the latter that we focus on here, given that many dykes are multiple and formed over considerable periods of time (Gudmundsson, 1995).

In the model, the fault zone is thus divided into a comparatively stiff core and soft damage subzones on either side of the core (cf. Browning and Gudmundsson, 2015; Fig. 15). The only loading is magmatic overpressure of 10 MPa in the dyke, as estimated above. The rock hosting the fault zone has a Young's modulus of 20 GPa, and Poisson's ratio 0.25, both of which are typical values for rocks similar to those in the Sirt Basin. In the first model (Fig. 15a) Young's modulus of the core is 10 GPa, and that of the damage subzones 1 GPa, whereas in the second model (Fig. 15c), the core is made very stiff (30 GPa). The models thus assume strain hardening, that is, a core that is stiffer (perhaps due do mineralisation and/or compaction or earlier dykes) than the damage zone. The numerical results (Fig. 15b, d) indicate that for both models the trajectories of maximum principal stress field σ_1 tend to rotate and become deflected towards the fault plane, suggesting that the fault may capture the dyke propagation path for a while. These numerical results imply that local stress field may, from time to time, favour dyke propagation along the fault zone, both for soft as well as for stiff steep normal faults, in which case the faults may have acted as parts of the dyke paths to the surface.

9.2. Future volcano-tectonic activity of the AHVP

Many of the volcanic features of the AHVP, particularly in its northern subzone, appear very recent, based on well-preserved inflation features such as tumuli and lava rises as well as modern age dating by Nixon et al. (2014) who concluded that the youngest lava flows are of late Holocene age (2.31 ka). It follows that it is likely that the AHVP has still the potential to erupt, that is, is still active. One indication of volcano-tectonic activity is earthquakes. An earthquake network, however, was established only very recently (past decade) in Libya, and given that there is generally not much seismic activity in the country, the information is so far limited.

Data on historical earthquakes have, however, been collected. And some of the recorded earthquakes may be associated with magmatism. For example, earthquake swarms have been reordered in Hun Graben

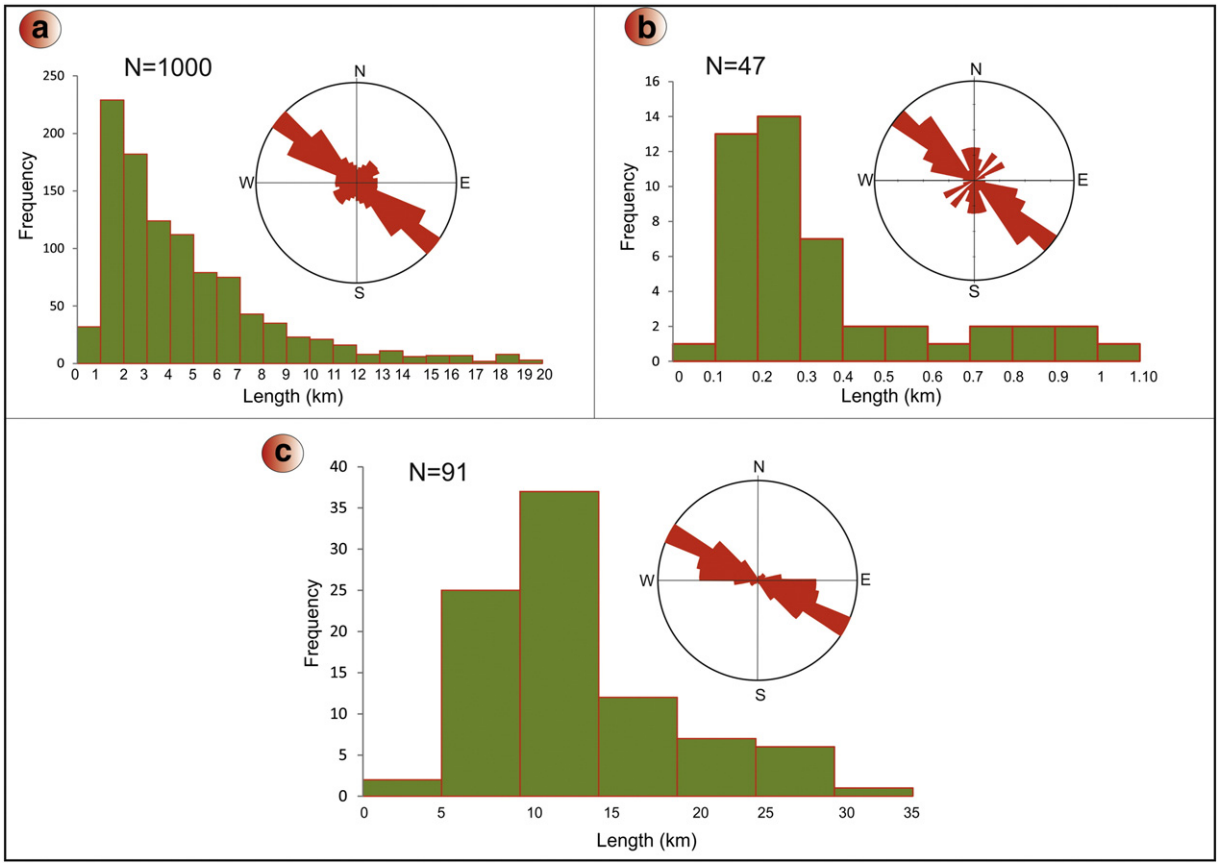

Fig. 11. Rose diagrams and frequency distributions of a) 1000 faults (mostly normal faults) mapped from available geological maps of the Al Haruj region, b) 47 dykes and volcanic fissures, c) 91 alignment of eruption points/centres. Length-size distributions of these lineaments are roughly lognormal.

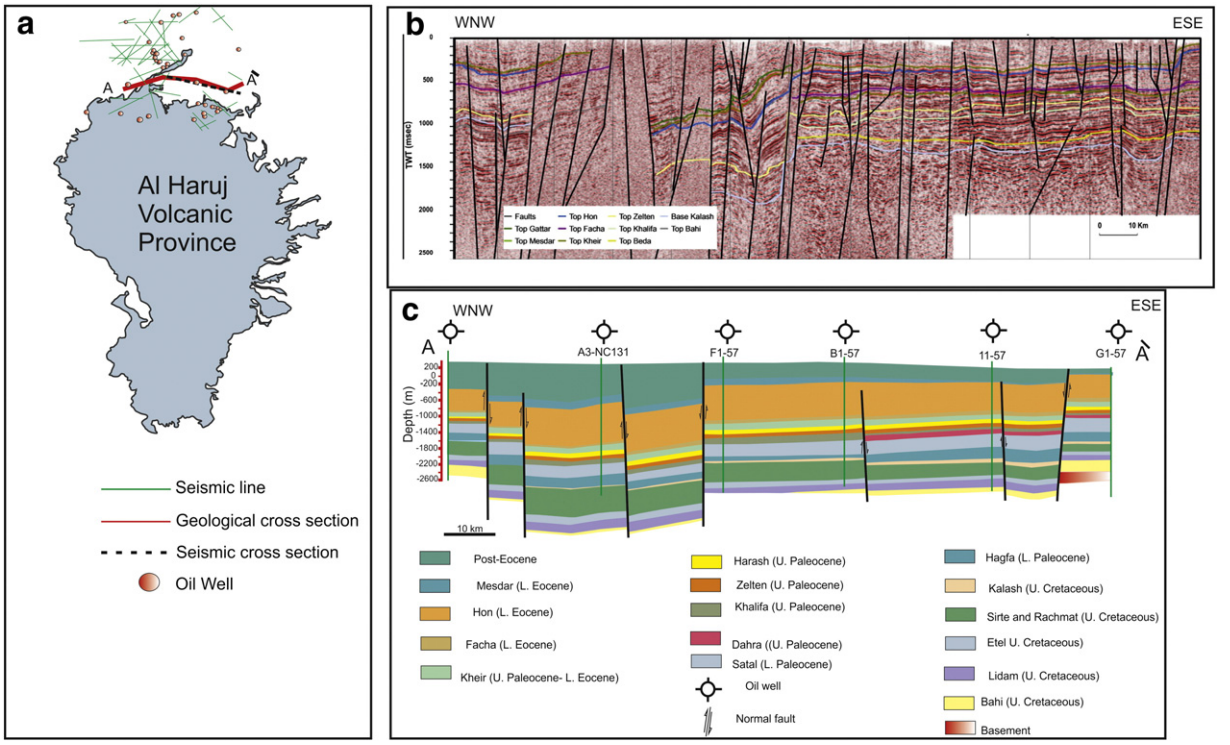

Fig. 12. a) Location of oil wells, seismic lines, and cross-sections in the northernmost of the AHVP. b) Seismic section, most of these high-angle normal faults (Abdunaser and McCaffrey, 2015). c). Geological cross section inferred from borehole data.
(Modified from Abdunaser and McCaffrey, 2015).

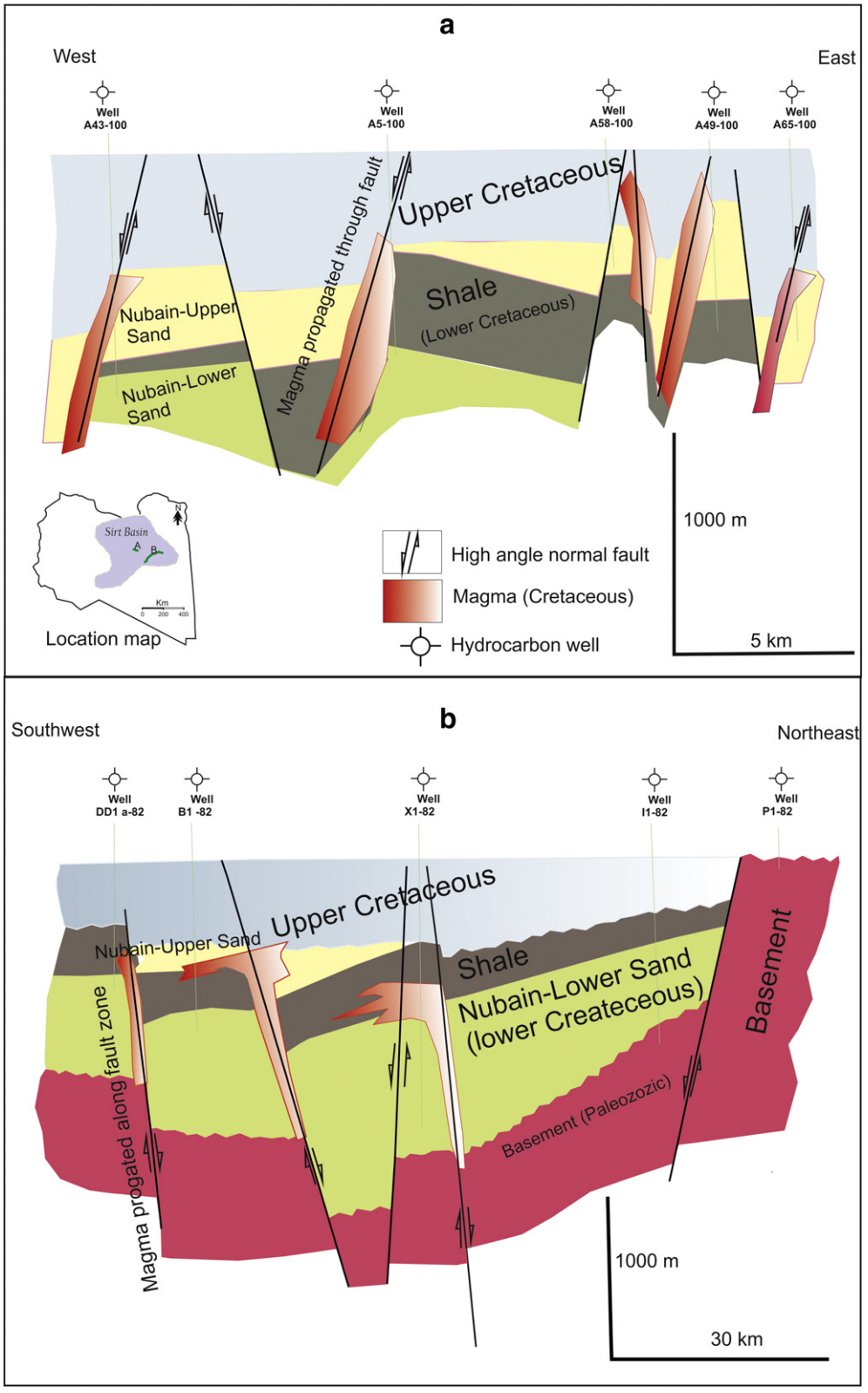

Fig. 13. Cross sections inferred from boreholes data in the Al Hameimat Trough, SE Sirt Basin. Both cross sections, a and b, show high-angle normal faults, some of which may have acted as channels for magma, that is, parts of dyke paths.
(Modified after Busrewil et al., 2012).

(northwestern Libya, Fig. 2) with earthquake magnitudes >M7.1 in 1935 and >M6 in 1939, 1940, 2000 and 2001, respectively (Hasen, 1983; Al-Heety, 2011). Earthquake swarms in volcanic regions are commonly related to magma migration, and could be so in these cases as well. Since the Hun Graben extends to the AHVP, the earthquake swarms, at least some of them, may be related to active magma

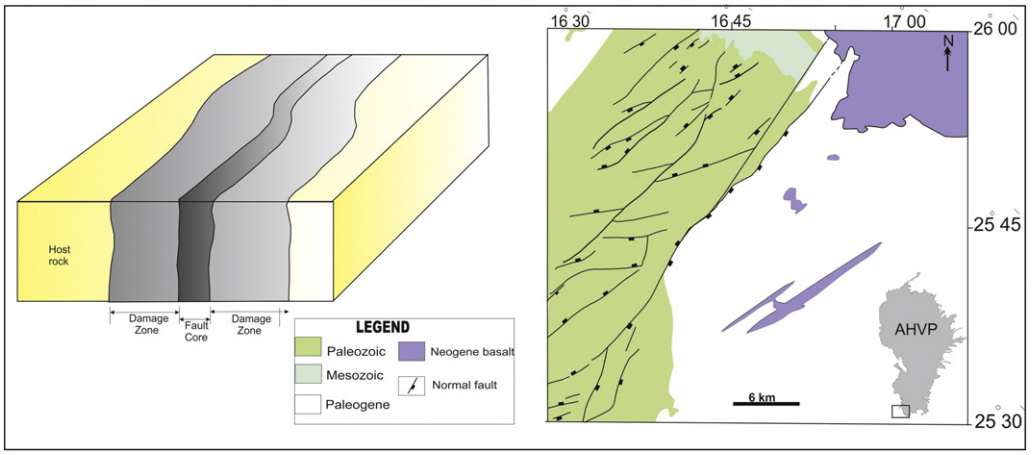

Fig. 14. Left: schematic model of the internal structure of a fault zone (here a strike-slip fault) consisting of a damage zone and a fault core (modified after Gudmundsson et al., 2010). Right: geological map showing part of pre-existing normal faults (Palaeozoic and Mesozoic) that may have very stiff cores favouring dykes using the faults as parts of their paths. (Modified from Less et al., 2006).

migration beneath or close to the AHVP. Also, earthquakes on active faults are commonly triggered by high fluid pressure. If some of the faults are used as paths for magma in AHVP (Bagnardi, 2014), the magmatic pressure along the faults would tend to trigger slip on the faults and earthquakes. All these will become better established in the coming years as the new seismic network in Libya collects more earthquake data. While it is not certain, it seems plausible that the AHVP is still being volcanically and tectonically active (Bardintzeff et al., 2012; Boote et al., 2012).

10. Conclusions

- The Al Haruj Intra-continental Volcanic Province (AHVP) in Libya is the largest part of an extensive volcanic province, covering an area

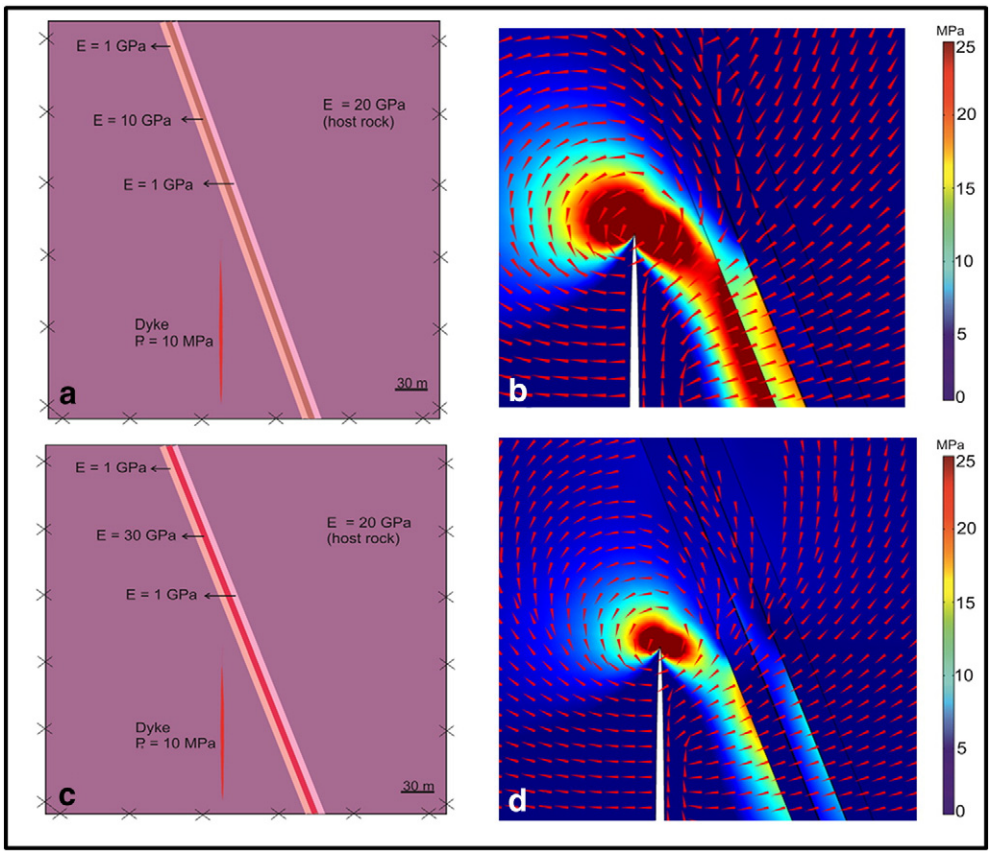

Fig. 15. a) Setup showing how the host rock and fault zone are modelled using different values for Young's modulus. The fault zone is modelled as a high-angle normal fault, similar in attitude to many normal faults observed in Al Haruj region and the Sirt Basin. b) Results of the numerical models. Large tensile stress σ_3 occurs in the area between dyke tip and fault plane. Trajectories of maximum principal stress σ_1 are rotated and could deflect the magma/dyke path into the fault plane. This and subsequent numerical model reveal the variation in the local stresses within fault zones. c) The fault core is modelled as a stiff layer (red layer) to simulate strain hardening (mineralisation, compaction) and/or previous dyke intrusions. d) Numerical model results displaying maximum compressive principal stress σ_1 are clearly deflected towards the fault plane.

of approximately 42,000 km^2. It is likely that the AHVP developed primarily during the early Pliocene to late Pleistocene, in response to tectonic rifting and evolution of the Sirt Basin, but it may still be active. Considerable attention has been focused on the AHVP in the last three decades, particularly with respect to its stratigraphy, geochemistry and geochronology. By contrast, volcano-tectonics of the area has received very little attention.

- The spatial distribution of around 432 eruption points or centres in the AHVP shows clustered distributions. Alignments of points/centres suggest that pre-existing structures, mainly along WNW to NW late Mesozoic-Cenozoic structures and along NE to NNE late Palaeozoic-early Mesozoic structures, exert some influence on the preferential of a magma pathway to reach the surface. The spatial distributions of volcanic eruptions reveal the presence of two maxima clustering of volcanoes.
- Volcanic fissures/crater rows are very common in the AHVP and mostly confined to the central and southernmost part of this region. Comparatively few dykes have been identified, but those that have occur mainly in elongated swarms outside the main volcanic system. The geometry of the volcanoes may be partly governed by pre-existing fractures and faults; which in turn play a significant role in the spatial distribution of volcanic fissures and dykes in the area.
- The magmatic overpressure of 47 dykes and volcanic fissures is estimated based on their aspect (trace length/thickness) ratios. Most of the obtained values indicate overpressures between around 8 MPa (when host-rock Young's modulus $E = 7$ GPa) and 19 MPa (when host-rock Young's modulus $E = 15$ GPa). These results are very reasonable and similar to those obtained from basaltic dykes in other volcanic regions.
- Numerical models were made to explore the local stress field around and within a fault zone when a dyke approaches it. In the models, the fault zone is divided into a comparatively stiff core (attributed to strain hardening) and softer damage zones on either side of the core. The numerical results indicate that the trajectories of maximum principal stress field σ_1 tend to rotate and become deflected towards the fault plane. Our findings suggest that steeply dipping faults, particularly normal faults, may capture propagating dykes for a while and act as parts of their paths.

Supplementary data to this article can be found online at http://dx.doi.org/10.1016/j.jvolgeores.2016.06.025.

Acknowledgements

AE thanks the Libyan Ministry of Higher Education for the financial support and John Browning and Marco Neri for very helpful review comments.

References

Abadi, A.M., van Wees, J.D., van Dijk, P.M., Cloetingh, S.A.P.L., 2008. Tectonics and subsidence evolution of the Sirt Basin, Libya. Am. Assoc. Pet. Geol. Bull. 92, 993–1027.
Abdunaser, K., McCaffrey, K., 2014. Rift architecture and evolution: the Sirt Basin, Libya: the influence of basement fabrics and oblique tectonics. J. Afr. Earth Sci. 100, 203–226.
Abdunaser, K., McCaffrey, K., 2015. Tectonic history and structural development of the Zallah-Dur al Abd Sub-basin, western Sirt Basin, Libya. J. Struct. Geol. 73 (2015), 33–48.
Abebe, T., Mazzarini, F., Innocenti, F., Manetti, P., 1998. The Yerer Tullu Wellel volcano-tectonic lineament: a transtensional structure in central Ethiopia and the associated magmatic activity. J. Afr. Earth Sci. 26, 135–150.
Al-Hafdh, N., El-Shaafi, A., 2015. Geochemistry and petrology of basic volcanic rocks of Jabal Al Haruj Al-Aswad, Libya. Int. J. Geosci. 6, 109–144. http://dx.doi.org/10.4236/ijg.2015.61008.
Al-Heety, E., 2011. Seismicity and seismotectonics of Libya: as an example of intraplate environment. Arab. J. Geosci. 6, 193–204. http://dx.doi.org/10.1007/s12517–011-0347-y (2011).
Ambrose, G., 2000. The geology and hydrocarbon habitat of the Sarir Sandstone, SE Sirt Basin, Libya. J. Pet. Geol. 23, 165–191.
Anketell, M., 1996. Structural history of the Sirt Basin and its relationship to the Sabratah Basin and Cyrenaican Platform, northern Libya. In: Salem, M.J., Busrewil, M.T., Misallati, A.A., Sola, M.A. (Eds.), The Geology of Libya.
Babiker, M., Gudmundsson, A., 2004. Geometry, structure and emplacement of mafic dykes in the Red Sea Hills, Sudan. J. Afr. Earth Sci. 38, 279–292.
Bagnardi, M., 2014. Dynamics of magma supply, storage and migration at basaltic volcanoes: geophysical studies of the Galápagos and Hawaiian volcanoes (PhD thesis) Scholarly Repository. Electronic Theses and Dissertations. University of Miami, USE.
Bardintzeff, J., Deniel, H., Guillou, B., Platevoet, P.T., Oun, K., 2012. Miocene to recent alkaline volcanism between Al Haruj and Waw an Namous (southern Libya). Int. J. Earth Sci. 101 (2012), 1047–1063.
Barnett, Z., Gudmundsson, A., 2014. Numerical modelling of dykes deflected into sills to form a magma chamber. J. Volcanol. Geotherm. Res. 281 (2014), 1–11.
Becerril, L., Galindo, L., Gudmundsson, A., Marales, J., 2013. Depth of origin of magma in eruptions. Sci. Rep. 3, 2762. http://dx.doi.org/10.1038/srep02762.
Bedard, J., Naslund, H., Nabelek, P., Winpenny, A., Hryciuk, M., Macdonald, W., Hayes, B., Steigerwaldt, K., Hadlari, T., Rainbird, R., Dewing, K., Girard, E., 2012. Fault-mediated melt ascent in a Neoproterozoic continental flood basalt province, the Franklin sills, Victoria Island, Canada. Geol. Soc. Am. Bull. 124, 723–736.
Boote, D., Dardour, A., Green, P., Smewing, J., Van Hoeflaken, F., 2012. Burial and unroofing history of the base Tanezzuft 'hot' Shale source rock, Murzuq Basin, SW Libya: new AFTA constraints from basin margin outcrops. 4th Sedimentary Basins of Libya Symposium: The Geology of Southern Libya, 17–20th November 2008, Tripoli, Libya.
Browning, J., Gudmundsson, A., 2015. Caldera faults capture and deflect inclined sheets: an alternative mechanism of ring dike formation. Bull. Volcanol. 77, 4. http://dx.doi.org/10.1007/s00445–014–0889-4 (2015).
Browning, J., Drymoni, K., Gudmundsson, A., 2015. Forecasting magma-chamber rupture at Santorini volcano, Greece. Sci. Rep. http://dx.doi.org/10.1038/srep15785.
Burke, K., 1996. The African plate, South African. J. Geol. 99, 341–409.
Busrewil, M., 1996. The volcanology of central Jabal al Haruj al Aswad volcanic province, Central Libya. The Geology of Sirt Basin vol. III. Elsevier, Amsterdam, pp. 331–345.
Busrewil, M., 2012. Evolution of Al Haruj Volcanic Province, Central Libya. Geol. South. Libya 3 (2012).
Busrewil, M., Suwesi, K., 1993. Geological Map of Libya 1: 250.000, Sheet: Al Haruj Al Aswad NG(33-4). Explanatory Booklet. Industrial Research Centre, Tripoli, p. 95.
Busrewil, M., Oun, K., Haman, M., 2012. Petrology and tectonic setting of Hameimaat Magmatic Rocks, SE Sirt Basin, Libya. Geol. South. Libya 3, 189–210 (2012).
Cartwright, J., Hansen, M., 2006. Magma transport through the crust via interconnected sill complexes. Geology 34, 929–932.
Chen, N., Dong, J., Chen, J., Dong, C., Shen, Z., 2014. Geometry and emplacement of the Late Cretaceous mafic dyke swarms on the islands in Zhejiang Province, Southeast China: insights from high-resolution satellite images. J. Asian Earth Sci. 7 (2014), 302–311.
Cvetković, V., Toljić, M., Ammar, A., Rundić, L., Trish, K.B., 2010. Petrogenesis of the eastern part of the Al Haruj basalts (Libya). J. Afr. Sci. 58, 37–50.
Delaney, P., Pollard, D., 1981. Deformation of host rocks and flow of magma during growth of minette dikes and breccia-bearing intrusions near Ship Rock, New Mexico. U.S. Geol. Surv. Prof. Pap. 1202.
Delaney, P., Pollard, D., Zlony, I., McKee, H., 1986. Field relations between dikes and joints: emplacement processes and paleostress analysis. J. Geophys. Res. 91, 4920–4938.
Drury, S., 2001. Image Interpretation in Geology. Blackwell Science, Nelson Thornes, UK, p. 290.
Farahat, S., Abdel Ghani, S., Aboazom, S., Asran, H., 2006. Mineral chemistry of Al Haruj low-volcanicity rift basalts, Libya: implications for petrogenetic and geotectonic evolution. J. Afr. Sci. 45, 198–212.
Francesco, M., D'Orazio, M., 2003. Spatial distribution of cones and satellite-detected lineaments in the Pali Aike Volcanic Field (southernmost Patagonia): insights into the tectonic setting of a Neogene rift system. J. Volcanol. Geotherm. Res. 125, 291–305.
Geshi, N., Kusumoto, S., Gudmundsson, A., 2010. Geometric difference between nonfeeders and feeder dikes. Geology 38, 195–198.
Gudmundsson, A., 1990. Emplacement of dikes, sills, and crustal magma chambers at divergent plate boundaries. Tectonophysics 176, 257–275.
Gudmundsson, A., 1995. Infrastructure and mechanics of volcanic systems in Iceland. J. Volcanol. Geotherm. Res. 64, 1–22.
Gudmundsson, A., 2011a. Rock Fractures in Geological Processes. Cambridge University Press, Cambridge http://dx.doi.org/10.1017/CBO9780511975684.
Gudmundsson, A., 2011b. Deflection of dykes into sills at discontinuities and magma chamber formation. Tectonophysics 500, 50–64.
Gudmundsson, A., Løtveit, I., 2012. Sills as fractured hydrocarbon reservoirs: examples and models. Geol. Soc. Lond., Spec. Publ. 374. http://dx.doi.org/10.1144/SP374.5.
Gudmundsson, A., Simmenes, T., Larsen, B., Philipp, S., 2010. Effects of internal structure and local stresses on fracture propagation, deflection,and arrest in fault zones. J. Struct. Geol. 32, 1643–1655.
Gudmundsson, A., Lecoeur, N., Mohajeri, N., Thordarson, T., 2014. Dike emplacement at Bardarbunga, Iceland, induces unusual stress changes, caldera deformation, and earthquakes. Bull. Volcanol. 76, 869. http://dx.doi.org/10.1007/s00445-0869-9.
Hansen, M., Cartwright, J., 2006. Saucer-shaped sill with lobatemorphology revealed by 3D seismic data: implications for resolving a shallow-level sill emplacement mechanism. J. Geol. Soc. Lond. 163, 509–523.
Hasen, H., 1983. Seismicity of Libya and Related Problems (Master thesis) Civil Engineer Department, Colorado state University, p. 108.
He, M.Y., Hutchinson, J.W., 1989. Crack deflection at an interface between dissimilar elastic materials. Int. J. Solids Struct. 31, 3443–3455.
Holt, S., Holford, S., Foden, J., 2014. New insights into the magmatic plumbing system of the South Australian Quaternary Basalt province from 3D seismic and geochemical

data. Aust. J. Earth Sci. 60, 797–816. http://dx.doi.org/10.1080/08120099.2013.865143.
Hutchinson, J.W., 1996. Stresses and failure modes in thin films and multilayers. Notes for a Dcamm Course Techincal University of Denmark, Lyngby (1–45 pp.).
Klitzsch, E., 2000. The structural development of the Murzuq and Kufra basins - significance for oil and mineral exploration. In: Sola, M.A., Worsley, D. (Eds.), Symposium on Geological Exploration in Murzuq Basin. Elsevier, Amsterdam, pp. 143–150.
Kusumoto, S., Geshi, N., Gudmundsson, A., 2013. Aspect ratios and magma overpressures of non-feeder dikes observed in the Miyake-jima volcano (Japan), and fracture toughness of its upper part. Geophys. Res. Lett. 40, 1–5. http://dx.doi.org/10.1002/grl.50284.
Le Corvec, N., Sporl, B., Rowland, J., Lindsay, J., 2013. Spatial distribution and alignments of volcanic centers: clues to the formation of monogenetic volcanic fields. Earth Sci. Rev. 124, 96–114.
Less, Gy., Turki, S. M., Suwesi, S. Kh., Peregi, L. F., Koloszar, L., Kalmar, J., Sherif, Kh., Csaszar, G., Gulasci, Z., Dalum, H., Al Tajuri, A., 2006. Explanatory Booklet. Geological Map of Libya 1: 250.000. Sheet: Waw Al Kabir NG 33-12. Industrial Research Centre, 295 p.
Lesti, C., Giordano, G., Salvini, F., Cas, R., 2008. Volcano tectonic setting of the intraplate, Pliocene-Holocene, Newer Volcanic Province (southeast Australia): role of crustal fracture zones. J. Geophys. Res. 113, B07407. http://dx.doi.org/10.1029/2007JB005110, 2008.
Magee, C., Jackson, C., Schofield, N., 2013. The influence of normal fault geometry on igneous sill emplacement and morphology. Geology 41, 407–410.
Martin, U., Né meth, K., 2006. How Strombolian is a "Strombolian" scoria cone? Some irregularities in scoria cone architecture fromthe Transmexican Volcanic Belt, near Volca'n Ceboruco, (Mexico) and Al Haruj (Libya). J. Volcanol. Geotherm. Res. 155 (1–2), 104–118.
Mohamed, M., 2014. Composition and Age of Cenozoic Volcanism in Libya (PhD thesis) University of Glasgow. Glasgow Theses Service.
Mouzughi, J., Taleb, T., 1981. Tectonic Elements of Libya (1:2,000,000). National Oil Corporation of Libya.
Nixon, S., Maclennan, J., White, N., 2014. Intra-plate magmatism of the Al Haruj Volcanic Field, Libya. Goldschmidt Conference Abstracts.
Pacific Aero Survey Co., 1979. Air borne geophysical survey Jabal Al Haruj Al Aswad area. Final Report. Qeb., Inc., Hayward, California (29 pp.).
Paulsen, T., Wilson, T., 2009. Structure and age of volcanic fissures on Mount Morning: a new constraint on Neogene to contemporary stress in the West Antarctic Rift, southern Victoria Land, Antarctica. Geol. Soc. Am. 1071–1089.
Peregi, Zs., Less, G. Y., Konrad, Gy., Fodor, L., Gulacsi, Z., Gyalog, L., Turki, S. M., Suwesi, S. Kh., Sherif, Kh., Dalub, H., 2003. Explanatory Booklet. Geological Map of Libya 1: 250.000. Sheet: Al Haruj Al Abyad NG 33-8. Industrial Research Centre, Tripoli, 248 p.
Planke, S., Rasmussen, T., Rey, S., Myklebust, R., 2005. In: Doré, A.G., Vining, B.A. (Eds.), Seismic characteristics and distribution of volcanic intrusions and hydrothermal vent complexes in the Vøring and Møre Basins.
Poland, P., Moats, P., Fink, H., 2008. A model for radial dike emplacement in composite cones based on observations from Summer Coon volcano, Colorado, USA. Bull. Volcanol. 70, 861–875. http://dx.doi.org/10.1007/s00445-007-0175-9.
Polteau, S., Ferré, C., Planke, S., Neumann, R., Chevallier, L., 2008. How are saucer shaped sills emplaced? Constraints from the Golden Valley Sill, South Africa. J. Geophys. Res. 113, B12104. http://dx.doi.org/10.1029/2008JB005620 (Article number B12104).
Qui, K., Gherryo, Y., Shatwan, M., Fuller, J., 2008. The application of the mechanical earth model on rejuvenation of a mature field in Libya. Copyright 2008, IADC/SPE Asia Pacific Drilling Technology Conference and Exhibition, Jakarta, Indonesia (16 pp.).
Rajesh, M., 2004. Application of remote sensing and GIS in mineral resource mapping an overview. J. Mineral. Petrol. Sci. 99, 83–103.
Tabatabaian, M., 2014. Comsol for Engineers. Mercury Learning and Information, Boston.
Thomson, K., Schofield, N., 2008. Lithological and structural controlson the emplacement and morphology of sills in sedimentary basins. J. Geol. Soc. Lond. Spec. Publ. 302, 31–44.
Thouless, M.D., Parmigiani, J.P., 2007. Mixed-mode cohesive-zone models for delamination and deflection in composites. In: Sørensen, B.F., Mikkelson, L.P., Lilhot, H., Goutianos, S., Abdul-Mahdi, F.S. (Eds.), Proceedings of the 28th Risø International Symposium on Materials Science: Interface Design of Polymer Matrix Composites, pp. 93–111 (Roskilde (Denmark)).
Tibaldi, A., 2015. Structure of volcano plumbing systems: a review of multi-parametric effects. J. Volcanol. Geotherm. Res. 298, 85–135. http://dx.doi.org/10.1016/j.jvolgeores.2015.03.023 (2015).
Wise, U., Funicello, R., Parotto, M., Salvini, F., 1985. Topographic lineament swarms: clues to their origin from domain analysis of Italy. Geol. Soc. Am. Bull. 96, 952–967.
Zakir, A., Quari, T., Mostafa, E., 1999. New optimizing technique for preparing lineament density maps. Int. J. Remote Sens. 20, 1073–1085.

Chapter 6: Distribution and size of lava shields on the Al Haruj al Aswad and the Al Haruj al Abyad Volcanic Systems, Central Libya

www.sciencedirect.com/science/article/pii/S0377027316302438

Journal of Volcanology and Geothermal Research

Abdelsalam Elshaafi and Agust Gudmundsson

Statement of contribution:

The origin idea and data collections were developed by AE

Analytical approach and numerical models were made by AE

The first draft and figures were prepared by AE with later critical revision done by co-author

Interpreted data along with conceptual model carried out by AE with substantial support from co-author

Journal of Volcanology and Geothermal Research 338 (2017) 46–62

Contents lists available at ScienceDirect

Journal of Volcanology and Geothermal Research

journal homepage: www.elsevier.com/locate/jvolgeores

Distribution and size of lava shields on the Al Haruj al Aswad and the Al Haruj al Abyad Volcanic Systems, Central Libya

Abdelsalam Elshaafi *, Agust Gudmundsson

Department of Earth Sciences, Royal Holloway University of London, Egham TW20 0EX, UK

ARTICLE INFO

Article history:
Received 5 August 2016
Received in revised form 28 February 2017
Accepted 10 March 2017
Available online 16 March 2017

Keywords:
Lava shields
Monogenetic volcanoes
Shield volcanoes
Eruption mechanisms
Magma reservoirs
Iceland
Galapagos
Hawaii

ABSTRACT

The Al Haruj Volcanic Province (AHVP) consists of two distinct volcanic systems. In the north is the system of Al Haruj al Aswad, covering an area of 34,200 km^2, while in the south the system of Al Haruj al Abyad, covering an area of 7,850 km^2. The systems have produced some 432 monogenetic volcanoes, primarily scoria (cinder) cones, lava shields, and maars. The density distribution of the volcanoes in each system, plotted as eruption points or sites, has a roughly elliptical surface expression, suggesting similar plan-view geometry of the magma sources, here suggested as deep-seated reservoirs. More specifically, the Al Haruj al Aswad magma reservoir has major and minor axes of 210 km and 119 km, respectively, and an area of 19,176 km^2, the corresponding figures for the Haruj al Abyad reservoir being 108 km and 74 km, for the axes, and 6209 km^2 for the area. We measured 55 lava shields on the AHVP. They are mostly restricted to the northern and southern parts of AHVP and date from late Miocene to (at least) the end of Pleistocene, while some may have been active into Holocene. In fact, although primarily monogenetic, some of the lava shields show evidence of (possibly Holocene) fissure eruptions in the summit parts. The early lava shields tend to be located at the edges of volcanic systems and with greater volumes than later (more central) shields. The average lava shield basal diameter is 4.5 km and height 63 m. There is strong linear correlation between lava shield volume and basal area, the coefficient of determination (R^2) being about 0.75. When 22 Holocene Icelandic lava shields are added to the dataset, for comparison, the correlation between volume and basal area becomes $R^2 = 0.95$. Numerical models suggest that the local stress fields favoured rupture and dyke injection at the margins of the source reservoirs during late Miocene – early Pliocene, in agreement with the distribution of the early, large-volume shields.

1. Introduction

The Al Haruj Intra-continental Volcanic Province (AHVP) is the largest part of the extensive volcanic field in Libya, which is regarded as a typical intraplate field (Fig. 1). The volcanic field developed during the late Miocene up to late Pleistocene and, presumably, continued to be active in Holocene. Its development has been linked to the tectonic evolution of the rifting of the Sirt Basin (Busrewil, 1996; Cvetkovic´ et al., 2010; Busrewil, 2012, Elshaafi and Gudmundsson, 2016). Age determinations of the AHVP have been made by many and using various techniques (Table 1). Most of these studies, e.g. Ade Hall et al. (1974), Peregi et al. (2003), Less et al. (2006), Cvetkovic´ et al. (2010), and Bardintzeff et al. (2012), indicate an active period of volcanism from the late Miocene to late Pleistocene. Nixon et al. (2011), however, used ^{3}He age dating method to infer that the Al Haruj volcanic activity continued until at least pre-historic time, namely to 2.31 ± 0.81 ka. Excellent well-persevered inflation features such as tumuli and lava rises from the last volcanic phase (phase VI) strongly support these young ages. In addition, Busrewil et al. (1996) and Busrewil (1996) suggest that the volcanic activity for the Al Haruj region commenced in the late Miocene and extended up to the pre-historic time, with the most recent lava flows (volcanic phases V, VI) being post-Neolithic in age. The older lava flows (Phases I, II, III and IV), however, were widely utilised for making Neolithic stone weapons.

The AHVP is made up essentially of substantial alkaline basalts to transitional basalts as well as subordinate sub-alkaline basalts, whereas more differentiated volcanic rocks are absent (Busrewil and Suwesi, 1993; Peregi et al., 2003; Al-Hafdh and Elshaafi, 2015). Klitzsch (1968) and Busrewil and Suwesi (1993) have suggested a scheme by which to divide the basaltic lava sequence into several major volcanic facies or generations based on the characteristics of the lava flows, as observed on aerial photographs, as well as morphological features, field relations, and degree of weathering, as observed in the field. This scheme has already been shown to be useful by later studies (e.g. Peregi et al., 2003; Less et al., 2006). For the southern part of the AHVP, in this way, dating of main six volcanic sequences shows that the earliest one is from the

* Corresponding author.
E-mail addresses: abdelsalamelshaafi@yahoo.co.uk (A. Elshaafi), a.gudmundsson@rhul.ac.uk (A. Gudmundsson).

http://dx.doi.org/10.1016/j.jvolgeores.2017.03.012
0377-0273/

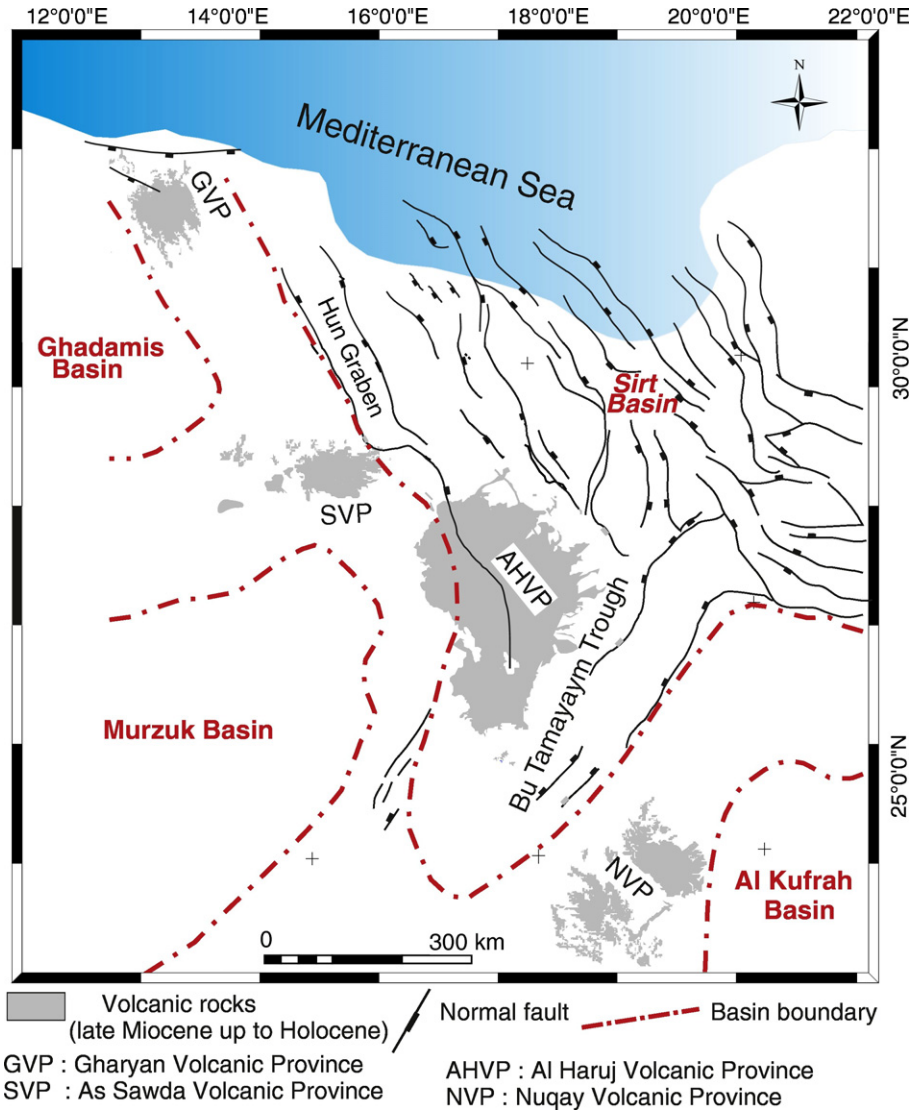

Fig. 1. Simplified geological map showing the distribution of the four main volcanic provinces in Libya and tectonic frame work of the Sirt Basin. The Al Haruj volcanic province (AHVP) is situated on the south-western margin of the Sirt Basin, central Libya. GVP; Gharayan Volcanic Province, SVP; As Sawda Volcanic Province; NVP; Nuqay Volcanic Province (modified from Mouzughi and Taleb, 1981; Abadi et al., 2008).

end of Miocene and the youngest one from the end of Pleistocene (Fig. 2A) (Table 1). Each volcanic phase is marked by multi-flow basaltic lobes (Peregi et al., 2003). As indicated above, however, volcanic activity in the AHVP appears to have continued into Holocene.

The average total thickness of basaltic lavas in the entire AHVP is small compared with the areal distribution of the volcanic flows. More specifically, the average sequence thickness is around 145 m in the central parts and gradually decreases to a few meters in the peripheral parts, based on measurement magnetic anomalies (Pacific Aero Survey, 1979; Peregi et al., 2003). We have crudely estimated the volume for each volcanic phase based on the average maximum thickness for each phase as measured in the field (Busrewil and Suwesi, 1993; Peregi et al., 2003). The results (Fig. 2B, C) suggest that the production rate for AHVP has generally decreased over time. For example, only 1730 km^2, or about 11.5 km^3, erupted during late Pleistocene-Holocene (0.30 Ma – 2.3 ka) whereas around 14,000 km^2, or about 231 km^3, erupted during the late Miocene - early Pliocene (7.94–3.67 Ma). Because some early lava flows are buried beneath subsequent flows, the areas and volumes of the early lavas are most likely underestimated compared with the areas and volumes of the later lavas, which are much better exposed. Thus the decline in lava production with time is clearly considerable, and may be greater than that indicated in Fig. 2.

There are a strong genetic relationships between most of the basaltic rocks from the various volcanic phases (e.g. Peregi et al., 2003; Less et al., 2006; Bardintzeff et al., 2012). These studies suggest that most of the rocks of the AHVP derived from a common parental mantle source with different degrees of partial melting.

The volcano-morphological features and thickness of lava flows in the AHVP have suggested two different palaeovolcanic systems rather than a single system (e.g. Peregi et al., 2003) (Fig. 3). The location of the exposed Eocene sedimentary rocks of the Wadi Thamat and Bishimah Formations coincides roughly to the boundary between two volcanic systems (Fig. 3A), as discussed in Section 3. The northern volcanic system is called the Al Haruj al Aswad subprovince and is characterised by more than a hundred metre thick volcanic pile in the central part. The thickness, however, gradually decreases to a few metres towards the periphery of the system (Pacific Aero Survey, 1979; Peregi et al., 2003; Less et al., 2006). The area of the system, calculated using ArcGIS 10.1 during this study, is about 34,200 km^2. The southern volcanic system is called the Al Haruj al Abyad subprovince, has a maximum thickness of about 20 m (Peregi et al., 2003), and covers an area of around 7,850 km^2. The A Haruj al Aswad system consists mainly of lava shields rising from a lava plateau, while the Al Haruj al Abyad system is primarily composed of clusters of crater cones, of scoria spatter, and

Table 1
Summarized results of age dating for the AHVP throughout the last four decades. There are generally consistent about the age of the Al Haruj province commenced from late Miocene in the range from 7.9 to 5.4 Ma until the late Pleistocene. But the modern age dating by Nixon et al. (2011) who used the ^{3}He technique inferred that the volcanism of the Al Haruj extended at least until 2.31 ± 081 ka.

Author (s) **Age dating method**	Ade Hall et al. (1974) (K/Ar)	Peregi et al. (2003) (K/Ar)	Less et al. (2006) (K/Ar)	Cvetkovic´ et al. (2010) (K/Ar)	Nixon et al. (2011) ^{3}He	Bardintzeff et al. (2012) Unspiked K/Ar
Volcanic Phase VI	0.4 Ma (late Pleistocene)	0.30–0.10 Ma (late Pleistocene)	–	0.5 ± 0.26 Ma (late Pleistocene)	2.31 ± 0.81 ka (Holocene)	0.2 ± 0.009 Ma (late Pleistocene)
Volcanic Phase V		0.50–0.30 Ma (middle to late Pleistocene)	–			
Volcanic Phase IV		1.22–0.50 Ma (middle Pleistocene)	–			
Volcanic Phase III		1.77–1.22 Ma (early Pleistocene)	–			
Volcanic Phase II		2.24–1.77 Ma (early Pleistocene)	3.31–1.77 Ma (late Pliocene-early Pleistocene)			
Volcanic Phase I		5.27–2.73 Ma (early to late Pliocene)	7.94–3.67 Ma (late Miocene to early Pliocene)			
	6.0 Ma (late Miocene)			5.4 ± 1.20 Ma (late Miocene)	----------	8.1 ± 0.22 Ma (late Miocene)

small lava shields which are aligned NW-SE to NNW-SSE (Martin and Németh, 2006). Generally, lava shields on the AHVP appear older than the scoria cones (Busrewil and Suwesi, 1993).

Busrewil and Suwesi (1993) suggest that the lava shields on the AHVP were primarily generated during two major eruptive stages separated by an interval of quiescence. The first eruptive stage is represented by most of the lava shields whereas the second stage is mainly marked by small cones primarily at the summits of the existing lava shields.

While the geochemistry and geochronology of the volcanic systems of AHVP have thus received considerable attention in the past four decades (Table 1), the distributions of the volcanoes, as regards size and location, have received little attention, as have the associated sources, the magma reservoirs. In this paper, we focus on the volcanism and tectonics of both the volcanic systems on the Al Haruj region, with a focus on the distribution in size and location of the lava shields, and discuss our finding in the light of possible effects of the post-rift stage of the Sirt Basin on production of magma and eruption of lava. The AHVP is located on the south-western margin of the Sirt Basin (Fig. 1).

The paper has three interconnected aims. The first is to provide density maps of monogenetic volcanoes (crater cones, lava shields, and maars) so as to define the dimensions of the two main volcanic systems and their inferred source magma reservoirs. A second aim is to provide data on the size and areal distributions of the lava shields, and compare them, as regards volume, with similar shields in Iceland. For comparison, polygenetic shield volcanoes from the Galapagos and Hawaii are included in some of the plots, but the focus is on comparison with the monogenetic and, in many ways, similar lava shields in Iceland. The third aim is to use numerical modelling results to explain, crudely, the size, age, and areal distribution of the lava shields in the AHVP with references to the local stresses and loading history of the inferred source magma reservoirs.

2. Data and methodology

In this study, we have compiled a data set for the lava shields of the AHVP. Based on geological maps, most of lava shields belong to the first and the third volcanic phases except that four lava shields were generated during the second volcanic phase. The methodology used during the present study combines georeferenced existing geological maps (Woller, 1984; Vesely, 1985; Busrewil and Suwesi, 1993; Peregi et al., 2003; Less et al., 2006) with multi-source high resolution remote sensing images available on Google Earth (2016) over the central part of Libya and digital elevation model (DEM) data collected by NASA Shutter Radar Topography Mission (SRTM). Google Earth imagery provides three-dimensional geospatial data through Keyhole Mark-up Language (KML). In the study area, the images have the high resolution of about 0.5–2.5 m (Abdunaser and McCaffrey, 2014). This high resolution makes it possible to locate and precisely map the lava shields and calculate their heights, areas and diameters in the frame of the Geographic Information System (GIS), using the published geological maps as guidance for their ages. This method is a powerful tool for volcano-tectonic studies when size, remoteness, arid and inhospitable region of study induces difficulties of ground-based access (Drury, 2001; Rajesh, 2004; Koch and Mather, 1997; Chorowicz and Deroin, 2003; Peña and Abdelsalam, 2006; Solomon and Ghebreab, 2008; Chen et al., 2014; Abdunaser and McCaffrey, 2014; Chorowicz and Benissa, 2016; Elshaafi and Gudmundsson, 2016). From these results the volume and average slope angle of shields have also been estimated.

2.1. Size, distribution and slope of lava shields

The basal radius and height of each lava shield on the AHVP were extracted from very high-resolution satellite imagery, using the same criteria to mark the margin of the volcano as used by Hasenaka (1994). The uncertainties or errors for our measurements are estimated at 10 ± 5%, partly based on comparison between measurement results on dykes and volcanic fissures obtained in the field and from satellite imagery (cf. Elshaafi and Gudmundsson, 2016). The basal radius of a volcano is calculated using standard trigonometry. That is, the height of the volcano is the difference between elevation of the summit and the elevation of the base and then the resulting right triangle gives the radius of the lava shield. Similarly, the average slopes of the lava shields were obtained from trigonometry. The results show that the lava shields on the AHVP are, in comparison with Icelandic shields, gently sloping (cf. Pike, 1978; Hasenaka, 1994).

The areas of the lava shields were calculated using ArcGlobe. A polygon-shape file was created in ArcCatalog, and then a polyline-shape file for ArcGlobe imported into ArcMap to calculate the area for individual lava shields. Because ArGIS uses planimetric algorithms to calculate areas, it follows that ArcGIS must work with a projected coordinate system (PCS) rather than geographic coordinate system (GCS).

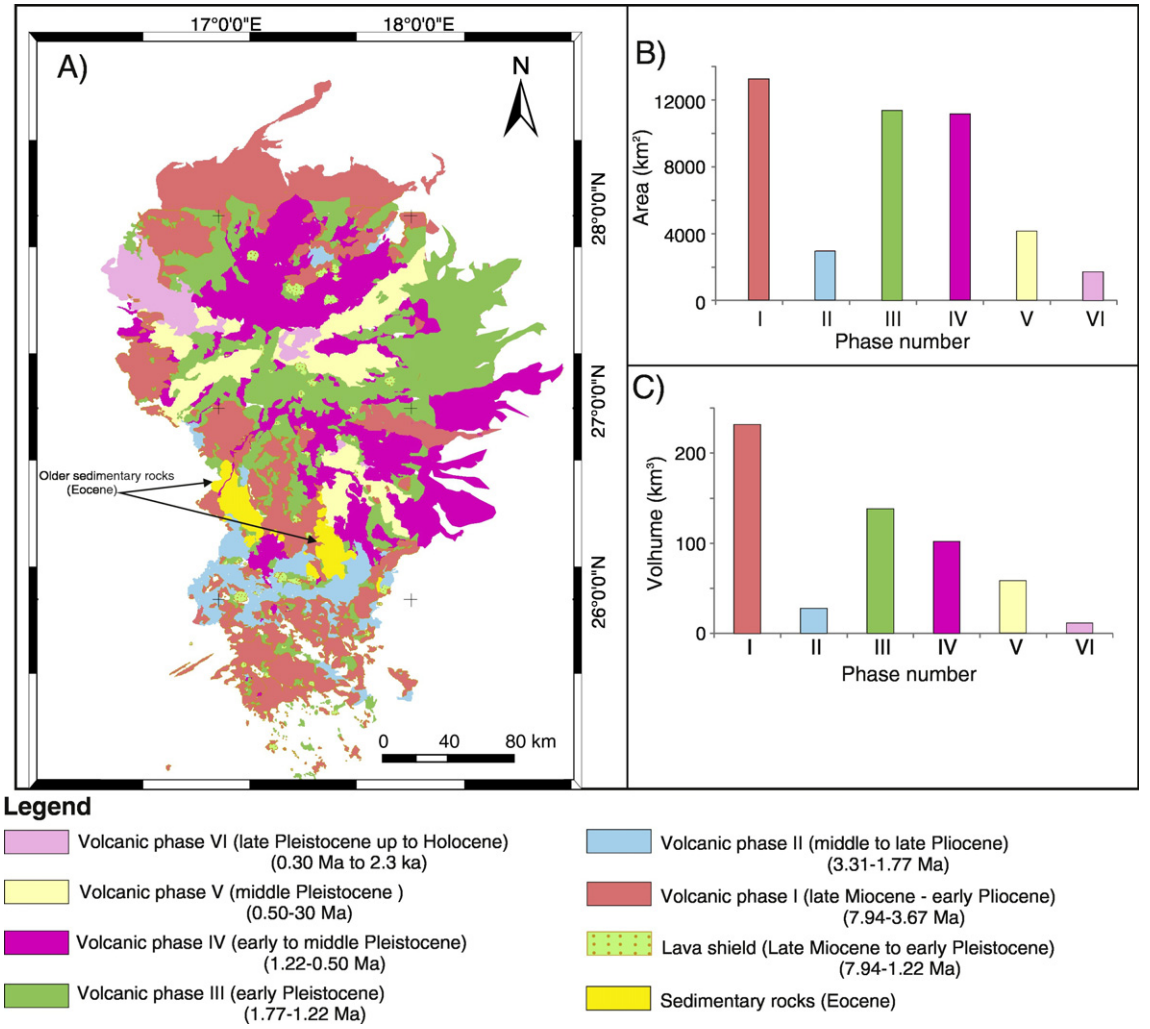

Fig. 2. A) Map showing the areal distribution and order of the six main volcanic facies or phases from the late Miocene up to Holocene. Based on the maps by Busrewil and Suwesi (1993), Peregi et al. (2003), Less et al. (2006). We considered the last volcanic phase continued until the Holocene based on the modern age dating by Nixon et al. (2011). Note the older sedimentary rocks for Wadi Thamat and Bishimah Formations (Eocene), indicated by dark yellow colour, were not covered by later Miocene-Holocene lava flows and seems to be the boundary or barrier between two rather different paleovolcanic systems; see text for more explanation. B) Histograms showing the total area covered by the volcanic phases, calculated using ArcGIS 10.1. C) Histograms showing the volume for each volcanic phase based on average maximum thickness measured in the field by Busrewil and Suwesi (1993) and Peregi et al. (2003). The volumes are generally decreased through the time.

The volumes of most lava shields were computed by approximating their shapes as truncated cones (Hasenaka, 1994). Here we consider lava shields as of cone or pyramid shape. Lava shields do not strictly have a cone shape, except the central parts (Rossi, 1997). However, the method can be used as a crude indicator of their volumes. More specifically, because of the small radius of the summit crater in most lava shields compared with their basal diameters, a very small error is introduced in the volume estimate even if the missing volume in the summit crater (the depression) is ignored. The approximation volume V of a lava shield is thus calculated as that of a circular cone, namely as follows:

$$V = \pi r^2 \frac{h}{3} \quad (1)$$

where r is the basal radius and h the maximum height of the lava shield. The volumes of lava shields are probably underestimates because a part of the lava flow field of each shield is buried beneath the lavas from later eruptions and thicknesses of the lava shields are usually imprecise (Andrew and Gudmundsson, 2007).

Frequency graphs and statistical analyses were made of lava shield location, height, basal radius, slope angle, area as well as volume to explore and evaluate the relationships between different lava shields and give a general view of the evolution of volcanism and tectonics in both volcanic systems. As regards location, the lava shields are essentially restricted to the north and south of the volcanic province and, as indicated, produced from the late of Miocene to Pleistocene (Peregi et al., 2003; Less et al., 2006) with possibly some activity in Holocene (Nixon et al., 2011). As explained, the lava shields themselves formed mostly from late Miocene to early Pleistocene, but there are indications of later fissure eruptions in their summit and central parts, some of which may be of Holocene age (Nixon et al., 2011). The early lava shields are generally located near the margins of the volcanic systems and the average volume of the early lava shields greater than that of later or more recent lava shields (Figs. 3; 4A).

Most lava shields on the AHVP are built up of pahoehoe lava flows (Busrewil and Suwesi, 1993; Peregi et al., 2003). Their basal diameters range between 1.5 km and 11.7 km and they have gentle slopes that range from 0.3° to 7°, with average around of 2°. They are thus very flat, that is, with very gentle slopes in comparison with many other lava shields, such as in Iceland (Rossi, 1997). They AHVP shields are generally steeper near the central summit crater than in the lava apron area, as is common for shields. Most of the lava shields

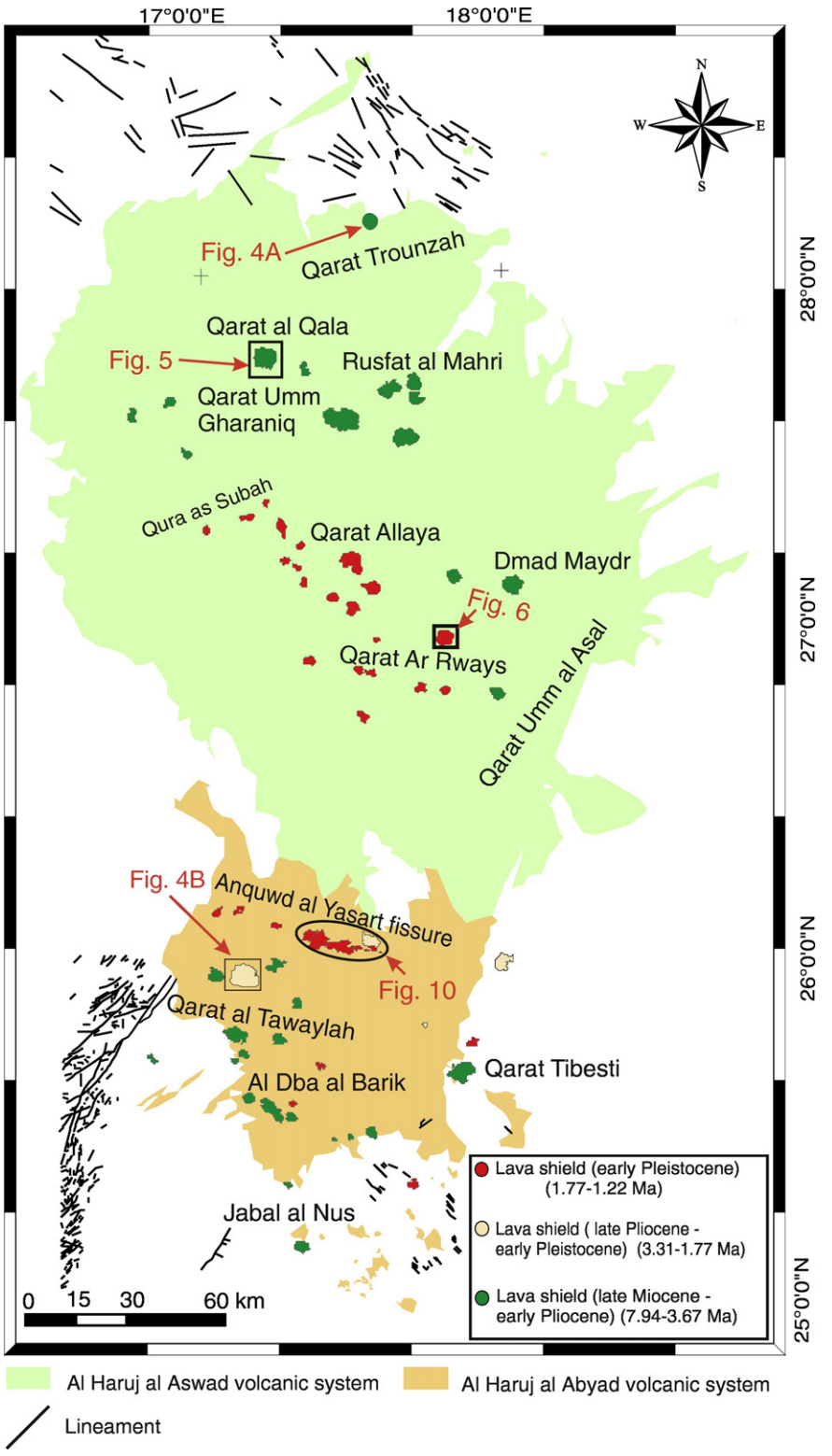

Fig. 3. Geological sketch map showing the two main volcanic systems based on geographical-geomorphological division and thickness sequence of lava flows that are consistent with the volcanoes density map in Fig. 11. Both volcanic systems constitute the largest volcanic province (AHVP) in Libya. The northern volcanic system (light green colour) is an order of a magnitude larger than the southern volcanic system (orange colour). Map shows the distribution of various lava shields on the AHVP and the sites of Figs. 4, 5, 6, 10. The early large lava shields occur mainly in the northernmost and southernmost parts of the volcanic province. Names of lava shields and their ages are taken from Busrewil and Suwesi (1993), Busrewil (2012), Peregi et al. (2003), and Less et al. (2006).

on the AHVP are marked by well-developed cones of pyroclastic breccias, agglutinates, and lava spatters at their summits. Some of these appear to have been issued from later volcanic fissures (Busrewil and Suwesi, 1993; Peregi et al., 2003; Less et al., 2006), some of which may be Holocene age (Fig. 4B). In addition, there are occasional small pit craters on the flanks of lava shields (cf. Busrewil and Suwesi, 1993), as are commonly seen on lava shields elsewhere, such as in Iceland (Rossi, 1997).

Most of the lava shields formed during the early volcanic phases (late Miocene to early Pleistocene) and can be classified into three groups according to age (Peregi et al., 2003; Less et al., 2006), namely:

i. Late Miocene – early Pliocene lava shield (7.94–3.67 Ma);
ii. Late Pliocene – early Pleistocene lava shield (3.31–1.77 Ma);
iii. Early Pleistocene lava shield (1.77–1.22 Ma).

Subsequently, eruptions occurred during the middle Pleistocene and into Holocene. These were mainly fissure eruptions, generating crater rows (of primarily scoria cones) up to several km long; one example is seen in Fig. 10. Some of the fissure eruptions, however, occurred in the summit areas of the lava shields, even if the lava shields are primarily monogenetic. The most recent eruption within the AHVP occurred 2300 years ago (Nixon et al., 2011). Hence the AHVP is likely to be still active, particularly the northern volcanic system.

The first group (i) is composed of the largest lava shields of the AHVP. The average height is 69 m, basal diameter 5.5 km, and volume 0.46 km^3. The sizes of these lava shields range up to large structures such as Qarat al Qala in the northernmost part of the Al Haruj al Aswad volcanic system (Fig. 5). A still larger one is Qarat Umm Gharaniq, one of the largest lava shields of the AHVP, whose height is 89 m, basal diameter 11.7 km, and volume 2.4 km^3. Most of the large lava shields are located in the northernmost part of the Al Haruj al Aswad volcanic system, except that the lava shield Qarat Umm Tibesti, with a volume of 1.25 km^3, is located in the northeast corner of the Al Haruj al Abyad volcanic system.

The second group (ii) of lava shields consists of only 4 shields and is confined to the south part of Al Haruj al Abyad volcanic system. The Qarat Tawaylah lava shield (Fig. 4A), the southernmost of the Al Haruj al Abyad system, belongs to this type. The lava shield area is around 46.8 km^2 and its height 49 m, yielding a volume of around 0.76 km^3. Many lava shields in this group may have been buried by subsequent lava flows, particularly in the central parts of volcanic systems, which may partly account for their scarcity. By contrast, the third group (iii) is composed of shields that are widely distributed within both the volcanic systems. These lava shields have average height of 68 m, basal diameter of 3.4 km, and volume of 0.23 km^3. They clearly look comparatively young (Fig. 6), but are smaller than the lava shields in the other two older groups (Fig. 7).

Lava shield volume and area show a reasonably strong linear correlation (Fig.7). With $R^2 = 0.7459$, the results mean that about 75% of the variation in volume of lava shields can be explained by, or predicted from, their variation in area. (Lava shield volume can, of course, also be taken as the independent variable and used to forecast or explain the variation in lava shield area.) Similar relationships are obtained for monogenetic lava shields in Iceland (Andrew and Gudmundsson, 2007); 22 Holocene Icelandic shields are included with the AHVP lava shields in Fig. 8. For comparison, we also include the large, polygenetic shield volcanoes on Hawaii (3 volcanoes) and Galapagos (12 volcanoes) together with the 22 from Iceland and 55 from the AHVP in Fig. 9. The radius and height of lava shields on the AHVP are clearly much closer to monogenetic lava shields in Iceland than polygenetic shield volcanoes on Hawaii and Galapagos (Fig. 9). On this logarithmic plot we have $R^2 = 0.6534$, but the straight line is actually a non-linear function, so that the correlation (using non-transformed axes) is really non-linear.

The typical monogenetic lava shields in Iceland consist of a central cone and a lava apron (Rossi, 1997). The central cone is roughly symmetrical and sloping in the range from 2° to 9° whereas the apron is typically of a roughly circular shape and extending for many kilometres with regional slopes from 0.2° to 5° (Rossi and Gudmundsson, 1996). Monogenetic lava shields, as in Iceland and AHVP, are believed to be formed in single eruptions, some of which may have lasted tens of years (Walker, 1965; Jakobsson et al., 1978: Gudmundsson, 1986; Andrew and Gudmundsson, 2007). The eruption usually commences with a fissure but then gradually becomes focused at several points so as to generate several overlapping small shields. In final state, the eruption becomes concentrated on the one large point that forms the main shield that buries the overlapping smaller shields (Gudmundsson, 2000; Andrew and Gudmundsson, 2007).

A lava shield consists of multi-flow lobes or units, features that can be easily recognised in the field as well as from satellite imagery. Some of these features may have be identified by earlier authors (e.g. Klitzsch, 1968; Busrewil and Suwesi, 1993) and given phase numbers to decipher whether multiple-flow lobes for each volcanic phase is the product of a single eruption, a multi-episode of a single eruption, or the result of totally different eruptions (Self et al., 1998). Based on field relations in the AHVP each volcanic phase is more likely the result of a single eruption than many eruptions. While each individual eruption begins with a volcanic fissure it may stop at any stage – so that a large lava shield is not a necessary the end stage (Gudmundsson, 1986; Gudmundsson, 2000; Andrew and Gudmundsson, 2007). Therefore, small overlapping cones may be initiated in an individual eruption from a segmented volcanic fissure as we have observed in many places in the Al Haruj al Abyad. For example, the 23-km-long Anquwd al Yasarat fissure, the longest one in the AHVP, produced five small lava shields and dozens of crater cones (Fig. 10) rather than a single large lava shield.

As indicated above, there was a gradual decrease in volume of lava shields and in the intensity of the volcanic phases through time. Also, the eruptive volumes in the Al Haruj al Aswad system are, on average,

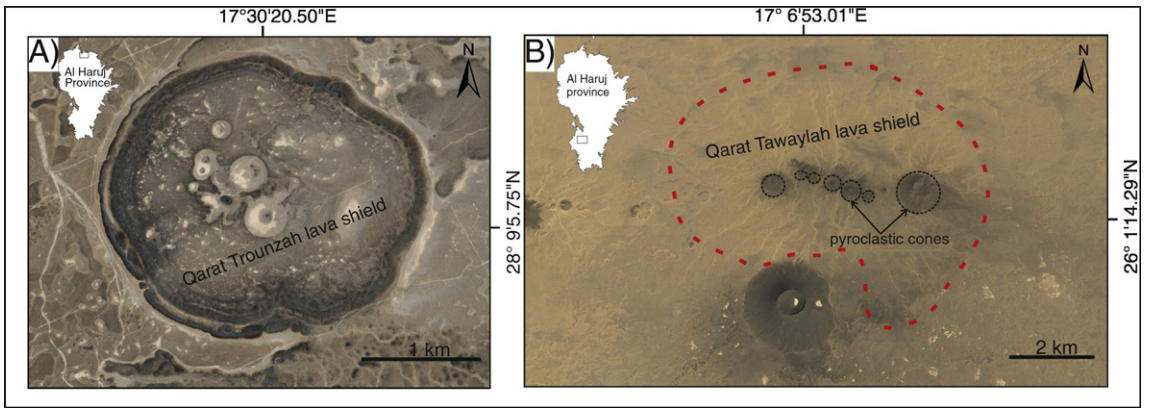

Fig. 4. A) Satellite imagery (adapted from Google Earth) showing the late Miocene – early Pliocene lava shield (Qarat Trounzah) which is located at the northernmost margin of the AHVP. B) Image showing the large lava shield Qarat Tawaylah (adapted from Google Earth), indicated by red broken line. The most recent eruptions are the dark volcanic cones in the summit area of the lava shield. The alignment of scoria cones are NW-SE in (A) and WNW-ESE in (B), coinciding with the orientation of the main fracture/fault zones in the western part of the Sirt Basin. The inset mapping shows location.

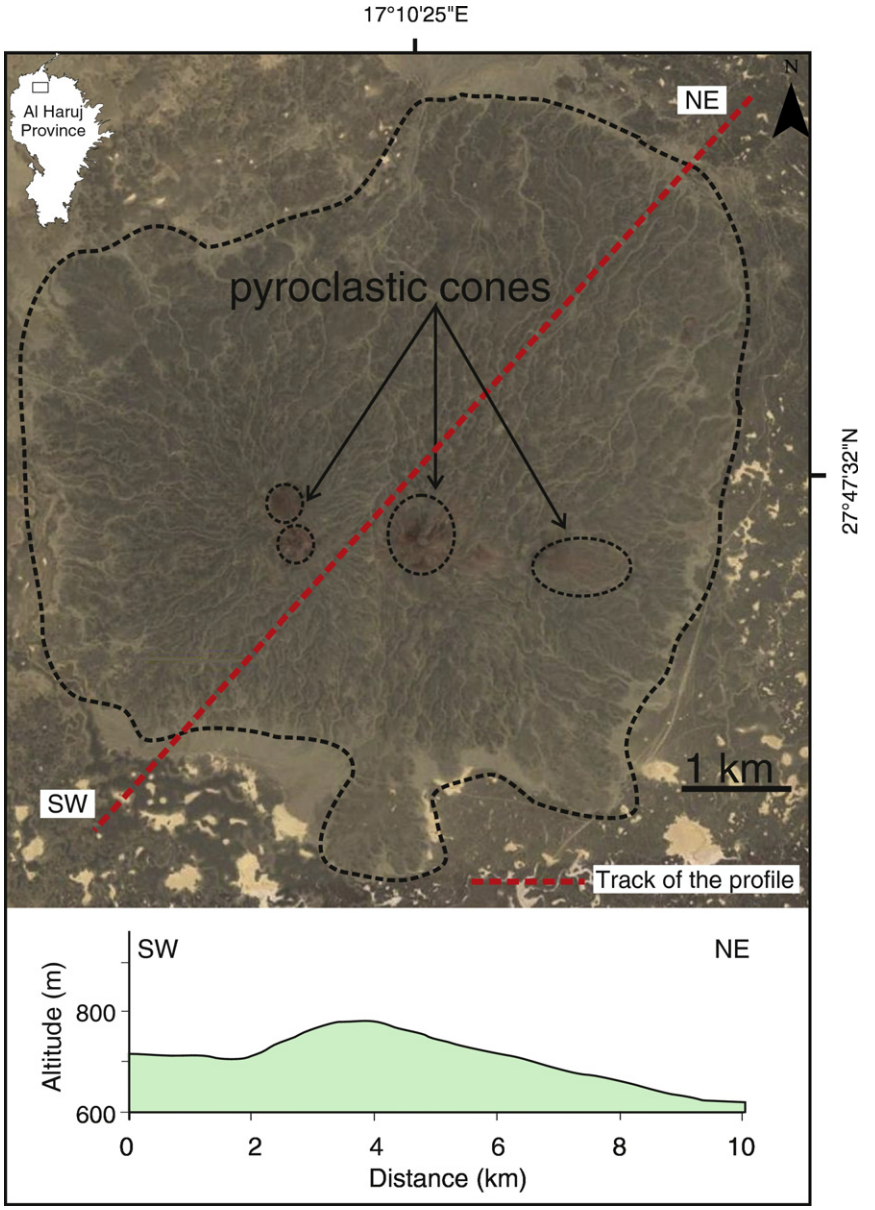

Fig. 5. Lava shield Qarat al Qala in the northernmost part of the AHVP (adapted from Google Earth). Small volcanic cones at the top of lava shield appear to be formed by later eruptions. NW-SE trending indicates a volcanic fissure. The lower graph shows the cross-section of the lava shield.

an order of magnitude larger than those in the Al Haruj al Abyad system (Fig. 2). This may suggests that the total volume during the lava shield phases produced by Al Haruj al Aswad is much than that produced during the same periods by Al Haruj al Abyad.

3. Spatial density of volcanic eruptions

The spatial distributions of 432 volcanic eruption sites have been examined and presented as an eruption-point density map, that is, as the number of eruption points per square kilometre (Fig. 11). For this task, ArcGlobe 10.1 was used to plot accurately the volcanic vents and polyline.shapefile was then imported to ArcGIS 10.1 to create the density map. Point density map calculates the number of points, here eruption points or sites, per square kilometre within a circular neighbourhood of a given radius and presents as intensity or magnitude contours. The spatial density map was drawn by ArcGIS 10.1 that used a search radius of 40 km to produce a more generalised output raster where all the volcanoes that fall within the neighbourhood (40 km) are used when calculating the density. Therefore the red spots in Fig. 11 represent the maximum density which then gradually decreases (indicated by the colours) away from the centre. The 40 km search radius highlights the crustal-scale distribution (Lesti et al., 2008). Only volcanoes with clear circumferences are used in making the map (Fig. 11), so as to reduce the possibility of including non-volcanic features. The volcanoes used are lava shields, scoria cones, spatter cones, and a few maars (the latter occur mainly in the southernmost part of the AHVP). The similarity of clustering or density of the eruption points in the north and south volcanic systems indicates that the mechanism of magma generation was most likely similar (Le Corvec et al., 2013). In addition, many of the eruption points are aligned and, apparently, follow pre-existing fractures, possibly used partly as channels. More details on the magmatism in AHVP and the tectonic activity in the nearby Sirt Basin are provided by Elshaafi and Gudmundsson (2016).

The spatial distribution of eruption points, presented as magnitude contours, can be subdivided into two main density subzones or subareas. One is in the northern part of the AHVP and mainly made up of lava

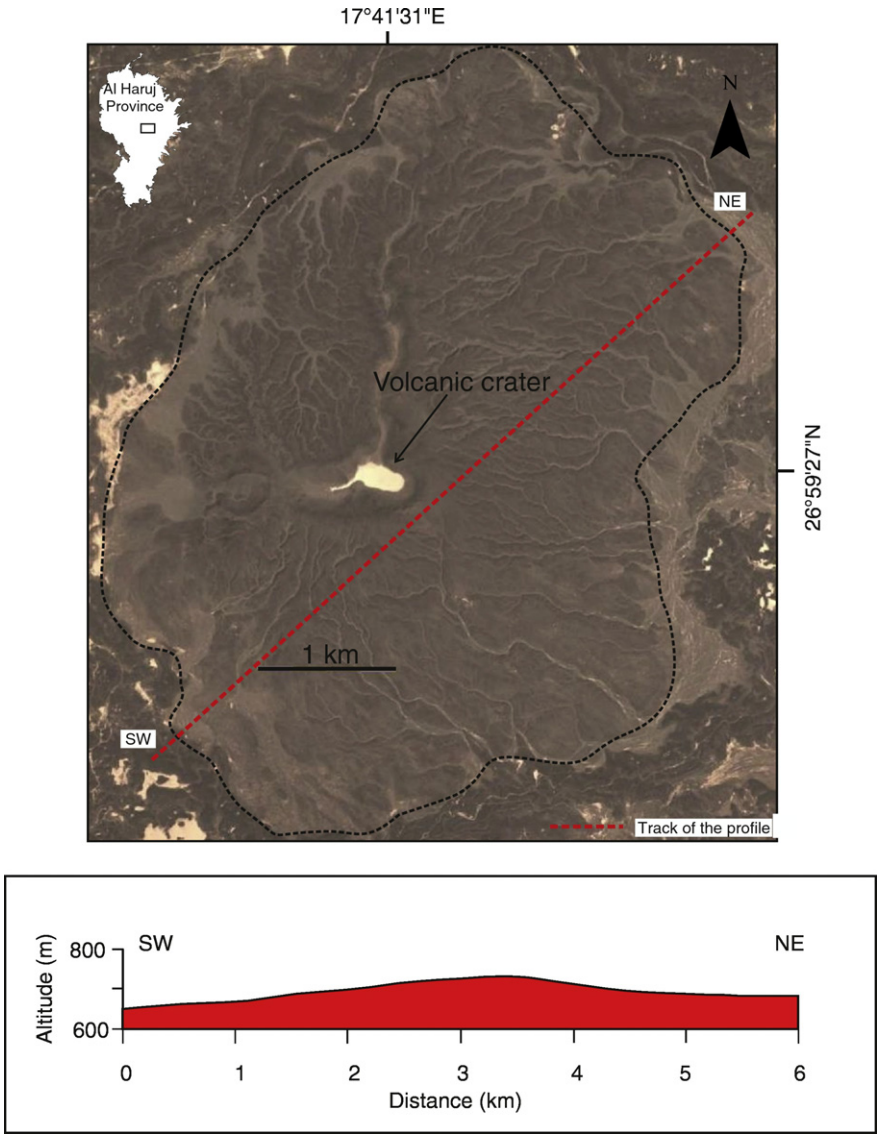

Fig. 6. Early Pleistocene lava shield Qarat Ar Rways in the southern part of the AHVP, inset map showing location (adapted from Google Earth). The lava shield is comparatively small and with un-weathered lava, suggesting young age. Also shown is a cross-section, indicating how gently sloping the shield is.

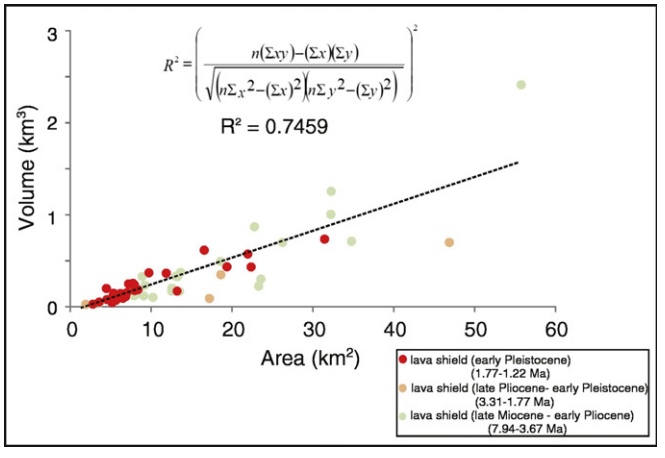

Fig. 7. Graph showing the relationship between area and volume of 55 lava shields on the AHVP. The coefficient of determination $R^2 = 0.7459$, where n is the number of lava shields while x and y are the area and volume for each lava shield respectively.

shields, as well as some scoria cones, including the youngest volcanoes in the area. The second subarea is in the southern part of the AHVP and contains mainly scoria cones or crater rows associated with volcanic fissures and small lava shields. The central area between these subareas has a very low density of eruption points (Fig. 11) and marks the boundary between the two volcanic systems identified in Fig. 3. The suggestion as to the boundary between the systems is supported the earlier studies (e.g. Peregi et al., 2003) which indicate that the Al Haruj Volcanic Province (AHVP) consists of two different paleovolcanic systems. We suggest that each system is supplied with magma from a specific magma reservoir. The density maps may be used as a crude indication of the geometry and location of the source magma reservoirs.

4. Magma reservoirs

The basalts of the AHVP show broad similarities, with only minor geochemical differences being recognised (Peregi et al., 2003; Less et al., 2006). The primary melts may have been generated by 1–5% melting of a garnet-peridotite mantle region. The depth of origin of the partial melts may then have extended to the depths of 80–150 km (Bardintzeff et al., 2012). However, Nixon et al. (2011) suggest that the melts of the

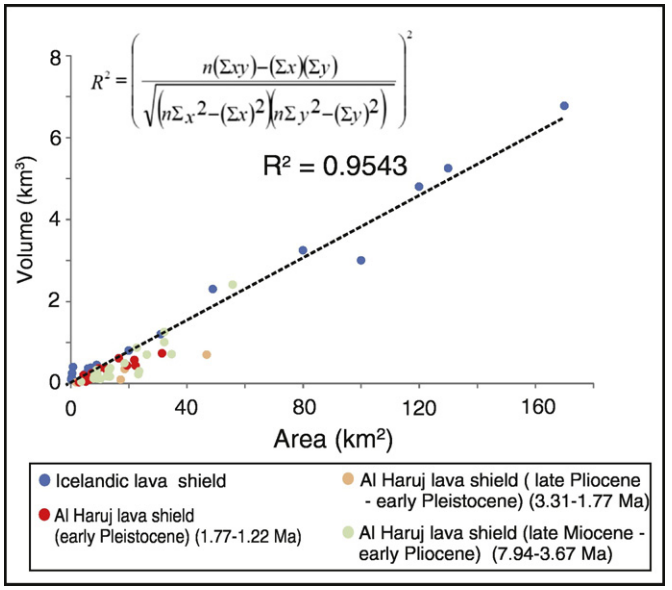

Fig. 8. Graph showing the relationship between area and volume of 55 lava shields on the AHVP and, for comparison, 22 Holocene shields on the Reykjanes Peninsula, Southwest Iceland. Data of Icelandic lava shields are taken from Jonsson (1978), Jakobsson et al. (1978), and Andrew and Gudmundsson (2007). The coefficient of determination R^2 = 0.9543.

AHVP were (and are) generated at depths of 70–74 km with a much higher melt fraction, namely between 13.5 and 18.9%.

The estimated equilibrium pressure values from studied peridotite xenoliths indicate that the magmas erupted at AHVP derive from magma reservoirs at temperatures of 850–950° C, pressures of 1–1.8 GPa, and thus from depths of 35–55 km (Peregi et al., 2003). By contrast, Nixon et al. (2011) suggest that fractional crystallisation of the primitive magma occurred at depths of 25–39 km and temperatures of 1215–1360° C. The location of the reservoirs would then be in the transition zone between the lowermost crust and upper mantle, as is also the depth of many magma reservoirs which form part of the

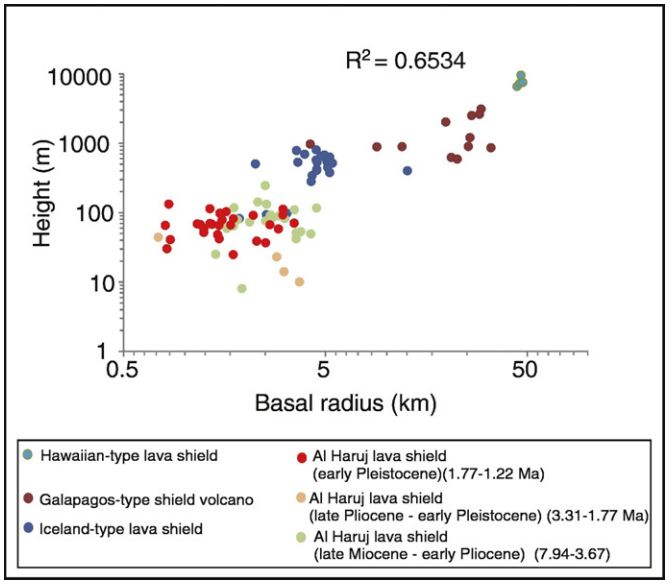

Fig. 9. Graph showing the relationship between basal radius and height of lava shields on the AHVP and in Iceland, as well as for selected shield volcanoes in the Galapagos (12 volcanoes) and Hawaii (3 volcanoes). Data of shield volcanoes from Galapagos and Hawaii are extracted from Whitford-Stark (1975) and Hasenaka (1994). The coefficient of determination R^2 = 0.6534.

partially molten 'magma layer' in Iceland (Gudmundsson, 1986, 2016; cf. Hermance, 1981; Schmeling, 1985). More detailed geophysical studies may help provide a better constrain on the magma layer in general and that of the reservoirs of the AHVP in particular.

The low-density magma, the lighter magma, tends to move upwards to the regions of minimum potential energy (Gudmundsson, 2011, 2016), and gradually forms layers (compartments) with high magma proportion, even totally molten pools, in the upper portions of the reservoirs (cf. Gudmundsson, 1987, 2012). Therefore, the magma content or proportion in the partially molten of upper parts magma reservoirs may be much greater than that in the lower parts (Gudmundsson, 1986, 1987).

The high degree of thermal maturity of shallow sediments as seen in oil wells in the western margin of the Sirt Basin indicates that more than one kilometre of sedimentary sequence was uplifted and eroded during the late Miocene (Gumati and Schamel, 1988; Abadi et al., 2008). Regional uplift during extension is commonly the effect of the excess pressure in and doming of a magma reservoir (Gudmundsson, 1986). The late Miocene uplift in the whole west part of the Sirt Basin is supported by the burial history of wells (QQQ1-11; aa1-11, Zallah trough) in northern part of the area of investigation (Gumati and Schamel, 1988; Abadi et al., 2008) (Fig. 12). Thus the crustal doming during the late Miocene and increased melt migration into the reservoirs may have led more elongated magma reservoirs in the vertical section (thicker reservoirs) and accumulation the lighter magma (basaltic magma) in the upper portions. As a result the locally thicker crustal parts between two magma reservoirs may have acted as crustal barrier so as to hinder magma to transport between reservoirs (Figs. 13) (Gudmundsson, 1986).

The main reason for uplift of the western part of the Sirt Basin during the late Miocene is still widely disputed, however. Some authors (e.g. Cloetingh and Van Wees, 2005) suggest that lithospheric doming was most likely associated with the mantle upwelling as found in many areas in Europe, where the asthenospheric rise caused decompression partial melting at various levels (Cvetkovic´ et al., 2010). Also, Nixon et al. (2011) suggest that extensive volcanism in the AHVP and larger parts of North Africa may be the result of diapiric upwelling plumes or hot fingers in the upper mantle. By contrast, Less et al. (2006) suggest that the relatively low temperatures obtained from studies of peridotite xenoliths do not support the existence of hotspot under the Al Haruj region during the time of the main volcanism but rather the presence of a relatively cold lithosphere. They suggest that the volcanism of the AHVP was related to the extension of the lithosphere, that is, passive rifting. The magmatism of the AHVP, however, post-dates the extension peak of the Sirt Basin. It follows that the thinning of lithosphere may not have had a direct relation to the melt generation. It is also noteworthy that the main volcanism took place at the south-western periphery of the Sirt Basin, which has a stretching factor of 1.1, rather than in the central part, which underwent significant thinning and has a stretching factor of 1.4. These values of stretching are derived from back-stripping geophysical results by Abadi et al. (2008).

4.1. Geometry of magma reservoir

The rough elliptical surface expression of the distribution of eruption points or volcanoes in the density map may be taken as an indication of ellipsoidal geometry of the magma reservoirs beneath the Al Haruj region (Fig.11). This follows from the observation that volcanic fields and volcanic systems tend to reflect the plan-view geometries of the source reservoirs (Gudmundsson, 2000, 2016), a conclusion that follows from stress-concentration considerations (Gudmundsson, 2011). It is well known that magma reservoirs may extend in a direction parallel to the maximum compressive stress σ_1 and perpendicular to the maximum tensile stress σ_3 (Gudmundsson, 1986). So if we take the reservoirs to be oblate ellipsoids, as a first approximation (Gudmundsson, 2016), the minor axis would be oriented NE-SW, that is, parallel to minimum principal compressive stress while major axis would be trending NW-SE, that is, in a direction parallel to maximum principal compressive stress (Fig. 11).

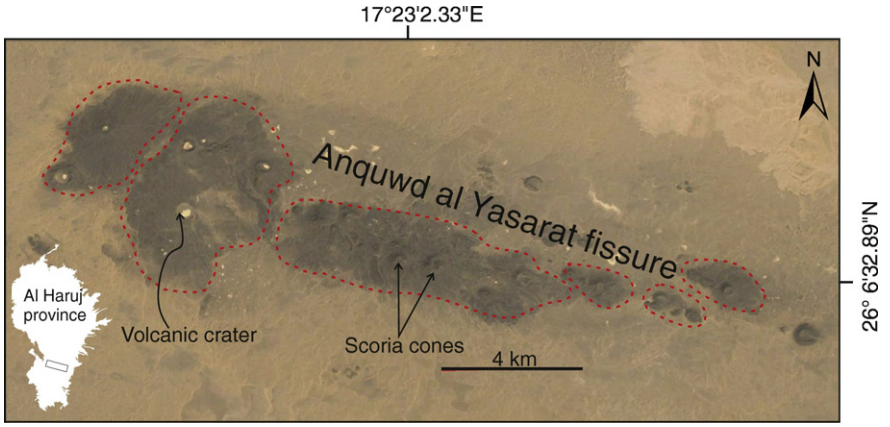

Fig. 10. Satellite imagery (adapted from Google Earth) showing one of the largest volcanic fissures on the AHVP (≈23 km long) whose lava flow and feeder dyke have a volume of about 4.16 km^3. The fissure has formed several small lava shields and dozens of scoria cones. The inset map shows the location of this volcanic fissure.

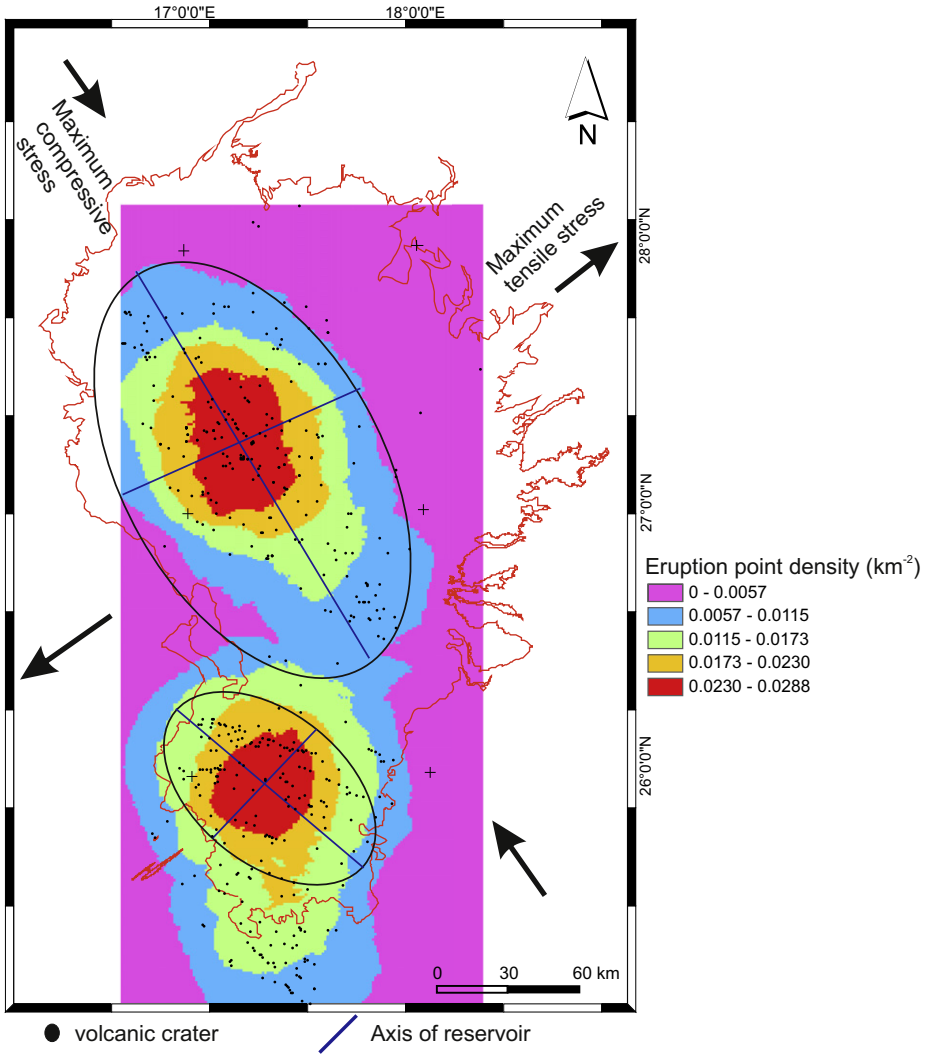

Fig. 11. Density map of volcanoes (eruption points) showing the magnitude (the number of eruption points that fall within a circular neighbourhood of 40 km) in order to highlight the crustal scale distribution. The red spots represent the maximum density which clearly corresponds to two rather different volcanic systems as follows: the Al Haruj al Aswad volcanic system in northern part and the Al Haruj al Al Abyad volcanic system in the southern part. Ellipsoidal geometry of both magma reservoirs beneath the Al Haruj region has been inferred from rough elliptical distributions of the magnitude of eruption points in the systems. The inferred magma reservoir is elongated parallel to maximum compressive stress, NW-SE, and perpendicular to maximum tensile stress, NE-SW, in the Sirt Basin.

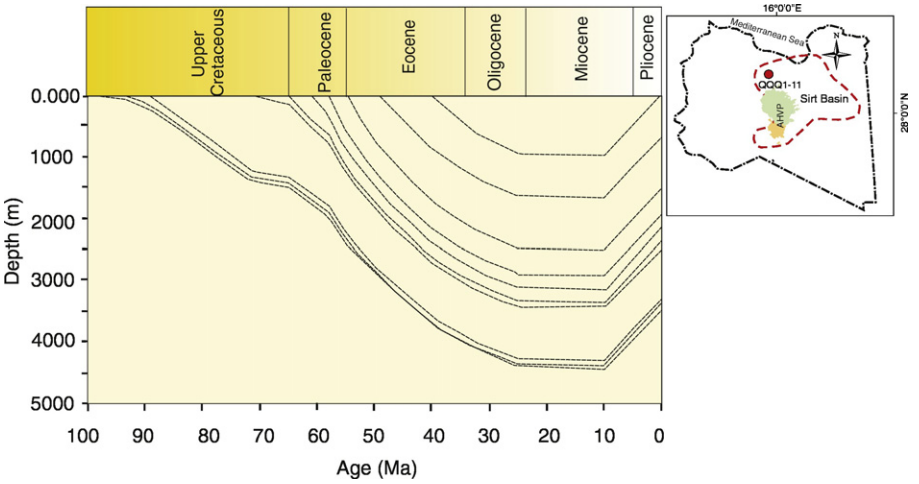

Fig. 12. Burial history of the western part of the Sirt Basin (well aa1-11, Zallah trough) showing that the regional uplift or doming of the area began during the late Miocene (Gumati and Schamel, 1988; Abadi et al., 2008). The inset map shows the location of the well QQQ1-11 which is near to the well aa1-11 at the Zallah trough.

The areas and lengths of the axes of the two magma reservoirs have been calculated through ArcGIS 10.1. We use the measured area of the Al Haruj al Aswad volcanic system, 19,176 km^2, and its major and minor axes of 210 km and 119 km, respectively. Also, for the Haruj al Abyad volcanic system, the area is 6209 km^2 and the major and minor axes are 108 km and 74 km, respectively. The volume of reservoir may be estimated if the thickness is known and vice versa, using the equation (Gudmundsson, 1986):

$$V_b = \frac{4}{3}AC \tag{2}$$

where V_b and C are the bulk volume and the half thickness of reservoir respectively, while A is the area.

Mechanical behaviour of magma reservoirs can be modelled as poroelastic (Machado, 1974; Blake, 1981; Wadge, 1981; Gudmundsson, 1987, 2016; Browning et al., 2015; Tibaldi, 2015). Thus the volumes of the reservoirs during individual eruptions in the AHVP may be roughly estimated by the following equation (Gudmundsson, 1987, 2016):

$$V_b = \frac{V_e}{p_e\varphi\left(\beta_m + \frac{\beta_b}{\varphi}\right)} \tag{3}$$

where V_e is the volume of eruptive material in a single eruption, φ is fraction porosity of the reservoir, p_e is the excess magmatic pressure in the reservoir, β_m and β_b are magma compressibility and bulk compressibility of the reservoir, respectively.

Here we assume that the magma reservoirs were generally located at an average depth of around 35 km, which corresponds to the boundary between the lower crust and upper mantle (Peregi et al., 2003; Nixon et al., 2011). The structural lithosphere of the Sirt Basin has been subdivided into several layers including upper mantle, lower crust, upper crust and uppermost crust. The latter involves Palaeozoic, Mesozoic and Cenozoic sediments (Ghanoush et al., 2014). The Moho discontinuity is estimated at around 35–40 km deep in southeast of the Sirt Basin while it is at around 26 to 33 km in the centre and northeast parts of the basin (Ghanoush et al., 2014). Thus, it seems plausible that the magma reservoirs are located at the boundary between the lower crust and upper mantle.

Elastic rock properties of the uppermost crust of the Sirt Basin have been measured on extracted drill cores samples as well as through downhole studies (Qui et al., 2008; Abdalkadeer et al., 2009). The mechanical properties of the deeper crustal parts were inferred from a global model for the Earth's crust based on seismic refraction data (Wienecke and Stadtler, 2014). The compression (V_p) and shear seismic velocities (V_s) of the main three crustal layers and the underlying mantle are given in Table (2). The values of Young's modulus for the upper crust, lower crust and the underlying mantle were calculated by using the compression and shear seismic velocities and densities from global model for the Earth's crust data based on the following equation (Jaeger and Cook, 1969):

$$E_d = \frac{V_s^2\rho\left[3\left(V_p^2/V_s^2\right)-4\right]}{\left(V_p/V_s\right)^2-1} \tag{4}$$

where E_d is dynamic Young's modulus, V_p is compression wave velocity, V_s is shear wave velocity and ρ the density of the rock. The static Young's modulus is commonly half the dynamic Young's modulus according to laboratory measurements (Clark, 1966; Cheng and Johnston, 1981; Gudmundsson, 1990; Gudmundsson, 2011). Therefore, the values of static Young's modulus in Table (2) are equal to half value of the dynamic Young's modulus.

Young's modulus for the layer 7 (the lower crust), which is most likely to host the magma reservoirs, is about 60 GPa (Table 3). The bulk modulus K for this layer can be calculated from the following equation (Gudmundsson, 2011):

$$K = \frac{E}{3(1-2\nu)} \tag{5}$$

where E is the static Young's modulus and ν is the Poisson's ratio whose common value for most solid rocks is around 0.25. Therefore, the compressibility β of layer 7 (the reciprocal of bulk modulus) is about 2.50×10^{-11} Pa^{-1} and compressibility of basaltic magma at 1100–1300° C is about 1.25×10^{-10} Pa^{-1} (Gudmundsson, 1987, 2016). At the time of reservoir rupture, the excess magmatic pressure is equal to the tensile strength of the host rock. Therefore, we may substitute excess pressure by tensile strength of the host rock in the Eq. (3) to obtain:

$$V_b = \frac{V_e}{\left(\varphi T_0\left(\beta_m + \frac{\beta_b}{\varphi}\right)\right)} \tag{6}$$

where T_0 is the tensile strength of the host rock.

The average unconfined compressive strength of the rocks in the Sirt Basin measured in laboratory tests is 36 MPa (Qui et al., 2008). Tensile strength has a well-known relation with unconfined compressive

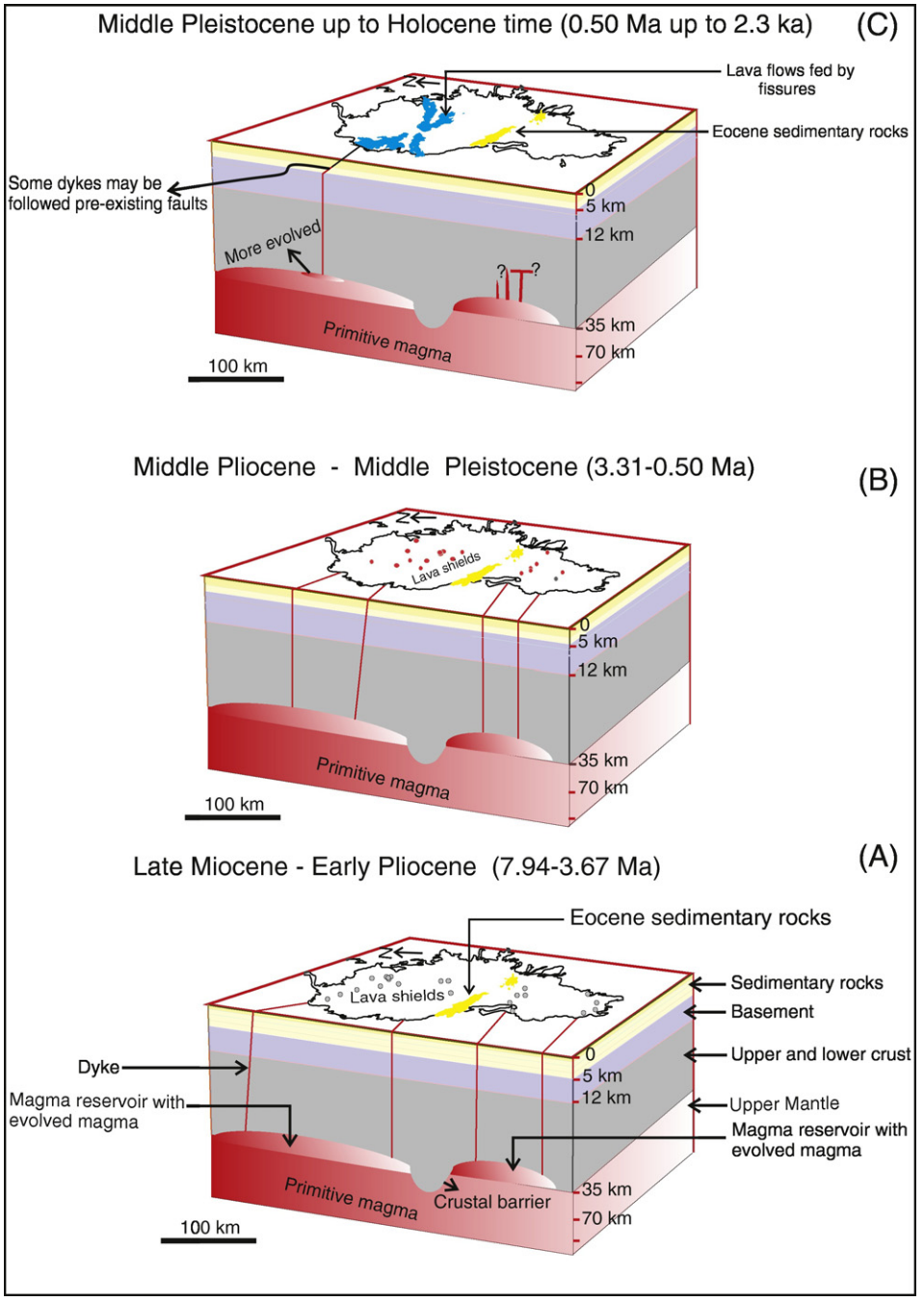

Fig. 13. Schematic illustration of the evolution the inferred magma reservoirs beneath the AHVP and some associated volcanism. Owing to fractional crystallisation the lighter (less dense) fraction of the basaltic magma tends to be accumulated in the uppermost part of the reservoir to form pools. While the locally thicker crust between two magma reservoirs may have acted as barrier to prohibit magma transport between them (cf. Gudmundsson, 1986). This barrier seems to correspond roughly with the Eocence sedimentary rocks of Wadi Thamat and Bishimah Formations (Eocene), indicated by dark yellow colour (data from Peregi et al., 2003). The schematic evolution is as follows. A) After the relaxation of the effect of compressive stresses at the bottom of lower crust, dykes would be injected from the margins of reservoir due to concentration of tensile stresses as seen in the numerical model results (Fig. 15), and much more eruptive material was produced during this period than in subsequent periods. Some dykes may use high angle pre-existing normal faults as part of their conduits in the uppermost of the crust (Elshaafi and Gudmundsson, 2016). B) The volcanic activity on the AHVP continued with slightly decreasing production until middle Pleistocene. C) Volcanic activity mainly ceased in the southern volcanic system in middle Pleistocene whereas activity in the north volcanic system continued, but with diminished lava production into Holocene, primarily as volcanic fissures forming crater rows. The basaltic rocks of the most recent volcanic eruptions are more evolved (cf. Asran and Aboazom, 2004; Farahat et al., 2006) than those in the earlier eruptions which indicates that they were erupted from the uppermost central part of northern magma reservoir (cf. Karaoğlu et al., 2017).

strength, but the relation depends somewhat on the rock type (Brook, 1993; Gudmundsson, 2011). Nazir et al. (2013) propose a relation between unconfined compressive strength (USC) and tensile strength T_0 of limestone on the form:

$$USC = 9.25T_0^{0.947} \tag{7}$$

This relation is very close to the well-known assumption that the ratio of compressive strength to tensile strength is approximately 10 (Sheorey, 1997; Gudmundsson, 2011). Accordingly, the average tensile strength of rocks in the Sirt Basin is around 4.2 MPa. This conclusion is in good agreement with the common in-situ tensile strength of typical solid rocks of 4–5 MPa (Haimson and Rummel, 1982; Schultz, 1995; Andrew and Gudmundsson, 2007; Gudmundsson, 2011).

Table 2
Dynamic and static elastic moduli for the Earth's crust and underlying mantle used in the numerical models. Densities and seismic velocities are taken from Global Model for the Earth's crust (Wienecke and Stadtler, 2014).

Layer	V_s (km/s)	V_p (km/s)	ρ (kg/m^3)	V_p/V_s	E_d (GPa)	E (GPa)
Upper crust	2.5	5	2600	2.00	44	22
Middle crust	3.65	6.6	2900	1.81	99	49
Lower crust	3.9	7.1	3050	1.82	120	60
Mantle	4.65	8.1	3350	1.74	181	90

Thus, from Eq. (6), and inserting the appropriate values for the parameters, the bulk volume of the reservoir is obtained from the following equation:

$$V_b = 2381\frac{V_e}{(1.25\varphi + 0.25)} \tag{8}$$

As we see here the volume of the reservoir needed to produce a given eruptive volume V_e depends upon the assumed magma fraction φ. For instance, if we assume the magma reservoir was totally molten ($\varphi = 1$) the volume of reservoir would be smaller ($\approx 1588V_e$) than if the same reservoir had only 0.25 magma fraction($\approx 4233V_e$).

Although the volume of a single eruption in the AHVP is often difficult to estimate, particularly since many individual volcanic phase or products could be formed in more than one volcanic eruption (as discussed earlier), the lava shields are generally believed to be monogenetic (Walker, 1965; Jakobsson et al., 1978: Gudmundsson, 1986, Gudmundsson, 2016). That is, the formation of each lava shield is thought to be related to one eruption, although some of the eruptions may have lasted for several years or more. Thus, most lava shields on the Al Haruj region may have assumed as formed in single eruptions where the whole reservoir may have supplied magma during the eruption.

The average volume of latest Miocene – early Pliocene lava shields on the Al Haruj al Aswad volcanic system is greater than the volume of same age lava shields on the Al Haruj al Abyad volcanic system, about 0.61 km^3 and 0.34 km^3, respectively. For a rough estimate of the average volume of a corresponding feeder dykes, the average length and thickness (opening) of volcanic fissures is 364 m and 1 m, respectively (Elshaafi and Gudmundsson, 2016), and its height (dip dimension), using the estimated magma source, is about 35 km depth. Thus the estimated average volume of the feeder dykes is about 0.013 km^3. Combining the feeder-dyke volume and the extrusive volumes, the average volume leaving the reservoir V_e for the two volcanic systems becomes 0.623 km^3 and 0.353 km^3. Hence the area of individual reservoir has been estimated from ArcGIS 10.1 and volume of reservoir may be estimated from Eq. (8) for individual volcanic eruption. Using these, the thickness of individual magma reservoir may be roughly estimated from Eq. (2).

If the uppermost part of the reservoir for the Al Haruj Aswad volcanic system were totally molten, then, from Eq. (8), the volume of that part of the reservoir which supplies magma during eruptions would be 990 km^3. If, however, the reservoir was partially molten with a porosity or magma fraction of 0.25 (cf. Gudmundsson, 2016; Karaoğlu et al., 2017), the bulk volume of reservoir would be 2637 km^3. The average volume of early lava shields in the Al Haruj al Abyad volcanic system is around 0.34 km^3 and the estimated average volume of the feeder dykes, assumed the same as for the northern volcanic system, about 0.013 km^3. It follows then that the volume of the corresponding reservoir would have to be 561 km^3 if the $\varphi = 1$ and 1494 km^3 if $\varphi = 0.25$. The thickness of the reservoir is estimated from Eq. (3) as about 78 m for the Al Haruj al Aswad volcanic system and as about 136 m for the Al Haruj al Abyad volcanic system when the reservoirs are assumed completely molten. By contrast, the thicknesses of the reservoirs for the north and south volcanic systems are around 206 m and 361 m, respectively, when the reservoirs are assumed partially molten ($\varphi = 0.25$). Notice that although we give the average thicknesses of the reservoirs to a metre, these are crude estimates and depend strongly on the assumed melt fraction φ and other factors, discussed below.

The estimated thickness values for the reservoirs are similar to those of thick sills, such as are exposed in many continental areas. It should be noted, however, that the reservoirs are likely to be much thicker. The thickness values indicated here, and below, refer primarily to the thickness of the uppermost parts of the reservoirs supplying magma to the individual eruptions (Gudmundsson, 1987, 2016). Under certain conditions, a larger part of the reservoir (that is, a much thicker layer) would contribute to the eruption – for example during major caldera or graben subsidence into the top of the reservoir (Gudmundsson, 2015, 2016). So, generally, the reservoirs may be much thicker than the above values – of the order of kilometres, as discussed further below.

There may also be an uncertainty in the assumption that each individual lava shield represents one magma flow from the reservoir. It is possible that several lava shields were formed simultaneously from a single reservoir, in which case the reservoir volume, in particular the reservoir thickness, would be increased significantly. For example, the Anquwd al Yasarat volcanic fissures appear to be erupted during a single eruptive cycle (Fig. 10) and fed from the same feeder dyke. This follows because the distances between the nearby segments tips are very small in comparison with the segment lengths. The segments are therefore functioning mechanically as single continuous fracture (Babiker and Gudmundsson, 2004; Gudmundsson, 2011). Hence we may also estimate the volume and thickness of the associate magma reservoir assuming that several lava shields were generated in a single long-lasting magma flow from the source reservoir, indicating a larger reservoir thickness than in the estimate above (the estimated reservoir area is essentially constant given the density distribution of the eruption points, Fig. 11, so only the thickness changes when the volume erupted during a single magma flow from the reservoir increases as would be the case if several lava shields were formed in a single flow out of the reservoir).

For these particular volcanic fissures (Anquwd al Yasarat) the volume of eruptive materials is estimated at about 4.17 km^3 using ArcGIS 10.1 (Fig. 10). The corresponding reservoir area would remain the same, but a thickness changes. For $\varphi = 0.25$ the thickness would be 4265 m and for $\varphi = 1.0$ (totally molten) the thickness would be 1600 m. These are both plausible thicknesses.

Whatever the magma fraction the reservoirs, only their uppermost parts normally supply magma to an eruption. This follows from general models on magma chambers/reservoirs (Gudmundsson, 1987, 2016) and is also in agreement with most basaltic rocks in the AHVP being moderately fractionated, with MgO value in the range 7 to 9% (Peregi et al., 2003; Busrewil and Suwesi, 1993; Farahat et al., 2006).

Table 3
Static Young's moduli, densities as well as thicknesses of the crustal layers used for the numerical models. Thicknesses and densities of the uppermost crust are extracted from gravity and magnetic model of the northeast Sirt Basin by Ghanoush et al. (2014).

Layer	Age	Thickness (km)	ρ (kg/m^3)	E (GPa)
Layer 1	Miocene	3.2	2250	11
Layer 2	Eocene-Oligocene	1.8	2300	14
Layer 3	Paleogene	1.1	2350	18
Layer 4	Mesozoic	2.9	2500	20
Layer 5	Paleozoic	3.3	2550	25
Layer 6	Upper and middle crust	8.7	2700	35
Layer 7	Lower crust	13	3050	60
Layer 8	Mantle	66	3350	90

5. Numerical model

The finite element method (FEM) is the most common numerical technique used for solving differential and partial differential equations

(Henk et al., 2013). Numerical models based on the finite element method can provide quantitative information on the local stresses field distribution around magma reservoirs. Numerical models can thus improve our understanding the volcanotectonic activity in areas such as the present one, in particular as regards region the stress-conditions for magma reservoir rupture, dyke injection and propagation with the potential to feed eruptions. Comsol Multiphysics (5.1), the finite element program used here, is a commercial multipurpose software (www.comsol.com).

We made several numerical models in order to explore the potential effects of uplift or doming of the western part of the Sirt Basin on the stress fields around magma reservoirs in the Al Haruj region. We conclude that the local stresses around the magma reservoirs are favourable to rupture and injection dyke during the late Miocene – early Pliocene boundary conditions.

5.1. Model setup

The lithosphere of the Sirt Basin has been subdivided into eight mechanical layers, comprising the upper mantle, lower crust, upper crust as well as uppermost crust with the Palaeozoic, Mesozoic and Cenozoic sedimentary rocks (Ghanoush et al., 2014), as already mentioned. Thus, the crust and underlying mantle of the western part of the Sirt Basin are here modelled as eight layers with various thicknesses, densities, and Young's moduli (Table 3; Fig. 14A). All the layers are assumed to have the same typical Poisson's ratio, 0.25, for solid rocks.

The magma reservoir was modelled as elliptical with a major axis of 193 km and located at a crustal depth of 35 km, namely at the crust-mantle boundary. The reservoir is, in some of the models, subject to a constant internal magmatic excess pressure (p_e) of 5 MPa, which corresponds to the typical in-situ tensile strength (T_0) of the host rocks in the Sirt Basin. There is, in addition, the tensile loading of 5 MPa associated with the regional stress field. Some models have, in addition, regional doming-related pressure at the bottom of the crust. All models are fastened at the lower boundary to avoid any rigid-body rotation and/or displacement. The numerical models then provide the magnitudes of the maximum principal tensile stresses as coloured contours (Figs. 14, 15).

5.2. Model result

In the first model (Fig.14B), we focus on the effect of doming due to excess magmatic pressure at the bottom of the crust. The doming is known to have been about 1000 m. Here the doming is generated by 20 MPa excess pressure at the depth of the crust-mantle boundary and extends under the entire western part of the Sirt Basin. More specifically, an entire 850 km wide zone is subject to doming at the bottom of lower crust. In addition there is 5 MPa extension at the boundary of the model, reflecting the extension associated with the Sirt Basin. By contrast, in the second model the uplift or doming is confined to the reservoirs of the volcanic systems themselves and their immediate surroundings (Fig. 15). Thus, the main difference between the models is that the model in Fig. 14B relates to general large-scale crustal doming over a wide area, including the western part of the Sirt Basin. By contrast, the model in Fig. 15 shows the local effect of excess pressure, expansion (and dome local doming) in the reservoirs themselves.

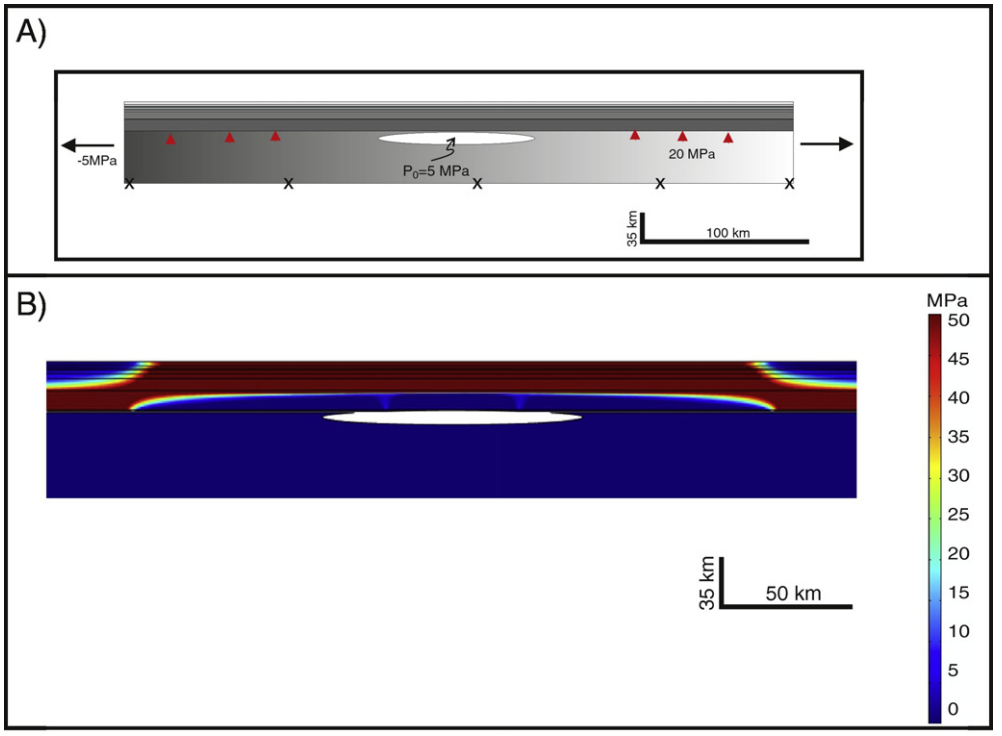

Fig. 14. A) Finite element model setup. An 850 km wide zone that represents the western part of the Sirt Basin was subject to uplift and doming during the late Miocene (Fig. 12), modelled with 20 MPa doming pressure, indicated by red cones. The deep seated magma reservoir is located at the boundary between the lower crust and upper mantle and is 193 km wide. The model is fastened at the lower boundary using a fixed constraint so as to avoid any rigid body rotation or displacement. Various elastic mechanical properties and thicknesses of the host rock are used in Table 3. Magma reservoir is modelled as an elliptical cavity with an excess magmatic pressure of 5 MPa. Tensile stress (−5 MPa) is applied as regional stress field, indicated by black arrows, to the far both boundary conditions of the model. B) Finite element model results. Colour contours represent the minimum compressive (maximum tensile) principle stress magnitudes. The regional uplift or doming may be generated compressive stress at the bottom of the lower crust and likely to be extended to the area surrounding magma reservoir. Compressive bending stresses, due to the doming, at the bottom of the curst would have prevented significant dyke injections and eruptions in late Miocene. Therefore, during this stage the volcano-tectonics are not suitable to trigger eruption. By contrast, the tensile stresses in the upper crust to reach theoretical values of several tens of mega-pascal (MPa) and would have reactivated and/or generated new fractures and faults, particularly normal faults, as are observed in the seismic lines of the western part of the Sirt Basin.

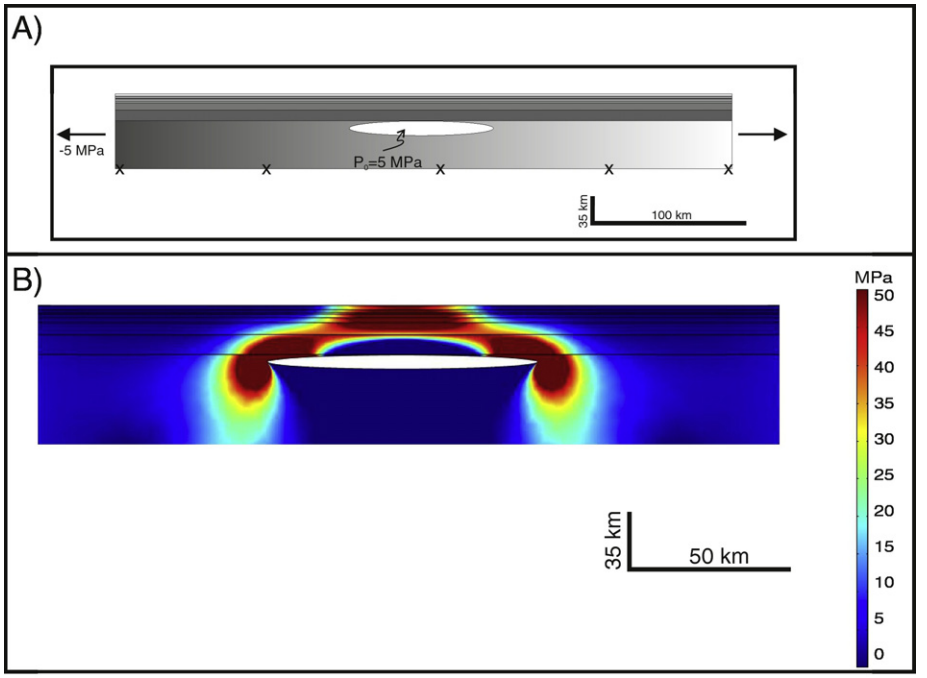

Fig. 15. A) Same model setup, mechanical layers, loading and boundary conditions as in Fig. 14A with the effect of doming of the lower crust removed from the model. The relaxation time to release the effect of compressive stresses at the bottom of the crust (Fig. 14) probably took several millions of years. Following this relaxation, excess magmatic pressure and contrast in mechanical properties of layers generated (B) maximum tensile stresses around margins of the magma reservoir and in the uppermost layers. These local stresses field encourage rupturing and injecting of dykes from its margins rather than the central part, in agreement with the location of most of the lava shields. Colour contours representing the minimum compressive (maximum tensile) principle stress.

The local stress field in the western part of the Sirt Basin was influenced particularly by doming in the late Miocene. The doming induces stresses which, in turn, depend on the mechanical properties of the crustal layers. The resulting variations in the ambient stress field in magnitudes and orientation are commonly referred to as stress perturbations and give rise to specific patterns referred to as the local stress field (Henk et al., 2013). The local stress field magnitudes reach several tens of megapascals (MPa) (Fig. 14B). We infer that the local palaeostress field controlled the generation and reactivation fractures in the area, in particular as observed in seismic lines of the western part of the Sirt Bain (cf. Abdunaser and McCaffrey, 2015).

In the second model (Fig. 15), we assume that the original doming stresses, resulting in compressive stresses at the crust over the 850 km wide area, have been somewhat reduced. This relaxation may have taken millions of years. After the relaxation of compressive stresses in the bottom of crust, at the crust-mantle boundary, the magma reservoir itself induces local tensile stresses around its margins. The induced tensile stresses around reservoir margins result in increased chances of reservoir rupture and injection of dykes, particularly from its margins to feed eruptions (Fig. 13 A). The eruptions may have been sustained in frequency until the middle Pleistocene (Fig. 13 B) and then declined in number and volume since the middle Pleistocene. Subsequently, the volcanic activity in the Al Haruj al Abyad system diminished much in middle Pleistocene whilst the magmatism and volcanism still continued at least Holocene near the centre of the magma reservoir of the Al Haruj al Aswad system, producing much smaller fissure eruptions with more evolved basaltic rocks than the earlier eruptions (i.e. Asran and Aboazom, 2004; Farahat et al., 2006; Cvetkovic´ et al., 2010) (Fig. 13 C).

6. Discussion and conclusions

This study focuses on monogenetic volcanoes in the AHVP area in the western part of the Sirt Basin in Libya. We show that the volcanoes form two density peaks or groups that can be distinguished as two separate volcanic systems. Each systems contains numerous monogenetic volcanoes, particularly crater cones, lava shields, and (some) maars. Each system is thought to be fed by a deep-seated and very extensive magma reservoir.

The lava shields on the AHVP are mostly gently sloping, based on the classification of Pike (1978). They are generally more gently sloping but otherwise roughly similar to many Holocene monogenetic lava shields in Iceland in terms of areas and volumes, although the largest shields in Iceland are considerably larger than those of the AHVP. By contrast, the lava shields of AHVP are many times smaller than the polygenetic shield volcanoes on Hawaii and Galapagos. The AHVP lava shields are regarded as being mostly monogenetic, that is, formed in single eruptions, some of which may have been of long duration.

The spatial distributions of the lava shields are essentially restricted to the north and south parts of the volcanic province. They were primarily formed in the period from late Miocene to early Pleistocene, but some volcanic activity may have continued into Holocene. In particular, there are indications of small fissure eruptions – some of which may be of Holocene age – in the summits of some lava shields. The early lava shields are mostly located at the margins of the volcanic systems and generally of larger volumes than later-formed shields – which are also geographically more widely distributed.

The volumes of an individual lava shields and areal distribution of volcanic phases gradually decrease with time. More specifically, the volumes of individual lava shields and sizes of the areas covered by volcanic phases in the Al Haruj al Aswad volcanic system is, on average, greater than similar eruptions and phases in the Al Haruj al Abyad volcanic system. It is clear that the total volume of lavas produced over a given time period in the northern volcanic system is much more than the total volume of lavas produced, during the same time, in the southern volcanic system.

Most of the eruption sites or points are concentrated in two areas within the AHVP. These distributions suggest the existence of associated separate magma reservoirs (Lesti et al., 2008) beneath the volcanic

systems, namely one reservoir beneath each system. Thus, we propose that the AHVP may be divided two distinct volcanic systems, each with its own source magma reservoir, a suggestion also made by other authors (i.e. Peregi et al., 2003). The two proposed volcanic systems are those of Al Haruj al Aswad and Al Haruj al Abyad.

From Eq. (8) the magma fraction of the reservoir presumably played a significant role in controlling the eruptive volumes at the surface. Due to the uncertainty about individual volcanic eruptions in the AHVP, we have made two assumptions to estimate bulk volumes and thicknesses of magma reservoirs that supplied magma to the eruptions of the AHVP. First, that each individual lava shield represents a single eruption. Second, that crater rows (volcanic fissures) and overlapping small lava shields represent single eruptions. Although the volume and thickness of parts of the reservoirs that supply magma to eruptions are quite different depending on which assumption is used, general considerations suggest that in nearly all the eruptions in the AHVP only the uppermost part of each reservoir supplied magma to the eruption. This means that the potential of the reservoirs – the maximum eruptive volumes that they can generate – is much greater than the typical volume (cf. Gudmundsson, 2015, 2016; Karaoğlu et al., 2017).

Several numerical models were made in order to investigate local variation in the stress field resulting from general doming of the area, as well as local loading by magma reservoirs through internal excess magmatic pressure and external tensile loading. We also include the effects of the mechanical properties of the layers that constitute the crustal segments forming the roofs of the magma reservoirs. Our finding in the first model, based on large-scale regional doming at the lower crust-upper mantle boundary, reveals that compressive stresses are generated in the lower part of the crust (tensile stresses in the upper part), and that these compressive stresses would tend to hinder dyke initiation and propagation to the surface. Thus, this type of loading is clearly not favourable for rupture of magma reservoir and dyke injection and eruption.

Following the doming and, then, gradual relaxation of compressive stresses in the bottom of crust – partly because of the effect of remote regional tensile rifting stress - excess magmatic pressure led to induced local tensile stresses around margins of magma reservoir. The relaxation time was presumably millions of years but eventually relaxed the compressive stresses around the magma reservoir. The relaxation seems to have continued during most of the Tortonian time to early Messinian time. Subsequently the volcanic activity began in the Al Haruj region at the Messinian time (Fig. 13A). The eruptions continued until the early Pleistocene (Fig. 13B), after which they gradually declined in volume and number, particularly since the middle part of the Pleistocene. The Al Haruj al Abyad volcanic system became more or less inactive in middle part of the Pleistocene while activity continued near the centre of the volcanic system of Al Haruj al Aswad, although with gradually smaller eruptive volumes, issued primarily in fissure eruptions, and producing more evolved basaltic rocks (Fig. 13C).

Acknowledgments

We thank the Libyan Ministry of Higher Education and Scientific Research for the financial support. We are grateful to the Editor Joan Marti and anonymous reviewers for comments which greatly improved the paper.

References

Abadi, A., van Wees, J., van Dijk, P., Cloetingh, S., 2008. Tectonics and subsidence evolution of the Sirt Basin, Libya. 92. AAPG Bulletin, pp. 993–1027 2008.

Abdalkadeer, K., Senturk, E., Norman, D., Goodman, M., Prada, M., Rivera, N., 2009. Changes in Near Wellbore Stress and Fracture Gradient Due to Cold Water Injection in a Sirte Basin Field, Libya. Copyright 2009. Society of Petroleum Engineers, Abu Dhabi, UAE (17 pp.).

Abdunaser, K.M., McCaffrey, K.J.W., 2014. Rift architecture and evolution: the Sirt Basin, Libya: the influence of basement fabrics and oblique tectonics. J. Afr. Earth Sci. 100, 203–226.

Abdunaser, K., McCaffrey, K., 2015. Tectonic history and structural development of the Zallah-Dur al Abd Sub-Basin, western Sirt Basin, Libya. J. Struct. Geol. 73:33–48. http://dx.doi.org/10.1016/j.jsg.2015.02.006.

Ade Hall, M., Reynolds, H., Dagley, P., Musset, G., Hubbard, B., Klitzsch, E., 1974. Geophysical studies of North African Cenozoic volcanic areas Al Haruj Al – Assuad, Libya. Can. J. Earth Sci. 11, 998–1006.

Al-Hafdh, N., Elshaafi, A., 2015. Geochemistry and Petrology of Basic Volcanic Rocks of Jabal Al Haruj Al-Aswad, Libya. Int. J. Geosci. 6:109–144. http://dx.doi.org/10.4236/ijg.2015.61008.

Andrew, R., Gudmundsson, A., 2007. Distribution, structure, and formation of Holocene lava shields in Iceland. J. Volcanol. Geotherm. Res. 168:137–154. http://dx.doi.org/10.1016/j.jvolgeores.2007.08.011.

Asran, A., Aboazom, A., 2004. Al-Haruj Tertiary basalts, Libya: petrological and geochemical approach. Proceedings of the 6th International Conference on the Geology of the Arab World (GAW6).

Babiker, M., Gudmundsson, A., 2004. Geometry, structure and emplacement of mafic dykes in the Red Sea Hills, Sudan. J. Afr. Earth Sci. 38, 279–292.

Bardintzeff, J., Deniel, H., Guillou, B., Platevoet, P., Télouk, Oun, K., 2012. Miocene to recent alkaline volcanism between Al Haruj and Waw an Namous (southern Libya) International Journal of Earth Sciences and Engineering. 101 pp. 1047–1063.

Blake, S., 1981. Volcanism and the dynamics of open magma chambers. Nature 289, 783–785.

Brook, N., 1993. The Measurement and Estimation of Basic Rock Strength. In: Hudson, J.A. (Ed.), Comprehensive Rock Engineering. 3, pp. 41–66.

Browning, J., Drymoni, K., Gudmundsson, A., 2015. Forecasting magma-chamber rupture at Santorini volcano, Greece. Sci. Report. http://dx.doi.org/10.1038/srep15785.

Busrewil, M., 1996. The volcanology of central Jabal al Haruj al Aswad volcanic province, Central Libya. The geology of Sirt Basin. III. Elsevier, Amsterdam, pp. 331–345.

Busrewil, M., 2012. Evolution of Al Haruj Volcanic Province, Central Libya. Geology of Southern Libya. 3, pp. 171–181.

Busrewil, M., Suwesi, K., 1993. Geological Map of Libya 1: 250.000, Sheet : Al Haruj Al Aswad NG(33-4). Explanatory Booklet. Industrial Research Centre, Tripoli (95pp).

Busrewil, M., Mriheel, I., Al Fasatwi, T., 1996. Volcanism, tectonism and hydrocarbon potentials of parts of Al Haruj area, SW Sirt Basin, Libya. The Geology of Sirt Basin. III. Elsevier, Amterdam 317-329.

Chen, N., Dong, J., Chen, J., Dong, C., Shen, Z., 2014. Geometry and Emplacement of the Late Cretaceous Mafic Dyke Swarms on the Islands in Zhejiang Province. Insights from high-resolution satellite images, Journal of Asian Earth Sciences, Southeast China, pp. 302–311.

Cheng, C., Johnston, D., 1981. Dynamic and static moduli. Geophys. Res. Lett. 39–42.

Chorowicz, J., Benissa, M., 2016. Remote sensing and field analysis of the Palaeozoic structural style inNW Libya: the Qarqaf arch a paleo-transfer fault zone between the Ghadamis and Murzuq basins. J. Afr. Earth Sci. 123, 272–293.

Chorowicz, J., Deroin, J., 2003. La télédétection et la cartographie géomorphologique et géologique. Editions Gordon & Breach, collection Geosciences (141 pp.).

Clark, G., 1966. Deformation moduli of rocks. Testing Techniques for Rock Mechanics. 402. American Society for Testing Materials, pp. 133–172.

Cloetingh, S., Van Wees, J., 2005. Strength reversal in Europe's intraplate lithosphere: Transition from basin inversion to lithospheric folding. Geology 33, 285–288.

Cvetkovic´, V., Toljic´, M., Ammar, N.A., Rundic´, L., Trish, K.B., 2010. Petrogenesis of the eastern part of the Al Haruj basalts (Libya). J. Afr. Earth Sci. 58, 37–50.

Drury, S., 2001. Image Interpretation in Geology. Blackwell Science, Nelson Thornes, UK (290 pp.).

Elshaafi, A., Gudmundsson, A., 2016. Volcano-tectonics of the Al Haruj Volcanic Province, Central Libya. J. Volcanol. Geotherm. Res. 325:189–202. http://dx.doi.org/10.1016/j.jvolgeores.2016.06.025.

Farahat, E., Abdel Ghani, M., Aboazom, A., Asranc, A., 2006. Mineral chemistry of Al Haruj low-volcanicity rift basalts, Libya: implications for petrogenetic and geotectonic evolution. J. Afr. Earth Sci. 45, 198–212.

Ghanoush, H., Imber, J., McCaffrey, K., 2014. Cenozoic Subsidence and Lithospheric Stretching Deformation of the Ajdabiya Trough Area, Northeast Sirt Basin, Libya. AAPG 2014 Annual Convention and Exhibition, Houston, Texas.

Gudmundsson, A., 1986. Mechanical aspects of postglacial volcanism and tectonics of the Reykjanes Peninsula, southwest Iceland. J. Geophys. Res. 91, 12711–12721.

Gudmundsson, A., 1987. Formation and mechanics of magma reservoirs in Iceland. Geophys. J. R. Astron. Soc. 91, 27–41.

Gudmundsson, A., 1990. Emplacement of dikes, sills, and crustal magma chambers at divergent plate boundaries. Tectonophysics, 176, 257–275.

Gudmundsson, A., 2000. Dynamics of volcanic systems in Iceland: example of tectonism and volcanism at juxtaposed hot spot and mid-ocean ridge systems. Annu. Rev. Earth Planet. Sci. 28, 107–140.

Gudmundsson, A., 2011. Rock Fractures in Geological Processes. Cambridge University Press, Cambridge http://dx.doi.org/10.1017/CBO9780511975684.

Gudmundsson, A., 2012. Magma chambers: formation, local stresses, excess pressures, and 674 compartments. J. Volcanol. Geotherm. Res. 237–238, 19–41.

Gudmundsson, A., 2015. Collapse-driven large eruptions. J. Volcanol. Geotherm. Res. 304, 1–10.

Gudmundsson, A., 2016. The mechanics of large volcanic eruptions. Earth Sci. Rev. 163: 72–93. http://dx.doi.org/10.1016/j.earscirev.2016.10.003.

Gumati, Y., Schamel, S., 1988. Thermal maturation history of the Sirte Basin, Libya. J. Pet. Geol. 205–218.

Haimson, B., Rummel, F., 1982. Hydrofracturing stress measurements in the Iceland research drilling project drill hole at Reydarfjordur, Iceland. J. Geophys. Res. 87, 6631–6649.

Hasenaka, T., 1994. Size, distribution, and magma output rate for shield volcanoes of the Michoac in-Guanajuato volcanic field, Central Mexico. Journal of Volcanology and Geothermal Research 63, 13–31.
Henk, A., Fischer, K., Kromuller, K., Wanger, D., Winter, I., 2013. Prediction of tectonic stresses and fracture Networks with geomechanical reservoir models. DGMK-Research Report 721. German Society for Petroleum and Coal Science and Technology.
Hermance, J., 1981. Crustal gensis in Iceland; geophysical constraints on crustal thickening with age. Geophys. Res. Lett. 8, 203–206.
Jaeger, J., Cook, N., 1969. Fundamentals of Rock Mechanics Methuen, London. (515 pp).
Jakobsson, S., Jónsson, J., Shido, F., 1978. Petrology of the western Reykjanes peninsula, Iceland. J. Petrol. 19, 669–705.
Jonsson, J., 1978. Jarofraedikort af Reykjanesskaga. Nation Energy Authority of Iceland (OS-JHD-7831).
Karaoğlu, O., Elshaafi, A., Salah, M., Browning, J., Gudmundsson, A., 2017. Large-volume lava flows fed by a deep magmatic reservoir atAğrı Dağı (Ararat) volcano, Eastern Turkey. Bull. Volcanol. http://dx.doi.org/10.1007/s00445-016-1098-0.
Klitzsch, E., 1968. Der Basalt vulkanismus des Djebel Haroudj, Ostfezzan, Libya. Geol. Rundsch. 57, 585–609.
Koch, M., Mather, P., 1997. Lineament mapping for groundwater resource assessment: a comparison of digital Synthetic Aperture Radar (SAR) imagery and stereoscopic Large Format Camera (LFC) photographs in the Red Sea Hills, Sudan. Int. J. Remote Sens. 18, 1465–1482.
Le Corvec, N., Sporl, B., Rowland, J., Lindsay, J., 2013. Spatial distribution and alignments of volcanic centers: clues to the formation of monogenetic volcanic fields. Earth Sci. Rev. 124, 96–114.
Less, G., Turki, S., Suwesi, K., Peregi, L., Koloszar, L., Kalmar, J., Sherif, K., Csaszar, G., Gulasci, Z., Dalum, H., Al Tajuri, A., 2006. Explanatory Booklet. Geological Map of Libya 1: 250.000. Sheet: Waw Al Kabir NG 33-12. Industrial Research Centre (295 pp.).
Lesti, C., Giordano, G., Salvini, F., Cas, R., 2008. Volcano tectonic setting of the intraplate, Pliocene-Holocene, Newer Volcanic Province (southeast Australia): role of crustal fracture zones. J. Geophys. Res. 113, B07407. http://dx.doi.org/10.1029/2007JB005110.
Machado, F., 1974. The search of magmatic resevoirs. In: Civetta, L., Gasparini, P., Luongo, Rapolla, A. (Eds.), Physcial Volcanology. Elsevier Science, New York, pp. 255–273.
Martin, U., Németh, K., 2006. How Strombolian is a "Strombolian" scoria cone? Some irregularities in scoria cone architecture from the Trans-mexican Volcanic Belt, near Volca´n Ceboruco, (Mexico) and Al Haruj (Libya). J. Volcanol. Geotherm. Res. 155, 104–118.
Mouzughi, A., Taleb, T., 1981. Tectonic Elements of Libya: Libya, National Oil Corporation, Scale 1:2,000,000, 1 Sheet.
Nazir, R., Momeni, E., Jahed Armaghani, D., Mohd, M., 2013. Correlation between confined compressive strength and indirect tensile strength of limestone rock samples. J. Geotech. Eng. 18 (Band. I).
Nixon, S., Maclennan, J., White, N., 2011. Generation of Alkali and Tholeiitic Basalts: The Al Haruj volcanic field, Volcanic and Magmatic Studies Group Annual Meeting, 5–7 January. Queens College, Cambridge.
Pacific Aero Survey, 1979. Air bone Geophysical Survey Jabal Al Haruj Al Aswad Area. Final Report. Qeb., Inc., Hayward, California.
Peña, S., Abdelsalam, M., 2006. Orbital remote sensing for geological mapping in southern Tunisia: implication for oil and gas exploration. African Earth Sciences]–>J. Afr. Earth Sci. 44, 203–219.
Peregi, Z., Less, G., Konrad, G., Fodor, L., Gulacsi, Z., Gyalog, L., Turki, S., Suwesi, S.Kh., Sherif, Kh., Dalub, H., 2003. Explanatory Booklet. Geological Map of Libya 1: 250.000. Sheet: Al Haruj Al Abyad NG 33-8. Industrial Research Centre, Tripoli (248 pp.).
Pike, R., 1978. Volcanoes on the inner planets: some preliminary comparisons of gross topography. Lunar and Planetary Science Conference 9th, pp. 3239–3273.
Qui, K., Gherryo, Y., Shatwan, M., Fuller, J., 2008. The application of the Mechanical Earth Model on Rejuvenation of A Mature Field in Libya. Copyright 2008. IADC/SPE Asia Pacific Drilling Technology Conference and Exhibition, Jakarta, Indonesia (16 pp.).
Rajesh, H., 2004. Application of remote sensing and GIS in mineral resource mapping – an overview. J. Mineral. Petrol. Sci. 99.
Rossi, M., 1997. Morphology of basaltic lava flow fields in Iceland. PhD Thesis, University of Turku, Finland.
Rossi, M., Gudmundsson, A., 1996. The morphology of flow-lobe tumuli on Icelandic lava shields. J. Volcanol. Geotherm. Res. 72, 291–308.
Schmeling, H., 1985. Partial melt below Iceland: a combined interpretation of seismic and conductivity data. J. Geophys. Res. 90, 105–110.
Schultz, H., 1995. Generation and equilibrium of olivine tholeiites in the northern rift zone of Iceland. A petrogenic study of the Blafjall table mountain. Journal of Volcanology and Geothermal Research 65, 161–179.
Self, S., Keszthelyi, L., Thordarson, T., 1998. The importance of pahoehoe. Annu. Rev. Earth Planet. Sci. 26, 81–110.
Sheorey, P., 1997. Empirical Rock Failure Criteria. A.A. Balkema, Rotterdam (176 pp.).
Solomon, S., Ghebreab, W., 2008. Hard-rock hydrotectonics using geographic information systems in the central highlands of Eritrea: implications for groundwater exploration. J. Hydrol. 349, 147–155.
Tibaldi, A., 2015. Structure of volcano plumbing systems: a review of multi-parametric effects. J. Volcanol. Geotherm. Res. 298:85–135. http://dx.doi.org/10.1016/j.jvolgeores.2015.03.023.
Vesely, J., 1985. Geological Map of Libya 1: 250.000 Sheet; Zallah NH 33-16. Explanatory Booklet. Industrial Research Centre, Tripoli (125 pp.).
Wadge, G., 1981. The variation of magma discharge during basaltic eruptions. J. Volcanol. Geotherm. Res. 11, 139–168.
Walker, G., 1965. Some Aspects of Quaternary Volcanism in Iceland. 49. Leicester Literary and Philosophical Society, pp. 25–40.
Whitford-Stark, J., 1975. Shield volcanoes. In: Fielder, G., Wilson, L. (Eds.), Volcanoes of the Earth, Moon, and Mars. St. Martins Press, New York, NY, pp. 66–74.
Wienecke, S., Stadtler, C., 2014. Asep + d Method: Identifying Anomalous Areas of the earth's Lower Crust, Publication Number EP 2791713 A1 (Patents).
Woller, F., 1984. Geological Map of Libya 1: 250.000, Sheet: Al Fuquaha NG 33-3. Explanatory Booklet. Industrial Research Centre, Tripoli (123 pp.).

Chapter 7: Emplacement and inflation of the Al-Halaq al Kabir lava flow field, central part of the Al Haruj Volcanic Province, Central Libya

Abdelsalam Elshaafi and Agust Gudmundsson

Contribution statement

Fieldwork conducted by AE from assistance Industrial Research Centre (IRC), Tripol, Libya.

Design of the work and analytical approach were developed by AE

Experiments carried out by AE at UCL with assistance from Nathaniel Forbes

Drafting the manuscript was made by AE and revising the manuscript critically from co-author

All illustrations, numerical and conceptual models were prepared by AE.

Data analysis and interpretation were done by AE with substantial support from co-author

Emplacement and inflation of the Al-Halaq al Kabir lava flow field, central part of the Al Haruj Volcanic Province, Central Libya

Abdelsalam Elshaafi[1], Agust Gudmundsson[1]

[1]Department of Earth Sciences, Royal Holloway University of London, Egham TW20 0EX, UK (abdelsalamelshaafi@yahoo.co.uk; a.gudmundsson@rhul.ac.uk)

Abstract

Numerous of lava rise plateaus and tumuli developed in the medial and distal portions of the Al-Halaq al Kabir lava flow field during the last eruption (sometime during the Holocene) in the central part of the Al Haruj Volcanic Province (AHVP). These inflation features can be used to understand better the lava emplacement mechanism in this part of the Al Haruj region where the widespread occurrence of tumuli and lava rises are good indicators of mode of emplacement. We report the results of detailed measurements of the maximum and minimum diameters in plan-view of 551 lava rises and 289 tumuli from the distal part of the Al-Halaq al Kabir lava field using ArcGIS and field observations. Tumuli and lava rise plateaus may be divided into subpopulations according to the abrupt change in the scaling exponents on log-log plots of their frequency versus diameters. The stiffness (Young's modulus) for the basaltic rocks in the study area is estimated in the range of 10-34 GPa. Numerical and analytical results show that theoretical maximum tensile stress in the inflated upper crust reaches 44 to 570 MPa. This theoretical stress is orders of magnitude higher than typical in-situ tensile strengths of rocks (0.5-9 MPa), which means that the tensile stresses are high enough to rupture the crust. These high tensile stresses are generated through crustal doming driven by a very low excess pressure (1 MPa or less). Our findings partly explain the abundance of tension fractures at the surface of the Al-Halaq al Kabir lava flow field. Tumuli observed in the area

are remarkably similar in morphology and aspect (height/width) ratios to the flow-lobe tumuli which have been studied in the medial and distal parts of Holocene Icelandic lava flow fields. This geometric similarity suggests that they may have been emplaced through an analogous mechanism of emplacement. The preferred thermally efficient internal pathways seem to have played a significant role in the transport of lava from the vent system to the distal portions of the lava flow field. These results of the mechanisms of formation of this lava flow field may also be of importance in connection with local biological extinction in the area. There appears to be a coincidence between the age of an initial volcanism in the AHVP ((≈7 Ma) and a fauna and flora local disappearance in the As-Sahabi area, NE the Sirt Basin, during Messinian-Zanclean time (≈7 to 5 Ma).

7.1 Introduction

Volcanic activity has commonly produced extensive basaltic lavas ranging from pahoehoe to aa types of lava flows (Walker 1991, Kilburn 2000; Nemeth et al., 2008). Lava flows are generally the most common volcanic features on the Earth and several of the solid planetary bodies and their satellites, particularly on Mars and Moon (Glaze et al., 2005; De Wet et al., 2014; Scheidt et al., 2014). The inflation structures, such as lava rise plateaus and tumuli, are the most abundant in pahoehoe lava flow field (Hon et al 1994; Self et al 1996; 1997, 1998; Walker, 1991; Keszthelyi&Pieri 1993; Chitwood, 1994; Rossi and Gudmundsson, 1996; Thordarson and Self 1998; Duraiswami et al., 2001) and a subsidiary in aa lava flow field (Calvari and and Pinkerton, 1998; Ducan et al., 2004). Pahoehoe lava flows are commonly associated with low effusion rate and relatively long-lived eruptions (Glaze et al., 2005). Lava rise plateaus, tumuli, lava-rise pits and inflation clefts are common inflation structures on the lava flow surfaces of

the Al Haruj Volcanic Province (AHVP), central Libya, and can be used in deciphering the emplacement mechanism of lava flow-field.

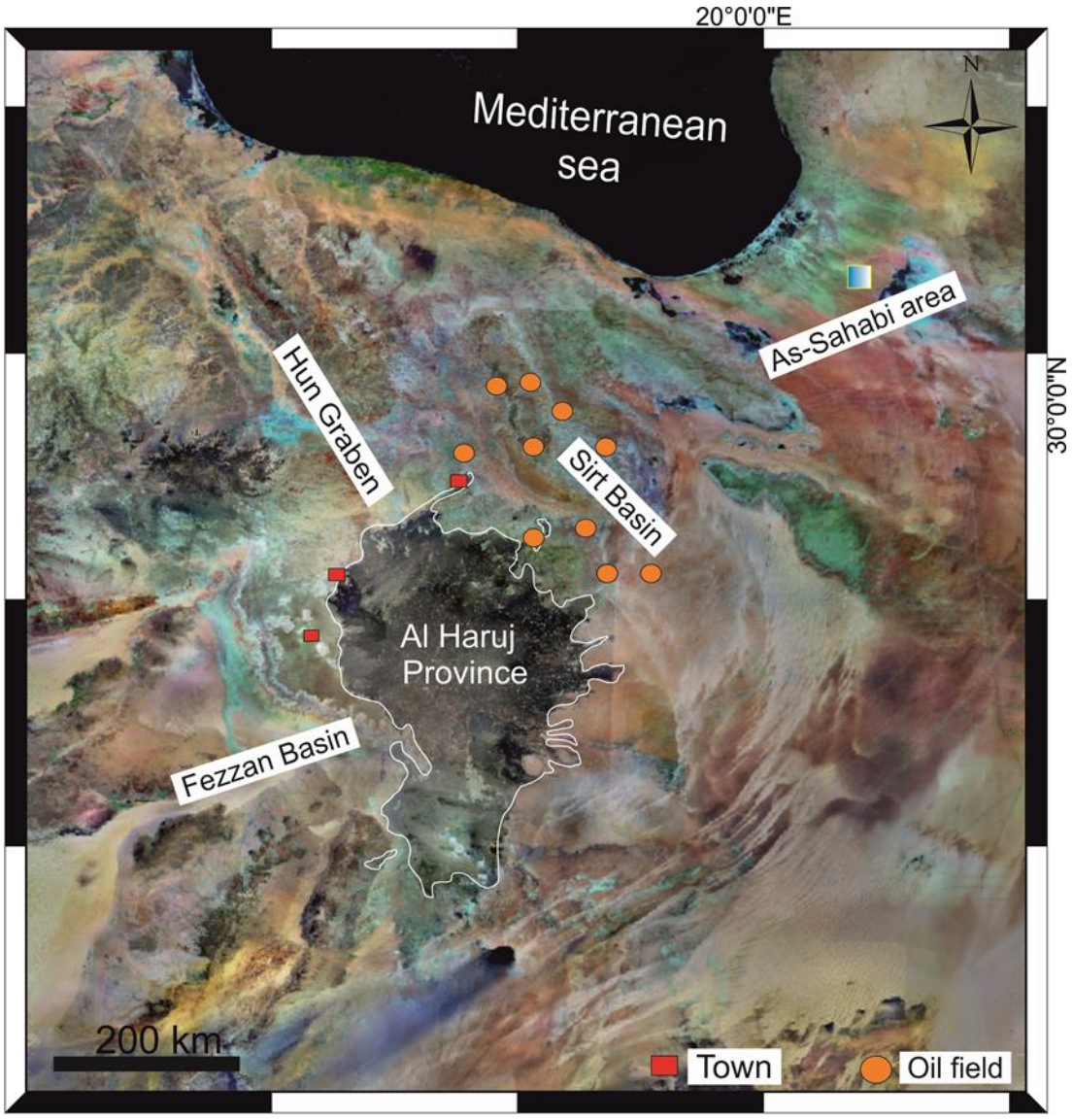

Figure 7.1. Landsat ETM+ image showing the extent of the Al Haruj Volcanic Province (AHVP), footprint-shaped, situated in the central part of Libya. The boundary of volcanic province is indicated by white line (adapted from Satellite Imaging Corporation). Orange circles and red boxes are indicated to locations of oil fields and towns in the Al Haruj region, respectively.

The result of new age dating by Nixon et al., (2011) of the last eruption on the Al Haruj volcanic province is indicated much younger (≈3.200 yrs) than earlier studies (≈0.1 Ma) (e.g., Peregi et al., 2003), This evidence along with a series of high magnitude earthquakes along the margin of the NW-SE trending Hun Graben, western Sirt Basin (Fig. 7.1), suggest that the Al Haruj region might still be potentially volcanically and seismically active. It follows that it is of fundamental importance to understand better the lava emplacement processes that formed the Al-Halaq al Kabir lava flow field.

Inflation structure is generally defined as positive topographic feature having various shapes with wide ranges of slope angles and characterised by three-part structural division of flow lobes; upper vesicular crust, crystalline core zone and lower vesicular crust (e.g., Hon et al., 1994; Thordarson and Self, 1998; Thordarson, 2000). The three-fold structural division are considered as keys for estimating duration and understanding better the emplacement mechanism of pahoehe flow lobes (Hon et al. 1994, Thordarson and Self, 1998). The crustal lifting or doming is occurred due to sustained supply of lava under an insulating crust (Rowland and Walker, 1987; Thordarson, 1995; Thordarson and Self, 1998, Duncan et al., 2004). The term inflation in pahoehoe flows was first introduced by Macdonald (1953) who gave a brief description of inflation feature but without mentioned the mechanism. Subsequently, Theilig (1986) and Walker (1991) described the formation of inflation structures. However, the first comprehensive and more reliable understanding of inflated pahoehe lava flows was done later by Hon et al. (1994) who have measured and observed low effusion an emplacement of active lava flows on Kilauea volcano, Hawaii. After that many studies have been used the results of Hon et al. (1994) and improved these crucial results in order to understand better the development, emplacement and duration of pahoehoe lava flow fields around the world (e.g., Thordarson 1995, Rossi and Gudmundsson, 1996; Self et al 1996, 1997, Keszthelyi et al 1997, Thordarson and Self, 1998; Thordarson, 2000; Thordarson et al., 2003;

Mattsson and Höskuldsson; 2005; Glaze et al., 2005; Thordarson, Sigmarsson, 2009). Walker (1991) has described various types of the tumuli and lava rise plateaus that are formed along the distance from the lava sources to the distal zone of pahoehoe lava flow-fields in Hawaii. He distinguished three types of tumuli in pahoehoe flow field in. Namely: (i) shallow slope tumuli, (ii) moderate slope tumuli and (iii) flow-lobe tumuli. Subsequently, Rossi and Gudmundsson (1996) focused on the morphology and formation of tumuli and lava rise plateaus on monogenetic shield volcanoes in Iceland. They mentioned that the flow lobe tumuli are mainly located at the medial and distal parts of the flow filed (≈9.5 km from vent) whilst the lava-coated and upper slope tumuli are essentially occurred at the proximal parts of flow fields. Also they found that the internal structure within the flow-lobe tumuli is identical to that of P-type flow lobes.

However, most tensional fractures are formed on surface of the pahoehoe flows during inflation processes rather than being cooling joint fractures (Anderson et al., 1999; Self et al., 2000). Inflation cracks represent brittle failure of the upper lava crust in response to expansion whereas columnar joints represent cooling when the flow of fresh lava terminated and the molten core became stagnant and less stress field. The highly irregular jointing of the lava crust is created due to instability of the lava crust during inflation processes (Thordarson and Self, 1998; Thordarson, 2000). The difference jointing styles indicates that jointing formed in several stages during emplacement pahoehoe lava flow fields and can be explained in the term of inflation rather than rapidly turbulent emplacement. Thordarson and Self (1998) used jointing style in the Roza Memebr, Columbia River Basalt Group (CRBG), as one criterion along with vesicularity pattern and crystallinity in order to recognise threefold structural division of P-type flow lobes and subsequently they employed these data to estimate the whole lava flow field duration. The overall morphology and general arrangement of internal structures of lava flow fields in the AHVP show characteristics

analogous to inflated pahoehoes flows have been observed by Rossi and Gudmundsson (1996) on monogenetic lava shields in Iceland and to that of which made up the distal sectors lava flows on Surtsey in Iceland have been described by Thordarson (2000).

7.2 Geological background of the Al Haruj Volcanic Province (AHVP)

The AHVP is one of the largest volcanic provinces in the North Africa, covering an area around 42,000 km^2 in the central part of Libya (Fig. 7.1) (Elshaafi and Gudmundsson, 2016). Vertical succession of basaltic flows with a thickness of few tens meter can be observed, and geophysical studies have indicated that the thickness attained by the lava pile is on average as much as 145 m in the central part (Peregi et al., 2003). While on the margins the lava pile decreases considerably in thickness to as less as few meters (Fig. 7.2). It has been postulated that the AHVP formed during the end of Miocene to Holocene time (Nixon et al., 2011). The AHVP is constituted dominantly of transitional to alkaline basaltic lava flows. The basaltic flows are intruded at a number of lava shields, scoria cones, spatter cones and numerous volcanic fissures that are speculated to represent feeder. The AHVP is widely believed to have erupted through numerous of fissures in the crust and spread laterally over considerable distances in addition to major eruptive centres which are located mainly in northern and southern parts of the volcanic province (Elshaafi and Gudmundsson, 2016; 2017).

Although inflation features are common in basaltic lava flows of the AHVP and extremely well-preserved, these features have not received any attention except the synoptic study of Nemeth et al. (2008) who describe the tumuli in the southernmost of the AHVP (Al Haruj al Abyad subprovince) and they have mentioned that there are similarity between type of tumuli in this part of

the AHVP and type of tumuli have been identified in Iceland by Rossi and Gudmundsson (1996). By contrast, significant works have been done on the AHVP in the past few decades concerning geochronology, petrology, and geochemistry.

Lithostratigraphic classification of basaltic lava flows on the AHVP has been done by Busrewil and Suwessi (1993); Peregi et al. (2003); Less et al. (2006), respectively. Basaltic flows have been grouped into six major volcanic phases according to their field relations and tonal variation of

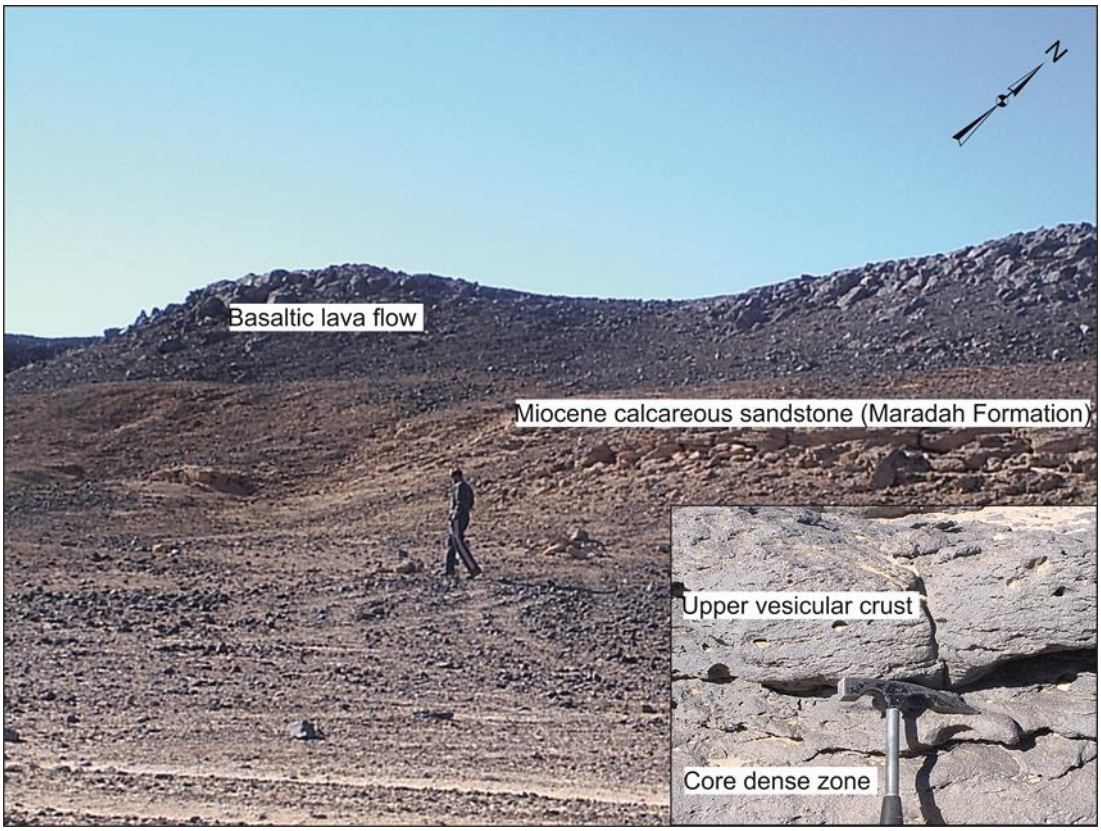

Figure 7.2. Field photograph showing the general morphology of a hummocky pahoehoe flow overlay the Miocene calcareous sandstone of Maradah Formation. The thickness of lava flow does not exceed few meters. The inset photograph showing the upper vesicular flow-lobe zone and core dense zone which is substantial evidence of endogenous growth during emplacement. Note the person provides scale.

various lava flow fields on the aerial photographs as well as age dating along with paleomagnetic measurements. There are not significant petrochemical variations between these six volcanic phases (Peregi et al., 2003; Less et al., 2006). It should be emphasised that each volcanic phase has been subdivided into the different mappable volcanic unit but with same age (Peregi et al., 2003, Less et al., 2006). Hummocky flows are quite common in the central part of the AHVP. They display a strong evidence of endogenous growth or inflation (Ninad et al., 2003) where flow-lobe consists mainly of a vesicular upper crust and a dense core zone but the lower vesicular zone is lacked observed (Fig. 7.2).

The Al-Halaq al Kabir lava field has been mapped by Busrewi and Suwesi (1993) as a mappable unit (6.1) follows the last volcanic phase (phase 6) and during this study, we treated this mappable unit as an individual flow field and remapped here as unit II (Fig. 7.3a, b). The terminology used in this paper to describe inflated pahoehoe lavas is revised from Walker (1991), Hon et al. (1994), Self et al. (1998), Rossi and Gudmundsson (1996) and Thordarson and Self (1998). The lava flow field is defined as a complex body that contains several lava flows (episodes) produced by individual volcanic eruptions and identified in the field on the basis field relations (Thordarson and Self, 1998; Thordarson and Hoskuldsson, 2008; Fig. 7.4a). A single volcanic eruption may consist of several eruptive episodes, which might take several months to years (Fig. 7.4a) (Fisher and Schmincke, 1984; Thordarson and Self, 1998; Thordarson, 2000; Németh and Kereszturi, 2015). The lava flow commonly consists of many flow lobes (Thordarson and Self, 1998). The flow lobe represents the smallest unit in pahoehoe flow field and has the characteristic three-part internal structural division as previously mentioned. The Al-Halaq al Kabir lava field is restricted nearly to the central part of the AHVP (Fig. 7.3a, b). Surface morphology of the Al-Halaq al Kabir lava-field is complicated by the preservation of tremendous of inflations structures seem to be developed over long-duration. Busrewil (1996)

propose that the Al Haruj volcanic activity may be extended up through the pre-historic time, where more recent lava flows (volcanic phase 6) may have been post-Neolithic in its age where the field observations indicate that this more recent basaltic lava flows on the AHVP did not use of pre-historic sites compared with the older volcanic phases that were abundantly being used.

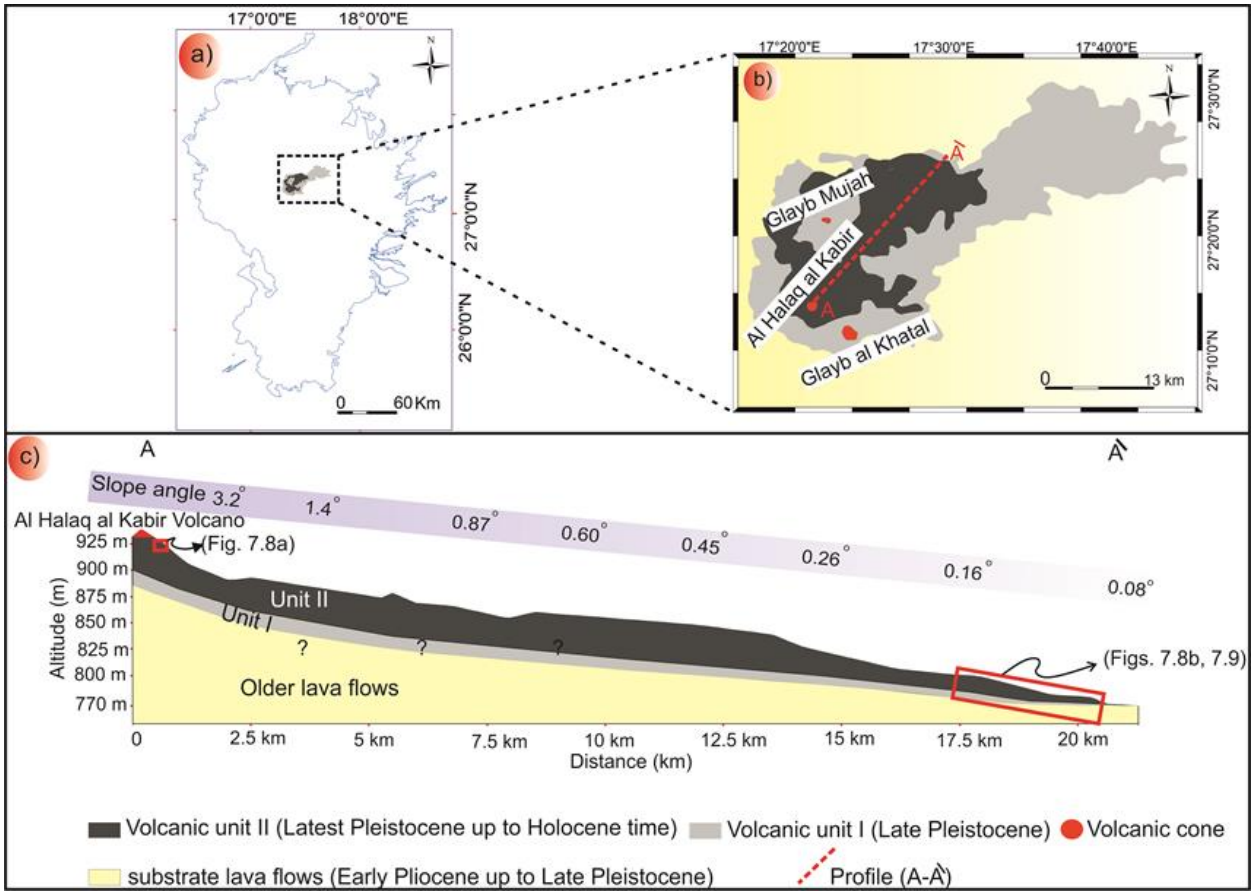

Figure 7.3. a) Simplified map showing the location of the study area which is located almost in the central part of the AHVP. b) Schematic map showing the extent of the Al-Halaq al Kabir flow-field (dark colour) covering partly the older volcanic unit I (grey colour). This lava flow field originated from a vent system and generally flowed NE over 20 km. Both volcanic units have been identified and mapped by Busrewil and Suwessi (1993). c) Profile illustrating the extent of the Al-Halaq al Kabir flow field in cross section. The slope angles along profile are indicated, the location of the cross-profile is shown in Figure 1c. Sites of figures (7.8a, b, 7.9) are shown.

Busrewil and Suwesi (1993) describe this lava flow field as pahoehoe lava flow having delicate ropy structures and festoon which is identical features in very young volcanoes field. In contrast, the equivalent flow unit in the south part of the AHVP described by Peregi et al. (2003) as fresh coal black aa lavas have a rough, clinkery or spiny surface that covered by sharp edges, lava blocks, large tension-fractures with small scattered pahoehoe lavas. However, the texture and mineral composition of this lava flow field are quite similar to basaltic rocks from the earlier volcanic phases. It is important to note that the petrographic differences between the basaltic rocks at the AHVP are significant in samples taken from the upper vesicular and deeper part of the single lava flow lobe than between the different flow fields. The relative abundance vesiculation structures and crystallinity along with jointing styles are the good indicators of three-part division of pahoehoe flow lobe (Thordarson and Self, 1998). The basaltic lavas at the AHVP generally consist of porphyritic intersertal texture with dominate of olivine as phenocrysts associated with clinopyroxene and laths of plagioclases and scattered of glass and minor calcite formed later which occupied some vesicles to form amygdaloidal.

The Al-Halaq al Kabir lava field (unit II) almost covered substratum and although it is thought to have been erupted from fissures, some basaltic flows seem to have come from the summit area of the Al-Halaq al Kabir volcano, where lava was erupted at around 933 m.a.s.l. (meters above sea level) on the north-eastern flank of the volcano and the flow-field extended down-slope to an altitude of around 800 m.a.s.l. (Fig. 7.3c). As the lava obviously encountered gentle slope, the flow spread out and began in endogenous as a result of inflation at few hundred meters from the volcano. The inflation occurred gradually due to sustained supply of fresh lava beneath the thickening upper thin solid crust. Continued inflation leads to the development of axial and circumferential clefts in response to the uplift and rupture of the brittle uppermost crust (Duraiswami et al., 2001).

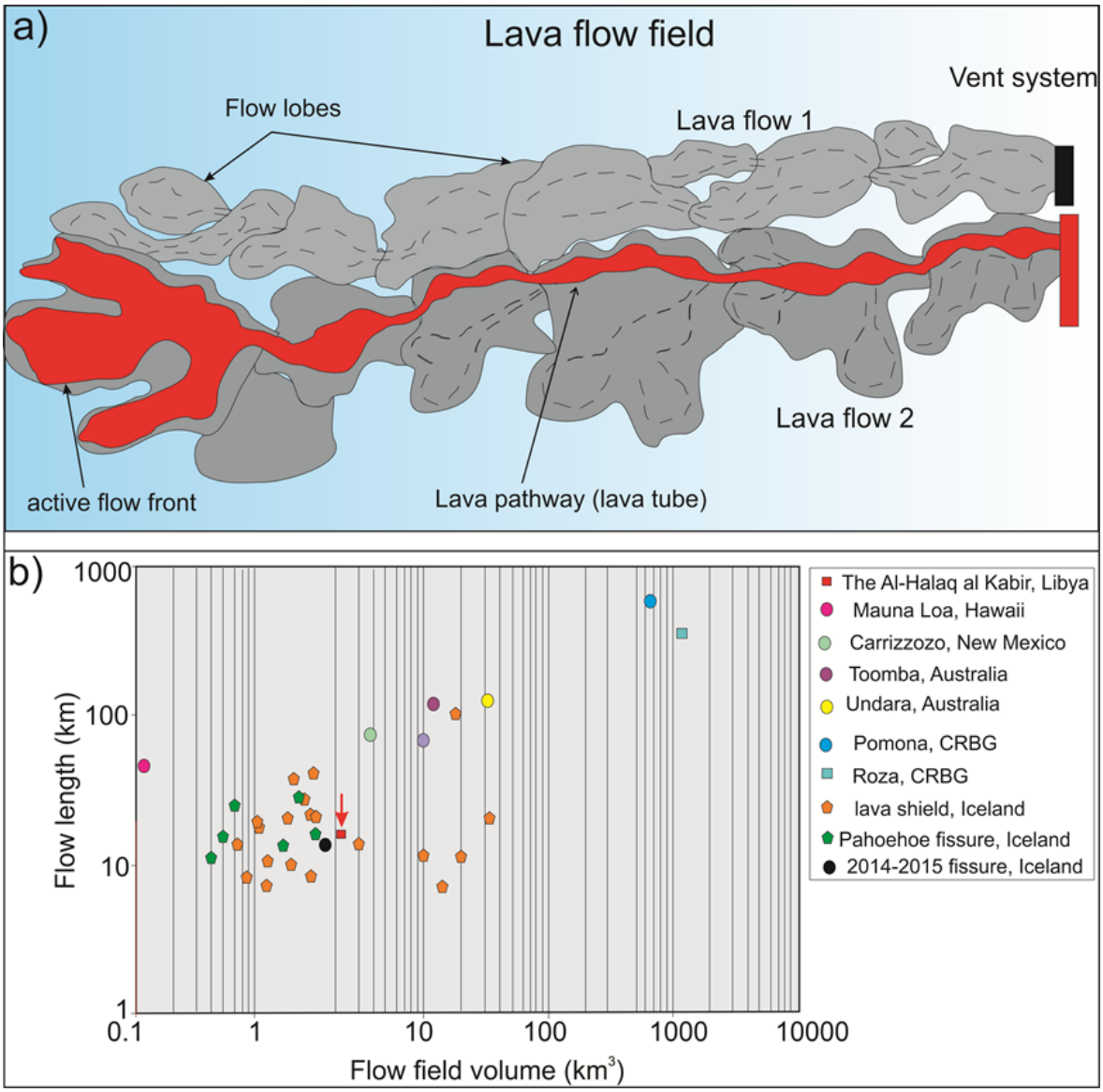

Figure 7.4. a) Cartoon of the development lava flow field. The lava flow field consists of two lava flows where each lava flow may be formed during effusive episode and composed of many flow lobes. Lava is transported from vent system to active flow front via thermally efficient lava tubes (modified from Thordarson and Hoskuldsson, 2008). b) Graph showing the relationship between volume and length of the Al-Halaq al Kabir lava flow field is indicated by red arrow, and, for comparison, 33 lava flow fields from various monogenetic and polygenetic volcanic provinces around the world (data from lava shields and pahoehoe fissures in Iceland are taken from Thordarson and Hoskuldsson, 2008, and 2014-2015 basaltic fissure in Iceland from Pedersen et al., 2017, whereas the rest of data are taken from Self and Thordarson, 1998).

This study explores the plan aspect (length/width) ratios of lava rise plateaus and tumuli within the Al-Halaq al Kabir flow field, where length is the maximum diameter, and width is the minimum diameter in plan-view in order to distinguish between various types of tumuli and lava rise plateaus and the mode of emplacement. These parameters are a crucial because of they could be applied to understanding remotely sensed observation of lava flows on other planetary surfaces (e.g., Moon and Mars) (cf. Self et al., 1998; Glaze et al., 2005; De Wet et al., 2014; Scheidt et al., 2014). Mapping of the lava flow field was executed by importing geological map and georeferenced images of the Al-Halaq al Kabir into ArcMap GIS software package. Shapefiles were used to trace margins. The Al-Halaq al Kabir flow field is representative the last volcanic eruption in this part of the Al Haruj region, without subsequent flows overlying the portion investigated. Therefore, it can precisely be tracing and mapping lava rise plateaus and tumuli on satellite imagery through ArcGIS 10.1. The surface morphology of this lava flow field is complex by the perseveration gigantic of inflation structures. Length (long axis) and width axes (short axis) on plan-view have been measured for these inflation structures at the distal portion of the flow field.

This lava flow field has systematic growth patterns suggesting they represent an individual volcanic eruption (cf. Mattsson and Hoskuldsson, 2005). Notwithstanding the thicknesses of these inflation features are difficult to measure precisely because there are a lack cross-sectional exposures, the thicknesses of lava rise plateaus were roughly estimated based on the difference of the altitude between inflation features and surrounding area (e.g., Fig. 7.5). This method is likely to give rise underestimation of the thickness due to do not take into account the older flow-lobes that are buried inside the lava field. Alternatively, thicknesses of some tumuli and lava rise pleatus have been measured precisely in the field (Fig. 7.6a, b). This flow field covered an area of around 220 km^2 and its thickness roughly estimate

around 10-15 m (Busrewil and Suwesi, 1993); accordingly its volume is about 2.2-3.3 km^3. These lavas reach lengths up to 20 km (Fig. 7.3c).

Figure (7.4b) is provided data on the volumes and lengths of many lava flow fields from difference volcanic provinces around the wold for comparison with the Al-Halaq al Kabir flow field. The volume and length of the Al-Halaq al Kabir are clearly much closer to monogenetic pahoehoe lava shield and

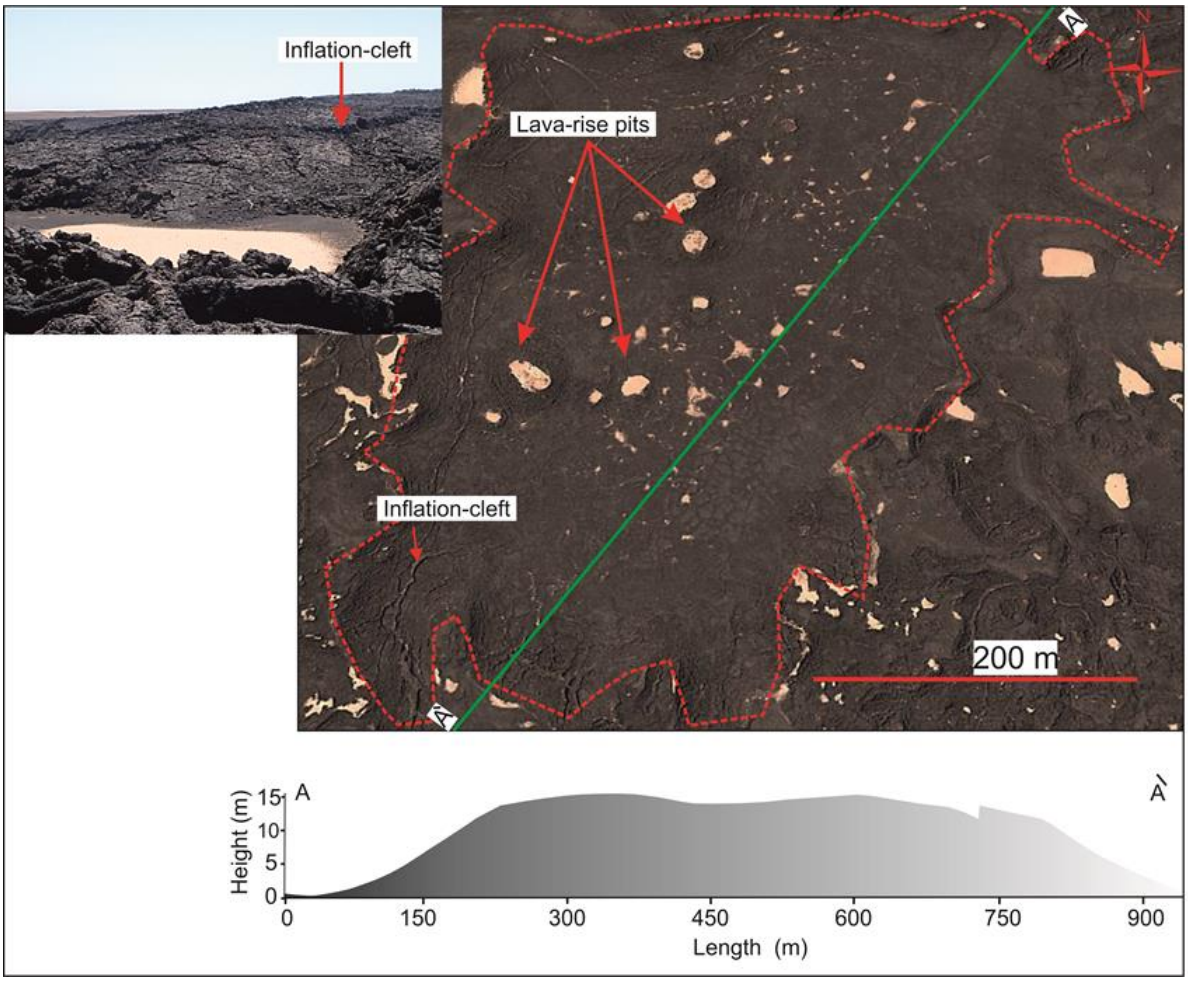

Figure 7.5. Large lava rise plateau with its surveyed cross-profile that is marked by a number of lava-rise pits. It is defined as plateau-shaped with marginal inflation clefts. The thickness or height is estimated around 15 m above the surrounding relief (adapted from Google Earth). The inset field photograph shows lava inflation cleft.

pahoehoe lava fissures in Iceland than polygenetic Large Igneous Province (LIP), created through flood basalt, such as Columbia River Basalt Group (CRBG).

The Al-Halaq al Kabir lava flow field most likely formed through subsurface inflation processes. Of particular interest is whether the Al-Halaq al Kabir was primarily one event occurring over several months or numerous events (several episodes) spread over several years or even decades. Geochemical variation and field observations cannot provide us to answer this question (e.g., Busrewil and Suwesi 1993; Peregi et al., 2003). Therefore, although the Halaq al Kabier lava field may be composed of several overlapping flows from different vents, vent system, which travelled tens of kilometres, the upper surface of most this flow-field preserves distinctive inflation features such as tumuli, lava rise pleatus, lava inflation clefts and lava rise pits that certainly formed over long period of time by endogenous processes beneath insulating crust during emplacement. The main aim of this paper is to present data on morphological, structural characteristic and quantitative analysis of lava rise plateaus and tumuli located within distal portion of this flow-field using a combination of Landsat imagery and field observations. Analytical and numerical modelling of inflation mechanism is used for improving our ability to interpret inflation features which led us to obtain definitive information on the evolution of volcanism in the central part of the AHVP. The implication of these observations for the characteristic lava emplacement mechanism will be discussed in more detailed in the future work for the other volcanic fields at the Libya's volcanism in general and AHVP in particular.

7.3 Inflation process and associated features

This flow field contains large number of inflation features, thus during this study, we have measured dimensions (maximum and minimum diameters) in plan-view (plan aspect ratio) of 551 lava rises and 289 tumuli on the north-eastern flank of the volcano at 100 m below the crater elevation and at around 20 km from the vent system that formed in the many pahoehoe flows emplaced in this eruption (Fig. 7.7). In analysing the surface morphology of the lava flow field,

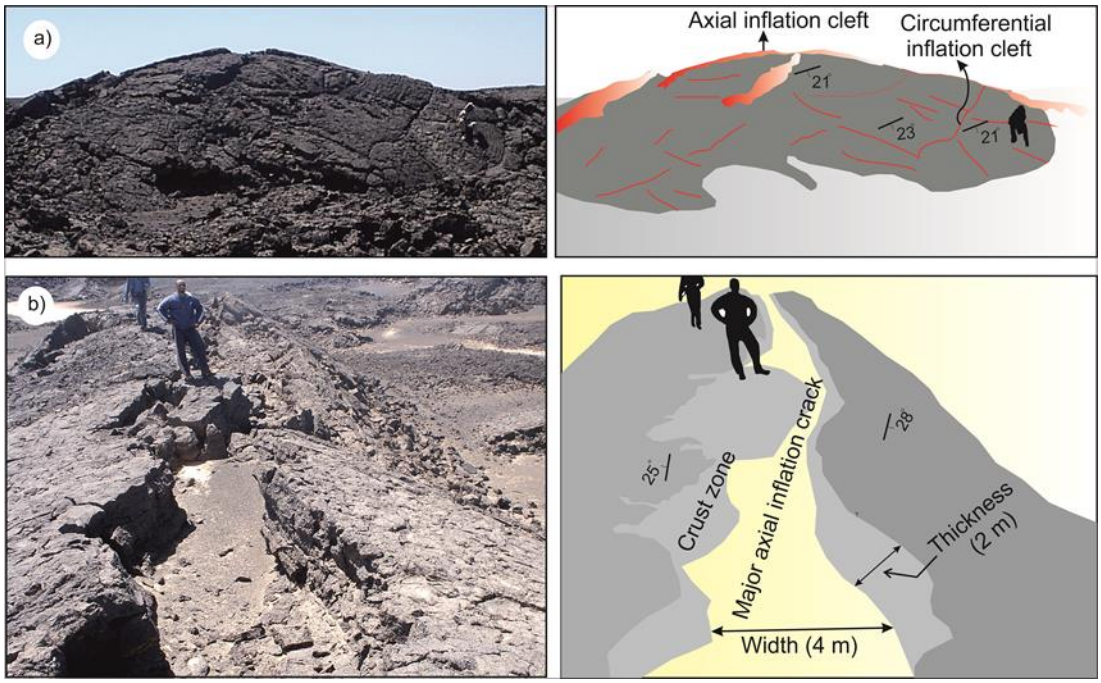

Figure 7.6. a) Photographic and schematic illustrations of tumulus and tumulus ridge. Note the axial and lesser fractures that are formed during the inflation process. b) Photographic and schematic of elongated tumulus which is characterized by large long and deep axial fracture. It is provided the direction of flow. The duration of this flow lobe is around 27 days based on cooling model equation $(t = 164.8H^2)$ of Hon et al. (1994) where t is the time in hours and H is the thickness of the upper vesicular in meters. The duration is probably underestimation due to the upper vesical crust is partly covered by sand dunes.

we determine; i) flow coated tumuli, ii) flow-lobe tumuli, iii) tumulus ridges, iv) lava rise plateaus, v) lava-rise pits and vi) lava inflation clefts. The flow coated tumuli observed within a few hundred meters from vent system that are marked by a typical around 4 meters high with plan aspect ratio 1.5 without distinguished lava inflation clefts (Fig. 7.8a). The flow coated tumuli in the AHVP are quite similar to flow coated tumuli that have been observed in Iceland by Rossi and Gudmundsson (1996). In contrary, other types occur abundantly in the medial and distal portions of the Al-Halaq al Kabir flow-field, and formed the majority of surface flow field (Figs. 7.8b, 7.9).

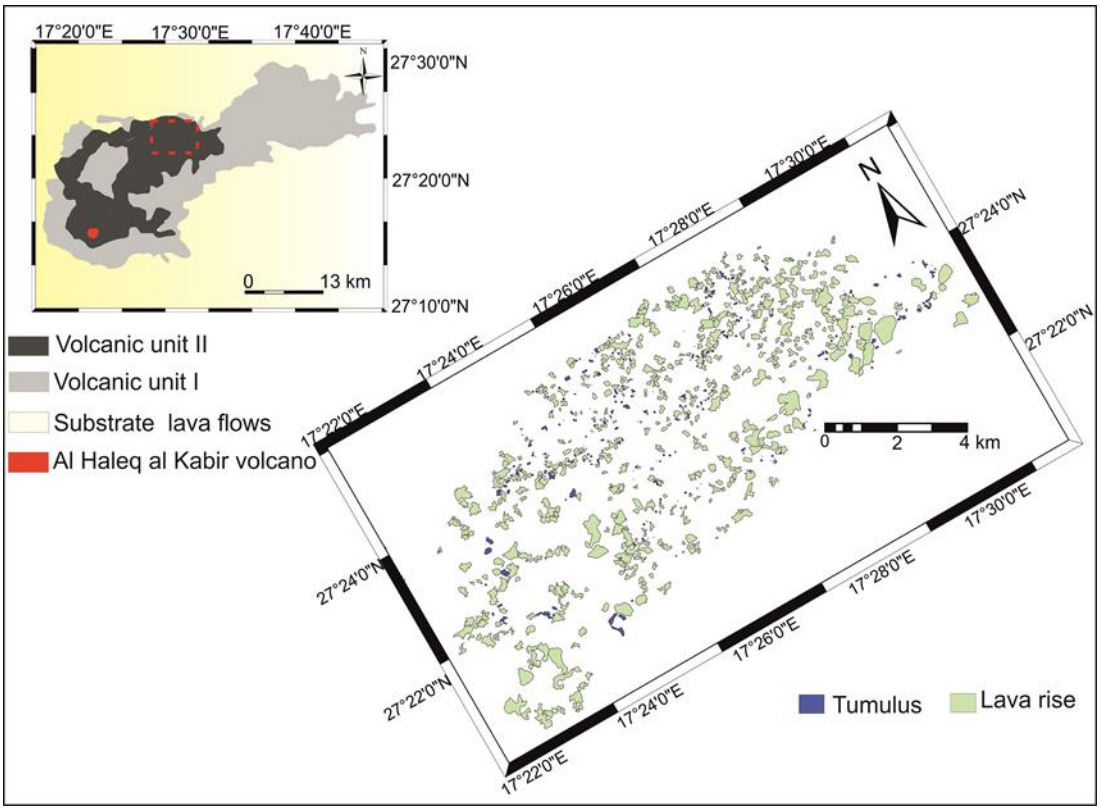

Figure 7.7. The lower map showing the areal distribution of 289 tumuli and 551 lava rise plateaus in the distal part of the Al-Halaq al Kabir lava flow field (volcanic unit II). The geometry and area of these inflation features have been measured precisely by ArcGIS. Dashed red square in the upper map is indicated the location. The flow direction is broad to the north-east.

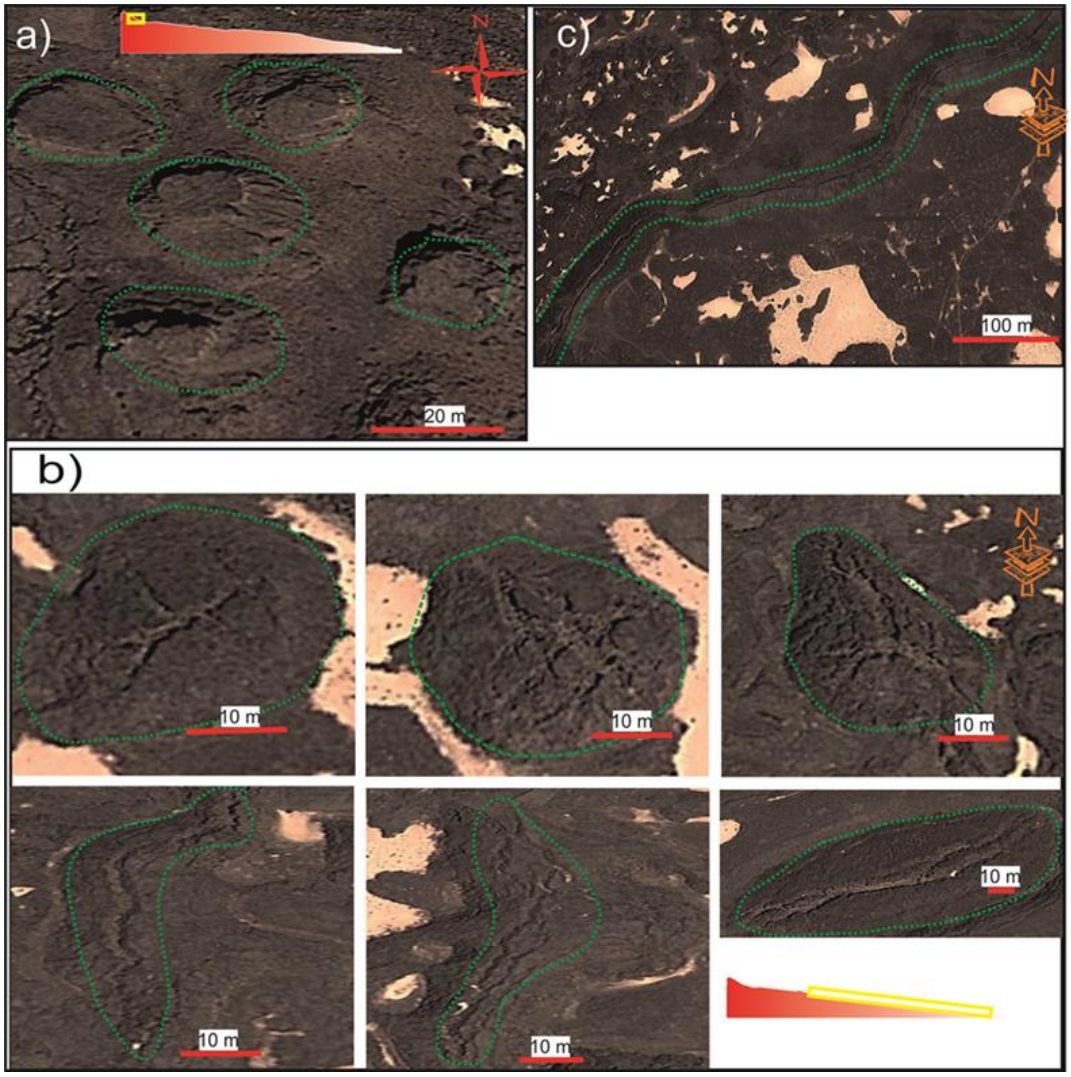

Figure 7.8. a) Satellite imagery (adapted from Google Earth) showing flow-coated tumuli that are located at a proximal part of the source. Note the absence of axial and circumferential cracks. b) Satellite imageries (adapted from Google Earth) showing various forms of flow- lobe tumuli at the distal part of the Al-Halaq al Kabir flow field. Note the abundance of axial and circumferential cracks (lava inflation clefts) and the gradual transition the morphology of tumuli from near source to the distal portion of the lava field. The locations of both images (a, b) are indicated by the yellow box on cross-profile. c) Preferred pathway might be used pre-existing drainage pattern to drain out lava lakes and this feature is predominately in the Al Haruj region.

Flow-lobe tumuli have generally cupola-shaped and marked by development axial cracks at the central part and circumferential cracks around margins that reveal the state of stress development during inflation processes (Walker, 1991; Rossi and Gudmundsson, 1996, Thordarson, 2000; De Wet et al., 2014; Scheidt et al., 2014). The tumulus ridges are created by inflation above relatively straight sections of preferred internal lava pathways (Thordarson and Hoskuldsson, 2008). Tumulus ridges (elongated tumuli) are marked by the presence of a prominent axial cleft and lesser clefts that are developed sub-parallel to the length or long axes. Therefore, they acted as tube-fed for the distribution of lava with thermally efficient to reach the middle and distal parts of flow field both as surface flows and within distributary tube system. There are numbers of tumulus ridges recognised on the satellite imagery and in the field (e.g., Figs. 7.6b, 7.8c). The morphological study of flow-lobe tumuli and tumulus ridges in the area of investigation shows that their major axes (length) range from 16 to 324 m and their minor axes (width) range between 11 to 141 m. The flow-lobe tumuli and tumulus ridges are semi-equant and elongated, respectively, on the basis of an aspect ratio of the major and minor axes in plan-view (Fig. 7.8b).

The tumulus ridges are genetically similar to flow-lobe tumuli, but more elongated in the direction of flow (Mattsson and Vuorinen, 2008; Nemeth et al., 2008). Flow-lobe tumuli are polygonal dome-shaped with various shapes (e.g., rectangles, triangles, hexagons, and octagons) are characterised by a system of inflation clefts arranged in a radial pattern and aspect ratio of major and minor axes is less than 1.5 (Fig. 7.8b). The vary aspect ratio of the elongated tumuli with respect to the flow-lobe tumuli may be attributed to the in situ inflation mechanism where the flow-lobe tumuli are formed by localised inflation of the upper lava crust overhead small pools in subsurface lava pathways in response to irregular underlying topography, while the tumulus ridges are formed by above relatively linear of the preferred pathways as mentioned earlier (Thordarson, 2000; Thordarson and

Hoskuldsson, 2008). By contrast, the geometry area of lava rise plateaus is commonly an order of magnitude larger than both types of tumuli. The lava rise plateau is defined as flat-topped and formed by uniform broad pahoehoe flow lobes (Walker, 1991; Thordarson, 2003). Lava inflation cleft in lava rise plateau are developed along the outer margins rather than the central part which can enable their interior surface to be uplifted with little or no disruption (De Wet et al., 2014; Scheidt et al., 2014) (Fig. 7.9).

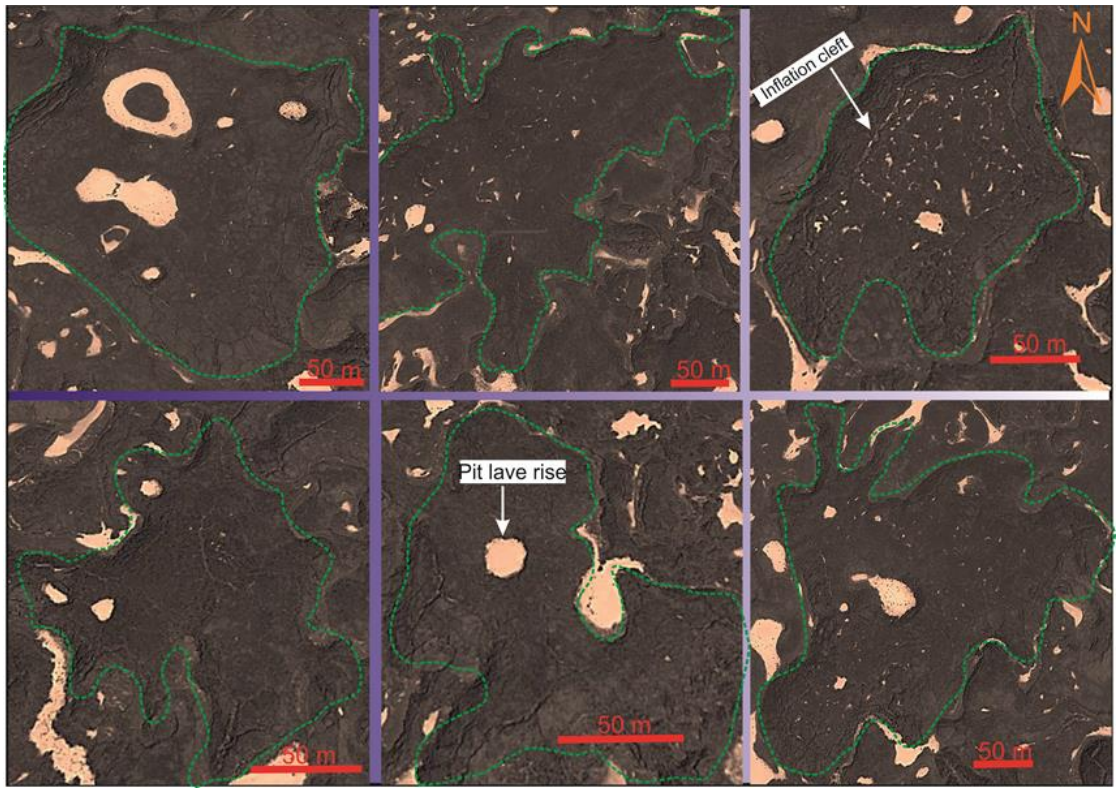

Figure 7.9. Satellite imageries (adapted from Google Earth) showing various forms of lava rise plateaus in plan-view. They are marked by flat-topped surface and circumferential cracks around margin that are indicated on bending during the inflation process. Circular and semi-circular lava-rise pits that are likely formed during inflation processes but the rate of inflation was under than surrounding parts of the flow; see text for more explanation.

The spatial distributions of tumuli and lava rise plateaus can be used to obtain information on the subsurface endogenous processes (Glaze et al.,

2005). Hence, micro-topography combined with effusion rate can have a significant influence on lava flow dynamics and the ultimate emplacement and morphology of inflation produced (Mattsson and Vuorinen, 2008). The morphometric of lava rise plateaus has long axes in the range from 88 to 717 m and short axes in the range between 23 to 495 m. Most of lava rise plateaus are roughly oval-shaped in plan-view based on an aspect ratio of the maximum and minimum axes or diameters.

Furthermore, throughout the Halaq al kabier flow field are numerous of depressions noticed among and within lava rises that seem to be as lava rise pits (Figs. 7.4, 7.9). Lava rise pits are localised areas, previously assigned to collapse or subsidence of lava tube system that commonly formed around lava rise plateaus due to the rate of inflation was lower than surrounding parts of the lava flow (Walker 1991; Self et al., 1998; Whitehead and Stephenson 1998; Thordarson and Hoskuldsson, 2008). Characteristics walls of lava rise pit are similar to the margins of lava rise plateaus (Walker 1991). Lava rise pits in the AHVP are similar to lava rise pits described within McCartys flow in New Mexico (De Wet et al., 2014; Scheidt et al., 2014). The difference in the dimensions of lava rises may be due to the original flow filling in the region of low relief. The Al Haruj region is characterised by wide-flat area with numerous isolated hills so that the flat low relief areas appear to be inverted during inflation and become lava rises and high topography areas have become as lava rise pits. Furthermore, the alignment of tumuli and lava rise plateaus in the field and from satellite imagery indicates the presence thermally efficient lava delivery beneath the Al-Halaq al Kab lava flow field during emplacement (cf. Duraiswami et al., 2001; Bernardi et al., 2015) (Fig. 7.10).

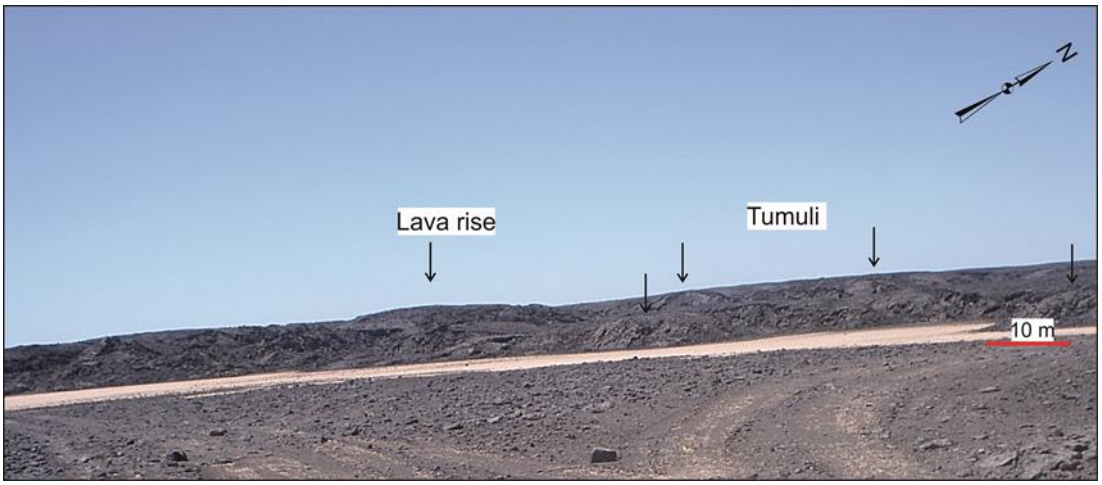

Figure 7.10. Panorama view showing lava rise plateaus and several tumuli. They are arranged in alignment that may be suggested the presence distributary lava tube system.

The length and width axes for both tumuli and lava rise plateaus show a linear correlation with coefficient determination (R^2) = 0.45 for tumuli and 0.60 for lava rises (Fig. 7.11a, b), whereas the correlation coefficient (R^2) was increased to 0.70 when plotted all (tumuli and lava rise plateaus) together (not shown here). Frequency distributions of their lengths (maximum diameters) are approximately followed normal distributions and directions of various lengths for both tumuli and lava rise plateaus have not preferentially orientated that are clearly consistent with the dendritic drainage pattern of the central part of the AHVP (Fig. 7.11c, d). The drainage pattern is a well-integrated pattern in the central part of the Al Haruj region formed by the main valleys with their tributaries branching and re-branching in many directions without systematic arrangement (Busrewil and Suwessi, 1993). It most likely reflects the orientation of the main feeder tubes in the lava field in various directions.

Tumuli display a characteristic of P-type flow-lobe where the upper vesicular crust and dense core zone as well as well-developed jointing are distinct whereas thin lower vesicular crust was lack observed (e.g., Fig. 7.12a, b). Tumuli observed in the study area, in the field, are remarkably similar in

morphology and aspect (height/width) ratios to the flow-lobe tumuli which have been studied in Holocene lava shields (monogenetic shield volcanoes) in Iceland by Rossi and Gudmundsson (1996) with coefficient of determination (R^2) = 0.834 (Fig. 7.13).

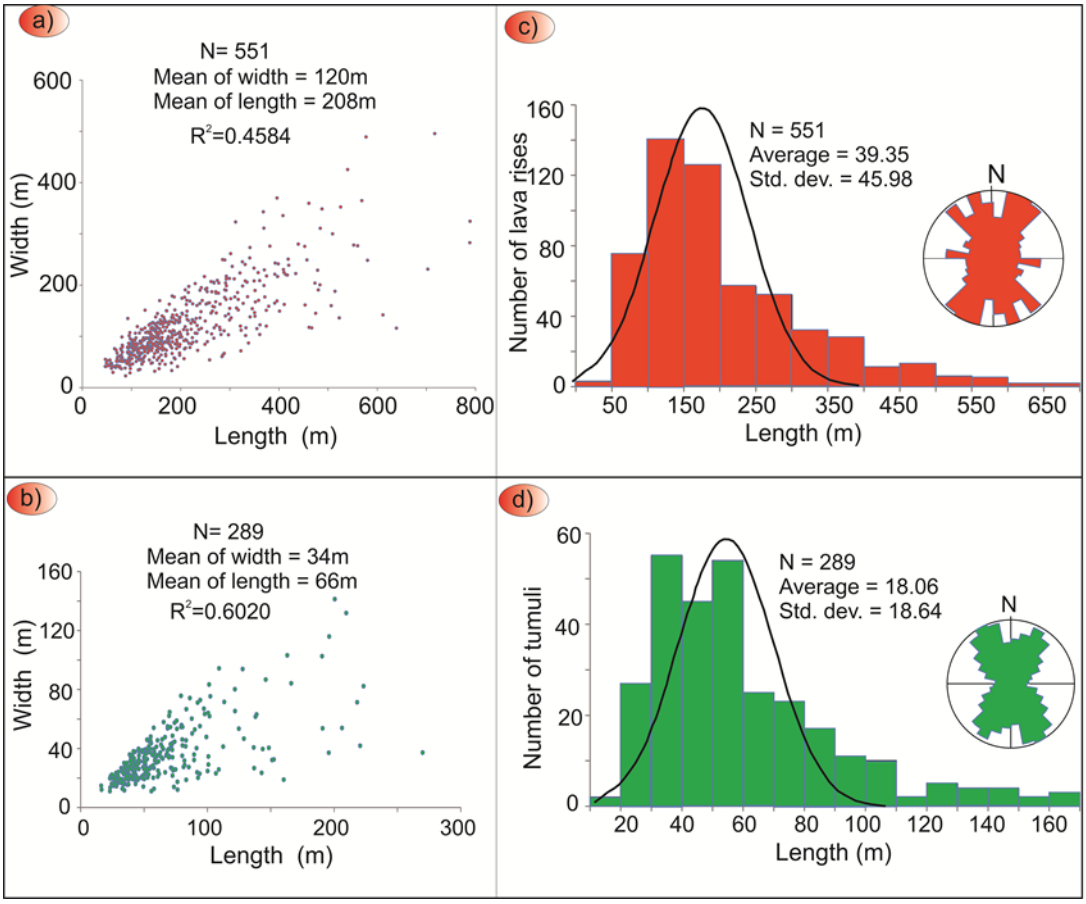

Figure 7.11. Graphs showing the correlation between the length and width in plan-view of lava rise plateaus (a) and tumuli (b). Both graphs show a positive correlation between two parameters. The N is the number of inflation feature, and R^2 is the coefficient of determination. Frequency distribution of lengths of lava rise plateaus (c) and tumuli (d) which are approximately followed normal distributions. The rose diagrams for lava rise plateaus (red colour) and tumuli (green colour) have not been clear preferential directions that are consistent with dendritic drainage pattern of the central part of the Al Haruj region. Note although the various dimensions between tumuli and lava rise plateaus, they have generally similar statistical trend relation.

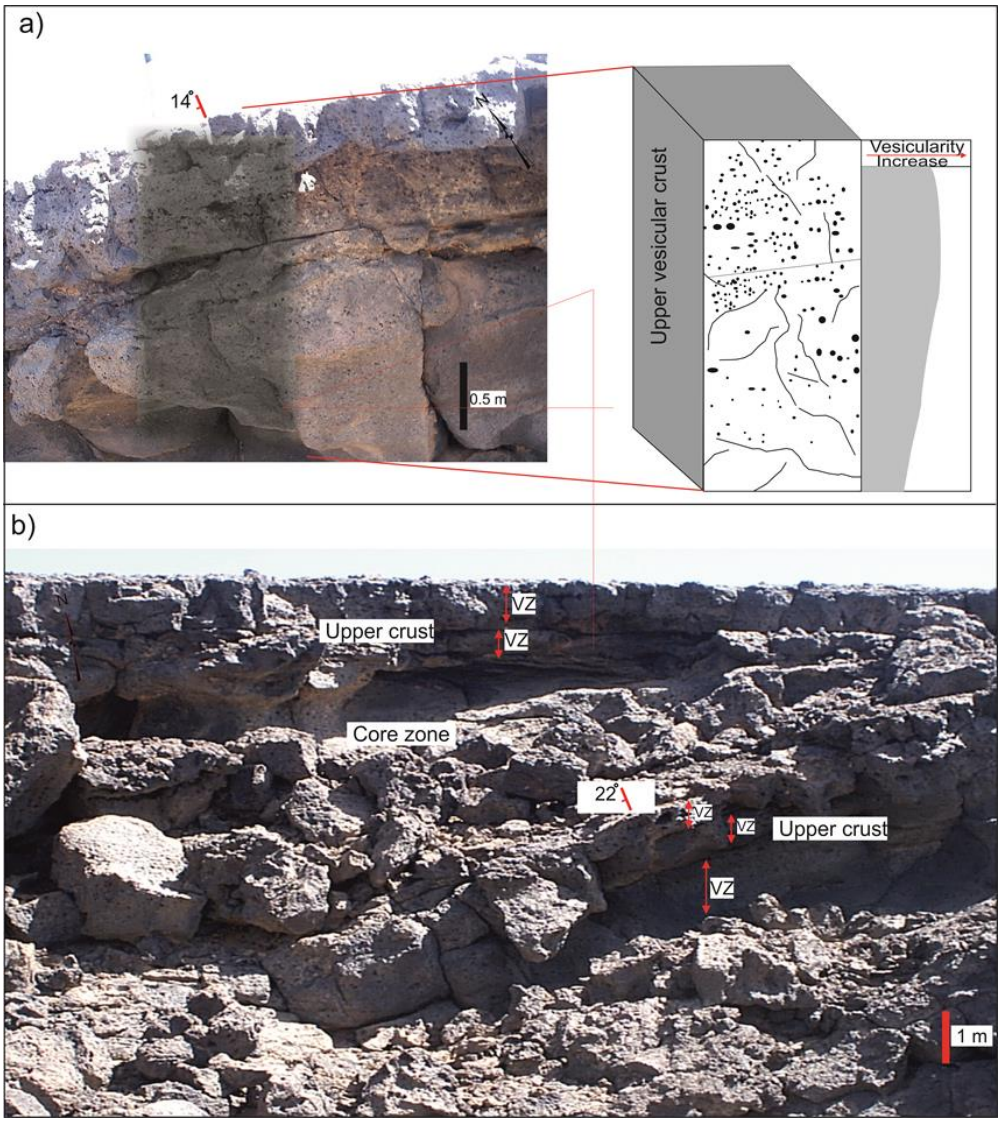

Figure 7.12. a) Field Photograph and graphic log display the upper vesicular crust of internal structure of tumulus. The tilting is around 14° in WNW direction. A number of vesicles is a decrease with depth and characterised by prismatic and irregular jointing. The thin lower vesicular crust and core zone is not exposed. The uppermost of lava crust is characterised by horizontal cracks that may be followed vesicle alignments. The duration of this flow lobe is approximately two months based on cooling model equation of Hon et al. (1994). b) Field photograph showing lava flow which consist of pahoehoe flow lobes. VZ is vesicular zones within the upper vesicular crust that formed during inflation processes. The flow lobe sheet seems to be overlapped the flow-lobe tumulus with flank tilting around 22°. The duration of this lava flow is roughly ten months.

Rossi and Gudmundsson (1996) recognised the flow-lobe tumuli in the distal part of the flow field (9.5 km from source) where slopes are very low, similar to present study site (at the distal portion of lava flow field with very low slope; Fig. 7.3c). This suggests that they were emplaced by an analogous mechanism.

7.4 Scaling exponents

There are very few previous studies (e.g., Rossi, 1999; Glaze et al., 2005) that have been used the quantitative statistical techniques to understand emplacement and inflation of lava flow fields. Therefore, we present new data on the trend and length measurements (maximum diameters) of tumuli and lava rises in the central part of the AHVP. The results of the measurements of a total of 289 tumuli and 551 lava rise plateaus are given in Figures (7.14; 7.11c, d), all of which belong to the Al-Halaq al Kabir lava flow field. The lengths of lava rise plateaus and tumuli on the Al Haruj region are statistical analysed through scaling exponent in order to obtain certain relations between the developments of inflation structures.

7.4.1 Power-law length distributions

Power laws are part of heavy-tailed distributions and marked by their yielding straight-line plots when data are plotted as bi-logarithmic plot (Gudmundsson, 2014). These tests have been applied to geological populations by Mohajeri and Gudmundsson (2012) and Gudmundsson and Mohajeri (2013). We, however, can find a frequency length distribution for inflation features from the power-law distribution equation (Williams, 1997; Mohajeri and Gudmundsson, 2012);

$$p(x) = Cx^{-D} \quad (7.1)$$

where $p(x)$ is the number of inflation features (tumuli or lava rises) in a binned or class histogram, C is a constant proportionality, and D is the scaling exponents. To take the logarithms for both sides of the values (x) and their probability $p(x)$ in order to know if they follow a power law;

$$\log(p(x)) = \log(C) - D\log(x) \quad (7.2)$$

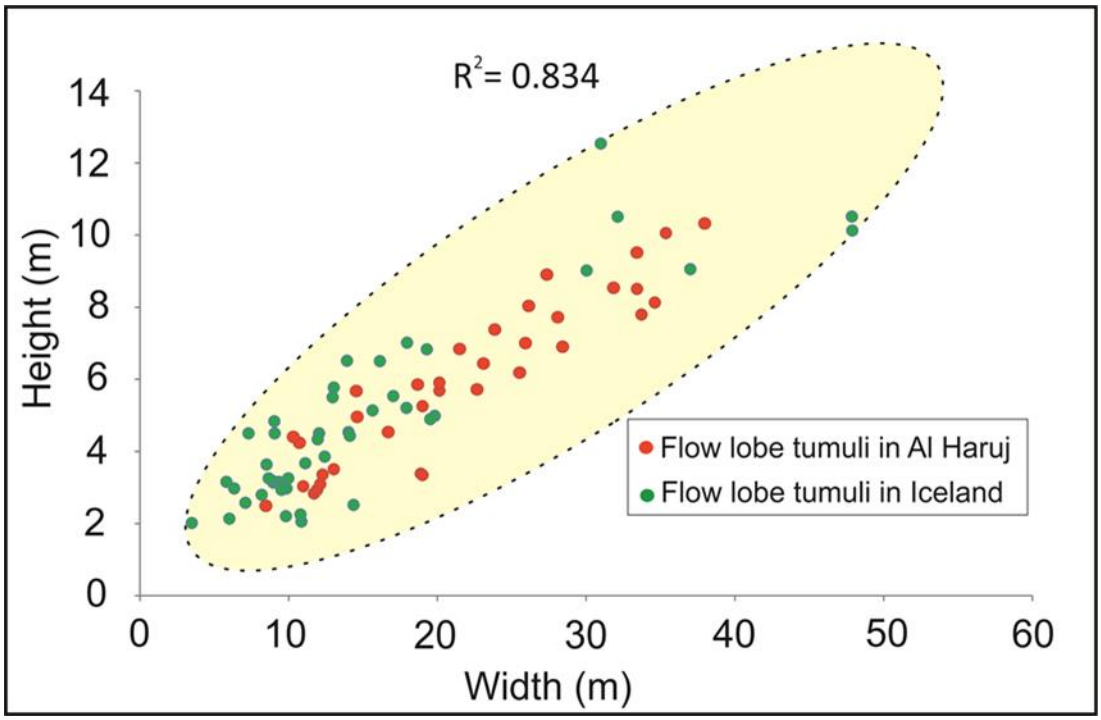

Figure 7.13. Graph showing the correlation between height (thickness) and width in cross-section of flow lobe tumuli in the AHVP measured in the field and Iceland for comparison. The graph shows a near-linear correlation between height and width in both volcanic provinces with the coefficient of determination (R) 0.834. Note the dimensions of flow tumuli in the Al Haruj region are located within the same field of the dimensions of flow-lobe tumuli in Iceland. The data for Iceland are taken from Rossi and Gududmunsson (1996).

The straight lines for tumuli and lava rises are indicated that they are followed a power-law (cf. Mohajeri and Gudmundsson, 2012) (Fig. 7.14b, e). The slope of the straight line that is scaling exponent depends mainly on the

size or width of class or bin. The cumulative frequency distributions of the lengths of tumuli and lava rises display power-law distribution (Mohajeri and Gudmundsson, 2012) (Fig. 7.14a, d). On logarithm plots, the deviation from a straight line are large that led to divide it into two straight lines (Fig. 7.14c, f). Therefore each line has a slope or scaling exponent. Various scaling exponents due to more than one slope are documented in many power-laws (Gudmundsson and Mohajeri, 2013). Each inflation feature may be analysed as a single population, and their trends follow approximately a normal distributions (Fig. 7.11c, d). Clearly, in the log-log plots for both tumuli and lava rise plateaus in Figure (7.14c, f) there is an abrupt change in slope and two straight lines forming like dogleg-shaped. The break in slopes of the lengths may be partly related to pre-existing topography combined with effusion rate (cf. Glaze, et al., 2005). It means that the different slopes or scaling exponents on the logarithm plots could refer to different inflation populations, based on Mohajeri and Gudmundsson (2012) who have mentioned that the breaks in the scaling exponents of the straight plots refer to different populations. Segments of tumuli that are shorter than 60 m in length have a much shallower straight line slope than that have longer lengths. Similarity, the lava rise plateaus also show an apparent abrupt change in the slope and two straight lines on the log-log plots (Fig 7.14f). The break occurs at around 200 m. It is evident that there is a break and slopes of the straight lines for both tumuli and lava rises and their scaling exponents change from 0.37 to 3.07 for tumuli and from 0.36 to 3.56 for lava rises, respectively.

The first population for tumuli is composed of lengths from 16 to 60 that are mostly flow-lobe tumuli and represent around 72% of the total exhibits a large number over broad areas and may be formed due to irregular underlying topography, while the second population primarily consists of tumulus ridges that appear to be elongated tumuli where pre-existing valleys

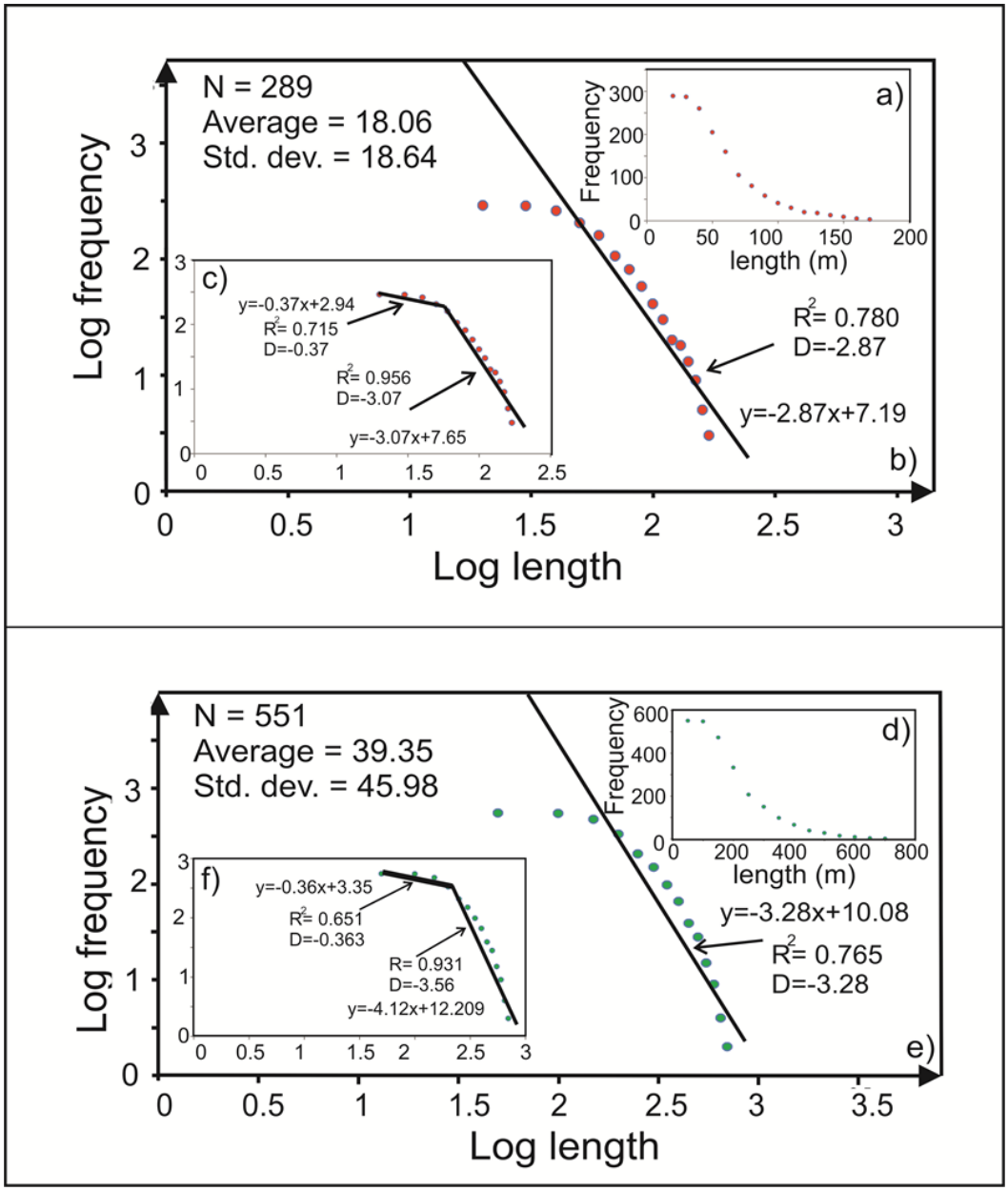

Figure 7.14. Scaling exponents for tumuli upper diagrams and lava rise plateaus lower diagrams. a) The cumulative frequency distribution of 289 lengths measured of tumuli using the class width of 10 m. b) A bi-logarithmic (log-log) plot of 289 lengths measured of tumuli. The straight line is suggested that it is followed a power law distribution. N is the number of inflation features, Std. dev is standard deviation, R^2 is the coefficient of determination, and D is the scaling exponents. c) The whole population of tumuli is divided into two populations based on an abrupt change in the scaling exponent or slope. d) The cumulative frequency distribution of 551 lengths measured of lava rise plateaus using bin width 50 m. e) A single line on a bi-logarithmic plot of the whole lava rise plateaus population. f) The whole lava rise plateaus population divided into two pupations based on abrupt change in slope.

played an important role to form this type of tumuli on the Al Haruj region. This result is in agreement with field observations of Németh et al. (2008) who have mentioned the large flow-lobe tumuli in the Al Haruj Abyad (the southern part the AHVP) are commonly elongated. Also, lava rise plateaus also divided into two populations based on the abrupt change in their scaling exponents. The paleo-topography seems to be partly controlled in determination their sizes. The first population seems to be the initial lava flow surface confined in smaller areas compared to the second population. It is possible the flow started narrow branches through pre-existing valleys that might have tended to pond in the vicinity of low topographic and slope and due to continued inflation via thermally efficient internal pathways result in the development of a vary inflation structures that can grow to considerable sizes as observed. The lengths of tumuli and lava rise plateaus on the lava flow surface are obviously systematically distributed and have identical statistical behaviour. Alternatively, the trends of lengths for these inflation features have not been clear preferential directions that are consistent with dendritic drainage pattern of the central part of the Al Haruj region (Fig. 7.11c, d).

Glaze et al. (2005) have used quantitative statistical analysis technique (Poisson distribution) to examine the spatial distribution of tumuli and lava rise plateaus on lava flow fields in Mauna Ulu, Hawaii, Thrainsskjoldur in Iceland and a lava flow Elysium Planitia on Mars in order to find relationship between these inflation structures and subsurface endogenous growth processes. They found that the spatial distributions of inflation features are systematically distributed in Iceland whereas randomly distributed in Hawaii and Mars. The random distribution in the space, consistent with Poisson distribution, may be generated due to random variations in paleo-topography or small-scale temporary preferred pathways, combined with very low slope. By contrast, the systematic distribution on the surface of lava flow field simply reflect permanent large-scale preferred pathways that led to establish

distributary tube systems directly beneath broad lava flow for long period of time (Glaze, et al., 2005). Also the spatial distribution of tumuli and lava rise plateaus on the surface the Al-Halaq al Kabir flow filed is remarkably different from the Poisson distribution on the basis of Glaze, et al. (2005) procedure. There thus may be some systematic manner controlling their mode of occurrence.

7.5 Modelling

7.5.1 Analytical model

The thicknesses of inflation features on the AHVP are quite small compared with their lengths and widths thus the basic assumptions in the general theory of plates are mostly valid for tumuli and lava rises (Szilard, 1974; Gudmundsson, 1986). The main purpose from modelling is to calculate the over-magmatic pressure and tensile stresses that caused inflation and tension fractures, respectively. The presence inflation clefts on the surface of lava rises and tumuli which indicate that vertical crustal displacement played an important role in the formation of inflation features (Rossi and Gudmundsson, 1996). Hence the elastic thin plate theory is suitable for the present problem. Considering an elliptical crustal plate theory for tumuli and lava rise plateaus on the AHVP is more fit than circular crustal plate theory as have been suggested by Rossi and Gudmundsson (1996) in Iceland where the average plan aspect (length/width) ratio for tumuli and lava rises in the Al Haruj region in range 1.81 and 2.01 respectively, as they are considerably more elongated in the direction of flow. So that during this study we propose the inflation feature as elliptical an elastic plate that is subjected to steady magmatic pressure at its lower boundary. The elliptical an elastic plate with a simply supported movable edge is subjected to

bending due to an effect of magmatic overpressure. The uppermost lava crust becomes fractured during the early stages of inflation process due to subject to maximum tensile stresses (expansion) so that it cannot prevent magma from squeeze out through it. In contrary, the viscoelastic crust is formed between upper crust and core molten zone and behaves as brittle at 800 - 1070^{o}C (Hon et al., 1994) (Fig. 7.15b). The viscoelastic crust is un-fractured and subject partly to compressive stresses during bending of the tumulus. Therefore, the viscoelastic crust acts to keep the magma interior the tumulus or lava rise during the inflation process (Hon et al., 1994; Rossi and Gudmundsson, 1996). The thickness of viscoelastic has been measured (0.2-0.4 m) in Hawaii (Hon et al., 1994). Nevertheless, during this study, four samples were collected from the Al-Halaq al Kabir flow filed in order to measure their Young's moduli as discussed in the next section. The Young moduli, then, have been used to calculate flexural rigidly for those rocks in order to estimate magmatic over-pressure caused inflation features.

7.5.1.1 Dynamic Young's modulus using ultrasonic wave velocities

Four cylindrical basaltic samples 25 mm in diameter and 38.7-26.6 mm long were obtained to calculate the dynamic elastic modulus through using ultrasonic wave velocities for the measure travel time for P and S-waves to cross sample at the Rock and Ice Physics Laboratory at University College of London (UCL). Four measurements (axial and radial) per individual core sample were prepared for these experiments for calculating the sample anisotropy by plotting the velocity as a function of azimuth. The anisotropy throughout the samples in different orientations is less than10% which indicates that the basaltic rocks at the AHVP can be considered as isotropic or weakly anisotropic. The time difference between the initial pulse and the first arrival was measured as the P-wave travelled through the sample. This procedure was repeated with polarized S-wave transducers, in order to

measure the travel time of an S-wave to cross the sample. The physical characteristics of the four core samples included in this study are shown in Figure (7.15).

The P and S-wave velocities and bulk density are utilised to calculate the dynamic Young's modulus based on this equation (Jaeger and Cook, 1969; Gudmundsson, 1990);

$$E_{dyn} = \frac{V_s^2 \rho \left[3\left(V_p^2 / V_s^2 \right) - 4 \right]}{\left(V_p / V_s \right)^2 - 1} \tag{7.5}$$

where E_{dyn} is dynamic Young's modulus, V_p is compression seismic velocity, V_s is shear seismic velocity, ρ represents the bulk density of the core sample where it is found from the average of mass and volume (kg/m^3) of four core samples.

Nevertheless, the relationships between the static and dynamic moduli for different types of rocks are somewhat complicated (Eissa and Kazi, 1988, Brotons et al., 2015). There are many studies have been done to estimate the relationship or correlation between the static and dynamic moduli for different types of rocks (e.g., Christaras et al., 1994; Brotons et al., 2015). In the laboratory measurements the dynamic modulus is around twice of the static modulus, but in the field, this ratio varies from 1.5 to 9.1 for volcanic rocks (Gudmundsson, 1990). However, Eissa and Kazi (1988) performed statistical relation to estimate the static from dynamic Young's modulus that may be crudely valid for all rock types as follows;

$$E_{st} = 0.74 E_{dyn} - 0.82 \tag{7.6}$$

Therefore, the static Young's modulus for the basaltic samples in the range 40-59 GPa with average 50GPa (Fig. 7.15), but the in-situ Young's modulus is likely to be lower (1.5 to 5 times) than the core-sample owing to the presence of fractures, cavities and planes of weakness (Gudmundsson, 2011). We thus assumed the in-situ static Young's modulus during this study in the range of 10-34 GPa.

The common differential equation of the vertical uplift of a plate subject to uniform over-magmatic pressure at lower boundary is given by the following equation (Gudmundsson, 1999);

$$D\nabla^2\nabla^2 w = p_o \qquad (7.7)$$

	Vp (m/s)	Vs (m/s)	Vp/Vs	density (kg/m^3)	E_{dyn}(GPa)	E_{st}(GPa)
Sample (1)	5688.71	3496.76	1.63	2758.82	80.71	58.91
	5680.57	3360.97	1.69	2758.82	76.70	55.94
	5646.14	3496.44	1.61	2758.82	80.20	58.53
	5811.46	3235.04	1.80	2758.82	73.65	53.68
Sample (2)	5708.23	3368.86	1.69	2787.25	77.99	56.89
	5594.59	3420.64	1.64	2787.25	78.36	57.17
	5844.25	3341.96	1.75	2787.25	78.26	57.09
	5844.25	3379.49	1.73	2787.25	79.50	58.01
Sample (3)	5527.28	2940.93	1.88	2755.31	62.08	45.12
	5518.63	3047.56	1.81	2755.31	65.54	47.68
	5479.66	3114.06	1.76	2755.31	67.41	49.06
	5469.99	3114.41	1.76	2755.31	67.35	49.02
Sample (4)	5503.26	3897.30	1.41	2553.97	77.34	56.41
	5488.20	3181.97	1.72	2553.97	64.48	46.90
	5558.15	3331.60	1.67	2553.97	69.14	50.34
	5390.85	3101.34	1.74	2553.97	61.54	44.72
	5313.12	2917.99	1.82	2553.97	55.84	40.50

Figure 7.15. Showing P and S-wave velocities, densities, dynamic and static moduli for four basaltic rocks from the study area. The values of static Young's modulus inferred from dynamic Young's modulus based on the equation of Eissa and Kazi (1988); see text for more explanation.

Where ∇^2 is the two-dimensional Laplace operator, w is a thickness of uplift or inflation and P_o is over magmatic-pressure. D is defined as is the resistance to bending of the plate and known as the flexural rigidity and can be found by this equation (Marti and Gudmundsson, 2000);

$$D = \frac{E_{st} d^3}{12(1-\nu^2)} \tag{7.8}$$

where E_{st} is the static Young's modulus, d is the effective thickness of the plate, and ν is the Poisson's ratio. The static young's modulus for basaltic rocks is in the range of 10-34 GPa as previously discussed, and the Poisson's ratio for most rocks is around 0.25 (Gudmundsson, 2011). The initial thickness of inflation features is a small fraction of its total thickness flow where the minimum thickness of lava emplacement is 0.2 to 0.5 m (Self et al., 1998). The effective thickness for inflation features is the thickness of viscoelastic (unfractured) rather than fractured upper crust (Rossi and Gudmundsson, 1996) as previously mentioned. Thus we assumed the average thickness of viscoelastic crust (0.30 m) as effective thickness to calculate flexural rigidity from Eq. (7.8) as D = 24 MNm when E_{st} = 10 GPa, and D = 82 MNm when E_{st} = 34 GPa.

The equation of the elliptical boundary is:

$$\frac{x^2}{a^2} + \frac{y^2}{b^2} = 1 \tag{7.9}$$

where x and y is cartesian coordinates and a is the half length of the plate and b is the half width of the plate (Fig. 7.16a).

The elliptical differential equation of the vertical uplift or deflection is given by (Gudmundsson, 1986);

$$w = \frac{p_o}{8D} \frac{\left(1 - \frac{x^2}{a^2} - \frac{y^2}{b^2}\right)^2}{\left(\frac{3}{a^4} + \frac{3}{b^4} + \frac{2}{(ab)^2}\right)} \tag{7.10}$$

where p_o is the over-magmatic pressure. The maximum uplift or displacement $(w_{\max})$ occurs at the centre, that is, where $x = 0$ and $y = 0$ then the Eq. 10 becomes;

$$w_{\max} = \frac{p_o}{8D} \frac{1}{\left(\frac{3}{a^4} + \frac{3}{b^4} + \frac{2}{(ab)^2}\right)} \tag{7.11}$$

Therefore, the over-magmatic pressure can be found by this relation;

$$p_o = \left[(w_{\max} 8D) \left(\frac{3}{a^4} + \frac{3}{b^4} + \frac{2}{(ab)^2}\right) \right] \tag{7.12}$$

Using the mean values for lengths and widths in plan-view for 289 tumuli and 551 lava rises have been measured during this study to estimate over-magmatic pressure that was needed for uplift or deflection of tumuli and lava rises on the Al Haruj region as follows; $a = 33m$ and $b = 17m$ and $w_{\max} = 5m$ for tumuli, whereas $a = 104m$ and $b = 60m$ and $w_{\max} = 15m$ for lava rise plateause. It follows from Eq. (12) the over-magmatic pressure p_o is 0.05 MPa when flexural rigidity D= 24MNm and p_o = 0.15 MPa when D = 82 MNm that needed for deflection tumulus. Our finding is generally agreement with the result of Rossi and Gudmundsson (1996) who have found the magmatic overpressure needed to form a typical flow-lobe tumulus in Iceland is in the range of 0.2 to 1 MPa. While the over-magmatic pressure is 0.002 MPa when D = 24MNm and p_o = 0.0.004 MPa when D= 82 MNm that were needed to form lava rise plateau.

The maximum tensile stress $\sigma_{\max}$ at surface of the crustal plate can be crudely estimated by the following relation (Gudmundsson, 1999);

$$\sigma_{\max} = \frac{3(3+\nu)\, p_o b^2}{8d^2} \tag{7.13}$$

All symbols are defined above; the maximum tensile stress at the surface of tumulus is 70-570 MPa while at the surface of lava rise is 44-150 MPa. The in-situ tensile strength of all rocks is commonly in the range of 0.5-9 MPa with most values between 2 and 5 MPa (Haimson, and Rummel, 1982; Gudmundsson, 2014). Therefore, the maximum tensile stress for both tumuli and lava rises is many orders of magnitude larger than the tensile strength of the basaltic upper crust (0.5-9 MPa) even though the over-magmatic pressure was very much small as we inferred in this study. Thus the viscoelastic crust played an important role to maintain the lava interior of the tumulus or lava rise during the inflation processes.

7.5.2 Numerical model

In the recent years, the increasing application of finite element methods in analysing structures and fluid flow that is an alternative procedure to analytical solutions. FEM models give more realistic results than other models where they can allow the implementation of mechanical heterogeneities within the Earth's crust (Bagnardi, 2014). Numerical models based on the finite element methods can provide quantitative information on the local stresses field distribution around inflation feature. Comsol Multiphysics (5.1) (www.comsol.com) is the finite element program used for the work described in this study. We have modelled the inflation feature as a homogenous layer with Young's modulus 25 GPa, density 2650 $kg\,m^{-3}$ and typical Poisson's ratio of 0.25. The over-magmatic pressure was modelled as loading 1MPa (Fig. 7.16b). We made a numerical model in order to explore

the potential effects of uplift or deflection due to the influence of magmatic overpressure beneath the rigid upper crust. We inferred that the tensile stresses around the upper crust are favourable to rupture and form axial and circumferential fractures. The result of numerical model displays the maximum tensile stress take places at the surface (Fig. 7.16b), then decline downward gradual to reach at the neutral surface (cf. Ugural, 1981; Rossi; Gudmundsson, 1996).

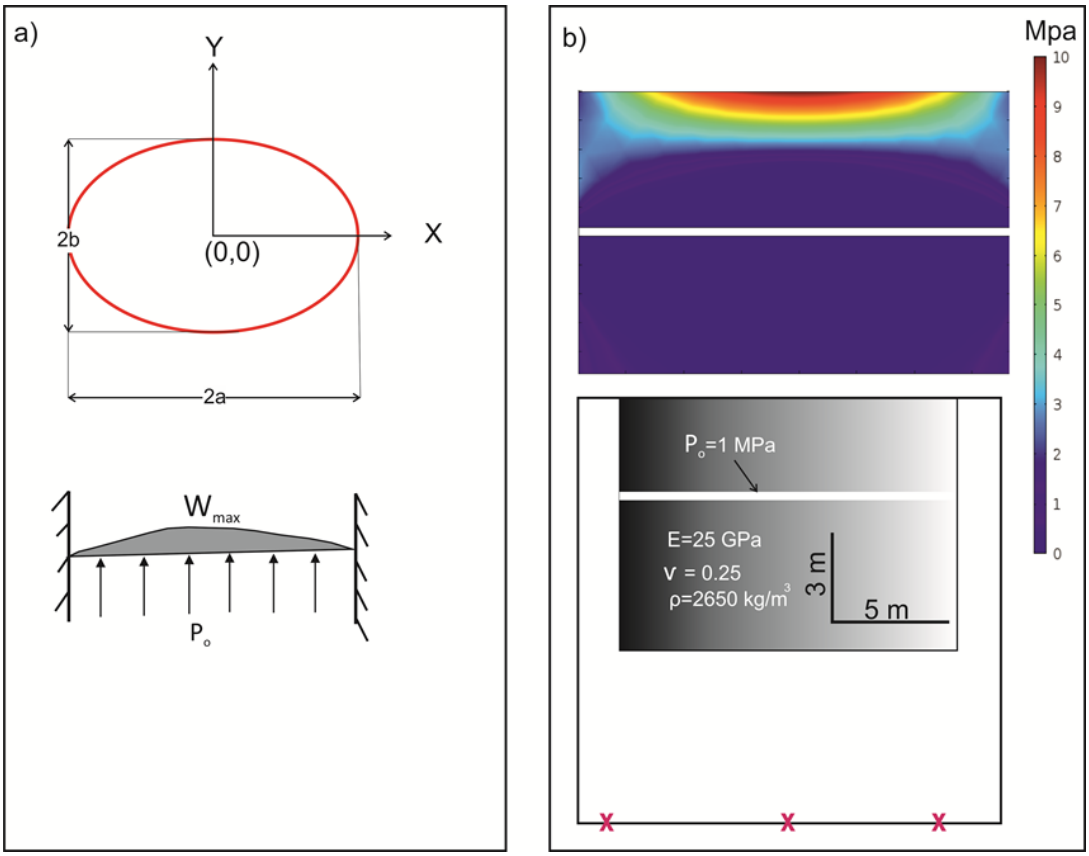

Figure 7.16 a) Elliptical plate with freely movable edge subject to bending due to over-magmatic pressure p_o. The length of the major axis (length) is 2a and length of minor axis (width) 2b. b) FEM (finite element model) results, colour contours represent the minimum principle compressive (maximum tensile) stress. The entire model is shown on grey rectangular in the lower inset diagram. The model is fixed at the lower part, indicated by red crosses, to avoid any rotation and displacement. The maximum tensile stress is concentrated at uppermost crust that caused tension fractures as we observed in the field and on satellite imagery, then decrease downward gradual to reach at the neutral surface (cf. Ugural, 1981; Rossi; Gudmundsson, 1996) and probably at this level the viscoelastic crust act to keep lava inside during inflation processes.

7.6 Discussion and conclusions

The Al-Halaq al Kabir flow field represents the last eruption in this portion of the AHVP based on the stratigraphic mapping of the AHVP. Therefore, it was selected to enable complete mapping of surface morphologies and identification of well-defined boundaries without subsequent flows overlying the part studied. The new age dating and field observations suggest that this eruption most likely occurred during the late Holocene (Busrewil, 1996; Nixon et al., 2011). This lava field appears to have low viscosity (high mobility) and feeding by lava tubes due travelled a great distance (around 22 km) (cf. Bernardi et al., 2015.) Field observations and remote sensing data suggest that an inflation mechanism (thickening by endogenous growth) played a significant role in the emplacement of the Al-Halaq al Kabir lava field. Tumuli, lava rise plateaus, lava rise pits and inflation clefts were formed by this mechanism, display certain diagnostic characteristics that are an indication of their emplacement mode. These inflation structures largely vary in their shape and size through the distance from the vent system to distal portions and seem to be mainly influenced by paleo-topography and the flux rate as well as its composition (Fig 7.17). There are a number of preferred path ways recognised on the satellite imagery and in the field that may be used pre-existing drainage pattern to drain out lava lakes.

The inflation structures on the surface of the Al-Halaq al Kabir are clearly followed a power-law and the roughly normal distribution. Scaling exponents results propose that the lava inflation structures are likely to be influenced by pre-existing topographic together with effusion rate variability, and the result in distributions of tumuli and lava rise plateaus. The tumulus ridges seem to be controlled by pre-existing channels or valleys to form elongated tumuli as more stable distribution pathways developed whereas smaller lengths represent localised or stationary inflation. Tumuli and lava rise plateaus

populations may be divided into subpopulations according to the abrupt change in the scaling exponents, ranging from D= 0.37 to 3.07 for tumuli and ranging from D= 0.363 to 3.56 for lava rises. The spatial distributions of tumuli and lava rise plateaus can be linked to network of lava transport beneath an insulating crust (Glaze et al, 2005). Tumuli from AHVP are morphologically similar to some Icelandic flow-lobe tumuli, suggesting a similar mechanism of emplacement. The tumuli and lava rise plateaus in Iceland are strongly related to persistent preferred internal pathways that produced a systematic distribution of inflation features. Therefore, the tumuli and lava rise plateaus on the surface of flow field in the AHVP are most likely correlated with preferred internal pathways thermally efficient that may be active at different times during the lava flow field emplacement. Furthermore, the alignment of tumuli and lava rise plateaus are clearly discernible in the field and on the satellite imagery which indicate that the distributary tube systems beneath the upper insulating crust. The pre-existing topography and flux rate are the most factors that may influence how and where inflation existence (Thordarson, 2000; Glaze et al., 2005; Thordarson and Hoskuldsson, 2008). These factors vary from place to place and sometimes within same lava flow field. The distribution of inflation structures in space might have begun as random, over time, the formation of lava tubes results in extremely efficient delivery of lava that led to a systematic clustering of the inflation features along these internal networks (cf. Glaze et al., 2005).

We inferred from analytical and numerical models that the potential tensile stresses at the surface of tumulus (170-570 MPa) and lava rise (44-150 MPa) are several orders of magnitude larger than the actual tensile strength (0.5-9 MPa) of basaltic rocks. Thus, the tensile strength of the lava crust is not high enough to resist the potential tensile stress during tumulus and lava rise formation, so that the crust will fracture, as we observed in the field and from satellite imagery. But, the viscoelastic crust is formed between upper crust and core molten zone and behaves as brittle at 800 - 1070^{o}C (Hon et

al., 1994) that had the responsibility to remain the magma inside during inflation processes.

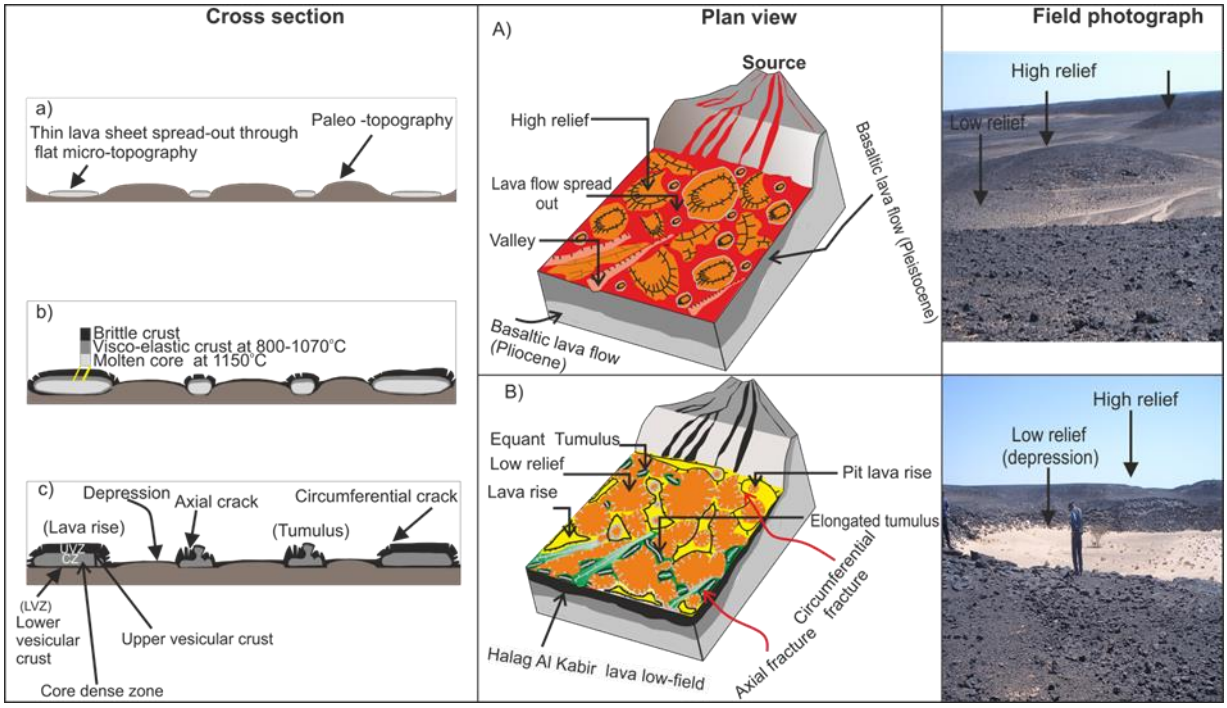

Figure 7.17. Cartoon showing the development of tumuli and lava rise plateaus in the study area. Cross sections on the left and plan views in the middle. Field photographs on the right to display natural of topography on the Al Haruj region that consists of a nearly flat-wide area within numerous isolated hills (upper photograph). a) and A) Lava flow spreads out through the low relief and thin crust was formed. b) The lava sustained a supply of magma beneath insulating crust and inflation began initially, in the meantime the viscoelastic formed beneath crust with thickness 20-40 cm at 800- 1070^{o} C (cf. Hon et al., 1994). The viscoelastic crust played an important role to keep magma inside during inflation process c) The tensile stress at the surface is much larger (44 to 570 MPa) than the tensile strength of basaltic rock (0.5-9 MPa) so that will be derived tension fractures on the surface as we observed in the field (see analytical and numerical model sections for more explanation). B) The plan-view of the present day of the Al-Halaq al Kabir flow-field where the paleo-topography inverted where the high relief becomes low relief (depression) and vice versa as seen in the lower field photograph.

Tumuli and lava rise plateaus are thought to be provided with magma from a tributary tube system that originates in overflow from several kilometres through fissures connected with the lava lake of lava sources (cf. Rossi and Gudmundsson 1996; Glaze et al., 2005). Therefore, if we assume the lava was delivered through distributary preferred pathways thermally efficient, the magma-static overpressure is $p_m = \rho_m g h$, where ρ_m is basaltic magma density (around 2650 Kg /m^3) and g is acceleration due to gravity (9.81 m/s^2) and h is the elevation difference. If this assumption were correct, there could be the elevation difference at the surface between the source lava lake and inflation structures on the Halaq al Kabier flow field (> 100 m) is sufficient to generate static overpressure ($\geq$2MPa) that easily caused these inflation structures due to tumulus and lava rise on the AHVP needed only less than 1 MPa to form them as discussed previously

The Al-Halaq al Kabir flow field is most likely formed during a single volcanic eruption (probably number of eruptive pulses) and the duration of this eruption was reasonable taken few months to several years on the basis of the thickness of the upper vesicular crust of inflated pahohe flow lobes, observed in the field. However, the production rate of the first volcanic eruption on the AHVP during Messinian-Zanclean time (≈7 to 3.6 Ma) (e.g., Less et al., 2006) is of course larger several factors than the last volcanic eruption during Holocene time. The decline in amount (production) of lava flows with time is undoubtedly considerable in the Al Haruj region (Elshaafi and Gudmundsson, 2017). In addition, monogenetic lava shields, as in Iceland and AHVP, are widely believed to be formed in single eruptions, some of which may have taken tens of years (Walker, 1965; Gudmundsson, 1986; Andrew and Gudmundsson, 2007; Thordarson and Hoskuldsson, 2008; Thordarson, Sigmarsson, 2009; Elshaafi and Gudmundsson, 2017). Thus if we presume both eruptions (initial and last eruptions) on the AHVP would have the similar emplacement mechanism, so the duration of the first volcanic eruption may be an order of magnitude greater than the last

eruption (probably years or even decades). If the eruptions would have taken many years (or decades) so replenishment primitive magma into the deep-seated reservoir could partly contribute to maintaining its excess magmatic pressure inside magma reservoir during the eruption (cf. Gudmundsson, 2016).

Similarly, many studies (e.g., Thordarson et al 1996; Thordarson and Self, 1998; Self et al., 1998; Wignall, 2001;Jahren, 2002, Burgess et al., 2017; Vaillant et al., 2017) propose that long-lived volcanic eruption, large basaltic eruptions, might be protracted and awful atmospheric impact due emission large amount of greenhouse gases (e.g., CO_2, CH_4) . Emissions of CO_2 might have induced considerable global warming and SO_2 global cooling if developed over a short interval (Olsen, 1999). There is apparent coincidence between the age of an initial volcanism in the AHVP and fauna and flora local extinctions in the As-Sahabi area, NE the Sirt Basin, during Messinian-Zanclean time (≈7 to 5 Ma) (Fig. 7.1) (Boaz, 2009 El-Shawaihdi et al., 2016). In addition , new important evidence is recently offered by Hounslow et al. (2017), who inferred on the basis of high-resolution chronology and magnetostratigraphy of the Neogene deposits in the Fezzan Basin, southwestern of the Sirt Basin that extremely aridity was taking place at Lake Megafezzan (a giant paleo-lake) after 11 Ma (Fig. 7.1). Causes of the local biological extinction in the Sirt Basin region remain under debate where some researches are connected this local disaster with the Mediterranean dramatically drawdown (as much as 1 km) during the end-Miocene (Messinian time) (5.96 to 5.33 Ma) and caused massive desiccation in the Mediterranean Sea, namely Messinian Salinity Crisis (MSC) (Gautier et al., 1994; Bache et al., 2009; El-Shawaihdi et al., 2016).

The individual effusive volcanic eruption could not cause alone massive aridification or local extinction although it certainly can do some local

disasters depends on the amount emission of greenhouse gases and duration of eruption. For instance, Kilauea eruption in Hawaii is considered as one of the most long-lived eruptions known on Earth. This volcano emitted nearly 2000 tons of SO_2 per day through 14 year (Elias et al 1993, Self and Thordarson, 1998). This volcanic fog caused serious eye and respiratory irritation in the population of Hawaii but does not have extensive awful atmospheric impact (Self and Thordarson, 1998). Other example, the 1783–1784 Laki eruption in Iceland is considered as one of the largest basaltic flood lava eruption in historical times (Thordarson et al., 2001; Thordarson et al., 2003). This volcanic eruption led to release more than 1.7 megatons of SO_2 per day and huge amount of dissolved HCl and HF during the first weeks of its duration (8 months) (Thordarson et al. 1996). This was led to thick dry fog that extended over large areas in Europe and Asia. This may be led to some environmental problems in Iceland at that time (Stothers, 1996). The remaining of sulfate aerosols in the stratosphere may be caused several years of extraordinarily low temperatures and awful weather in many portions on Earth (Fiacco et al, 1994, Thordarson and Self, 1997).

Nevertheless, the linked between volcanism and ecologically catastrophic climate throughout the geological record are still debated in the literature and various interpretations based on new geochemical and isotope data are available (e.g., Burgress et al., 2017, Vaillant et al., 2017). Thus, in order to assess whether the duration along with amount of volatile content liberated during individual volcanic eruption as listed above may have influenced the local biological extinction in the Sirt Basin area, we should be needed further research in the AHVP to accurate quantify eruption durations by using drilling core barrels due to the lack of exposures. The core barrels can be used to examine the changes in vesiculation structures along with petrographic texture and jointing style that are excellent indicators of the transitional from crystalline core zone to upper vesicular crust (Thordarson, 1995; Self et al., 1997: Cashman and Kauahikaua, 1997; Thordarson and Self, 1998). In

addition, the detailed petrographic investigation would be a good test to estimate the pre and post eruption volatile material of the glass in inclusions trapped in phenocrysts (pre-eruption) and degassed lava matrix (post-eruption) (cf. Self et al., 1998). Such data is also essential condition for forecasting and assessment hazards of the AHVP.

Acknowledgments

We are grateful and acknowledged N. Inskip for heavily assistant for preparation samples and measurement of dynamic Young's modulus at the Rock and Ice Physics Laboratory at University College of London (UCL). We are also indebted to the Industrial Research Centre (IRC), Tripoli, for their encouragement and kind support during fieldwork. This work has been funded by the Libyan Ministry of Higher Education and Scientific Research.

References

Anderson, S., Stofan, E., Smrekar, S., Guest, J., Wood B., 1999. Pulsed inflation of pahoehoe lava flows: implications for flood basalt emplacement. Earth and Planetary Science Letters, 168, 7–18.

Andrew, R., Gudmundsson, A., 2007. Distribution, structure, and formation of Holocene lava shields in Iceland. Journal of Volcanology and Geothermal Research 168, 137–154. doi:10.1016/j.jvolgeores.2007.08.011.

Boaz, N., 2009. Libya before the Sahara: The vanished world of the Eo-Sahabi Valley. Published by the International Institute for Human Evolutionary Research Integrative Centers for Science and Medicine 2565 Siskiyou Boulevard, Suite 4/1L Ashland, OR 97520, U.S.A. 1, 1–12.

Bagnardi, M., 2014. Dynamics of Magma Supply, Storage and Migration at Basaltic Volcanoes: Geophysical Studies of the Galápagos and Hawaiian Volcanoes. PhD thesis. University of Miami, USE. Scholarly Repository. Electronic Theses and Dissertations.

Brotons, V. Toma´s, R., . Ivorra S., Grediaga, A., Martı´nez-Martı´nez, J., Benavente, D.,Go´mez-Heras, M., 2015. Improved correlation between the static and dynamic elastic modulus of different types of rocks. Materials and Structures, 49, 8, p. 3021–3037.

Burgess, S., Muirhead, J., Bowring, S., (2017). Initial pulse of Siberian Traps sills as the trigger of the end-Permian mass extinction. Nature communications, 8: 164, doi:10.1038/s41467-017-00083-9

Busrewil, M., Suwesi, S.,1993. Geological Map of Libya 1 : 250.000, Sheet : Al Haruj Al Aswad NG(33-4). Explanatory Booklet. Industrial Research Centre, Tripoli, p. 95.

Busrewil, M. T., 1996. The volcanology of central Jabal al Haruj al Aswad volcanic province, Central Libya. The geology of Sirt Basin, Elsevier, Amsterdam. . III, 331-345.

Calvari, S., and H. Pinkerton (1998), Formation of lava tubes and extensive flow field during the 1991–1993 eruption of Mount Etna, Journal of Geophysical Research 103, 27,291– 27,301.

Chitwood, L.A., 1994. Inflated basaltic lava-examples of processes and landforms from central and southeast Oregon. Oregon Geology, 56, 11–21.

Christaras, B, Auger. F., Mosse, E.,1994. Determination of the moduli of elasticity of rocks. Comparison of the ultrasonic velocity and mechanical resonance frequency methods with direct static methods. Materials and Structures, 27, 222–228. doi:10.1007/bf02473036.

De Wet A., Hamilton, C. Bleacher, J., Garry, B., 2014. Lava Mars and the Earth: A comparative study of inflated and distributed flows.

Published by Keck Geology Consortium. 27th annual Symposium Volume. ISBN: 1528–7491.

Dill, K., Bromberg, S. 2003. Molecular Driving Forces: Statistical Thermodynamics in Chemistry and Biology; Taylor and Francis: London, UK.

Duncan, A., Guest, J., Stofan, E., Anderson, S., Pinkerton, H., Calvari, S., 2004. Development of tumuli in the medial portion of the 1983 aa flow-field, Mount Etna, Sicily. Journal of Volcanology and Geothermal Research, 132, 173–187.

Duraiswami, R., Bondre, N., Dole, G., Phadnis, V., Kale, V., 2001. Tumuli and associated features from the western Deccan Volcanic Province, India. Bulletin of Volcanology, 63, 435–442. DOI 10.1007/s004450100160.

Elias T, Sutton AJ, Stokes JB. 1993. Current SO2 emissions at Kilauea Volcano: quantifying-scattered degassing sources. Eos, EGU publications, 74:670–71

Elshaafi, A., Gudmundsson, A., 2016. Volcano-tectonics of the Al Haruj Volcanic Province, Central Libya, Journal of Volcanology and Geothermal Research, 325, 189–202. http://dx.doi.org/10.1016/j.jvolgeores.2016.06.025.

Elshaafi, A., Gudmundsson, A., 2017. Distribution and size of lava shields on the Al Haruj al Aswad and the Al Haruj al Abyad Volcanic Systems, Central Libya. Journal of Volcanology and Geothermal Research, 228, 46-62.

El-Shawaihdi, M., Mozley, P., Boaz, N., Salloum, F., Pavlakis, P., Muftah, A., Triantaphyllou, M., 2016. Stratigraphy of the Neogene Sahabi units in the Sirt Basin, northeast Libya. Journal of African Earth Sciences, 118, 87- 06.

Fisher, R., Schmincke, H., 1984. Pyroclastic rocks. Springer, Heidelberg, pp 1–474.

Eissa E, Kazi A.,1988. Relation between static and dynamic Young´s Moduli of rocksInternational Journal of Rock Mechanics and Mining, 25, 479–482. doi:10.1016/0148-9062(88)90987-4.

Fiacco, R., Thordarson, T.,, Germani, M.,, Self, S., Palais, J. 1994. Atmospheric aerosol loading and transport interpreted from ash particles and acidity due to the 1783–1784 Laki eruption in the GISP2 ice core. Quat. Res. 42, 231–40.

Glaze, L., Anderson, S., Stofan, E., Baloga, S., Smrekar, S., Statistical distribution of tumuli on pahoehoe flow surfaces:Analysis of examples in Hawaii and Iceland and potentialapplications to lava flows on Mars. Journal of Geophysical Research, 110, 1-14.

Gudmundsson, A., 1986. Mechanical aspects of postglacial volcanism and tectonics of the Reykjanes Peninsula, southwest Iceland. Journal of Geophysical Research, 91, 12711–12721.

Gudmundsson, A.,1990. Emplacement of dikes, sills, and crustal magma chambers at divergent plate boundaries. Tectonophysics, 176, 257–275.

Gudundmusson, A. 1999. Postglacial crustal doming, stresses and fracture formation with application to Norway. Tectonophysics, 307, 407–419.

Gudmundsson A., 2011. Rock fractures in geological processes. Cambridge University Press, Cambridge. doi: 10.1017/ CBO9780511975684. p. 592.

Gudmundsson, A., 2014. Elastic energy release in great earthquakes and eruptions. Frontiers in Earth Science. 10, 1-12. doi: 10.3389/feart.2014.00010.

Gudmundsson, A., 2016. The mechanics of large volcanic eruptions. Earth-Science Reviews, 163, 72–93.

Gudmundsson, A., Mohajeri, N. 2013. Relations between the scaling exponents, entropies, and energies of fracture networks. Bull.

Geol.Soc. France 184, 377–387. doi:10.2113/gssgfbull.184.4–5.373.

Haimson, B. Rummel, F., 1982. Hydrofracturing stress measurements in the Iceland research drilling project drill hole at Reydarfjordur, Iceland. Journal of Geophysical Research, 87, 6631–6649.

Henk, A., Fischer, K., Kromuller, K., Wanger, D., Winter, I., 2013.Prediction of Tectonic Stresses and Fracture Networks with Geomechanical Reservoir Models. DGMK-Research Report 721. German Society for Petroleum and Coal Science and Technology. p. 216.

Hon, K., Kauahikaua, J., Denlinger, R., McKay, K., 1994. Emplacement and inflation of pahoehoe sheet flows observation and measurements of active lavas on Kilauea volcano, Hawaii. Geol. Soc. Am. Bull. 106, 351–370.

Hounslow, M., White, H., Drake, N., Salem, M., El-Hawat A., McLaren, S., Karloukovski, V., Noble, S., Hlal, O., 2017. Miocene humid intervals and establishment of drainage networks by23 Ma in the central Sahara, southern Libya. Gondwana Research, 4, 118–137.

Jaeger, J., Cook, N., 1969. Fundamentals of Rock Mechanics. Methuen, London, 515 pp.

Jahren, A., 2002. The biogeochemical consequences of the mid-Cretaceous superplume. Journal of Geodynamics, 34, 177–191.

Keszthelyi L., Pieri, D., 1993. Emplacement of the 75-km-long Carrizozo lava flow field, south-central New Mexico. Journal of Volcanology and Geothermal Research. 59,,59–75.

Keszthelyi, L., Self S, Thordarson T., 1997. Application of recent studies on the emplacement of basaltic lava flows to the Deccan Traps. Journal of the Geological Society of India. Less, G., Turki, S., Suwesi, K., Peregi, L., Koloszar, L., Kalmar, J., Sherif, K., Csaszar, G., Gulasci, Z., Dalum, H., Al Tajuri, A.,

2006. Explanatory Booklet. Geological Map of Libya 1: 250.000. Sheet: Waw Al Kabir NG 33– 12.

Macdonald, G., 1953. Pahoehoe, aa, and block lava. American Journal of Science, 251, 169–91.

Mattsson, H., Hoskuldsson, A., 2005. Eruption reconstruction, formation of flow lobe tumu1i and eruption duration in the 5900 BP Helgafell lava field (Heimney), south Iceland. Journal of Volcanology and Geothermal Research, 147, 157–-172.

Mattsson, H., Vuorinen, J., 2008. Emplacement and inflation of natrocarbonatitic lava flows during the March–April 2006 eruption of Oldoinyo Lengai, Tanzania. Bulletin of Volcanology, 71, 301–311. DOI 10.1007/s00445-008-0224-z.

Mohajeri, N., Gudmundsson, A. 2012. Entropies and Scaling Exponents of Street and Fracture Networks. Entropy, 14, 800–833; doi:10.3390/e14040800. ISSN 1099–4300.

Marti, J., Gudmundsson, A., 2000. The Las Cañadas caldera (Tenerife, Canary Islands): an overlapping collapse caldera generated by magma-chamber migration. Journal of Volcanology and Geothermal Research, 103, 161–173.

Mauro, I., Bertotto, G., Jalowitzki, T., Orihashi, Y., Ponce, A., 2015. Emplacement history and inflation evidence of a long basaltic lava flow located in Southern Payenia Volcanic Province, Argentina. Journal of Volcanology and Geothermal Research 293, 46–56.

Muftah, A., Pavlakis, P., Godelitsas, A., Gamaletsos, P., Boaz, N. 2013. Paleogeography of the Eosahabi River in Libya: New insights into the mineralogy, geochemistry and paleontology of Member U1 of the Sahabi Formation, north-eastern Libya. Journal of African Earth Sciences, 78, 86–96.

Nemeth, K., Haller, M., Martin, U., Rossi, C., Massafero, G., 2008. Morphology of lava tumuli from Mendoza, Patagonia

(Argentina) and Al-Haruj (Libya). Z. Geomorphology, 52, 181–194.

Németh, K., Kereszturi, G., 2015. Monogenetic volcanism: personal views and discussion. International Journal of Earth Sciences, 104, 2131–2146.

Ninad, R., Raymond, A. Duraiswami R., 2003. Morphology an emplacement of flows from the Deccan Volcanic Province, India. Bulletin of Volcanology, 66:29–45. DOI 10.1007/s00445-003-0294-x.

Nixon, S., Maclennan, J., White, N., 2011. Intra-plate magmatism of the Al Haruj Volcanic Field, Libya. Goldschmidt Conference Abstracts.

Olsen, P. 1999. Giant lava flows, mass extinctions and mantle plumes. Science, 284, 604–605.

Pedersen G., Höskuldsson, A., Dürig, T., Thordarson, T., . Jónsdóttir, S., Riishuus, M., Óskarsson, B., Dumont, S., Magnusson, E., Gudmundsson, M., Sigmundsson, F., DrouinV., Gallagher, C., Askew, R., Gudnason, J., Moreland, W., Nikkola, P., Reynolds, H., Schmith, J., the IES eruption team, 2017. Lava field evolution and emplacement dynamics of the 2014–2015basaltic fissure eruption at Holuhraun, Iceland, Journal of Volcanology and Geothermal Research, 340,155–169.

Peregi, Z., Less, G., Konrad, G., Fodor, L., Gulacsi, Z., Gyalog, L., Turki, S., Suwesi, K., Sherif, K., Dalub, H., 2003. Explanatory Booklet. Geological Map of Libya 1: 250.000. Sheet: Al Haruj Al Abyad NG 33-8. Industrial Research Centre, Tripoli, p. 248.

Rossi, M., J.999. Plan-curvature effect on the formation of tumuli on shield volcanoes: an example from Leitin lava flow field in Iceland, Zeitschrift für Geomorphologie,114, 1– 10.

Rossi, M., Gudmundsson, A., 1996. The morphology of flow-lobe tumuli on Icelandic lava shields. Journal of Volcanology and Geothermal Research 72, 291–308.

Rowland, S., Walker, G., 1987. Toothpaste lava: characteristics and origin of a lava structural type transitional between pahoehoe and aa. Bulletin of Volcanology, 49, 631–641.

Scheidt, S., Hamilton, C., Zimbelman, J., Bleacher, J., Garry, W., De Wet, A., Crumpler, L., 2014. Lava rise plateaus and inflation pits within the Mc-cartys flow, New Mexico, USA. 45th Lunar and Planetary Science Conference.

Self S, Thordarson Th, Keszthelyi L, Walker GPL, Hon K, et al. 1996.Anewmodel for the emplacement of the Columbia River Basalts as large inflated pahoehoe sheet lava flow fields. Geophysical Research Letters. 23, 2689–92

Self, S., Thordarson, T., Keszthelyi. L. . 1997. Emplacement of continental flood basalt lava flows. In AGU Geophys. Monogr. Large Igneous Processes, ed. JJ Mahoney, M Coffin.

Self, S., Keszthelyi, L., Thordarson, T., 1998. The importance of pahoehoe. Annual Review of Earth and Planetary Sciences, 26, 81–110.

Self, S., Keszthelyi, L., Thordarson, T., 2000. Discussion of: 'Pulsed inflation of pahoehoe lava flows: implications for flood basalt emplacement,' by Anderson et al. Earth and Planetary Science Letters, 179, 421–423.

Stothers, R.,. 1996. The great dry fog of 1783. Climatic Change ,32, 79–89

Suleiman, A., Doser, D., 1995. The seismicity, seismotectonics and earthquake hazards of Libya, with detailed analysis of the 1935 April 19, M=7.1 earthquake sequence. Geophysical Journal International, 120, 312–322.

Szilard, R., 1975. Theory and analysis of plates, classical and numerical methods, Prentice-Hall, Englewood Cliffs, N. J. p. 253.

Theilig, E,. 1986. Formation of pressure ridgesand emplacement of compound basaltic lava flows. PhD thesis. Ariz. State Univ., Tempe.212 pp.

Thordarson T., 1995. Volatile release and atmospheric

effects of basaltic fissure eruptions. PhD thesis. Univ. Hawaii, Manoa, Honolulu.

580 pp.

Thordarson, T., 2000. Physical volcanology of lava flows on Surtsey, Iceland:A preliminary report. Suurtesy Research. Reylzjavik, 11, 109-126.

Thordarson, T., Höskuldsson, A., 2008. Postglacial volcanism in Iceland, Jokull - The Icelandic Journal of Earth Sciences, 58, 197-228.

Thordarson, T., Sigmarsson, O., 2009. Effusive activity in the1963–67 Surtsey eruption, Iceland: flow emplacement and growth of small lava shields. In: Thordarson, T., G. Larsen,S. Self, S. Rowland and Á. Höskuldsson eds. Studies in Volcanology: The Legacy of George Walker. Geological Society, London, Special Publications.

Thordarson, T., Self, S., Miller, D., Larsen, G., Vilmundardóttir, G., 2003. Sulphur release from flood lava eruptions in the Veiðivötn, Grímsvötn and Katla volcanic systems, Iceland. In: Oppenheimer, C., D. M. Pyle and J. Barclay eds. Volcanic Degassing. Geological Society, London, Special Publications. 213, 103–121.

Thordarson T., Self, S., 1997. Atmospheric and environmental effects of the 1783-84 AD Laki eruption. Glob. Planet. Change. In revision Thordarson, T., Self, S., 1996. Sulphur, chlorine and fluorine degassing and atmospheric loading by the Roza eruption, Columbia River Basalt Group, Washington, USA. Journal of Volcanology and Geothermal Research, 74, 49–73.

Thordarson, T., Self, S., Óskarsson, N., Hulsebosch, T., 1996.Sulfur, chlorine, and fluorine degassing and atmospheric loading by

the 1783–1784 AD Laki (Skaftár Fires) eruption in Iceland. Bulletin of Volcanology. 58, 205–225.

Thordarson, T., Self, S., 1993. The Laki (Skaftár Fires) andGrímsvötn eruptions in 1783–1785. Bulletin of Volcanology, 55, 233–263.

Ugural, A. 1981. Stresses in plates and shells. McGraw-Hill, New York, NY, p.317.

Vaillant, M., Barnes, S., Mungall, J., Mungall, L., 2017. Role of degassing of the Noril'sk nickel deposits in thePermian–Triassic mass extinction event. Proceedings of the National Academy of Sciences of USA. 14, 2485–2490.

Volkenstein, M., 2009. Entropy and Information; Birkhauser: Berlin, Germany.

Walker, G., 1965. Some aspects of Quaternary volcanism in Iceland, Leicester Literary and Philosophical Society, 49, 25–40.

Walker, G., 1991. Structure and origin by injection of lava under surface crust, of tumuli, lava rises, 'lava-rise pits', and 'lava-inflation clefts' in Hawaii. Bulletin of Volcanology, 53, 546-558.

Whitehead, P., Stephenson, P., 1998. Lava rise ridges of the Toomba basalt flow, North Queensland, Australia. Journal of Geophysical Research, 103, 371–382.

Wignall, P., 2001. Large igneous provinces and mass extinctions. Earth-Science Reviews, 53, 1–33.

Chapter 8: Mechanical interaction between volcanic systems in Libya

Tectonophysics

Abdelsalam Elshaafi and Agust Gudmundsson

Contribution statement:

The origin idea, data collections, methodology and creation of 2-dimensional and 3-dimesional models were conducted by AE.

Analysis and interpretation of numerical results were done by AE and specifically support input from co-author.

Writing the initial draft was made by AE and later revising the manuscript for important intellectual content from co-author

Illustrations were prepared by AE.

Mechanical interaction between volcanic systems in Libya

Abdelsalam Elshaafi[1], Agust Gudmundsson[1]

[1]Department of Earth Sciences, Royal Holloway University of London, Egham TW20 0EX, UK (abdelsalamelshaafi@yahoo.co.uk; a.gudmundsson@rhul.ac.uk)

Abstract

The spatial distributions of monogenetic volcanoes, primarily volcanic craters, within the four principal volcanic provinces of Libya are examined and presented on volcano density maps. Six main volcanic clusters have been identified, referred to as volcanic systems. Remarkably, the Al Haruj (AHVP) and Nuqay (NVP) volcanic provinces have double-peak density distributions, while Gharyan (GVP) and Sawda (SVP) volcanic provinces have single-peak density distributions. We interpret each density peak as corresponding to a separate volcanic system, so that there is a total of six systems in these four provinces. There was an overlap in volcanic activity in these provinces with at least three simultaneously active. We propose that each of the 6 volcanic systems was/is supplied with magma from a large sill-like reservoir, similar in lateral dimensions to the systems/clusters themselves. Numerical results show zones of high tensile and shear stresses between the reservoirs that coincide roughly with the main swarms of extension (dykes and volcanic fissures) and shear (faults) fractures in the areas. The most recent volcanic eruptions in Libya fall within the modelled high-stress concentration zones, primarily eruptions in the volcano Waw an Namus and the Holocene Al Mashaqaq lava flow. There are no known eruptions in Libya in historical time, but some or all the volcanic systems may have had one or more arrested historical dyke injections. In particular, part of the recurrent seismic events in the Hun Graben in the northwest Libya may be related to dyke propagation and arrest. If some of the inferred magma

reservoirs are still fluid, as is likely, they pose earthquake and volcanic hazards to parts of Libya, particularly to the city of Gharyan (population about 45,000) and Zallah town (population about 8,000), as well as to many oil-field operations.

Keywords: volcano distribution, volcanotectonics, volcanic system, magma reservoir, volcano interaction, crustal stresses

8.1 Introduction

Libya is located on the Mediterranean part of the African shield, which includes basins of Sirt, Ghadamis, Murzuq and Al Kufrah. The Sirt Basin, in central Libya, is regarded as the youngest among the other Palaeozoic sedimentary basins (Fig. 8.1) (Suleiman and Doser, 1995). Libya has four main volcanic provinces. From northwest to southeast, these are as follows (Fig. 8.1): (i) The Gharyan Volcanic Province (GVP), which is situated in the south-western Tripoli; (ii) the Sawda Volcanic Province (SVP), which is located between GVP and (iii) the Al Haruj Volcanic Province (AHVP) at the central part of Libya; and (iv) the Nuqay Volcanic Province (NVP), which is located close to Tibesti massif at the Libyan-Chadian border (Elshaafi and Gudmundsson, 2016). In addition, there are some small volcanic areas and structures, such as massif of Al Hasawinah, southwest of SVP, and the ring-dyke, Jabal Awayant, located in the south-easternmost Libya (Busrewil and Wadsworth, 1980). The AHVP is regarded as still volcanically active. This conclusion rests on recent geochronological data by Nixon et al. (2011) as well as extremely well-preserved inflation features such as tumuli and lava rises that strongly support young ages. The lava flows of these four volcanic provinces are primarily of alkali to transitional basalts while more evolved volcanic rocks such as trachyte and phonolite are not observed in the AHVP but being subsidiary in the other volcanic provinces (e.g., Stuart et al., 2014).

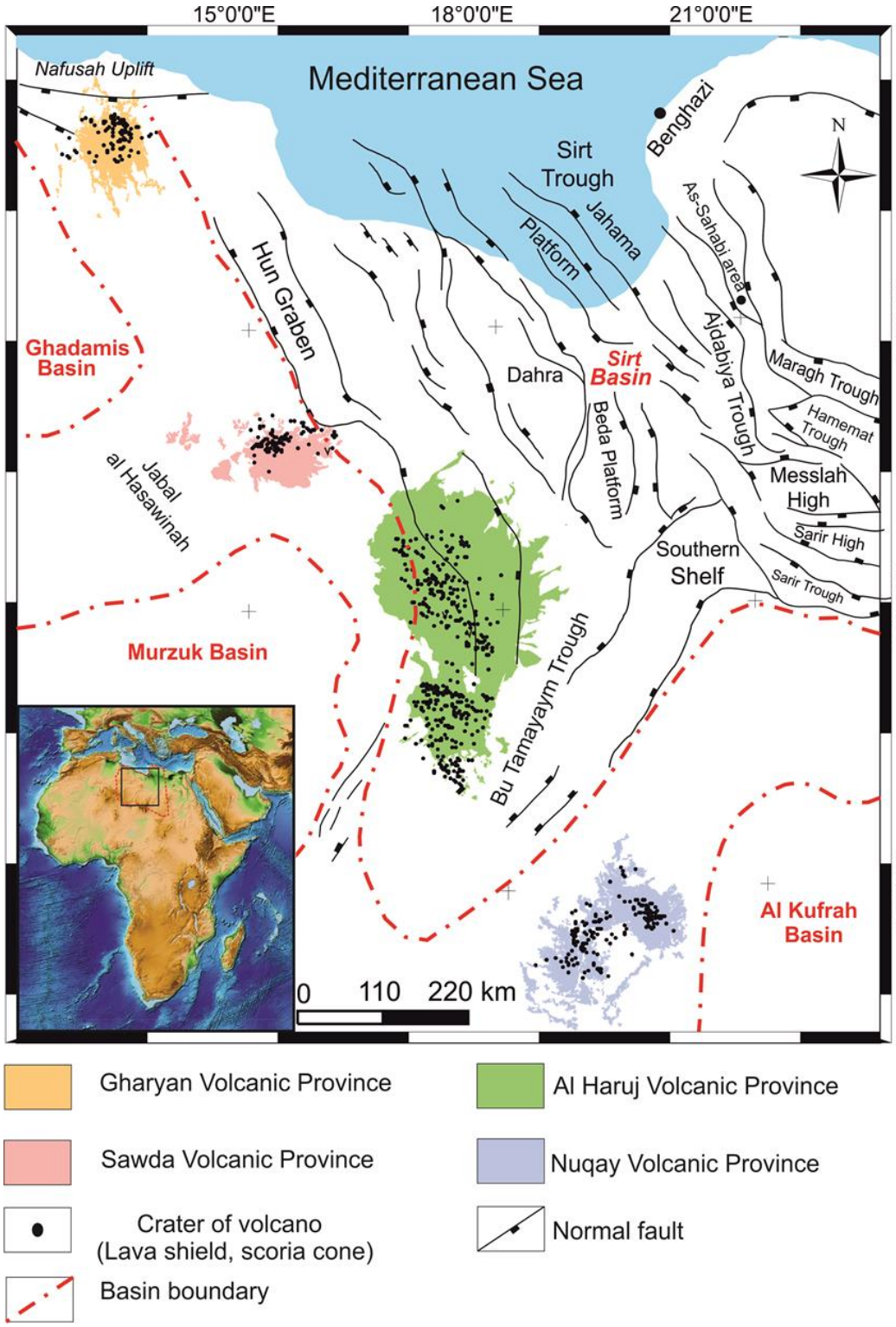

Figure 8.1. Simplified tectonic map of Libya showing the distribution of main volcanic provinces as well as the sedimentary basins. The four principal volcanic provinces are obviously arranged NW–SE direction. Inset map shows the location of these volcanic provinces in Africa. The normal faults are taken from Mouzughi and Taleb (1981) and Abadi et al. (2008).

The main evidence for the four principal volcanic provinces in Libya is that volcanism occurs primarily within well-defined areas whose long axes coincide with ancient structural elements. All the provinces show considerable volcanotectonic similarities, particularly in the mechanism and products of volcanic eruption (alkali to mildly alkali basalts) as well as in their ages (Klitzsch, 1971; Mohamed, 2014; Radivojević et al., 2015). The volcanic provinces form a general NW–SE trend, are of Miocene – Quaternary age, and cover a total area of about 65,000 km^2 (Figs. 8.1 and 8.2). They occur mostly at the intersections between the main regional pre-existing structural elements in Libya (Klitzsch, 1971; Busrewil, 2012). Although together the provinces form one of the largest volcanic fields in North Africa, they have not been previously investigated in detail as regards their volcanotectonic evolution.

New age determinations during the past few years show that volcanism in Libya was to a degree simultaneous, that is, overlapped, during certain periods of time in three of the provinces (Nixon et al., 2011; Bardintzeff et al., 2012; Stuart et al., 2014; Radivojević et al., 2015). Before these new age determinations, it was generally though that volcanism in Libya showed a gradual decrease in their age from the northwest, namely the Gharyan Volcanic Province, towards the southeast, that is, to the Nuqay Volcanic Province (e.g., Hegazi, 1999). These new age data, indicating simultaneous activity in most of the volcanic provinces over certain periods of time, encourage us to test the potential of a mechanical interaction between the provinces, and in particular their volcanic systems. The interaction is most likely to have occurred during late Miocene – Pliocene, but may have continued to some extent so long as the associated reservoirs were active as partially or (more rarely) totally fluid bodies. Some magma reservoirs are active for many millions or years, occasionally tens of millions of years, in which case mechanical interaction is possible over the same time periods (Gudmundsson et al., 2008).

Potential mechanical interaction between volcanic systems and individual polygenetic volcanoes (stratovolcanoes, basaltic edifices, central volcanoes) has received increasing attention in recent years. Such an interaction, where it exists, is important as regards general volcanotectonic development of the associated volcanoes/volcanic systems, mixing of magmas between them, and forecasting their volcanic eruptions. Recent studies on mechanical interaction between volcanoes include geodetic measurements in the Galapagos Islands, where there is strong evidence for mechanical interactions between basaltic edifices (central volcanoes) in close proximity (Amelung et al., 2000). There is also abundant evidence of mechanical interactions between central volcanoes in Iceland, particularly in the part of the volcanic zones located above the Iceland Mantle Plume (Andrew and Gudmundsson, 2008; Gudmundsson et al., 2008). Similarly, there is evidence for mechanical interaction between some central volcanoes in the Kenyan Rift of Africa (Biggs et al., 2016). Here we made several numerical models in order to explore the potential mechanical interaction between volcanoes in Libya.

To explore the potential interaction between volcanic systems in Libya we use the spatial distributions of monogenetic volcanoes, primarily volcanic craters, within the four principal volcanic provinces to define 6 potentially interacting volcanic systems. We propose that each volcanic system is supplied with magma from a sill-like reservoir, that is, a reservoir that is thin in relation to its lateral dimensions which are assumed similar to those of the associated volcanic system. The reservoirs are assumed located at the crust-mantle boundary. We then model numerically the stresses around and in-between the proposed magma reservoirs developed partly as a result of northeast-southwest extension perpendicular to the main trend of the volcanic systems and the nearby Sirt Basin (Fig. 8.1).

8.2 Geological and tectonic setting

It is only in the last four decades that the plate-tectonic history of Libya has become reasonably well understood. This understanding is primarily the result of intensive research during which deep seismic profiling and deep drilling of oil wells have extended to the entire territory of Libya, providing extensive new subsurface datasets (Hallet, 2002; Peregi et al., 2003; Less et al., 2006). During the general tectonic development of the North Africa there

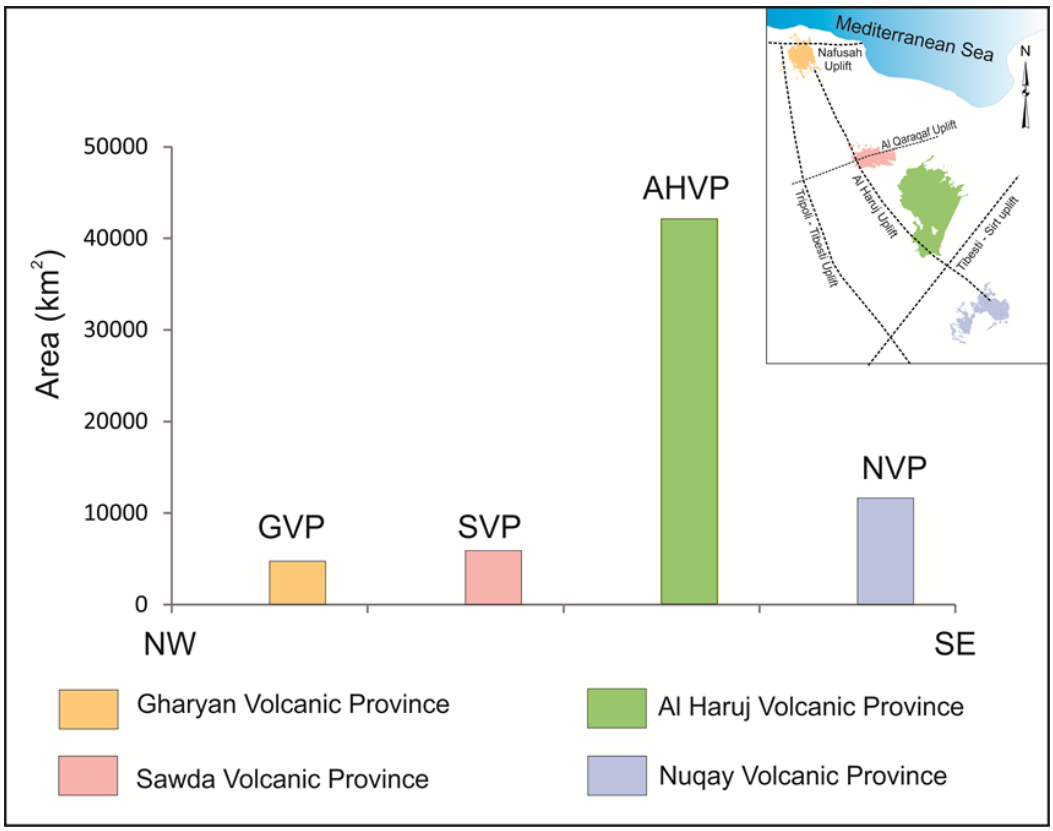

Figure 8.2. Graph showing the area for each an individual volcanic province in Libya. The Al Haruj Volcanic Province (AHVP) represents the largest one, covering area around 42,000 km^2 while the Gharyan Volcanic Province (GVP) represents the smallest one with area around 4,494 km^2. The inset map shows two main orthogonal pre-existing structural trends based on Woller and Fediuck (1980).

have been several periods of extensions followed by compression (Klitzsh, 1971). The major tectonic episodes in Libya include the Pan-African, Caledonian and Hercynian orogenies (Peregi et al., 2003). Tectonic deformations during Cretaceous, middle Tertiary through Miocene, and Holocene also produced major structural and tectonic features. However, the effects of major tectonic events were generally broadly distributed, and compressional folds are not common (Goudarzi, 1980; Less et al., 2006; Al-Heety, 2013; Chorowics and Benissa, 2016). In general terms, during the Palaeozoic and early Mesozoic the Libyan tectonics was controlled by the evolution of Gondwana and Pangaea, whereas through the late Mesozoic and Cenozoic times the tectonics was controlled by the evolution of Tethys and the Mediterranean sea, the North Africa being situated on the leading edge of Gondwana (Hallet, 2002; Peregi et al., 2003; Al-Hafdth and Elshaafi, 2015).

The African plate ceased to move relative to European plate during the Palaeocene (Rosenbaum et al., 2002). Subsequently, the Palaeocene and Eocene were marked by magmatism and ring-dyke intrusions, dated as Eocene at Jabal Awayant, at the border between Libya, Sudan and Egypt (Woller and Fediuk, 1980; Andre, et al. 1991). Simultaneously, there was uplift and erosion in western Libya which may be interpreted as the result of upwelling mantle plume, as well as continued extensive subsidence in the whole of the Sirt Basin (Hallet, 2002). In Oligocene the movement of the African plate relative to Eurasian plate changed much, which led to several major changes in the western Mediterranean. Subsidence of the Hun Graben occurred during this period, and major subsidence was still taking place in northern part of the Ajdabiya Trough, eastern part of the Sirt Basin (Hallet, 2002; Abadi et al., 2008) (Fig. 8.1). Moreover, sedimentation of the Oligocene was affected by the upper Eocene – early Oligocene uplift and erosion. The broad carbonate platforms in the early Tertiary have represented a major hydrocarbon reservoir in the Sirt Basin (Hallet, 2002). In addition, the Arabian shield began to break up from the African plate

throughout the opening of the Red Sea during this period (Bosworth et al., 2005; Al-Kwatli et al., 2012).

The Dead Sea was subject to strike-slip faulting during mid-late Miocene, reflecting the east-northeast tilting and minor folding of the Sirt Basin (Hallet, 2002). Following that the motion of the African plate relative to the European plate changed from north-northeast to northwest which led to rejuvenation Hyrecian faults. During this period there was thrusting and wrench faulting offshore of Libya, formation of marine sedimentary rocks in Cyrenica (Jabal

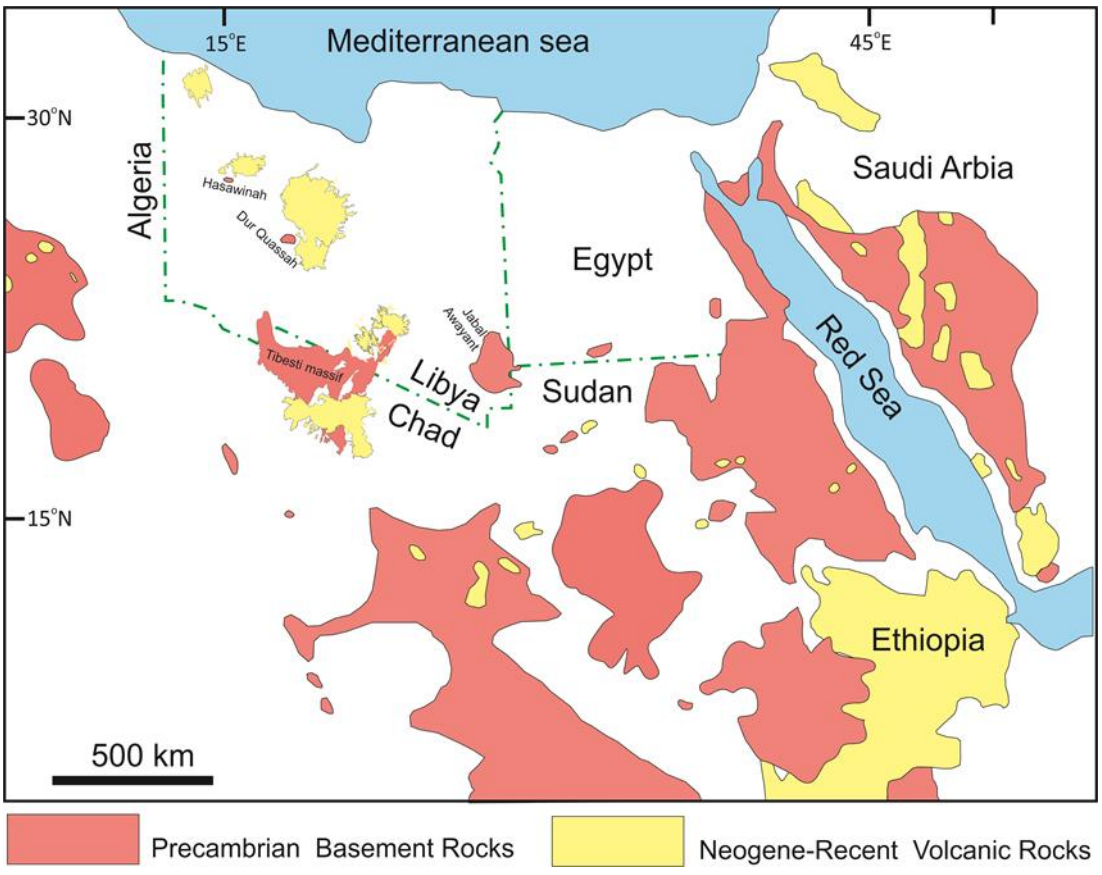

Figure 8.3. Map showing the relationship between the late Phanerozoic volcanic rocks with the basement outcrops in the North Africa (modified after Vail, 1971and Guiraud et al., 2000). Note there is obviously coincidence between the volcanism of Libya and the axial trend of the basement outcrops.

Al Akhadar area), NE Libya, as well as the effusion of large volumes of basaltic lava flows, which were erupted along the axis of the Palaeozoic Tripoli –Tibesti Uplift which follows the NNW–SSE trend from the Gharyan volcanic field at the coast of Mediterranean Sea, through the AHVP, to the Nuqay field at the southernmost Libya (Anketell, 1996, Abadi et al., 2008). The Tripoli – Tibesti Uplift is considered by many authors to be located at the junction between two African plates (East and West plates), partly based on paleo-stress studies (Hallett, 2002). In the late Miocene (Messinian time) the sea level in the Mediterranean dropped as much as 1 km, which resulted in a salinity crisis. The Messinian event has been evidenced by the layers of evaporites that are exposed in the Sahabi area, west of the city of Ajdabia, and in oil wells in the Sabratah Basin (Hallett, 2002). In addition, there is apparently a coincidence between the age of main volcanisms in Libya (late Miocene) and the fauna and flora local extinctions in the As-Sahabi area, north-eastern part of the Sirt Basin, during Messinian-Zanclean time (≈7 to 5 Ma) (Boaz, 2009).

While considerable progress has recently been made as regards our knowledge of the plate-tectonic history of Libya, there is still lack in geophysical information on crustal structure of the entire of Libyan Territory (e.g. Peregi et al., 2003; Abadi et al., 2008; Elshaafi and Gudmundsson, 2017). The most relevant recent information may be summarised as follows. Ghanoush et al. (2014) used gravity and magnetic modelling to estimate crustal thickness variations in the eastern part of the Sirt Basin. They divided the lithospheric into different layers, more specifically the upper mantle, the lower crust, and the upper crust. The upper crust involves Palaeozoic, Mesozoic and Cenozoic sediments. Most recently, Lemnifi et al. (2017) used receiver function constraints (RFs) from data obtained for the first time from 15 seismic broadband stations from the Libyan Center for Remote Sensing and Space Science to map, crudely, the seismic structure. In the present study, however, we use constant average static Young's modulus of 40 GPa and a constant Poisson's ratio of 0.25 for the entire crust.

8.3 Volcano-tectonic evolution

The Neogene – Quaternary volcanism is widespread within the African and European plates, partly reflecting the change in the plate-tectonic regime and associated change in the regional stress field (Cloetingh and VanWees, 2005; Abadi et. al., 2008). Changes in patterns of mantle convection contemporaneous with hot mantle plumes seem to be among the main causes of the flood basalt volcanism (Wilson and Guiraud, 1998; Abadi et. al., 2008).

In general terms, the volcanic provinces on Libya are spatially related to main two structural trends; early Palaeozoic structural elements of a prevalent NW–SE to NNW–SSE direction (parallel to the Red Sea) and late Palaeozoic to Mesozoic structures (Hercynian Orogeny) with a general E–W to ENE–WSW trend (parallel to east Africa rifts). These two structural element trends represent regional structures, which have played a significant role in the geological evolution of Libya's volcanism at large scale (Woller and Fediuk, 1980; Al-Hafdth and Elshaafi., 2015; Fig. 8.2). The basement beneath the main volcanic provinces in Libya is restricted to the overlap of Palaeozoic and Mesozoic structural elements, and creates the boundaries of sedimentary basins (Hallet, 2002). The Precambrian crystalline rocks in the Libyan territory are exposed in narrow and comparatively small areas such as Jabal al Hasawinah, west of Sawda, in Dur Quassah west of the AHVP, as well as in the Tibesti massif at Libyan – Chadian border (Al-Hafdth and Elshaafi., 2015; Fig. 8.3). Within these specific areas with their particular crustal structures and tectonic development during Palaeozoic and Mesozoic period the four major volcanic provinces in Libya formed during the Tertiary to Holocene time (Busrewil and Oun, 1991; Goudarzi, 1980; El¬Makhrouf, 1988; Less et al., 2006).

Vail (1971) suggests that the late Phanerozoic volcanic activity in North Africa occurred over a wide area and was coincident with the outcrops of basement rocks (Fig. 3). It is clear that the major volcanic fields in Libya are strongly correlated to the current elevated basement areas (Fig. 8.3). The basement highs seem to reflect some form of subcrustal arching where magma may have preferentially penetrated. Alternatively, the magma might have had difficulty in piercing thick sedimentary sequence that may be acted as barriers to the formation of surface volcanoes (the injected dykes, if any, being arrested or deflected into sills within the sedimentary piles) between the main volcanic systems on Libya's Tertiary (Vail, 1971, Al-Hafdth and Elshaafi., 2015; Elshaafi and Gudmundsson, 2017). The geochemistry, petrology and geochronology of the volcanic provinces of Libya have recently been discussed in detail (e.g., Bardintzeff et al., 2012; Mohamed, 2014; Al-Hafdh and Jafeer, 2015; Radivojević et al., 2015). Accordingly, we present only a brief summary of their characteristics.

8.3.1 Gharyan Volcanic Province (GVP) (late Miocene to Pleistocene)

The Gharyan Volcanic Province, with an area of 4,494 km^2, is the smallest among four main volcanic fields in Libya (Fig. 8.2). It forms a generally continuous sheet of volcanoes and lava flows in the central part of Jabal Nafusah, which has been active from late Miocene to late Pleistocene and lies at the intersection of two major structural elements. These are the NNW–SSE trending Tripoli – Tibesti Uplift axis formed in the early Palaeozoic and the E–W trending Nafusah Uplift formed during the late Palaeozoic to Mesozoic time (Woller and Fediuk, 1980; Goudarzi, 1980; Busrewil and Suwesi, 1993) (Fig. 8.2).

The province is made up of three distinct phases: (1) An early phase of extensive basaltic plateau that is made up of hypersthene normative lavas.

(2) A second phase of small phonolitic domes and trachyte. (3) A third phase which is characterised by lavas of basanitic composition (Almond et al., 1974; Al-Hafdh and Jafeer, 2015). The new age dating for the major pluses of basalt volcanism in this volcanic province using Ar/Ar chronology by Stuart et al.(2014) indicates that the volcanism of the Gharyan province is contemporaneous with the volcanism in both the Al Haruj and Nuqay volcanic provinces (from the end of Miocene to Pleistocene). This new age dating results are strongly difference with previous age determinations that were thought the initial volcanism in this region at 55-50 Ma (Eocene) (e.g., Almond et al., 1974).

8.3.2 Sawda Volcanic Province (SVP) (Miocene)

The Sawda Volcanic Province is situated in the westernmost of the Sirt Basin at the intersection of the early Palaeozoic the Al Haruj Uplift with the late Palaeozoic to Mesozoic Al Qarqaf Uplift (Woller and Fediuk, 1980; Fig. 8.2). This volcanic province covers an area of approximately 5,902 km^2, but this figure may be an underestimate because of lack of geological maps at the detail available for this volcanic field. Further to the southwest of the Sawda province, the volcanic field of Jabal al Hasawinah is tectonically related to the Tertiary reactivation of two intersecting major elements in south Libya, early Palaeozoic NNW–SSE Tripoli –Tibesti Uplift and the Hercynian ENE–SW, Al Qarqaf Uplift (Woller and Fediuk, 1980). These tectonic movements occurred during the evolution of two neighbouring structural domes on an N–S axis (namely Wadi Bardan and Wadi Darman domes), in which cores the basement granite of Pan-African Orogeny is exposed (Busrewil and Oun, 1991). However, the volcanic rocks of Sawda and al Hasawinah consist of alkaline and tholeiite basalts with phonolitic and gabbroic rocks being subordinate (Woller, 1978, Busrewil and Suwesi, 1993). The modern age dating of Jabal Al Hasawinah and Sawda suggests that their basalts were

erupted significantly earlier (23-10 Ma) than those of the other volcanic provinces (Stuart et al., 2014).

8.3.3 Al Haruj Volcanic Province (AHVP) (late Miocene up to Holocene time)

The Al Haruj Volcanic Province (AHVP) is the largest one in Libya. It developed from the end of Miocene up to Holocene and has been linked to the tectonic evolution of the rifting of the Sirt Basin (Cvetkovic et al., 2010; Elshaafi and Gudmundsson, 2016). The Al Haruj Volcanic Province consists of two distinct volcanic systems: Al Haruj al Aswad in the north covers an area of 34,200 km^2 while Al Haruj Al Abyad in the south covers area 7,850 km^2 (Elshaafi and Gudmundsson, 2017). The greatest number of volcanic eruptions, the greatest density, is concentrated in two areas in the AHVP. We suggest that each of these density peaks or volcanic systems was and possibly still is supplied with magma from an individual magma reservoir beneath the system (Elshaafi and Gudmundsson, 2017). The AHVP primarily made of alkaline to transitional basalts as well as subordinate sub-alkaline, whereas more differentiated volcanic rocks are not observed (Busrewil and Suwesi, 1993; Peregi et al., 2003; Less et al., 2006; Al-Hafdth and Elshaafi, 2015).

8.3.4 Nuqay Volcanic Province (NVP) (Middle Miocene to Pleistocene)

This volcanic province has been affected by two main volcanic events or episodes (Radivojević et al., 2015). The first event occurred from the middle Miocene up to the Pliocene and produced mainly alkaline to sub-alkaline basaltic rocks (transitional). The second event extends from late Pliocene up through Pleistocene and produced basanite spatter to scoria pyroclastic cones and subsidiary flow-lobes lava flow (Radivojević et al., 2015) that are

apparently consistent with age and composition of the main volcanic phases of the Haruj Volcanic Province (AHVP). The NVP covers area around 11,655 km^2 and is considered the second largest volcanic province in Libya. The modern age dating for the main volcanic provinces in Libya during the last years by Nixon et al. (2011), Bardintzeff et al. (2012), Staurt et al. (2014) and Radivojević et al. (2015) suggest that the volcanic activity for these volcanic provinces may have occurred over same period of time rather than, as previous thought, gradually decreasing in age from northwest to southeast.

8.3.5 Geodynamic framework

Many different models have been suggested for the geodynamic framework of the Libyan volcanism. Some authors suggest that the Neogene - Quaternary volcanism of Libya was related to the passage of the African plate over a fixed asthenosphere hotspot or plume (e.g., Hegazi, 1999). This is currently not regarded as a very plausible model because the time-related migration of volcanic provinces does not fit well with the movement of the African plate (Farahat et al., 2006; Mohammed, 2014; Radivojević et al., 2015). By contrast, Almond et al. (1974) suggest that intra-continental volcanism of Libya was most likely the result of North Africa being situated on a fracture zone extending from Cameroon through Chad with a prolongation traced from Tibesti to Nuqay and the trending northwest the Al Haruj and Gharyan volcanic provinces. Similarly, Bardintzeff et al. (2012) propose that Libyan volcanism may be caused by reactivation of pre-existing regional basement faults associated with lithospheric extension and asthenospheric upwelling as a result of tectonic interaction between the African and European plates.

Tomographic results of Lie´geois et al. (2005) do not support the existence of a mantle plume or plumes beneath Libyan volcanic provinces. Their model

proposes that the shallow mantle is warmer, with primitive magma or melt at depths of 80 to 150 km below Libyan volcanic provinces. Farahat et al. (2006) suggest that the Libyan volcanic rifts are most likely related to the large Afro-Arabian rift system that extends from Turkey to Mozambique. This rift system is thought to have developed episodically rather than continuously. Radiometric age dating results of the eastern rift in Kenya are generally occurred with ages of Libyan volcanic activity that extends from Miocene up to Holocene time. Therefore, the Libya's volcanism is usually though to be related to tectonic processes rather than a mantle plume (Peregi et al., 2003; Less et al., 2006; Bardintzeff et al., 2012).

Mantle-plume models have also been proposed for the volcanism in Libya. One such model, Nixon et al. (2011) suggest that the primitive magma of the Al Haruj province originated at depths of 70 for tholeiite and 74 km for alkali basalts, and that fractional crystallisation occurred at depths of 25-39 km and temperatures between 1215^{o}C and 1360^{o}C. Also they propose that the North African Tertiary volcanisms can be explained by diapiric upwellings or hot fingers originating in the upper mantle. Hence, the origin of volcanisms in Libya and North Africa at large scale is clearly ambiguous and still under debate. Nevertheless, the petrographic and geochemical similarity between various basaltic rocks from the four volcanic provinces and little or no evidence on crustal contamination (e.g., Stuart et al., 2014) indicate that most of the basaltic rocks derived from common parental sources with different degree of partial melting.

8.4 Spatial density of volcanic eruptions: methods and results

The spatial distributions of volcanic eruptions or monogenetic volcanoes within the principal volcanic provinces in Libya were examined and are presented on a volcano-density map (Fig. 8.4). We used the published

geological maps created by Industrial Research Centre (IRC), Tripoli, from the 1980s until 2006 as part of the programme of regional mapping of whole Libya of 1: 250,000 scale. These studies use tonal variations on Landsat images together with aerial photographs of different scales as well as field observations to identify different types of volcanic shapes and features. Therefore these geological maps are considered the most recent and accurate studies on the Libyan territory.

ArcGIS 10.1 (www.esri.com) was used to georeference raster images of the geological maps of these volcanic provinces as a guide to plot the craters of these volcanoes. A volcano-density map is defined as the frequency of eruption sites or centres that fall within the neighbourhood of each raster cell. A neighbourhood is defined as an area around each cell centre. The total or cumulative number of eruptive sites or centres is then divided by the area of the neighbourhood to obtain the density. The spatial density map was drawn by ArcGIS used a search radius of 35 km to produce a more generalised output raster. The 35 km search radius (corresponding roughly to the crustal thickness) was used for the creation of the density map (Lesti et al., 2008). The main vents, that is, the eruption centres or sites, are lava shields, scoria cones, spatter cones, and maars. We identified 432 volcanic monogenetic eruption sites (including scoria cones, spatter cones, lava shields and few maars) in the Al Haruj Volcanic Province. Of these, 55 are lava shields, 8 are maars, and 369 spatter and scoria cones. For other volcanic provinces the eruption sites are mapped as vents or volcanic craters rather than grouped into the specific types above. The total number monogenetic eruption sites in the six volcanic systems is 831 where 432 in the AHVP, 180 in NVP, 116 in SVP and 103 in GVP.

The volcanic eruptions are obviously clustered throughout a substantial part of Libya (Fig. 8.4). The density map, however, show that six main volcanic clusters have been identified in this study. Interestingly, the Al Haruj and

Nuqay volcanic provinces have double density peaks, that is, each is composed of two subzones or subareas. The middle area or boundary between two subzones has the lowest eruption density that most likely represents the boundary or barrier between separate volcanic systems (cf. Andrew and Gudmundsson, 2007; Elshaafi and Gudmundsson, 2017). By contrast, Gharyan and Sawda volcanic provinces have a single density peak, that is, a single volcanic system. Cluster of volcanoes are primary WNW–ESE trending, roughly coinciding with the general trend of the main crustal fractures zone in the area (Fig. 8.4). The crustal thickness may be variable along the zone of volcanism in Libya, as defined by the trend of the four volcanic provinces. Each volcanic system is thought to be supplied with magma from a source reservoir which mainly draws magma from a limited region where the crustal thickness attains a relative minimum (cf. Gudmundsson, 2016). The regions of local minimum crustal thickness, that is, the reservoirs strongly correlate with the elevated basement areas.

Because of their double-peak density distributions, the Al Haruj and Nuqay volcanic provinces may be subdivided into two distinct volcanic systems where each system has specific magma reservoir. The basalts from various volcanic provinces exhibit broad similarities; only minor geochemical differences are recognised (Peregi et al., 2003; Less et al., 2006; Al-Hafdh and Jafeer, 2014; Stuart et al., 2014; Radivojević et al., 2015), suggesting that the composition of the source reservoirs are also similar. There are no available geophysical data as to the depths of the reservoirs. As indicated above, Nixon et al. (2011) suggest that fractional crystallisation of the primitive magma for the Al Haruj volcanic province occurred at depths of 25-39 km and temperatures of 1215-1360^{o}C. Therefore, a layer at approximately this depth probably represents the transition zone between the lowermost crust and upper mantle and may correspond to the location of the reservoirs as a part of perhaps a larger and more general ‘magma layer’ as in Iceland (Hermance, 1981; Schmeling, 1985; Gudmundsson, 1987).

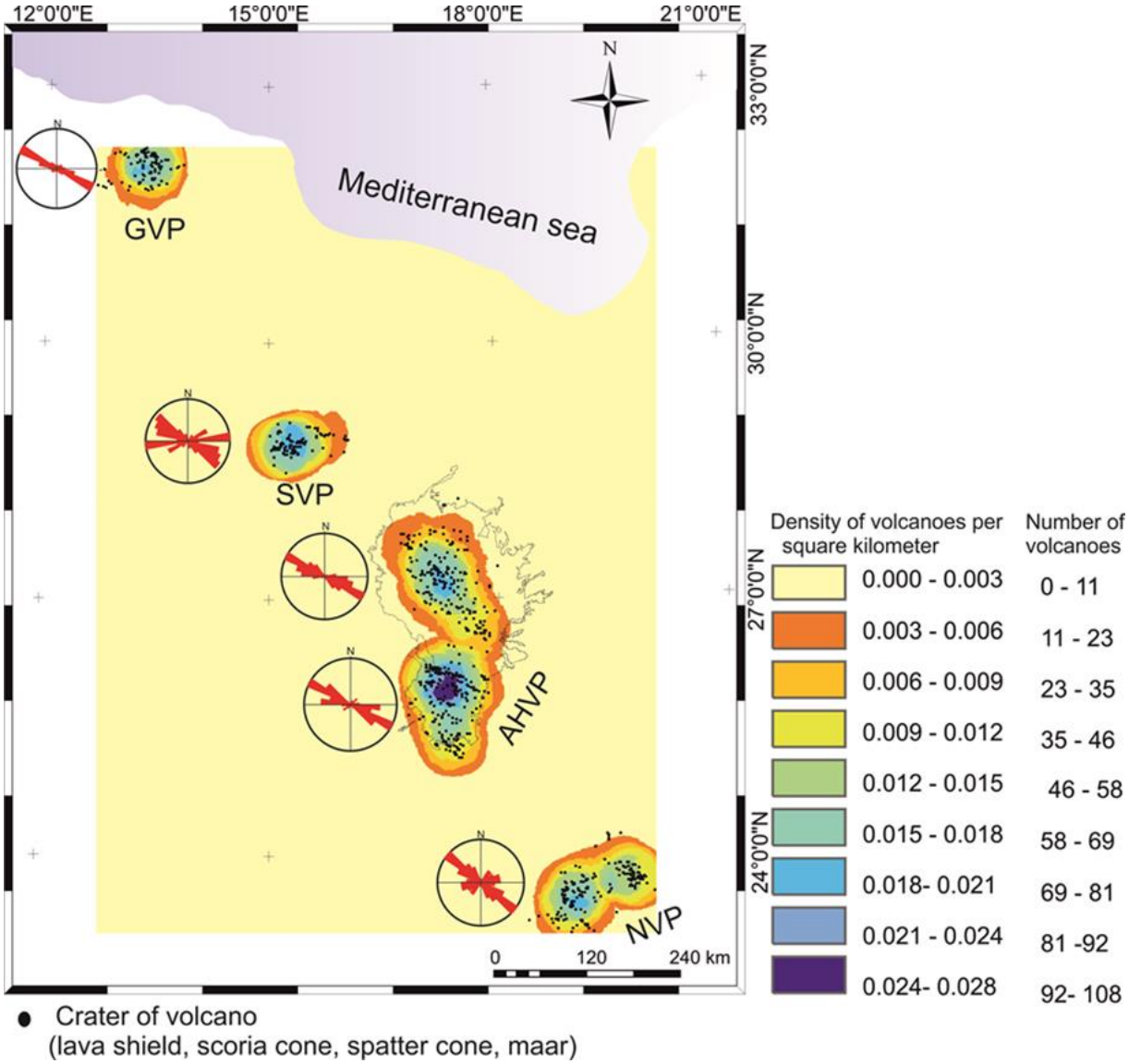

Figure 8.4. Volcano density map on the Libyan territory was created by using ArcGIS10.1, a circular neighbourhood with a given radius 35 km. Both of the Al Haruj (AHVP) and Nuqay (NVP) Volcanic Provinces may be subdivided into two volcanic systems based on the maxima clustering of volcanic craters. Whereas the Gharyan (GVP) and Sawda (SVP) Volcanic Provinces have only single maxima volcanic craters. Spatial alignments of volcanoes are plotted in rose diagrams.

Because of lack of data on the depth of magma reservoirs in the other volcanic provinces, during this study we assume the magma reservoirs for all four volcanic provinces occurred at around 35 km and that this depth corresponds roughly to the crust-mantle boundary in central Libya (Ghanoush et al., 2014). It follows that, in the present model, the volcanism

in all the four provinces was supplied with magma directly from reservoirs in the lower crust or at the crust-mantle boundary rather than through shallow magma chambers. The model is supported by seismic and geochemical evidence for any shallow magma chambers beneath the volcanic provinces.

8.5 Modelling

All the models here are numerical and used the finite element method. The finite-element method (FEM) represents the most common technique for solving differential and partial differential equations (Henk et al., 2013). Numerical models based on the finite-element method are easily used to provide quantitative information on the local stresses around magma reservoirs, such as those of interest here. These stress fields, in turn, greatly improve our understanding of the volcanotectonics in the region because in situ stress fields, partly determined by concentration of stresses around thereservoirs, largely control fault slip and dyke emplacement, hence of seismicity and volcanism, in the zone hosting the volcanic provinces. Comsol Multiphysics (5.1) is the finite element program used for the work described in this paper. It is commercial large-scale multipurpose finite element software (www.comsol.com).

We made several two-dimensional (2-D) and three-dimensional (3-D) numerical models in order to explore the potential mechanical interaction between the six volcanic systems. To simplify our models we modelled the Earth's crust as a homogenous and isotropic layer with a Young's modulus of 40 MPa, corresponding to the average Young's modulus of the crust in central Libya (Elshaafi and Gudmundsson, 2017) and a Poisson's ratio of 0.25, as is typical of most solid rocks (Gudmundsson, 2006, 2016). In the 2-D models, the magma reservoirs were modelled as circular holes with magmatic excess pressure of 5 MPa at a crustal depth of 35 km

corresponding to the crust-mantle boundary, the depth of the reservoir inferred and discussed above. In the 3-D models, the reservoirs are modelled as oblate ellipsoids (penny shaped or sill-like) with a thickness of 2 km. All the reservoirs in all the models have a diameter of 66 km, using the sizes of the volcanic systems inferred by tracing the crudely defined boundary of the systems from the density maps of volcanic or eruption sites (Fig. 8.5).

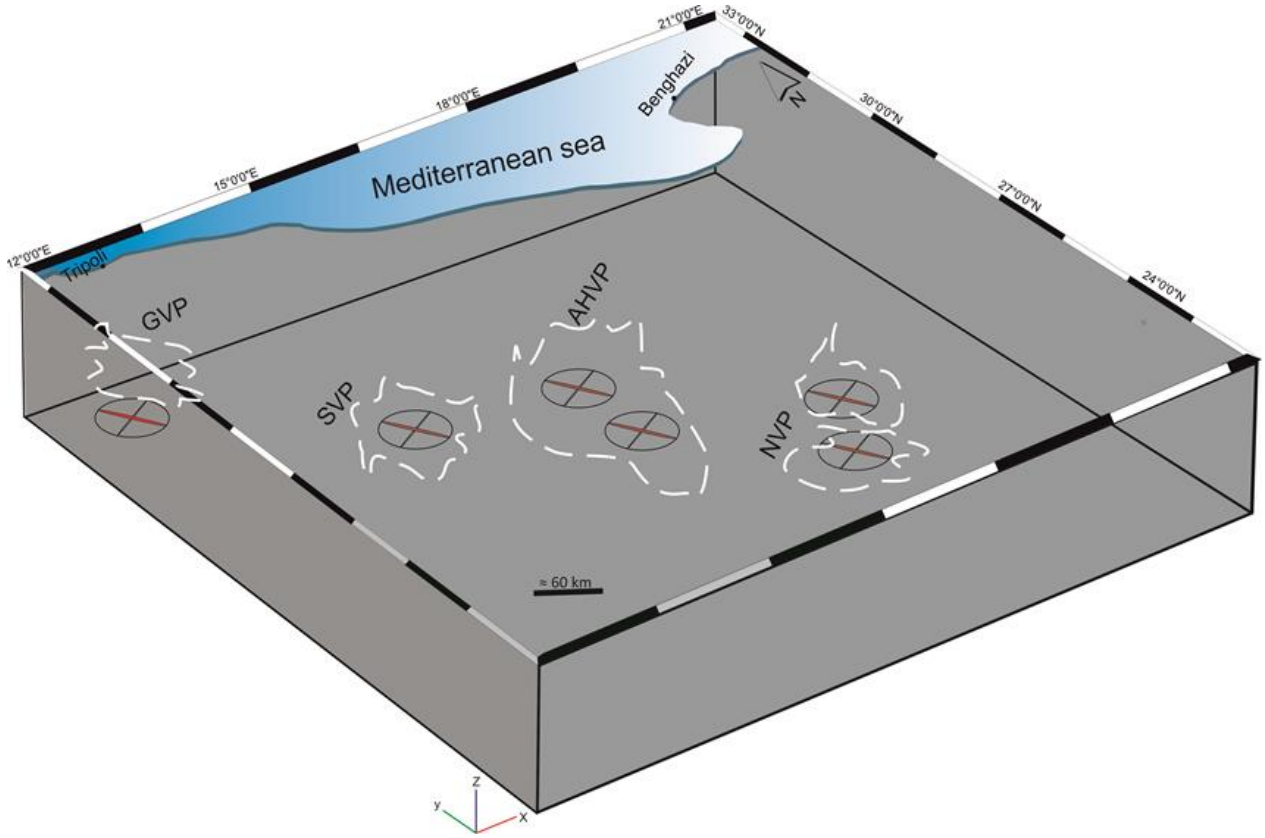

Figure 8.5. Volcanic systems in Libya shown here as six roughly circular areas at the surface of a crustal block where both AHVP and NVP have double magma reservoirs while the GVP and SVP have only a single magma reservoir. The magma reservoir for each volcanic system can be approximated as oblate ellipsoid or, in geological terms, sill-like. They are here assumed circular in plan-view, so that the length and width are equal, namely 66 km. Each magma reservoir has an amplitude or thickness (vertical dimension) of 2 km as indicated by the red colour. The scale is approximately correct for reservoir lateral dimensions but thicknesses of the reservoirs and the crustal are exaggerated several times. This geometry is used as a basis for the 2-D and 3-D numerical models presented in Figs. 8.7 and 8.8. The dashed white lines represent the boundary of the volcanic province at the Earth's surface.

The size of the reservoir associated with the Al Haruj al Aswad volcanic system (northern part of the AHVP) (Fig. 8.4) may be somewhat larger, but generally the reservoir size should reflect the size of the associated system which, in turn, should correspond to the general distribution of eruption sites at the surface. As a rule, the larger the reservoir in relation to the distance between them, then, for a given loading, the larger will be the mechanical or stress interaction. We think, however, that in this case the estimated sizes of the reservoirs are very reasonable.

The regional loading on the reservoirs is extensional rifting of 5 MPa, that is, external tensile stress of this magnitude. The direction of loading, that is, the extension vector, is oriented NE–SW (Fig. 8.6), as follows from the orientation of grabens and normal faults in central Libya, particularly in and associated with the Sirt Basin (Fig. 1), and is also in agreement with general field and remote data (Peregi et al., 2003; Less et al., 2006). The regional tensile loading parallel with the extension vector is chosen as 5 MPa so as to be in agreement with the commonly measured maximum in situ tensile strength (T_o) of rock (Gudmundsson and Brenner, 2003; Gudmundsson, 20016, Elshaafi and Gudmundsson, 2017). The tensile stress at the surface cannot exceed the maximum in situ tensile strength, and is thus generally less than 6 MPa (Gudmundsson et al., 2007). The tensile stress is often relative at depths exceeding about one kilometre, that is, is not negative but rather reduces the compressive stress at that depth (Gudmundsson, 2006). At the contact of a fluid-filled body, such as a totally molten top of a magma reservoir, then, for certain loadings, the tensile stress becomes negative, that is, is absolute. All models were fastened at the corners to avoid any rotation and/or displacement (Fig. 8.7). The numerical model images presented here show snapshots of the magnitudes of the maximum principal tensile σ_3 and shear τ stresses that occur as coloured contours and trajectories of maximum compressive principal stress σ_1 occurs as arrows (Fig. 8.7).

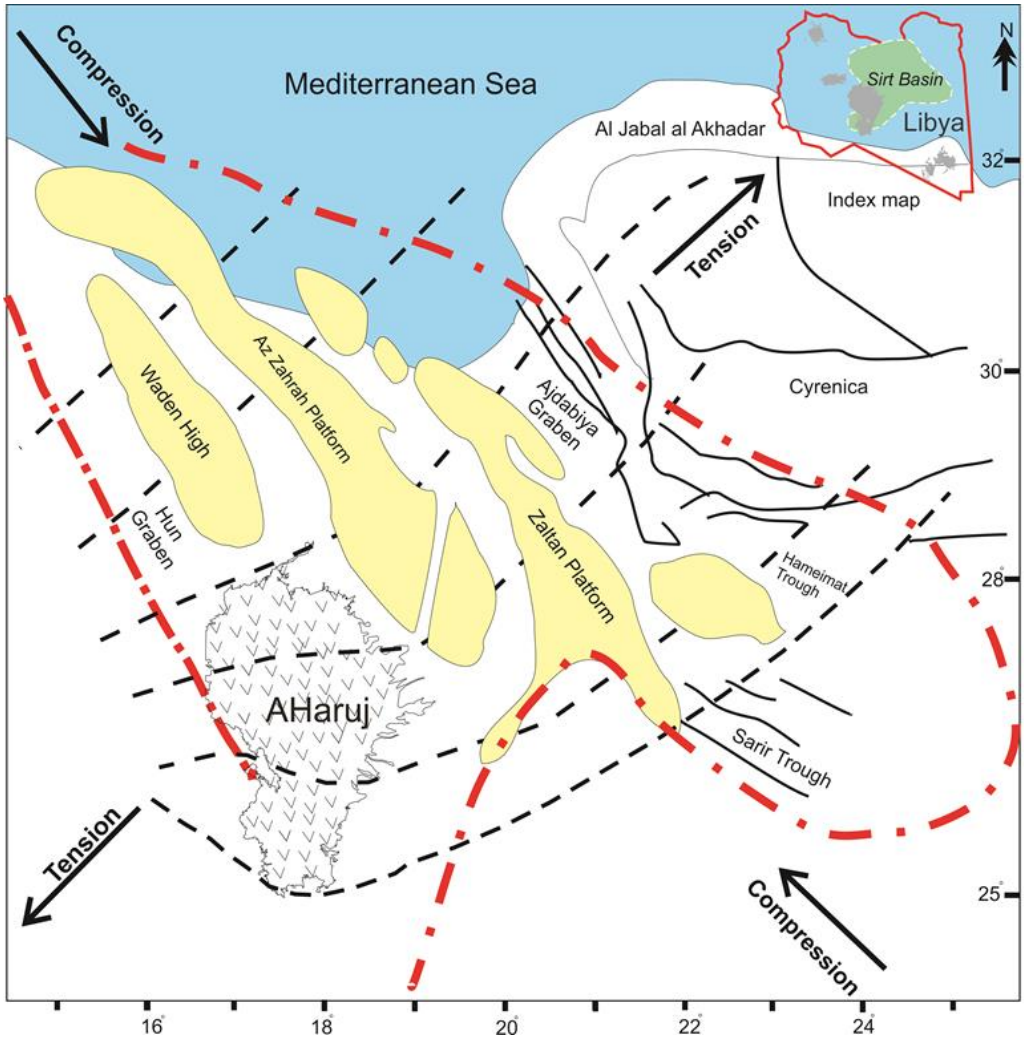

Figure 8.6. Map showing the main structural elements of the central part of Libya trend generally NW–SE. Dashed black lines indicate trajectories of the maximum tensile stress in NE–SW direction (modified after Anketell, 1996; Less et al., 2006).

8.6 Mechanical interaction between magma reservoirs

Mechanically, the magma reservoir beneath each volcanic system may be modelled as an elastic inclusion where there is an abrupt contrast in elastic properties between magma reservoir and the crustal host rocks (Andrew and Gudmundsson, 2007). Young's modulus or stiffness is the primary constant used to measure difference in elastic properties between the matrix (here the

host rock) and the inclusion (here the magma reservoir) (Savin, 1961; Nemat-Nasser and Hori, 1999; Jaeger et al., 2007).

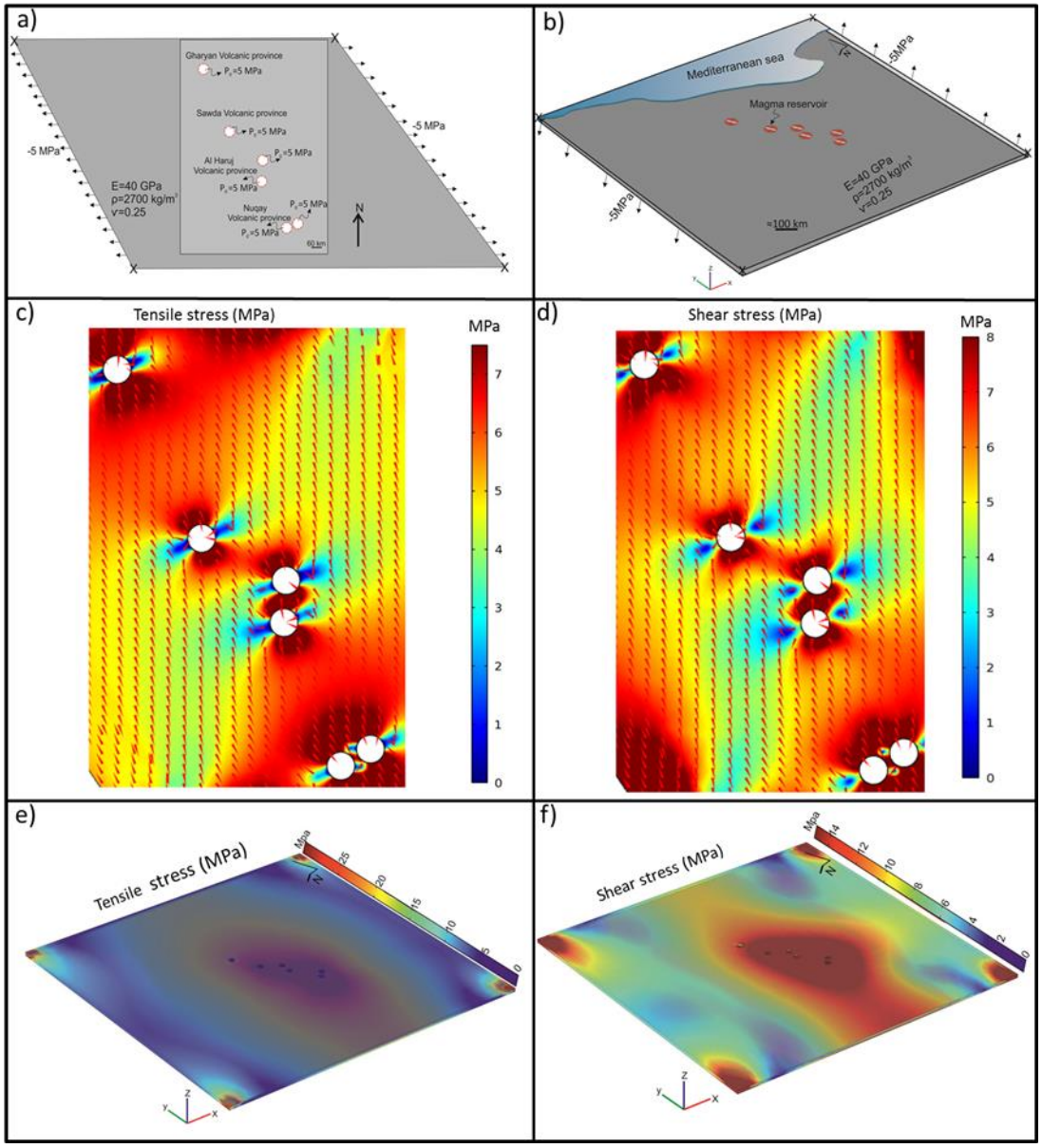

Figure 8.7. a) 2-D model setup showing the locations of magma reservoirs modelled as hole with diameter 66 km. b) 3-D model setup showing the locations of magma reservoirs modelled as oblate ellipsoids, that is, as penny-shaped or sill-like with a diameter of 66 km and thickness of 2 km. The magma reservoirs are given an excess magmatic pressure of 5 MPa. The direction of tension applied to models and indicated by the arrows with 5 MPa. Both the 2-D and the 3-D models assume a homogenous and isotropic crustal segment with a density of 2700 kg/m^3, a Poisson's ratio of 0.25, and a Young's modulus of 40 GPa. c) and d) 2-D numerical model results for tensile σ_3 and shear τ stresses in mega-pascals. High tensile σ_3 and shear τ stresses clearly occur around each individual magma reservoir. There are

also apparently stress concentration zones between nearby volcanic systems and thus likely mechanical interaction between volcanic systems. Red cones indicate the directions (trajectories) of the maximum compressive principal stress σ_1. These generally coincide with the overall directions of the stress-concentration zones, thereby indicating likely dyke (and volcanic fissure) and normal fault strikes. e) and f) 3-D numerical model results for the principal tensile stress σ_3 and the shear stress τ. The potential zones for mechanical/stress interactions between nearby volcanic systems remain basically similar to those yielded by the 2-D model results in c) and d).

The inclusion, the magma reservoir, may be softer or stiffer than its matrix, the host rock. During this study we assume the magma reservoir was totally molten, so that its Young's modulus is zero and the inclusion reduces to a hole, when modelled as a two-dimensional structure, and as a cavity, when modelled as a three-dimensional structure (Andrew and Gudmundsson, 2008). By contrast, when a magma reservoir is totally solidified it forms a pluton which is generally stiffer, that is, with a higher Young's modulus, than surrounding host rock. It follows that fossil magma chambers and reservoirs, that is, plutons, can and commonly do act as elastic inclusions that modify the associated stress fields. Cavities and inclusions in an elastic body result in stress concentrations and thus change the local stress field. If the cavities/inclusions are comparatively (in relation to their sizes) close to each other, then the entire regional stress field in the area may be modified so as to encourage mechanical interaction between reservoirs/chambers and associated volcanic systems (Gudmundsson et al., 2007).

The main volcanic provinces are clearly arranged NW–SE with various distance between nearby provinces and their volcanic systems. The average distance between GVP and SVP is around 379 km while the average distance between SVP and Al Haruj al Aswad volcanic system (northern part of AHVP) is around 106 km. The average distance between Al Haruj al Abyad (the southern part of AHVP) and Nuqay volcanic province (NVP) is around 214 km (Fig. 8.4). All the reservoirs were modelled as either circular holes (2-D) or as oblate ellipsoids or penny-shaped (3-D), that is, essentially

as thin sills with lateral dimensions, diameters, of 66 km, as inferred from the density maps, and (for the 3-D models) thicknesses of 2 km. However, we also made models to with different diameters for the reservoirs. For example, modelling Al Haruj al Aswad as with nearly a double diameter of around 120 km and Al Haruj Al Abyad as with a diameter of 80 km, the rest of the reservoirs being of diameter 66 km. The stress magnitudes were greater for the larger reservoirs, but the geometries of the stress-concentration zones, hence the potential zones for mechanical interaction between systems, remained generally similar as when all the reservoirs had the standard 66 km diameter (Appendix B). The typical stress fields are presented in Fig. 8.7. The results show the magma reservoirs to be connected by zones of high tensile σ_3 and shear τ stresses.

The results also show that the stress fields generated between the magma reservoirs of the 2-D and 3-D models are basically similar. A simultaneous activity between nearby volcanic systems may have resulted in shared seismic swarms and dyke injections (Gudmundsson et al., 2008). The trajectories of maximum compressive stress σ_1 and zones of high tensile stress σ_3 are extremely useful to indicate potential sharing of dykes between volcanic systems and volcanoes in general, as well as indicating likely strike direction of tension fractures and normal faults. For the latter, zones of shear stress τ provide additional information as to the likely sites for the formation or rejuvenation of normal faults (Andrew and Gudmundsson, 2008). The results of models show that high tensile σ_3 and shear stress τ concentration zones connect the nearby reservoirs and associated volcanic systems. These stress zones generally coincide with dominating fracture trends (mostly normal faults) in the area. There is a clear mechanical interaction between northern part of the AHVP and SVP and between southern part of the AHVP and NVP (Fig. 8.7). But there is also a mechanical interaction between GVP and SVP, even though they are separated by a comparatively great distance.

As presented above, all the magma reservoirs are modelled as very soft inclusions, that is, as fluid holes. To take into account that the volcanism of SVP was significantly earlier than that in the other volcanic provinces we modelled the magma reservoir for this province as a stiff elastic inclusion (really a pluton), with a Young's modulus of 82 GPa (average stiffness of gabbro), and thus stiffer than surrounding host rock, at 40 GPa (Fig. 8.8a). The other magma reservoirs were again modelled as holes with excess pressure of 5 MPa (Fig. 8.8b, c). The results, however, in this model were not very different from results in that a mechanical or stress interaction is predicted by the zones of tensile σ_3 and shear stress τ between pluton of SVP and still active reservoirs of the nearby volcanic provinces (Fig. 8.8). The details of the stress fields/zones are of course different between the models in Figs. 8.7 and 8, as expected, but the results show that plutons nearby active magma reservoirs/chambers can have significant stress effects and encourage the generation of local stress fields that would not occur in the absence of the pluton. Thus the results show the importance of taking the rock heterogeneity, particularly the existence of large plutons, into account when modelling stress fields around active magma chambers/reservoirs.

8.7 Discussion

Libya, situated on the northern part of the Mediterranean foreland of the African shield, has encountered a significant intraplate tectonism, volcanism through its history, and currently has some seismicity indicating tectonic and possible intrusive activity (Suleiman and Doser, 1995). We present density maps of the spatial distributions of monogenetic volcanoes within the four principal volcanic provinces of Libya. The maps define six main volcanic clusters, each of which is here regarded as a volcanic system. The difference in number between systems and provinces is because the Al Haruj and Nuqay volcanic provinces may be subdivided, based on the density map, into

two distinct volcanic systems each. We propose that each volcanic system, in turn, was supplied with magma from a separate reservoir.

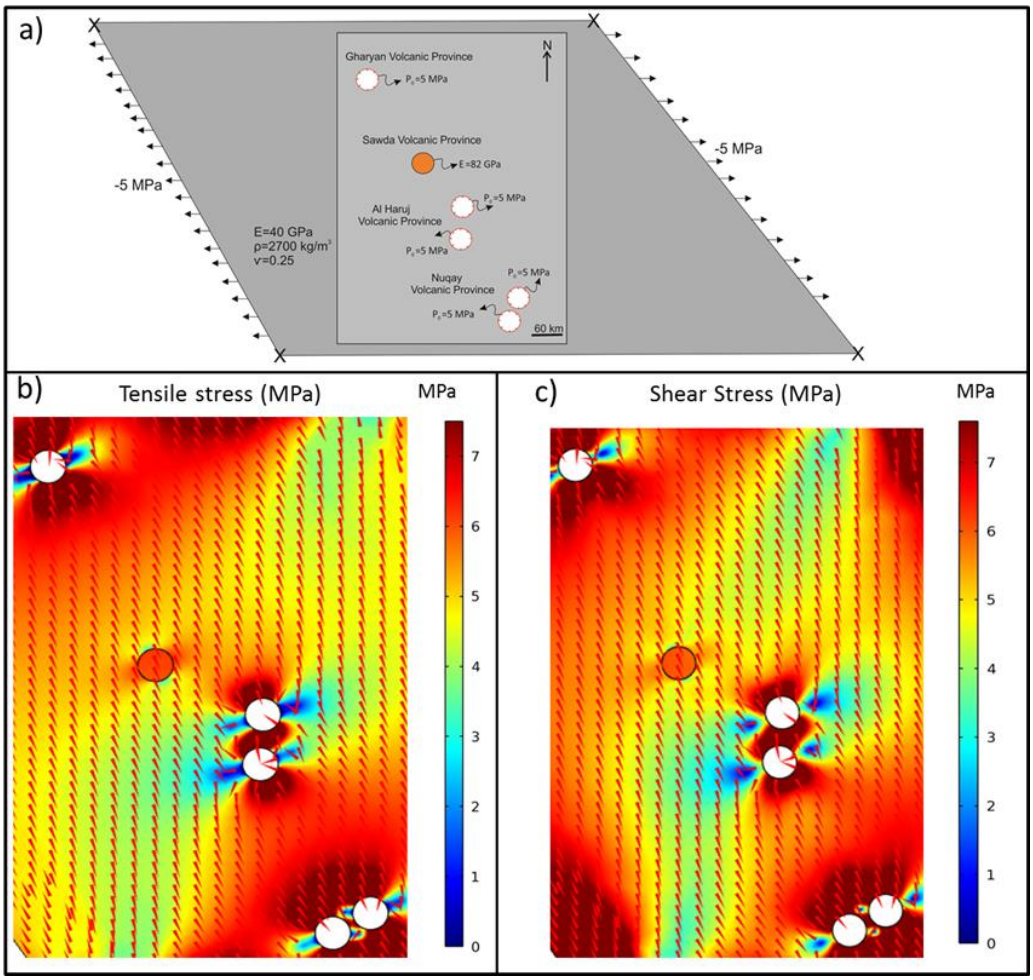

Figure 8.8. a) 2-D model setup is the same as that shown in Fig. 7a except the magma reservoir of the SVP modelled as much stiffer than surrounding host rock with a Young's modulus of 82 GPa. There are b) tensile σ_3 and c) shear τ stresses concentration zones between nearby volcanic system which indicate that the mechanical interactions should be possible. See text for more explanation.

The crustal thickness is likely to be variable along the main Libyan volcanic area. The magma reservoirs are then located at the regions of local minimum crustal thickness which, in turn, are strongly correlated to the current areas of elevated basement (Fig. 8.3). It is important to note that the extensive field studies in Iceland and seismological data in Hawaii indicate that the percentage of feeder-dykes is low (commonly as low as 10-20%) compared with arrested or deflected dykes at various level within the Earth's crust

(commonly 80-90%) due to abrupt contrasting mechanical properties at segments of the Earth's crust (Chastin and Main, 2003; Gudmundsson and Philipp, 2006). In addition, the magma reservoirs are long-lived fluid-filled structures and, for most of time, in lithostatic equilibrium with their host rocks.

One remarkable feature about the volcanism in Libya is that it is largely apparently 'off-rift'. That is, if the Sirt Basin is regarded as the main rift, then most of the volcanic provinces are at and just west of the southwest margin of the Sirt Basin. Off-rift volcanism is common worldwide and there have been many models proposed to explain it (e.g., Gudmundsson et al., 1996; Pinel and Jaupart, 2003; Gudmundsson, 2006; Maccaferri et al., 2014; Roman and Jaupart, 2014). There is, however, little evidence of volcanism in the Sirt Basin. It therefore follows that although the Sirt Basin is a rift structure – a major graben structure – it is not clear that it has any extensive magma reservoirs that could supply magma (through inclined dyke or sheet propagation) to the off-rift volcanism southwest of the rift. By contrast, the available evidence indicates – which is also one major conclusion of this paper that the volcanic provinces west of the Sirt Basin are fed essentially in vertical flow through dykes injected from sill-like, laterally extensive magma reservoirs located at the crust-mantle boundary and directly beneath the provinces. More specifically, we suggest that each of the six identified volcanic systems has an extensive magma reservoir which fed all the monogenetic volcanoes that constitute the systems.

The numerical models presented here show clear high tensile σ_3 and shear-stress (von Mises) τ concentration zones between all the volcanic systems. Mechanical interaction between them was, therefore, presumably considerable during the active times. There is a clear mechanical interaction between northern part of the AHVP and SVP and between southern part of the AHVP and NVP. But there is also a mechanical interaction between GVP and SVP, even though they are at great distance from each other. The stress

concentrations zones change their orientation and geometry slightly from the northwest to the southeast.

The stress-concentration zone and trajectories of maximum compressive stress σ_1 between southern part of AHVP and NVP trends NW–SE while the trend of stress concentration zone and trajectories of maximum compressive stress σ_1 between Al Haruj Al Abyad and Al Haruj Al Aswad is NNE–SSW. The tensile σ_3 and shear τ stresses between northern part of AHVP and SVP and the trajectories of maximum compressive stress σ_1 strike WNW–ESE then return in the stress concentration zone between GVP and NVP to NW–SE direction. The stress concentration zones among volcanic systems are obviously consistent with the strike of faults within the region. The directions of maximum principal compressive stress σ_1 and high tensile stress σ_3 can be used to infer likely dyke sharing between nearby volcanic systems whereas the trajectories of maximum principal compressive stress σ_1 and von Mises or shear stress τ can be used to indicate the formation or rejuvenation of shear fractures or seismogenic faulting (Andrew and Gudmundsson, 2008); in the present case, primarily normal faulting.

There is considerable observational evidence supporting the results of the numerical models. The more recent volcanic eruptions in Libya occur in the areas between the main volcanic systems. More specifically, in the Waw an Numus Volcano, situated in the area between northern part of NVP and southern part of the AHVP, and also the Holocene Al Mashaqaq lava flow, which erupted in the area between northernmost part of the AHVP and SVP (Fig. 8.9). In addition, the western part of the Sirt Basin is characterised by large swarms of tectonic fractures and numerous crater rows/volcanic fissures at the surface and a dense swarm of high angle normal faults at deeper crustal levels, these being recognized in seismic data (e.g., Abdunaser, McCaffrey, 2015). Thus the stress concentration zones due to

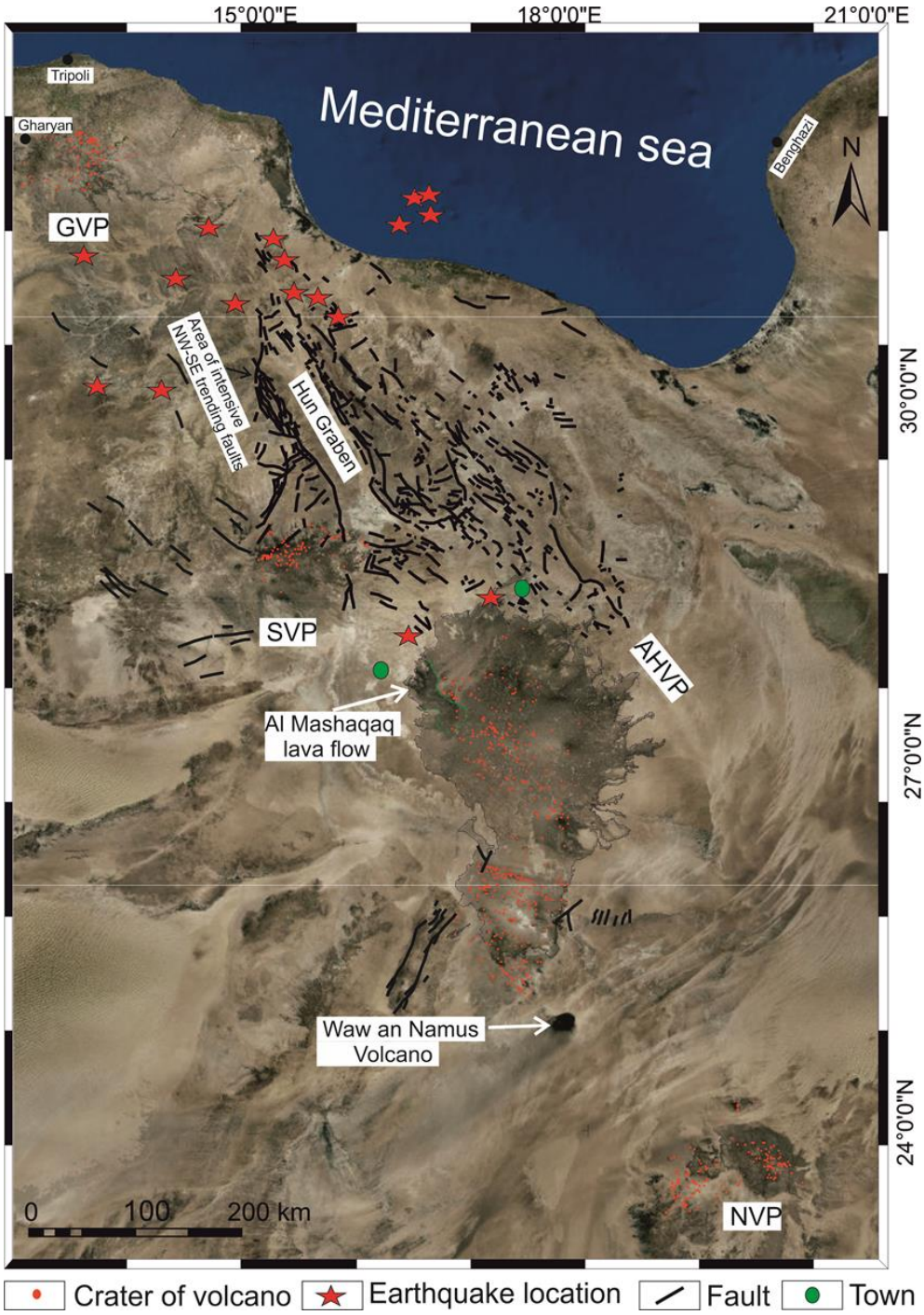

Figure 8.9. Satellite imagery, (adapted from Google Earth), showing the distribution of volcanic craters throughout Libyan territory and epicentres of earthquakes recorded in the past one hundred years as well as master and auxiliary faults around the Hun Graben area. Note the more recent volcanic eruptions (such as Waw an Namus and Holocene Al Mashaqaq lava flow, indicated by white arrow) and the earthquakes around the Hun Graben are clearly coincidence with stress concentration zones between the volcanic systems that inferred from numerical models (Figs. 7, 8). Locations of earthquakes are taken from Suleiman and Doser (1995) and faults from Abdunaser (2015).

mechanical interaction between magma reservoirs may partly contribute to generate these extension and shear fractures.

The alignment of volcanisms in Libya along the axis of the Palaeozoic Tripoli-Tibesti Uplift may relate to the mechanical interaction between the volcanic and contribute to a favourable orientation for the generation of stress-concentration zones. A series of high magnitude earthquakes have also been recorded along the margin of the NW–SE trending Hun Graben, western Sirt Basin, during historical time (Fig. 9). This recording includes one of the largest historical earthquakes recorded in Africa with magnitude 7.1 on 9th April 1935, showing that that this region is seismically quite active (Suleiman and Doser, 1995). By contrast the eastern part of the Sirt Basin is seismically less active, which may be partly due to the lack of volcanism in that part. Some of these earthquakes in the western part of the Sirt Basin have estimated focal depths at 21±3 km (Suleiman and Doser, 1995), which is comparatively close to the estimation depth of fractional crystallization and magma reservoir at the Al Haruj region (25-39 km) (Nixon et al., 2011).

The seismic swarm in the vicinity of Hun Graben area appears to be consistent with high shear concentration stress zone between GVP and SVP (Fig. 8.7c). In addition, the Gharyan area appears to be seismically active; a seismometer in the Gharyan region, southwest Tripoli, operated for six hours in 1977 and during this time recorded three moderate earthquakes (Kebeasy 1980; Suleiman and Doser, 1995). One problem seismicity studies in Libya in the past decades is the absence of seismic monitoring stations. The first Libyan seismological network has been installed only in 2005 (Al-Heety, 2013). So that the actual number of earthquakes in Libya and their location are poorly known. In addition, faults have not been sufficiently investigated to yield the certain information about recent activity needed to be able to predict earthquake occurrence in Libya (Hassen, 1983).

The inferred shear-stress zones due mechanical interaction between SVP and GVP may contribute to seismogenic faulting as is supported by the number of large earthquakes that have been documented along the margin of the NW–SE trending Hun Graben (Figs. 7c, 8.9). Although there are no evidence for eruptions in Libya during the historical time, many or perhaps all the volcanic systems may have been subject to one or more dyke injections during this period. It follows that the seismic events in Hun Graben area could be associated with dyke propagation, where the dyke eventually became arrested and thus did not erupt. More detailed geophysical studies and geodetic data in the future may help us to obtain a better constraint on Libyan tectonism and magmatism.

8.8 Conclusions

- This study focuses on the volcanism and tectonism of the four main volcanic provinces of Libya, using field data and numerical models.
- Six main monogenetic volcanic clusters are identified in this study. Each cluster is interpreted as a volcanic system supplied with magma from a separate magma reservoir. Each reservoir is thought to occupy a region of local and relative crustal-thickness minimum. These local minimum crustal thicknesses, and thus the inferred reservoirs, coincide with areas of elevated basement.
- Numerical models show strong stress interaction between the magma reservoirs. In particular, stress concentration zones and trajectories of maximum compressive stress σ_1 between nearby volcanic systems may encourage simultaneous volcanic and tectonic events, seismogenic faulting, and dyke sharing between volcanic systems.
- The modelled stress-concentration zones agree well with the distribution of the major tectonic features in this part of Libya.
- The numerical models show that the mechanical interaction decreases as the distance between nearby volcanic systems

increases. Thus, the great distance between GVP and SVP is presumable the main reason for comparatively little mechanical interaction between them compared with the much greater interaction between SVP and northern part of AHVP.

- Seismic events in Hun Graben (e.g., M7.1, on April/1935) area may have been related to dyke propagation that eventually became arrested and thus did not result in an eruption.
- If magma reservoirs are still active fluid-filled structures, they may pose a significant earthquakes and volcanic risk to the city of Gharyan (population >45.000), the towns of Zallah (population >8.000) and Al Fuqaha (population >6.000 population), as well as to many oil fields.

Acknowledgements

AE thanks the Libyan Ministry of Higher Education for the financial support. We thank John Browning and an anonymous reviewer for helpful comments.

References

Abadi, A, van Wees, J., van Dijk, P., Cloetingh, S., 2008. Tectonics and subsidence evolution of the Sirt Basin, Libya. AAPG Bulletin, 92, 993–1027.

Abdunaser, K., 2015. Satellite Imagery for Structural Geological Interpretation in Western Sirt Basin, Libya: Implication for Petroleum Exploration. Geosciences 2015, 5(1): 8-25DOI: 10.5923/j.geo.20150501.02.

Abdunaser, K., McCaffrey, K., 2015. Tectonic history and structural development of the Zallah-Dur al Abd Sub-Basin, western Sirt Basin, Libya. Journal of Structural Geology, 73, 33–48. http://dx.doi.org/10.1016/j.jsg.2015.02.006.

Al-Hafdh, N. Elshaafi, A., 2015. Geochemistry and Petrology of Basic Volcanic Rocks of Jabal Al Haruj Al-Aswad, Libya. International Journal of Geosciences, 6, 109-144.

Al-Hafdh, N., Gafeer, A. 2015. The petrology and geochemistry of Gharyan volcanic province of NW Libya. Journal of African Earth Sciences, 104, 71–102.

Al-Hafdh, N. Elshaafi, A., 2015. Geochemistry and Petrology of Basic Volcanic Rocks of Jabal Al Haruj Al-Aswad, Libya. International Journal of Geosciences, 6, 109-144.

Al-Kwatli, M., Gillot, P. Zeyen, H., Hildenbrand, A. Al Gharib, I., 2012. Volcano-tectonic evolution of the northern part of the Arabian plate in the light of new K–Ar ages and remote sensing: Harrat Ash Shaam volcanic province (Syria). Tectonophysics, 580, 192–207.

Almond, D., Busrewil, M., Wadsworth, W., 1974. The Gharian Tertiary volcanic province of Tripolatania, Libya. Geological Journal, 9, 8-17.

Andre, L., Klerky, J., Busrewil, M., 1991. Geochemical and Rb-Sr isotopic data on felsic rocks from the Jabal Awaynat alkaline intrusive complex (SE Libya). Third Symposium on the Geology of Libya, (eds. M.J. Salem and M.T Busrewil and A.M. Ben Ashour), Elsevier, Amsterdam, 7, 2511–2528.

Andrew, R., Gudmundsson, A., 2007. Distribution, structure, and formation of Holocene lava shields in Iceland. Journal of Volcanology and Geothermal Research. 168, 137–154.

Andrew, R., Gudmundsson, A., 2008. Volcanoes as elastic inclusions: Their effects on the propagation of dykes, volcanic fissures, and volcanic zones in Iceland. Journal of Volcanology and Geothermal Research, 177, 1045–1054.

Anketell, M., 1996. Structural history of the Sirt Basin and its relationship to the Sabratah Basin and Cyrenaican Platform, northern Libya, in M. J. Salem, M. T. Busrewil,A. A. Misallati, and M. A. Sola, eds., The geology of Libya.

Amelung, F., Jonsson, S., Zebker, H. Segall, P., 2000. Widespread uplift and “trapdoor” faulting in Galapagos volcanoes observed with radar interferometry. Nature, 407, 993-996.

Bardintzeff, J., Deniel, H. Guillou, B. Platevoet, P. Télouk, Oun, K., 2012. Miocene to recent alkaline volcanism between Al Haruj and Waw an Namous (southern Libya) Journal of African Earth Sciences,101, 1047–1063.

Biggs, J., Robertson, E., Cashman, K., 2016. The lateral extent of volcanic interactions during unrest and eruption. Nature Geoscience, 9, 308-311, doi: 10.1038/ngeo2658.

Boaz, N., 2009. Libya before the Sahara: The vanished world of the Eo-Sahabi Valley. Published by the International Institute for Human Evolutionary Research Integrative Centers for Science and Medicine 2565 Siskiyou Boulevard, Suite 4/1L Ashland, OR 97520, U.S.A. 1, 1–12.

Bosworth, W., Huchon, P., McClay, K., 2005. The Red Sea and Gulf of Aden basins. Journal of African Earth Sciences, 43, 334–378.

Busrewil, M., 2012. Evolution of Al Haruj Volcanic Province, Central Libya. Geology of Southern Libya, 2012, vol. 3. . In: 4th Sedimentary Basins of Libya Symposium: the Geology of Southern Libya, 17– 20th November 2008, Tripoli, Libya.

Busrewil, M., Wadsworth, W., 1980. Preliminary chemical data on the volcanic rocks of Al Haruj area, central Libya. In: The Geology of Libya (eds. M. J. Salem and M. T. Busrewil), London Academic Press, 3, 1077-1080.

Busrewil, M. Oun, K., 1991. Geochemistry of the Tertiary alkaline rocks of Jabal al Hasawinah, west central Libya. Third Symposium on the Geology of Libya, vol. 7 (eds. M.J. Salem and M.T. Busrewil and A.M. Ben Ashour), Elsevier, Amsterdam, 2587-2598.

Busrewil, M., Suwesi, S., 1993. Geological Map of Libya 1: 250.000, Sheet : Al Haruj Al Aswad NG(33-4). Explanatory Booklet. Industrial Research Centre, Tripoli, p. 95.

Chastin, S., Main, I., 2003. Statistical analysis of daily seismic event rate as a precursor to volcanic eruptions. Geophysical Research Letters, 30, DOI: 10.1029/2003GL016900

Chorowicz, J. Benissa, M., 2016. Remote sensing and field analysis of the Palaeozoic structural style inNW Libya: The Qarqaf arch a paleo-transfer fault zone between the Ghadamis and Murzuq basins. Journal of African Earth Sciences, 123, 272-293.

Cloetingh, S., Van Wees, J., 2005. Strength reversal in Europe's intraplate lithosphere: Transition from basin inversion to lithospheric folding: Geology, 33, 285–288.

Cvetkovic,´ V., Toljic´ , M., Ammar, N.A., Rundic´, L., Trish, K., 2010. Petrogenesis of the eastern part of the Al Haruj basalts (Libya). Journal of African Earth Sciences, 58, 37–50.

El – Makhrouf, A. 1988. Tectonic interpretation of Jabal Eghei area and its regional application to Tibesti orogenic belt, South Central Libya. Journal of African Earth Sciences, 7, 945–967.

Elshaafi, A., Gudmundsson, A., 2016. Volcano-tectonics of the Al Haruj Volcanic Province, Central Libya, Journal of Volcanology and Geothermal Research, 325.189–202.

Elshaafi, A., Gudmundsson, A., 2017. Distribution and size of lava shields on the Al Haruj al Aswad and the Al Haruj al Abyad Volcanic Systems, Central Libya. Journal of Volcanology and Geothermal Research, 228, 46-62.

Farahat, .S., Abdel Ghani, S., Aboazom, A., Asranc, A., 2006. Mineral chemistry of Al Haruj low-volcanicity rift basalts, Libya: implications for petrogenetic and geotectonic evolution. Journal of African Earth Sciences45, 198–212.

Ghanoush, H., Imber, J., McCaffrey, K., 2014. Cenozoic Subsidence and Lithospheric Stretching Deformation of the Ajdabiya Trough Area, Northeast Sirt Basin, Libya. AAPG 2014 Annual Convention and Exhibition, Houston, Texas.

Goudarzi, G., 1980. Structure – Libya. In : The Geology of Libya (eds.) Salem, M. J., and Busrewil, M. T., London Academic press, 3, 879–892.

Gudmundsson, A., 1987. Formation and mechanics of magma reservoirs in Iceland. Geophys. Geophysical Journal of the Royal Astronomical Society, 91, 27-41.

Gudmundsson, A., 2006. How local stresses control magma-chamber ruptures, dyke injections, and eruptions in composite volcanoes. Earth-Science Reviews 79, 1–31.

Gudmundsson, A., 2016. The mechanics of large volcanic eruptions. Earth-Science Reviews, 163, 73–92.

Gudmundsson, A., Bergerat, F., Angelier, J., 1996. Off-rift and rift-zone palaeostresses in Northwest Iceland. Tectonophysics, 255, 211-228.

Gudmundsson, A., Brenner, S., 2003. Loading of a seismic zone to failure deforms nearby volcanoes: a new earthquake precursor, Terra Nova, 15, 187–193.

Gudmundsson, A., Philipp, S., 2006. How local stress fields prevent volcanic eruptions. Journal of Volcanology and Geothermal Research, 158, 257–268.

Gudmundsson, A., Friese, N., Andrew, R., Philipp, S., Ertl, G. Letourneur, L., 2008. Effects of dyke emplacement and plate pull on mechanical interaction between volcanic systems and central Volcanoes in Iceland. In: Hoskuldsson, A., Sparks, R. S. J. & Thordarson, T (eds): Volcanic Processes: The Legacy of G.P.L. Walker (the “Walker Volume”). Geological Society London, Special Publications.

Guiraud, R., Mbaigane, D., Carretier, S., Dominguez, S., 2000. Evidence for a 6000 km length NW-SE-striking lineament in north Africa: the Tibesti Lineament. Journal of the Geological Society, 157, 99. 897–900.

Hallett, D., 2002. Petroleum geology of Libya. Elsevier, Amsterdam, p. 503.

Hasen, H., 1983. Seismicity of Libya and related problems. Master thesis. Civil Engineer Department, Colorado state University, p. 108.

Hegazy, H., 1999. Tertiary volcanics in Libya: evidence for the direction and rate of the African plate motion. Proceeding of the 4th International Conference on Geochemistry. Alexandria University, Egypt, 401–419.

Henk, A., Fischer, K., Kromuller, K., Wanger, D., Winter, I., 2013. Prediction of Tectonic Stresses and Fracture Networks with Geomechanical Reservoir Models. DGMK-Research Report 721. German Society for Petroleum and Coal Science and Technology. p. 216.

Hermance, J., 1981. Crustal gensis in Iceland; Geophysical constraints on crustal thickening with age, Geophysical Research Letters, 8, 203–206.

Jaeger, J., Cook, N., Zimmerman, R., 2007. Fundamentals of Rock Mechanics, fourth edition. Blackwell Publishing Ltd.. 515 pp.

Kebeasy, R., 1980. Seismicity and seismotectonics of Libya, in The Geology of Libya, 3, 955-963, eds Salem, M.J. & Busrewill, M.T., Academic Press, London.

Klitzsch, E., 1971. The structural development of parts of North Africa since Cambrian time. In: Gray, C. (Eds.). First symposium on the Geology of Libya. Fac. Science, Univ. Libya, Tripoli, 253–262.

Lemnifi, A., Elshaafi, A., Browning, J., El Ebadi, S., Gudmundsson, A., 2017. Crustal thickness beneath Libya and the origin of partial melt beneath AS Sawda Volcanic Province from receiver-function constraints. Submitted in Journal of Geophysical Research - Solid Earth.

Less, G., Turki, S., Suwesi, K., Peregi, L., Koloszar, L., Kalmar, J., Sherif, K., Csaszar, G., Gulasci, Z., Dalum, H., Al Tajuri, A., 2006. Explanatory Booklet. Geological Map of Libya 1: 250.000. Sheet: Waw Al Kabir NG 33- 12. Industrial Research Centre, p. 295.

Lesti, C., Giordano, G., Salvini, F., R. Cas R.,2008. Volcano tectonic setting of the intraplate, Pliocene-Holocene,Newer Volcanic Province (southeast Australia): Role of crustal fracture zones. Journal of Geophysical Research. 113, 1–11.

Lie´geois J., Benhallou A, Azzouni-Sekkal, A., Yahiaoui, R., Bonin, B., 2005. The Hoggar swell and volcanism: reactivation of the Precambrian Tuareg shield during Alpine convergence and West African Cenozoic volcanism. In: Foulger GR, Natland JH, Presnall DC, Anderson DL (eds) Plates, plumes, and paradigms. Geological Society of America Special paper, 388,379–400.

Maccaferri, F., Rivalta, E., Keir, D., Acocella, V., 2014. Off-rift volcanism in rift zones determined by crustal unloading. Nature Geoscience, 7, 297-300, doi:10.1038/ngeo2110

Stuart, F., Masoud, A., Mark, D., 2014. The origin of Cenozoic magmatism of Libya. Geophysical Research Abstracts, Vol. 16, EGU2014-15877.

Mouzughi, A., Taleb, T., 1981, Tectonic elements of Libya: Libya, National Oil Corporation, scale 1:2,000,000, 1 sheet.

Nemat-Nasser, S., Hori, M., 1999. Micromechanics: Overall Properties of Heterogeneous Materials. Elsevier, Amsterdam.

Nixon, S., Maclennan, J., White, N., 2011. Intra-plate magmatism of the Al Haruj Volcanic Field, Libya. Goldschmidt Conference Abstracts.

Peregi, Z., Less, G., Konrad, G., Fodor, L., Gulacsi, Z., Gyalog, L., Turki, S., Suwesi, S., Sherif, Kh., Dalub, H., 2003. Explanatory Booklet. Geological Map of Libya 1: 250.000. Sheet: Al Haruj Al Abyad NG 33-8. Industrial Research Centre, Tripoli, p. 248.

Pinel, V., Jaupart, C., 2003. Magma chamber behavior beneath a volcanic edifice. Journal of Geophysical Research, 108, doi: 10.1029/2002JB001751

Radivojević, M., Toljić, M., Turki, S., Bojić, Z., Šarić, K., Cvetković, V., 2015. Neogene to Quaternary basalts of the Jabal Eghei

(Nuqay) area (south Libya): Two distinct volcanic events or continuous volcanism with gradual shift in magma composition? Journal of Volcanology and Geothermal Research, 293, 57–74.

Roman, A., Jaupart, C., 2014. The impact of a volcanic edifice on intrusive and eruptive activity. Earth and Planetary Science Letters, 408, 1-8.

Rosenbaum, G., Lister, G., Duboz, C., 2002. Relative motions of Africa, Iberia and Europe during Alpine orogeny. Tectonophysics, 359, 117 – 129.

Savin, G., 1961. Stress Concentration A round Holes. Pergamon, New York.

Schmeling, H., 1985. Partial melt below Iceland: A combined interpretation of seismic and conductivity data, Journal of Geophysical Research, 90, 10, 105-10.

Suleiman, A., Doser, D., 1995. The seismicity, seismotectonics and earthquake hazards of Libya, with detailed analysis of the 1935 April 19, M=7.1 earthquake sequence. Geophysical Journal International,120, 312–322.

Vail, J., 1971. Dikes swarms and volcanic activity in Northeastern Africa. In : (ed.) Gray, C. Faculty of Science University of Libya, Tripoli. 341 – 347.

Wilson, M., Guiraud., R., 1998. Late Permian to Recent magmatic activity on the African-Arabian margin of Tethys, in D. S. Macgregor, R. T. J. Moody, and D. D. Clark-Lowes, eds., Petroleum geology of North Africa: Geological Society (London) Special Publication,132, 231–263.

Woller, F., Fediuk, F., 1980. Volcanic rocks of Gabal as Sawda. In: Salem, M. J., Busrewil, M. T. (eds.), The Geology of Libya, London Academic Press, 3, 1081 – 1093.

Woller, F., 1978. Geological Map of Libya 1: 250.000, Sheet; Al Washkah NH 33 – 15. Explanatory Booklet. Industrial Research Centre, Tripoli, p. 104.

Chapter 9: Central volcanoes and caldera collapses at the late Miocene – late Pleistocene Tibesti Volcanic Province, NW Chad

Abdelsalam Elshaafi and Agust Gudmundsson

Contribution statement:

The initial idea, data collections, methodology and creation of models were conducted by AE and support input from co-author

Analysis and interpretation of numerical results were done by AE and specifically support input from co-author.

Writing the initial draft was made by AE and later revising the manuscript for important intellectual content from co-author

Figures were prepared by AE.

Central volcanoes and caldera collapses at the late Miocene – late Pleistocene Tibesti Volcanic Province, NW Chad

Abdelsalam Elshaafi[1], Agust Gudmundsson[1]

[1]Department of Earth Sciences, Royal Holloway University of London, Egham TW20 0EX, UK (abdelsalamelshaafi@yahoo.co.uk; a.gudmundsson@rhul.ac.uk)

Abstract

The Tibesti Volcanic Province (TVP) represents the second largest among the five Gharyan – Tibesti volcanic provinces and covers an area around 29,000 km^2. The TVP, in the north-western part of Chad, shows considerable difference in terms of volcano-tectonic processes, eruptive style and production of volcanic materials from other four volcanic fields in Libya, although they are mostly contemporaneous from the late Miocene to Quaternary and may have derived from the common mantle source. The variations of volcanic products along the TVP range from contemporaneous basaltic to acidic, during the end of Miocene to late Pleistocene indicate that the magma in this volcanic field may be derived from a double magma source, in contrast to other most volcanic provinces in Libya. Field observations and numerical model results suggest that basaltic magma (scoria cones) at the periphery of the volcanic province may be derived from a deeper magma reservoir in the lower crust while the more evolved rhyolite and ignimbrites most likely are obtained from a shallow crustal magma chamber. The presence of a shallow magma chamber for an extended period of time (> 1Ma) has modified the in situ stress fields beneath this volcanic region and generated volcano-tectonic elements which may be superimposed on the pre-existing regional lineaments which define two preferential directions; a NW–SE and NE–SW. The evolution of the TVP is characterised by constructive episode (between 8 and 7–5 Ma), and then destructive episode (between 7-5 and 0.43 Ma) where the constructive (inflation process) period involves the accumulation of volcanic materials to

form central volcanisms, whereas destructive periods (deflation processes) involve vertical collapse calderas due to volcano-tectonic forcing and produced the large-volume volume of ignimbrites (>100 km^3). Here we present many numerical models with various loadings to understand better the volcano-tectonic evolution and spatial and temporal distribution of the major volcanic units. Our findings suggest that the stress fields associated with excess magmatic pressure or regional field stress as loading are favourable to form a volcano cone fed by radial dykes and inclined sheets and mostly associated with small-volume eruptions. While stress fields associated with the uplift doming at the lower crust owing to the accumulation of magma are favourable for initiation ring-faults at the surface or at shallow depth and emplacement of ring-dykes from lateral ends of existence shallow crustal magma chamber that subsequently led to subsidence block roof (piston-like caldera subsidence) to squeeze out much magma. In fact, some basaltic lava flows and mixing lava andesitic-trachyte are usually followed each an individual collapse caldera that may be derived from infrequently dykes from deeper magma reservoir or from the floor of the former magma chamber. These lavas are mainly recognised around rims of calderas that might be used the pre-existing ring-faults planes as conduits.

9.1 Introduction

The Tibesti Massif or the Tibesti Mountains is located in the central Sahara desert, mostly in north-western Chad and extend into north-eastern Niger and southern Libya which covers the area around 100,000 km^2 (Permenter and Oppenheimer 2007; Deniel et al., 2015) (Fig. 9.1a). It is a dome with elevations in excess 3,000 m above the sea level with late Miocene to late Pleistocene volcanic field in the southern half of the mountains which covers area around 29,000 km^2. The Tibesti Volcanic Province (TVP), at the north-western of Chad, is considered as the southernmost extension of the four main volcanic provinces in Libyan territory. They are organised from NW to SE as follows; Gharyan Volcanic Province (GVP) is located in the north-

western Tripoli, As Sawda Volcanic Province (SVP) is situated between GVP and the Al Haruj Volcanic Province (AHVP) at the central part of Libya, and Nuqay Volcanic Province (NVP) is located farther south close to Tibesti massif at the Libyan – Chadian border (Fig. 9.1a) (Bardintzeff et al., 2012; Elshaafi and Gudmundsson, 2016). Those five volcanic fields represent the Neogene – Quaternary outpouring volcanic activity which covering a total area exceeds 95,000 km^2 (Fig. 9.1a). There are great differences between the Tibesti Volcanic Province (TVP) and other volcanic provinces in regards to volcano-tectonic process, the eruptive style, and volume of volcanic materials although there are mostly contemporaneous at the end of Miocene and onward. The lava flows of Libya's volcanism are generally predominated by alkali to transitional basaltic rocks with a minor amount of phonolites and trachyte which are only associated with primary basaltic rocks at GVP and NVP (e.g., Staurt et al., 2014; Radivojević et al., 2015). While the surface of TVP is almost entirely made mostly of ignimbrites, trachyte, and basaltic lava flows along with minor recent andesitic-trachyte (Deniel et al., 2015).

Although the TVP is enormous and the second largest in size among the Tibesti – Gharyan volcanic provinces, very little is known about it due to a series of sporadic clashes and conflicts at Libyan – Chadian border, at Tibesti Massif, since 1979 to 1989 between Libyan and Chadian forces and remain extremely challenging and hazardous to ground-based access this region particularly during present-day. Therefore, most of the literature dates back to the early fifties and seventies, by Wacrenier et al. (1958); who established the first geological map. Subsequently, Vincent (1960, 1963, and 1970) has provided valuable data on the geology and structure of the Tibesti massif. Then, Malin (1977) mentioned from remote sensing data that Elysium Mons and the Martian volcanoes (e.g., Olympus Mons and the Tharsis Montes) are comparable the volcanoes within the Tibesti mountains (e.g., Emi Koussi) and he inferred that the sources of magma for these volcanic provinces are stationary relative with respect to the surface (Permenter and Oppenheimer 2007). Furthermore, the modern studies on this fascinating volcanic region are also still very few and sparse commonly by Guiraud et al.

(2000); Gourgaud and Vincent (2004); Permenter and Oppenheimer (2007); Deniel et al. (2015).

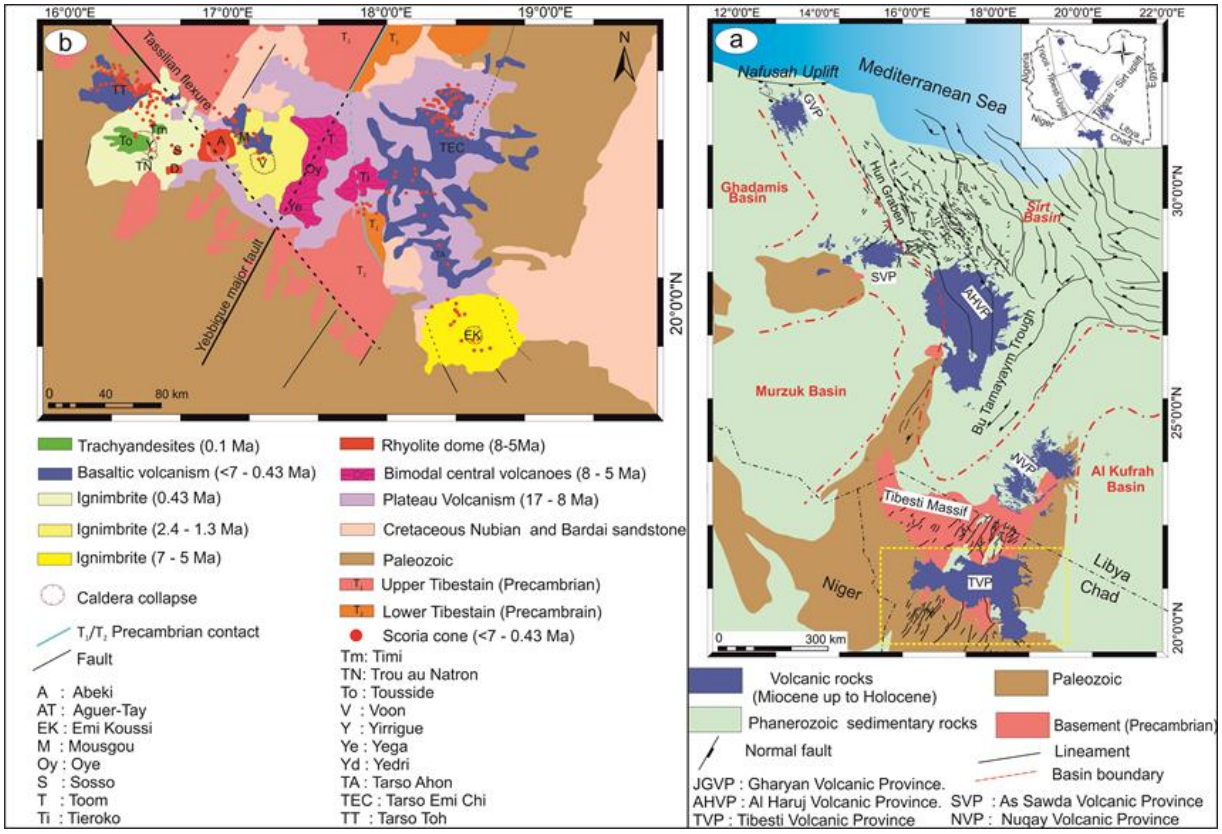

Figure 9.1. a) Simplified geological map showing the distribution of the main Tibesti – Gharyan volcanic provinces which are generally arranged NW-SE direction (modified from Abadi et al., 2008; Deniel et al., 2015). The inset map shows main orthogonal pre-existing structural trends based on Woller and Fediuck (1980). The dashed orange box shows the location of Fig. 9.1b. b) Volcanotectonic map of the Tibesti Volcanic Province showing the distribution of the five main volcanic units and tectonic framework. Three collapse calderas are indicated by yellow colours with associated large volume of ignimbrites (> 100km^3) that are aligned with an NW-SE linear trend. Three bimodal central volcanoes are marked by pink colour that are extended NE-SW trend along Yebbigue major fault. Scoria cones are indicated by red spots and mainly concentrated at the margin of province as well as around collapse calderas. The Precambrian rocks were divided into the Lower Tibestain (T1) and Upper Tibestain (T2) (modified from Permenter and Oppenheimer, 2007; Deniel et al., 2015).

In general terms, the five Tibesti – Gharyan volcanic provinces are spatially related to main two structural trends; early Palaeozoic structural elements of a prevalent NW–SE to NNW–SSE and late Palaeozoic to Mesozoic

structures (Hercynian Orogeny) with ENE–WSW trend (Fig. 9.1a) (Woller and Fediuk, 1980). These two orthogonal regional elements are likely to be inherited from the previous basement construction of those volcanic fields. These two preferential structural elements have played a significant role in the geological evolution of the North Africa (Woller and Fediuk, 1980). It is interesting to note that the basement beneath the main volcanic provinces in the North Africa is restricted to the overlap of ancient structural elements, and creating the boundaries of sedimentary basins (Fig. 9.1a). The Precambrian crystalline rocks are exposed in restricted and comparatively small areas in Libyan territory such as Jabal al Hasawinah, west of As Sawda volcanic field and inlier of Dur Quassah west of the Al Haruj Volcanic Provine while in a large area at Tibesti massif at Libyan – Chadian border (Fig. 9.1a). Therefore, it appears to be that the attenuation of the Earth's crust within these specific areas during the Proterozoic, Palaeozoic and Mesozoic period is one of the main contributions that encourage to the outflowing of principal volcanic provinces during the Neogene to Quaternary period (Busrewil and Oun, 1991; Goudarzi, 1980; El-Makhrouf, 1988; Less et al., 2006).

Vail (1971) suggests that the late Phanerozoic volcanic activities of the whole North Africa have occurred over a wide area and coincident with the outcrops of basement rocks. However, the major volcanic fields in the North Africa are strongly correlated to the current basement elevated areas. The basement highs seem to be reflected some form of subcrustal arching or swelling where magma might have preferentially penetrated, alternative this might be difficulty in piercing thick sedimentary sequence that may be acted as a crustal barrier between the main volcanic provinces (Vail, 1971, Elshaafi and Gudmundsson, 2017). The Tibesti –Gharyan volcanic provinces seem to be on a terrane boundary between Neoproterozoic high-grade metamorphic rocks to the east and Neoproterozoic-Palaeozoic low-grade rocks to the west (El-Makhrouf, 1988; Keppie et al., 2011). Schafer et al. (1980) suggest that this volcanism line trend NW–SE, is related to the Cretaceous boundary between the NW and SE African subplates which was reactivated during the

late Miocene due to the convergence between Africa and Europe (Bardintzeff et al ., 2012).

9.2 Geological and tectonic setting

The Neogene to Quaternary volcanic activity within the North Africa is extensive and reflected a change in the plate tectonic regime, most likely related to the changing stress fields and patterns of mantle convection (Cloetingh and VanWees, 2005; Abadi et. al., 2008), simultaneous with hot mantle plumes appear to be the main cause of the flood basalt volcanism (Wilson and Guiraud, 1998; Abadi et. al., 2008). Many models have been suggested for the geodynamic setting of the North Africa's volcanism as well as the origin of magma is still widely under debate and poorly understood. For instance, Bardintzeff et al. (2012) pointed out that these volcanisms caused by reactivation of pre-existing regional basement faults associated with lithospheric extension and asthenospheric upwelling as a result of the relative interaction of the African and European plates. While tomographic model of Lie´geois et al. (2005) does not support the existence mantle plumes beneath these volcanic provinces, this model assumed that the shallow mantle is warmer, prevailing the depth or primitive magma between 80 to 150 km beneath the region, which is consistent with the low He^3/He^4 isotope signature of Gharyan xenoliths supposing an origin of their common HIMU-FOZO component with the upper mantle.

By contrast, Burke (1996) suggests that the mantle plumes beneath the African plate at the upper mantle caused the doming or swelling due to the very slowly drifting African plate with related to hotspots or actually immobile during the last 35 Ma (Begg et al., 2009). Those volcanic fields appear to be corresponding to weakness and up-doming areas (Peregi et al., 2003; Permenter and Oppenheimer, 2007). Gourgaud and Vincent (2004) have been identified the presence mantle plume beneath the TVP from a

geochemical signature. Nixon et al. (2011) suggest that the North African Tertiary volcanisms can be explained by diapiric upwellings or warm fingers originating in the upper mantle. Keppie et al. (2011) propose conceptual model based on geophysical and geological constraints to depict the geometry of the super-plume or channel plume underlain the North Africa that can laterally feed geographically discrete volcanic fields analogous the Afar plume (cf. Ebinger and Sleep, 1998; Begg et al., 2009). This model has been suggested the Hoggar Massif, in Algeria, was fed by mafic basaltic magma from the Tibesti–Al Haruj plume that flowed westwards and then southwards into the Hoggar Massif and locations of volcanic fields are controlled by pre-existing regional faults.

However, the structural features, geological history and description of principal volcanic units on the TVP have recently been discussed in detail by Deniel et al. (2015). Accordingly, we present here a brief summarised of their key features, focusing in this paper on the aspects most relevant for local and regional stress fields that are favourable to form central volcanoes and collapse calderas and areal distribution of scoria basaltic cones. The basement rocks underlying the TVP were emplaced during the Late Precambrian (Pan-African orogeny), accompanied by intense deformation, shearing and metamorphism and subdivided into the Lower Tibestain (T_1) and Upper Tibestain (T_2) which are separated by unconformity or contact (Fig. 9.1b). The former basement unit is exposed in the eastern part and made up of high-grade metamorphic rocks while the latter basement unit consists of low-grade metasedimentary rocks (Deniel et al., 2015). It was followed by post-orogenic magmatism until the early Cambrian intruded by different types of granites and elucidated as the early manifestation of the Caledonian orogeny (Klitzch, 2000; Peregi et al., 2003, Deniel et al., 2015). The Caledonian orogeny was accompanied by the formation of the NW–SE trending for more than several hundred kilometres, long extensional structures, such as Tripoli – Tibesti Uplift that is subparallel to the Al Haruj Uplift and among others. The TVP is also influenced by perpendicular structures during the Hercynian orogeny (late Jurassic – early Cretaceous)

were superimposed over the earlier Pan-African system (Fig. 9.1a). The NE–SW striking Sirt – Tibesti uplift (Sirt Arch) has been formed during this period. The elevated Precambrian of central Sahara was actively eroded during most of the Palaeozoic and produced a large volume of clastic materials and subsequently largely formed the Palaeozoic hydrocarbon reservoirs in the Murzuq Basin, SW Libya (Peregi et al., 2003; Fig. 9.1a). Deniel et al. (2015) suggest that the volcano-tectonic in the TVP was influenced by two tensional lines, namely, the great NW–SE Tassilian flexure to the southwest and a major NE –NNE Yebbigue fault zone to the east (Fig. 9.1b). They are obviously more or less consistent with two orthogonal regional structures elements that were interpreted by Woller and Fediuk (1980).

9.2.1 Main volcanic units at the Tibesti Volcanic Province

In the Tibesti mountains, a large volume of late Miocene - late Pleistocene volcanic rocks (TVP) is exposed in the southern part and have been classified into five main volcanic units by Deniel et al. (2015), based on field relationships, volcanological, geochronological data and petrological studies, as follows; a) Plateau volcanism (17-8 Ma) consists of alkaline olivine basalts covering area around 29,000 km^2 associated with trachytic to phonolite plugs and this volcanic unit represents the oldest volcanic rocks in the TVP. This volcanic unit was contemporaneous with basaltic lavas of the As Sawda Volcanic Province (SVP), central Libya, which has been dated between 16 and 8 Ma (Ade-Hall et al. 1974; Woller and Fediuk 1980; Bardintzeff et al., 2012). The plateau volcanism on the TVP seems to be erupted episodically rather than continuous where it was interrupted by sedimentary deposits among layers of basaltic rocks. b) The second volcanic unit, it spreads toward central part of the province at the end of Miocene (between 8 and 5 Ma), forming four large compositionally bimodal volcanic centres, namely; Yega, Oye, Toom and Tieroko (Fig. 9.1b). Those central volcanoes are exposed over an area about 2.700 km^2 and form an eroded plateau. Each central volcano consists of two distinct stages. The first stage consists mainly

of basaltic lava created at the margins while the second stage consists of mainly rhyolites lava flow and formed at the core (Deniel et al., 2015). This volcanic unit was followed by c) third volcanic unit, multiple collapse calderas, which most likely associated with significant up-doming at the bottom of the crust led to collapse three major calderas respectively, and produced three large ignimbrites as much as 100 km^3, namely; Voon caldera (7–5 Ma), Emi Koussi caldera (2.4–1.33 Ma), and Yirrigue caldera (0.43 Ma) (Deniel et al., 2015). d) The recent basaltic volcanism resuming again after initial basaltic plateau (volcanic unit a) at 7–5 Ma which produced scoria pyroclastic cones and basaltic lavas. This fourth volcanic unit is apparently consistent with age and composition of the first volcanic phase at the Haruj Volcanic Province (AHVP) which has been dated between 7.9 Ma to 3.6 Ma (Less et al., 2006; Bardintzeff et al., 2012). Some of the basaltic lavas occurred along rims of calderas and interior of the calderas.

However, each major caldera-forming episode coincided with termination of rhyolite activity and the initiation of mafic volcanism around the rim of caldera and migration of the focus of further ignimbrite to other places of the Tibesti region due the local stress field associated around the old magma is not favourable to feed it from deeper magma reservoir so that the new magma chamber would be formed on either or both sides of the old magma chamber (Fig. 9.2). We will discuss this mechanism in more detail in the discussion section. e) Last volcanic unit on the TVP has been observed at a rim of Yirrigue caldera in the Tarso Tosside Volcanic Complex and produced andesitic-trachyte (100 ka). This volcanism as well as Tarso Tousside and Emi Koussi fumarole are considered as potentially volcanically active (www.volcano.si.edu) (Permenter and Oppenheimer, 2007). However, the present distribution of the main volcanic units on the TVP is given in Figure (9.1b), it is only a guideline to whole the volcanic province which involves delineation of different types of volcano-tectonic elements together with their assignment to the relevant volcanic events. Consequently, we will build up the present work according to this comprehensive and concise division was provided by Deniel et al. (2015).

Additionally, the main volcanic units were examined here in more detail using ArcGIS 10.1 and multi-source high-resolution remote sensing images, for instance, the satellite imagery available on Google Earth (2016) for the central Sahara desert. Digital elevation model (DEM) and data collected by the NASA Shutter Radar Topography Mission (SRTM) were also used. Google Earth imagery provides three-dimensional geospatial data through Keyhole Mark-up Language (KML). In the TVP, the images are detailed enough so as to provide high-resolution of about 0.5–2.5 m multispectral at nadir as well as considerably enhanced by extremely good preservation of volcanic features because the aridity of the region (Permenter and Oppenheimer, 2007; Abdunaser and McCaffrey, 2014; Elshaafi and Gudmundsson, 2016, 2017) and allow us to measure the geometry of volcanoes, azimuth, and thickness of inclined sheets and dykes. The present work confirms that high-resolution remote sensing is an effective and efficient complementary tool to traditional field measurements for volcanological

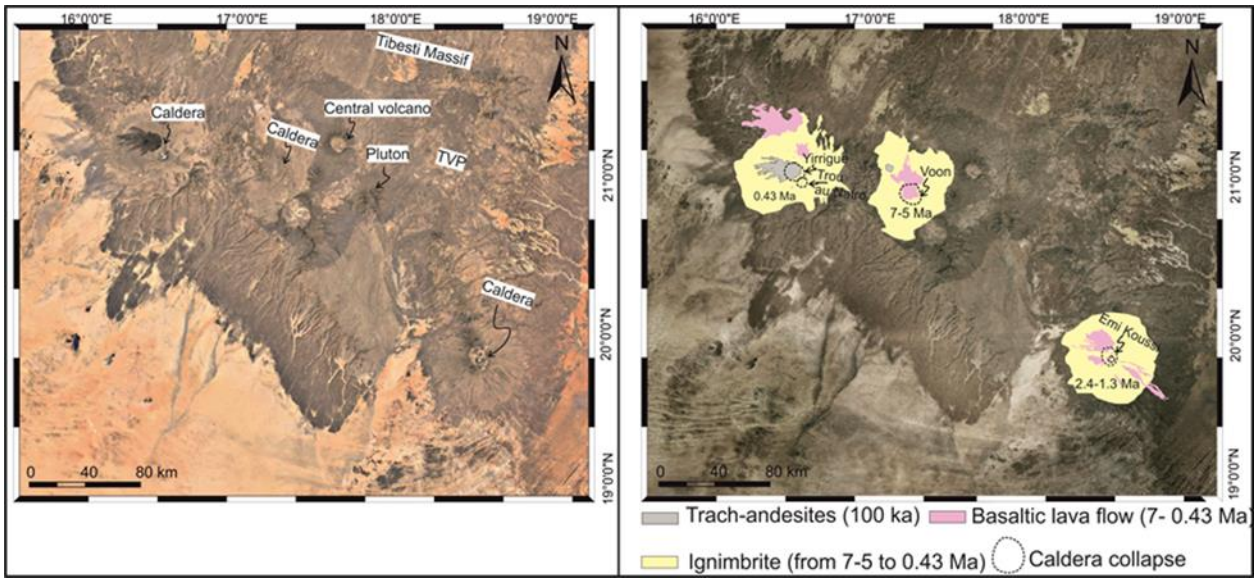

Figure 9.2. Satellite imagery (adapted from Google Earth) covers the TVP and shows the locations of three collapse calderas and central volcanoes (left image). Note each large ignimbrite eruption (indicated by yellow colour) was followed by the basaltic and andesitic-trachyte (indicated by pink and gray colours, respectively). Yellow colours represent the area covering by ignimbrite and have been estimated by ArcGIS 10.1 as follows: Yirrigue Caldera 3,223 km^2, Voon Caldera 2,777 km^2 and Voon Caldera 2,167 km^2.

examination in arid and remote and hazardous regions (cf. Drury, 2001; Rajesh, 2004; Permenter and Oppenheimer, 2007; Chen et al., 2014; Abdunaser and McCaffrey, 2014; Elshaafi and Gudmundsson, 2016) such the TVP. The geometry of each volcanic unit is defined by its length, width (diameters), area, volume and depth or thickness. ArcGlobe 10.1 was used to plot the scoria cones, then the shape files of scoria cones imported into ArcMap10.1 that were added to the map through georeferenced raster images of the geological maps of the TVP prepared by Permenter and Oppenheimer (2007); Deniel et al. (2015) as a baseline (Fig. 9.1a, b).

The main aim of this work is to provide a model to explain the formation of the central volcanoes (constructive structure) and calderas (destructive structure) as a consequence of the existence of a shallow magma chamber. Finite element methods (FEM) are used here to calculate the local stress field associated with magma chamber to better understand the volcano-tectonics mechanism for this region. Magma chambers are modelled here as a hole within the Earth's crust and subject to various loading conditions. The three primary loading conditions considered are (i) the excess magmatic pressure within magma chamber, (ii) tensile stresses represent the remote field stress as well as (iii) the compressive stress at the bottom of the crust during the end of Miocene due to accumulation magma and caused regional swelling or uplift. The results indicate that the uplift doming at the lower crust played major role to generate three major calderas respectively, while excess magmatic pressure and far-field stress as loadings are only favoured to form constructive volcano (radial dykes, inclined sheets and regional dykes) rather than collapse caldera (ring-faults and ring-dykes). Basaltic lavas are mainly produced at peripheral of province and meantime followed each collapse caldera, but the intermediate and acid rocks are mostly produced in the central volcanoes and collapse calderas (Fig. 9.1b).

The evolution of the TVP is characterised by constructive episode (between 8 and 7-5 Ma), and then destructive episode (between 7–5 and 0.43 Ma) where the constructive (inflation process) period involves accumulation of

volcanic materials for formation central volcanism (volcanic unit b) whereas destructive period (deflation process) involve vertical collapse calderas and produced huge volume of ignimbrites and most likely associated with ring faults and ring dykes (volcanic unit c). Interruptions between ignimbrites activity were characterised by widespread basaltic to andesitic-trachyte volcanism and like this phenomenon has been observed in many collapse calderas worldwide, for instance, the Las Canada caldera in Tenerife (Marti and Gudmundsson, 2000).

Stratigraphic and geochronological data show that during the development of calderas the focus of felsic volcanic activity migrated with time from centre of the volcanic province at Voon caldera (7-5 Ma) and then to the southwest at Emi Koussi caldera (2.4–.33 Ma), and finally moved to the northeast at Yirrigue caldera (0.43 Ma) (Fig. 2). The conceptual, analogue and analytical modelling of Marti and Gudmundsson (2000) for overlapping collapse calderas generated by magma chamber migration seems to be applicable for the caldera collapses on the Tibesti volcanic province although there are spaces separated between nearby calderas in the TVP rather than overlapping as we discussed in later sections. The dimensions (diameters), maximum depth below the top of the caldera, geometry area and eruptive volume of ignimbrites associated with each individual caldera on the TVP are summarised in Table (9.1). These eruptive volumes have been estimated by Deniel et al. (2015) that most likely are a crude measure of the effective minimum magma volume that left the magma chamber during eruption due to the effects of erosion and buried by later eruptions. This volcanic province is likely fed by double magma sources, in contrary to other volcanic provinces in Libya (Fig. 9.3a). One magma chamber is most likely located within the Earth's crust and mainly produced more evolved lava flow while deeper magma chamber (magma reservoir) at the lower crust or at crust-mantle boundary produced mainly less evolved lava flows. Temporal and spatial of various style and productions of volcanisms on the TVP can be a understanding better in the terms of volcano-tectonics processes and numerical models.

9.3 Conditions for magma chamber rupture and dyke emplacement

The magma chamber is typical formed within the Earth's crust over considerable periods of time at depths from a few kilometres to several tens of kilometres below the free surface with various great sizes from hundreds to thousands cubic kilometres or even more in other planetaries (Gudmundsson, 2008; Gudmundsson, 2014). Magma chamber may be developed from an original sill absorbs the magma of many dykes whilst it is still liquid or, alternatively, due to merge nearby sills into a large one

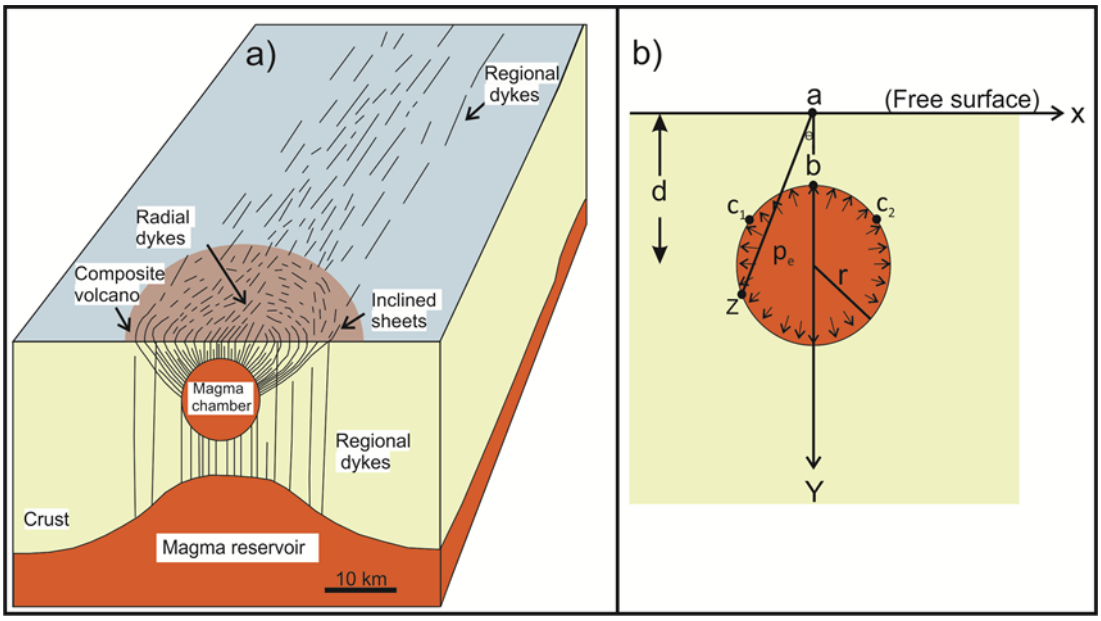

Figure 9.3. a) Schematic diagram illustration the volcanic field may be fed by double magma sources. The shallow magma chamber provided magma through radial dykes and inclined sheets whereas the deeper magma reservoir provided primitive magma through regional dykes (modified from Gudmundsson et al., 2008). Shallow magma chambers are the sources of bimodal central volcanoes as well as collapse calderas at the TVP while deep-seated reservoir may be the source of monogenetic basaltic rocks at the periphery of the province. b) The simplified illustration of spherical magma chamber at shallow depth d subject to magmatic excess pressure p_e. The maximum tensile stress σ_{max} occurs at the boundary at points c_1 and c_2 once the angle θ reaches a maximum. The tensile stress σ_b at a point b is equal to internal magmatic excess pressure p_e while at point a depends mainly on the radius r and depth d of the magma chamber (see text for more explanation) (modified from Gudmundsson, 1990).

(Gudmundsson, 1990). The condition for rupture of a magma chamber and emplacement of dykes when the following equation is satisfied (Gudmundsson, 2011);

$$p_l + p_e = \sigma_3 + T_0 \quad (9.1)$$

where p_l is the lithostatic pressure, p_e is the magmatic excess pressure (above the lithostatic pressure) in the magma chamber prior dyke emplacement and T_0 is the tensile strength of the host rock at the wall of the chamber, σ_3 denotes the minimum compressive principal stress, here is given by its absolute value (positive), and perpendicular to the dyke emplacement. Since magma chambers are long-lived fluid-filled structures which normally rupture not regularly in comparison with their lifetime and commonly in lithostatic equilibrium with host rock so that $\sigma_3 = p_l = \sigma_1$ (maximum principal compressive stress) and excess pressure p_e is zero in the chamber at every point at its surface. But for unrest period the excess pressure p_e must be positive in the chamber and condition to be satisfied is $p_e = T_0$ due to (i) magma replenishment from deeper source or (ii) through gas exsolution from its magma or (iii) reduce the minimum principal compressive stress σ_3 owing to extension (Gudmundsson, 2012). The in-situ tensile strength T_0 of rocks in range of 0.5 and 9 MPa with most common values being 2–4 MPa (Haimson and Rummel, 1982; Amadei and Stephansson, 1997). Thus we used here the maximum excess magmatic pressure for magma chamber is 5 MPa for all numerical models.

Once magma chamber ruptures the over magmatic pressure (driving or net pressure) has the responsibility to form a fluid-driven fracture and then magma filled extension fractures and crystallised to form sheets (Gudmundsson, 2015). The sheets are classified into inclined sheet, dyke/sill depending on its attitude relative to the host rocks. Dykes are mainly vertical or close to vertical while inclined or cone sheets are relatively tilting (Fig. 9.3a) and sills are commonly horizontal (Tibaldi, 2015). As the dyke or

inclined sheet begins to propagate up into the roof of the chamber, the magmatic overpressure in the fluid-driven fracture becomes (Gudmundsson, 2011):

$$p_o = p_e + (\rho_r - \rho_m)gh + \sigma_d \quad (9.2)$$

where ρ_r is the average density of the crustal layers which the dyke dissects, ρ_m is the magma density (assumed constant), g is acceleration due to gravity (assumed constant), h is the dip dimension above magma chamber and σ_d is the differential stress at the level where the dyke is observed (Gudmundsson, 1990; Gudmundsson, 2011).The magmatic overpressure p_0 measures the difference between the total magmatic pressure and maximum tensile principal stress σ_3, which acts normal to the dyke, and increases so long as the buoyancy term $(\rho_r - \rho_m)gh$ is positive on its path towards the surface. During fissure eruptions, the overpressure p_0 has large effects on the effusion rate (Gudmundsson, 1990; Gudmundsson, 2011; Kusumoto et al., 2013). The over magmatic pressure at the Al Haruj Volcanic Province, central Libya, has been estimated of 8–19 MPa by Elshaafi and Gudmundsson (2016), even though the excess magmatic pressure commonly does not exceed 5 MPa as indicated above.

In fact, the majority of dykes propagated from magma chamber that are arrested or deflected at various levels of the Earth's crust (Gudmundsson, 2014; Elshaafi and Gudmundsson, 2016). In case of deflection led to form an initial sill as previously mentioned due to three main mechanisms, namely i) stress barriers (layers where the principals stresses have turned so as to become unsuitable to dyke emplacement . ii) The Cook-Gordon debonding or delamination (induced dyke-parallel tensile stress opens the contact ahead of the propagating dyke tip). iii) Clastic mismatch mechanism (relates to abrupt change in Young's modulus across a contact in relation to the contact properties and material toughness). Further details of the arrested

and deflection of dykes are given by Browning and Gudmundsson (2015) and Elshaafi and Gudmundsson (2016).

9.4 Mechanism of constructive central volcanoes

Field observations and geophysical studies suggest that the geometry of long-lived magma chambers approaches the ideal geometry of spherical or ellipsoidal rather than being irregular in shape, particularly during the end stages of their evolutions (Gudmundsson, 1988, Gautenb et al., 1989, Gudmundsson, 1990; Gudmundsson and Nilsen, 2006; Gudmundsson, 2008). Therefore if we assume magma chamber circular geometry at depth (d) and radius r and subject to an internal magmatic excess pressure p_e (Fig. 3b), the stress fields associated with magma chamber is given by this equation (Savin, 1961, Gudumundsson1998);

$$\sigma_b = p_e(1+2\tan 2\theta) \tag{9.3}$$

where σ_b is the tensile stress along the boundary of the chamber and θ is the angle between the vertical axis and tangent (AZ) to the boundary of the magma chamber. The maximum tensile stress occurs at the both sides (c_1 and c_2) of the chamber where the angle reaches a maximum at these points. On the top of the chamber at point b the tensile stress is equal to magmatic excess pressure p_e. The maximum tensile stresses $\sigma_{\max}$ has been recorded at point c_1 and c_2 when the radius r of chamber is close to central depth d of the magma chamber and can be found by this relation (Gudmundsson, 1998) (Fig. 9.3b);

$$\sigma_{\max} = \frac{p_e\left(d^2+r^2\right)}{\left(d^2-r^2\right)} \tag{9.4}$$

Caldera	Age (Ma)	Legth (km)	Width (km)	Maximum Depth (km)	Area (km^2)	Eruptive Volume (km^3)
Yirrigue	0.43	15.2	13.15	0.387	3223	150
Emi Koussi	2.4-1.3	12	12	0.356	2777	Unknown
Voon	7-5	15.8	13.6	0.308	2167	130

Table 9.1. The cross-sectional area, maximum depth and eruptive material (area and volume) associated with each major collapse caldera at the TVP. The ages and eruptive volumes are taken from Deniel et al. (2015).

All symbols are as defined above. Once d is > 1.73 r, the maximum tensile stresses at both sides of chambers at points c_1 and c_2 is greater than maximum tensile stress at the free surface above magma chamber at point a (Gudmundsson,1998) and vice versa.

Deeply eroded in the TVP, probably several kilometres (Vincent 1970; Deniel et al., 2015), particularly at Tieroko extinct central volcano, is very helpful for understanding the similar three-dimensional structure of the active magma chambers (cf. Gudmundsson, 1998) (Fig. 9.4a). Extinct crustal magma chambers of different sizes and depths occur in deeply eroded volcanic regions and commonly associated with swarms of inclined sheets, radial dykes, ring faults, and ring dykes or concentric dykes such as Iceland and Scotland (Gudmundsson, 1998; Upton, 2004). The swarms of inclined sheets and radial dykes occur at flanks of Tieroko extinct central volcano and can be traced to pluton (cf. Deniel et al., 2015) (probably the uppermost part of extinct magma chamber) (Fig. 9.4a). Some of the inclined sheets seem to be arrested at various levels due to an abrupt change in the mechanical properties between layers, particularly changes in stiffness (Young's modulus) of those layers (Fig. 9.5a) (Elshaafi and Gudmundsson, 2016).

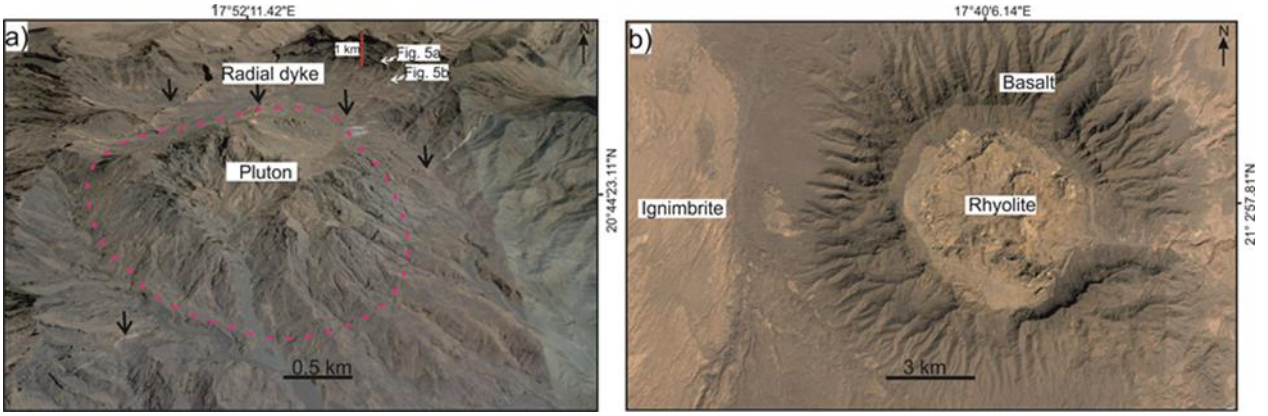

Figure 9.4. a) Satellite imagery (adapted from Google Earth) showing the deeply eroded Tieroko extinct central volcano. The black arrows indicate the radial dykes (lighter tune than surrounding) that may be injected from the uppermost of the magma chamber and seem to be comparatively thick ones. The exposed part of the chamber, pluton, is at a depth few kilometres below the initial top of the associated volcano (cf. Deniel et al., 2015). The white arrows provided the locations Figure (9.5a, b). b) Composite central volcanoes consist of two distinct volcanic phases. The first phase made up of basaltic and emplaced around the margin while the second phase consisted of rhyolite and emplaced at the central part. The description and names of both volcanic phases are taken from Deniel et al. (2015).

The cross-cutting relationships also indicate that the radial dykes (probably acidic) were mostly emplaced after inclined sheets (probably basaltic) (Fig. 9.5b). The inclined sheets (less evolved) apparently formed from deeper part of magma chamber while radial dykes formed from the uppermost part (more evolved). The distribution of radial dykes and inclined sheets indicates the existence of at least two magma sources (two magma chambers) or stratified/compartments being due to the difference between the density of felsic and mafic magma (buoyancy effects) within the same magma chamber where the high density may accumulate at the floor while light density tend to move toward the top of the magma chamber (cf. Gudmundsson, 2012).

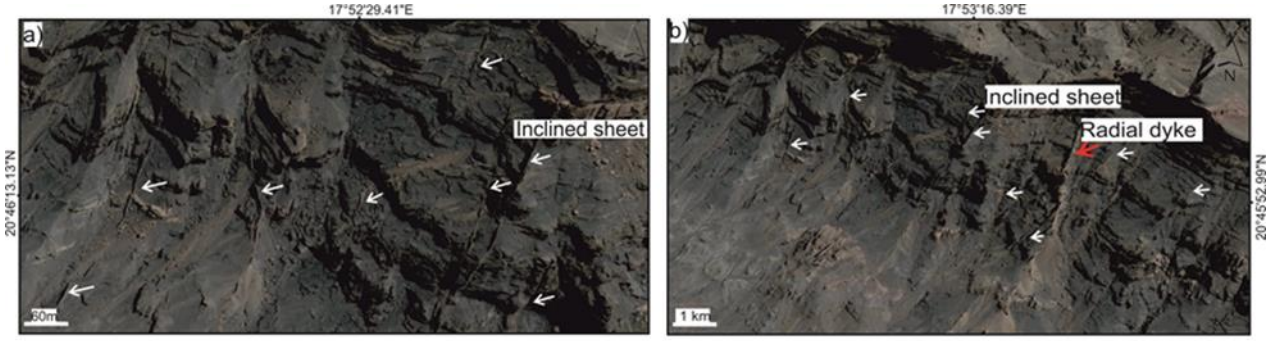

Figure 9.5. a) Swarms of inclined sheets indicated by white arrows, in the eroded Tieroko extinct central volcano (located in Figure 9.4a). They may be basaltic and mostly 0.5-3 m thick. b) Rhyolitic radial dyke (indicated by red arrow) cross-cutting the inclined sheet that may be assumed younger than basaltic inclined sheets (indicated by white arrows).

In addition, the morphology and stratigraphy of Toom central volcano strongly support this assumption, where it consists of two distinct volcanic generations (bimodal) (Fig. 9.4b). The first generation made up of less evolved volcanic rocks (basaltic rocks) whereas the second generation made up of more evolved volcanic rocks (rhyolite) (Vincent, 1970; Permenter and Oppenheimer, 2007; Deniel et al., 2015). At the contacts with the Tieroko pluton, the dips of the host rocks increase sharply toward top of the edifice from 10^{o} to as much as 20^{o}. It may be indicated that the magma chamber/pluton generates space for itself partly through forceful intrusion, primarily by bending or uplift the layers above and below (cf. Gudmundsson, 2012; Barnett and Gudmundsson 2014). Nevertheless, the presence of a shallow magma chambers beneath the region for long period of time (>1Ma) has indeed affected the stress field on the TVP (cf. Gudmundsson, 1998, 2015, 2016; Karaoglu et al., 2017) and caused volcanotectonic elements which may have superimposed on the pre-existing regional lineaments which define two preferential directions; NW–SE and NE–SW as already stated.

Hence we made many numerical models using the finite-element methods (FEM) to study in detail stress fields associated with magma chamber on the Tibesti Volcanic Province. The finite element methods (FEM) represent the

most common technique for solving differential and partial differential equations (Henk et al., 2013; Hickey and Gottsmann, 2014). Numerical models based on the finite element methods provide quantitative information on the local stresses field distribution around magma chamber and magma reservoir and greatly improve our understanding the volcanotectonics in this region because in situ stress field is of fundamental importance in volcanotectonics to explain the concentration stress zones around the magma chamber that may be trigger of volcanisms, ring faults as well as seismic activity. Comsol Multiphysics (5.1) is the finite element program used for the work described in this paper. It is commercial large-scale multi-purpose finite element software (www.comsol.com), and for more details of the standards modelling procedure can be found in Deb (2009).

Magma chamber can be modelled as a finite size cavity or penny-shaped in a three-dimensional model or as a hole for a two-dimensional model, the hole in elastic host rock when still magma or as an elastic inclusion when crystallised (pluton) which concentrate stresses when loaded (Andrew and Gudmundsson, 2007; 2008). Extinct stiffness magma chamber may be generated local stress field difference from active magma chamber due to varying in elastic modulus. The active magma chamber may have zero Young's modulus while the fossil magma chamber is usually higher young's modulus than the host rock. However, in the present work, we modelled magma chamber as hole with diameter 14 km and a top at 7 km depth, in both common geometries, spherical or oblate ellipsoidal (sill-like), in an elastic host rock subject to magmatic overpressure of 5 MPa as the only loading (Figs. 9.6a, 9.7a). The effects of gravity are taken into account automatically due to we used excess magmatic pressure rather than total pressure (Gudmundsson, 2012). The cross-sectional area of the associated magma chamber at the TVP has been roughly estimated from the geometry of the collapse calderas (Marti et al., 1994; Marti and Gudmundsson, 2000; Acocella, 2007) (Table 9.1). Additionally, we roughly estimated the top depth of magma chamber from Tieroko extinct central volcano. If we assume this pluton represents the uppermost part of the extinct crustal magma chamber

and taking into account the thickness of eroded (probably several kilometres) (Deniel et al., 2015). Therefore, the top depth of magma chamber in the TVP most likely located within few kilometres where the results of numerical models are not sensitive significant to the depth of the magma chamber.

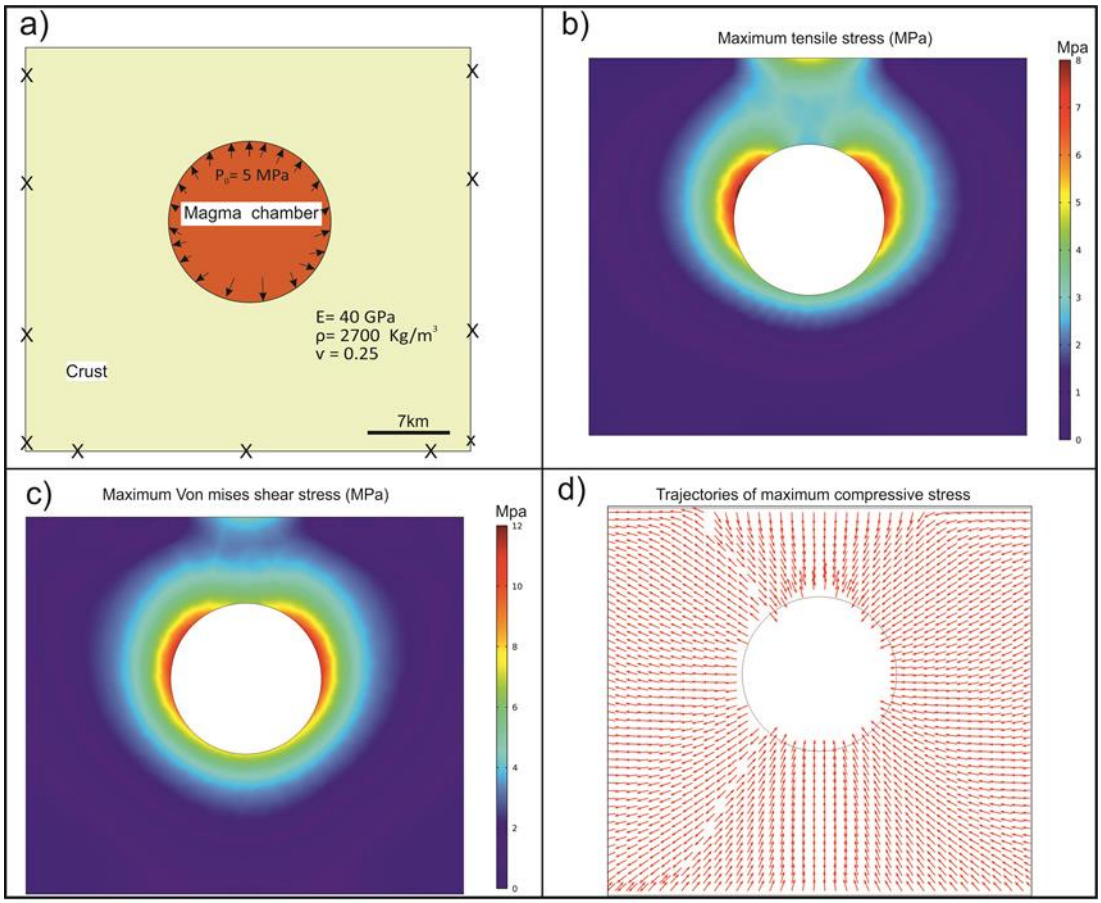

Figure 9.6. a) Model outline showing circular magma chamber a top at depth 7 km with diameter 14 km subject to internal magmatic excess pressure 5 MPa as the only loading. The model is fastened at the outer boundary using a fixed constraint to avoid any rotation or displacement. Colour contours showing the magnitude of the maximum principal tensile stress σ_3 (b) and von Mises shear stress τ (c) in mega-pascals. The maximum stresses have occurred at the boundary that are consistent with the analytical model (Fig. 3b). d) Showing the trajectories of the maximum principal compressive stress σ_1 so that a fluid-driven fracture (usually a dyke or an inclined sheet) are commonly propagated parallel trajectories.

To simplify our models, we modelled the crust as homogenous layer with static Young's modulus for the crust 40 GPa corresponding to the average static Young's modulus for the upper crust (Wienecke and Stadtler, 2014; Elshaafi and Gudmundsson, 2017), and Poisson's ratio of most rocks around 0.25 (Gudmundsson, 2011). The typical results are presented in Figures (9.6 b, c, 7b, and c), generally yield similar results. They show, first of all, the maximum principal tensile and shear stresses generated around the margins of both shapes of magma chambers (spherical and sill-like magma chamber). The local tensile stress σ_3 satisfies (8-10 MPa) the condition for failure or rupture of magma chamber Eq. (9.1) because the magnitude of tensile stress exceeds the tensile strength of the host rocks (most commonly 2-4 MPa) (Amadei and Stephansson, 1997; Gudmundsson, 2008).

Dykes or inclined sheets essentially are extension fracture so that it follows the trajectories of the maximum compressive principal stress σ_1 (cf. Gudmundsson, 2011) (Figs 9.6d, 9.7d). Hence the magma driven-fractures would have propagated in all directions like radial from the source where the driven-fractures propagate from the central part would be more vertical (dyke) than driven-fractures propagate from both sides (inclined sheets). These modelling results are greatly coincidence with field observations at Tieroko eroded central volcano (Figs. 9.4a, 9.5a, b). To test the effect of remote or regional stress field we again made several numerical models using Comsol (www.comsol.com). We used the same crustal properties, Young's modulus of 40 GPa and a Poisson's ratio of 0.25 as in the previous models. We used only loading 5 MPa (Fig. 9.8a) as represent regional extensional stress field, NE – SW direction, because absolute tensile stress at close to the surface or within few kilometres cannot go-over the in situ tensile strength of the host rocks (commonly 4-5 MPa) (Haimson and Rummel, 1982;Schultz, 1995; Amadei and Stephansson, 1997; Gudmundsson, 2008).

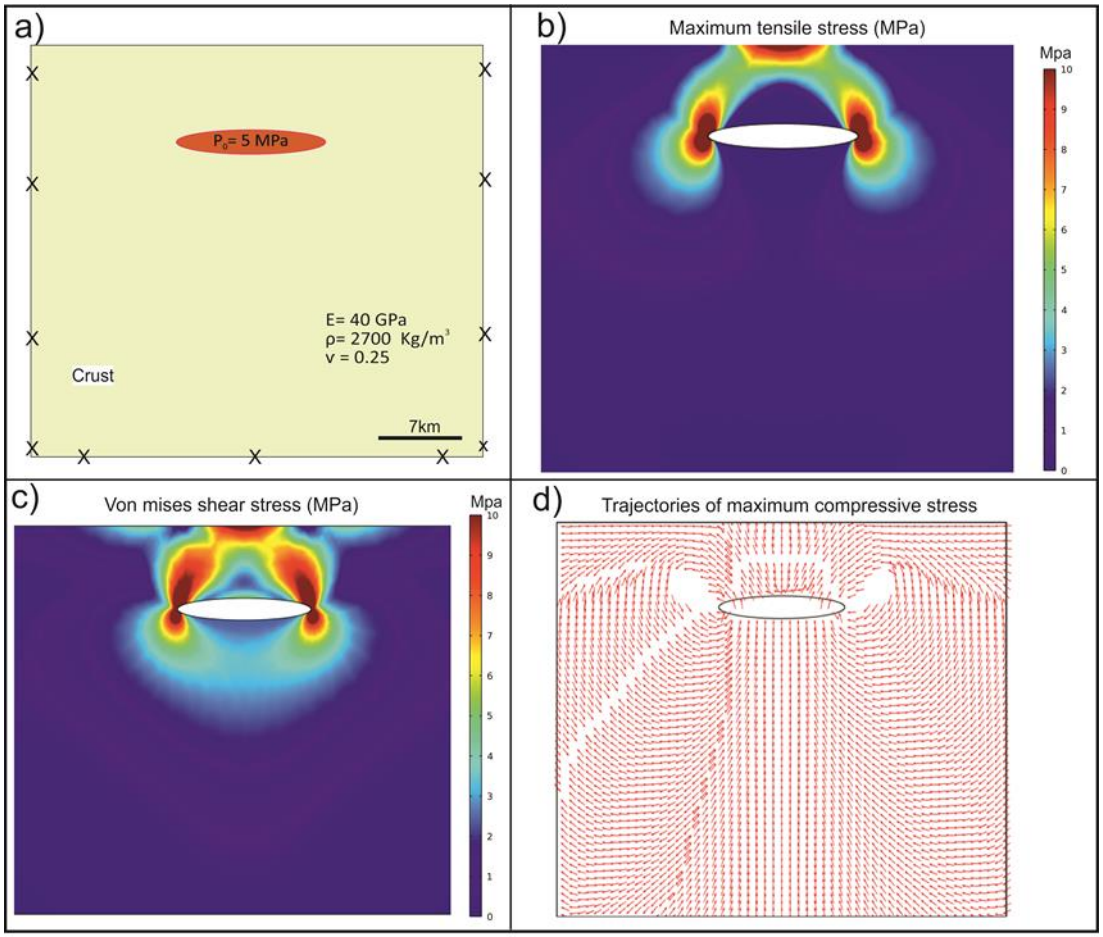

Figure 9.7. a) Model outline showing sill-like magma chamber a top at depth 7 km with diameter 14 km and 2 km thick subject to internal magmatic excess pressure 5 MPa as the only loading. The results of model yield similar as in circular magma chamber Figure (9.6). The maximum tensile principal stress σ_3 (b) and von Mises shear stress τ (c) occurred at lateral ends of the magma chamber and in the centre of free surface. d) Driven-fractures propagated from the magma chamber parallel to the trajectories of maximum principal compressive stress σ_1.

The results (Fig. 9.8b, c) show that while the maximum tensile σ_3 and shear τ stresses concentration above the magma chamber rather than margins and the trend trajectories of the maximum principal compressive stress σ_1 is generally vertical and would favour the formation vertical dykes rather than inclined sheets (Fig. 9.8d) as we observed in the previous models. So that the radial dykes and inclined sheet in the Tieroko eroded centre volcano most likely generated by local stress fields associated with magma chamber due to excess magmatic pressure rather than regional stress field. The latter

could be partly responsible for formation vertical dyke from the deeper magma reservoir rather than inclined sheets from the shallow crustal magma chamber. Our findings are in good agreement with field observations and modelling deeply eroded, extinct central volcanoes by Gudmundsson (1998) in Iceland. In addition, we made the same modelling for spherical magma chamber under same loading and boundary conditions, and we found the same results for sill-like magma chamber, are not shown here.

9.5 Mechanism of caldera collapse

Caldera is one of the most important volcano-tectonic features of the TVP and still poorly documented and understood. Collapse caldera is generally defined as an elliptical or spherical in plan-view with depression in range of few hundred meters and their diameters greater than one kilometre and commonly being 10 km (Marti and Gudmundsson, 2000; Gudmundsson, 2008; Gudmundsson, 2015). It frequently occurs along steeply dip-slip faults, so as to either inward-dipping (normal fault) or outward-dipping (reverse fault), consequently existence shallow crustal magma chamber (Fig. 9.9) (Gudmundsson, 2015; 2016). Many of ring-faults used as magma conduit during collapse calderas and formed ring dykes (Browning and Gudmundsson 2015). The caldera collapse can be subdivided into two groups based on the types of volcanoes to which they belong (Francis, 1993; Lipman, 2000; Radebaugh et al., 2001; Krassilnikov and Head, 2004; Cole et al., 2005; Gudmundsson, 2008). The first group mainly belongs to basaltic shield volcanoes such as Hawaii and Galapagos and have mean maximum diameters in range 6-7 km while the second group is belong to composite (central) volcanoes and have diameters in the range 18-19 km (Radebaugh et al., 2001). There are three major collapse calderas, in addition to small nested-calderas, that have been identified on the TVP with diameters in the range 12-16 km (Fig. 2.9). They are very close to the second group rather than the first group (Table 9.1). The calderas on the TVP have been partly filled with lava flows to their rims and interior (Fig. 9.10 a, b), similar to many other calderas worldwide.

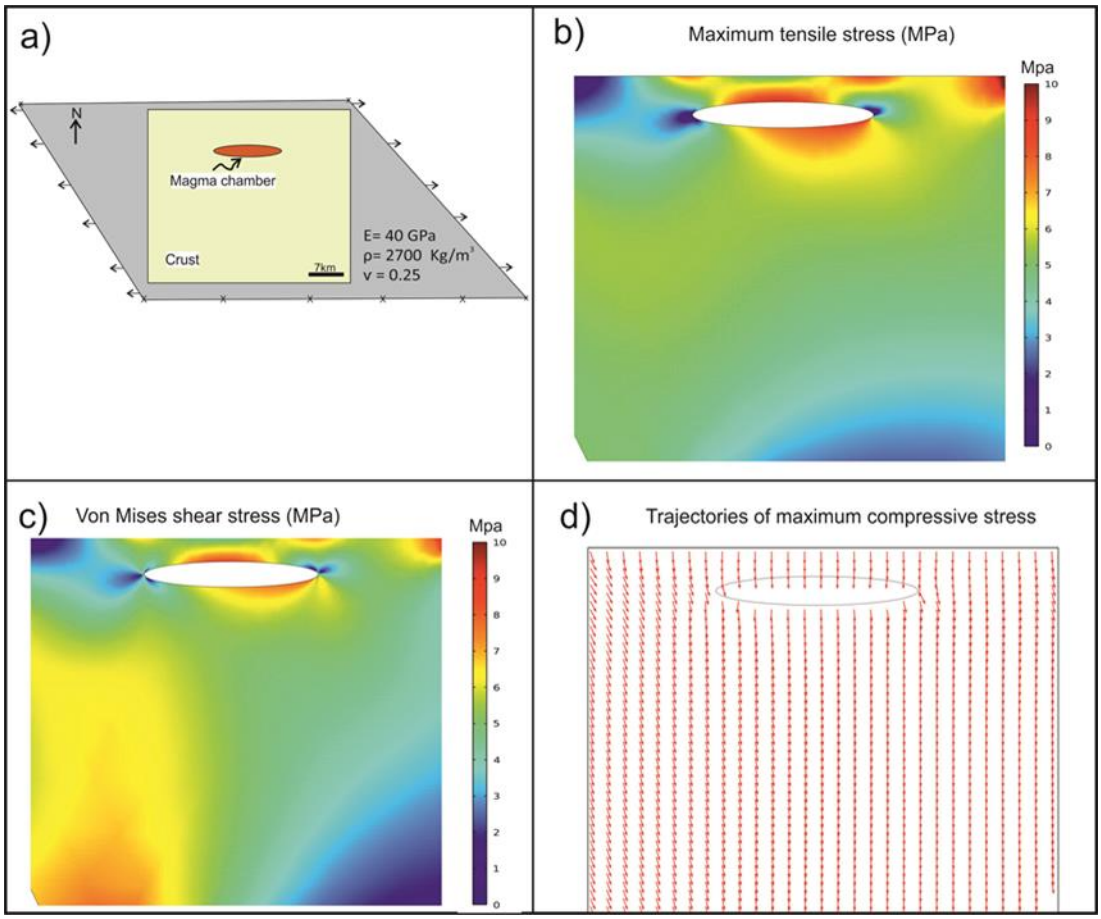

Figure 9.8. a) Model setup showing the sill-like magma chamber a top at 7 km and 14 km wide and 2 km thick in homogeneous crust with stiffness 40 GPa. Note the direction of tension applied to the model demonstrated by arrows. It is a tensile stress of 5 MPa only as a loading. The maximum tensile stress σ_3 (b) and von Mises shear stress τ (c) occurred at the top and bottom of the magma chamber rather than later ends. d) Stress trajectories (trends) of the maximum principal compressive stress σ_1.

While many different models have been suggested for explain the relationship between ring faults and existence shallow crustal magma chamber into which the caldera block subsides (Walker, 1984, Marti et al., 1994; Burov and Guillou-Frottier, 1999; Acocella et al., 2004; Folch and Marti, 2004; Gray and Monaghan, 2005), little attempts have obviously made to clarify their mechanics (Gudmundsson, 2007; 2008). It is well known that the ring-fault must create at the surface prior the block subsidence take places (Gudmundsson, 2008). The ring-faults are commonly inward-dipping (normal faults) at the TVP, becoming vertical with depth that caused

subsided blocks of collapse calderas and associated with huge volumes of ignimbrite, more than 100 km^3, associated with each individual caldera, (Deniel et al., 2015; Table 9.1). Inward-dipping ring-faults can be generated when volcanic province containing volcano is subject to doming or extension force, particularly in rift zones and in continental grabens. When the inward-dipping is close to vertical, the ring-dyke is likely to propagate; consequently, the magma chamber may squeeze out large fraction, and sometimes effectively all, the magma in the chamber (Gudmundsson, 2015, 2016). However, the ring-fault displacement (volcano-tectonic forcing) and composition of magma (gas-rich magma) played a very significant role to squeeze out a much higher volume of magma than the frequency or ordinary poroelastic eruption. Because excess magmatic pressure p_0 drops rapidly during ordinary eruptions and therefore is not capable to produce these huge volumes at the TVP, whereas the ring-faults and gas-rich magma generally can permanently maintain the excess pressure as longer than the ordinary eruption to keep a fluid-driven fracture open at its contact with the chamber until the eruption comes to an end thereby producing large eruption (cf. Gudmundsson, 2015; 2016).

Deniel et al. (2015) propose that some of the ring-faults/ring-dykes on Yirrigue caldera may be buried by subsequently the post-caldera Tousside complex (Fig. 9.10a). Different loading conditions and magma chamber geometries (spherical or sill-like) are deeply investigated by Gudmundsson et al. (1997), Gudmundsson and Nilsen (2006); Gudmundsson (1998, 2007, 2008) in order to improve our understanding the mechanism of formation ring-fault (volcano-tectonic forcing) and caldera stability and why some of them associated with huge volcanic eruptions (many tens cubic kilometres). Attention should be drawn to the fact that collapse calderas are not always associated with massive eruptive material where the volume of eruptive materials depend mainly on the dipping of ring-fault (inward-dipping, or outward-dipping) and composition of the magma. Further more details about

caldera collapse mechanisms and the associated eruptions are given by Gudmundsson (2015, 2016).

In general terms, it is well known that the caldera collapse conditions depend strongly on the shape of the magma chamber, loading conditions as well as Young's moduli of the host rocks (Gudmundsson and Nilsen, 2006). The geometry and size of magma chamber are generally changeable during its evolution so that only specific shapes of magma chambers are favourable for formation collapse calderas such as oblate ellipsoidal while others such as prolate ellipsoidal, are unlikely to generate local stress field for formation collapse caldera (Gudmundsson, 1998, 2007, 2008). Therefore the ordinary poroelestic eruptions in collapse calderas, through radial dykes and inclined sheets, are considerable more regular than initiation, or renewed slip on an existing ring-fault (Newall and Dzurisin, 1988; Gudmundsson, 2008). The stress field associated with various geometries of magma chamber through its lifetime may favour injections numerous of inclined sheets and dykes whereas the stress field associated with magma chamber for formation or slips on the existing ring-faults persists is uncommonly (Gudmundsson, 2007). Based on well-documented field observations by Gudmundsson (1998, 2008), the shear stress τ and the near-surface tensile stress σ_3 must apex at both sides of magma chamber as well as at the radial distance at the free surface to form a ring-fault, owing to most of ring faults and ring dykes initiate at the lateral ends of the associated magma chamber. However, the ring-fault is essentially shear fracture, and hence the local shear stress τ field must be satisfied the condition of failure criterion (Gudmundsson, 2007, 2008).

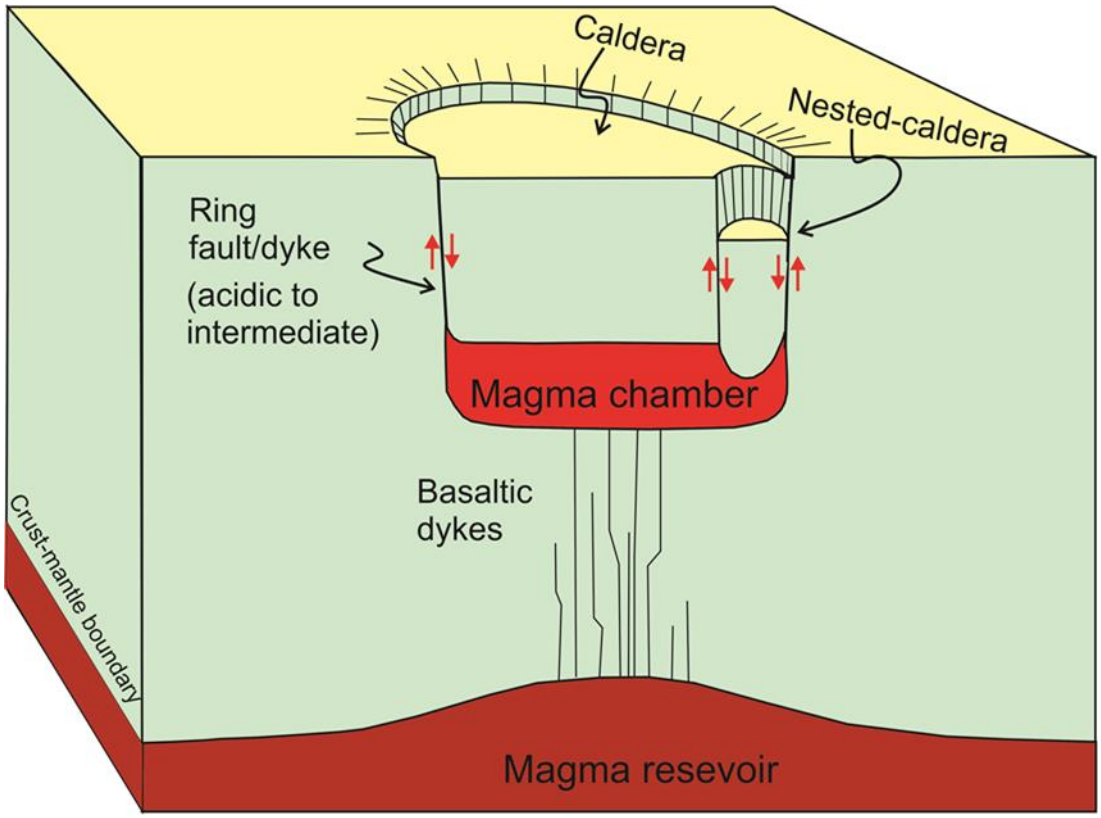

Figure 9.9. Schematic illustration of collapse caldera that is commonly associated with existence shallow crustal magma chamber. The cross-sectional area of magma chamber can be achieved from geometry area of a caldera. Most of the collapse calderas occur in the volcanic provinces when magma accumulates at the lower crust to cause upwelling or doming much larger than the diameter of the existence shallow crustal magma chamber. The ring-fault slip is played a significant role to squeeze out much magma and generated large eruption. Nested collapse caldera is commonly associated with older and larger caldera at the centre or margin such as Tou au Natron a nested caldera within the larger Yirrigue collapse caldera at the NE Tibesti Volcanic Province (Fig. 9.10a) (modified from Gudmundsson, 2007).

In the above models, the maximum surface tensile σ_3 and von Mises shear τ stresses occurred due to either excess magmatic pressures p_e (Figs. 9.6, 9.7) or extensional regional stress field (Fig. 9.8) that are mainly concentrated at the point above the centre of magma chamber rather than its lateral edges, accordingly those stresses fields are not at a suitable location

to promote ring-fault or ring-dyke formation while being favourable to radial dyke and inclined sheet injection as we have discussed earlier. We thus made again some numerical models using Comsol (www.comsol.com) in order to test the stress field that is favourable for formation or slip on pre-existing ring-faults. We used the same crustal properties, Young's modulus of 40 GPa and a Poisson's ratio of 0.25 as in the previous models. Underlying the crustal segment is a magma reservoir with a width 50 km.

We used only loading 10 MPa (Fig. 9.8a) as representing the magma accumulation and excess pressure or stress at the base of the crustal segment, resulting doming of an area much larger than that of the shallow magma chamber and then most likely subsequently caused collapse caldera (Williams and McBirney, 1979; Lipman, 1984; Komuro, 1986; Marti and Gudmundsson, 2000, Gudmundsson, 2007, 2008). The primitive magma generated due to partial melting at the upper/lower mantle boundary (≈ 670 km depth) travels buoyantly through the mantle, displacing denser asthenosphere, and ultimately accumulated at the crust-mantle boundary (Permenter and Oppenheimer, 2007). Due to the lack of the geophysical data on the Tibesti massif, we assume that the magma reservoir (accumulation of magma) was generally located at average depth around 35 km, which generally corresponds to the boundary (Moho discontinuity) between the lower crust and upper mantle in the central and southern Libya (Ghanoush et al., 2014). This depth is also quite consistent with depth of magma reservoir in the Al Haruj Volcanic Province (AHVP), central Libya (Peregi et al., 2003; Nixon et al., 2011; Elshaafi and Gudmundsson, 2017). The thickness of crust at TVP $(\approx 35km)$ seems to be sensible due to Tibesti massif is located on a stable cratonic with lithospheric thickness around 130-140 km (Ebinger and Sleep,1998; Permenter and Oppenheimer 2007).

The magma chamber is modelled as elliptical shape field-scale with a major axis 14 km and at depth 7 km, to a first approximation (Fig. 9.11a). The

spherical magma chamber is not suitable for formation ring-faults within homogenous Earth's crust (Gudmundsson, 1998, Gudmundsson and Nilsen, 2006), but in fact is suitable under-specific Young's modulus for the layer hosting magma chamber (Gudmundsson, 1998; 2008) and are beyond the scope of the present work. The models show doming at the bottom of the crust due to accumulation of magma that led to generate the maximum tensile stress σ_3 at the margin of magma chamber about 3.5 MPa (Fig. 9.11b, c) whereas at the free surface above the chamber the maximum tensile stress σ_3 shows two peaks at around 5.5 MPa (Fig. 9.11b, d). Furthermore, the von Mises shear stress τ at the margin of the chamber reaches about 9 MPa while at the free surface above the chamber has two peaks of about 4.5 MPa (Fig. 9.12a, c).

Shear strength τ_0 of most rocks has been estimated from stress drop of earthquakes between 1 MPa to 10 MPa, and is most commonly 3-6 MPa (Kanamori and Anderson, 1975; Kanamori, 1977; Gudmundsson, 2016), while the tensile strength T_0 has a comparatively lower range and mostly around 2-4 MPa (Amadei and Stephansson, 1997; Gudmundsson, 2012). In addition, the tensile T_0 and shear τ_0 strengths of the country rocks may be slightly reduced due to thermal effects of the active magma chamber (Browning et al., 2016). Thus the conditions for ring-fault initiation at the free surface and at the shallow depth seem to be suitable (cf. Gudmundsson et al., 1997; Gudmundsson 1998, 2007, 2008). Maximum tensile σ_3 and shear τ stresses at the lateral ends of the magma chamber and the radial distance from the surface point above the centre of the chamber appear to be coincided and in the similar range of tensile T_0 or shear strength τ_0 of ordinary rocks. So that those in situ stress fields are likely to trigger ring-fault initiation or slip on an existing ring-faults on the surface as well as the emplacement of ring-dykes from margins of the magma chamber (cf., Gudmundsson 1998, 2007, 2008). It is important to note that those stress concentrations above the margins of the associated shallow magma

chamber rarely occur in the global volcanic fields to form caldera collapse in comparison with ordinary poroelastic eruptions (Gudmundsson 2015; 2016).

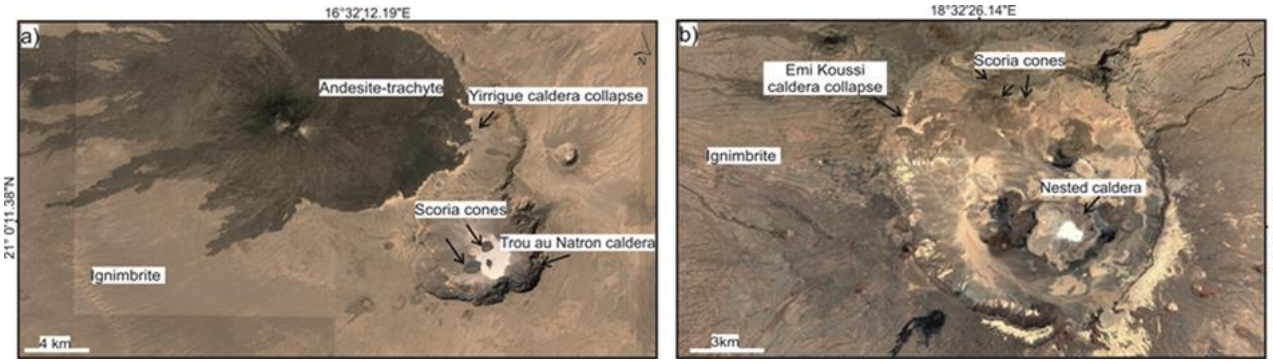

Figure 9.10. Satellite imageries (adapted from Google Earth) exhibit two main collapse calderas at the TVP. a) Yirrigue caldera collapse (0.43 Ma) associated with nested Trou au Natron caldera and followed by recent andesitic-trachyte (100 ka) at its margin. b) Emi Koussi caldera collapse (2.4–1.3 Ma) associated with nested unknown caldera at the central part and followed by scoria cones along its margin and in the central part as well. Note the ignimbrites for both calderas cover the huge area (>100 km^3).

9.6 Discussion and conclusion

9.6.1 Magma supply by double magma sources

The variety of volcanic products along the TVP range from contemporaneous basaltic to acidic, during the end of Miocene to late Pleistocene, propose that the magma in this volcanic field may be comparatively derived from double magma sources while the Al Haruj Volcanic Province, central Libya, is commonly supplied through single magma reservoir, most likely at the crust-mantle boundary (cf. Peregi et al 2003; Less et al 2006; Nixon et al., 2011), although both volcanic provinces have generally occurred in the same period. However, the more evolved acidic volcanic rocks (rhyolite, trachyte and ignimbrite) on the TVP are commonly concentrated in the central part of the edifice while the less evolved basaltic rocks are distributed along its

margins and meantime followed collapse caldera in the central parts as well (Fig. 9.1b).

In general terms, some of dykes were injected from the central part of the deeper magma reservoir seems to be deflected into initial sill within the uppermost crust, due to abrupt changes in the mechanical properties of the crustal rocks and thereby generate potential magma chamber as previously stated. Whereas some less evolved dykes could be propagated directly to the surface and feeding eruption. Field observations and the numerical model results are generally agreed with this assumption, where basaltic magma (scoria cones) can be observed around the periphery of the volcanic edifice while more evolved (rhyolite and ignimbrite) as well as some basalt are present mainly in the central part. In fact, similar this distribution is well known and documented in other volcanic edifices, such as Ağrı Dağı volcanic field, eastern Turkey (Karaoğlu et al., 2017).

Several of central volcanoes (composite volcanoes) and collapse calderas at the TVP are poorly documented and understood, particularly regarding of their relationship to volcano-tectonic forcing. These volcanisms seem to be superimposed on the two preferential regional pre-existing lineaments where the central volcanoes (Yega, Oye and Toom) are well- developed along NE–SW trend (Deneil et al., 2015), while the collapse calderas (Voon, Emi Koussi and Yirrigue) are roughly alignment along NW–SE direction (Fig. 9.1b). We thus made here two sets of numerical models in order to better understand the mechanism and volcano-tectonic process that led to form these constructive (8–5Ma) and followed by destructive (7–5 Ma to 0.43 Ma) volcanic units respectively. The results of the first suite numerical models indicate that the local stress fields around magma chamber and on the free surface due to excess magmatic pressure p_0 or regional stress field are likely to encourage only the emplacement of dykes or inclined sheets and produced commonly small range in eruptive volume most commonly being

between 0.01 km^3 and 0.1 km^3 (Karaoğlu et al., 2005; Gudmundsson, 2016). In addition, it is well-known that the geometry and size of magma chamber change considerably during its evolution and consequently the local stress field (Gudmundsson, 1998). Thus the cross-cutting between sheets at the Tieroko extinct central volcano is controlled by in situ stress field around chamber rather than regional stress field.

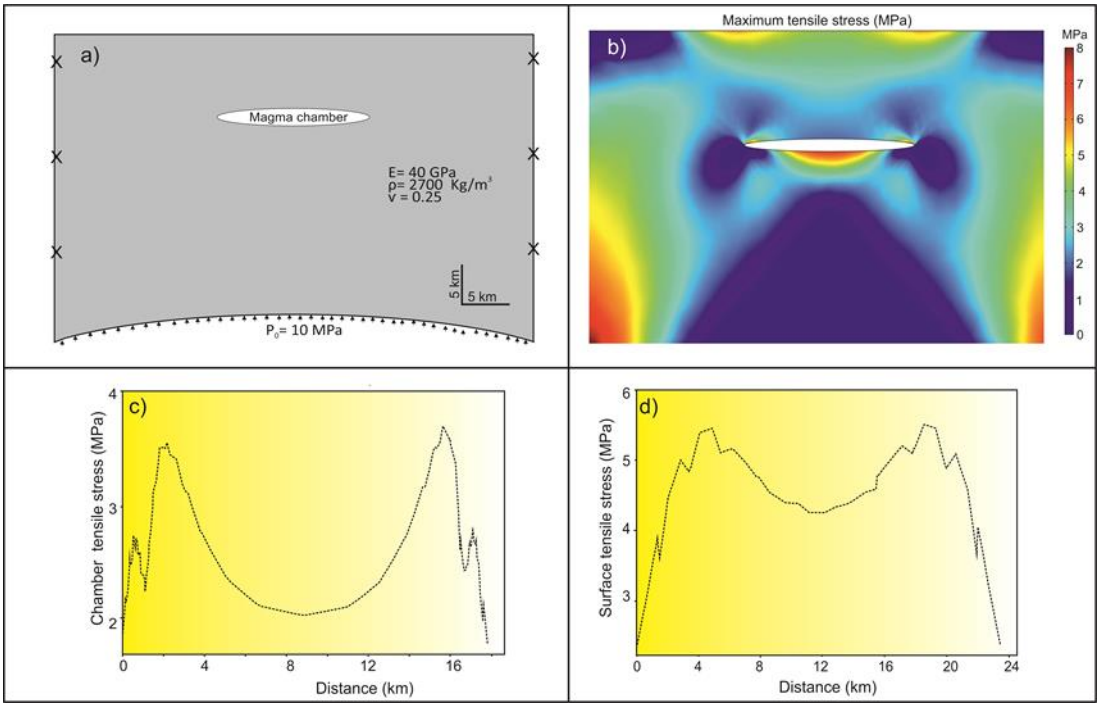

Figure 9.11. a) . Model outline showing ellipse (sill-like) magma chamber a top at 7 km, wide 14 km, and thickness 2 km in homogeneous crust with average young's modulus 40 GPa, 35 km thick and 50 km wide, subject to compressive stress, p_e 10 MPa, at the lower crust due to an accumulation of magma. b) The result of modelling showing the magnitude of the maximum principal tensile stress σ_3. c) Graph exhibiting the maximum principal tensile stress σ_3 at the upper boundary of the magma chamber. d) Graph showing the maximum principal tensile stress σ_3 at the free surface.

In contrast, the other models suite considered the effect of doming at the lower crust due to an accumulation of magma. The results of the second suite of models indicate that the doming at the lower crust might have extensive effects on the associated local stress fields that may have acted in harmony to encourage initiation ring-faults at surface or at the shallow depth

as well as injection of ring-dykes from the lateral ends of the chamber and then led to produce sometimes huge volume eruptions as much as 100 km^3 as occurred and observed on the TVP.

9.6.2 Caldera collapse and generated new magma-chamber

The rough elliptical surface expressions of scoria cones on the TVP may be taken as an indication of an elliptical geometry of the magma reservoir beneath this volcanic region, to a first approximation (Fig. 9.13a). It follows from the observations that volcanic fields and volcanic systems tend to reflect the plan-view geometries of the source reservoirs (Gudmundsson, 2000). Hence, the long axis of the deeper reservoir would be roughly 365 km while its short axis crudely 193 km (Fig. 9.13a). For comparison, the long axis of collapse calderas at the TVP is around 12-16 km (Table 9.1). Thus the doming area at the lower crust is very much larger than the crustal magma chamber and most likely played a significant role to form collapse caldera (Williams and McBirney, 1979; Lipman, 1984; Komuro, 1986, Marti and Gudmundsson, 2000).

The late Miocene uplift in the whole western part of the Sirt Basin, central Libya, is well provided by the burial history of oil wells (QQQ1-11; aa1-11), situated at the western margin of the Sirt Basin (Gumati and Schamel, 1988; Abadi et al., 2008). Also, the high degree of thermal maturity of shallow sediments inferred that more than one kilometre (probably several) of a sedimentary sequence was uplifted and eroded during the late Miocene in the whole western part of the Sirt Basin (Gumati and Schamel, 1988; Abadi et al., 2008). This regional uplift seems to be impacted on the whole Tibesti – Gharyan volcanic provinces. As a result undoubtedly the crustal doming during the end of Miocene and increased melt migration into the magma reservoirs beneath most of the Tibesti – Gharyan volcanic provinces in general and the TVP in particular might have led to elongated magma

reservoirs in the vertical section and accumulation of magma at the crust-mantle boundary. Therefore, the magmatic excess pressure in the

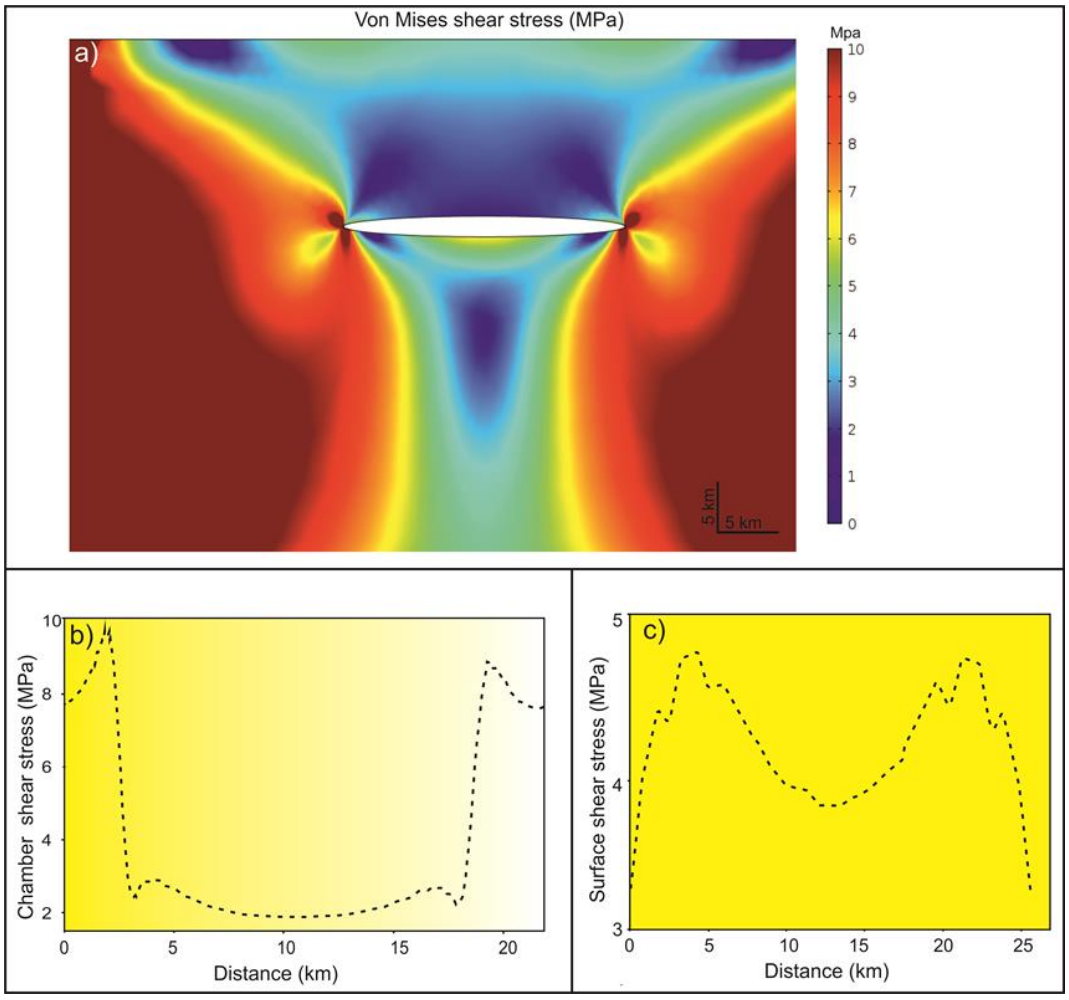

Figure 9.12. a) Same model setup, loading and boundary conditions as in Fig. 11a. a) The result of modelling showing the magnitude of the von Mises shear stress τ around magma chamber and at the free surface in Mega-pascal. b) Graph showing the von Mises shear stress τ at the upper boundary of the magma chamber. c) Graph showing the von Mises shear stress τ at the free surface.

magma reservoir at the crust-mantle boundary may have caused crustal doming of the hosting the three major collapse calderas. Accordingly, the collapse calderas on the TVP can be investigated in the light of the conceptual model is given by Marti and Gudmundsson (2000). This model

has provided how and under what stress condition overlapping collapse calderas generated by magma migration. In addition, this model is applicable for explaining magma chamber migration in regions where plate or continent is very slowly drifting such as African plate (i.e. Burke 1996; Begg et al., 2009), because bending tensile stress σ_3 controls the location of dyke injection frequently for a significant period rather than a fast drifting plate.

As a result of magma accumulation at the bottom of the crust, the central part of the crustal segment hosting the collapse calderas are subject to compressive stress while the lateral ends are subject to tensile stress (Fig. 9.13b). Hence the compressive stress, above the central deeper magma reservoir, might be difficult for dyke to penetrate and replenish the old shallow magma chamber (cf. Marti and Gudmundsson, 2000). By contrast, the tensile stress σ_3 on the lateral sides of the deeper magma reservoirs is likely to encourage repeatedly dyke injection. Each individual collapse caldera on the TVP appears to be formed at the end of each cycle. Once the magma chamber full-grown (more evolved) and when it has assembled large volume of ignimbrite magma (gas-rich magma), the tectonic-volcanic forcing (slip of the ring-faults) may be led to the subsidence roof of the associated felsic magma chamber and produce huge eruptive materials (ignimbrites). Meanwhile, the tensile stress σ_3 in the lower crust is most likely favourable frequently dyke emplacement and new magma chamber formation to either side of the old magma chamber and hence magma chamber migration rather than replenishment of the old magma chamber (cf. Marti and Gudmundsson, 2000). The migration of the magma chamber on the TVP inferred from field-relations and geochronological data (Deniel et al., 2015) (Fig. 9.13b).

The first caldera collapse (Voon caldera) occurred at the end of Miocene (7-5Ma) that may be simultaneous with the first volcanic phase at the Al Haruj Volcanic Province (AHVP) (7–3.5 Ma) (Less et al., 2006, Bardintzeff et al ., 2012). Furthermore, the local stress field around the deeper magma

reservoir, following the Voon caldera collapse existed, might be difficult and infrequently for dykes to feed the Voon chamber (old chamber) while the stress field is

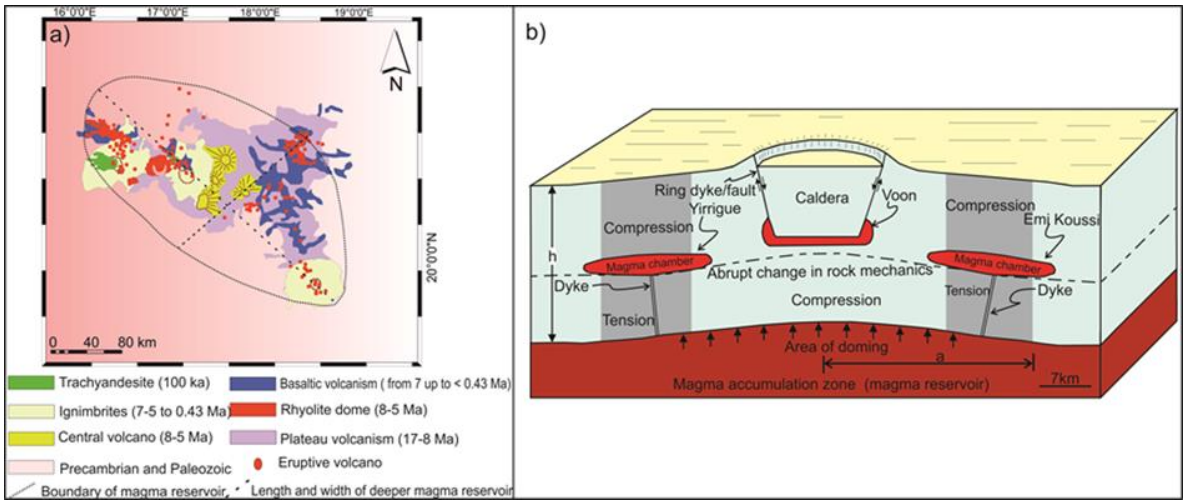

Figure 9.13. a) Simplified geological map of the TVP showing areal distribution of scoria cones (red spots) (7-0.43 Ma) that may be used to roughly estimate the dimensions of deeper magma reservoir. b) Conceptual model illustration the mechanism of overlapping collapse calderas and generated new magma chamber, is given by Marti and Gudmudsson (2000). This prediction model seems to be fit with the mechanism of collapse calderas at The TVP. The compressive stress above the deeper magma reservoir is making difficult for dyke piercing to feed Voon magma chamber while tensile stresses on the lateral ends of deeper magma reservoir are most likely suitable to encourage frequently dykes to form Emi Koussi magma chamber within uppermost crust at the right lateral margin at the SW of the TVP. After the destruction of Emi Koussi magma chamber, the local stress field may have suitable to form the third new magma chamber (Yirrigue magma chamber) at the lateral left end, at the NE of the TVP, a is the radius width of the deeper magma reservoir and h is the depth of the crust (modified from Marti and Gudmudsson, 2000).

suitable to frequently injection of dykes from margins of the deeper reservoir. Thus the new magma chamber may be created in the NW part of the TVP (Emi Koussi caldera, 2.4–1.3 Ma) (Figs. 9.2, 9.13b). This new magma chamber seems to be taken around 2.5 Ma based on the available geochronological data (Deneil et al., 2015). This period appears overestimate to form acidic magma from primitive magma (cf. Marti and

Gudmundsson, 2000). Subsequently, however, after the collapse of the second magma chamber, the new third magma chamber (Yirrigue caldera, 0.43 Ma) may be formed at the northwestern part of the TVP which spent around 1 Ma to form the rhyolitic magma from primitive magma. This period may be more reasonable to form acidic magma chamber (cf. Marti and Gudmundsson, 2000). It is important to note that the basaltic and mixing magmas were usually followed each collapse caldera that might have derived from the floor of the former destructive shallow magma chamber as compartment such as magma mixing and mingling (andesitic- trachyte) of Tousside volcanic complex (100 ka) followed the last caldera collapse (Yirrigue caldera, 0.43 Ma) or through infrequently dykes injected from deeper magma reservoir that may be unusual to overcome the unfavourable compressive local stress field. Most of the basaltic lavas are distributed along rims of calderas (e.g., Fig. 9.10a) due to most likely basaltic magma used pre-existing ring-faults/ring-dykes as conduits (cf. Browning and Gudmundsson, 2015; Elshaafi and Gudmundsson, 2016).

Acknowledgements

We are grateful to the Libyan Ministry of Higher Education for financial support.

References

Abadi, A., van Wees, J., van Dijk, P., Cloetingh, S., 2008. Tectonics and subsidence evolution of the Sirt Basin, Libya. AAPG Bulletin, 92, 993-1027.

Abdunaser, K., McCaffrey, K., 2014. Rift architecture and evolution: the Sirt Basin, Libya: the influence of basement fabrics and oblique tectonics. Journal of African Earth Sciences, 100, 203–226.

Acocella, V., 2007. Understanding caldera structure and development: and overview of analogue models compared to natural calderas. Earth-Science Reviews, 85, 125–160.

Acocella, V., Funiciello, R., Marotta, E., Orsi, G., de Vita, S. 2004. The role of extensional structures in experimental calderas and resurgence. Journal of Volcanology and Geothermal Research, 129, 199–217.

Ade-Hall, M., Reynolds, H., Dagley, P., Musset, G., Hubbard, B., Klitzsch, E. 1974. Geophysical studies of North African Cenozoic volcanic areas Al Haruj Al– Assuad, Libya. Canadian Journal of Earth Science, 11, 998-1006.

Amadei, B., Stephansson, O., 1997. Rock Stress and its Measurement. Chapman & Hall, London.

Andrew, R., Gudmundsson, A., 2007. Distribution, structure, and formation of Holocene lava shields in Iceland. Journal of Volcanology and Geothermal Research, 168, 137–154. doi:10.1016/j.jvolgeores.2007.08.011.

Andrew, R., Gudmundsson, A., 2008. Volcanoes as elastic inclusions: Their effects on the propagation of dykes, volcanic fissures, and volcanic zones in Iceland. Journal of Volcanology and Geothermal Research, 177, 1045–1054.

Bardintzeff, J., Deniel, H. Guillou, B. Platevoet, P. Télouk, Oun, K., 2012. Miocene to recent alkaline volcanism between Al Haruj and Waw an Namous (southern Libya) Int. Journal of African Earth Sciences, 101, 1047–1063.

Barnett, Z., Gudmundsson, A. 2014. Numerical modelling of dykes deflected into sills to form a magma chamber. Journal of Volcanology and Geothermal Research 281, 1–11.

Begg, G. Griffin, W., Natapov, L., O'Reilly, S., Grand, S., O'Neill, C., Hronsky, J., Djomani, Y., Swain, C., Deen, T., Bowden, P., 2009. The lithospheric architecture of Africa: Seismic tomography, mantle petrology, and tectonic evolution. Geosphere, Geological Society of America. 5 23–50.

Browning, J., Gudmundsson, A., 2015. Caldera faults capture and deflect inclined sheets: an alternative mechanism of ring dike formation. Bulletin of Volcanology, 77: 4DOI 10.1007/s00445-014-0889-4.

Browning, J., Meredith, P., Gudmundsson, A. 20016. Cooling-dominated cracking in thermally stressed volcanic rocks. Geophysical Research Letters 43, doi:10.1002/2016GL070532

Burke, K., 1996. The African plate, South African. The Journal of Geology. 99, 341–409.

Burov, E., Guillou-Frottier, L., 1999. Thermomechanical behaviour of large ash flow calderas. Journal of Geophysical Research, 104, 23081–23109.

Busrewil, M. Oun, K., 1991. Geochemistry of the Tertiary alkaline rocks of Jabal al Hasawinah, west central Libya. Third Symposium on the Geology of Libya, (eds. M.J. Salem and M.T. Busrewiland A.M. Ben Ashour), Elsevier, Amsterdam, 7, 2587–2598.

Chen N., Dong J. Chen, J., Dong C., Shen, Z., 2014. Geometry and emplacement of the Late Cretaceous mafic dyke swarms on the islands in Zhejiang Province, Southeast China: Insights from high-resolution satellite images, Journal of Asian Earth Sciences, 7, 302–311.

Cole, J., Milner, D., Spinks, K. 2005. Calderas and caldera structures: a review. Earth-Science Reviews, 69, 1-26.

Cloetingh, S., Van Wees, J., 2005. Strength reversal in Europe's intraplate lithosphere: Transition from basin inversion to lithospheric folding: Geology, 33, 285–288.

Deb, D.,2009. Finite Elment Method, (Concepts and Applications in Geomchanics). New Delhi. 2nd edition, p. 269.

Deniel, C., Vincent, P., Beauvilain, A., Gourgaud, A. 2015. The Cenozoic volcanic province of Tibesti (Sahara of Chad): major units, chronology, and structural features. Bulletin of Volcanology.

Drury, S., 2001. Image Interpretation in Geology. Blackwell Science, Nelson Thornes, UK, p. 290.

Ebinger, C., Sleep N.1998. Cenozoic magmatism throughout East Africa resulting from impact of a single plume. Nature, 395, 1788–1791.

El–Makhrouf, A. 1988. Tectonic interpretation of Jabal Eghei area and its regional application to Tibesti orogenic belt, South Central Libya. Journal of African Earth Sciences, 7. 945–967.

Elshaafi, A., Gudmundsson, A., 2016. Volcano-tectonics of the Al Haruj Volcanic Province, Central Libya, Journal of Volcanology and Geothermal Research. 325, 189–202.

Elshaafi, A., Gudmundsson, A., 2017. Distribution and size of lava shields on the Al Haruj al Aswad and the Al Haruj al Abyad Volcanic Systems, Central Libya (accepted), Journal of Volcanology and Geothermal Research.

Folch, A., Marti, J., 2004. Geometrical and mechanical constraints on the formation of ring-fault calderas. Earth and Planetary Science Letters, 221, 215–225.

Francis, P., 1993. Volcanoes: a Planetary Perspective. Oxford University Press, Oxford.

Lipman, P.W. 2000. Calderas. In: Sigurdsson, H. (ed) Encyclopedia of Volcanoes. Academic Press, San Francisco, 643–662.

Gautneb, H., Gudmundsson, A., Oskarsson, N., 1989. Structure, petrochemistry, and evolution of a sheet swarm in an Icelandic central volcano. Geological Magazine, 126, 659-673.

Ghanoush, H., Imber, J., McCaffrey, K., 2014. Cenozoic Subsidence and Lithospheric Stretching Deformation of the Ajdabiya Trough Area, Northeast Sirt Basin, Libya. AAPG 2014 Annual Convention and Exhibition, Houston, Texas.

Goudarzi, G., 1980. Structure – Libya. In : The Geology of Libya (eds.) Salem, M. J., and Busrewil, M. T., London Academic press, 3, 879– 892.

Gourgaud, A. Vincent, P. 2004. Petrology of two continental alkaline intraplate series at Emi Koussi volcano, Tibesti, Chad. Journal of Volcanology and Geothermal Research, 129, 261–290.

Gray, J., Monaghan, J., 2004. Numerical modelling of stress fields and fracture around magma chambers. Journal of Volcanology and Geothermal Research, 135, 259–283.

Gudmundsson, A.,1990. Emplacement of dikes, sills, and crustal magma chambers at divergent plate boundaries. Tectonophysics, 176, 257–275.

Gudmudsson, A., Marti, J., Elisenda, T., 1997. Stresses fields generating ring faults in volcanoes. Geophysical Research Letters, 24, 1559–1562.

Gudmundsson, A., 1998. Formation and development of normal-fault calderas and the initiation of large explosive eruptions. Bulletin of Volcanology, 60, 160–170.

Gudmundsson, A., 2000. Dynamics of volcanic systems in Iceland: example of tectonism and volcanism at juxtaposed hot spot and mid-ocean ridge systems. Annual Review of Earth and Planetary Sciences, 28, 107–140.

Gudmundsson, A., 2007. Conceptual and numerical models of ring-fault formation. Journal of Volcanology and Geothermal Research, 164, 142–160.

Gudmundsson, A., 2008. Magma-chamber geometry, fluid transport, local stresses, and rock behaviour during collapse-caldera formation. In: Gottsmann, J., Marti, J. (Eds.), Caldera Volcanism: Analysis, Modelling and Response. Developments in Volcanology,10. Elsevier, Amsterdam, p. 313–349.

Gudmundsson A., 2011. Rock fractures in geological processes. Cambridge University Press, Cambridge. doi: 10.1017/ CBO9780511975684. p. 592.

Gudmundsson, A., 2012. Magma chambers: formation, local stresses, excess pressures, and compartments. Journal of Volcanology and Geothermal Research , 237–238: 19–41.

Gudmundsson, A., 2014. Elastic energy release in great earthquakes and eruptions. Frontiers in Earth Science. 1–11. doi: 10.3389/feart.2014.00010.

Gudmundsson, A., 2015. Collapse-driven large eruptions. Journal of Volcanology and Geothermal Research, 304, 1–10.

Gudmundsson, A., 2016. The mechanics of large eruptions. Earth-Science Reviews, 163, 72–93.

Gudmundsson, A., Nilsen, K. 2006. Ring faults in composite volcanoes: structures, models, and stress fields associated with their formation. In: De Natale, G., Kilburn, C., Troise, C. (eds), Mechanisms of Activity and Unrest at Large Calderas. Geological Society London Special Publications, 269, p. 83-108.

Gumati, Y., Schamel, S., 1988. Therma maturation history of the Sirte Basin, Libya: Journal of Petroleum Geology, 11, 205–218.

Haimson, B. Rummel, F., 1982. Hydrofracturing stress measurements in the Iceland research drilling project drill hole at Reydarfjordur, Iceland. Journal of Geophysical Research, 87, 6631–6649.

Henk, A., Fischer, K., Kromuller, K., Wanger, D., Winter, I., 2013.Prediction of Tectonic Stresses and Fracture Networks with Geomechanical Reservoir Models. DGMK-Research Report 721. German Society for Petroleum and Coal Science and Technology, p. 216.

Hickey, J., Gottsmann, J., 2014. Benchmarking and developing numerical Finite Element models of volcanic deformation. Journal of Volcanology and Geothermal Research, 280, 126–130.

Kanamori, H., 1977. The energy release in great earthquakes. Journal of Geophysical Research, 82, 2981–2987.

Kanamori, H., Anderson, D., 1975. Theoretical basis for some empirical relations in seismology. Bulletin of the Seismological Society of America, 65, 1073-1095.

Karaoğlu, Ö. Özdemir, Y., Tolluoğlu, AÜ., Karabıyıkoğlu, M., Köse, O., Froger, JL. 2005. Stratigraphy of the volcanic products around Nemrut Caldera: implications for reconstruction of the Caldera Formation. Turkish Journal of Earth Sciences, 14, 123–143.

Karaoğlu, Ö., Browning, J., Bazargan, M., Gudmundsson, A.. 2016. Numerical modelling of triple-junction tectonics at Karlıova, Eastern Turkey, with implications for regional magma transport. Earth and Planetary Science Letters, 452, 152–170.

Karaoğlu, O. Elshaafi, A., Salah, M., Browning, J., Gudmundsson, A., 2017. Large-volume lava flows fed by a deep magmatic reservoir atAğrı Dağı (Ararat) volcano, Eastern Turkey. Bulletin of Volcanology. 1–16.

Keppie, J., Dostal, J., Murphy, J., 2011. Complex geometry of the Cenozoic magma plumbing system in the central Sahara, NW Africa. International Geology Review. 53, 1576-1592.

Klitzch, E., 2000. The structural development of the Murzuq and Kufra basins significance for oil and mineral exploration, In: Sola, M. A. and Worsley, D. (Ed.). Geological exploration of the Murzuq basin. Elsevier, Amsterdam, 143-150.

Komuro, H., 1986. Experiments on cauldron formation: a polygonal cauldron and ring fractures. Journal of Volcanology and Geothermal Research. 31, 139–149.

Krassilnikov, S., Head, W., 2004. Calderas on Venus and Earth: comparison and models of formation. Lunar and Planetary Science, 35, 1531.

Kusumoto, S., Geshi, N., Gudmundsson, A., 2013. Aspect ratios and magma overpressures of non-feeder dikes observed in the Miyake-jima volcano (Japan), and fracture toughness of its upper part. Geophysical Research Letters, 40, 1–5, http://dx.doi.org/10.1002/grl.50284.

Less, G., Turki, S. , Suwesi, S., Peregi, L. , Koloszar, L., Kalmar, J., Sherif, K., Csaszar, G., Gulasci, Z., Dalum, H., Al Tajuri, A., 2006. Explanatory Booklet. Geological Map of Libya 1 : 250.000. Sheet : Waw Al Kabir NG 33- 12. Industrial Research Centre, p. 295.

Liégeois J., Benhallou, A., Azzouni-Sekkal, A., Yahiaoui, R., Bonin, B. 2005. The Hoggar swell and volcanism: reactivation of the

Precambrian Tuareg shield during Alpine convergence and West African Cenozoic volcanism. In: Foulger GR, Natland JH, Presnall DC, Anderson DL (eds) Plates, Plumes, and Paradigms, Special Papers - Geological Society of America, 388, 379–400.

Lipman, P. 1984. The roots of ash flow calderas in western North America: windows into the tops of granitic batholiths. Journal of Geophysical Research, 89, 8801–8841.

Malin, M. 1977. Comparison of volcanic features of Elysium (Mars) and Tibesti (Earth). Geological Society of America Bulletin, 88, 908–919.

Marti, J., Ablay, G., Reshaw, T., Sparks, J. 1994. Experimental studies of collapse calderas. Geological Society, London, Special Publications, 151, 919–929.

Marti, J., Gudmundsson, A. 2000. The Las CanÄadas caldera (Tenerife, Canary Islands): an overlapping collapse caldera generated by magma-chamber migration. Journal of Volcanology and Geothermal Research, 103, 161–173.

Mohamed, M., 2014. Composition and age of Cenozoic volcanism in Libya. PhD thesis. University of Glasgow. Glasgow Theses Service.

Newhall, C., Dzurisin, D., 1988. Historical Unrest of Large Calderas of the World. U.S. Geological Survey Bulletin, 2, p. 1108.

Nixon, S., Maclennan, J., White, N., 2011. Intra-plate magmatism of the Al Haruj Volcanic Field, Libya. Goldschmidt Conference Abstracts.

Peregi, Z., Less, G., Konrad, G., Fodor, L., Gulacsi, Z., Gyalog, L., Turki, S., Suwesi, S., Sherif, Kh., Dalub, H., 2003. Explanatory Booklet. Geological Map of Libya 1: 250.000. Sheet: Al Haruj Al Abyad NG 33-8. Industrial Research Centre, Tripoli, p. 248.

Permenter, J., Oppenheimer, C.2007. Volcanoes of the Tibesti massif (Chad, northern Africa). Bulletin of Volcanology, 69, 609–626.

Radebaugh, J., Keszthelyi, L.P., McEwen, A.S., Turtle, E.P., Jaeger, W., Milazzo, M., 2001. Paterae on Io: a new type of volcanic caldera? Journal of Geophysical Research, 106, 33005-33020.

Radivojević, M., Toljić, M., Turki, S., Bojić, Z., Šarić, K., Cvetković, V., 2015. Neogene to Quaternary basalts of the Jabal Eghei (Nuqay) area (south Libya): Two distinct volcanic events or continuous volcanism with gradual shift in magma composition? Journal of Volcanology and Geothermal Research, 293, 57–74.

Rajesh, M., 2004. Application of remote sensing and GIS in mineral resource mapping an overview. Journal of Mineralogical and Petrological Sciences, 99, 83–103.

Schäfer K, Kraft K., Häusler, H., Erdmann, J. 1980. In situ stresses and palaeostresses in Libya. In: Salem MJ, Busrewil MT (eds) The geology of Libya. Academic Press, London, 3, 907–922.

Scholz, C., 1990. The Mechanics of Earthquakes and Faulting. Cambridge University Press, Cambridge.

Tibaldi, A., 2015. Structure of volcano plumbing systems: A review of multi-parametric effects. Journal of Volcanology and Geothermal Research, 298, 85–135. http://dx.doi.org/10.1016/j.jvolgeores.2015.03.023.

Upton, B., 2004. Volcanoes and the Making of Scotland. Dunedin Acad. Press, Edinburgh.

Vail, J., 1971. Dikes swarms and volcanic activity in Northeastern Africa. In : (ed.) Gray, C. Faculty of Science University of Libya, Tripoli. 341– 47.

Vincent, P. 1960. Dynamismes et structures des volcans rhyolitiques du Tibesti occidental et central. Rev Geogr Phys Geol 2, 229–237.

Vincent, P.1963. Les volcans tertiaires et quaternaires du Tibesti occidental et central (Sahara du Tchad). Mémoires BRGM 23. Thesis 1st part, University of Paris.

Vincent P. 1970. The evolution of the Tibesti volcanic province, eastern Sahara. In: Clifford TN, Gass IG (eds) African magmatism and tectonics. Oliver and Boyd, Edinburgh, 301–319.

Wacrenier P, Hudeley H, Vincent P. 1958. Notice explicative de la carte géologique provisoire du Borkou-Ennedi-Tibesti au 1:1,000,000e. Direction des mines et de la géologie AEF, Brazaville.

Walker, G., 1984. Down sag calderas, ring faults, caldera sizes, and incremental caldera growth. Journal of Geophysical Research, 89, 8407–8416.

Wienecke, S., Stadtler, C., 2014. Asep+d method: identifying anomalous areas of the earth's lower crust, Publication number EP 2791713 A1, Patents.

Williams, H., McBirney, A., 1979. Volcanology. W.H. Freeman, New York.

Wilson, M., Guiraud., R., 1998. Late Permian to Recent magmatic activity on the African-Arabian margin of Tethys, in D. S. Macgregor, R. T. J. Moody, and D. D. Clark-Lowes, eds., Petroleum geology of North Africa: Geological Society (London) Special Publication, 132, 231–263.

Woller, F., Fediuk, F. 1980. Volcanic rocks of Jabal as Sawda. In: Salem, M.J., Busrewil,M.T. (Eds.), The Geology of Libya III. Academic Press, London, 3 1081–1093.

Chapter 10: Discussion and critical evaluation

10.1 Evaluation the pre-existing fracture zones and magmatic overpressure

Although considerable attention has been focused on the AHVP in the last few decades (e.g., Busrewil and Wadsworth, 1980; Busrewil and Suwesi, 1993; Peregi et al., 2003; Less et al., 2006; Cvetkovic et al., 2010, Nixon et al., 2011; Bardintzeff et al., 2012; Busrewil, 2012; Mohamed, 2014), the volcano-tectonic aspects along with mechanism of lava flow fields emplacement are still poorly documented and understood. Some studies, however, of the Al Haruj Volcanic Province (AHVP) have suggested the magma migrated partly along crustal fractures (e.g., Klitzsch, 2000; Less et al., 2006) but the exact process of magma channelling along such weakness has not been evaluated. In chapter 5 (Elshaafi and Gudmundsson, 2016) we have offered the first detailed volcano-tectonics study in this region for constraining why and how magma reaches the surface in the AHVP, and what is the relation between the volcanic activity in AHVP and the tectonic activity in the nearby Sirt Basin.

It is well known that pre-existing fractures can significantly influence magma propagation where dykes use partly pre-existing structures, primarily joints but sometimes high-angle (primarily normal) faults, to form their paths (Delaney et al., 1986; Valentine and Krogh, 2006; Bedard et al., 2012; Schofield et al., 2012; Magee et al., 2013; McClay et al., 2013;; Tibaldi, 2015; Browning and Gudmundsson, 2015, Maccaferri et a., 2014; 2015). For example, late Cretaceous basaltic rocks within the Nubain clastics in Al Hameimat trough, NE Sirt Basin, were firmly controlled by pre-existing extensional faults that most likely have used high angle normal faults as magma paths (Busrewil et al., 2012). In addition, McClay et al. (2013) inferred from two-dimensional and three-dimensional well-images seismic

data in the Carnarvon Basin, NW Shelf, Australia, that some dykes partly used the pre-existing Jurassic – early Cretaceous extensional faults as channels where normal faults are strongly controlled on the morphologies of the dykes in this rifting basin. We considered the interaction between a mechanically fault and a propagating dyke using numerical approach where the fault zone modelled as stiff core and soft damage subzones on either side of the core. Our results infer that steeply normal dipping faults may capture propagating dykes of a while and perform as parts of their paths in the uppermost of the Earth's crust. Field observations generally confirm this conclusion where alignments eruptive vents or row cones show the dominating strike of volcanic fissures/feeder-dykes as the WNW–ESE to NW–SE, coinciding with the orientation of one of main fracture/fault zones in the Sirt Basin.

The magmatic overpressure along the dyke is inversely proportional to Young's modulus and the strike dimension of dyke while it is directly proportional to the width or thickness of dyke (cf. Gudmundsson, 1990). In fact, the thickness and magmatic overpressure is lesser close to the causative source than at the surface of the Earth's crust. Therefore, the strike dimension of dyke appears to increase with depth in the crust in order to maintain the volume rate of magma flow at the lower portion of the dyke equal to that in the upper portion (Fig. 10.1) (White, 1974; Gudmundsson, 1990; 2011). The strike dimension of dyke may thus be much longer at the top of the magma reservoir than at higher crustal levels (Fig. 10.1).

The lack of subsurface data and deeply exposure areas at the AHVP makes difficultly in measuring thickness and length of dykes at depth. We, therefore, have taken average dyke (length/width) ratio at the surface to approximately estimate magmatic overpressure, assumed its constant along the length (dip dimension) of the dyke at any particular depth below the surface, at the time of formation of the dyke. The maximum thickness of dyke is taken as the average measured thickness. The uncertainties or errors in our

measurements are estimated at 10 ±5% based on measured dimensions of some dykes and volcanic fissures in the field which were then compared with measurements from satellite imagery. The average dyke (length/thickness) ratio of 421 indicates approximately magmatic overpressures during the associated fissure eruptions of 8–19 MPa (depending on host-rock elastic properties). These results are very rational and similar to those obtained from basaltic dykes in other volcanic fields.

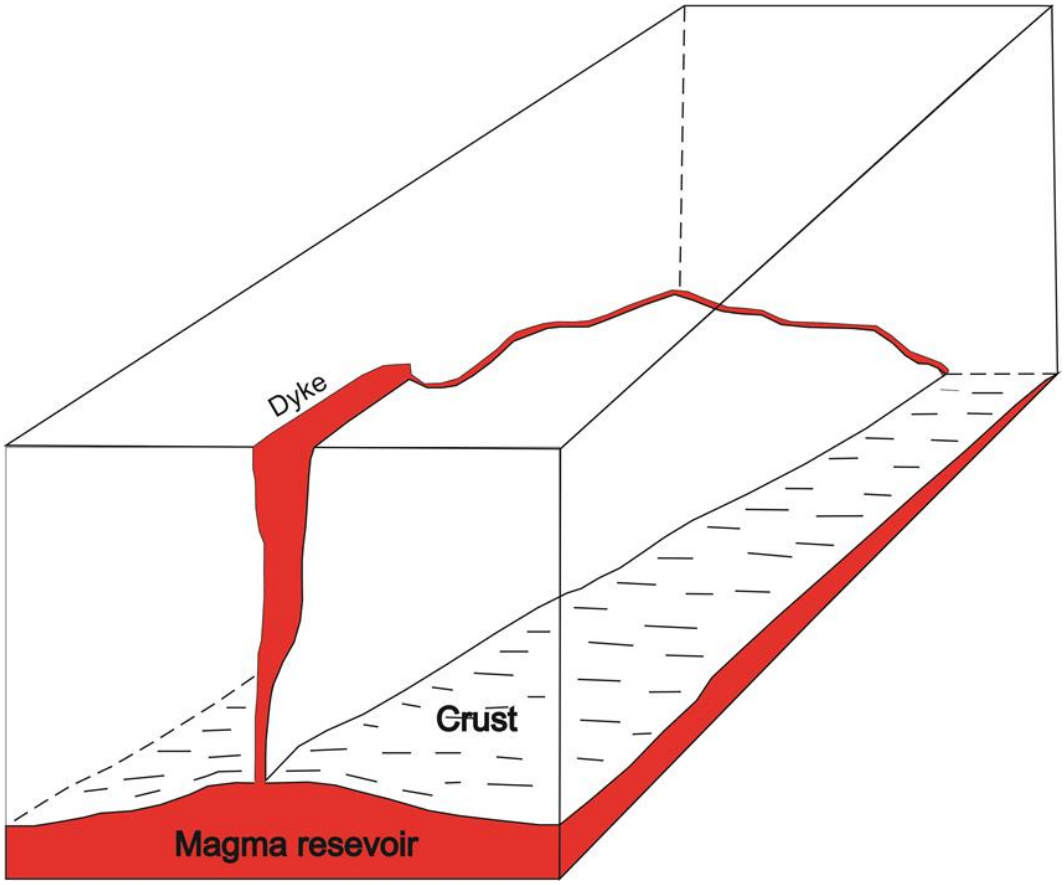

Figure 10.1. Schematic diagram showing the strike dimension of dyke increases with depth in the crust while the thickness decreases. Dyke should be much longer at the top of the causative source than at the surface of the volcanic pile. The thickness of dyke is exaggerated much many times in order to explain the variation along the dip of dyke. Not to scale (modified from Gudmundsson, 1990).

The percentage of feeder-dykes, however, is very low compared with arrested or deflected dykes (non-feeder dykes) at various levels within the Earth's crust on basis of the seismological data in Hawaii (Chastin and Main,

2003) and extensive field observations of eroded rift zones, such as in Iceland, where at any particular dyke swarm increases with depth below initial surface (Torfason, 1979; Gudmundsson and Philipp, 2006). The numerical approach used during this study to understand better how arrest or deflect of dyke can take place concerning the three main arrest mechanisms.

10.2 Assessment the size and geometry of magma reservoirs

Despite initially the AHVP appearing as a single volcanic system, based on the geographical-geomorphological criteria and the thickness of basaltic sequence to be composed of two different paleo-volcanic systems (e.g., Peregi et al., 2003). One of the results of Chapter 6 (Elshaafi and Gudmundsson, 2017) supports this division since the AHVP consists actually of double volcanic systems rather than single volcanic system based on the volcanoes density map. The density distribution of 432 monogenetic volcanoes in the AHVP plotted as eruption points. There are several key points of information which are included through the construction of the density eruptions map. The maxima values of eruption points density do not exactly correspond to those with more dots (eruption points) owing to the point density map calculate the density of features around each output raster cell as the number of points that fall within a circular neighbourhood (Silverman, 1986). A neighbourhood is defined around each raster cell centre, and the cumulative number of points that fall within the neighbourhood is calculated and divided by the area of the neighbourhood (Silverman, 1986). During this study, we assume that the radius of a circular neighbourhood is 40 km to highlight the crustal-scale distribution of eruption sites/monogenetic volcanoes, and output raster cell size of 1 km (Lesti et al., 2008). Large values of radius either 40 km or 35 km produce a more generalised density raster and do not change effectively the calculated density values. Because of more points will fall inside the larger neighbourhood, and this number will be divided by a larger area when calculating the density. The main effect of a larger radius is that density is

calculated using a larger number of points. The absolute values for volcanoes for each class can be obtained by multiply density (km^{-2}) for each bin in the area of a circular neighbourhood.

The rough elliptical surface expression of the distribution of eruption points in the density map can be taken as an indication of an ellipsoidal geometry of the magma reservoirs beneath the AHVP. This conclusion derives from extensive field observations since volcanic systems tend to reveal the plan view geometries of the source magma reservoirs due to stress-concentration considerations (Gudmundsson, 2000, 2016). More specifically the density maps of the monogenetic volcanoes used to estimate the lateral cross-sectional area of the associated source magma reservoirs. We do not have any other means of estimated the sizes or areas of the magma reservoirs since they have not generated large collapse calderas and detailed geophysical studies are lacking. The size distribution of the lava shields follows from the measurements made and relates to the volumes that the associated reservoirs are able to erupt. The term lava shield is used here so as to avoid confusion with larger polygenetic shield volcanoes (central volcanoes) in many regions such as and Galapagos and Hawaii.

Comparison lava shields with the size distribution of similar volcanoes in other and much better known areas such as Iceland is to improve our understanding the volcanism in Libya. The coefficient of determination between AHVP and Iceland is very high and that the lava shields from Iceland and Libya have similar scaling laws, even if the Icelandic lava shields range more widely regarding of areas and volumes. These indicate similarities in eruptive mechanisms and aspect (volume/area) ratios. Simple model was used in the present study to estimate crudely volumes of lava shields, and the error involved in assuming the lava shields to be cone-shaped takes into account that they are flat near the margins/edges and commonly much steeper near the centre – the cone part, but regard this approach as the most appropriate for the present study.

Basaltic volcanism in an ordinary poroelastic eruption commonly much less than 0.1% of the magma in a reservoir can flow out of it with the potential of forming dyke and a lava flow. Therefore, very much larger poroelastic reservoir is needed than the volumes of individual lava flows or lava shields (cf. Gudmundsson, 2016). Due to the much different sizes of the reservoirs the amount of magma derived from the northern part, Al Haruj al Aswad Volcanic System, is an order of a magnitude larger than that produced by the southern part, Al Haruj al Abyad Volcanic System (Fig. 10.2a). Because of uncertainty about individual volcanic eruptions in the AHVP, we have made two assumptions to estimate bulk volumes and thicknesses of magma reservoirs that supplied magma to the eruptions of the AHVP. The estimated areas and volumes of the reservoirs, however, are based on various mechanical simplifications and approximations and will doubtless have to be refined and worked out in greater detail in the light of seismic, magnetotelluric and gravity studies.

The results of numerical approaches indicate that the maximum principal tensile stresses concentrate around the lateral ends of the magma reservoir after the gradually released of compressive stress at the bottom of crust owing to late Miocene uplifted. Hence the initial dykes for early lava shields are most likely injected from margins of magma reservoir rather than central parts (Fig. 10.2a). This conclusion is supported by the geographical distribution of the lava shields. There is a clear likelihood for late Miocene–Pliocene lava shields to be situated near the peripherals of both volcanic systems, that is, roughly above the margins of the magma reservoirs. There are many examples around the world support this phenomenon such as lava shields in Iceland (Andrew and Gudmundsson, 2007).

We have also applied the same analytical and numerical techniques for estimating the volume of the magma reservoir supplying each individual basaltic volcanic eruption and association local stress field around source magma reservoir at Ağrı Dağı stratovolcano, Eastern Turkey (Appendix C).

We calculated the total injected materials for two of the most recent basaltic eruptions at this volcanic pile. The erupted materials of Lava flow I are around 3.2 km^3 while the lava flow II is around 0.6 km^3. Massive eruptions from the Ararat volcano complex potentially pose a risk to the population of Eastern Turkey and hence understanding these volcanic systems is important.

It is abnormal for stratovolcanoes to produce large volume effusive eruptions without an element of local volcano-tectonic forcing (e.g., subsidence of collapse caldera and graben). Therefore, this study integrated different data (analytical, numerical models, seismic tomographic images along with some geochemical data) in order to better understanding the conditions that triggered the emplacement large two basaltic lava flows at Ağrı Dağı (Ararat) volcano in the absence of volcano-tectonic forcing. We propose two scenarios to clarify the difference in volume of two basaltic lava flows. One scenario is that the absolute reservoir volume decreased between the two eruptions. This is possible, but not very likely since the likely time between the eruptions is not very large in comparison with the lifetimes of large reservoirs. The second scenario includes reservoir compartments. Future field investigations will be needed to provide robust petrology and geochemistry for various volcanic flows. This study may be encouraging further research of this interesting stratovolcano particularly which is located near inhabitant area and consequently may raise a significant risk as already mentioned.

10.3 Mechanical interaction due to magma reservoir, their effects on propagation of fractures

The magma reservoirs in the upper mantle, at its contact with the crust, can live several million years or more. So that they are considered as concentrate stresses and hence the potential for mechanical or stress

interaction between the nearby magma reservoirs, particularly when located away from plate boundaries as in the Libya's magmatism. New high-resolution geochronology for the main volcanic provinces in Libya conclude that volcanism in Libya was to a degree simultaneous, that is, overlapped, during certain periods of time. Chapter 8 presents new data on volcanic eruption centres and combines this data with a suite of finite element numerical models in order to infer the relative location of magma reservoirs and resultant stress concentration in Libyan territory. The spatial distributions of monogenetic volcanoes (lava shield, spatter cones, scoria cone and maars) within the four principal volcanic provinces of Libya are examined and presented on a density map (radius of a circular neighbouring 35 km). The results show that there are obviously six main volcanic clusters, each of which is regarded as a volcanic system. The magma reservoir beneath each volcanic system was assumed as totally molten, therefore, the Young's modulus is zero and the inclusion reduces to a hole, when modelled as a two-dimensional and three-dimensional structure.

The magma reservoirs assumed at around 35 km and that this depth corresponds roughly to the crust-mantle boundary in the central Libya (Ghanoush et al., 2014; Lemnifi et al., 2017). This depth also is largely consistent with many earthquakes that occurred in Libya during the past century have depths between 30 km and 35 km (Al-Heety, 2013) as well as fractional crystallization of the primitive magmas at the AHVP is also thought to have occurred at similar depths, namely in reservoirs at depths of 25-39 km (Nixon et al., 2011). Numerical model results show strong stress interaction between the magma reservoirs. More specifically, stress concentration zones and trajectories of maximum compressive stress between nearby volcanic systems may encourage simultaneous volcanic and tectonic events, seismogenic faulting, and dyke sharing between volcanic systems. The model stress concentration zones agree well with the distribution of the major faults and more recent eruptions. Seismic events in Hun Graben (e.g. M7.1, on April/1935) area may have been related to dyke

propagation that eventually became arrested and thus did not result in an eruption.

Currently and first of its kind geophysical study in Libyan territory by Lemnifi et al. (2017) who have used receiver function constraints (RFs) from data obtained from recent available broadband seismic stations; fifteen seismic stations belonging to the Libyan Center for Remote Sensing and Space Science and three seismic stations publically. This study inferred that the observed high Vp/Vs (κ) ratios of 1.91 at one station located in the As Sawda Volcanic Province. It is indicated the presence of partial melt at the crust-mantle boundary (≈35 km) (Lemnifi et al., 2017). Additionally, modern age dating at the Al Haruj Volcanic province concludes that the volcanism in this region continued until recent time and magmatic differentiation took place at 25-39 km (Nixon et al., 2011). If magma occupies beneath Libyan territory in reservoirs, as seen in the suite of numerical models during this study, then the volcanic systems may pose significant earthquakes and volcanic risks. Further geophysical studies are still needed in the future in order to obtain better constraints on the deep structure of the lithosphere beneath this region.

10.4 Future volcano-tectonic activity

The northernmost part of the AHVP seems to be very recent based on the latest precise age determinations along with excellent preservation of tumuli and lava rise plateaus (chapter 7). Thus it is likely that the AHVP has still the potential to erupt, that is, is still active. A major problem for the seismicity studies of Libya in the past decades was the absence of any extensive seismological network until 2005 at which time the first Libyan seismological network was established (Al-Heety, 2013). Lemnifi et al. (2017) have used data collection from 2005 to 2009 and that allowed deducing in much greater detail than has been possible before the depth of Moho in various parts of

Libya and the origin of the partial melt beneath central Libya as mentioned previously.

However, information on historical earthquakes has been collected, and some of these recorded earthquakes may be associated with magmatism. For instance, earthquake swarms have been reordered in Hun Graben, with earthquake magnitudes >M7.1 in 1935 and > M6 in 1939, 1940, 2000 and 2001, respectively (Hassen, 1983; Al-Heety, 2013). In addition, the Gharyan area appears to be seismically active; a seismometer in the Gharyan region, southwest Tripoli, operated for six hours in 1977 and during this time recorded three moderate earthquakes (Kebeasy 1980; Suleiman and Doser, 1995). Earthquake swarms in volcanic regions are commonly related to magma migration (Bagnardi, 2014) and could be so in these cases as well. Since the Hun Graben extends to the AHVP, the earthquake swarms, at least some of them, may be related to active magma migration beneath or close to the AHVP. Also, earthquakes on active faults are commonly triggered by high fluid pressure. If some of the faults are used as paths for magma in AHVP, the magmatic pressure along the faults would tend to trigger slip on the faults and earthquakes (cf. Bagnardi, 2014). It is well-known that dyke-induced seismicity can be utilised to detect the location of the intrusion and assess whether the dyke is most likely to erupt in a certain region (Maccaferri et al., 2015). All these will become a well-established in the next years as the new seismic network in Libya collects more earthquake data. Meanwhile, it is not yet well defined; it appears likely that Libya volcanism at least in the central part is potentially volcanically and tectonically active.

10.5 Emplacement and inflation of lava flow field

Detailed analyses of tumuli and lava rise plateaus using field observations, and remote sensing data provide an understanding mechanism emplacement of the Al-Halaq al Kabir lava flow field. Endogenous growth beneath insulating lava crust played a significant role in the emplacement of Holocene basaltic lava flows in central part of the AHVP. Tumuli, lava rise plateaus, lava rise pits and inflation clefts were formed by this mechanism, display certain diagnostic characteristics that are an indication of their emplacement mode. These inflation structures largely vary in their shape and size through the distance from the vent system to middle and distal parts and seem to be mainly influenced by paleo-topography and the effusion rate as well as lavas composition. There are a number of preferred path ways recognised on the satellite imagery and in the field that may be used pre-existing drainage pattern to drain out lava lakes.

Few previous studies (e.g., Rossi, 1999; Glaze et al., 2005) have been used the spatial and temporal distribution of inflation features on lava flow surfaces in a statistical technique. Therefore, the statistical quantitative analyses are used in the present work to infer that the tumuli and lava rise plateaus on the surface of the Al-Halaq al Kabir clearly follow a power-law distribution, and there also are strong relationship between width (minimum diameter) and length (maximum diameter) in plan-view of various tumuli and lava rise plateaus with correlation coefficient (R^2) 0.70. In addition, scaling exponents results indcate that the lava inflation structures are likely to be influenced by pre-existing topographic together with effusion rate variability, and the result in distributions of tumuli and lava rise plateaus. The tumulus ridges seem to be controlled by pre-existing channels or valleys to form elongated tumuli as more stable distribution pathways developed whereas smaller lengths represent localised or stationary inflation. Tumuli and lava rise plateaus populations may be divided into subpopulations according to the abrupt change in the scaling exponents, ranging from D= 0.37 to 3.07 for tumuli and

ranging from D= 0.363 to 3.56 for lava rises. The spatial distributions of tumuli and lava rises can be linked to network of lava transport beneath an insulating crust (Glaze et al, 2005).

Glaze et al. (2005) have utilised Poisson probability distribution in order to study the distribution in the space of tumuli and lava rise plateaus on lava flow fields in Hawaii, Iceland and on Mars in order to connect between these inflation structures and subsurface endogenous growth processes. They inferred that the spatial distributions of inflation features are systematically distributed in Iceland whereas randomly distributed in Hawaii and on Mars. The random distribution in the space, consistent with Poison probability distribution, may be generated due to random variations in paleo-topography or small-scale temporary preferred pathways, combined with very low slope. In contrast, the systematic distribution on the surface of lava flow field simply reflect permanent large-scale preferred pathways that led to establish distributary tube systems directly beneath broad lava flow for long-duration (Glaze, et al., 2005). Also the spatial distribution of tumuli and lava rise pleatus on the surface the Al-Halaq al Kabir flow filed is remarkably different from the Poisson distribution on the basis of Glaze, et al. (2005) procedure. There thus may be some systematic manner controlling their occurrence. Tumuli from AHVP are morphologically similar to some Icelandic flow-lobe tumuli, suggesting a similar mechanism of emplacement. The tumuli and lava rise plateaus in Iceland are strongly related to persistent preferred internal pathways that produced a systematic distribution of inflation features. Thus, the tumuli and lava rise plateaus on the surface of flow field in the AHVP are most likely correlated with preferred internal pathways that may be active at different times during the lava flow field emplacement.

Numerical and analytical results demonstrate that the potential tensile stress in the inflated upper crust is an order of a magnitude larger than the actual tensile strength of rocks (around 0.5-6 MPa) (Gudmundsson, 2011). Thus, the tensile strength of the lava crust is not high enough to resist the potential tensile stress during inflation process, so that the crust will fracture, as observed in the field and from satellite imagery. The viscoelastic crust is formed between upper crust and core molten zone and behaves as brittle at 800 - 1070^{o}C (Hon et al., 1994) that most likely has the responsibility to keep lava inside during inflation processes. As mentioned above the AHVP might be still volcanically and seismically active. Consequently, it is of fundamental importance to understand the processes that give rise inflation structures on the AHVP. Such an understanding is essential condition for forecasting and may be applied for understanding remotely sensed observation of lava flows where Mars has large inflation strucutres on their surfaces that morphologically resemble those that exist today on the AHVP (cf. Glaze et al., 2005; De Wet et al., 2014).

The duration to of the Al-Halaq al Kabir lava flow field might be taken several months or even years on the basis of the thickness of the upper vesicular crust of inflated pahohe flow lobes, observed in the field, particularly for large tumulus and lava rise plateau. If the eruption would have taken many years (or decades) so replenishment primitive magma into the deep-seated reservoir could partly contribute to maintaining its excess magmatic pressure at around 5 MPa inside magma reservoir during the eruption (cf. Gudmundsson, 2016). Long-lived volcanic eruptions may be correlated with ecologically catastrophic climate change due to extensive input of volatiles into atmosphere (e.g. Self et al., 1998; Wignall, 2001; Jahren, 2002). Emissions of CO_2 might have induced considerable global warming and SO_2 global cooling if developed over a short interval (Self and Thordarson, 1998; Olsen, 1999). For example, there is a considerable consistency between the great Siberian flood basalts with the Permian-Triassic mass extinction event (Kamo et al., 2003; Pirajno, 2004; Vaillant et al., 2017).

There is apparent coincidence between the age of an initial volcanism in the AHVP and local fauna and flora local extinctions in the As-Sahabi area, NE the Sirt Basin, during Messinian-Zanclean time (≈7 to 5 Ma) (Fig. 7.1) (Boaz, 2009 El-Shawaihdi et al., 2016). In addition, Hounslow et al., (2017) have recently concluded based on high-resolution chronology and magnetostratigraphy of the Neogene deposits in the Fezzan Basin, southwestern of the AHVP, that extremely aridity was taken place at Lake Megafezzan (a giant paleo-lake) after 11 Ma (late Miocene).

The linked between volcanism and a awful environmental impact is still widely under debate in the literature, for example, Burgess et al. (2017) have currently discussed new study published in Nature Communications in order to a new understanding of the role of volcanism in driving extinctions. They also have linked between Large Igneous Provinces (LIPs) and ecologically catastrophic climate, but they argue that the underground magma have triggered abrupt climate warming and mass extinction more effectively than an epic outpouring of lava. Based on Burgess's hypothesis, the thick sequence of sediments in the Sirt Basin (> 4 km) consists mainly of carbon-bearing rocks such as limestone and dolomite. When these carbonate rocks intruded by subvolcanic network of magmas that led to cooking those sediments as well as organic-rich sediments and subsequently largely liberates greenhouse gases (e.g., CO_2 and CH_4). Nevertheless, causes of fauna and flora local extinctions in Sirt Basin remain under debate and poorly understood. Further researches in the AHVP and Libya's volcanism at larger scale should be needed in the future to accurate quantify eruption durations and amount of volatile materials liberated during eruption e.g. using drilling core barrels and other techniques. Such data are also important for predict and assessment hazards of the AHVP.

10.6 Mechanics of caldera collapse and generated new magma chamber

The variety of volcanic products along the Tibesti Volcanic Province (TVP) range from under-saturation basaltic rocks to over-saturation acidic rocks during the late Miocene up through the end of Pleistocene indicate that magma may be comparatively produced from double magma sources. By contrast, the various basaltic rocks of the AHVP from six volcanic phases are a strong genetic relationship and most likely derived from the common parent magma source at a crust-mantle boundary (Fig. 10.2). The volcano-tectonic aspects, eruptive styles and size of eruptive materials of the volcanic provinces contain shallow magma chambers, in addition to deep-seated magma reservoirs, which are more complicated than volcanic provinces have only deeply seated magma reservoirs.

Field observations and numerical model results suggest that basaltic magma at the margins of the TVP may be injected from the deeper magma reservoir at the lower crust whilst the more evolved rhyolite and ignimbrite most likely were derived from shallow crustal magma chamber (Fig. 10.2b). Some basaltic lavas are concentrated along rims of the caldera that seem to be utilized the pre-existing ring-faults/ring-dykes as channels as already discussed in chapter 5 (Elshaafi and Gudmundsson, 2016). The collapse calderas of the TVP are one of the most significant volcano-tectonic features and still poorly documented and understood due to a series of sporadic clashes and conflicts at Libyan – Chadian border for many decades. The present work was built-up on the comprehensive and concise division which was done by Deniel et al. (2015) who have classified the TVP into five main volcanic units based on detailed field relationships, volcanological, geochronological and petrological data. The cross-sectional area of the associated magma chamber at the TVP has been estimated from geometry of the collapse calderas (Marti et al., 1994; Marti and Gudmundsson, 2000;

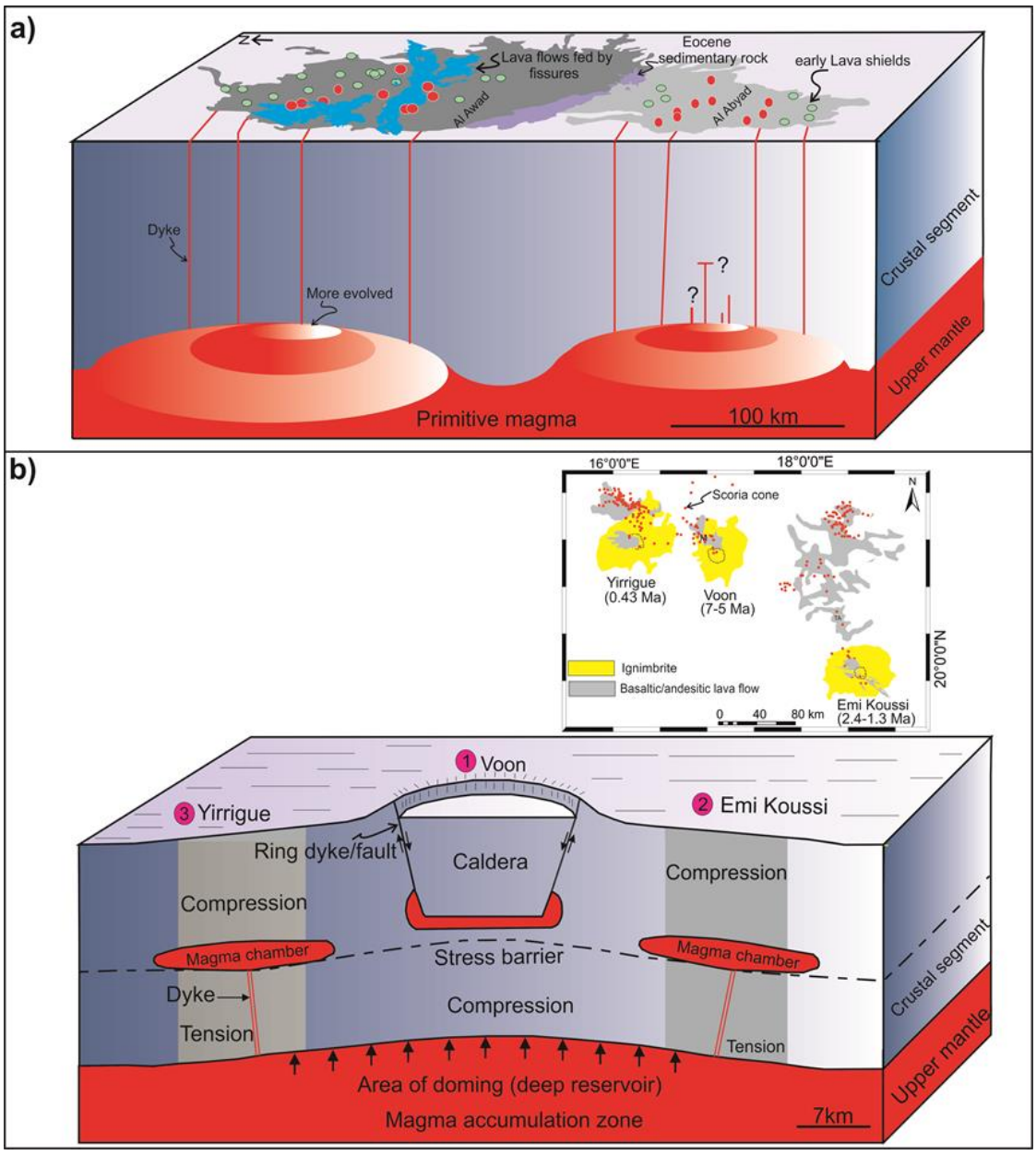

Figure 10.2. Schematic illustrations show the main volcano-tectonic aspects at the AHVP and TVP, respectively. a) The AHVP was fed only by deep-seated magma reservoirs at crust-mantle boundary. The bulk volume magma reservoir of the Al Haruj al Aswad volcanic system, northern portion, is larger than the Al Haruj al Abyad volcanic system, southern portion. Consequently, the much larger amount of injective materials was produced from the northern volcanic system than the southern volcanic system. The boundary between two volcanic systems is marked by older Eocene sedimentary rocks, indicated by purple colour. The initial dykes would be injected from the lateral ends of reservoir then gradually moved toward the central part alongside diminished lava production and more evolved basaltic magma. Some dykes may utilise high angle pre-existing faults partly of their paths in the uppermost of the crust. b) The variations of volcanic product at the TVP indicate that the magma may be comparatively produced from double magma sources rather than single magma reservoir as the AHVP although both these

volcanic provinces are contemporaneous from the late Miocene to Pleistocene and probably into Holocene. The simplified geological map at right corner shows the evolved acidic volcanic rocks that are mainly concentrated at the central part of the province whereas the less evolved basaltic rocks and scoria cones are mostly distributed along peripherals as well as in the central part followed each collapse caldera. The conceptual model shows three collapse calderas respectively that are aligned along pre-existing regional element NW–SE trend. The doming area at the crust-mantle boundary is most likely played an important role in forming collapse caldera as seen in the numerical modelling results. The compressive stress above the central deeper magma reservoir performed as stress barrier and made difficulty for dyke to penetrate and replenish the oldest caldera, Voon (7-5 Ma). Alternatively, the maximum tensile stress on the lateral ends of the deep reservoir is most favourable frequently dyke injection to from new magma chamber; see Chapter 9 for further explanation about caldera collapse and generated new magma chamber.

Acocella, 2007) and depth of magma chamber from initial surface inferred from Tieroko extinct central volcano where assumed this pluton represents the uppermost part of the extinct crustal magma chamber and taking into account the thickness of eroded may be several kilometres (Deniel et al., 2015).

The evolution of the TVP, however, is characterised by constructive episode (8-5 Ma), and consequently destructive episode (5-0.43 Ma) where the constructive period involves accumulation of volcanic materials to form central volcanisms whereas destructive period involves vertical collapse calderas due to volcano-tectonic forcing and produced huge volume of ignimbrites (>100 km^3). The Volcano-tectonic forcing keeps the magmatic excess pressure in the magma chamber until a longer time of the eruption, thereby squeezing out an extraordinarily large fraction of the magma, probably most content of the chamber. By contrast, an ordinary poroelastic eruption as occurred in the AHVP, the excess magmatic pressure in the magma reservoir rapidly reduced and consequently produced less than 0.1% of the bulk volume of the reservoir. It is interesting to note that the basaltic/andesitic lava flows were commonly followed each collapse caldera that would have derived from the former destructive shallow magma

chamber as compartment such as magma mixing and mingling (andesitic-trachyte) of Tousside volcanic complex (100 ka) followed the last collapse Yirrigue caldera (0.43 Ma) or through infrequently dykes injected from deeper magma reservoir.

The numerical approaches with various loadings during this study are greatly improved our understanding the volcano-tectonic evolution and spatial and temporal distribution of the major volcanic units at the TVP. The model of Marti and Gudmundsson, (2000) for overlapping collapse calderas in the Las Canada caldera in Tenerife appears to be applicable for the caldera collapses on the TVP. Therefore, the collapse calderas on the TVP examined in the light of this conceptual model. This model illustrated how and under what stress condition overlapping collapse calderas generated by magma migration. The model also is able to clarify magma chamber migration in a region where a plate is very slowly drifting or stationary as African plate because bending maximum tensile principal stress the location of dyke injection frequently for the significant period rather than a fast drifting plate. Furthermore, the present model explains the lacks or misunderstood in a spatial progression of collapse calderas as raised by Permenter and Oppenheimer (2007). The first collapse caldera, Voon Caldera (7-5 Ma) interpreted as to have initiated in the central TVP, subsequently, caldera migrated to the eastern at Emi Koussi Caldera (2.4-1.3 Ma) then developed to the westernmost part at Yirrigue Caldera (0.43 Ma). Nevertheless, geophysical and volcanology investigations will certainly be needed to further establish the details of the TVP development through better constrain on the shallow magma chambers and volcano-tectonic forcing (ring faults).

Chapter 11: Summary and future work

11.1 Summary

The Al Haruj intra-continental Volcanic Province (AHVP), situated at the southwestern periphery of the Sirt Basin, hosts the most extensive and recent volcanic activity in Libya, covering an area around 42,000 km^2. The AHVP is considered a typical within the plate interior. The northernmost part of the AHVP seems to be very recent based on the latest precise age determinations (cosmogenic ^{3}He exposure) (Nixon et al., 2011), along with excellent preservation of tumuli and lava rise plateaus. Thus it is likely that the AHVP has still the potential to erupt, that is, is still active. Volcanic fissures/crater rows are very common in the AHVP and mostly confined to the central and southernmost part of this region. Comparatively few dykes have been identified, but those that have occur mainly in elongated swarms outside the main volcanic system.

The geometry of the volcanoes may be partly governed by pre-existing fractures and faults; which in turn play a significant role in the spatial distribution of volcanic fissures and dykes in the area. The alignments eruptive vents/crater rows at the AHVP display the dominating strike of volcanic fissures/feeder-dykes as WNW–ESE to NW–SE and NE to NNE, coinciding with the predominate orientations of main pre-existing fracture/fault zones in the Sirt Basin. Preferred numerical models and field observations suggest that some feeder-dykes may have utilised steeply dipping faults, particularly normal faults, as part of their paths to the surface. Thus the various orientations of volcanic fissures are likely to be partly controlled by the directions of pre-existing faults. Despite the great depth of origin of the magma (≈ 35 km) at the AHVP, the magmatic overpressure during the associate fissure eruptions and dyke emplacement of 8–19 MPa

(depending on the Young's modulus of host-rock) which is similar to that of typical regional feeder dykes in many other areas.

One of the findings of this thesis suggests that the AHVP consists of double volcanic systems rather than single volcanic system based on the volcano-density map. The monogenetic volcanoes (lava shields, scoria cones, spatter cones, and maars) in the AHVP form two distinct density groups which are interpreted as separate volcanic systems. Each system is believed to be fed by a deep-seated and very extensive magma reservoir. The density distribution of the volcanoes in each system, plotted as eruption points or sites (a total 432 sites), has a roughly elliptical surface expression, suggesting similar plan-view geometry of the source reservoirs. This conclusion derives from extensive field observations, where volcanic systems tend to reflect the plan view geometries of the source magma reservoirs due to stress-concentration considerations (cf. Gudmundsson, 2000, 2016). From the eruptive volumes and the density distributions of the volcanoes, the bulk volumes of the reservoirs were estimated. Numerical models are used to investigate local variation in the stress field resulting from general doming of the area during the late Miocene, as well as local loading by magma reservoirs, including the effects of various mechanical properties of the crustal layers, so as to explain the variation in the spatial and temporal of the volcanic activity in this part of Libya.

Due to uncertainty to calculate volume of single volcanic eruption in the AHVP, two assumptions have been made to estimate bulk volumes and thicknesses of magma reservoirs that supplied magma to the eruptions. Basaltic volcanism in an ordinary poroelastic eruption commonly much less than (≈ 0.1%) of the magma in a reservoir can flow out of it with the potential of forming dyke and a lava flow. Hence, very much larger poroelastic reservoir is needed than the volumes of individual lava flows or lava shields. The results of numerical approaches indicate that the maximum principal tensile stresses concentrate around the lateral ends of the magma reservoir

at the AHVP after the gradually released of compressive stress at the bottom of crust due to late Miocene uplifted. In turn, the initial dykes for early lava shields are most likely injected from margins of magma reservoir rather than central parts. This conclusion is supported by the geographical distribution of the lava shields. There is a clear likelihood for late Miocene – Pliocene lava shields to be situated near the peripherals of both volcanic systems, that is, roughly above the margins of the magma reservoirs.

The spatial distributions of 831 monogenetic volcanoes (lava shields, scoria cones, spatter cones and maars) within the four principal volcanic provinces of Libya (Gharyan, Sawda, Al Haruj, Nuqay volcanic provinces) are examined and presented on a volcano- density map. The results show that there are evidently six main volcanic clusters, each of which is regarded as a volcanic system. Each volcanic system is thought to have been supplied with magma from a deep-seated reservoir so that an individual magma reservoir may have existed beneath each maximum amount of volcanic cones, most likely at the crust-mantle boundary. The magma reservoir beneath each volcanic system was assumed as totally molten, so that the Young's modulus is zero and the inclusion reduces to a hole, when modelled as two-dimensional and as oblate ellipsoids (penny shaped or sill-like) when modelled as three-dimensional structure. Numerical model results show strong stress interaction between the magma reservoirs. More specifically, stress concentration zones and trajectories of maximum compressive stress between nearby volcanic systems may encourage simultaneous volcanic and tectonic events, seismogenic faulting, and dyke sharing between volcanic systems. The model stress concentration zones agree well with the distribution of the major faults and Holocene eruptions. There are no known eruptions in Libya in historical time, but some, perhaps all, the volcanic systems may have had one or more arrested historical dyke injections. In particular, part of the recurrent seismic events (e.g., M7.1, on April/1935) in the Hun Graben in the northwest Libya may be related to dyke propagation and arrest. If some of the inferred magma reservoirs are still fluid, as is likely, they pose earthquakes and volcanic risks to many parts of Libya.

Detailed analyses of tumuli and lava rises using field observations, and remote sensing data provide an understanding an inflation and emplacement mechanism of the Al-Halaq al Kabir lava flow field, central part of the AHVP. The thickening by endogenous growth seems to be played a significant role in the emplacement of Holocene basaltic lava flow field in the central part of the AHVP. Tumuli and lava rise plateaus, commonly formed by this mechanism, display certain diagnostic characteristics that are an indication of their emplacement mode. Tumuli observed in the area are remarkably similar in morphology, internal structure and aspect (height/width) ratios to the tumuli which have been studied in the distal portions of Icelandic lava flow fields. It suggests that they have been emplaced by an analogous mechanism. The tumuli and lava rise plateaus in Iceland are strongly related to persistent preferred internal pathways that produced a systematic distribution of inflation features (cf. Glaze et al., 2005). Therefore, the tumuli and lava rise plateaus on the surface of flow field in the AHVP are most likely correlated with preferred internal pathways that may be active at different times during the lava flow field emplacement. Furthermore, the alignment of tumuli and lava rise plateaus are clearly discernible in the field and on the satellite imagery which indicate the presence distributary tube systems beneath the upper crust.

The preferred pathways seem to be responsible for thermally efficient lava delivery from the vent system to the distal portion (≈22 km) of the lava flow field in the central part of the AHVP. The paleotopography combined with flux flow rate are the most parameters that may influence the formation of inflation feature. Numerical and analytical results demonstrate that the potential tensile stress in the inflated upper crust is an order of a magnitude larger than the actual tensile strength of rocks. Thus, the tensile strength of the lava crust is not high enough to resist the potential tensile stress during inflation process, so that the crust will fracture, as observed in the field and from satellite imagery. In contrast, the viscoelastic crust played a significant role to keep lava inside during inflation processes.

The Tibesti Volcanic Province (TVP) represents the second largest among the five Gharyan – Tibesti volcanic provinces, covering an area of approximately 29,000 km^2. There are great differences between the TVP and other Libya's volcanism although they have generally occurred in the same period of time. These differences are as regards to volcano-tectonic aspects, the eruptive styles and production of volcanic materials. The variations of volcanic products along the TVP range from contemporaneous basaltic to acidic (rhyolite and ignimbrite), during the end of Miocene to late Pleistocene indicate that the magma in this volcanic field may be derived from a double magma sources. Alternatively, the Libya's volcanism, particularly the AHVP, is commonly supplied through single magma reservoir, most likely at the crust-mantle boundary. Field observations and numerical model results suggest that basaltic magma (scoria cones) at the periphery of the TVP may be derived from a deeper magma reservoir in the lower crust or at crust-mantle boundary while the more evolved rhyolite and ignimbrites most likely were obtained from a shallow crustal magma chamber.

The presence of a shallow magma chamber for an extended period of time (> 1Ma) has modified the in situ stress fields beneath TVP and generated volcano-tectonic elements which may be superimposed on the orthogonal pre-existing regional lineaments. The evolution of the TVP is characterised by constructive episode (between 8 and 7–5 Ma), and then destructive episode (between 7-5 and 0.43 Ma) where the constructive (inflation process) period involves the accumulation of volcanic materials to form central volcanisms, whereas destructive periods (deflation processes) involve vertical collapse calderas due to volcano-tectonic forcing and produced the large-volume of ignimbrites (>100 km^3). The numerical approaches with various loadings used during this study are greatly improved our understanding the volcano-tectonic evolution and spatial and temporal distribution of the major volcanic units at the TVP. The numerical model results suggest that the stress fields associated with excess magmatic pressure or regional field stress as loading are only favourable to form a

volcano cone fed by radial dykes and inclined sheets and mostly associated with small-volume eruptions (<1 km^3). While stress fields associated with the uplift doming at the lower crust due to the accumulation of magma are favourable for initiation ring-faults at the surface and at shallow depth and emplacement of ring-dykes from lateral ends of existence shallow crustal magma chamber that subsequently led to subsidence block roof (piston-like caldera subsidence) and squeeze out much magma (>100 km^3). In fact, some basaltic lava flows and mixing lava andesitic-trachyte are commonly followed each an individual collapse caldera that may be derived from infrequently dykes from deeper magma reservoir or from the floor of the former magma chamber. The basaltic and andesitic lava flows are mainly recognised around rims of calderas that might be used the pre-existing ring-faults planes as conduits. The collapse calderas on the TVP are examined in the light of the model of Marti and Gudmundsson (2000). This model has illustrated how and under what stress condition overlapping collapse calderas can be generated by magma migration. The preferred model has also explained the misunderstood in the spatial and temporal progression of collapse calderas throughout the TVP.

11.2 Future work

High-quality deep subsurface data, such as two-dimensional and three-dimensional seismic reflection, borehole and petrological data from the Sirt Basin will be undoubtedly needed in the future research to further provide magma-fault interaction and identify geometry, distribution, and timing of subsurface magmatism in the Sirt Basin.

Unmanned Aerial Vehicles (UAVs) surveys are recently increasingly employed in order to obtain ultra-high resolution mapping (≈10mm/pixel) in much shorter time interval than would be commonly achievable through conventional grid mapping (Bemis et al., 2014). This new technique also

provides access to vertical and instable exposures (Bemis et al., 2014). Therefore, the UAVs will be used as a powerful tool in the near-future researches to easily collect data from size, remoteness and inhospitable field areas induce difficulties of ground-based access and unsafe exposures, such the AHVP and the TVP.

A series of volcanic activity in the central part of Libya during the end of Miocene might have been partly caused the local fauna and flora extinctions in the As-Sahabi area, NE the Sirt Basin, and hyper-aridity in Megafezzan Lake, SW Sirt Basin. This speculation result within the limits of data is only set forth about a possible link between local biological extinction, super-aridity, and volcanism in the Sirt Basin area, central Libya and this will doubtless demand very close scrutiny in the future. Detailed petrographic and geochemistry studies would be a good test to estimate the pre and post eruption volatile materials of the glass in inclusions trapped in phenocrysts (pre-eruption) and degassed lava matrix (post-eruption) as well as detectable geochemical record for an increase greenhouse gases (e.g., CO_2 and CH_4) in lacustrine sediments, fossil soils and fossil plant anatomy (cf. Olsen, 1999; Burgess et al., 2017). In addition, drilling core barrels can be used to estimate duration of eruption. Such data is also extremely important for forecasting and assessment hazards of the AHVP.

I currently collaborate with work with Missouri University of Science and Technology, Rolla, Missouri, USA, in order to measure precisely crustal thickness beneath Libya and the origin of partial melt beneath AS Sawda Volcanic Province from receiver-function constraints. We have used receiver function constraints (RFs), for the first time, from data obtained from recent available broadband seismic stations; fifteen seismic stations belonging to the Libyan Center for Remote Sensing and Space Science (LCRSSS) and three seismic stations publically. This study has preliminarily inferred that the observed high Vp/Vs (κ) ratios of 1.91 at one station located in the As Sawda Volcanic Province. It is indicated the presence of partial melt at the

crust-mantle boundary (≈35 km). This new finding indicates that the magma reservoir beneath this region is most likely still active, consequential generating significant earthquakes and volcanic hazards. More geophysical studies, such heat flow data, magnetotelluric, gravity studies and geothermal data, will be certainly needed in the future in order to obtain better constraints on the deep structure and magma chamber/reservoir in other parts of Libyan territory.

Finally, my results in this thesis on the volcanism and tectonics, along with mechanism of lava emplacement in Libya and adjacent areas are largely new and the methods may be used for other similar regions, in addition to being of great value for volcanological studies in the North Africa at large scale. Thus this thesis enhances the departmental profile, provides scientific advance, and involves international collaboration. I shall, on returning to Libya, present some of my results to the general public and motivate the Libyan National Oil Corporation (NOC) to pay special attention for the risk of the Holocene volcanism and associated earthquakes as well as evaluate the volumetric effects of the magmatism on the generation, migration and trapping of hydrocarbons due to number of oil fields are located in the AHVP. Also, I will strongly encourage the Libyan Center for Remote Sensing and Space Science (LCRSSS) to install permanent and denser broadband seismic stations coverage, particularly at volcanic areas.

Bibliography

Abadi, A., 2002. Tectonics of the Sirt Basin, inferences from tectonic subsidence analysis, stress inversion and gravity modelling: Ph.D. thesis, Vrije Universiteit, Amsterdam, p. 187.

Abadi, A., van Wees, J., van Dijk, P., Cloetingh, S., 2008. Tectonics and subsidence evolution of the Sirt Basin, Libya. AAPG Bulletin, 92, 993–1027.

Abdel-al, M., Abdel-Karim, El-Nuri M., Ramadan, Mohamed, R., Embashi .2013. Multiphase Alkaline Basalts of Central Al-Haruj Al-Abyad of Libya: Petrological and Geochemical Aspect. Journal of Geological Research, 2013, p. 12.

Abdunaser, K., McCaffrey, K., 2014. Rift architecture and evolution: the Sirt Basin, Libya: the influence of basement fabrics and oblique tectonics. Journal of African Earth Sciences, 100, 203–226.

Acocella, V., 2007. Understanding caldera structure and development: and overview of analogue models compared to natural calderas. Earth-Science Reviews, 85, 125–160.

Ade-Hall, M., Reynolds, H., Dagley, P., Musset, G., Hubbard, B., Klitzsch, E. 1974. Geophysical studies of North African Cenozoic volcanic areas Al Haruj Al – Assuad, Libya. Canadian Journal of Earth Science, 11, 998–1006.

AGOCO (Arab Gulf Oil Company), 1980. Geology of stratigraphic giant – the Messlah oil field. In: Salem, M.J., Busrewil, M.T. (Eds.),

The Geology of Libya Volume II. Academic Press, London, 521–536.

Al-Hafdh, N., Gafeer, A. 2015. The petrology and geochemistry of Gharyan volcanic province of NW Libya. Journal of African Earth Sciences, 104, 71–102.

Al-Hafdh, N. Elshaafi, A., 2015. Geochemistry and Petrology of Basic Volcanic Rocks of Jabal Al Haruj Al-Aswad, Libya. International Journal of Geosciences, 6, 109-144.

Al-Heety, E., 2013. Seismicity and seismotectonics of Libya: as an example of intraplate environment. Arabian Journal of Geosciences, 6, 193–204.

Al-Kwatli, M., Gillot, P. Zeyen, H., Hildenbrand, A. Al Gharib, I., 2012. Volcano-tectonic evolution of the northern part of the Arabian plate in the light of new K–Ar ages and remote sensing: Harrat Ash Shaam volcanic province (Syria). Tectonophysics, 580, 192–207.

Almond, D., Busrewil, M., Wadsworth, W., 1974. The Gharian Tertiary volcanic province of Tripolatania, Libya. Geological Journal ,9, 17–28.

Ambrose, G., 2000. The geology and hydrocarbon habitat of the Sarir Sandstone, SE Sirt Basin, Libya. Journal of Petroleum Geology, 23,165–191.

Anderson, D., 1998. The edges of the mantle, in: M. Gurnis et al. (Eds.), The Core-Mantle Boundary Region, American Geophysical Union, Washington, DC, 255-–271.

Anderson, D., 2000. The thermal state of the upper mantle: no role for mantle plumes, Geophys. Res. Lett. 27, 3623–3626.

Andre, L., Klerky, J., Busrewil, M., 1991. Geochemical and Rb-Sr isotopic data on felsic rocks from the Jabal Awaynat alkaline intrusive complex (SE Libya). Third Symposium on the Geology of Libya, vol. 7 (eds. M.J. Salem and M.T Busrewil and A.M. Ben Ashour), Elsevier, Amsterdam, 2511–2528.

Andrew, R., 2008. Volcanotectonic Evolution and Characteristic Volcanism of the Neovolcanic Zone of Iceland. PhD thesis, p. 130.

Andrew, R., Gudmundsson, A., 2007. Distribution, structure, and formation of Holocene lava shields in Iceland. Journal of Volcanology and Geothermal Research. 168, 137–154.

Anketell, J., Ghellali, S., 1991. A paleogeologic map of the Pre-Tertiary surface in the region of the Jifarah Plain and its implication to the structural history of the northern Libya. In: Salem, M.J., Sbeta, A.M., Bakbak, M.R. (Eds.), The Geology of Libya, volume VI, 2381–2406.

Anketell, J.M., Kumati, S.M., 1991. Structure of Al Hufrah region - western Sirt Basin, G.S.P.L.A.J. In: Salem, M.J., Belaid, M.N. (Eds.), The Geology of Libya, volume V, 2353–2370.

Anketell, J., 1996. Structural history of the Sirt Basin and itsrelationship to the Sabratah Basin and Cyrenaican Platform,northern Libya, in M. J. Salem, M. T. Busrewil,A. A. Misallati, and M. A.

Sola, eds., The geology of the Sirt Basin: Amsterdam, Elsevier, 3, 57–87.

Assaf, H., Corpel, J., Megerisi, M., El Mabruk, H., 1973. Preliminarily exploration work on the radioactive anomalies at Dor El Goussa area. Internal report. Industrial Research Centre, Tripoli.

Asran, A., Aboazom, A., 2004. Al-Haruj Tertiary basalts, Libya: petrological and geochemical approach. In: Proceedings of the 6th International Conference on the Geology of the Arab World, (GAW6).

Azzouni-Sekkal, A., Bonin, B., Benhallou, A., Yahiaoui, R., Liègeois, J.P., 2007. Cenozoic alkaline volcanism of the Atakor massif (Hoggar, Algeria). In: Beccaluva, L., Wilson, M., Bianchini, G. (Eds.), Cenozoic Volcanism in the Mediterranean Area. Geological Society of America, special paper, 418, 321–340.

Babiker, M., Gudmundsson, A., 2004. Geometry, structure and emplacement of mafic dykes in the Red Sea Hills, Sudan. Journal of African Earth Sciences 38, 279–292.

Bache, F., Olivet, J., Gorini, C., Rabineau, M., Baztan, J., Aslanian, D., Suc, J., 2009. Messinian erosional and salinity crises: View from the Provence Basin (Gulf of Lions, Western Mediterranean). Earth and Planetary Science Letters, 286, 139-157.

Baird, D., Aburawi, R., Bailey, N., 1996. Geohistory and petroleum in the central Sirt Basin, in M. J. Salem, M. T. Busrewil, A. A.

Misallati, and M. A. Sola, eds., The geology of the Sirt Basin: Amsterdam, Elsevier, 3, 3–56.

Bagnardi, M., 2014. Dynamics of Magma Supply, Storage and Migration at Basaltic Volcanoes: Geophysical Studies of the Galápagos and Hawaiian Volcanoes. PhD thesis. University of Miami, USE. Scholarly Repository. Electronic Theses and Dissertations.

Bardintzeff, J., Deniel, H. Guillou, B. Platevoet, P. Télouk, Oun, K., 2012. Miocene to recent alkaline volcanism between Al Haruj and Waw an Namous (southern Libya) Int. Journal of African Earth Sciences, 101, 1047–1063.

Bardintzeff, J., Leyrit, H., Guillou, H., Guille, G., Bonon, B., Giret, A., Brousse, R., 1994. Geochemical Journal. 28, 489-515.

Barnett, Z., Gudmundsson, A. 2014. Numerical modelling of dykes deflected into sills to form a magma chamber. Journal of Volcanology and Geothermal Research, 281, 1–11.

Barr, F., Weegar, A., 1972. Stratigraphic nomenclature of the Sirt Basin, Libya: Tripoli, Petroleum Exploration Society of Libya, p. 179.

Barry, T.,Self, S., Kelley, S..; Reidel, S., Hooper, P., Widdowson, M., 2010. "New 40Ar/39Ar dating of the Grande Ronde lavas, Columbia River Basalts, USA: Implications for duration of flood basalt eruption episodes", Lithos, 118, 213–222.

Beccaluva L, Bianchini G, Ellam RM, Marzola M, Oun KM, Siena F, Stuart F., 2008. The role of HIMU metasomatic components in the North African lithospheric mantle: petrological evidence

from the Gharyan lherzolite xenoliths, NW Libya. In: Coltorti M,Gre´goire M (eds) Metasomatism in Oceanic and Continental Lithospheric Mantle. Geological Society London Special Publications, 293, 253–277.

Becerril, L., Galindo L., Gudmundsson, A. Marales J., 2013. Depth of origin of magma in eruptions. Scientific reports. 3 : 2762 | DOI: 10.1038/srep02762.

Bedard, J., Naslund H., Nabelek P., Winpenny A., Hryciuk M., Macdonald W., Hayes B., Steigerwaldt K., Hadlari T., Rainbird R., Dewing K., Girard E., 2012. Fault-mediated melt ascent in a Neoproterozoic continental flood basalt province, the Franklin sills, Victoria Island, Canada. Geological Society of America Bulletin, 124, 723–736.

Begg, G. Griffin, W., Natapov, L., O'Reilly, S., Grand, S., O'Neill, C., Hronsky, J., Djomani, Y., Swain, C., Deen, T., Bowden, P., 2009. The lithospheric architecture of Africa: Seismic tomography, mantle petrology, and tectonic evolution. Geosphere, Geological Society of America. 5; 23–50.

Bellair, P., Freulon, J. M., Lefrance, J. M., 1952. Les eruptions volcaniques de l´Hruj el Assoued (Saharal oriental), Academy of science, Paris, ,234. 2460 –2461.

Belliar, P., Freulon, J. Lefranc, J., 1952. Les eruptions volcaniques de L Haruj Assoued (Sahara oriental). Academy of science, Paris, 234, 2460–2461.

Belhaj, F. 1996. Palaeozoic and Mesozoic stratigraphy of eastern Ghadamis and western Sirt Basins. First Symposium on the Sedimentary Basins of Libya,Geology of the Sirt Basin, (eds. M.J. Salem,A.J. Mouzughi and O.S. Hammuda), Elsevier, Amsterdam, 1, 57–96.

Bellini, E., Massa, D., 1980. A stratigraphic contribution to the Palaeozoic ofthe southern basins of Libya. In: Salem, M.J., Busrewil, M.T. (Eds.), Second Symposium on the Geology of Libya, Academic Press, London, 1, 3–56.

Bemis, S., Micklethwaite, S., Turner, D., James, M., Akciz, S., Rhiele, S., Bangash, H., 2014. Ground-based and UAV-Based photogrammetry: A multi-scale, high-resolution mapping tool for structural geology and paleoseismology. Journal of Structural Geology, 69, 163-178.

Benson, P., Meredith, P., Platzman, E., White, E., 2005. Pore fabric shape anisotropy in porous sandstones and its relation toelastic wave velocity and permeability anisotropy under hydrostatic pressure. International Journal of Rock Mechanics and Mining Sciences, 42, 890–899.

Bezan, M., 1996. The Paleocene sequence in Sirt Basin, in M. J. Salem, M. T. Busrewil, A. A. Misallati, and M. A.Sola, eds., The geology of the Sirt Basin: Amsterdam, Elsevier, 1, 97–118.

Bingöl, E., Bal, I., Can, N., 1989. Geological map of Turkey, scale 1:2000000, General Directorates of Mineral Research and Exploration, Ankara, Turkey.

Binks, R., Fairhead, J., 1992. A plate tectonic setting for Mesozoic rifts of west and central Africa. Tectonophysics, 213, 141–151.

Boaz, N., 2009. Libya before the Sahara: The vanished world of the Eo-Sahabi Valley. Published by the International Institute for Human Evolutionary Research Integrative Centers for Science and Medicine 2565 Siskiyou Boulevard, Suite 4/1L Ashland, OR 97520, U.S.A. 1, 1–12.

Boote, D., Clark-Lowes, D., Traut, M., 1998. Palaeozoic petroleum systems of North Africa. In: MacGregor, D.S., Moody, R.T.J., Clark-Lowes, D.D. (Eds.), Petroleum Geology of North Africa, Geological Society Special Publication, London, 132, 7–68.

Boote, D.., Dardour, A., Green, P.., Smewing, J., Van Hoeflaken, F., 2012. Burial and unroofing history of the base Tanezzuft 'hot' Shale source rock, Murzuq Basin, SW Libya: new AFTA constraints from basin margin outcrops. In: 4th Sedimentary Basins of Libya Symposium: the Geology of Southern Libya, 17– 20th November 2008, Tripoli, Libya.

Bosworth, W., 2008. North Africa – Mediterranean present-day stress field transition and implications forfractured reservoir production in the Eastern Libyan Basins. Geology of East Libya 2008, 4, 123-138.

Bosworth, W., Huchon, P., McClay, K., 2005. The Red Sea and Gulf of Aden basins. Journal of African Earth Sciences, 43, 334–378.

Bosworth, W., Strecker, M., 1997. Stress field changes in the Afro-Arabian Rift system during the Miocene to Recent period: Tectonophysics, 278, 47–62.

Bosworth, W., Strecker, M., Blisniuk, P., 1992. Integration of East African paleostress and present-day stress data: implications for continental stress field dynamics. Journal of Geophysical Research, 97, 11851–11865.

Boyce, J., 2013. The Newer Volcanics Province of southeastern Australia: a new classification scheme and distribution map for eruption centres, Australian Journal of Earth Sciences, 60, 449–462.

Brenchiley, J., Marshall, J., Garden, G., Robbertson, B., Long, B. Meidla, D., Hings, L., Anderson, T.,1994. Bathymetric and isotopic evidence for a short lived late Ordovician glaciation in a greenhouse period. Geology, 22, 295–298.

Brotons, V. Toma´s, R., . Ivorra S., Grediaga, A., Martı´nez-Martı´nez, J., Benavente, D.,Go´mez-Heras, M.,.2015. Improved correlation between the static and dynamic elastic modulus of different types of rocks. Materials and Structures, 49, 3021–3037.

Browning, J., Gudmundsson, A. 2015. Caldera faults capture and deflect inclined sheets: an alternative mechanism of ring dike formation. Bulletin of Volcanology 77: 4, 1–13.

Browning, J.,2015. Thermo-mechanical effects of magma chambers and caldera faults. PhD thesis. Royal Holloway University of London. p. 178.

Burgess, S., Muirhead, J., Bowring, S., 2017. Initial pulse of Siberian Traps sills as the trigger of the end-Permian mass extinction. Nature communications, 8: 164, doi:10.1038/s41467-017-00083-9

Burke, K., Dewey, J., 1974. Two plates in Africa during the Cretaceous?: Nature, 249, 313–316.

Burrough, P., Frank, A.,1996. Geographic Objects with Indeterminate Boundaries. GISDATA Series, Taylor & Francis, London, p. 352.

Busrewil, M., 2012. Evolution of Al Haruj Volcanic Province, Central Libya. Geology of Southern Libya, 2012, vol. 3. . In: 4th Sedimentary Basins of Libya Symposium: the Geology of Southern Libya, 17– 20th November 2008, Tripoli, Libya.

Busrewil, M., Oun, K. Haman, M., 2012. Petrology and Tectonic Setting of Hameimaat Magmatic Rocks, SE Sirt Basin, Libya. Geology of Southern Libya, 2012, 3, 189-210.

Busrewil, M., 1996. The volcanology of central Jabal al Haruj al Aswad volcanic province, Central Libya. The geology of Sirt Basin, Elsevier, Amsterdam. Vol. III, 331-345.

Busrewil, M., Mriheel, I., Al Fasatwi, T., 1996. Volcanism, tectonism and hydrocarbon potentials of parts of Al Haruj area, SW Sirt Basin, Libya. In: The geology of Sirt Basin, Elsevier, Amterdam, III, 317–329.

Busrewil, M., Suwesi, S., 1993. Geological Map of Libya 1 : 250.000, Sheet : Al Haruj Al Aswad NG(33-4). Explanatory Booklet. Industrial Research Centre, Tripoli, p. 95.

Busrewil, M. Oun, K., 1991. Geochemistry of the Tertiary alkaline rocks of Jabal al Hasawinah, west central Libya. Third Symposium on the Geology of Libya, (eds. M.J. Salem and M.T. Busrewil and A.M. Ben Ashour), Elsevier, Amsterdam, 7, 2587–2598.

Busrewil, M., Wadsworth, W., 1982/83. The basalts and associated lherzolite xenoliths of Waw-an-Namus volcano, Libya. Libyan J. Sci., 12, 19-28.

Busrewil, M., Wadsworth, W., 1980. Preliminary chemical data on the volcanic rocks of Al Haruj area, central Libya. In: The Geology of Libya (eds. M. J. Salem and M. T. Busrewil), London Academic Press, 3, 1077–1080.

Calvari, S., and H. Pinkerton (1998), Formation of lava tubes and extensive flow field during the 1991–1993 eruption of Mount Etna, Journal of Geophysical Research 103, 27,291– 27,301.

Cahen, L., Senelling, J., Vail, R., 1984. The geochronology of Africa: Oxford, Clarendon Press, p. 512.

Capitanio, F., Faccenna, C., Funiciello, R., 2009. Opening of Sirte Basin: result of slab avalanche? Earth and Planetary Science Letters, 285, 210–216.

Capitanio, F., Faccenna, C., Funiciello, R., Salvini, F., 2012. Recent Tectonics of Tripolitania, Libya: An Intraplate Record of Mediterranean subduction. Geological Society, London, Special Publications, 357, 319–328.

Cartwright, J., Hansen, D.M., 2006. Magma transport through the crust via interconnected sill complexes. Geology 34, 929–932.

Cashman, K., Kauahikaua, J., 1997. Re-evaluation of vesicle distributions in basaltic lava flows. Geology, 25, 419– 422.

Cazenave,A., A. Souriau, K., Dominh, 1989. Global coupling of Earth surface topography with hotspots, geoid and mantle heterogeneities, Nature, 340, 54–57.

Dessert C., , Dupré, B., François,L., Schott, J., Govind, C., ; Sujit, B., 2001."Erosion of Deccan Traps determined by river geochemistry: impact on the global climate and the 87Sr/86Sr ratio of seawater". Earth and Planetary Science Letters. 188: 461.

Chastin, S., Main, I., 2003. Statistical analysis of daily seismic event rate as a precursor to volcanic eruptions. Geophysical Research Letters, 30, DOI: 10.1029/2003GL016900

Chen, N., Dong J. Chen, J., Dong, C., Shen, Z., 2014. Geometry and emplacement of the Late Cretaceous mafic dyke swarms on the islands in Zhejiang Province, Southeast China: Insights from high-resolution satellite images, Journal of Asian Earth Sciences, 302–311.

Chorowicz, J. Benissa, M., 2016. Remote sensing and field analysis of the Palaeozoic structural style in NW Libya: The Qarqaf arch a paleo-transfer fault zone between the Ghadamis and Murzuq basins. Journal of African Earth Sciences, 123, 272–293.

Chorowicz, J., Deroin, J., 2003. La télédétection et la cartographie géomorphologique et géologique. Editions Gordon & Breach, collection Geosciences, p. 141.

Chorowicz, J., Bardintzeff, J., Rasamimanana, G., Chotin,P., Thouin, C., Rudant, J., 1997. An approach using SAR ERS images to relate extension fractures to volcanic vents: Examples from Iceland and Madagascar: Tectonophysics, 271, 263–283.

Christaras, B., Auger, F., Mosse, E., 1994. Determination of the moduli of elasticity of rocks. Comparison of the ultrasonic velocity and mechanical resonance frequency methods with direct static methods. Materials Structures , 27, 222–228.

Clemens J. Mawer, C.,1992. Granitic magma transport by fracture propagation. Tectonophysics, 204, 339–360.

Cloetingh, S., Van Wees, J., 2005. Strength reversal in Europe's intraplate lithosphere: Transition from basin inversion to lithospheric folding: Geology, 33, 285–288.

Cloetingh, S., Ziegler, P.. Beekman, F., Andriessen, P., Matenco, L., . Bada, G., Garcia-, D., Castellanos, Hardebol, N., Dezes, P., Sokoutis, D., 2005, Lithosphere memory, state of stress and rheology: Neotectonic controls on Europe's intraplate continental topography: Quaternary Science Reviews, 24, 241–304.

Conant, L.Goudarzi, G., 1967. Stratigraphic and tectonic framework of Libya. AAPG Bulletin, 51, 719–730.

Corti, G., 2009. Continental rift evolution: From rift initiation to incipient break-up in the Main Ethiopian Rift, East Africa. Earth-Science Reviews, 96, 1–53.

Courel, L., Aı¨t Salem, H., Benaouiss, N., Et-Touhami, M., Fekirine, B., Oujidi, M., Soussi, M., Tourani, A., 2003. Mid-Triassic to Early Liassic clastic/evaporitic deposits over the Maghreb Platform. Palaeogeography, Palaeoclimatology, Palaeoecology, 196, 157–176.

Courtillot, V., Renne, P., 2003. On the ages of flood basalt events. Geoscience, 335, 113–140.

Courtillot, V., A. Davaille, J. Stock, B., 2003, Three distinct types of hotspots in the Earth's mantle, Earth and Planetary Science Letters, 205, 295-308,Craig, J., Jackson, J., Priestley A., McKenzie D., 2011. Earthquake distribution patterns in Africa: their relationship to variations in lithospheric and geological structure, and their rheological implications. Geophysical Journal International 185, 403–434.

Cvetkovic,´ V., Toljic´ , M., Ammar, N.A., Rundic´, L., Trish, K., 2010. Petrogenesis of the eastern part of the Al Haruj basalts (Libya). Journal of African Earth Sciences, 58, 37–50.

Deb, D.,2009. Finite Elment Method, (Concepts and Applications in Geomchanics). New Delhi. 2nd edition, p. 269.

Delaney P., Pollard D., ZIony I., McKee H., 1986. Field relations between dikes and joints: emplacement processes and paleostress analysis. Journal of Geophysical Research, 91,4920–4938

Delaney, P., Pollard , D., 1981. Deformation of host rocks and flow of magma during growth of dikes and breccia-bearing intrusions near Ship Rock, New Mexico, U.S. Geological Survey Publications, p. 1202.

Deniel, C., Vincent, P., Beauvilain, A., Gourgaud, A. 2015. The Cenozoic volcanic province of Tibesti (Sahara of Chad): major units, chronology, and structural features. Bulletin of Volcanology 77: 74DOI 10.1007/s00445-015-0955-6.

Desio, A.1937. Geologia emorfologia del Fezzan. In: Sahara Italiano – Fezzan Oasidi Gat. R. Soc. Geogr. It. I, 39–94.

Desio, A., 1936. Riasunto sulla constituzione geologica del Fezzan. Bol. Soc. Geol. Ital., 55, 319–356.

Desio, A., 1935. Studi geologic sulla Cirenica, Orientale. Missi one Scientifica della. R. Accad. d'Italia acufra, Rome. p. 480.

Desio, A.,1934. Lo Hruj. Le vie Ital., 3, p. 83–130.

Dercourt, J., Gaetani, M., Vrielynck, B., Barrier, E., Biju-Duval, B., Brunet, M.F., Cadet, J.P., Crasquin, S., Sandulescu, M. (Eds.), 2000. Atlas Peri-Tethys, Palaeogeographical maps. CCGM/CCMW, Paris, 24 maps and explanatory notes, I–XX, p. 269.

Dercourt, J., Ricou, L., Vrielynck, B. (Eds.), 1993. Atlas Tethys Palaeoenvironmental Maps.Gauthier-Villars, Paris, p. 307.

Dercourt, J., Zonhain, L., Ricou, L.,Kazmin, G., Pichon, X., Knipper, A.,Granjacquet, C., Sbortchitkov, I.,Getssant, J., Lepvrier, D., Boulin, J.,Sibuet, L., Savostin, O., Westphal, M.,Bazhenov, M.,Lauer, L., Bijuduval,B., 1986. Geological evolution of the

Tethys belt from the Atlantic to the Pamirs since the Lias. Tectonophysics, 123. 241–315.

Deunff, J., Massa, D., 1975. Palynologie et stratigraphic du Cambro-Ordovicien (Libye nordoccidentale) .C.R. Acad. Sci, Paris. Ser. D, 281, 21–24.

De Wet A., Hamilton, C. Bleacher, J., Garry, B., 2014. Lava Mars and the Earth: A comparative study of inflated and distributed flows. Published by Keck Geology Consortium. 27th annual Symposium Volume. ISBN: 1528–7491.

Dodge Y., 2003. The Oxford dictionary of statistical terms. ISI. ISBN: 9780199206131.

Drury, S., 2001. Image Interpretation in Geology. Blackwell Science, Nelson Thornes, UK, p. 290.

Ebinger, C., Sleep N.1998. Cenozoic magmatism throughout East Africa resulting from impact of a single plume. Nature, 395, 1788–1791.

Echikh, K., Sola, M., 2000. Geology and hydrocarbon occurrences in the Murzuq Basin, SW Libya. Symposium on Geological Exploration in Murzuq Basin (eds. M.A. Sola and D. Worsley), Elsevier, Amsterdam, 175–222.

Echikh, 1998. Geology and hydrocarbon occurrences in the Ghadames Basin, Algeria, Tunisia, Libya. In:Petroleum Geology of North Africa, Geological Society. Special Publication, 132, 109–130.

El-Hawat, A., Missallati, A.,Bezan, A., Taleb, T., 1996. The Nubian Sandstone in the Sirt Basin and its correlatives, in M. J.

Salem, M. T. Busrewil, A. A. Misallati, and M. A. Sola, eds., The geology of the Sirt Basin: Amsterdam, Elsevier, 2, 3–30.

El–Makhrouf, A., 1996. The Tibisti-Sirt orogenic belt, Libya, G.S.P.L.A.J. First Symposium on the Sedimentary Basins of Libya, Geology of the Sirt Basin, (eds. MJ. Salem, M.T. Busrewil, A.A. Misallati and M.J. Sola), Elsevier, Amsterdam, 3, 137–154.

El–Makhrouf, A. 1988. Tectonic interpretation of Jabal Eghei area and its regional application to Tibesti orogenic belt, South Central Libya. Journal of African Earth Sciences, 7, 945–967.

Elshaafi, A., and Gudmundsson, A., 2017. Distribution and size of lava shields on the Al Haruj al Aswad and the Al Haruj al Abyad Volcanic Systems, Central Libya. J. Journal of Volcanology and Geothermal Research, 1-17.

Elshaafi, A., Gudmundsson, A., 2016. Volcano-tectonics of the Al Haruj Volcanic Province, Central Libya, Journal of Volcanology and Geothermal Research, 325.189–202.

Eissa E, Kazi A.,1988. Relation between static and dynamic Young´s Moduli of rocks. International Journal of Rock Mechanics and Mining, 25, 479–482.

El-Shawaihdi, M., Mozley, P., Boaz, N., Salloum, F., Pavlakis, P., Muftah, A., Triantaphyllou, M., 2016. Stratigraphy of the Neogene Sahabi units in the Sirt Basin, northeast Libya. Journal of African Earth Sciences, 118, 87- 06.

Farahat, .S., Abdel Ghani, S., Aboazom, A., Asranc, A., 2006. Mineral chemistry of Al Haruj low-volcanicity rift basalts, Libya: implications for petrogenetic and geotectonic evolution. Journal of African Earth Sciences, 45, 198–212.

Fairhead, D., 1988. Mesozoic plate tectonic reconstructions of the central South Atlantic Ocean: The role of the west and central Africa rift system: Tectonophysics, 155, 181–191.

Fairhead, J., Binks, R., 1991. Differential opening of the central and southatlantic oceans and the opening of the West African rift system. Tectonophysics, 187, 191–203.

Fairhead, J., Green, C., 1989. Controls on rifting in Africa and the regional tectonic model for the Nigeria and east Niger rift basins. Journal of African Earth Sciences, 8, 231–249.

Fisher, R., Schmincke, H., 1984. Pyroclastic rocks. Springer, Heidelberg, pp 1–474.

Finetti, I., Del Ben, A., 2000. Crustal stratigraphy and tectono-dynamics of the Pelagian Sea region from new 'CROP' seismic data (abstract only).Second Symposium on the Sedimentary Basins of Libya, Geology of Northwest Libya, p. 42.

Fodor, L., Turki, S.M., Dalob, H., Al-Gerbi, A., 2005. Fault-related folds and along-dip segmentation of breaching faults: syn-diagenetic deformation in the southwestern Sirt Basin, Libya. Terra Nova, 17, 121–128.

Francesco, M., D'Orazio, M., 2003. Spatial distribution of cones and satellite-detected lineamentsin the Pali Aike Volcanic Field

(southernmost Patagonia): insights into the tectonic setting of a Neogene rift system. Journal of Volcanology and Geothermal Research, 125, 291–305.

Futyan, A. Jawzi, A., 1996, The hydrocarbon habitat of the oil and gas fields of north Africa with emphasis on the Sirt Basin, in M. J. Salem, M. T. Busrewil, A. A. Misallati, and M. A. Sola, eds., The geology of the Sirt Basin: Amsterdam, Elsevier, 2, 287–307.

Galushkin, Y., 2016. Non-standard Problems in Basin Modelling. DOI 10.1007/978-3-319-33882-8.

Gautier, F., Clauzon, G., Suc, J., Cravatte, J., Violanti, D., 1994. Age and duration of the Messinian salinity crisis. C.R. Acad. Sci., Paris (IIA) 318, 1103–1109.

Gealey, W., 1988. Plate tectonic evolution of the Mediterranean–Middle East region: Tectonophysics, 155, 285–306.

Ghanoush, H., Imber, J., McCaffrey, K., 2014. Cenozoic Subsidence and Lithospheric Stretching Deformation of the Ajdabiya Trough Area, Northeast Sirt Basin, Libya. AAPG 2014 Annual Convention and Exhibition, Houston, Texas.

Glaze, L., Anderson, S., Stofan, E., Baloga, S., Smrekar, S., Statistical distribution of tumuli on pahoehoe flow surfaces:Analysis of examples in Hawaii and Iceland and potentialapplications to lava flows on Mars. Journal of Geophysical Research, 110, 1-14.

Goudarzi, G., 1980. Structure – Libya. In : The Geology of Libya (eds.) Salem, M. J., and Busrewil, M. T., London Academic press, 3, 879–892.

Goudarzi, G., 1970. Geology and mineral resources of Libya – A reconnaissance. U.S. Geological Survey Publications, 660, p. 104.

Gough, D., Bell, J., 1981. Stress orientation from oil well fractures in Alberta and Texas. Canadian Journal of Earth Sciences, 18, 638–645.

Gourgaud, A. Vincent, P., 2004. Petrology of two continental alkaline intraplate series at Emi Koussi volcano, Tibesti, Chad. Journal of Volcanology and Geothermal Research, 129, 261–290.

Gras, R., Thusu, B., 1998. Trap architecture of the Early Cretaceous Sarir Sandstone in the eastern Sirt Basin, Libya, in S. D. Macgregor, J. T. R., Moody, and D. D. Clark-Lowes, eds., Petroleum geology of North Africa: Geological Society (London) Special Publication, 132, 317–334.

Gras, R., 1996. Structural style of the southern margin of the Messlah High. In:Salem, M.J., El-Hawat, A.S., Sbeta, A.M. (Eds.), The Geology of Sirt Basin. Elsevier,Amsterdam, III, 201–210.

Grosfils, E., 2007. Magma reservoir failure on the terrestrial planets: Assessing the importance of gravitational loading in simple elastic models. Journal of Volcanology and Geothermal Research, 166, 47–75.

Gudmundsson, A., 2016. The mechanics of large eruptions. Earth-Science Reviews, 163, 72–93.

Gudmundsson, A., 2015. Collapse-driven large eruptions. Journal of Volcanology and Geothermal Research, 304, 1–10.

Gudmundsson A.,2012. Magma chambers: formation, local stresses, excess pressures, and 674 compartments. Journal of Volcanology and Geothermal Research. 237–238, 19–41.

Gudmundsson A., 2011. Rock fractures in geological processes. Cambridge University Press, Cambridge. doi:10.1017/ CBO9780511975684, p. 592.

Gudmundsson, A.,1990. Emplacement of dikes, sills, and crustal magma chambers at divergent plate boundaries. Tectonophysics, 176, 257–275.

Gudmundsson, A., Løtveit, I., 2012. Sills as fractured hydrocarbon reservoirs: examples and models. Geological Society of London, Special Publication, 374, 251–271.

Gudmundsson, A., Friese, N., Andrew, R., Philipp, S., Ertl, G. Letourneur, L., 2008. Effects of dyke emplacement and plate pull on mechanical interaction between volcanic systems and central Volcanoes in Iceland. In: Hoskuldsson, A., Sparks, R. S. J. & Thordarson, T (eds): Volcanic Processes: The Legacy of G.P.L. Walker (the “Walker Volume”). Geological Society London, Special Publications.

Gudmundsson, A., Philipp, S., 2006. How local stress fields prevent volcanic eruptions. Journal of Volcanology and Geothermal Research, 158, 257–268.

Guiraud, R., Bosworth, W., Thierry, J., Delplanque, A., 2005. Phanerozoic geological evolution of northern and central Africa: an overview. Journal of African Earth Sciences, 43, 83–143.

Guiraud, R., Issawi, B., Bosworth, W., 2001, Phanerozoic history of Egypt and surrounding areas, in P. A. Ziegler, W. Cavazza, A. H. F. Robertson, and S. Crasquin-Soleau, eds., Peri-Tethys memoir 6: Peri-Tethyan rift/wrench basins and passive margins: Me´moires Museum National d'Histoire Naturalle, Paris, 186, 469–509.

Guiraud, R., Mbaigane, D., Carretier, S., Dominguez, S., 2000. Evidence for a 6000 km length NW-SE-striking lineament in north Africa: the Tibesti Lineament. Journal of the Geological Society, London, 157, 897–900.

Guiraud, R., Bosworth, W., 1997. Senonian basin inversion and rejuvenation of rifting in Africa and Arabia: Synthesis and implications to plate-scale tectonics: Tectonophysics, 282, 39–82.

Guiraud, R., Bellion, Y., 1995. Late Carboniferous to Recent geodynamic evolution of west Gondwanian cratonic Tethyan margins, in A. Nairn, J. Dercourt, and B. Verielynk, eds., Basins and margins: The Tethys Ocean: New York, Plenum, 8, 101–124.

Guiraud, R., Binks, R., Fairhead, J., Wilson, D., 1992. Chronology of geodynamic setting of the Cretaceous–Cenozoic rifting in west and central Africa: Tectonophysics, 213, 227–234.

Guiraud, R., Maurin, J., 1992. Early Cretaceous rifts of Western and Central Africa: an overview. Tectonophysics, 213, 153–168.

Gumati, Y., Kanes, W., 1985. Early Tertiary subsidence and sedimentary facies, north Sirt Basin, Libya: AAPG Bulletin, 69, 39–52.

Gumati, Y., Schamel, S., 1988.Thermal maturation history of the Sirte Basin, Libya: Journal of Petroleum Geology, 11, 205–218.

Gumati, Y., Nairn, A., 1991. Tectonic subsidence of the Sirt Basin, Libya: Journal of Petroleum Geology, 14, 93–102.

Hall, R., 2014. Shot notice and introduction for ArcGIS 10.1, p. 79.

Hallett, D., 2002. Petroleum Geology of Libya. Elsevier, Amsterdam, p. 503.

Hallett, D., El Ghoul, A., 1996. Oil and gas potential of the deep troughs areas in the Sirt Basin, Libya in M. J. Salem, A. S. El-Hawat, and A. M. Sbeta, eds., The geology of Sirt Basin: Amsterdam, Elsevier, 7, 455–484.

Hammuda, O., van Hinte, J., Nederbragt, S., 1991. Geohistory analysis mapping in the central and southern Tarabulus Basin, northwest offshore of Libya, in M. J. Salem, O. S. Hammuda, and B. A. Eliagoubi, eds.,The geology of Libya: Amsterdam, Elsevier, 4, 1657–1680.

Hansen, D.M., Cartwright, J., 2006. Saucer-shaped sill with lobate morphology revealed by 3D seismic data: implications for resolving a shallow-level sill emplacement mechanism. Journal of the Geological Society, London, 163, 509–523.

Hasenaka,. T., 1994. Size, distribution, and magma output rate for shield volcanoes ofthe Michoac in-Guanajuato volcanic field, Central Mexico. Journal of Volcanology and Geothermal Research, 63, 13–31.

Hassen, H., 1983. Seismicity of Libya and related problems. Master thesis. Civil Engineer Department, Colorado state University, p. 108.

Hegazy, H., 1999. Tertiary volcanics in Libya: evidence for the direction and rate of theAfrican plate motion. Proceeding of the 4th International Conference on Geochemistry. Alexandria University, Egypt, 401–419.

Henk, A., Fischer, K., Kromuller, K., Wanger, D., Winter, I., 2013. Prediction of Tectonic Stresses and Fracture Networks with Geomechanical Reservoir Models. DGMK-Research Report 721. German Society for Petroleum and Coal Science and Technology, p. 216.

Hickey, J., Gottsmann, J., 2014. Benchmarking and developing numerical Finite Element models of volcanic deformation. Journal of Volcanology and Geothermal Research, 280, 126–130.

Hickey, J., Gottsmann, J., del Potro, R., 2013. The large-scale uplift in the Altiplano-Punaregion of Bolivia: a parametric study of source characteristics and crustal rheology using finite element analysis. Geochemistry Geophysics Geosystems Journal. 14, 540–555.

Himmali, A., Oun, K., 1991. The volcanics of sheet Zallah, NH 33-16: a reappraisal. First Symposium on the Sedimentary Basins of Libya, Geology of the Sirt Basin, (eds. M.J. Salem,M.T. Busrewil, A.A. Misallati and M.J. Sola), Elsevier, Amsterdam, 3, 347–356.

Holt, S., Holford. S., Foden, J. 2014. New insights into the magmatic plumbing system of the South Australian Quaternary Basalt province from 3Dseismic and geochemical data, Australian Journal of Earth Sciences, 60, 797–816.

Hon, K., Kauhikaua, J., Denlinger, R., MacKay, K., 1994. Emplacement and inflation of pahoehoe sheet flows: observations and measurements of active lava flows on Kilauea Volcano, Hawaii. Geological Society of America Bulletin, 106, 351–370.

Hornemann, F., 1802. Tagebuch seiner Reise von Cairo mach Murzok der Hauptstdt des Konigreiches Fezzan in Africa in den Jahren 1797 and 1979: Weimar. Aus der deutschen Handschrift herausge – geben von Carl Koning.

Houghton, B., Wilson, C., Smith, I., 1999. Shallow-seated controls on styles of explosive basaltic volcanism: a case study from New Zealand. Journal of Volcanology and Geothermal Research 91, 97–120

Hounslow, M., White, H., Drake, N., Salem, M., El-Hawat A., McLaren, S., Karloukovski, V., Noble, S., Hlal, O., 2017. Miocene humid intervals and establishment of drainage networks by23 Ma in the central Sahara, southern Libya. Gondwana Research, 4, 118–137.

Issawi, B., 1972. Review of Upper Cretaceous-Lower Tertiary Stratigraphy in central and southern Egypt. Bulletin American Association of Petroleum Geologists, 56, 1448–1463.

Jaeger, J., Cook, N., Zimmerman, R., 2007. Fundamentals of Rock Mechanics, 4th edition. Blackwell Publishing Ltd., p.515.

Jahren, A., 2002. The biogeochemical consequences of the mid-Cretaceous superplume. Journal of Geodynamics, 34, 177–191.

Jankovics, E., Harangi, S., Kiss, B., Ntaflos, T., 2012. Open system evolution of the Fuzes-to alkaline basaltic magma, western Pannonian Basin; constraints from mineral textures and compositions. Lithos, 140, 25–37

Janssen, M., Stephenson, R., Cloetingh, S., 1995. Temporal and spatial correlation between change in plate motions and evolution of rifted basin in Africa: Geological Society of America Bulletin, 107, 1317–1332.

Johnston A. 1989. The seismicity of "Stable Continental Interiors" Proceedings of the NATO Advanced Research Workshop on causes and effects of earthquakes of passive margins and in areas of postglacial rebound on both sides of the north Atlantic, Vordirgborg, Denmark, 299–327.

Jurak, L., 1978. Geological map of Libya, Sheet Jabal Al Hasawnah (NH33–14): Tripoli, industrial research centre, scale 1:250,000, p. 74.

Kamo, S., Czamanske, G., Amelin, Y., Fedorenko, V., Davis, D., Trofimov, V. 2003. Rapid eruption of Siberian flood-volcanic rocks and evidence for coincidence with the Permian-Traissic

boundary and mass extinction at 251 Ma. Earth and Planetary Science Letters, 214, 75–91

Karakhanian, A., Djrbashian, R., Trifonov, V., Philip, H., Arakelian, S., Avagian, A., 2002. Holocene–historical volcanism and active faults as natural risk factors for Armenia and adjacent countries,. Journal of Volcanology and Geothermal Research 113, 319–344.

Karaoğlu, O. Elshaafi, A., Salah, M., Browning, J., Gudmundsson, A., 2017. Large-volume lava flows fed by a deep magmatic reservoir atAğrı Dağı (Ararat) volcano, Eastern Turkey. Bulletin of Volcanology. DOI 10.1007/s00445-016-1098-0

Karaoğlu, Ö., Browning, J., Bazargan, M., Gudmundsson, A., 2016. Numerical modelling of triple-junction tectonics at Karlıova, Eastern Turkey, with implications for regional magma transport. Earth and Planetary Science Letters ,452:152–170

Karaoğlu, Ö., Özdemir, Y., Tolluoğlu, A., Karabıyıkoğlu, M., Köse. O., Froger, J., 2005. Stratigraphy of the volcanic products around Nemrut Caldera: implications for reconstruction of the Caldera Formation. Turkish Journal of Earth Sciences, 14, 123–143.

Kebeasy, R., 1980. Seismicity and seismotectonics of Libya, in The Geology of Libya, 3, 955-963, eds Salem, M.J. & Busrewill, M.T., Academic Press, London.

Kheirkhah, M., Allen, M., Emami, M., 2009. Quaternary syn-collision magmatism from the Iran/Turkey borderlands. Journal of Volcanology and Geothermal Research, 182, 1–12.

Klitzch, E., 2000. The structural development of the Murzuq and Kufra basins significance for oil and mineral exploration, In: Sola, M. A. and Worsley, D. (Ed.). Geological exploration of the Murzuq basin. Elsevier, Amsterdam, 3, 143–150.

Klitzsch, E., 1971. The structural development of parts of North Africa since Cambrian time. In: Gray, C. (Eds.). First symposium on the Geology of Libya. Faculty Science, University Libya, Tripoli, 253–262.

Klitzsch, E., 1970. Die Structurgeschichte der Zentralsahara: Neue Erkenntnissezum Bau und der Palaeogeographieeines Tafellandes. GeologischeRundschau, 59, 459-527.

Klitzsch, E., 1968. Der Basalt vulkanismus des Djebel Haroudj, Ostfezzan, Libya. Geologische Rundschau, 57, 585-609.

Klitzsch, E., 1967. Geology of the northeast flank of the Muruzk Basin. In; South – Central Libya and North Chad (ed. J. J. Williams) Petroleum Exploration Society Libya. 8th Annular Conference, 19-32.

Koch, M., Mather, P., 1997. Lineament mapping for groundwater resource assessment: A comparison of digital Synthetic Aperture Radar (SAR) imagery and stereoscopic Large Format Camera (LFC) photographs in the Red Sea Hills, Sudan. International Journal of Remote Sensing, 18, 1465–1482.

Kröner, A., 1991. The Pan-African belt of north-eastern and eastern Africa, Madagascar, southern India, Sri Lanka and east

Antarctica; Terrane amalgamation during formation of the Gondwana Supercontinent, in: Thorwiehe, U., Schandelmeier, H. (Eds.), Geoscientific research in Northeast Africa. Rotterdam, Netherlands, A.A., Balkema, 963, 3–9.

Kumati, S., 1981. The geology of the Hofra region, Sirte Basin, Libya (S.P.L.A.J.). Ph.D Thesis. University of Manchester, p. 231.

Kusumoto, S., Geshi, N., Gudmundsson, A.., 2013. Aspect ratios and magma overpressures of non-feeder dikes observed in the Miyake-jima volcano (Japan), and fracture toughness of its upper part. Geophysical Research Letters, 40, 1–5.

Le Corvec, N., Sporl., B. Rowland, J., Lindsay, J., 2013. Spatial distribution and alignments of volcanic centers: Clues to the formation of monogenetic volcanic fields. Earth-Science Reviews, 124, 96–114.

Lemnifi, A., Elshaafi, A., Browning, J., El Ebadi, S., Gudmundsson, A., 2017. Crustal thickness beneath Libya and the origin of partial melt beneath AS Sawda Volcanic Province from receiver-function constraints. Journal of Geophysical Research - Solid Earth, Revised.

Le Pichon, X., Bergerat, F.,Roulet, M., 1988. Plate kinematics and tectonics leading to the Alpine belt formation: A new analysis, in S. Clark, B. C. Barchfiel, and J. Suppe, eds., Processes in continental lithospheric deformation: Geological Society of America Special Paper, 218, 111–131.

Lie´geois J., Benhallou A, Azzouni-Sekkal, A., Yahiaoui, R., Bonin, B., 2005. The Hoggar swell and volcanism: reactivation of the Precambrian Tuareg shield during Alpine convergence and West African Cenozoic volcanism. In: Foulger GR, Natland JH, Presnall DC, Anderson DL (eds) Plates, plumes, and paradigms. Geological Society of America, Special paper, 388,379–400.

Less, G., Turki, S., Suwesi, K., Peregi, L., Koloszar, L., Kalmar, J., Sherif, K., Csaszar, G., Gulasci, Z., Dalum, H., Al Tajuri, A., 2006. Explanatory Booklet. Geological Map of Libya 1: 250.000. Sheet: Waw Al Kabir NG 33- 12. Industrial Research Centre, p. 295.

Lesti, C., Giordano, G., Salvini, F., R. Cas R.,2008. Volcano tectonic setting of the intraplate, Pliocene-Holocene,Newer Volcanic Province (southeast Australia): Role of crustal fracture zones. Journal of Geophysical Research. 113, 1–11.

Lustrino, M., Cucciniello, C., Melluso, L., Tassinari, C., De Gennaro, R., Serracino, M., 2012. Petrogenesis of Cenozoic volcanic rocks in the NW sector of the Gharyan volcanic field, Libya. Lithos 155, 218–235.

Maccaferri, F., Acocella, V., Rivalta, E., 2015. How the differential load induced by normal fault scarps controls the distribution of monogenic volcanism, Geophysical Research Letters, 42, 7507–7512, doi:10.1002/2015GL065638.

Maccaferri, F., Rivalta, E., Keir, D., Acocella, V., 2014. Off-rift volcanism in rift zones determined by crustal unloading. Nature Geoscience, 7, 297-300, doi:10.1038/ngeo2110.

Magee, C., Muirhead, J., Karvelas, A.,Holford, S., Jackson, C., Bastow, I., Schofield, N., Stevenson, C., McLean, C., McCarthy, W., Shtukert, O., 2016. Lateral magma flow in mafic sill complexes: Geosphere, 12, 1–33.

Magee C, Jackson C., Schofield N., 2013. The influence of normal fault geometry on igneous sill emplacement and morphology. Geology 41:407–410.

Malin, M.,1977. Comparison of volcanic features of Elysium (Mars) and Tibesti (Earth). Geological Society of America Bulletin, 88: 908–919.

Marti, J., Gudmundsson, A. 2000. The Las CanÄadas caldera (Tenerife, Canary Islands): an overlapping collapse caldera generated by magma-chamber migration. Journal of Volcanology and Geothermal Research, 103, 161–173.

Marti, J., Ablay, G., Reshaw, T., Sparks, J. 1994. Experimental studies of collapse calderas. Journal of the Geological Society, London, 151, 919–929.

Martin U., Ne´meth K., 2006. How Strombolian is a ‘‘Strombolian’’ scoria cone? Some irregularities in scoria cone architecture from the Trans-Mexican Volcanic Belt, near Volca´n Ceboruco, (Mexico) and Al Haruj (Libya). Journal of Volcanology and Geothermal Research, 155, 104–118.

Mattsson,, H., Hoskuldsson, A. 2005. Eruption reconstruction, formation of flow-lobe tumuli and eruption duration in the 5900 BP Helgafell lava field (Heimaey), south Iceland. Journal of Volcanology and Geothermal Research, 47, 157– 172.

McClusky, R., Reilinger, S., Mahmoud, D., Ben Sari, A., 2003. Taeleb GPS constraints on Africa (Nubia) and Arabia plate motions. Geophysical Journal International, 155, 126–138.

McKenzie, D., 1978. Some remarks on the development of sedimentary basins: Earth and Planetary Science Letters, 40, 25–31.

McClay, K., Scarselli, N., and Jitmahantakul, S., 2013, Igneous intrusions in the Carnarvon Basin, NW Shelf, Australia, in Keep, M., and Moss, S.J., eds., The sedimentary basins of Western Australia IV: Proceedings of the Petroleum Exploration Society of Australia Symposium:Perth, Petroleum Exploration Society of Western Australia, 1–20.

Middlemost, E., 1975. The basalt clan. Earth Sciences Review. 11, 337-364.

Stuart, F., Masoud, A., Mark, D., 2014. The origin of Cenozoic magmatism of Libya. Geophysical Research Abstracts, Vol. 16, EGU2014-15877.

Modi,C., Kumari, P., Sharma, V., 2016. Reflection/refraction of qP/qSV wave in layered self-reinforced media. Applied Mathematical Modelling, 40, 8737-8749.

Montgomery, S., 1994. Ghadames Basin and Surrounding Areas: Structure in Tectonics, Geochemistry and Field Summaries. Petroleum Frontiers, p. 78.

Mouzughi, A., Taleb, T., 1981. Tectonic elements of Libya: Libya, National Oil Corporation, scale 1:2,000,000, 1 sheet.

Muftah, A., 1996, Agglutinated foraminifera from Danian sediment of northeastern Sirt Basin, in M. J. Salem, M. T. Busrewil, A. A. Misallati, and M. A. Sola, eds., The geology of the Sirt Basin: Amsterdam, Elsevier, 1, 233–242.

Muftah, A., Pavlakis, P., Godelitsas, A., Gamaletsos, P., Boaz, N. 2013. Paleogeography of the Eosahabi River in Libya: New insights into the mineralogy, geochemistry and paleontology of Member U1 of the Sahabi Formation, north-eastern Libya. Journal of African Earth Sciences, 78, 86–96.

Nagao, K., Matsuda, J., Kita. I., Ercan, T., 1989. Noble gas and carbon isotopic compositions in Quaternary volcanic area in Turkey. Bull Geomorphol. 17, 101–110.

Nakamura, K., 1977. Volcanoes as possible indicators of tectonicstress orientation- Principles and proposal. Journal of Volcanology and Geothermal Research, 2, 1–16.

Nakamura, K., Jacob, K., and Davies, J., 1977, Volcanoes as possible indicators of tectonic stress orientation—Aleutians and Alaska: Pure and Applied Geophysics,115, 87–112.

Németh,, K., Haller, M., Martin, U., Rossi, C., Massafero, G., 2008. Morphology of lava tumuli from Mendoza, Patagonia

(Argentina) and Al-Haruj (Libya). Z. Geomorphology, 52, 181–194.

Németh, K., Kereszturi, G., 2015. Monogenetic volcanism: personal views and discussion. International Journal of Earth Sciences, 104, 2131–2146.

Nemeth, K., Suwesi, K., Peregi, Z., Gulacsi, Z., and Ujszaszi, j., 2003. Plio/Pleistocene Flood Basalt Related Scoria and Spatter Cones, Rootless Lava Flows and Pit Craters, Al Haruj Al Abiyad, Libya. Geolines 15, 107–112.

Nixon, S., Maclennan, J., White, N., 2011. Generation of alkali and tholeiitic basalts: The Al Haruj volcanic field, Volcanic and Magmatic Studies Group Annual Meeting, 5-7 January. Queens College, Cambridge.

.Nyblade, A., Suleiman, I., Roy, R., Pusell, B., A., Suleiman, A., Doser, D., Keller, R.,1996. Terrestrial heat flow in the Sirt Basin, Libya, and the pattern of heat flow across northern Africa. Journal of Geophysical Research, 101, 17,737–17,746.

Olsen, P. 1999. Giant lava flows, mass extinctions and mantle plumes. Science, 284, 604–605

Overweg, A., 1851. Geognostische Bemekungen auf der Reise von Philippeville uber Tunis nach Tripoli und von hier nach Murzuc in Fezzan. Z. Geol. Ges. N. F., Berlin, 3, 93–102.

Oun, K., Menuge, J., Himmali, A., 1998. Geology, geochemistry, geochronology and tectonic evolution of the Dur al Qussah basement inlier. Industrial Research centre, Tripoli, p. 106.

Pacific Aero Survey , 1979. Air bone Geophysical Survey Jabal Al Haruj Al Aswad Area. Final Report. Qeb., Inc. Hayward, California, p. 29 .

Parfitt, E., 2004. A discussion of the mechanisms of explosive basaltic eruptions. Journal of Volcanology and Geothermal Research, 134, 77–107

Parsons, M., Azgaar, A., Curry, J., 1980. Hydrocarbon occurrences in the Sirte Basin, Libya, in A. D. Miall, ed., Canadian Society Petroleum Geologists Memoir, 6, 723–732.

Pawellek, T., 2007. A Field Guidebook to the Geology of Sirt Basin, Libya. Gutenberg Press, Malta, RWE fieldtrip guide books. Tripoli, p. 102.

Paulsen, T., Wilson, T., 2009. Structure and age of volcanic fissures on Mount Morning: A new constraint on Neogene to contemporary stress in the West Antarctic Rift, southern Victoria Land, Antarctica. Geological Society of America, 1071–1089.

Pearce, J., 1990. Genesis of collision volcanism in Eastern Anatolia, Turkey. Journal of Volcanology and Geothermal Research, 44, 189–229.

Pedersen G., Höskuldsson, A., Dürig, T., Thordarson, T., . Jónsdóttir, S., Riishuus, M., Óskarsson, B., Dumont, S., Magnusson, E., Gudmundsson, M., Sigmundsson, F., DrouinV., Gallagher, C., Askew, R., Gudnason, J., Moreland, W., Nikkola, P., Reynolds, H., Schmith, J., the IES eruption team, 2017. Lava

field evolution and emplacement dynamics of the 2014–2015basaltic fissure eruption at Holuhraun, Iceland, Journal of Volcanology and Geothermal Research, 340,155–169.

Peña, S., Abdelsalam, M., 2006. Orbital remote sensing for geological mapping in southern Tunisia: implication for oil and gas exploration. Journal of African Earth Sciences, 44, 203–219.

Pesce, A., 1966. Uau en Nammus – South central Libya and Northern Chad. Excursions fὺhrer der petroleum Exploration Society of Libya, Tripoli, 47– 51.

Permenter, J., Oppenheimer, C., 2007. Volcanoes of the Tibesti massif (Chad, northern Africa). Bulletin of Volcanology, 69, 609–626.

Peregi, Z., Less, G., Konrad, G., Fodor, L., Gulacsi, Z., Gyalog, L., Turki, S., Suwesi, S., Sherif, Kh., Dalub, H., 2003. Explanatory Booklet. Geological Map of Libya 1: 250.000. Sheet: Al Haruj Al Abyad NG 33-8. Industrial Research Centre, Tripoli, p. 248.

Philip, J., 2003. Peri-Tethyan neritic carbonate areas: distribution through time and driving factors. Palaeogeography, Paleo-climatology, Paleoecology, 196, 19–37.

Pik R, Marty B, Hilton, D. 2006. How many plumes in Africa? The geochemical point of view. Chemical Geology, 226, 100–114.

Pindel, J., Dewey, J., 1982. Permo-Triassic reconstruction of western Pangea and the evolution of the Gulf of Mexico/Caribbean region. Tectonics, 179–211.

Pirajno, F., 2004. Hotspots and mantle plumes: global intraplate tectonics, magmatism and ore deposits. Mineralogy and Petrology, 82, 183–216

Planke, S., Rasmussen, T., Rey, S., Myklebust, R., 2005. Seismic characteristics and distribution of volcanic intrusions and hydrothermal vent complexes in the Vøring and Møre Basins. In: Doré, A.G., Vining, B.A. (Eds.).

Pollard, D., Fletcher, R., 2005. Fundamentals of Structural Geology. Cambridge University Press, Cambridge, p. 500.

Pollard, D., Segall p., 1987, Theoretical displacement and stresses near fractures in rocks: With application to faults, points, veins, dykes,and solution surfaces, in Fracture Mechanics of Rock, edited by B. K., Atkinson, Academic Press, London, 277–349,

Potere, D., 2008. Horizontal Positional Accuracy of Google Earth's High-Resolution Imagery Archive. Sensors, 8, 7973-7981.

Priestley, K., McKenzie D., 2006. The thermal structure of the lithosphere from shear wave velocities, Earth and Planetary Science Letters, 244, 285–301.

Qui, K., Gherryo, Y., Shatwan, M., Fuller, J.,2008. The application of the Mechanical Earth Model on Rejuvenation of A Mature Field in Libya. IADC/SPE Asia Pacific Drilling Technology Conference and Exhibition, Jakarta, Indonesia, p. 16.

Reidel, Stephen P., 2005. "A Lava Flow without a Source: The Cohasset Flow and Its Compositional Members", Journal of Geology, 113, 1–21,

Radivojević, M., Toljić, M., Turki, S., Bojić, Z., Šarić, K., Cvetković, V., 2015. Neogene to Quaternary basalts of the Jabal Eghei (Nuqay) area (south Libya): Two distinct volcanic events or continuous volcanism with gradual shift in magma composition? Journal of Volcanology and Geothermal Research, 293, 57–74.

Rajesh, H.,2004. Application of remote sensing and GIS in mineral resource mapping – an overview. Journal of Mineralogical and Petrological Sciences, 99, 83–103.

Rasul, S., 2000. Cambrian microplankton from central Sirt Basin (abstract only). Intern. Workshop on North African Micropalaeontology for Petroleum exploration. Univ. Coll. London, 21–25 August 2000. Book of abstracts, p. 64.

Reinecker, J., Heidbach, O., Tingay, M., Connolly, P.,Muller, B., 2015. The 2015 release of the World Stress Map. (available online at www.world-stress-map.org).

Ricou, L.1994. Tethys reconstructed: plates, continental fragments and their boundaries since 260 Ma from central America to south-eastern Asia. Geodinamica Acta, 7, 169–218.

Richards, M., Duncan R., Courtillot, V., 1989. Flood basalts and hot spot tracks: Plume heads and tails, Science246 (1989) 103–107.

Ritsema, A., 1975. The contribution of the study of seismicity and earthquake mechanisms to the knowledge of Mediterranean geodynamic processes, in Progress in Geodynamics, Amsterdam, 142–153.

Rohlich, P., 1991, Tectonic development of Al Jabal Al Akhdar, in M. J. Salem and M. T. Busrewil, eds., The geology of Libya: London Academic Press, 923–931.

Rogers, J., 1980. Uranium in Pan-African Belts. In: Salem, N.J., Busrewil, M.T. (Eds.), Geology of Libya, Al-Fateh Univ, Tripoli, 907–922.

Rosenbaum, G., Lister, G., Duboz, C., 2002. Relative motions of Africa, Iberia and Europe during Alpine orogeny. Tectonophysics, 359. 117–129.

Rossi, M., Tonna, M., Larbash, M., 1991. Latest Jurassic–Early Cretaceous deposits in the subsurface of the eastern Sirt Basin (Libya): Facies and relationships with tectonics and sea level changes, in M. J. Salem, A.M. Sbeta, and M. R. Bakbak, eds., The geology of Libya: Amsterdam, Elsevier, 6, 2212–2225.

Rossi, M., 1999. Plan-curvature effect on the formation of tumuli on shield volcanoes: an example from Leitin lava flow field in Iceland, Zeitschrift für Geomorphologie, 114, 1– 10.

Rossi, M., Gudmundsson, A., 1996. The morphology of flow-lobe tumuli on Icelandic lava shields. Journal of Volcanology and Geothermal Research, 72, 291–308.

Saadi, N., Abdel Zaher, M., El-Baz, F., Watanabe, K., 2001. Integrated remote sensing data utilization for investigating structural and tectonic history of the Ghadames Basin, Libya. International Journal of Applied Earth Observation and Geoinformation,13, 778–791.

Salem, M., 2014. Jebel Al-Haruj: Biggest volcanic field in Libya with heritage and economic value. Libya Herald. The independent Libya Online, p. 4.

Sato, H., Aramaki, S., Kusakabe, M., Hirabayashi, J., Sano, Y.,Nojiri, Y., Tchoua, F., 1990. Geochemical difference of basalts between polygenetic and monogenetic volcanoes in the central part of the Cameroon volcanic line, Geochemical Journal, 24, 357–370.

Sanver, M., 1968. A palaeomagnetic study of Quaternary volcanic rocks from Turkey. Physics of the Earth and Planetary Interiors, 1, 403–421.

Schäfer, K., Kraft, K., Hausler, H., Erdman, J., 1980. In situ stresses and paleostresses in Libya. In: Salem, N.J., Busrewil, M.T. (Eds.), Geology of Libya, Al-Fateh University, Tripoli, 907–922.

Schofield, J., Brown, D., Magee, C., Stevenson, T., 2012. Sill morphology and comparison of brittle and non-brittle emplacement mechanisms, Journal of the Geological Society, 169, 127–141.

Schroter, T., 1996. Tectonic and sedimentary development of the central Zallah trough (west Sirt Basin, Libya), in M. J. Salem, M. T. Busrewil, A. A. Misallati, and M. A. Sola, eds., The geology of the Sirt Basin: Amsterdam, Elsevier, 3, 123–135.

Scotese, C., McKerrow, W., 1990. Revised world maps an introduction, in: McKerrow, W.S., Scotese, C.R. (Eds.), Paleozoic

Paleogeography and Biostratigraphy. Geological Society of America Bulletin, 12, 1–21.

Scott D., Stevenson, D., 1986. Magma ascent by porous flow. Journal of Geophysical Research, 91,9283–9296.

Self S, Thordarson Th, Keszthelyi L, Walker GPL, Hon K, et al. 1996.Anewmodel for the emplacement of the Columbia River Basalts as large inflated pahoehoe sheet lava flow fields. Geophysical Research Letters. 23, 2689–92

Self, S., Thordarson, T., Keszthelyi. L. 1997. Emplacement of continental flood basalt lava flows. In AGU Geophys. Monogr. Large Igneous Processes, ed. JJ Mahoney, M Coffin.

Self, S., Keszthelyi, L., Thordarson, T., 1998. The importance of pahoehoe. Annual Review of Earth and Planetary Sciences, 26, 81–110.

Semtner, A. Klitzsch, E., 1994. Early Paleozoic of the northern Gondwanan margin: new evidence for Ordovician-Silurian glaciation. International Journal of Earth Sciences. 83, 743–751.

Sestini, G., 1984. Tectonic and sedimentary history of the NE African margin (Egypt-Libya). In: J.E. Dixon and A.H.F. Robertson (Editors), The Geological Evolution of the Eastern Mediterranean. Geological Society London Special Publications, 17, 161–175.

Shegewi, O., 1992. Onshore and offshore basins of northeast Libya: their origin and hydrocarbon potential. In: Ph.D. Thesis, University South Carolina, p. 607.

Sevensen H., Corfu F., Polteau S., Hammer., Planke S., 2012. Rapid magma emplacement in the Karoo Large Igneous Province. Earth and Planetary Science Letters, 325–326, 1–9.

Silverman, B.. 1986. Density Estimation for Statistics and Data Analysis. New York: Chapman and Hall, p. 177.

Sinha, N. Mriheel, Y., 1996. Evaluation of subsurface Palaeocene sequence and shoal carbonates, south central Sirt Basin, in M. J. Salem, M. T. Busrewil, A. A. Misallati, and M. A. Sola, eds., The geology of the Sirt Basin: Amsterdam, Elsevier, 2, 153–196.

Skogseid, J., 1994. Dimensions of Late Cretaceous–Palaeocene northeast Atlantic rift derived from Cenozoic subsidence: Tectonophysics, 240, 225–247.

Skuce, G., 1996. Forward modeling of compaction above normal faults: An example from the Sirt Basin, Libya, in P. G. Buchanan and P. A. Nieuwland, eds., Modern development in structural interpretation, validation and modeling: Geological Society Special Publication, 99,135–136.

Solomon, S., Ghebreab, W., 2008. Hard-rock hydrotectonics using geographic information systems in the central highlands of Eritrea: Implications for groundwater exploration. Journal of Hydrology, 349, 147–155.

Stuart, F., Masoud, A., Mark, D., 2014. The origin of Cenozoic magmatism of Libya. Geophysical Research Abstracts, Vol. 16, EGU2014-15877

Stampfli, 2001. In: Stampfli, G. (Ed.), Geology of the Western Swiss Alps. A Guidebook, Mémoires de Géologie (Lausanne), 36, p. 195.

Suleiman, A., Albini, P., Migliavacca, P., 2004. A short introduction to historical earthquakes in Libya. Annals of Geophysics, 47, N. 2/3, April/June 2004.

Suleiman, A., Daba, I., Abdurazag, E., 2001. Seismicity of Sirt and surrounding areas. Detailed investigations and future planning, in First Conference on the Natural Resources in the Sirt Area, Sirt, Libya, p. 13 (in Arabic).

Suleiman, A. Doser, D.,1995. The seismicity, seismotectonics and earthquake hazards of Libya, with detailed analysis of the 1935 April 19, M = 7.1 earthquake sequence. Geophysical Journal International, 120, 312–322.

Suleiman, A., Magee, C., Jackson, C., Fraser, A., 2017. Igneous activity in the Bornu Basin, onshore NE Nigeria; implications for opening of the South Atlantic. Journal of the Geological Society of London. 1–12, https://doi.org/10.1144/jgs2016-107

Sutcliffe, O., Adamson, K., Ben Rahuma, 2000. The geological evolution of the Palaeozoic rocks of western Libya: a review and field guide. Second Symposium on the Sedimentary Basins of Libya, Geology of northwestern Libya. Field Guide. Earth Sciences Society of Libya. p. 93.

Suter, M., Quintero, O., and Johnson, C., 1992, Active faults and state of stress in the central part of theTrans-Mexican volcanic belt, Mexico: 1. The Venta deBravo fault: Journal of Geophysical Research, 97,11,983–11,993.

Tawadros, E., 2001. Geology of Egypt and Libya. A.A. Balkema, Rotterdam, p. 468.

Tibaldi, A., 2015. Structure of volcano plumbing systems: A review of multi-parametric effects. Journal of Volcanology and Geothermal Research, 298, 85–135.

Thomson D., Hutton D.,2004. Geometry and growth of sill complexes: insights using 3D seismic from the North Rockall Trough. Bulletin of Volcanology, 66, 364–375.

Thomson, K., Schofield, N.,2008. Lithological and structural controlson the emplacement and morphology of sills in sedimentary basins. Geological Society London Special Publications, 302, 31–44.

Thusu, B., 1996. Implication of the discovery of reworked and in situ late Palaeozoic and Triassic palynomorphs on the evolution of Sirt Basin, Libya. In: Salem, M.J.,U Mouzughi, Hammuda, O.S. (Eds.), The Geology of Sirt Basin, Elsevier, Amsterdam, I, 455–474.

Thordarson, T., 2000. Physical volcanology of lava flows on Surtsey, Iceland:A preliminary report. Suurtesy Research. Reylzjavik, 11, 109-126.

Thordarson, T., Sigmarsson, O., 2009. Effusive activity in the1963–67 Surtsey eruption, Iceland: flow emplacement andgrowth of small lava shields. In: Thordarson, T., G. Larsen,S. Self, S.

Rowland and Á. Höskuldsson eds. Studies in Volcanology:The Legacy of George Walker. Geological Society, London, Special Publications.

Thordarson, T., Höskuldsson, A., 2008. Postglacial volcanism in Iceland, Jokull - The Icelandic Journal of Earth Sciences, 58, 197-228.

Thordarson, T., Self, S., Miller, D., Larsen, G., Vilmundardóttir, G., 2003. Sulphur release from flood lava eruptions in the Veiðivötn, Grímsvötn and Katla volcanic systems, Iceland. In: Oppenheimer, C., D. M. Pyle and J. Barclay eds. Volcanic Degassing. Geological Society, London, Special Publications. 213, 103–121.

Thordarson T., Self, S., 1997. Atmospheric and environmental effects of the 1783-84 AD Laki eruption. Glob. Planet. Change. In revision Thordarson, T., Self, S., 1996. Sulphur, chlorine and fluorine degassing and atmospheric loading by the Roza eruption, Columbia River Basalt Group, Washington, USA. Journal of Volcanology and Geothermal Research, 74, 49–73.

Thordarson, T., Self, S., Óskarsson, N., Hulsebosch, T., 1996.Sulfur, chlorine, and fluorine degassing and atmospheric loading by the 1783–1784 AD Laki (Skaftár Fires) eruption in Iceland. Bulletin of Volcanology. 58, 205–225.

Thordarson, T., Self, S., 1993. The Laki (Skaftár Fires) andGrímsvötn eruptions in 1783–1785. Bulletin of Volcanology, 55, 233–263.

Torfason, H., 1979. Investigations into the structure of southeastern Iceland. Ph.D. Thesis, Univ. of Liverpool, ,p. 587.

Türkünal, S.,1980. Doğu ve Güneydoğu Anadolu'nun jeolojisi. TMMOB Jeoloji Mühendisleri Odası.

Unrug, R., 1996. Geodynamic map of Gondowana supercontinent assembly, scale 1: 10,000,000. Bur.Rech. Geol. Min. Orleans.

Unternehr, P., Curie, D., Olivet, J.L., Goslin, J., Beuzart, P., 1988. South Atlantic fits and intraplate boundaries in Africa and South America. Tectonophysics, 155, 169–179.

Valentine, G., 2012. Shallow plumbing systems for small-volume basaltic volcanoes, 2: evidence from crustal xenoliths at scoria cones and maars. Journal of Volcanology and Geothermal Research 223, 47–63

Valentine, G., Graettinger, A., Sonder, I., 2014. Explosion depths for phreatomagmatic eruptions. Geophysical Research Letters, 41, 3045–3051.

Valentine, G., de Vries B., 2014. Unconventional maar diatreme and associated intrusions in the soft sediment-hosted Mardoux structure (Gergovie, France). Bulletin of Volcanology, 76, 1–16

Valentine, G., Cortes, J., 2013. Time and space variations in magmatic and phreatomagmatic eruptive processes at Easy Chair (Lunar Crater Volcanic Field, Nevada, USA). Bulletin of Volcanology, 75, 1–13

Valentine, G., White, J., 2012. Revised conceptual model for maar diatremes: subsurface processes, energetics, and eruptive products. Geology, 40, 1111–1114

Valentine, G., Krogh. K., 2006. Emplacement of shallow dikes and sills beneath a small basaltic volcanic center–The role of pre-existing structure (Paiute Ridge, southern Nevada, USA), Earth and Planetary Science Letters, 246, 217–230.

Vaillant, M., Barnes, S., Mungall, J., Mungall, L., 2017. Role of degassing of the Noril'sk nickel deposits in thePermian–Triassic mass extinction event. Proceedings of the National Academy of Sciences of USA. 14, 2485–2490.

Van der Meer, F., Cloetingh, S. 1993. Intraplate stresses and subsidence history of the Sirt Basin (Libya): Tectonophysics, 226, 37–58.

Van Houten, F., 1983, Sirt Basin, north-central Libya, Cretaceous rifting over a fixed mantle hotspot? Geology, 11, 115–118.

Van Houten, F., 1980. Latest Jurassic–Early Cretaceous regressive facies, northeast African craton: AAPG Bulletin, 64, 857–867.

van Otterloo, J., Cas ,R., Sheard, M., 2013. Eruption processes and deposit characteristics at the monogenetic Mt. Gambier Volcanic Complex, SE Australia: implications for alternating magmatic and phreatomagmatic activity. Bulletin of Volcanology, 75, 1–21

Vesely, J., 1985. Geological Map of Libya 1: 250.000 Sheet; Zallah NH 33-16. Explanatory Booklet. Industrial Research Centre, Tripoli, p. 125.

Vincent P. 1970. The evolution of the Tibesti volcanic province, eastern Sahara. In: Clifford TN, Gass IG (eds) African magmatism and tectonics. Oliver and Boyd, Edinburgh, 301–319.

Vincent, P.1963. Les volcans tertiaires et quaternaires du Tibesti occidental et central (Sahara du Tchad). Mémoires BRGM 23. Thesis 1st part, University of Paris.

Vincent, P. 1960. Dynamismes et structures des volcans rhyolitiques du Tibesti occidental et central. Rev. Geogr. Phys. Geo., l 2, 229–237.

Wennekers, J., Wallace, N., Abugares, I., 1996. The geology and hydrocarbons of the Sirt Basin: A synopsis, in M. J. Salem, A. J. Mouzoughi, and O. S. Hammuda, eds., The geology of the Sirt Basin: Amsterdam, Elsevier, 1, 3–56.

Wacrenier P, Hudeley H, Vincent P. 1958. Notice explicative de la carte géologique provisoire du Borkou-Ennedi-Tibesti au 1:1,000,000e. Direction des mines et de la géologie AEF, Brazaville.

Westaway, R., 1996. Active tectonic deformation in the Sirt Basin and its surroundings. In: Salem, M.J., Busrewil, M.T., Misallati, A.A., Sola, M.J. (Eds.), First Symposium on the Sedimentary Basins of Libya, Geology of the Sirt Basin, Elsevier, Amsterdam, 3, 89–100.

Westaway, R., 1990. The Tripoli, Libya, earthquake of September 4, 1974: implications for the active tectonics of the central Mediterranean. Tectonics, 9, 231–248.

Wilson, M., 2007. Igneous Petrogenesis A global Tectonic approach. 9th Springer, p. 465

White, F., 1974. Viscous Fluid Flow. McGraw-Hill, New York, N.Y., p. 725.

White, R., McKenzie, D., 1989. Magmatism at rift zones: The generation of volcanic continental margins and flood basalts. Journal of Geophysical Research: Solid Earth, 94, 7685–7729.

Wignall, P., 2001. Large igneous provinces and mass extinctions. Earth-Science Reviews, 53, 1–33

Wilson, M., Guiraud, R., 1992. Magmatism and rifting in west and central Africa from Late Jurassic to Recent time: Tectonophysics, 213, 203–255.

Wilson, M., Guiraud., R., 1998. Late Permian to Recent magmatic activity on the African-Arabian margin of Tethys, in D. S. Macgregor, R. T. J. Moody, and D. D. Clark-Lowes, eds., Petroleum geology of North Africa: Geological Society (London) Special Publication 132, 231–263.

Winter, N., 2010. An introduction to igneous and metamorphic petrology, Prentice Hall PTR, p. 702.

Wise, D., Funicello, R., Parotto, M., Salvini, F., 1985.Topographic lineament swarms: Clues to their origin from domain analysis of Italy. Geological Society of America Bulletin, 96, 952-967.

Woller, F., 1984. Geological Map of Libya 1: 250.000, Sheet: Al Fuquaha NG 33-3. Explanatory Booklet. Industrial Research Centre, Tripoli, p.123.

Woller, F., Fediuk, F., 1980. Volcanic rocks of Gabal as Sawda. In: Salem, M. J., Busrewil, M. T. (eds.), The Geology of Libya, London Academic Press, 3, 1081– 093.

Yahiaouia, R., Dautriab J., Alardb O., Boschb D., Azzouni-Sekkalc, d. , Bodinierb J., 2014. A volcanic district between the Hoggar uplift and the Tenere Rifts: Volcanology, geochemistry and age of the In-Ezzane lavas (Algerian Sahara) Journal of African Earth Sciences, 92, 14–20.

Yılmaz, Y., Guner, Y, Saroglu, F., 1998. Geology of the Quaternary volcanic centres of the East Anatolia. Journal of Volcanology and Geothermal Research, 85, 173–210.

Zakir, F., Quari, M., Mostafa, M.,1999. New optimizing technique for preparing lineament density maps. International Journal of Remote Sensing, 20, 1073–1085.

Ziegler, P., 1992. Plate-Tectonics. Plate moving mechanisms and rifting. Tectonophysics, 215, 9–34.

Ziegler, P., 1988. Evolution of the Arctic-North Atlantic and the western Tethys: AAPG Memoir 43, p. 198.

Zoback, M., World Stress Map team, 1989. Global patterns of tectonic stress. Nature. 341, 291-2YX.

Appendix A

Supplementary data of Elshaafi and Gudmundsson (2016) (Chapter 5)

I

Length, thickness, orientation and aspect (length/thickness) ratios of 47 dykes and volcanic fissures mapped from satellite imagery.

number	Length (m)	thickness (m)	Azimuth	Length/thickness
1	445	0.83	136°	536
2	1100	1.15	127°	957
3	513	0.8	143°	641
4	550	0.83	137°	663
5	373	0.56	149°	666
6	183	0.53	110°	345
7	169	0.56	140°	302
8	920	1.25	150°	736
9	825	1.15	133°	717
10	128	0.42	82°	305
11	143	0.63	133°	227
12	230	0.59	127°	390
13	234	0.69	77°	339
14	159	0.74	73°	215
15	236	0.98	45°	241
16	205	0.63	60°	325
17	193	0.51	17°	378
18	290	0.72	144°	403
19	57	0.44	137°	130
20	183	0.83	87°	220
21	166	0.69	145°	241
22	151	0.63	128°	240
23	197	0.73	147°	270
24	217	0.71	158°	306
25	725	1.1	162°	659
26	315	0.84	157°	375
27	307	0.75	133°	409
28	233	0.83	109°	281
29	221	0.67	25°	330
30	189	0.63	27°	300
31	245	0.83	159°	295
32	196	0.61	120°	321
33	167	0.59	150°	283
34	364	0.82	140°	444
35	1133	2.1	99°	540
36	450	0.98	50°	459
37	237	0.79	152°	300
38	340	0.8	102°	425
39	771	1.12	100°	688
40	230	0.79	51°	291
41	245	0.59	169°	415
42	320	0.69	23°	464
43	210	0.48	85°	438
44	219	0.49	135°	447
45	926	1.25	139°	741
46	817	1.1	96°	743
47	345	0.89	133°	388

Appendix A

Supplementary data of Elshaafi and Gudmundsson (2016) (Chapter 5)

II

Schematic illustration the tectonic evolution of the Al Haruj region subdivided into five main deformation phases from the late Precambrian to Holocene. The data is based on field observations as well as interpretation of aerial photographs and satellite imagery (modified from Peregi et al., 2003).

Deformation Phase	Age	Stress axes
V	Late Miocene - Quaternary	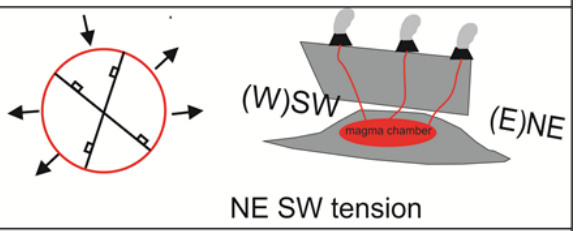
IV	Paleocene - Oligocene	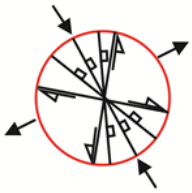 NE- SW to E- W tension NW-SE to N-S compression
III	Late Carboniferous	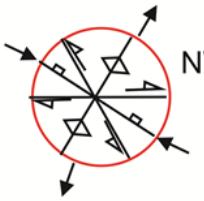 NW-SE compression
II	Early Paleozoic	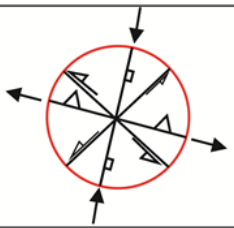 N-S Compression
I	Late Neoproterozoic - early Cambrian	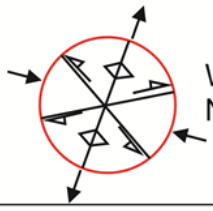 WNW-ESE compression NNE-SSE tension

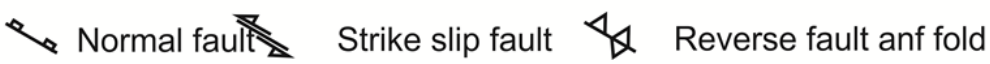 Normal fault Strike slip fault Reverse fault anf fold

Appendix A

Supplementary data of Elshaafi and Gudmundsson (2016) (Chapter 5)

III

Map showing the main structural elements of the Sirt Basin trend NW-SE. Dashed black lines indicate σ_3 stress trajectories that show slight changes at the southernmost of the AHVP (modified after Anketell, 1996; Less et al., 2006).

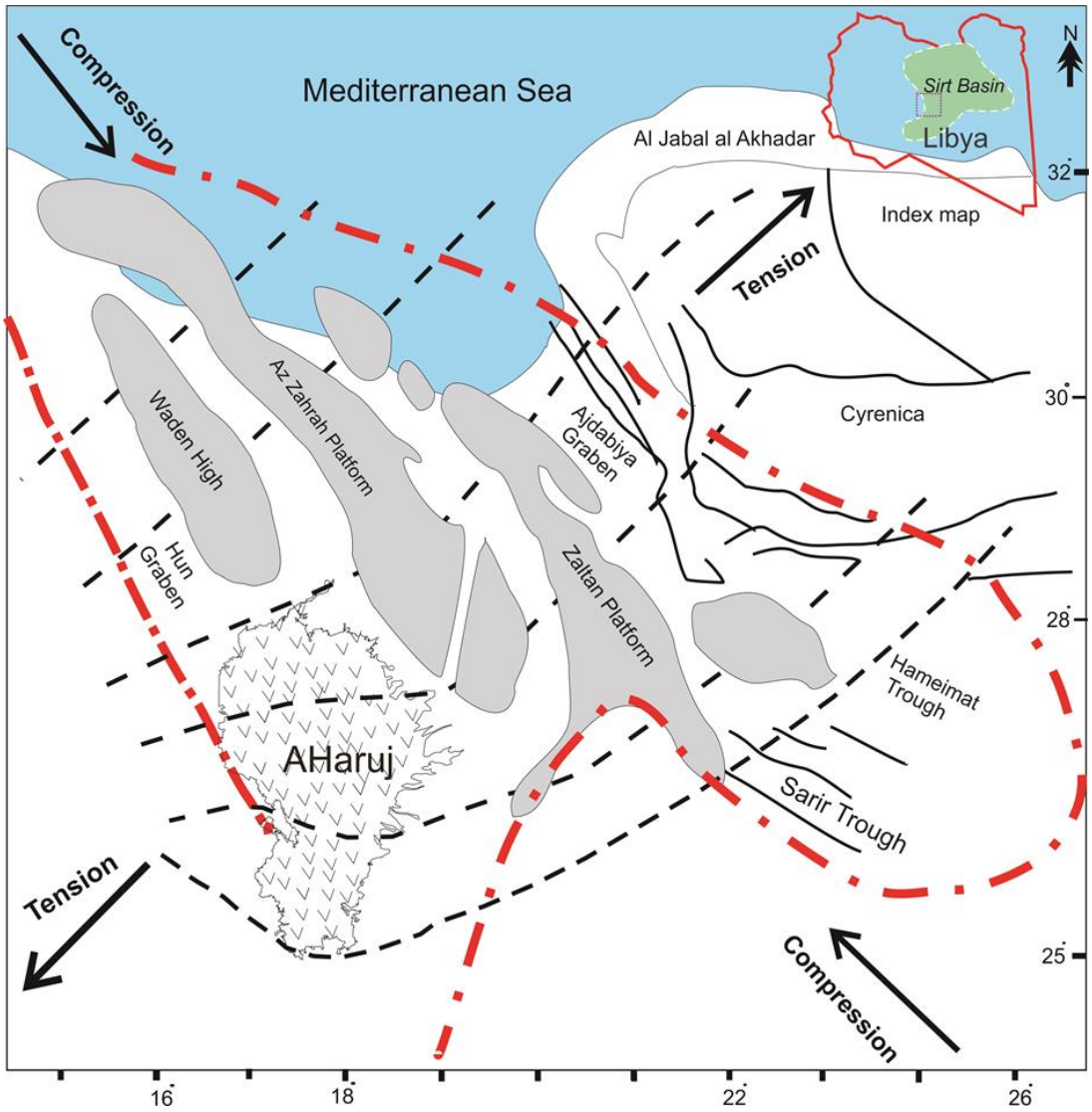

Appendix B

Supplementary data of Elshaafi and Gudmundsson (second revision in Tectonophysics) (Chapter 8)

I

Block model showing the tensile stress resulting from magma reservoirs and far-field extensional stress throughout Libyan territory. Applied the tensile boundary load is 5 MPa and excess magma pressure is 5 MPa in each magma reservoir. GVP; Gharyan Volcanic Province, SVP; Sawda Volcanic Province, AHVP; Al Haruj Volcanic Province, NVP; Nuqay Volcanic Province.

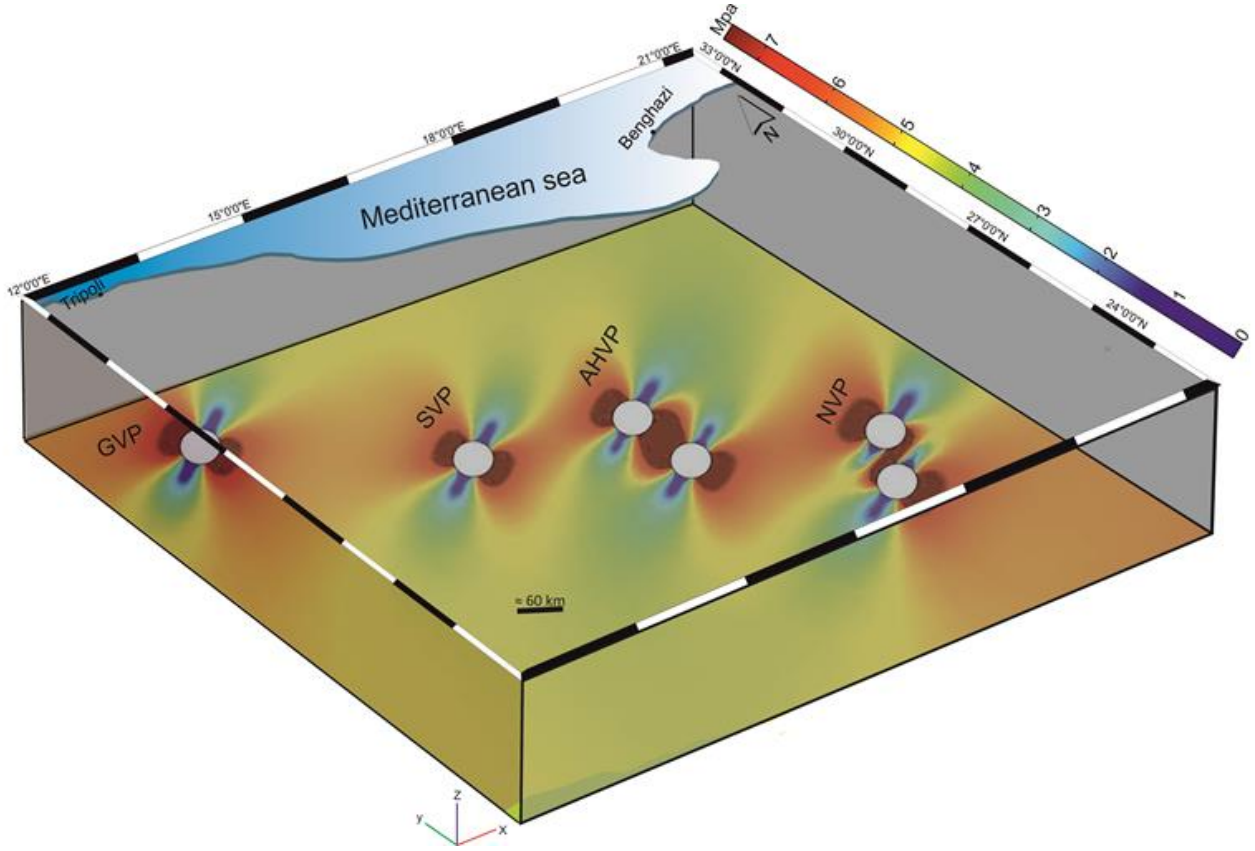

Appendix B

Supplementary data of Elshaafi and Gudmundsson (second revision in Tectonophysics) (Chapter 8)

II

The numerical model results, tensile stress on the left side and shear stress on the right side, with various diameters of magma reservoir in the range from 66 km to 120 km. The Haruj al Aswad volcanic system modelled with nearly a double diameter of around 120 km and the Al Haruj Al Abyad volcanic system as with a diameter of 80 km, the rest of the reservoirs being of diameter 66 km. It is interesting to note that the potential zones for mechanical interaction between volcanic systems remained generally as similar and effectively as Figure 7.

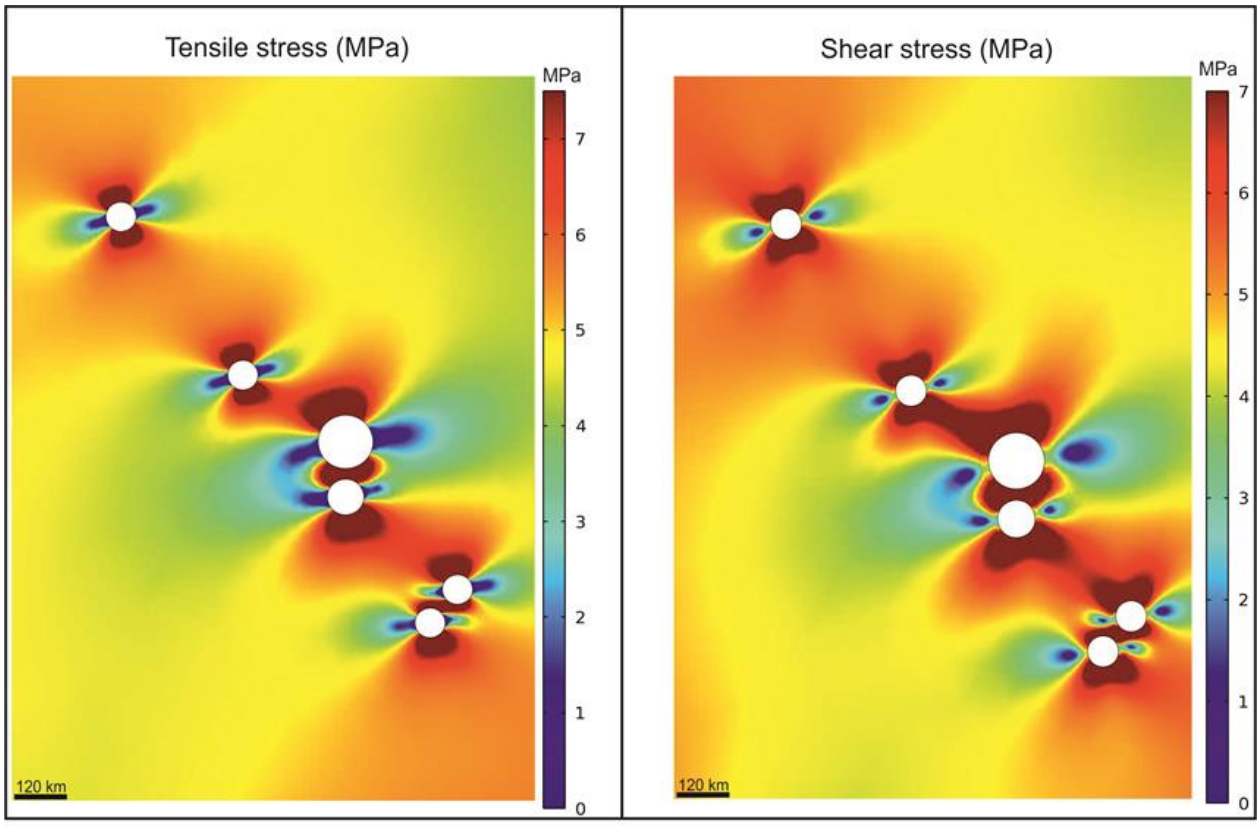

Appendix C

Large-volume lava flows fed by a deep magmatic reservoir at Ağrı Dağı (Ararat) volcano, Eastern Turkey

I

Bulletin volcanology

Özgür Karaoğlu & Abdelsalam Elshaafi & Mohamed K. Salah & John Browning & Agust Gudmundsson

Bull Volcanol (2017) 79:15 DOI 10.1007/s00445-016-1098-0

Contribution statement:

The initial idea and creation of numerical models were conducted by ÖK and AE and support input from co-authors

Measurements using ArcGIS conducted by AE

Analytical approach was developed by AE

Writing the initial draft was made by ÖK and AE and later revising the manuscript for important intellectual content from all authors

Tomographic images and their analysis and interpretation were conducted by MS

Illustrations were prepared by ÖK and support input by AE

All authors contributed to improve the final manuscript.

Bull Volcanol (2017) 79:15
DOI 10.1007/s00445-016-1098-0

RESEARCH ARTICLE

Large-volume lava flows fed by a deep magmatic reservoir at Ağrı Dağı (Ararat) volcano, Eastern Turkey

Özgür Karaoğlu[1,2] · Abdelsalam Elshaafi[2] · Mohamed K. Salah[3] · John Browning[4] · Agust Gudmundsson[2]

Received: 22 August 2016 / Accepted: 28 December 2016

Abstract Ağrı Dağı (Ararat), whilst being the tallest volcano in Turkey, is largely understudied. Two predominant peaks, Greater and Lesser Ağrı, make up the main edifice, which has been built during four main phases. The most recent phase consisted of two volcanic eruptions. The respective surface area and volume of the first volcanic eruption were estimated at 96 km^2 and 3.2 km^3, whereas those of the second eruption were much smaller with the surface area and volume estimated at 25 km^2 and 0.6 km^3. It is unusual for stratovolcanoes to produce basaltic eruptions of more than 3 km^3, although these and larger volumes are not uncommon in flood basalt-type eruptions. Large basaltic eruptions from stratovolcanoes normally require volcano-tectonic forcing (e.g. subsidence of collapse caldera and graben). However, there is no evidence for such volcano-tectonic forcing, during the most recent eruptions at Ağrı Dağı (Ararat), and therefore, their comparatively large volume basaltic lavas need to be explained in a different way. Here, we present an analytical method for calculating the source volume needed to supply magma to the eruptions at Ağrı Dağı. We found that the lava flow of 3.2 km^3 was likely fed by a very large magma reservoir (~13,000 km^3), while the second flow of 0.6 km^3 was fed by a reservoir of a much smaller effective size (or ~2000 km^3). 'Effective size' depends on what fraction of the reservoir participates in the eruption. We propose that the entire reservoir supplied magma to the larger eruption, but only one of its compartments (about one fifth of the total volume of the reservoir) supplied magma to the smaller eruption. Although seismic tomography indicates a magma reservoir at great depths (>20–30 km) below the Ağrı Dağı volcano, geochemical constraints on some of the later-formed rocks suggest an interaction between a shallow chamber (at 8–10-km depth) and the deep reservoir approximately 0.5 Ma. We provide numerical models whose results indicate that dykes injected from the lateral margins of the deep-seated reservoir are more likely to reach the surface directly rather than replenish the shallow magma chamber, suggesting also that the compartment for the second eruption was at the margin of the reservoir.

Keywords Large eruptions · Magma chambers · Magma reservoirs · Volcano-tectonic forcing · Crustal stresses · Numerical models

Editorial responsibility: V. Acocella

Electronic supplementary material The online version of this article (doi:10.1007/s00445-016-1098-0) contains supplementary material, which is available to authorized users.

✉ Özgür Karaoğlu
ozgur.karaoglu@deu.edu.tr; cougarforever@gmail.com

[1] Department of Geological Engineering, Eskişehir Osmangazi University, 26040 Eskişehir, Turkey

[2] Department of Earth Sciences, Royal Holloway University of London, Egham TW20 0EX, UK

[3] Department of Geology, American University of Beirut, Riad El Solh, Beirut 1107 2020, Lebanon

[4] Department of Earth Sciences, University College London, Gower Street, London WC1E 6BT, UK

Introduction

Magma or melt transport in the mantle is somewhat different from magma transport in the upper crust. Magma in the mantle, and partly in the lower crust, ascends by porous flow (Scott and Stevenson 1986). At shallower crustal levels, magma ascent is primarily through magma-driven fractures, that is, dykes. Dyke initiation and propagation are known to be partly controlled by regional stress fields, particularly those

Published online: 24 January 2017

induced by crustal extension (e.g. Gudmundsson 1990, 2006; Daniels et al. 2012; Le Corvec et al. 2013; Maccaferri et al. 2014; Tibaldi 2015). Reservoirs which are underlying the shallow magma chamber may directly supply magma to areas outside of the stratovolcano (Gudmundsson 2006). Thus, less evolved magmas can erupt at the margins of stratovolcanoes while more evolved magmas erupt within the central parts of the stratovolcano.

Long-lived (>1 My) major volcanic edifices, such as a stratovolcano, a caldera volcano or a large shield volcano (basaltic edifice), are commonly supplied with magma from a comparatively shallow crustal magma chamber (Browning et al. 2015; Gudmundsson 2016; Karaoğlu et al. 2016), while active, a shallow magma chamber acts as a sink for magma from a deeper magma source (or reservoir) (Gudmundsson 2012; Le Corvec et al. 2013). If new magma is injected from a deeper source during an eruption, that magma is likely to be of high density and may accumulate at the floor of the magma chamber (Coppola et al. 2009; Gudmundsson 2012). For an eruption to occur, the necessary conditions are that the magma chamber or reservoir (deep-seated magma chamber) ruptures and a fluid-driven fracture is able to propagate from the chamber to the surface (Gudmundsson 2012). There is a close relationship between the excess chamber pressure (p_e) and magma recharge volume. At the most active volcanoes, rupture probability based on increasing excess pressure within the shallow chamber allows forecasts of dyke formation to be made in real time during magma recharge events (Browning et al. 2015). Stratovolcanoes in Turkey, or elsewhere, are commonly fed by shallow crustal magma chambers with estimated volumes that commonly range from about 5 to 500 km^3 (e.g. Chester 1993). Lavas issued from stratovolcanoes commonly range in volume between 0.01 and less than 0.1 km^3. Whilst these small eruption volumes can be considered 'normal', more voluminous eruptions are known to erupt at stratovolcanoes such as the 1981 lateral blast event at Mt. Saint Helens, USA (2.5 km^3), the Plinian eruption of Krakatoa, Indonesia, in 1881 (18–21 km^3), the 1991 dome collapse of Mt. Unzen, Japan (1 km^3), and the Plinian eruption of Mt. Nemrut, Eastern Turkey (2.5 km^3) (Karaoğlu et al. 2005). Such events cannot be considered normal as they are often associated with some degree of volcano-tectonic forcing, particularly graben or caldera formation or slip. By volcano-tectonic forcing, we mean processes where the strain energy needed for displacement on a ring fault of a caldera or the boundary faults of a graben is primarily of tectonic origin and the displacement cause reduction in volume and shrinkage, of the chamber/reservoir source. The volume reduction maintains the magmatic excess pressure in the source until the very end of the eruption, thereby squeezing out an exceptionally large fraction of the magma in the source and producing a large eruption (Gudmundsson 2015, 2016). As said, we do not find evidence of volcano-tectonic forcing of this kind for these two eruptions and therefore seek alternative explanations for their sizes.

The type and composition of magma feeding an eruption can also influence the eruptive volume. For example, eruptions of felsic magmas commonly produce somewhat larger volumes than mafic ones, as exemplified by the eruption of Puyehue-Cordon Caulle, which produced a rhyolitic lava flow of volume 0.5 km^3 (Tuffen et al. 2013). Nevertheless, large-volume basaltic lava flows are commonly associated with flood basalt events such as the Deccan Plateau and the Columbia Basalt Plateau (Reidel et al. 2013).

It is seemingly rare for stratovolcanoes to produce both normal-size eruptions and large-volume effusive eruptions without an element of local volcano-tectonic forcing (Gudmundsson 2015, 2016). The Ağrı Dağı volcano, however, seems to exhibit such rare behaviour. Where most of the lavas that make up Ağrı Dağı were produced in relatively small eruptions (<0.1 km^3), two massive basaltic lava flows with total volume exceeding 3.8 km^3 formed roughly during the period between the peak activities of the Greater and Lesser Ağrı volcano. There is currently no explanation as to why such voluminous eruptions occurred during this time.

At the height of 5165 m, Ağrı Dağı (Ararat) is the tallest volcano in Turkey and comprised two main peaks: Greater and Lesser Ağrı (Fig. 1). The most recent eruption (<0.5 Ma) of Ağrı Dağı occurred at 39° 30′ 20″ N/44° 22′ 23″ E and produced two generations of basaltic lava flows. The former volcanic eruption occupies an area of about 96 km^2 and a volume of around 3.2 km^3, while the later volcanic eruption was much smaller with an area of 25 km^2 and a volume of 0.6 km^3 (Fig. 1). The exact age difference between these lava flows, however, is unknown. The nearest major population centres (about 145,000 inhabitants) are only 6 km away from the volcano. Many of the stratovolcanoes in Eastern Turkey are poorly studied and understood, particularly in terms of their relationship to the current tectonics. This is an important issue because Ağrı Dağı and other neighbouring volcanoes are situated close to major strike-slip faults and areas of triple junction tectonics (Fig. 1).

The Ağrı Dağı volcano covers the largest area (~1100 km^2) of any volcano in Turkey. The volcano has erupted 1150 km^3 of volcanic materials over its ~1.5 Ma of activity (Yılmaz et al. 1998) (Fig. 2). There are no calderas or grabens dissecting the volcano, which is in contrast with the common calderas on most stratovolcanoes in Eastern Turkey, such as the Nemrut caldera (Karaoğlu et al. 2005). The orientations of the parasitic cones and main volcanic fissures indicate that the dominant direction of tension in the area is NW–SE (e.g. Karakhanian et al. 2002). Dextral faults are common and form several pull-apart structures, some of which may be linked to volcanic activity (Karakhanian et al. 2002).

Ağrı Dağı is a typical stratovolcano mostly built up by calc-alkaline volcanic rocks (Yılmaz et al. 1998, Fig. 2). Initial products (pre-cone phase) observed in the eastern part of the volcano are mainly intermediate (dacitic and andesitic in

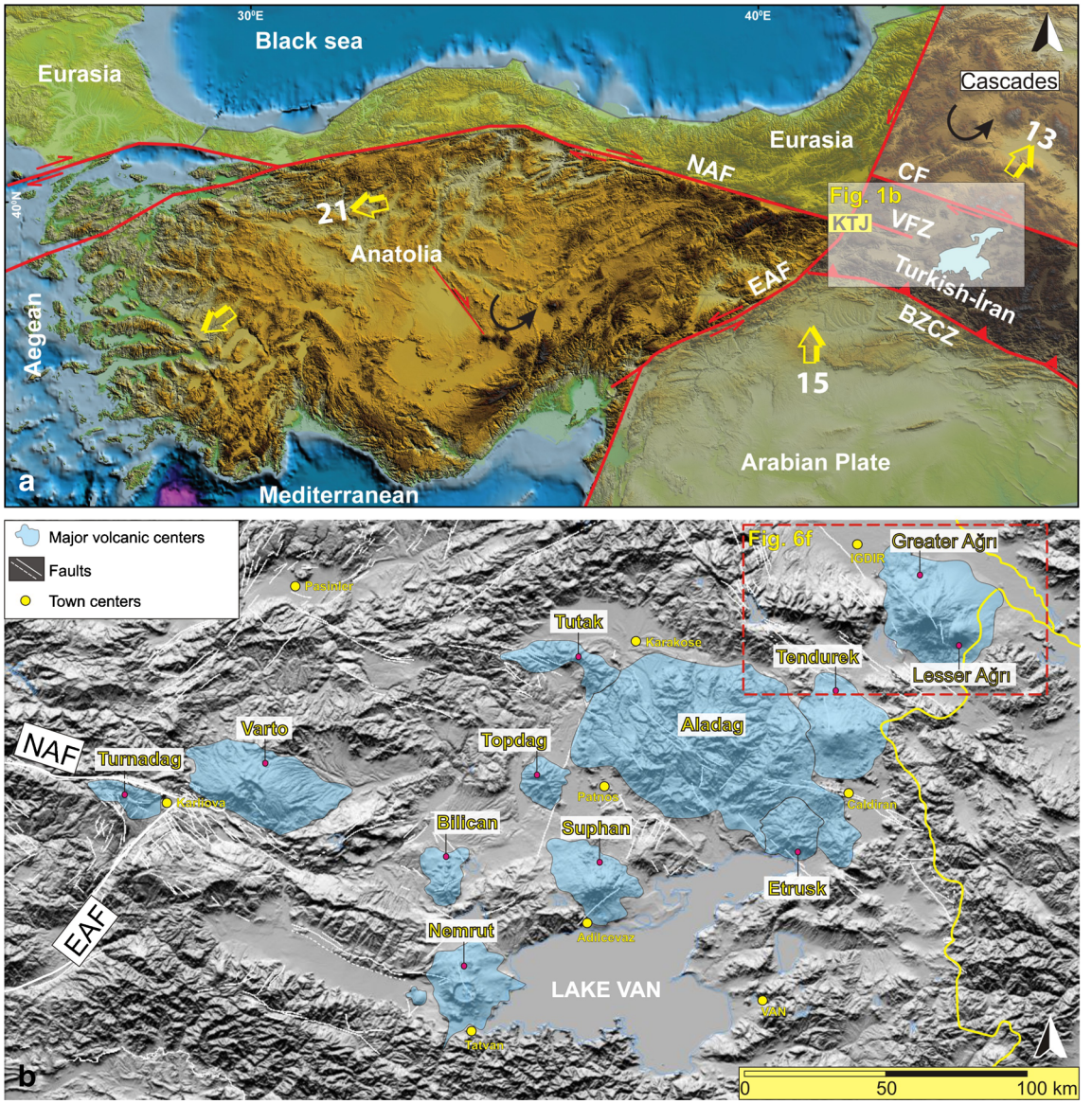

Fig. 1 **a** Map of the tectonic framework of Turkey. **b** Middle Miocene to recent volcanic centres in Eastern Turkey and location of population centres on a DEM-derived map. *NAF* North Anatolian Fault, *EAF* Eastern Anatolian Fault, *KTJ* Karlıova Triple Junction, *VFZ* Varto Fault Zone

composition) pyroclastic rocks and lavas (e.g. Yılmaz et al. 1998). K-Ar radiometric age data show that the oldest lavas are basaltic and were erupted between 1.51 and 1.09 Ma ago (Sanver 1968; Pearce et al. 1990). Basaltic lava flows overlay the oldest volcanic rocks. Following the first eruptive stages, the main cone of the volcano was built up mostly by andesite and dacite lavas. The last stage (flank eruption phase) is represented by alternating andesitic and basaltic lava flows from the main cone and parasitic scoria spatter cones on the flanks. During the last and most recent phase, basaltic lava flows were particularly dominant at the margin of the Ağrı Dağı volcano (Fig. 2).

One objective of this paper is to provide models that give insights into the magma storage systems feeding the Ağrı Dağı volcano and how their characteristics can account for the contrasting eruption volumes issued at the volcano. More specifically, we aim to find the feeding mechanism of the large-volume basaltic lava flows. Furthermore, in the absence of evidence of volcano-tectonic forcing contributing to the generation of the lava flows, we seek an alternative mechanism for their comparatively large sizes. In particular, we propose that the entire reservoir supplied magma during the eruption of the larger and more primitive lava flow. By contrast, we suggest that only a small compartment within the reservoir supplied magma during the eruption of the smaller and more evolved lava flow.

Geochemical constraints indicate that the Ağrı Dağı volcano was predominantly constructed from acidic to intermediate lavas and the later-formed rocks indicate an interaction between a shallow chamber (at 8–10-km depth) and the deep

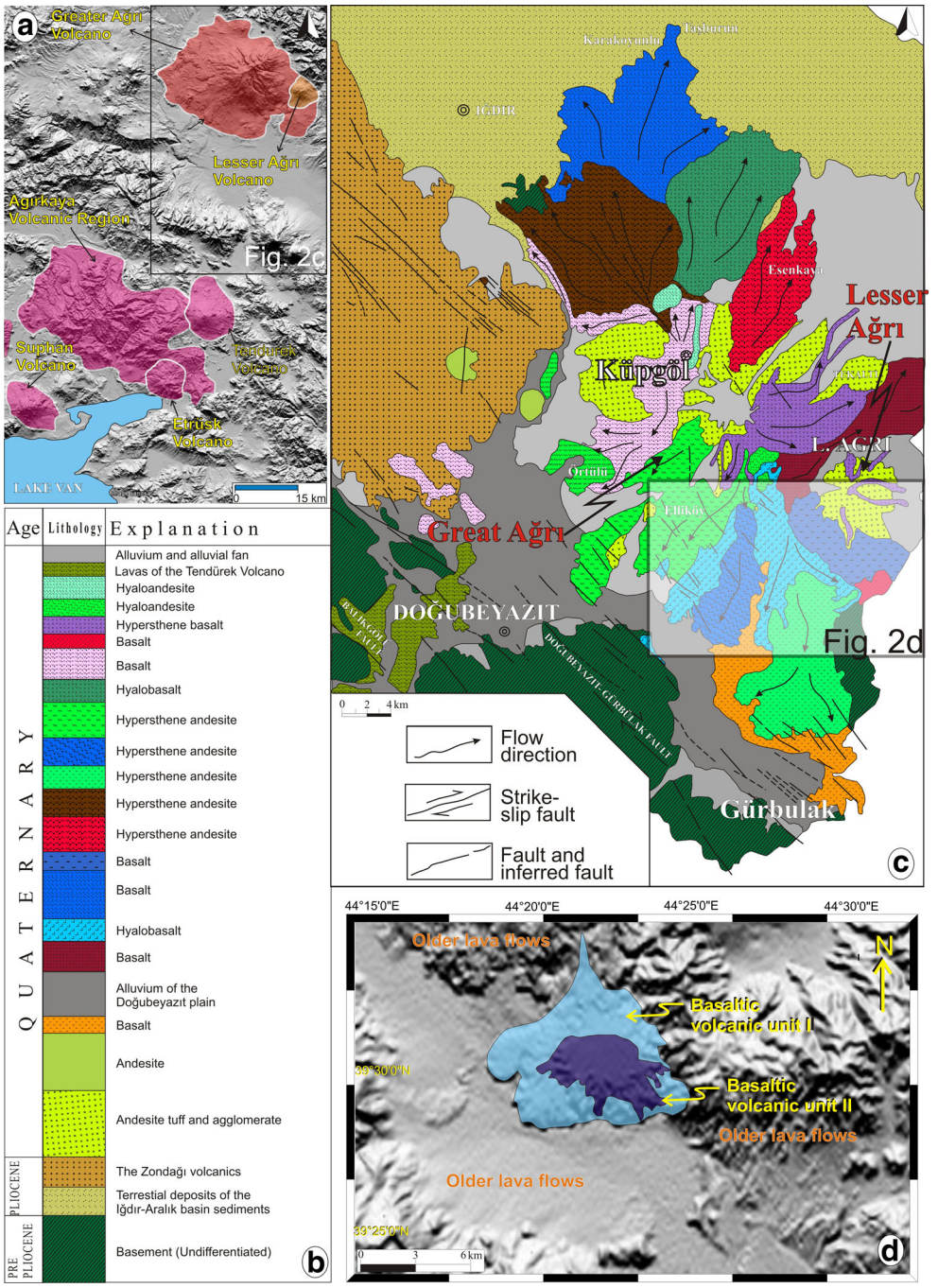

Fig. 2 **a** Ağrı Dağı volcano and surrounding region. **b** Volcano stratigraphy of the Ağrı Dağı volcano. **c** Geological map of the Ağrı Dağı volcano. **d** Geological map of the last two basaltic lava eruptions, flows I and II

reservoir. As such, we have developed numerical models to study how of the magma systems of Ağrı Dağı volcano interact over time. These models are combined with approximate estimations as to the volume of the magma system underlying the Ağrı Dağı volcano in order to understand how and why such comparatively voluminous lavas can be erupted from stratovolcanoes such as Ağrı Dağı. The results provide information which is vital for understanding such large eruptions, particularly because they pose a significant threat to nearby population centres (e.g. Small and Naumann 2001).

Geological setting and geochemistry of the Ağrı Dağı volcano

The East Anatolian High Plateau (EAHP) displays a very complex volcano-tectonic history of continental collision. After the closure of the Neotethyan Ocean as a result of Africa-Eurasian convergence (Barka 1992; Okay and Tüysüz 1999; Bozkurt 2001), syn- and post-collisional magmatisms dominate in the EAHP since the Middle Miocene (15 My, Lebedev et al. 2010). Four stages of Neogene-Quaternary volcanism have been identified:

Middle Miocene (15.0–13.5 Ma), Late Miocene (10–9 Ma), Pliocene (5.8–3.7 Ma) and Quaternary (1.0–0.4 Ma) (Lebedev et al. 2010). Quaternary stratovolcanoes (e.g. Nemrut, Suphan, Ağrı Dağı volcanoes, Fig. 1) and shield volcanoes (e.g. Tendürek) on the Eurasian Plate produce predominantly calk-alkaline-type eruptive materials (e.g. Pearce et al. 1990; Keskin et al. 1998; Yılmaz et al. 1998; Keskin 2007, Lustrino et al. 2010), with minor alkaline igneous rocks (e.g. Innocenti et al. 1976, 1980; Pearce et al. 1990; Keskin et al. 1998; Yılmaz et al. 1998; Alici et al. 2001; Keskin 2007). Lustrino et al. (2010) proposed that extensive volcanic activity on the Arabian plate, such as Karacadağ shield volcano, surfaced on a 35–40-km-thick crust mostly during the Late Miocene to Quaternary, with the production of large amounts of alkaline basic rocks (Pearce et al. 1990; Ercan et al. 1990; Notsu et al. 1995). The formation of Ağrı Dağı volcano has been tectonically linked to slab break-off and delamination in intraplate settings overlying hot asthenosphere through transtension (Yılmaz et al. 1998; Shabanian et al. 2012; Selçuk et al. 2016).

Recent seismic tomography studies have documented that the crust in Eastern Turkey has an average thickness of 65 km; it is thinner than average in the south, about 38 km (Arabian foreland (Angus et al. 2006; Ozacar et al. 2008; Cakir et al. 2000; Zor et al. 2003) (Fig. 1). Many studies suggest that the lithospheric mantle may be either completely absent (e.g. Al-Lazki et al. 2003) or very thin (e.g. Angus et al. 2006; Ozacar et al. 2008) beneath Eastern Turkey. Three controversial views have been expressed as to the origin of volcanism in Eastern Turkey; namely (i) that the region is reformed by melting and cooling of the asthenosphere and is as such an older lithospheric mantle (Keskin 2007); (ii) that, on average, a 20-km-thick lithosphere may have resulted from cooling of the asthenosphere from 15 to 7 Ma (Angus et al. 2006); and (iii) slab break-off of a northward subducting slab belonging to the northern branch of the Neotethyan ocean (e.g. Şengör et al. 2003; Keskin 2007). The crustal stress field has likely changed dramatically in the past 10 to 5 Ma (Örgülü et al. 2003). These seismic- and petrology-based studies indicate that the uppermost mantle is partially molten and that the asthenosphere is close to the base of the crust, consistent with the existence of volcanism in the region (Örgülü et al. 2003).

The volcano stratigraphy of the Ağrı Dağı volcano was mapped by Yılmaz et al. (1998). Geological observations and published data (Türkünal 1980; Bingöl et al. 1989) show that 14 different types of geological units represent the stratigraphy of the region around the Ağrı Dağı volcano (Appendix Table 1). A cone-building phase produced mostly basaltic but rarely andesite rocks between 0.68 and 0.5 Ma (Sanver 1968; Pearce 1990). The final stages of activity resulted in flank eruptions between 0.3 and 0.04 Ma (Sanver 1968; Pearce 1990; Ercan et al. 1990; Notsu et al. 1995), and the most recent activity which occurred 20,000 years ago produced mostly andesitic lavas (Nagao et al. 1989). Since this period, the volcano has been dormant, although there were unrest periods characterised by increased seismicity in 2500–2400 BC and 1840 AD (Karakhanian et al. 2002).

Here, we consider the most recent basaltic lava flows erupted during the cone-building and flank eruption phases (<0.5 Ma), which are located on the southern flank of the Greater Ağrı Dağı volcano (lava flows I and II, Fig. 3). The flows are easily distinguishable from the older basaltic lava flows (lava flow III, Fig. 3) by colour and lack of both erosion and alteration. These most recent basaltic lava flows were erupted from a NW–SE aligned series of scoria cones dated at 0.5 Ma (Sanver 1968). The origin of those basaltic lava flows is poorly constrained in terms of petrology because previous sampling localities were not spatially defined (e.g. Pearce et al. 1990; Yılmaz et al. 1998). Generally, though, the volcanic rocks of the Ağrı Dağı volcano are classified through a wide compositional range from trachy-basalt, tephrite/basanite, basaltic andesite, andesite, dacite and rhyolite (Fig. 4a) (e.g. Pearce et al. 1990; Nagao et al. 1989; Kheirkhah et al. 2009). A significant feature of the genesis and evolution of Quaternary magmas in Ağrı Dağı is the absence of basalt on the plot although the petrography shows them as basalt (Fig. 4). MORB-normalised trace element content of selected basaltic rocks is shown in Fig. 4b. The basaltic lava flows at the main cone of the Ağrı Dağı are more enriched in LREE than the marginal lavas (Fig. 4b).

Injected material and reservoir volume

In order to estimate the relative contribution of a shallow magma chamber and the contribution of a deeper magma reservoir to the eruptions of Ağrı Dağı, we calculated first the total volume of injected materials, that is, magma volume leaving the chamber/reservoir during the eruption, from the lava flows I and II. In this study, we used ArcGIS 10.1 to calculate the geometry and area of the Quaternary basaltic lava flows I and II (Fig. 3). The maximum thickness for each flow was estimated based on the elevation difference with the surrounding area using a Shuttle Radar Topography Mission (SRTM) compiled digital elevation model (DEM). The thickness of each individual lava flow increases from the margins to the centre, and so, the greatest thickness was recorded at the centre of each flow that appears to be similar to lava shield (Fig. 2).

We can make an approximation to the shape and emplacement style of a lava shield. The volume of a lava shield is generally computed by approximating its shape as a truncated cone for flat-topped volcanoes or a pyramid for a volcano with a distinct peak (Hasenaka 1994). Therefore, during this study, the volume of each lava flow is calculated by approximating its shape to a cone, namely as

$$V_e = a\left(h/3\right) \quad (1)$$

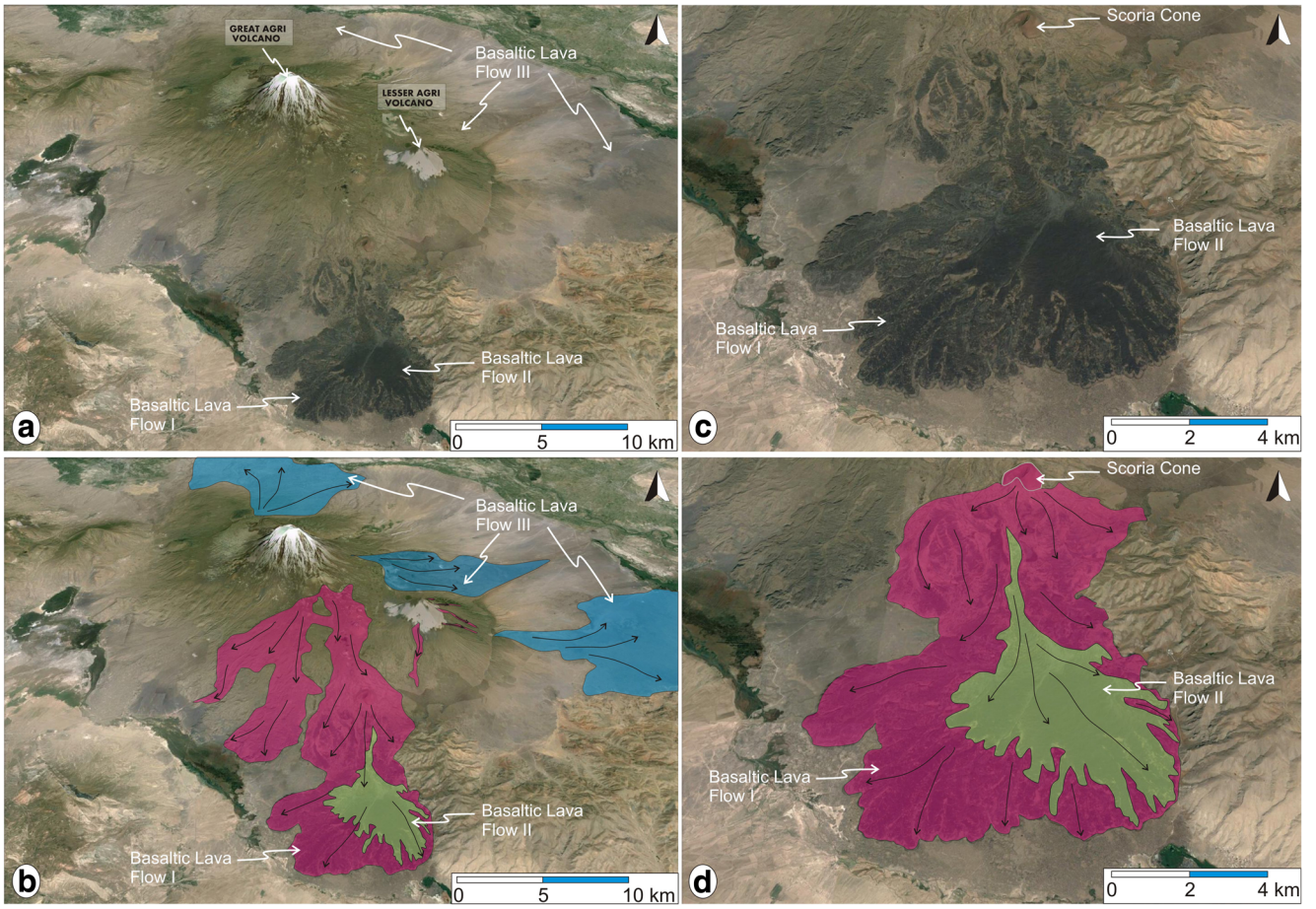

Fig. 3 The last basaltic/most basaltic lava flows around Ağrı Dağı volcano. **a**, **b** Google Earth images of basaltic lava flows at around the Great and Lesser Ağrı Dağı volcanoes. **c**, **d** Images of the most recent lava flows (I–II)

where V_e is the volume of the volcanic unit, a is the area, and h is the maximum thickness of the unit. The area of the base of each individual volcanic unit was calculated using ArcGIS. The volume of eruptive surface materials is somewhat uncertain because part of the flow may be partially submerged by younger thick lava sequences (Andrew and Gudmundsson 2007). The total volume of the injected material is a combination of the volume of an individual lava flow on the surface and the volume of the feeder dyke that fed the eruption. There are no available data in the study area on dyke geometries, such as length (strike dimension), thickness and depth (dip dimension), to calculate the volume of feeder dykes. As such, we use rough estimations of the average volume of dykes in Eastern Turkey, where the volumes do not exceed 0.004 km^3 (Karaoğlu et al. 2016). Therefore, the error produced in the total injected material due to neglected volume of feeder dyke is very small.

The total injected material or magma *Ve* from Eq. (1) for lava flow I is around 3.2 km^3 (±0.1 km^3), while the total injected material for lava flow II is around 0.6 km^3 (±0.02 km^3). Both volumes are quite similar to the sizes of monogenetic Holocene lava shields on the Reykjanes Peninsula, West Iceland, where the volume lava flow II is approximately the same size of the picrite lava shields, while the volume lava flow I is approximately the size of the olivine-tholeiite shields (Andrew and Gudmundsson 2007). The primary picrite or olivine basaltic magmas in Iceland are believed to come from deep magma reservoirs rather than crustal shallow magma chambers (Meyer et al. 1985).

It is known that magma can accumulate at the crust-mantle boundary, which is commonly the situation for deep-seated reservoirs. A deep reservoir may directly feed surface eruptions or form a shallow magma chamber in the upper or middle crust. Such shallow chambers can form due to abrupt changes in the mechanical properties of the crustal rocks, particularly changes in stiffness (Young's modulus) of those rocks (Barnett and Gudmundsson 2014). In areas of intense magmatism such as Iceland, the crust-mantle boundary is commonly referred to as the magma layer (Hermance 1981; Bjornsson 1983;

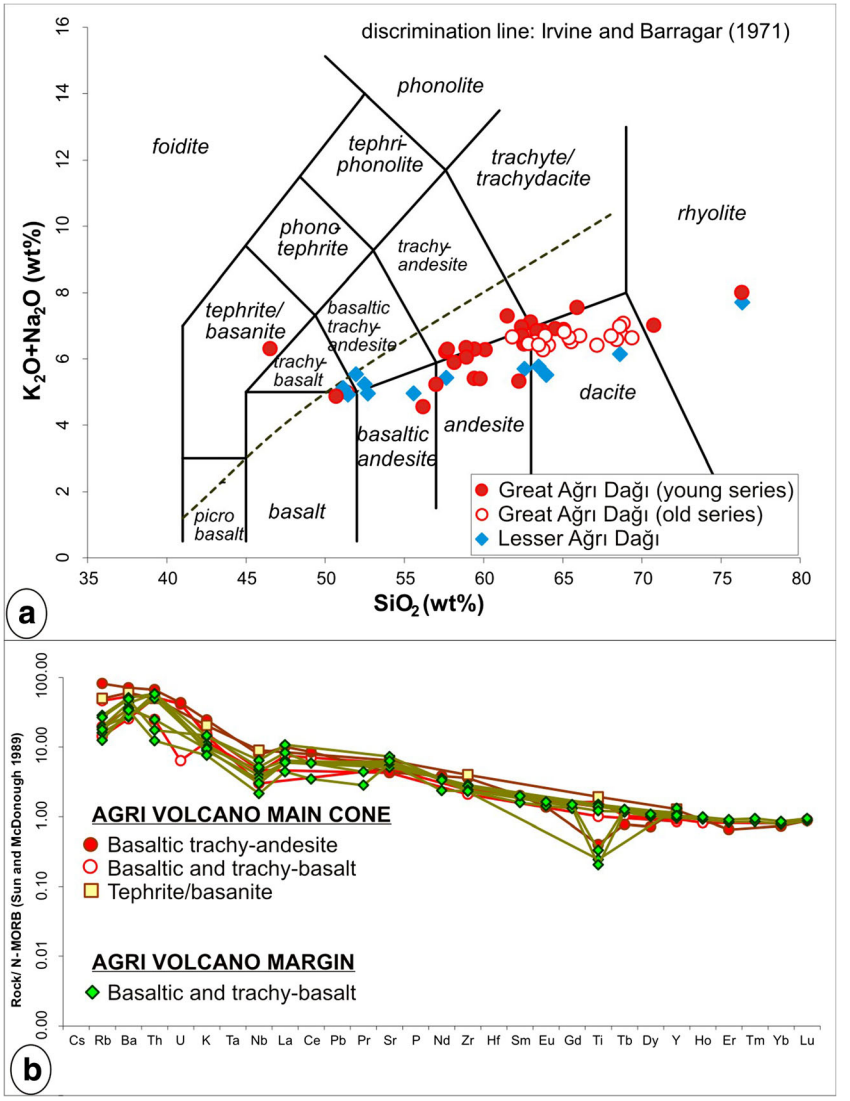

Fig. 4 **a** $K_2O + Na_2O$–SiO_2 (TAS) (LeMaitre 2002) diagram for the rock samples around Ağrı Dağı volcano (data taken from Gulen 1984; Pearce et al. 1990); alkaline-subalkaline line is according to Irvine and Baragar (1971). **b** MORB-normalised multi-element diagrams for the volcanic rocks of the basaltic/most basaltic rock samples around Ağrı Dağı volcano (data taken from Gulen 1984; Pearce et al. 1990; Kheirkhah et al. 2009). Normalising values are from Sun and McDonough (1989)

Gudmundsson 1987). The porosity or melt fraction differs through a magma reservoir due to buoyancy and reduced potential energy such that magma tends to move towards the top (shallowest depth) of the reservoir. Therefore, the greatest melt fraction is normally in the uppermost compartments of the reservoir and gradually decreases with depth (Richter and McKenzie 1984). The average melt fraction throughout a reservoir is commonly assumed at 0.25 (e.g. Richter and McKenzie 1984). The melt fraction of the lowest parts of a chamber may be higher if the reservoir is continuously supplied with new primitive melt or magma from deeper sources in the mantle, for example, from the upper parts of a mantle plume (Gudmundsson 1987). The mechanical behaviour of a magma reservoir can be modelled to a first approximation as a poroelastic material (Gudmundsson 1986, 2016; Tibaldi 2015). Hence, the volume of a magma source during individual eruptions may be roughly estimated from Eq. 2 and is given by the following (Gudmundsson 1987, 2016; Browning and Gudmundsson 2015):

$$V_b = \frac{V_e}{p_e \phi \left(\beta_m + \frac{\beta_b}{\phi} \right)} \tag{2}$$

where V_e is the volume of injected material in a single eruption, ϕ is the fractional porosity of the reservoir, p_e is the excess magmatic pressure in the reservoir, and β_m and β_b are the magma compressibility and bulk compressibility of the reservoir, respectively.

Magmatic excess pressure in the reservoir can be considered nearly equal to the in situ tensile strength of the host rock at the time of rupture (Elshaafi and Gudmundsson 2016). The

average in situ tensile strength of the upper crust in Eastern Turkey is around 3.5 MPa (Gurocak et al. 2012). Compressibility is a measure of the relative volume change of a fluid or solid as a response to change in stress. The static compressibility of basaltic magma β_m at 1100–1300 °C is around 1.25×10^{-10} Pa^{-1} (Murase and McBirney 1973). The Young's modulus for the lowermost crust in Eastern Turkey is around 35 GPa at a depth of 20 km (e.g. Gurocak et al. 2012: Karaoğlu et al. 2016). The bulk modulus (K) for this part of the crust can be calculated from the following relation:

$$K = \frac{E}{3(1-2\nu)} \tag{3}$$

where E is the Young's modulus and ν is the Poisson's ratio, whose average value for most solid rocks is around 0.25 (Gudmundsson 2011). Hence, the compressibility of the crust in Eastern Turkey $\left(\frac{1}{K}\right)$ is around 4.28×10^{-11} Pa^{-1}.

From Eq. (2), if we assume the magma reservoir as partially melted with an average porosity of 0.25 throughout the reservoir as previously mentioned, the volume of the reservoir would be as follows:

$$V_b = 3858 \times V_e \tag{4}$$

This equation can be applied to estimate the volume of magma within a reservoir supplying magma to individual eruptions. From Eq. (4), the volume of the magma reservoir during the first eruption (lava flow I) is around 12,345 km^3. By contrast, the volume of the magma reservoir during the second eruption (lava flow II) is at 2403 km^3, that is less by a factor of about 5. A much larger reservoir is thus needed to give rise to the first lava flow than the second lava flow, as expected, assuming that the reservoir's elastic properties remained the same for both eruptions. To explain this difference in reservoir size and related aspects during these eruptions, we created a suite of numerical models which investigate the distribution of stresses around a deep magma reservoir, with some constraints from seismic tomography.

Seismic tomography models

Low-velocity anomalies obtained from seismic tomography models can be used to detect magma chambers and reservoirs at depth. The seismic velocity model derived by Salah et al. (2011) is used to construct five vertical cross sections of P-wave velocity across the area of Ağrı Dağı volcano. This model is constructed through the application of the seismic tomography method of Zhao et al. (1992, 1994) on P-wave (primary wave) arrival times in Eastern Anatolia. This method has been applied successfully on arrival times collected from seismic events occurring in different tectonic circumstances. The method is adaptable to a general velocity structure, which includes several seismic velocity discontinuities of complex topography. Initially, a 3-D grid net is set in the model space to express the 3-D velocity variations; the seismic velocities are taken as unknown parameters. Velocity at any point in the model is calculated by linear interpolation of the velocity values at eight grid nodes surrounding that point. The method uses an efficient 3-D ray-tracing scheme which accurately calculates travel times and ray-paths. More details about the method can be found in the study by Zhao et al. (1992, 1994, 2012).

The Eastern Turkey data set comprises 31,730 P-wave arrival times generated by 7380 seismic events, which were recorded by 39 seismic stations distributed relatively uniformly in the study area. Analysis of ray path coverage (both in plan and vertical views) and the results of a checkerboard resolution test and the hit count rates all imply that the obtained velocity anomalies are reliable features down to a depth of 45 km (Salah et al. 2011). P-wave velocity along the selected five cross sections is shown in Fig. 5. The model shows that prominent low P-wave velocity zones are visible at a depth range of 20–30 km beneath cross sections 1–3 which strike in a NW–SE direction. Cross sections 4 and 5 run in an NE-SW direction and exhibit low P-wave velocities that extend to the base of the upper crust (Fig. 5). These low P-wave velocity zones most likely indicate the occurrence of partial melt, which can be interpreted as magma reservoirs beneath Eastern Anatolia (Hearn 1999; Calvert et al. 2000; Zor et al. 2003). These low-velocity zones seem to be consistent with previous seismological observations such as inefficient S_n propagation and low P_n velocity (Rodgers et al. 1997; Al-Lazki et al. 2004).

Numerical models

Whilst the seismic tomography data clearly indicate the presence of a deep reservoir, there is little evidence in the tomography for a shallow magma chamber. However, geochemical constraints indicate that a shallow chamber was active approximately 5 Ma. As such, we built a suite of numerical models to test the stress conditions generated by different arrangements of magma chambers. The objective is to understand which conditions favour eruptions and how could the relative size and location of those eruptions change due to the magma chamber arrangement.

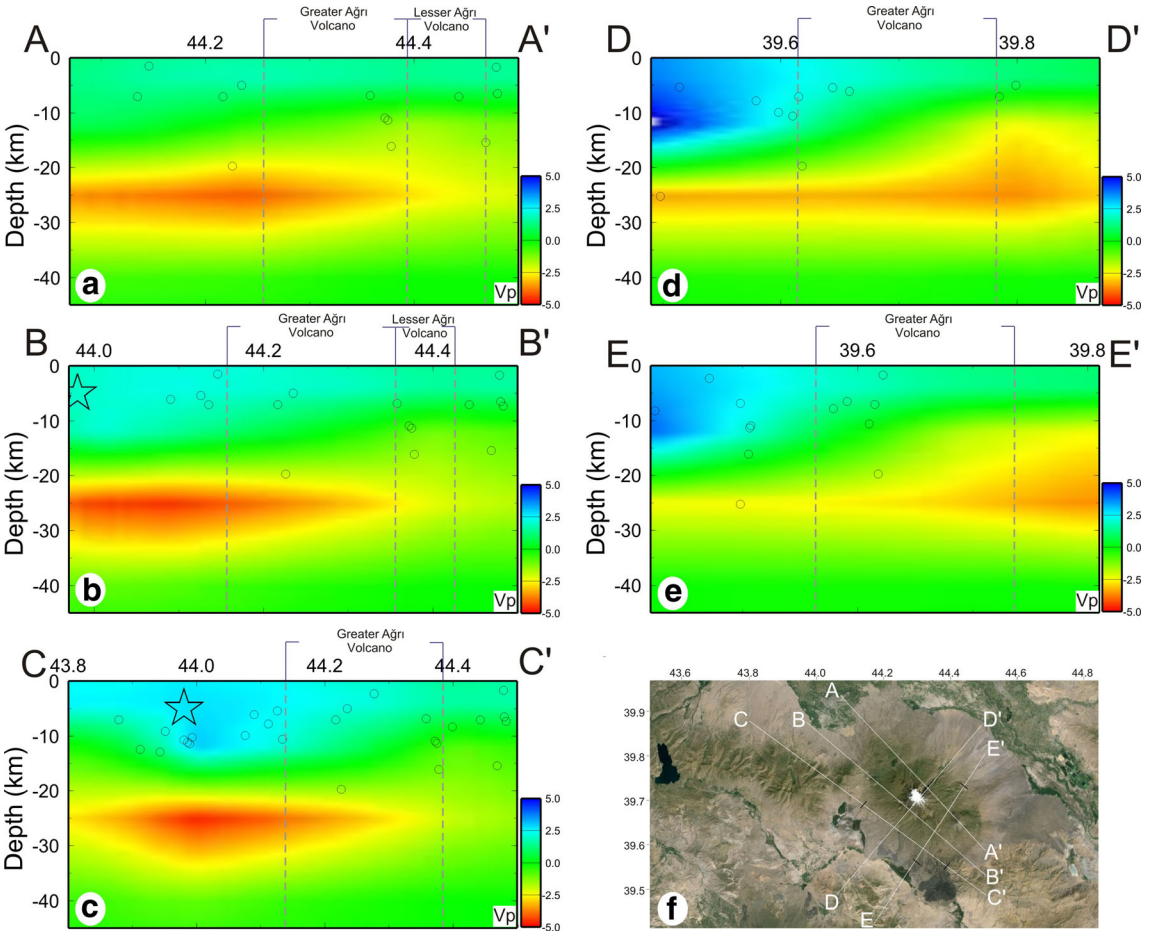

Fig. 5 **a**–**e** Five vertical cross sections of P-wave velocity beneath the area of the Ağrı Dağı volcano (see Fig. 1 for the location of the cross sections). Low velocities are shown in *red*, whereas high velocities are shown in *blue*. *Large stars* and *small circles* show, respectively, the location of moderate/large earthquakes ($M \geq 5.0$) and the microseismic activity in a 30-km-wide zone around the profile. The perturbation scale (±5%) is shown to the *right*. **f** The locations for these seismic profiles on the map

The numerical models were built and solved using the finite element program COMSOL (www.comsol.com; cf. Zienkiewicz 1979; Deb 2006). The models are based on the real geological setting of the Ağrı Dağı volcano as interpreted from field measurements, seismic wave profiles and InSAR data (Cavalié and Jónsson 2014) (Fig. 6). All models are two dimensional where the magma chambers and reservoirs are modelled as cavities or holes with prescribed loads given at their boundaries to simulate overpressure (Gudmundsson 2011; Gerbault 2012) (Fig. 6).

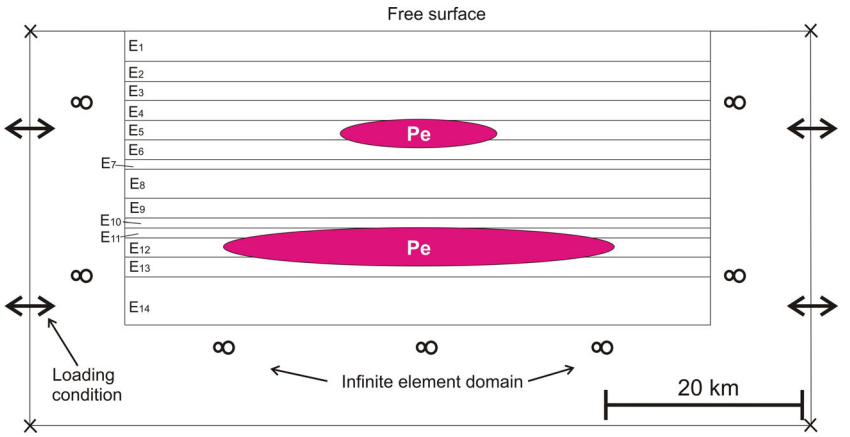

Fig. 6 Two-dimensional numerical model setups. The 2-D example shown represents the geology of an E-W striking profile through Ağrı Dağı volcano. All 2-D models are layered $E_{(1–14)}$ with each unit assigned a different value of Young's modulus. Magma chambers, represented as cavities, are given an excess pressure of 5 to 15 MPa

Model set-up

The geometry of our 2-D models is based upon a simplified E-W striking profile through the Ağrı Dağı volcano (Fig. 6). The magma sources in our models are elliptical, which is likely a simplification of real magma chamber geometries (e.g. Gudmundsson 2012; Le Corvec et al. 2015; Karaoğlu et al. 2016). Although it has been shown previously that topography can play a role in distributing near-surface stresses, the primary focus of our investigation is on the stress differences resulting from different boundary conditions applied to the magma chamber itself, where the host-rock properties as well as the depth, shape and size of the chamber are of main concern. Thus, we assume flat topography in all models. The 14 different geological units as mechanical layers used in our models are based on direct geological observations and published literature (Yılmaz et al. 1998) (Fig. 6). The values used to calculate depth of the magma chamber encompass all of these mechanical layers.

The depths of shallow magma chambers are commonly located within a few kilometres of the ground surface (cf. Gudmundsson 1998). In this study, we assume the magma chamber depth to be 8 km, although results are not sensitive to the shallow chamber depth. The depth of the deep-seated magma reservoir is inferred from tomographic data at around 20 km. In Fig. 6, we show only the model along an E-W strike. We performed two models, in order to investigate different eruption volumes, i.e. (i) very large magma storage configuration for lava flow I (i.e. ~13,000 km^3) and (ii) a smaller lava flow II (i.e. ~2000 km^3). We assumed two magma storage regions: (1) a deeper and larger reservoir at a depth of 20 km (with a diameter of 40 km and a thickness of 7 km) and (2) a shallow magma chamber at 8-km depth (with a diameter of 16 km and a thickness of 5 km (Fig. 7a, b). The second model shows the same shallow magma chamber at 8-km depth (with a diameter of 16 km and a thickness of 2 km) but with a much smaller-volume deeper reservoir at 20-km depth (with a diameter of 30 km and thickness of 3 km (Fig. 7c, d).

In this model, both magma chambers are residing within a heterogeneous, anisotropic elastic half space with Young's modulus (E) varying between individual layers from 50 to 20 GPa, as shown in Appendix Table 1. The shallower magma chamber is modelled considering two criteria: first, that most stratovolcanoes are fed by shallow chambers and, second, that geological data (some magma mingling textures in the rocks) and geochemical records indicate the existence of a shallow magma chamber beneath the volcano. The deeper magma reservoir is modelled based on our seismic tomography data. It was assumed that the shallower magma chamber has a maximum diameter of 16 km to a first approximation (Fig. 7a, b), whereas the deeper chamber or reservoir has a maximum diameter of 40 km for the first volcanic eruption to correspond the shrinkage of the volume of reservoir with the time. Poisson's ratio (ν) does not vary significantly between individual layers; thus, in the models, we use a constant typical value of 0.25 (Gudmundsson 2011). The E-W striking profile hosts predominantly horizontal layers where the layer thicknesses are taken from geological measurements (Fig. 2) and given in Appendix Table 1. All models are fixed at the corners, with boundary loads applied at the west and east edges and a free surface (a region free from shear stress) prescribed on the upper edge (Earth's surface).

In addition to boundary loads prescribed at the edge of the models, to simulate tectonic stressing, we also load the internal cavities to simulate excess magma pressure, which is 5 MPa in Fig. 6. Magma chamber rupture and dyke injection

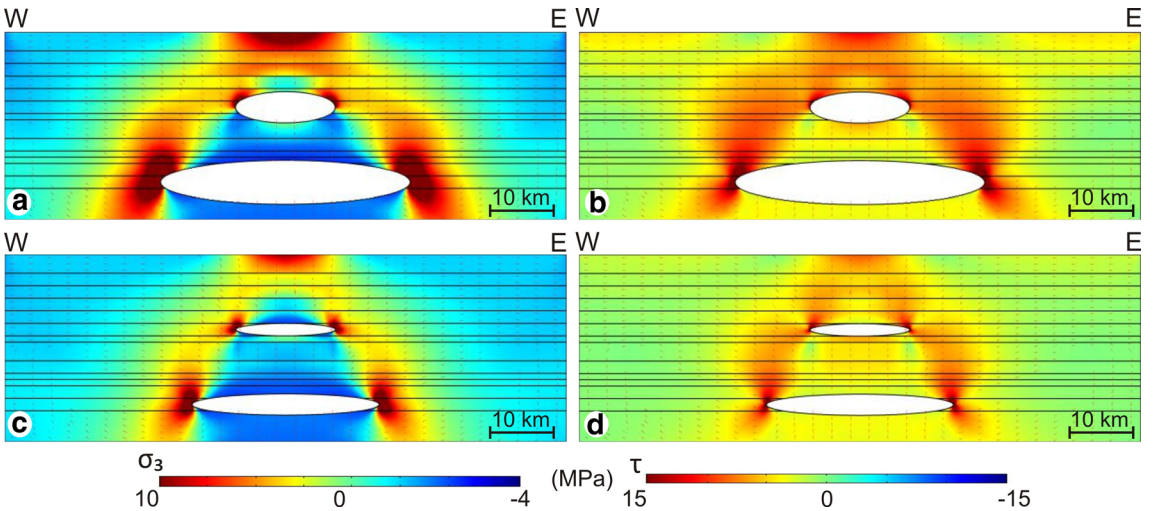

Fig. 7 Modelled stresses induced by excess magmatic pressure (p_e) inside a shallow chamber of diameter 16 km and a deep reservoir of diameter 40 km. **a** Magnitudes of the minimum principal compressive (maximum tensile) stress (σ_3). **b** Magnitude of von Mises shear stresses (τ) The excess magmatic pressure in each chamber is 5 MPa and is the only loading. Parts **c**, **d** show the same arrangement of shallow chamber and deep reservoir, but in this case, the reservoir is reduced in size with diameters of 16 and 30 km, respectively

occur when the tensile stresses at any point at the boundary of the chamber/reservoir reach the tensile strength of the rock (0.5 to 9 MPa) (Amadei and Stephenson 1997). Laboratory tensile strengths of rocks reach up to about 30 MPa, but the in situ tensile strengths are between 0.5 and 9 MPa, the most common values being 2–4 MPa (Gudmundsson 2011). By using excess pressure in the chamber/reservoir rather than total pressure, the effects of gravity are automatically considered (cf. Gudmundsson 2012). We use a triangular mesh with a maximum element size of 16 m and a minimum element size of 2 m. Our simplified models show that the most likely area of chamber rupture and surface eruption is fed by interconnected magma reservoirs and shallow and deeper magma chambers (Fig. 7).

Results

To explore the potential magma propagation paths in the shallow crust beneath the Ağrı Dağı volcano, we constructed a numerical model (Fig. 7). It is first necessary to consider the stress required for magma chamber rupture. In the simplest terms, a magma chamber roof will rupture and inject a dyke (or an inclined sheet) when (Gudmundsson 1990, 2011)

$$p_l + p_e = \sigma_3 + T_o \quad (5)$$

where p_l is the lithostatic pressure and p_e is the excess pressure in the magma chamber, σ_3 is minimum principal compressive stress in the host rock, and T_0 is the tensile strength of the host rock, which ranges from 0.5 to 9 MPa (Amadei and Stephenson 1997), and the average in situ tensile strength of the upper crust in East Turkey is around 3.5 MPa (in agreement with the common in situ tensile strength range given previously). When a chamber roof has failed in tension and a dyke is initiated, then the magma follows the path or trajectories of maximum principal compressive stress, σ_1 (Gudmundsson 2011). Here, we present first the results on crustal stresses induced solely by magmatic excess pressure within each chamber, ignoring initially the effects of any regional tectonic loading. In Fig. 7, we show the magnitudes of the minimum principal compressive (maximum tensile) stress, σ_3, and von Mises shear stress, τ.

In an E-W profile, the maximum tensile and shear stresses concentrate at the lateral margins of each magma chamber and at the Earth's surface above the magma chamber. Complex stress patterns and interactions occur at depth due to the attitude and mechanical properties of the layers (Fig. 7a). There is a stress concentration zone or link between the deeper magma reservoir and the shallow chamber (Fig. 7b). Our model indicates that if magma propagates from the edge of the deeper reservoir, it can reach the surface without interaction with the shallow chamber (Fig. 7a, b). However, this is partially dependant on the size and position of the deeper reservoir with respect to the shallow chamber. When the reservoir is smaller (Fig. 7c), there is more likelihood of interaction with the shallow chamber. Here, the results show that the deeper magma reservoir has two options, so as to either (1) feed the volcanic edifice from the lateral margins or (2) replenish the shallow magma chamber. Dykes that propagate from the central part will not feed an eruption but instead charge the shallow magma chamber. These models indicate that most lava flows at the central part of the volcano will produce more evolved lavas compared to those lavas fed from the reservoir margins.

Discussion

Magma discharge mechanism

Field studies and stratigraphy of the volcano indicate three major andesitic and two basaltic lava flow eruption cycles, with tens of intermediate-composition lava stacks, from cone building to late stage of the Ağrı Dağı volcano (Fig. 2; Yılmaz et al. 1998). We focus on the latest basaltic lava flows (~0.5 Ma; Sanver 1968) which record a single magmatic pulse and path from chamber to the surface. The combined volume of lava flows I and II represents only 0.06% of the volume of the estimated magma reservoir.

The variety of volcanic products along Ağrı Dağı volcano ranges from contemporaneous intermediate (dacitic and andesitic) to basic (basaltic) eruptions, indicating that the magma in this volcanic edifice may be derived from double magma chambers rather than a single magma source. The more evolved intermediate volcanic rocks (e.g. dacite and andesite) are generally concentrated at the central part of the edifice, while the less evolved basaltic rocks are distributed at the margin. The injection of dykes from the central part of the deeper magma chamber (magma reservoir) could feed the shallow magma chamber, while dyke injection from the margin of the deeper magma reservoir can propagate directly to the surface to feed eruptions. Field observations and the numerical models are consistent with this distribution, where less evolved magma can be observed around the periphery of the volcanic edifice, whereas more evolved lava flows are present around the central part.

The results of the numerical model, supported by geochemical data, indicate that dyke injection from the central part of a deep magma reservoir could feed a shallow magma chamber. The magma arriving at the shallower depths could then begin a fractionation or differentiation process prior to the chamber rupture condition ($p_e = T_0 \approx 5$ MPa) being reached. Thus, we suggest that the shallow magma chamber produces more evolved magma (e.g. the young andesitic rocks of age 0.1–0.02 Ma; Nagao et al. 1989), whereas the deep-seated magma reservoir produces the older and less evolved lavas (e.g. 0.3–0.049-Ma basaltic rock).

The magma reservoir volume underneath Ağrı Dağı appears to have reduced considerably over a period of 0.5 Ma. Our models indicate a volume reduction from 12,345 km^3 for lava flow I to 2403 km^3 for lava flow II. Magma storage shrinkage has been interpreted at other volcanic provinces such as in Iceland (Andrew and Gudmundsson 2007) and at the Al Haruj Volcanic Province, central Libya (Elshaafi and Gudmundsson 2016) (Fig. 8).

The first volcanic eruptions may be envisaged as injection from the margins of the deeper part of reservoir, whereas the second volcanic units may be injected from the uppermost part of the reservoir where more fractionated (lighter) basaltic rocks form. These basaltic magmas tend to occupy the uppermost part of a reservoir due to buoyancy. This process might explain why the volume of the reservoir changed substantially through time.

The sizes and areas of individual volcanic eruptions are mainly dependent on the sizes of the source magma chambers. There are many examples around the world showing that individual volcanic eruptions can occur on the order of several hundred square kilometres and have volumes exceeding several cubic kilometres. In fact, the largest basaltic lava flows reach estimated volumes of thousands of cubic kilometres (Fig. 8). Much more commonly, however, lava flows cover only small areas and have volumes less than 0.5 km^3. As an example of a large historical lava flow, the 1783 Laki lava in Iceland covers 565 km^2 and has a volume of about 15 km^3 (Fig. 8). Also, some prehistorical (mainly 16–17 Ma old) individual lava flows of the Columbia River Plateau exceed volumes of 1000 km^3. By contrast, the lava flow erupted during the Krafla Fires in North Iceland, 1975–1984, covers an area of 0.3 km^2 and its volume is about 0.17 km^3 (Tryggvason 1984), while Etna lava flow for the 1991–1993 eruption has an area of 7.2 km^2 and an estimated volume between 0.022 and 0.072 km^3 (Harris et al. 2000) (Fig. 8). Many eruptions of 1–10 km^3 and even larger can be explained by local volcano-tectonic forcing (e.g. Gudmundsson 2015, 2016) or continuous supply from a large deeper reservoir to the shallow chamber during the eruption (Gudmundsson 1987). By contrast, normal or small eruptions are usually less than 0.1 km^3 and commonly fed by crustal shallow magma chambers with little or no continuous magma replenishment from a large deeper reservoir during the eruption (Gudmundsson 1987, 2016). Thus, in the absence of evidence for local volcano-tectonic forcing, we assume that both lava flows I and II were emplaced from a deep reservoir in a normal eruption. This

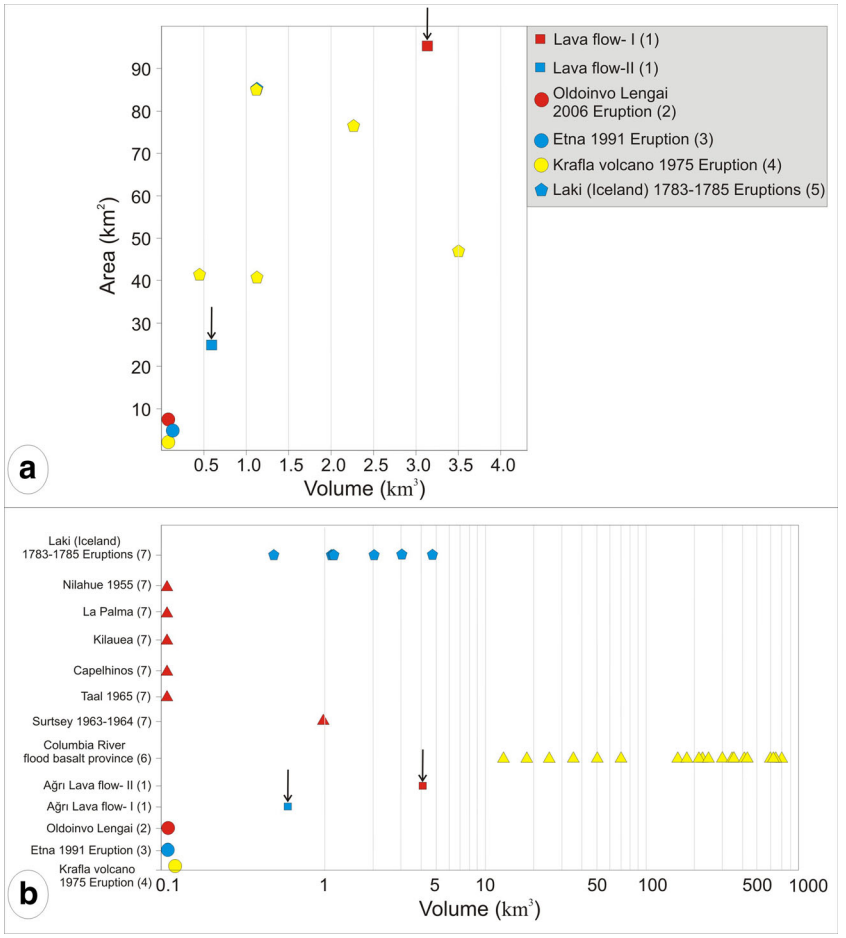

Fig. 8 **a** Area vs. volume constraints of some single lava discharge ratios for composite volcanoes and volcanic regions. **b** Volume compilation for some historical eruptions. (*1*) This study; (*2*) Kervyn et al. (2008); (*3*) Harris et al. (2000); (*4*) Tryggvason (1984); (*5*) Thordarson and Self (1993); (*6*) Reidel et al. (2013); (*7*) White and Houghton (2000). *Arrows* highlighting the last two basaltic eruptions of Ağrı Dağı volcano

notion is supported by the chemistry of the lavas, which indicates primitive magma, particularly of the larger lava flow.

To explain the difference in the volumes and chemistry of the lava flows, there are several possibilities. One possibility is that the size or volume of the entire reservoir decreased greatly between the two eruptions, in which case reduction in 'effective size' corresponds to reduction in true size. This possibility cannot be ruled out, but the reduction in size would then have to have happened within the time period of, at maximum, a few hundred thousand years (the lava flows are younger than 500,000 years). This is possible, but not very likely given that reservoir feeding volcanic systems, such as in Iceland, are commonly active for 0.5–1 Ma (Gudmundsson 2006, 2012), and in many other areas, similar reservoirs are active for as long as millions of years. We, therefore, propose that the second smaller eruption was supplied with magma from only a part of the reservoir, that is, for a compartment within the reservoir (see Gulen 1984 for discussion of the origin of the lavas). This suggestion is supported by the second and smaller lava flow being more evolved than the first and larger flow. It is clear particularly at the margin area of the Ağrı Dağı volcano (e.g. Kheirkhah et al. 2009). Thus, we suggest that only a fraction of the entire reservoir, a compartment (cf. Gudmundsson 2012), contributed to the second eruption, thereby, partly at least, explaining their volume and chemical differences. Based on our calculations, the volume of that compartment is 2403 km^3 or roughly one fifth that of the entire reservoir. Formation and maintenance of compartments in magma sources are discussed by Gudmundsson (2012). Furthermore, based on our numerical studies, this compartment was most likely at one of the margins of the reservoir.

Tomography

The tomographic data indicate the presence of an active deep magma reservoir having low P-wave velocities that extend to the base of the upper crust (Fig. 5). The magma reservoir may extend between 20 and 30 km in depth and 35–45 km in width, showing a NW–SE-elongated tabular form (sill-like shape) in the crust (Fig. 5a–c). A diapiric-shaped dyke injection extending to the upper level of the crust in a NE–SW-oriented profile (Fig. 5d) is clearly observed. In all profiles, we note that diapiric-shaped dyke injection feeding the main vent of the Ağrı Dağı volcano is not aligned below the main volcanic centres (Fig. 5a–d). It seems that there is no magma source below the Lesser Ağrı Dağı volcano. Greater Ağrı Dağı volcano is not situated directly over the centre of the large deeper reservoir. This suggests that the reservoir may have migrated laterally following constructing of the Ağrı Dağı volcano during the past 1.5 Ma. The shallow magma chamber may be fossilised as a plutonic body directly below the Ağrı Dağı volcano, which would not be possible to detect it with tomographic imaging.

At least four historical volcanic eruptions are known to have occurred from Ağrı Dağı volcano (Karakhanian et al. 2002): (i) pyroclastic flow in 1840 AD from Greater Ağrı Dağı volcano, (ii) unclear eruption type in 1450 AD from the SE slope of the Lesser Ağrı Dağı volcano, (iii) unclear eruption type in late third–early fourth century AD from Greater Ağrı Dağı volcano and (iv) explosive eruption-pyroclastic flow in 2500–2400 BC from the N–NE slope of Greater Ağrı Dağı volcano. Taking into account the huge magma reservoir below the volcano, even a small future eruptive event coupled with volcano flank instabilities could therefore pose a threat to the large populations living around Ağrı Dağı volcano, in Eastern Turkey and in the Armenian province.

Numerical models in the geological context

Our general numerical results provide insights into the mechanism of magma movement from a deep magma reservoir to the surface. Such a process can occur in two predominant ways: (i) the magma is fed directly to the surface from the lateral margins of the deep reservoir, or (ii) when the magma of deep origin is injected from the central part of the reservoir, the magma path (the dyke) connects with a shallow chamber which, in turn, ruptures and propagates a dyke to the surface. In the second case, any erupting magma is then technically fed from the shallow chamber. Despite the tomography data which support an active deep magma reservoir (20–30 km in depth), the huge volume of intermediate and acidic lavas constructed at Ağrı Dağı stratovolcano (see Fig. 2) and other large stratovolcanoes most likely requires the formation of a shallow magma chamber.

When taken together, all of our results indicate that the bulk volume of the reservoir appears to be considerably reduced between the time of erupting lava flow I and lava flow II. The smaller size of the later magma reservoir increases the likelihood of interaction with the shallow chamber, assuming that it has not already solidified which seems to be the case in Ararat volcano. Regardless of the size of each individual chamber, the conditions for rupture remain the same, namely that the excess pressure must exceed the tensile strength of the wall rocks (Eq. 5). In both cases tested numerically (Fig. 7), we found that this failure is most likely at the margins of the chamber. Therefore, the more evolved basaltic magma, which remains inside the reservoir during the quiescence between eruptions, may be mobilised vertically due to buoyancy effects to form compartments in the reservoir (Gudmundsson 2012), which subsequently ruptures when Eq. 5 becomes satisfied again (Fig. 7c).

Basaltic rocks generated in lava flow II are generally more fractionated than lava flow I, which is exactly as expected. The lack of data concerning the petrogenesis and geochemistry for both volcanic flows makes further analysis challenging. We therefore encourage a systematic field survey which

would greatly improve the understanding of Ağrı Dağı volcano. We hope that these results encourage further research into this volcano.

Conclusions

1. We calculated the total erupted materials V_e for two of the most recent basaltic eruptions at the Ağrı Dağı volcano. Lava flow I is around 3.2 km^3, while the lava flow II is around 0.6 km^3. In addition, we present an approach for estimating the volume of the reservoir supplying each individual volcanic eruption. The effective reservoir volumes obtained were 12,345 and 2403 km^3 for lava flows I and II, respectively.
2. Results of seismic tomography reveal a low-velocity zone at a depth range of 20–30 km below the northwest part of the Ağrı Dağı volcano, which is interpreted to be a deep magma reservoir. We did not find strong evidence of a shallow magma reservoir from the present velocity models, implying that the shallow magma chamber has already been solidified.
3. We explore two scenarios to explain the difference in volume of these two flows. One is that the absolute reservoir volume decreased between the two eruptions. This is possible, but not very likely since the likely time between the eruptions is not very large in comparison with the lifetimes of large reservoirs. The other scenario involves reservoir compartments. In this scenario, while the less evolved lavas around the volcano were fed only by a deep reservoir, a comparatively small compartment within the reservoir contributed magma to the eruption, which generated lava flows I and II at Ağrı Dağı volcano. In this view, the calculated reservoir volume of 2403 km^3 for issuing lava flow II thus corresponds to that compartment and is about one fifth of the total volume of the reservoir.
4. The combined results from tomography models and analytical calculations were used to prepare a suite of numerical models. By simulating various crustal loading situations, we show the most likely stress state that promoted feeder-dyke propagation to erupt lava flows I and II. Our data are useful in estimating the potential source of future eruptions at Ağrı Dağı volcano. The interpretation of our numerical models suggests that Ağrı Dağı volcanism has been periodically fed by a deep-seated magma reservoir at 20–30-km depth.
5. The basaltic magma feeding Ağrı Dağı stratovolcano is enriched in LILE, which indicates an interaction just below the volcano between the shallow magma chamber and the deeper magma reservoir. However, less evolved basaltic volcanic rocks at the margin of the Ağrı Dağı volcano were presumably fed by a deeper magma reservoir with no interaction with the shallow chamber.

Acknowledgements Özgür Karaoğlu is supported by The Scientific and Technological Research Council of Turkey (TUBITAK) International Postdoctoral Research Fellowship Programme. John Browning is supported by NERC project NE/N002938/1. We are grateful to the Editor Valerio Acocella and the reviewers, Alessandro Tibaldi and an anonymous reviewer, for comments which greatly improved this work. This study is dedicated to the memory of Okan Delibaş.

References

Alici P, Temel A, Gourgaud A, Vidal P, Gundogdu MN (2001) Quaternary tholeiitic to alkaline volcanism in the Karasu Valley, Dead Sea rift zone, Southeast Turkey: Sr-Nd-Pb-O isotopic and trace-element approaches to crust-mantle interaction. Int Geol Rev 43(2):120–138

Al-Lazki A, Seber D, Sandvol E, Turkelli N, Mohamad R, Barazangi M (2003) Tomographic Pn velocity and anisotropy structure beneath the Anatolian plateau (eastern Turkey) and the surrounding regions. Geophysc Res Lett 30:24. doi:10.1029/2003GL017391

Al-Lazki AI, Sandvol E, Seber D, Barazangi M, Turkelli N, Mohamad R (2004) Pn tomographic imaging of mantle lid velocity and anisotropy at the junction of the Arabian, Eurasian and African plates. Geophys J Int 158:1024–1040. doi:10.1111/j.1365-246X.2004.02355x

Amadei B, Stephenson O (1997) Rock stress and its measurement. Chapman and Hall, London

Andrew RE, Gudmundsson A (2007) Distribution, structure, and formation of Holocene lava shields in Iceland. J Volcanol Geoth Res 168(1):137–154

Angus DA, Wilson DC, Sandvol E, Ni JF (2006) Lithospheric structure of the Arabian and Eurasian collision zone in Eastern Turkey from S-wave receiver functions. Geophys J Int 166:1335–1346

Barka AA (1992) The North Anatolian fault zone. Ann Tecton 6:164–195

Barnett ZA, Gudmundsson A (2014) Numerical modelling of dykes deflected into sills to form a magma chamber. J Volcanol Geoth Res 281:1–11

Bingöl E, Bal I, Can N (eds) (1989) Geological map of Turkey, scale 1: 2000000, General Directorates of Mineral Research and Exploration, Ankara, Turkey

Bjornsson H (1983) A natural calorimeter at Grimsvötn; an indicator of geothermal and volcanic activity. Jökull 33:13–18

Bozkurt E (2001) Neotectonics of Turkey—a synthesis. Geodin Acta 14: 3–30

Browning J, Gudmundsson A (2015) Caldera faults capture and deflect inclined sheets: an alternative mechanism of ring dike formation. B Volcanol 77(1): 1–13

Browning J, Drymoni K, Gudmundsson A (2015) Forecasting magma-chamber rupture at Santorini volcano, Greece. Sci Rep 5:15785. doi:10.1038/srep15785

Cakir O, Erduran M, Cinar H, Yılmazturk A (2000) Forward modeling receiver functions for crustal structure beneath station TBZ (Trabzon, Turkey). Geophys J Int 140:341–356

Calvert A, Sandvol E, Seber D, Barazangi M, Roecker S, Mourabit T, Vidal F, Alguacil G, Jabour N (2000) Geodynamic evolution of the lithosphere and upper mantle beneath the Alboran region of the western Mediterranean: constraints from travel time tomography. J Geophys Res 105(B5):10871–10898

Cavalié O, Jónsson S (2014) Block-like plate movements in eastern Anatolia observed by InSAR. Geophys Res Lett 41:26–31

Chester D (1993) Volcanoes and society. Edward Arnold, London

Coppola D, Piscopo D, Staudacher T, Cigolini C (2009) Lava discharge rate and effusive pattern at piton de la Fournaise from MODIS data. J Volcanol Geoth Res 184(1):174–192

Daniels KA, Kavanagh JL, Menand T, Stephen JSR (2012) The shapes of dikes: evidence for the influence of cooling and inelastic deformation. Geol Soc Am Bull 124(7–8):1102–1112

Deb D (2006) Finite element method, concepts and applications in geomechanics. PHI Learning Private Limited, New Delhi

Elshaafi A, Gudmundsson A (2016) Volcano-tectonics of the Al Haruh Volcanic Province, Central Libya. J Volcanol Geoth Res 325:189–202

Ercan T, Fujitani T, Madsuda JI, Notsu K, Tokel S, Tadahide UI (1990) Dogu ve güneydogu Anadolu Neojen-Kuvaterner volkanitlerine iliskin yeni jeokimyasal, radyometrik ve izotopik verilerin yorumu: M.T.A Dergisi 110:143–164

Gerbault M (2012) Pressure conditions for shear and tensile failure around a circular magma chamber; insight from elasto-plastic modelling. Geol Soc Lond Spec Publ 367(1):111–130

Gudmundsson A (1986) Mechanical aspects of postglacial volcanism and tectonics of the Reykjanes Peninsula, Southwest Iceland. J Geophys Res-Solid 91(B12):12711–12721

Gudmundsson A (1987) Geometry, formation and development of tectonic fractures on the Reykjanes peninsula, southwest Iceland. Tectonophysics 139(3–4):295–308

Gudmundsson A (1990) Emplacement of dikes, sills and crustal magma chambers at divergent plate boundaries. Tectonophysics 176:257–275

Gudmundsson A (1998) Magma chambers modeled as cavities explain the formation of rift zone central volcanoes and their eruption and intrusion statistics. J Geophys Res 103:7401–7412

Gudmundsson A (2006) How local stresses control magma-chamber ruptures, dyke injections, and eruptions in composite volcanoes. Earth-Sci Rev 79:1–31

Gudmundsson A (2011) Rock fractures in geological processes. Cambridge University Press, Cambridge

Gudmundsson A (2012) Magma chambers: formation, local stresses, excess pressures, and compartments. J Volcanol Geoth Res 237–238: 19–41

Gudmundsson A (2015) Collapse-driven large eruptions. J Volcanol Geoth Res 304:1–10

Gudmundsson A (2016) The mechanics of large eruptions. Earth Sci Rev. doi:10.1016/j.earscirev.2016.10.003

Gulen L (1984) Sr, Nd, Pb isotope and trace element geochemistry of calc-alkaline and alkaline volcanics, Eastern Turkey. Doctoral dissertation, Massachusetts Institute of Technology

Gurocak Z, Solanki P, Alemdag S, Zaman MM (2012) New considerations for empirical estimation of tensile strength of rocks. Eng Geol 145:1–8

Harris AJL, Flynn LP, Garbeil H, Mouginis-Mark P, Okubo C, Pilger E, Dean K (2000) Detecting and monitoring volcanic hot spots from space. In: Mouginis-Mark PJ, Crisp JA, Fink JH (eds) Remote sensing of active volcanism monograph. Am Geophys Union, Washington, pp 139–159

Hasenaka T (1994) Size, distribution, and magma output rate for shield volcanoes of the Michoac in-Guanajuato volcanic field, Central Mexico. J Volcanol Geoth Res 63:13–31

Hearn TM (1999) Uppermost mantle velocities and anisotropy beneath Europe. J Geophys Res 104:15123–15139

Hermance JF (1981) Crustal genesis in Iceland: geophysical constraints on crustal thickening with age. Geophysc Res Lett 8(3):203–206

Innocenti F, Mazzuoli R, Pasquare G, Redicat di Brozolo F, Villari L (1976) Evolution of the volcanism in the area of interaction between the Arabian, Anatolian and Iranian plates (Lake Van, Eastern Turkey). J Volcanol Geoth Res 1:103–112

Innocenti F, Mazzuoli R, Pasquare G, Serri G, Villari L (1980) Geology of the volcanic area north of Lake Van (Turkey). Geol Rundsch 69: 292–322

Irvine TN, Baragar WRA (1971) A guide to the chemical classification of the common volcanic rocks. Can J Earth Sci 8:523–548

Karakhanian A, Djrbashian R, Trifonov V, Philip H, Arakelian S, Avagian A (2002) Holocene–historical volcanism and active faults as natural risk factors for Armenia and adjacent countries. J Volcanol Geoth Res 113:319–344

Karaoğlu Ö, Özdemir Y, Tolluoğlu AÜ, Karabıyıkoğlu M, Köse O, Froger JL (2005) Stratigraphy of the volcanic products around Nemrut Caldera: implications for reconstruction of the Caldera Formation. Turk J Earth Sci 14:123–143

Karaoğlu Ö, Browning J, Bazargan M, Gudmundsson A (2016) Numerical modelling of triple-junction tectonics at Karlıova, Eastern Turkey, with implications for regional magma transport. Earth Planet Sc Lett 452:152–170

Kervyn M, Ernst GG, Klaudius J, Keller J, Kervyn F, Mattsson HB, Belton F, Mbede E, Jacobs P (2008) Voluminous lava flows at Oldoinyo Lengai in 2006: chronology of events and insights into the shallow magmatic system. B Volcanol 70(9):1069–1086

Keskin M (2007) Eastern Anatolia: a hot spot in a collision zone without a mantle plume. In: Foulger GR, Jurdy D (eds) Plates, plumes, and planetary processes. Geol Soc Am Spec Pap 430:693722

Keskin M, Pearce JA, Mitchell JG (1998) Volcano-stratigraphy and geochemistry of collision-related volcanism on the Erzurum-Kars Plateau, North Eastern Turkey. J Volcanol Geoth Res 85:355–404

Kheirkhah M, Allen MB, Emami M (2009) Quaternary syn-collision magmatism from the Iran/Turkey borderlands. J Volcanol Geoth Res 182(1):1–12

Le Corvec N, Menand T, Lindsay J (2013) Interaction of ascending magma with pre-existing crustal fractures in monogenetic basaltic volcanism: an experimental approach. J Geophys Res-Sol Ea 118(3): 968–984

Le Corvec N, McGovern PJ, Grosfils EB, Galgana G (2015) Effects of crustal-scale mechanical layering on magma chamber failure and magma propagation within the Venusian lithosphere. J Geophys Res 120(7):1279–1297

Lebedev VA, Sharkov EV, Keskin M, Oyan V (2010) Erratum: geochronology of Late Cenozoic volcanism in the area of Lake Van, Turkey: an example of developmental dynamics for magmatic processes. Dokl Earth Sci 433(2):1031–1037

LeMaitre RW (2002) Igneous rocks: a classification and glossary of terms: recommendations of the International Union of Geological Sciences. Subcommission on the Systematics of Igneous Rocks. Cambridge University Press, Cambridge

Lustrino M, Keskin M, Mattioli M, Lebedev V, Chugaev A, Sharkov E, Kavak O (2010) Early activity of the largest Cenozoic shield volcano in the circum-Mediterranean area: Mt. Karacadag SE Turkey. Eur J Mineral 22:343–362

Maccaferri F, Rivalta E, Keir D, Acocella V (2014) Off-rift volcanism in rift zones determined by crustal unloading. Nat Geosci 7(4):297–300

Meyer PS, Sigurdsson H, Schilling JG (1985) Petrological and geochemical variations along Iceland's neovolcanic zones. J Geophys Res-Solid 90(B12):10043–10072

Murase T, McBirney AR (1973) Properties of some common igneous rocks and their melts at high temperatures. Geol Soc Am Bull 84(11):3563–3592

Nagao K, Matsuda JI, Kita I, Ercan T (1989) Noble gas and carbon isotopic compositions in Quaternary volcanic area in Turkey. Bull Geomorphol 17:101–110

Notsu K, Fujitani T, Ui T, Matsuda J, Ercan T (1995) Geochemical features of collision-related volcanic rocks in central and eastern Anatolia, Turkey. J Volcanol Geoth Res 64:171–192. doi:10.1016/0377-0273(94)00077-T

Okay AI, Tüysüz O (1999) Tethyan sutures of northern Turkey. Geol Soc Spec Publ 156:475–515

Örgülü G, Aktar M, Türkelli N, Sandvol E, Barazangi M (2003) Contribution to the seismotectonics of Eastern Turkey from moderate and small size events. Geophysc Res Lett 30(24)

Ozacar AA, Gilbert H, Zandt G (2008) Upper mantle discontinuity structure beneath East Anatolian Plateau (Turkey) from receiver functions. Earth Planet Sc Lett 269:426–434

Pearce JA et al (1990) Genesis of collision volcanism in Eastern Anatolia, Turkey. J Volcanol Geotherm Res 44:189–229

Reidel SP, Camp VE, Tolan TL, Martin BS (2013) The Columbia River flood basalt province: stratigraphy, areal extent, volume, and physical volcanology. Geol Soc Am Spec Pap 497:1–43

Richter FM, McKenzie D (1984) Dynamical models for melt segregation from a deformable matrix. J Geol 92:729–740

Rodgers AJ, Ni JF, Hearn TM (1997) Propagation characteristics of short-period Sn and Lg in the Middle East. B Seismol Soc Am 87:396–413

Salah MK, Sahin S, Aydin U (2011) Seismic velocity and Poisson's ratio tomography of the crust beneath east Anatolia. J Asian Earth Sci 40: 746–761. doi:10.1016/j.jseaes.2010.10.021

Sanver M (1968) A palaeomagnetic study of Quaternary volcanic rocks from Turkey. Phys Earth Planet Inter 1:403–421

Scott DR, Stevenson DJ (1986) Magma ascent by porous flow. J Geophys Res-Sol Ea 91(B9):9283–9296

Selçuk-Sağlam S, Erturaç MK, Nomade S (2016) Geology of the Çaldıran Fault, Eastern Turkey: age, slip rate and implications on the characteristic slip behaviour. Tectonophysics 680:155–173

Şengör AMC, Özeren S, Genç T, Zor E (2003) East Anatolian high plateau as a mantle supported, north-south shortened domal structure. Geophysc Res Lett 30. doi:10.1029/2003GL017858

Shabanian E, Acocella V, Gioncada A, Habibolllah G, Belier O (2012) Structural control on volcanism in intraplate post collisional settings: Late Cenozoic to Quaternary examples of Iran and eastern Turkey. Tectonics 31:TC3013

Small C, Naumann T (2001) The global distribution of human population and recent volcanism. Global Environmental Change Part B Environmental Hazards 3(3):93–109

Sun SS, McDonough W (1989) Chemical and isotopic systematics of oceanic basalts: implications for mantle composition and processes. Geol Soc Lond Spec Publ 42:313–345

Thordarson T, Self S (1993) The Laki (Skaftár Fires) and Grímsvötn eruptions in 1783–1785. B Volcanol 55(4):233–263

Tibaldi A (2015) Structure of volcano plumbing systems: a review of multi-parametric effects. J Volcanol Geotherm Res 298:85–135

Tryggvason E (1984) Widening of the Krafla fissure swarm during the 1975–1981 volcano-tectonic episode. Bull Volcanol 47:47–69

Tuffen H, James MR, Castro JM, Schipper CI (2013) Exceptional mobility of an advancing rhyolitic obsidian flow at Cordón Caulle volcano in Chile. Nat Commun 4

Türkünal S (1980) Doğu ve Güneydoğu Anadolu'nun jeolojisi. TMMOB Jeoloji Mühendisleri Odası.

White JDL, Houghton B (2000) Surtseyan and related phreatomagmatic eruptions. Encyclopedia of volcanoes. Academic, San Diego, p 495–513

Yılmaz Y, Guner Y, Saroglu F (1998) Geology of the Quaternary volcanic centres of the East Anatolia. J Volcanol Geoth Res 85:173–210

Zhao D, Hasegawa A, Horiuchi S (1992) Tomographic imaging of P- and S-wave velocity structure beneath northeastern Japan. J Geophys Res 97:19909–19928

Zhao D, Hasegawa A, Kanamori H (1994) Deep structure of Japan subduction zone as derived from local, regional and teleseismic events. J Geophys Res 99:22313–22329

Zhao D, Yanada T, Hasegawa A, Umino N, Wei W (2012) Imaging the subducting slabs and mantle upwelling under the Japan Islands. Geophys J Int 190:816–828

Zienkiewicz OC (1979) The finite element method. McGraw-Hill, New York, p 787

Zor E, Sandvol E, Gurbuz C, Turkelli N, Seber D, Barazangi M (2003) The crustal structure of East Anatolian plateau from receiver functions. Geophysc Res Lett 30. doi:10.1029/2003GLO18192

Appendix C

Supplementary data of Özgür Karaoğlu & Abdelsalam Elshaafi & Mohamed Salah & John Browning & Agust Gudmundsson (2017)

II

Stratigraphic columnar section of the Ağrı and Lake Van region (data taken from Türkünal, 1980). (u_l): thickness; E: Young's modulus; ρ_r: the average density of the host rock; v: Poisson's ratio.

AGE			LITHOLOGY	EXPLANATION	(u_l)	E		v	ρ_r
CENOZOIC	Quaternary	Holoc. / Pleistocene		Basaltic andesite, andesitic basalt and andesitic, rhyolitic, trachitic lavas	3000	E_1	35	0.25	3200
	Tertiary	Upper Pliocene		Alternation of sandstone, siltstone, mudstone and limestone	2500	E_2	30	0.25	2600
		Miocene		Alternation of limestone sandstone, and marl	3000	E_3	40	0.25	2500
		Oligo-Miocene		Alternation of sandstone, siltstone, and mudstone	2000	E_4	20	0.25	2500
		Upper Eocene		Variations of gabro, diabase rocks, pelagic sediments and limestones	2500	E_5	35	0.25	2800
		Lower-Middle Eocene		Alternation of sandstone, calcarenite, limestone, marl and mudstone	3000	E_6	40	0.25	2500
		Upper Paleocene		Limestone	2000	E_7	50	0.25	2500
				Alternation of sandstone, marl and mudstone	3000	E_8	25	0.25	2500
MESOZOIC	Jurassic-Cretaceous			Variations of gabro, diabase rocks, pelagic sediments and limestones	2200	E_9	35	0.25	2800
				Ultrabasic rocks	2000	E_{10}	45	0.25	3100
				Alternation of meta volcanic, meta ophiyolite, and metasedimanter rocks	1500	E_{11}	50	0.25	3200
				Alternation of platform type marl, limestone, calcarenite and metamorphic rocks	2000	E_{12}	40	0.25	2500
				Metasedimentary rocks	2000	E_{13}	35	0.25	2700
	Paleozoic			Metamorphites: Gneiss, granitic gneiss, amphibolite schist, micaschist,quartziteschist, marble, sericite-chlorite schist, calc-schist and phyllate	5500	E_{14}	40	0.25	3100